SCUDO

Doctoral Dissertation

Doctoral Program in Energetics (36th Cycle)

Urban Energy Atlas for a Sustainable development

PhD Canditate

Silvia Santantonio

Supervisors

Prof. G. Mutani, Supervisor

Prof. C. Bertani, Co-Supervisor

Summary

Higher level of liveability and sustainability are the main goals in urban areas, where the building stock account as a major source of climate changing emissions (IEA, 2020). They can be reached through the reduction of GHG emissions, the implementation of the energy security and affordability (e.g. energy poverty) and the liveability of outdoor spaces. The increase in distributed renewable energy production and the reduction of energy consumption is encouraged by the UN Sustainable Development Goals (SDGs), the European Green Deal and the decarbonization plans of the European Climate Pact. Nowadays, it is strongly evident the importance of resilient energy systems in the attempt of climate change, pandemic, and energy crisis. More sustainable and resilient cities should rely on national and regional strategic planning, in which the energy issue is integrated within the decision-making processes, as it can drive to the economic development and social innovation of local communities. In Italy, to address the vulnerabilities generated by the post-pandemic crisis, the National Recovery and Resilience Plan (PNNR) has been launched: all the six strategic topics include the concept of energy sustainability and funds are allocated to energy related projects at local scale. Therefore, sustainable energy policies should be defined to be adaptable to every context and scale. The energy assessment should consider simultaneously all different scales from the territorial to the building level, as the territorial energy planning should become a fundamental component of the existing territorial regulatory framework. This can occur referring to:

- a place-based approach that highlight opportunities and criticalities specific to each context to optimize the local energy demand and supply from the available RES energy mix,
ensuring the long-term sustainability of local economic development.
- a holistic approach, able to integrate with the existing environmental, social, and economic policies and the territorial and urban plans to ensure the sustainability of interventions.

Therefore, the energy planning of territories requires supporting models and tools in exploring the spatial distribution of energy consumption, local RES, GHG emissions and liveability of urban environment (e.g thermal comfort conditions), integrating different levels of analysis at proper scales and comparing different scenarios. Decline energy policies to each specific context can contribute in overcoming local constraints and defining flexible measures. Referring to the scientific research field of Urban-Scale Energy Models (USEM), all different parameters that contribute to the electrical and thermal energy consumption of buildings must be considered to meet the local energy demand with the available RES generation, optimizing the morphology of the built environment and the available local energy production. A mutual influence between urban context and every building exists: urban morphology and local climate are crucial to assess the building energy performance at different level. In fact, the novelty of this kind of modelling consists of the conversion of energy-related variables from validated Urban Building Energy Models (UBEM) in new input parameters defined at a larger scale to assess energy consumption and producibility at district, urban or territorial scale. These models make use of Geographic Information System (GIS) software and tools to process different data, scaling through different spatial levels. They provide for the possibility to apply a very flexible methodology, adapting it to the peculiarities of each case study and allowing its replicability. The advantage of a GIS-based methodology stands in achieving reliable results with short-time simulations, as required in larger-scale energy assessments.

This research takes part from an existing GIS-based engineering energy model already validated within the previous work of my research group. It has been designed to evaluate the space heating energy consumption both at building and district scale at monthly and hourly level, as it is based on

a dynamic-energy balance of buildings with the calibration and optimization of some parameters (sky view factor, solar exposition, urban canyon aspect ratio) to consider the urban context.

The main objective of this work is the implementation of the GIS-based engineering energy model, modelling the ventilation loads and the number of air changes per hour (ach), according to the building characteristics, the urban context, and the local climate conditions. Since the ventilation aspect has not yet been studied on an urban scale in the GIS-based engineering energy model, the aim of this research is to delve deeper into the evaluation of ventilation loads at neighbourhood scale considering how local climatic conditions and urban morphology influence the air flow rate inside each building, which consequently affects building energy performance, indoor air quality and thermal comfort conditions. According to this, the research activity has been organized in steps to investigate: i) how the terrain roughness and obstacles affect the wind speed and direction inside urban canyons at urban scale, influencing wind path and momentum, generating windward/leeward zones, turbulence, and pressure variation on building facades; ii) how the combined effect of wind-driven and buoyancy can generate air flows inside building zones, applying parametric models at building scale to calculate the air flow rate due to infiltrations through building envelopes; iii) how the ventilation loads due to infiltration, intended as thermal gains or losses, affect the monthly and hourly variation of the Air Change per Hours (ACH) parameters and consequently the thermal energy balance equation for building space heating and cooling.

Regarding the first step, this work investigates specific GIS tools and remote sensing techniques to retrieve physical-based model at urban scale based on interactions with spatial geometries. Q-GIS plug-in based on morphometric methods is studied allowing to define the spatial distribution of aerodynamic parameters as a function of morphometric parameters with digital surface model (DSM) as input data and the real environment as application field. Starting from it, a place-based methodology is proposed to calculate: i) the wind speed variation at local scale as a function of roughness elements morphology, ii) the spatial distribution of the height of boundary canopy layer at neighbourhood scale to apply proper wind profile laws, iii) the horizontal and vertical distribution of incident wind speed along buildings' facades to determine air flow rate inside building (considering only the natural wind-driven effect). The GIS place-based methodology is applied at building and bock of building scale to a case study in Turin and results are compared with the one of validated parametric tools (*Cpcalc+).* From the analysis of the main limits of this methodology, concerning the impossibility of adjusting the wind speed inside urban canyons, derives the second step of investigation regarding the evaluation of wind paths and momentum inside urban street canyons where turbulent flows occur due to the presence of roughness elements (buildings).

A lack of investigation in this research field regards the evaluation of urban airflows pattern in non-isothermal conditions. The proposed methodology is applied at urban level to several zones in the city of Turin, after having identified classes of the urban canyons as representative of the whole city, considering two important parameters: the aspect ratio and the canyon axis orientation. Seasonal hourly variations of the local climatic conditions are assessed to include all the effective hourly variations during a whole climatic year. The results of these analyses carried out in GIS constitute the boundary conditions provided to the research group of the DIMEAS department which is responsible for the 2D CFD simulations that are processed. The goal of CFD analysis is to acquire velocity vector fields in the dominium, considering the combined effect of cross wind-driven and thermal buoyancy in different local climatic conditions, and to evaluate how vortical structures are affected by the urban geometry. The objective is to adjust the reference hourly wind speed obtained from local weather station at specific points in the canyon positioned near the windward and leeward facades of buildings

at interesting heights above the ground. Results from CFD simulations allow to describe the boundary conditions of the air flow model at urban scale that implemented in the third step of this research.

This part of the work concerns the definition and application of an air flow lumped parameters model that is designed to consider the combined effect of cross natural ventilation, wind-driven and buoyancy on air flow rate at building level. Initially a single-zone model is analysed, considering only the effect of wind-driven cross-ventilation; levels of complexity are gradually inserted into the model, moving to multidimensional models: a two-zones air flow model, including the buoyancy effect and then the three-zones air flow model. The last model represents a promising solution which can entail a good balance between the physical phenomena's description, the great number of input data, the detailed description of the building: a model that is synthetic enough to be applied to all buildings in an urban area. The building is schematized in a finite number of interconnected zones, represented by nodes and links, which describe the displacement of the air flow in space. Nodes and links are the elements of a network system whose relationships are describe in mathematical terms by the zero-dimensional multizone lumped parameter model based on the theory of oriented graphs. In a three-zones air flow model, ten links connect two heated zones representing the apartments identified below the local displacement height, one no-heated zone, representing the building shaft, and four external nodes, representing the outdoor environmental conditions around the building's facades. The calculated air flow rate is due only to infiltrations, depending on the characteristics of leakages, openings, and buildings; hourly pressure variations consider both dynamic and potential contributions, and the stack-effect, according to different climate conditions for each class of urban canyon. Based on the theory of mass and energy conservation, the non-linear equations system associated to the network, is solved by an iterative procedure using the Newton-Raphson numerical method. In particular, the *fsolve* function and the trust-region algorithm in *MatLab* software are chosen as a numerical method to find the zeros of the functions. Several trials have been done to define the proper tolerance criteria and initial values, that are fundamental to achieve model convergence. The resulting hourly air flow rate is then used to calculate the hourly air changes per hours (ach) in each of the three indoor zones and for the whole building. According to the hourly variation of local climate condition and the characteristics of the urban canyon in which a building is sited, this methodology allow to evaluate the hourly variation of the number of ach for each building in a case study zone at urban scale.

The results of the 3-zone air flow model constitute a new dataset that can be used as optimization and calibration parameters of the GIS-based engineering energy model for the hourly space heating consumption of residential building. It provides a wide and exhaustive case history describing the hourly variation of ach values for any building examined, that can replace the fixed ach values used in the energy model. Then, int the energy assessment of the energy performance of buildings, the contribution of each thermal gain and loss in the thermal energy balance can be evaluated separately, with a focus on ventilation loads. Relying on open-source software with high level of integrability provides for the possibility to implement the proposed methodology with existing plug-in for application at larger spatial scale with simulations that last just few hours. Among the possible applications of the presented place-based methodology, there is its integration in a digital platform to simulate urban energy scenarios, combining ventilation assessment. It provides for the possibility of mapping an entire city, helping policy makers, urban planners, public administration, and citizens in architectural and urban planning capable of exploiting the morphological peculiarities of the built environment to increase the energy efficiency of buildings and make urban space more liveable.

Contents

Nomenclature

Nomenclature – *symbols and units*

Symbol	Quantity	Unit
alt	Altitude	m (asl)
ach	Air changes per hour	1/h
A	Area	m^2
C	thermal capacities	$[kJ \cdot m^{-2} \cdot K^{-1}]$
c_a	air specific heat	$J \cdot kg^{-1} \cdot K^{-1}$
Cd	Discharge Coefficient	-
Cp	Pressure Coefficient	-
DirV	Wind direction (undisturbed flow)	0°(N)
$GtCO_{2e}$		$GtCO_{2e}$
g	Gravity	m/s^2
g	solar transmittance of glass	
H	Height of the canyon	m
he	Convective exchange capacity	W/m^2K
H/W	Aspect ratio (Height-to-Width)	-
K	Leakage coefficient	-
I_b	Direct normal solar irradiation	W/m^2
I_d	Diffuse solar irradiation	W/m^2
I_{inc}	Incident solar irradiation	W/m^2
$\dot{m}$	Air flow rate	Kg/s
n	Type of flux motion (coeff.)	-
P_{atm}	Atmospheric pressure	Pa
p_{dyn}	Dynamic pressure	Pa
p_s	Static pressure	Pa
p_{pot}	Potential pressure	Pa
Re	Reynolds number	
S/V	surface-to-volume ratio	-
t	time	h,s
T_{air}	Air temperature	°C, K
T_{s-a}	Sol-air temperature	°C, K
T_{ai}	indoor air temperature	°C, K
T_{ae}	external air temperature	°C, K

Symbol	Quantity	Unit
U	thermal transmittances	$[W \cdot m^{-2} \cdot K^{-1}]$
U	Wind velocity (undisturbed flow)	m/s
v	Wind velocity (inside canyon)	m/s
vol	Volume	m^3
W	Width of the canyon	m
z	Height from the ground	m
z_H	Mean Height	m
z_{Hmax}	Maximum height	m
z_{Hstd}	Height variability	m
z_0	*Roughness length*	m
z_d	*Zero-plane displacement height*	m
α	Absorption factor	-
β	Sun incident angle on building facade	°
ΔP	Pressure variation between nodes	Pa
ΔT	Temperature variation inside canyon	K
θ	Wind direction (undisturbed flow)	0°(N)
υ	Roughness parameters	-
ρ	Air density	Kg/ m^3
δ	height of the boundary layer	m
σ_H	variability of roughness	-
λ_p	Plan Area Index	-
λ_f	Frontal Area Index	-
φ_I	heat flow rate from internal gains	W
φ_{sol}	heat flow rate from solar gains	W
φ_C	heat flow rate from the cooling system	W
φ_H	heat flow rate from the heating system	W
φ_T	heat flow rate by transmission	W
φ_V	heat flow rate by ventilation	W

Nomenclature – *subscripts*

C	Celsius degree	***op***	opening
K	Kelvin degree	**out**	outdoor
i	generic node	***ref***	reference
in	internal/indoor	**sh**	shaft
L	links associated to a node		
leak	leakage		
1, 2, 3, 4	external nodes	**a,b,c**	Internal nodes and zones
a', a'', b', b'', c', c'', c''', c"	internal nodes at leakage level		

Nomenclature – *acronyms*

ABL	Atmospheric Boundary Layer	**MOS**	Main Orientation of the Street
AI	Artificial Intelligence	**NC**	Narrow Canyon
AIC	Akaike Information Criterion	**NDVI**	Normalized Difference Vegetation Index
BCR	Building Coverage Ratio	**PAD**	Plan area density
BD	Building Density λp	**PCA**	Principal Component Analysis
BEM	Building Energy Modeling	**PNIEC**	Integrated National Plan for Energy and Climate
BFA or λs	Building frontal area	**PNRR**	Italian National Recovery and Resilience Plan
CFD	Computational Fluid Dynamic	**RC**	reduced-order resistor capacitor (RC) models
CEC	Citizens Energy Community	**REC**	Renewable Energy Community
DEM	Digital Elevation Model	**RES**	Renewable Energy Source
DHN	District Heating Network	***RSL***	Roughness Sub-Layer
DSM	Digital Surface Model	***SAGA***	System for Automated Geoscientific Analysis
DSO	Distribution System Operators	**SAR**	Side Aspect Ratio

DTM	Digital Terrain Model
EC	Energy Community
EU	European Union
FAR	Frontal Area Ratio
GAR	Green Area Ratio
GFAR	Gross floor area ratio
GHG	Green House Gases
GIS	Geographic Information System
HVAC	Heating, Ventilation and Air Conditioning
HDD	Heating Degree Days
HCSE	Heteroskedasticity-Consistent Standard Errors
IPCC	Intergovernmental Panel on Climate Change
ISL	Internal Sub-Layer
ISTAT	Italian census database
LC	Large Canyon
MC	Medium Canyon
ML	Machine Learning
SCD	Street Canyon Density
SVF	Sky View Factor
TS	Thermodynamic system
UBEM	Urban Building Energy Modeling
UBL	Urban Boundary Layer
UC	Urban Canyon
UCL	Urban Canopy Layer
UMEP	Urban Multi-scale Environmental Predictor
UN	United Nation
USEM	Urban System Energy Modeling
USBEM	Urban Scale Building Energy Modeling
VIF	Variance Inflation Factor
VEG	Vegetation Area Density
WIN	Winter (season)
WCF	Winward Cold Facade
WHO	World Health Organization
WS	Weather Station
WWF	Windward Warm Facade

List of Figures

Chapter 1 – Energy atlas for sustainable development

1. Introduction and motivation

In the last report of the Intergovernmental Panel on Climate Change (IPCC) [1], the responsibility of the human activities in causing the global warming is unequivocally presented and it is principally related to the emissions of greenhouse gases (GHG), reaching a global surface temperature of +1.1°C above 1850–1900 in 2011–2020.

Over 2010–2019, global GHG emissions have continued to increase with ongoing contribution from unsustainable energy use, land use, lifestyles and patterns of consumption and production across countries: a record high of 57.4 $GtCO_{2e}$ has been reached in 2022, growing by 1.2 per cent (0.6 $GtCO_{2e}$) from the previous year. This rate is slightly above the average rate in the decade preceding the COVID-19 pandemic (2010–2019), when GHG emissions growth averaged 0.9 per cent per year, but is slower than the emissions growth of the 1990s (1.2 per cent per year) and 2000s (2.2 per cent per year). Around the 75% of global GHG emission contributions come from cities and urbanized contexts [2].

The climate change issue is nowadays affecting many climate extremes in many regions across the world. Adverse impacts on human health, on economies and society, on food, water and energy security are actually evident. Vulnerable communities who have historically contributed the least to current climate change are disproportionately affected [1].

Climate changes, pandemic, and energy prices crisis have highlighted the centrality of the energy topic [4]. The concept of cities and the management of energy consumption and production have been exported to the developing countries and now there is an energy problem that affects almost all the world, due to the high use of fossil fuels imported from abroad.

More than half of the world's population resides in urban areas, and the projections to 2050 confirm the growth trend [5] . Higher levels of liveability and sustainability are the main goals in high-dense urban areas, where the building stock account as a major source of climate changing emissions [6]. Despite the transportation and industrial activities that can strongly differ among cities, the building sector is commonly a key-contributor in affecting urban environmental sustainability.

In 2022, 96% of the European urban population was exposed to concentrations of fine particulate matter above the health-based guideline level set by the World Health Organization (WHO) [7]. Data from 2021 show that Central-eastern Europe and Italy reported the highest concentrations of particulate matter, primarily due to the burning of solid fuels for domestic heating and their use in industry [7]. Air pollution emissions have declined in the last two decades, resulting in better air quality. Despite this improvement, air pollution remains the largest environmental health risk in Europe. Exposure to fine particulate matter and nitrogen dioxide levels is linked to asthma, heart disease and stroke. air pollution can considerably impact Europe’s economy due to increased healthcare costs, reduced life expectancy, and lost working days across sectors. It also damages vegetation and ecosystems, water and soil quality, and local ecosystems.

Since the 1980s, the EU has adopted strict policies on air quality. The European Commission has proposed an updated Directive on ambient air quality and cleaner air for Europe, with a key goal being to bring EU standards closer to recommendations from the WHO report [8]. The challenges of rising temperatures and air pollution in cities are linked to current energy systems based on the use of fossil fuels in all sectors, including the energy consumption of buildings.

In fact, the 74.5% of the European population live in urban contexts [9]; here, the building sector is responsible of the 36% of total GHG emissions [10], while the residential building sector accounts for the 28% of final energy-uses [Eurostat database, available here https://ec.europa.eu/eurostat/web/main/home, last access on June 25, 2024]. Higher levels of urban sustainability can be reached through the reduction of GHG emissions, the implementation of the energy security and affordability (e.g. energy poverty) and the liveability of outdoor spaces.

To implement a *Clean Energy Transition* achieving carbon neutrality by 2050 international strategies and policies have been implemented, whose main objectives are the increase of energy self-sufficiency, security, and equity with a reduction of GHG emissions, especially in the critical high-density urban environments. The increase in distributed renewable energy production and the reduction of energy consumption is also encouraged by the *UN Sustainable Development Goals* (SDGs) adopted by the United Nation [11].

The *European Green Deal* [12] has increased its climate ambition aiming in transforming the EU into a modern, resource-efficient and competitive green economy with the *Fit for 55% package*. More specifically, the EU aims to: reduce greenhouse gas emissions by 55% compared to 1990 levels, achieve a share of at least 32% of energy from renewable sources in total energy consumption, increase energy efficiency by 32.5%, reduce CO_2 emissions in transport by 50-55%, promote low-carbon industrial production with the help of more sustainable technologies, encourage electrification in the energy mix, strengthen the internal energy market and promote the development and use of green hydrogen.

Among the key principles of the *European Green Deal* and to achieve the goals set by the *Paris Agreement 2015* [13], the *Clean Energy for all Europeans Package*, proposed in November 2016, sets eight legislative acts, among which there are two important directives. These have directly influenced the national and local energy policies of the state members in shifting towards an energy territorial planning. The Renewable Directive- RED II (2001/2018/EU) [14] o*n promoting the use of Renewable Energy Source*, it contains the definition the *Renewable Energy Communities (REC)*, and the so called, Electricity Directive (2019/944/ EU) [15] *on common rules for the internal market for electricity* addresses the *Citizen Energy Communities (CEC*).

These directives declare two legal entities: *the Citizens Energy Communities (CEC)* in which citizens, Small-Medium Enterprises (SME) and local authorities, cooperate in the generation, consumption, distribution, storage, supply of energy, or in providing energy efficiency and service management (regardless of renewable energies); the *Renewable Energy Communities (REC)* that owns the objective of providing, through renewable energy production and sharing activities, environmental, economic and social benefits to the community, without contemplating electricity distribution activities. These two new energy subjects can boost the European energy transition towards more sustainable, competitive, and secure energy systems, enhancing the active role of citizens, collective participation and action, the strengthening of renewable and distributed energy production and therefore a more territorial dimension of energy systems.

In the transposition of the EU Directive into the current Italian regulatory framework, this new energy configurations have been implemented by the objectives set up by the national energy plans. The Integrated National Plan for Energy and Climate (PNIEC) 2030 [16] set ambitious objectives in achieving the 65% of RES production in electricity consumption, the 40.5% of renewables in gross final energy consumption, a reduction of GHG emission (-62% compared to 2021), and promoting the energy self-consumption; this last directly related to the Energy Communities configurations.

The PNIEC is divided into five dimensions, which follow the European Union guidelines and highlight specific purposes to be met by 2030:

- Decarbonisation, reducing emissions and increasing renewable energy in the electricity, heat and transport sectors.
- Energy efficiency, implementing directives on energy efficiency and on energy performance of buildings, focusing on renovation, electrification, thermal insulation and automation.
- Energy security: better managing the challenges generated by war events, market volatility and fuel prices, and security of infrastructures for energy supplies.
- Internal market: integrating European energy markets and strengthening Italy's role as a European energy hub.
- Research, innovation and competitiveness: developing new technologies and the promotion of competitiveness in the energy sector.

In addition, to address the vulnerabilities generated by the post-pandemic crisis, the Italian National Recovery and Resilience Plan 2021 (PNNR) [17] has been launched: all the six strategic topics include the concept of energy sustainability and funds are allocated to energy related projects at local scale. Among the six missions, the *green revolution and ecological transition* (mission 2) is made up of four components; among them, the most relevant to the energy topic are the ones that concern the *renewable energy, hydrogen, network and sustainable mobility* (component n.2) and the *energy efficiency and energy retrofit of buildings* (component 3).

On the availability of energy source throughout the territory and on the energy security, the sustainable development of countries can be based. The energy security means to guarantee the continuity of supply, even in the occurrence of catastrophic events, and to ensure physical and economic energy accessibility for all citizens. Both conditions can be achieved by self-producing the demanded energy, relying on technologies that exploit local renewable energy sources (RES).

To faster energy transition processes an overall optimization of the site-specific energy demand and supply is necessary using a systemic perspective and setting multiple evaluation indicators, among which there are the self-sufficiency and the carbon neutrality.

The most critical areas, in terms of high-energy demand and low renewable energy sources are the urban environments, especially high-dense built cities.

A very crucial challenge for the European policies is how to reach high level of energy self-sufficiency in high-density urban contexts, boosting available but scarce renewable energy sources (RES) to satisfy a demand that must necessarily be reduced [18]. The high-energy intensity and the numerous technical and regulatory constraints, together with the low availability of RES, require a shift in the spatial scale of the energy analysis: from the local scale (i.e., building or block of building scale) to the urban and territorial scale.

Nowadays, it is strongly evident the importance of resilient energy systems in the attempt of climate change, pandemic, and energy crisis. More sustainable and resilient cities should rely on national and regional strategic planning, in which the energy issue is integrated within the decision-making processes, as it can drive to the economic development and social innovation of local communities.

Therefore, sustainable energy policies should be defined to be adaptable to every context and scale. The energy assessment should consider simultaneously all different scales from the territorial to the building level, as the territorial energy planning should become a fundamental component of the existing territorial regulatory framework.

According to these premises, the planning of energy supply and demand becomes a fundamental process, the scale of which must necessarily extend to the territorial scale. In this way it is possible to deal with the dispersed and discontinuous nature of renewable sources, evaluating the convenience between the use of storage systems and the differentiation and optimization of the energy mix to exploit different energy sources.

Territorial energy planning is required to manage the complexity due to the multiplicity of subjects and networks, the different spatial and temporal scales, the dynamics and mutual influences that exist between them, but also the different objectives to be achieved which can create conflicts. The potential of this level of investigation is given by the possibility of providing an overall vision capable of predicting real and contextual opportunities and critical issues, capable of orienting policies and strategies, choosing between possible scenarios. This can happen without relying on in-depth studies which require time and resources with the risk of hindering the translation of the actions envisaged by the plans into concrete projects.

The territorial energy planning can occur referring to:

- a place-based approach that highlight opportunities and criticalities specific to each context to optimize the local energy demand and supply from the available RES energy mix, ensuring the long-term sustainability of local economic development.
- a holistic approach, able to integrate with the existing environmental, social, and economic policies and the territorial and urban plans to ensure the sustainability of interventions.

Therefore, the energy planning of territories requires supporting models and tools in exploring the spatial distribution of energy consumption, local RES, GHG emissions and liveability of urban environment (e.g thermal comfort conditions), integrating different levels of analysis at proper scales and comparing different scenarios. Decline energy policies to each specific context can contribute in overcoming local constraints and defining flexible measures.

1.1. Scientific research framework

In this study the main scientific research framework regards the place-based approach on energy models to investigate the natural and anthropogenic urban environment, including the spatial relationships between objects to tackle the complexity of the urban energy systems. In present days, place-based energy planning has become a discussed tool. This integration can ensure the identification of more effective and context-adapted energy models for a sustainable development of territories [19].

Referring to the scientific research field of Urban-Scale Energy Models (USEM), all different parameters that contribute to the electrical and thermal energy consumption of buildings must be considered to meet the local energy demand with the available RES generation, optimizing the morphology of the built environment and the available local energy production. A mutual influence between urban context and every building exists: the local climate and the urban morphology are fundamental to assess the building energy performance at different level.

In fact, the novelty of this kind of modelling consists in the conversion of energy-related variables from validated Urban Building Energy Models (UBEM) in new input parameters defined at a larger scale to assess energy consumption and producibility at district, urban or territorial scale.

The Geographic Information Systems (GIS) can have a significant role in the identification of proper energy models at urban scale and in their application [20]. It provides for the possibility to geo-

reference all the energy-related information at any territorial scale, and perform qualitative and quantitative analysis, including spatial analysis [21]. GIS tools can support decision-makers and urban planners thanks to the visualization of realistic and multilayer representations of energy consumptions through a spatiotemporal dimension [22].

The Urban-Scale Energy Models (USEM) can make use of Geographic Information System (GIS) software and tools to process different data, scaling through different spatial levels. They provide for the possibility to apply a very flexible methodology, adapting it to the peculiarities of each case study and allowing its replicability. The advantage of a GIS-based methodology stands in achieving reliable results with short-time simulations, as required in larger-scale energy assessments.

The place-based approach characterized by a multiscale and multidisciplinary features is functional to decline global strategies into local effective actions [23]. Among the advantages of applying the place-based approach on energy modelling there is the opportunity to increase a great flexibility in energy assessment for different cities and communities in different environmental, socio-economic contexts and legislative and regulatory frameworks. The place-based USBEM can support strategic territorial and urban energy planning in redistributing sustainability targets, exploiting opportunities and compensating constraints of each local context.

Delving into the possibility of implementing USBEM models with the place-based approach, Urban Scale Building Energy Modelling allows to describe spatial correlation of the interdependent systems of buildings, and to manage mutual influence between local and larger scale physical phenomena [24]. It means relying on energy models to assess spatial distribution of energy consumption of buildings, integrating it with local available RES production and comparing different scenarios of interventions. Different typologies of USBEM can be implemented with the place-based approach.

The main advantages concern the possibility to select the more effective energy model or tool in each case study application; thanks to an increase in the number, the typology, and when possible, the accuracy of energy-related variables.

Moreover, this allows to properly identify local energy policies and plans, including in every energy model environmental, socio-economic, and technical input data that is known can have an important impact on the actual and future energy scenarios [25] . To sum up, a place-based approach combined with energy consumption models of buildings at urban scale can be a promising tool assessment to identify the most effective solution to improve energy efficiency in each territory [26].

1.2. Research gap

Reviews of the existing energy models and tools without (presented in detail in the next chapter) reveal that among the main disadvantages for their application is related to the large amount of input data that are required to run simulations, most of which are often not available and provided by not accessible databases. Few energy models and tools at urban scale are able to simulate all buildings of an entire city without exceed in simulation times and computational effort requiring specific resources. Therefore, most of them have limitations in describing the real urban energy distribution and energy related context of a certain case study.

To sum up, simple and easily applicable models are needed, sufficiently accurate to provide reliable results with flexible approach and fast simulations, and that can harmonize different type of variables relying on accessible public and available database in order to ensure replicability and updating of assessments.

1.3. Research objective and novelty

The most effective model typologies for assessing and optimizing the energy demand and supply are the process-driven (engineering) energy models. By the adjustment of some variables, they can verify different and future scenarios. For this reason, in addition to the possibility of model predictions, they offer the possibility of distinctly determining the contribution of each energy related variable and evaluating its weight in relation to the overall result.

The work here presented aim to introduce an improvement to an already existing engineering energy model for the evaluation of the energy consumption for space heating and cooling of residential buildings on a territorial scale, assessing the fluctuation of ventilation load as a function of the air tightness of buildings, and the surrounding context, including urban morphology and microclimate.

This physic-based process-driven engineering energy model is also a USBEM and GIS-based model already implemented with a place-based approach. It has already validated within previous works [27] to assess the space heating energy consumption both at building and district scale at monthly and hourly level.

The main goal of the doctoral research activity has been to delve deeper into the aspect of urban natural ventilation which had not yet been studied on an urban scale in the GIS-based engineering energy model. The goal is to model the ventilation loads and provide hourly values of the number of air changes per hour (ach) to be applied in the energy model, according to the building characteristics, the urban context, and the local climate conditions. This has required the evaluation of ventilation loads at neighbourhood scale considering how local climatic conditions and urban morphology influence the air flow rate inside each building, which consequently affects building energy performance, indoor air quality and thermal comfort conditions.

The main purpose has been the definition of a physic-based and GIS-based methodology at different spatial scale to investigate urban ventilation as a physical phenomenon that varies according to scale.

The place-based methodology here proposed aim to integrate physic equations and the use of GIS to consider local characteristics of the real built environment. This improvement consent to increase the number and quality of energy-related variables through geo-databases, to comprehend the relationships behind spatial patterns, to rely on new tools appropriately selected to be adapted to the research's objectives, optimizing techniques to analyze any territory and city.

Starting from the premises above, this work deals with methodology and models that describe the spatial interrelationship within the urban components, together with temporal variation of physical phenomena influencing energy consumption.

This research investigates the use of USBEM with a place-based approach focusing on the urban ventilation evaluations at different scale with the objective to:

- describe the specific characteristics of urban natural ventilation that influence the energy consumption of buildings in urban environments
- adjust or adapt existing assessments tools to describe urban and building ventilation related parameters characteristics and their spatial distribution
- define site-specific parameters and threshold values considering all real specificities and constrain of a case study

The main features of this research activity, throughout all the steps in which it is declined, consist of a:

- place-based approach to implement site-specific energy modelling according to the accessibility of spatial information, databases, and spatial correlations-tools
- inter-scalability approach (multi-level) to manage and harmonize data at different spatial-temporal scales
- multidisciplinary and holistic approach to include and describe the complexity of urban energy systems, considering the mutual influence between energy, environmental, socio-economic and governance features.

The main contribution of this work in the scientific research field is the introduction of the place-based approach into a GIS-based methodology that describes the spatial-temporal relationships of urban natural ventilation phenomena and its impact on energy consumption modeling within the complex system of urban environments.

The novelty of this kind of modelling consists of the use of open-source GIS software (Q-GIS), accessible input database already used by urban planning, and the definition and conversion of energy-related variables at a larger scale as new input parameters for the energy model with the possibility to scaling through different spatial levels while maintaining and rather implementing the level of data accuracy. As represented in the flow chart in Figure 1, the overall research activity has been organized into three main steps to investigate:

1) how the presence of roughness elements affects wind speed and direction at urban scale, influencing wind path and momentum, generating windward and leeward zones, turbulence, and pressure variation on building facades; The output of this analysis is the assessment of the wind velocity as function of the height from the ground Vz [$m \cdot s^{-1}$], applying physical law of wind profiles, and focusing on the challenging objective to assess turbulent flows that occur inside urban canyons due to the combination of the two main driving forces of wind-driven and thermal gradient effects.

2) how the combined effect of wind-driven and buoyancy generate pressure variation on building facades and air flows inside building zones, focusing on air flow rate due to infiltrations through building envelope; the output of this analysis in the assessment of the Air Change per Hours parameters (ACH) [h^{-1}], applying multizone air flow lumped parameter model based on the mass and energy conservation law;

3) how the monthly and hourly Air Change per Hours (ACH) parameters affected the ventilation loads in the thermal energy balance equation for building space heating and cooling, as thermal gains or losses of the GIS-based energy model to optimize the evaluation of hourly energy consumption of buildings.

Relying on open-source software with high level of integrability provides for the possibility to implement the existing GIS plug-in to apply the methodology at larger spatial scale with simulations that last just few hours. Mapping the entire city can help policy makers, urban planners, public administration, and citizens in architectural and urban planning capable of exploiting the morphological peculiarities of the built environment to increase the energy efficiency of buildings and make urban space more liveable. All evaluations can be collected in Urban energy Atlas and digital platforms that can support effective local energy policies through the optimization of the urban form.

This work is fully consistent with the purposes of the international national and regional energy strategies and policies, whose main objectives regard the increase of the energy self-sufficiency,

security, and equity with a reduction of GHG emissions, especially in critical high-density urban environments.

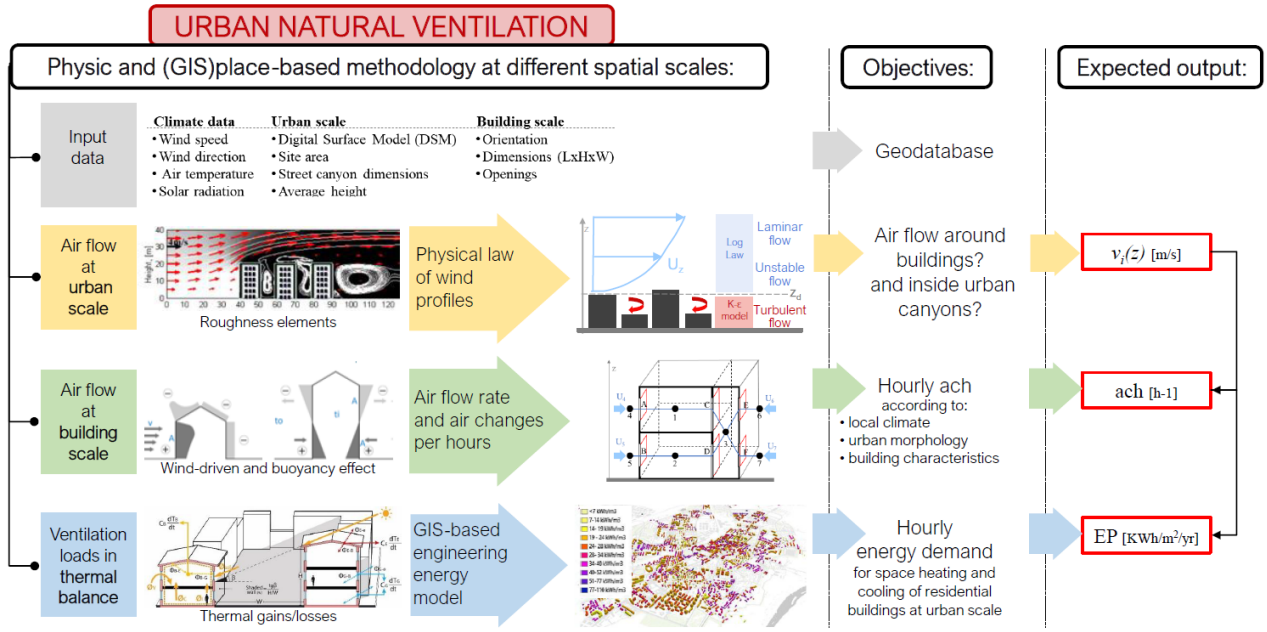

Fig. 1 - Flowchart of the overall research study on urban natural ventilation.

1.4. Thesis structure

The doctoral thesis is organized in five chapters structured as follow.

This chapter introduces the main context of the research activity, presenting the crucial challenges related to the energy transition and the motivations that lead to the need of energy sustainable strategies and planning. After introducing the main scientific research framework, the second part describes the research objectives, novelty and its contribution on the research field.

Chapter two introduce an overview of the existing energy model and tools to assess building consumption for space heating and cooling. In the first part, the state of the art is summarized, according to literature review: several energy modelling types are presented and compared, classifying them according to the modelling types, approaches and scales of application. An example of a annual data-driven (statistical) model is reported. It is a study that has been published in the journal *TECNICA ITALIANA-Italian Journal of Engineering Science* [28]. Even if it deals with the annual electric energy consumption, it constitutes an example of a GIS-based statistical energy model with a place-based and multidisciplinary approach in which energy-related variables concerning socio-economic input data are considered to implement the model in predicting annual energy consumption at municipal level.

The second part of this chapter describes the previous mentioned GIS-based and place-based process-driven engineering energy model that this research aims to implement providing hourly values of the air change per hours parameters (ach). To better understand how the physic-based model works, the thermal energy balance is presented with a focus on the ventilation loads that are directly affected by the ach parameters. Finally, the GIS place-based process-driven model is presented in its application at the block of building scale to a case study in the city of Turin. The work has been presented at the *38th International Conference on Heat and Mass Transfer (UIT)*, held in Cassino (Italy), on June 21st-

23rd, 2021 and published in the *Journal of Physics: Conference Series* [29]. The work evaluates how the urban morphology and local climate influence cooling energy demand of buildings. After re-scaling the input parameters to apply the model at the block of building scale, the results of the hourly space cooling energy demand has been compared to the ones of others energy consumption tool and model, validating the GIS-based model.

Chapter three focuses on modelling the urban local wind environment at urban scale and inside urban canyons. After introducing physical laws of wind profiles, different model and tools are compared to find the best solution to describe wind pattern at urban level. QGIS tools are studied and a selected QGIS plug-in is applied to calculate aerodynamic parameters at neighbourhood scale, correcting wind speed in presence of roughness elements and assessing the spatial variation of wind pressure across windward and leeward buildings' façades. Compared to existing parametric models, this flexible methodology considers real obstructions and spatial relationships between buildings, providing short-term simulations even at larger scale. The methodology has been applied to a real case study at district scale in Turin: the work has been presented at the *5th Building Simulation Applications Conference (BSA 2022)*, held in Bolzano (Italy), on June 29th – July 1st 2022, and published in *the BSA Conference Proceedings* [30].

The second part of this chapter describes a GIS-based methodology to assess wind paths and momentum inside urban canyons where turbulent flows occur. 2D-CFD simulations are processed to investigate urban airflows patterns in non-isothermal conditions and for classes of aspect ratio. The results are used to create a final database describing patterns of wind speed; this place-based approach allows to create specific database for all building within a zone or a city of any real case study application. In this work, results of a case study district in Turin have been assessed. The methodology has been presented at the *8th AIGE/IIETA International Conference and 18th AIGE 2023 Conference on "Energy Conversion, Management, Recovery, Saving, Storage and Renewable Systems"* held in Turin (Italy) on June 14th-15th 2023.

Chapter four deal with the evaluation of the air flow at building scale. In the first part, fundamentals of natural ventilation at building scale are studied, considering physical properties of phenomena and the main variables that influence the air flow rate to be calculated. Existing models and tools have been compared, among which the lumped parametric model has been chose to implement the GIS-place-based methodology. A brief description of the evolution of the proposed model is presented; part of this analysis has been presented at the *4th IEEE International Conference and Workshop Óbuda on Electrical and Power Engineering (CANDO-EPE)*, held in Budapest (Hungary) on November 17th-18th 2021 and it has been published in the *IEEE Conference Proceedings* [31].

In the second part, a three-zone air flow lumped parameters model is implemented to assess the hourly variation of the air changes per hour (ach), considering the combined effect of wind-driven and buoyancy, generating pressure variations and air flow motion through leakages on building envelope. The methodology has been presented at the *8th AIGE/IIETA International Conference and 18th AIGE 2023 Conference on "Energy Conversion, Management, Recovery, Saving, Storage and Renewable Systems"* held in Turin (Italy) on June 14th-15th 2023, with applications on case study at urban scale in the city of Turin. Results can be used to calibrate and optimize the GIS-based engineering energy model, evaluating the ventilation loads of thermal energy balance and the overall building energy performance. In addition, the GIS-place-based methodology consents to spatialized results and create urban energy atlas on urban ventilation characteristics for the real urban environment. Example of mapping a case study urban area to define critical zones are reported to show how this methodology can help policy makers, urban planners, and public administration in adapting energy policies

exploiting the morphological peculiarities of the built environment to increase the energy efficiency of buildings, optimizing the urban form.

Chapter five summaries the main results of this doctoral research and introduces the outlook.

Chapter 2 – Energy consumption modelling

Chapter overview

This chapter introduces an overview of the existing energy model and tools to assess building consumption for space heating and cooling. In the first part, the state of the art is summarized, according to literature review: several energy modelling types are presented and compared, classifying them according to the modelling types, approaches and scales of application. An example of an annual data-driven (statistical) model is reported. It is a study that has been published in the journal *TECNICA ITALIANA-Italian Journal of Engineering Science* [28]. Even if it deals with the annual electric energy consumption, it constitutes an example of a GIS-based statistical energy model with a place-based and multidisciplinary approach in which energy-related variables concerning socio-economic input data are considered to implement the model in predicting annual energy consumption at municipal level.

The second part of this chapter describes the previous mentioned GIS-based and place-based process-driven engineering energy model that this research aims to implement providing hourly values of the air change per hours parameters (ach). To better understand how the physic-based model works, the thermal energy balance is presented with a focus on the ventilation loads that are directly affected by the ach parameters. Finally, the GIS place-based process-driven model is presented in its application at the block of building scale to a case study in the city of Turin. The work has been presented at the *38th International Conference on Heat and Mass Transfer (UIT)*, held in Cassino (Italy), on June 21st-23rd, 2021 and published in the *Journal of Physics: Conference Series* [29]. The work evaluates how the urban morphology and local climate influence cooling energy demand of buildings. After re-scaling the input parameters to apply the model at the block of building scale, the results of the hourly space cooling energy demand have been compared to the ones of others energy consumption tool and model, validating the GIS-based model.

2.1. State of the art and literature review

In this paragraph a synthetic description of the different energy consumption models and tools is presented. In literature a wide variety of modelling exist. The state of the art presented below consider only energy model for evaluating building consumption for space heating and cooling. Different criteria can be used to classify them to find the best model for each case study. Many literature reviews agree in classifying models according to the scale of model implementation (2.1.1), the hierarchy of input data (2.1.2) and the modelling type (2.1.3).

Many authors agree that integrated urban energy models facilitate the identification of accurate, time-efficient, and feasible solutions, and that they have a great potential in supporting energy efficiency and management solutions at city scale, orienting urban and regional building energy planning for a sustainable development of the built environment [32]. However, they should face the challenge of describing the complexity of the urban energy systems; this requires resources, time and effort, in addition to insufficient and often inaccessible spatial data [33], [34], and [35].

2.1.1. Type and scale of energy modelling: from BEM to USBEM

A very consistent scientific literature exist on the topic of Building Energy Modeling (BEM): models implemented at individual building level whose results are up scaled to urban level, usually according to archetypes. It is common knowledge that it is no longer sufficient to simulate building energy demand assuming them as isolated objects from their surrounding microclimate and built context, or the energy systems in which are inserted [36] . More recently, building energy studies have been shifting from individual building to cluster and city-level evaluations [37] .

To include the geometrical relationships between buildings and the surrounded built-context, Urban Building Energy Modeling (UBEM) and Urban Scale Energy Model (USEM) have gradually replaced BEM providing large-scale simulations concerning different urban morphologies and building typologies [38]. In literature, UBEM are define as the method used for bottom-up city-scale energy modeling of buildings that includes physical model of heat and mass transfer in and around buildings [35]. UBEM is a multi-disciplinary and complex research scientific field, in which a compromise between quality and accuracy of data, adaptability of the model, computational effort and simulation time must be achieved [39]. USEM focus on the optimization of energy network systems, and usually the building stock is modeled with a low level of detail, while UBEM primarily models as a possible input to design optimized energy system at different scale [39]; the two approaches can converge together, addressing Urban Scale Building Energy Modeling (USBEM). Currently, this new type of modeling constitutes a promising field of research, even if it is a necessary reminder but there is no unique modelling solution for specific urban environments. Many literature reviews provide overviews of existing modelling, tools, and platforms, detailing their capacity to address relevant aspects of urban energy assessment [36], [40].

2.1.2. Energy modelling approaches: Top-down and Bottom-up

Regarding the hierarchy of input data and the modeling strategy, two approaches can be categorized: top-down and bottom-up approaches.

Top-down modeling relies on aggregated information to describe the relation between the energy demand and associated drivers, usually socio-economic and climate variables. Energy consumption is estimated from long-term relationships that link energy use and drivers of different nature: socio-econometric, technical or physical models [39]. They are vastly used since are simply models that rely only on aggregated historical data and not on detailed technological descriptions. However, due to their dependency on historical macroeconomic energy trends and statistical data, these models are less suitable to assess changes in technologies and their contribution on future energy demand, while are suitable for a broad and aggregated large-level scale of analysis [25]. In addition, top-down modelling cannot be used to predict future energy trends since it is based on past interconnections without any precise spatial or temporal detail correlation.

Bottom-up models are built from extensive disaggregated data of individual buildings of which the energy demand is estimated and can be aggregated in many ways. This type of modeling can formulate clusters of buildings with similar features at different scales, considering not only geometrical characteristics. They are suitable models for the identification of energy efficiency solutions and the impact of their implementation on the urban energy demand. For this reason, it is considered the ideal modeling type for in-depth urban scale building analysis [33].

2.1.3. Modelling and tools: Data-driven, Process-driven and Hybrid

Several scientific reviews [41], [39] agree in classifying USBEM into three main groups, according to the scale of model implementation: data-driven or black box models, process-driven or white-box models, and hybrid or grey-box models.

Data-driven modeling.

In this category are comprised statistical and Artificial Intelligence (AI) approaches, that can be based on Machine Learning (ML) techniques. Both statistical and ML models rely on regression algorithms of increasing level of complexity to identify the more accurate association between the energy demand of buildings and parameters selected as influential; they require large amounts of data to train and validate the model [42].

The bottom-up statistical models can easily represent relations between the individual energy-use of buildings and the buildings' characteristics and socioeconomic indicators. Statistical models are widely used since they consists into short-term simulations and fast-processing; these features collide with the difficulty in describing energy patterns, the complexity of real energy systems and detailed descriptions of peculiarities of a case study [43].

ML provides high computational capacity that allows to consider stochastic variables, identify patterns between output data, creating clusters of samples, and improving the accuracy of model predictions. ML algorithms have restricted application fields, due to their dependency on predictors' identification that are necessarily derived from the training dataset; when implemented at urban scale, ML can be very high time-consuming [44]. Several tools exist for energy analysis from statistical models [45] (e.g., *EnergyProforma, CRECM*) and for energy benchmarking and analysis from ML models [46], [47], (e.g., *DUE-S, DUE-B*).

Process-driven modeling.

The process-driven energy models, also known as engineering or physic-based models, are based on physical principles to calculate the energy performance of buildings [48]. The computation of the required energy consumption is driven from physical and technological characteristics of individual buildings: a complete set of data for the detailed description of several physical phenomena and their interaction at different scale is necessary. Compared to other methods, this type of modeling has the highest level of flexibility in evaluating technological developments and energy efficiency scenarios and its results are characterized by a higher spatiotemporal detail.

According to the simulation method, it is possible to further breakdown process-driven modeling into two groups: reduced-order resistor capacitor (RC) models and detailed multizone dynamic thermal simulation models [39]. The first make use of RC models in which, usually, each building is represented by a single thermal zone; the second use detailed dynamic heat balance equations of the walls, zones and energy systems, including energy balance equations between buildings and outdoor environment. These models can consider buildings' geometry and characteristics, people behavior, urban parameters describing the morphology of the built environment, and local and microclimate variables.

Among the many simulation engines and tools, the most used are: *CityBES, UMI,Simstadt, UrbanOPT, MIT's UBEM, CitySim, SEMANCO* [36] and *CityGM*. These tool can be used to describe the mechanisms of the transfer of energy in buildings; their application fields is wide and flexible:

after the validation of the model, the energy balance equations is adaptable to any case study context and to any multiple spatial-temporal scales [27].

The main criticalities concern the models' applicability, in relation to their specific need for extensive empirical data not always available, and the models' accuracy, in considering uncertainties and stochastic variables that do not follow physical phenomena, particularly for occupant behavior profiles [49]. These limitations motivate the use of hybrid models.

Hybrid modeling.

This new modeling type can be intended as the synthesis between process-driven modeling and data-driven modeling, combining into a more sophisticated model the best features of both approaches; in detail, the high computational efficiency of the data-driven models and the capacity of explaining physical relationships of the process-driven models [50]. In addition, synergy allows each model to overcome its own criticalities. In the hybrid models, the buildings are usually modeled according to their physical characteristics, as in the process-driven models, while energy-related data, mainly stochastic variables, is obtained from analysis of the historical energy use intensity (as in the statistical models).
Ranges of variability proper of some energy-related variables (e.g., user profiles) can be selected by ML technique and this can support the process-driven model and contribute to better calibrate the resulting hybrid model [51]. Conversely, it is possible to introduce some physical-based correlations into a data-driven model. Generally, physical-based modelling is more advantageous for USBEM with place-based approach due to the possibility to describe the dependency of variables on spatial morphology, as USBEM consist in site-specific applications.
Many studies agree in appreciating hybrid models for their better performances, their ability to handle unexpected trends and complex situations with high levels of data accuracy [52]. The number of tools (e.g., *SimStadt, TEASER, CEA*) that permit the combination of data-driven and process-driven models is currently increasing, [53], [54].

2.2. Annual data-driven (statistical) model

In this paragraph an example of an annual data-driven (statistical) energy model is presented. It is a study that has been published in the journal *TECNICA ITALIANA-Italian Journal of Engineering Science* [28]. This work deals with the annual electric energy consumption; it constitutes an example of a GIS-based statistical energy model with a place-based and multidisciplinary approach in which energy-related variables concerning socio-economic input data are considered to implement the model in predicting annual energy consumption at municipal level. To motivate the choice of this model at the municipal scale a brief introduction is necessary.

Many countries and cities around the world are trying to achieve the goal of the decarbonization of energy systems, envisaging an increase in the use of electric energy in all sectors. It is expected a widespread conversion to electric energy vector, even for uses that were not yet contemplated, especially regarding the residential building sectors. To better re-organize the existing electrical systems ensuring supply to the future energy demand, it is necessary to predict future electric consumption in each sector. As reported by [41], building characteristics are not enough to predict building energy consumption, but also occupant behaviour information are needed to deeper understand residential energy demand; in most cases, prohibitive cost of surveys and privacy issues

in collecting data contribute to a poor understanding of residential electric consumption. In line with the European energy transition goals, local energy policies are including economic and environmental concerns in energy security and efficiency strategies, with the aim to define proper solutions for each territory. The European directives are trying to empower local institutions (municipalities) to let them drive the energy transition. New energy entities named Renewable Energy Communities (REC) have been defined [14] as social instruments that can boost local energy efficiency interventions and low-carbon systems improvement through a bottom-up path. The REC are based on the balanced composition of members, both in terms of renewable production and profiles of energy demand, with the goal to optimize the energy exchange between stakeholders, and to ensure economic and environmental advantages for the whole community. To do that, consideration in urban planning must be done, and energy consumption must be investigated at a local scale.

The aim of this work is the evaluation of the demand of electric energy of residential buildings at municipal scale, according to selected energy-related variables. The goal is to define a methodology based on multiple linear regression model that can predict residential annual electric consumption and that can be replicated in any case study at municipal scale.

The analysis is performed using open-source software: the tool *Q-GIS* for the harmonization of several databases, and the calculation of climatic and urban variables, and the statistical software *R* for the implementation of statistical techniques; in detail, the principal components analysis to evaluate the main energy-related variables and the multiple linear regression to predict electric consumption of the case studies to which the model is applied.

2.2.1. Case study

This work analyses the case study of the 1,206 municipalities in Piedmont, the North-West Region in Italy. This territory is analysed considering its climatic-environmental and socio-economic characteristics. All the information come from the regional database *Geoportale Piemonte* (technical regional map *BDTRE*, updated to 2019, available at http://www.geoportale.piemonte.it/), the Digital Terrain Model (DTM), the Digital Surface Models (DSM), and the Italian census database *ISTAT* (updated to 2011, available at https://www.istat.it. All input data are georeferenced in the Q-GIS environment. For all the characteristics, in Table 1 are shown the main statistical parameters evaluated considering all the observed municipalities. Incomplete information is checked in the pre-processing phase, and outliers observations are removed.
The area of the region is vast (25,387 km^2) and characterized by a heterogeneous morphology, including different types of environmental context (mountains, hills, and plain areas), with an average altitude of 421 m asl. Local climatic input data are obtained from the Regional environmental protection agency (*ARPA*); the Heating Degree Days (HDD) are calculated, according to the UNI 10349-3:2016, assigning the correspondent climatic zone to each municipality (E 1-3 and F 1-4, in Table 2). Many of the municipalities (892) is in the climatic zone E (i.e. HDDE < 3000 °C), 309 municipalities are in zone F (i.e. HDDF ≥ 3000 C), the 74% and the 26% of all municipalities, respectively.
The total population in the region is 4,363,916 inhabitants (*ISTAT 2011*), and the average population density is around 153 inhabitant/km^2. To create homogeneous groups of municipalities, are defined: seven categories of population (*P*), and three groups (*LP-Low, MP-Medium, HP-High*). In Table 2 is reported the number of municipalities belonging to these categories. Residential buildings represent the 91% of the entire built context; the 66% of them are occupied. The average floor area for each person correspond to 49.6 $m^{2,}$ with an average total floor area per building of 106.63 m^2.

The annual electricity consumption data is provided by the Piedmont Region technical office, obtained from the Distribution System Operators (DSOs) [55]. Selecting only the observations with complete information, 1,201 municipalities are selected, considering annual energy consumption data from the year 2010 to the year 2016), excluding the year 2011 because of missing data.

Table 1. Climate, socio-economic, and built context characteristics of case study.

Characteristics		Statistical parameters			
Climatic-environmental		**min**	**max**	**median**	**average**
Area [km^2]		0.7	203.7	13.4	21.0
Altitude [m asl]		76.0	2,035.0	334.0	420.4
HDD [°C/yr]		2,422	5,165	2,766	2,883
Socio-economical					
Population [no. inhab]		42	101,952	1,015	2,868
Density [inhab/ km^2]		0.5	2,830.8	81.4	153.0
Foreigner [% on tot pop]		0	22.3	5.4	6.1
Age [% on tot pop]	0-19 /20-69 /70-99	16 /64 /20	16 /64 /20	16 /65 /19	16 /64 /20
Education Diploma [% on tot pop]	Primary School /Jr. High School /Sr. High School /University	8 /18 /10 / 0	57 /49 /50 /30	27 /35 /30 / 7	28 /34 /30 / 8
Occupation	Workforce (W) /NoW [% on tot pop]	22 /33	66 /77	51 /49	51 /49
	Employed (E) /NoE [% on tot W]	8 / 0	100 / 20	95 / 5	95 / 5
	Homemakers /Students / Fixed income /Others [% on tot NoW]	2 / 0 /24 / 0	38 /26 /88 /31	16 /11 /65 / 8	15 /11 /66 / 8
Income	[€/yr/n. of taxpayer]	6,737	36,415	19,436	19,367
Families [% on tot n.]	1 member / 2 members / 3 members / 4 members / 5 members / 6 or more members	16 /12 / 1 / 0 / 0 / 0	81 /41 / 32 / 24 / 10 / 4.8	35 /29 /19 /12 / 2.6 / 0.7	38 /28 /18 /12 / 2.6 / 0.8
Residential Built Heritage					
Year of construction [% on tot buildings]	Before 1918 1919 – 1945 1946 – 1960 1961 – 1970 1971 – 1980 1981 – 1990 1991 – 2000 2001 – 2005 After 2005	0 / 0 / 0 / 0 / 0 / 0 / 0 / 0 / 0	98 /91 /63 /44 /59 /46 /25 /18 /21	34 /12 / 8 /10 /10 / 5 / 4 / 2 / 2	37 /16 /10 /11 /11 / 6 / 4 / 3 / 2
Number of floors [% on tot buildings]	1 floor / 2 floors / 3 floors / 4 or more floors	0 / 1 / 0 / 0	97 /96 /82 /72	7 / 62 /24 / 2	9 /61 /25 / 4
Maintenance condition [% on tot buildings]	Optimal / Good / Mediocre / Worst	0 / 1 / 0 / 0	98 /99 /80 /23	29 /50 /14 / 1	31 /51 /16 / 2

Table 2. Municipalities according to population and climatic zone categories.

Climatic	LP					MP	HP
Zone	p<350	350<p<750	750<p<1500	1500<p<3000	3000<p<5000	5000<p<50000	p>50,000
E1	2	3	14	8	4	5	1
E2	32	68	92	86	38	65	3
E3	65	110	125	80	47	44	-
F1	77	49	33	25	16	12	1
F2	37	18	11	1	1	-	-
F3	12	4	1	-	1	-	-
F4	7	1	2	-	-	-	-

2.2.2. Methodology: input data and regression model

This study develops a GIS-based methodology implemented by statistical techniques to investigate the most important drivers of the residential electric energy consumption. Achieving the best accuracy of results depends on the reliability of input data and the quality of available public databases. The analysis has been performed using the open-source Q-GIS software and the statistical software *R* version 4.0.0 with a final input geo-database made up by 1,201 observations (municipalities) and 117 variables related to residential electric consumptions.
The following steps summarize the methodological framework of this study:

A. Statistical distribution of energy consumption data.
B. Identification of the independent variables.
C. Univariate and multivariate analysis technique
D. Multiple linear regression model.
E. Influence of independent variables.

Step A - Statistical distribution of energy consumption data.
Starting from the observations of 1,201 municipalities, the frequency distribution of energy consumption data is evaluated separately for each of the six-years with the most used statistical analysis techniques. Comparing each consumption year to the previous and the next ones, anomalous observations are individually evaluated. Then, a cut-off of the maximum variation is set arbitrarily to 0.3, eliminating observations that vary more than 30%. A final database is realized with 1,186 municipalities. *Cullen and Frey* chart is used to inspect the probability distribution: after checking the Normal and Log-Normal distributions graphically, the goodness of fit is evaluated: histogram and probability density functions are drawn together [56]. To evaluate whether the energy consumption significantly vary trough years, the *ANOVA test* is applied.

Step B - Identification of independent variables.
To combine the socio-demographic and environmental characteristics to the already analyzed energy consumption data of the 1,186 municipalities, the GIS tool is used to georeferenced residential electric energy consumption at municipal scale. The spatial reference of the socio-economic and the built environment characteristics is the census sections. The available 2011 ISTAT census database is harmonized using GIS tool and all information is assigned to the municipal area (layer). In some cases, variables are transformed, creating new variables: absolute values are calculated in percentage of the total value.

Step C - Univariate and multivariate analysis techniques.
The univariate statistical methods (i.e., the *Pearson's rho* [ρ]) are used to assess the correlation among variables and between each variable and the output data. Collinear variables are identified creating a correlation matrix and then, these are removed to avoid singularity of the matrix of correlation.
The *Principal Component Analysis (PC*A) is chosen to highlight variables that mainly explain data variability and then to create homogeneous groups of observations.
The measure of adequacy of PCA is referred to the *Kaiser-Meyer-Olkin factor*. Hierarchical clustering is performed applying the criterion of Ward on the selected principal components, based on the multidimensional variance. From the PCA it is possible to obtain the cluster dendrogram that is cut off at 1.0 height to create homogeneous groups. to identify. Uninfluential variables are identified evaluating graphically the contribution of variables to the main principal component.

Step D - Multiple linear regression model.

The electric energy consumption was estimated using a linear regression model, which is the most used statistical technique, as expressed by Eq. (1):

$$Y_i = \beta_0 + \beta_1 \cdot x_{i1} + \cdots + \beta_p \cdot x_{ip} + \varepsilon_i \quad (1)$$

where, Y_i is the annual electric consumption (dependent variable), x_{ij} are the independent variables, β_j are the estimated coefficients and ε_i correspond to the random errors of each observation i.

The Ordinary Least Squares (OLS) method is used to identify the model expressed by Eq. (1), considering that standard errors must be independent and normally distributed. Observed values y_i (i=1, …, N) are written as Eq. (2):

$$y_i = b_0 + b_1 \cdot x_{i1} + \cdots + b_p \cdot x_{ip} + e_i \quad (2)$$

where, b_j are the least squares estimates of β_j (j=0,1, …, p) and e_i (i=1, …, N) are the residuals.

A multiple linear regression model sets the following conditions: linear dependency, no multicollinearity among variables, normality of ε_i, and homoscedasticity among ε_i.

Then, the stepwise method is performed considering both the backward and forward directions in order to check the linear model, minimizing the *Akaike Information Criterion (AIC),* and selecting influential variables. The automatic selection procedure of the stepwise method combines backward elimination steps and the forward ones; for each regressor, the first computes the t-ratio and eliminate absolute value smaller than the pre-determined threshold value; if the corresponding t-ratio is greater than the threshold value, the forward step adds a new variable.

The resulting model must be control, checking the normality and homoscedasticity of the residuals, and multicollinearity of the variables. This can be done by assessing the *Variance Inflation Factor (VIF*). Since in regression analysis, the homoskedasticity is a crucial assumption, this work test it through the probability graphs (*Q-Q-plot*) and the scatter plot of (residuals) predicted values and normality. Influential points observations are identified graphically with the diagnostic graph of the outlier and leverage, removing observations, that have (*Student*) residuals and leverage values higher than 2 standard deviations. Then, the analysis is repeated.

The *Breusch–Pagan* and the *White diagnostic tests* are performed to assess the model's accuracy in predicting values. The *White test* is conducted also to evaluate the homoscedasticity of residuals, considering the following hypotheses:

$$H_0: \sigma_i^2 = \sigma^2 \quad (3)$$

$$H_i: \exists_{i,j}\ such\ that\ \sigma_i^2 \neq \sigma_j^2 \quad (4)$$

According to the null hypothesis (Eq. 3), residuals have constant variance (σ^2) and this does not show any pattern; the alternative hypothesis (Eq. 4) implies a not constant variance among residuals, and this requires a variance-stabilizing transformation to reach more accurate variables estimators. To reduce the heteroscedasticity the *Heteroskedasticity-Consistent Standard Errors (HCSE or White correction)* is performed: it allows to fit the regression model containing heteroscedastic residuals [57]. In a multiple regression model characterized by multicollinearity the dependent variable is affected by the independent variables, and it can be difficult to determine their reciprocal influence. The *Variance Inflation Factors (VIF)* is used to assess the validity of multiple regression. The VIF is intended as the reciprocal (R_j^2) of the inverse of the coefficient of determination (R^2) of an independent variable x_j, according to Eq. (5):

$$VIF_j = \frac{1}{1-R_j^2} \quad (5)$$

The VIF describes the proportional increase of β_j variance, considering its discrepancy from the scenario of completely uncorrelated explanatory variables. On the threshold value calculated as Eq. (6) is referred the evaluation criteria:

$$VIF < \max\left(10, \frac{1}{1-R_{model}^2}\right) \quad (6)$$

where, R^2 *model* is the R-squared of the regression model.
Variables with high VIF are transformed and analysis is repeated. The coefficient of determination R^2 is used to assess the model adequacy, as it corresponds to the variance proportion of the dependent variable, predicted from the independent variables. The adjusted R^2 (Adj R^2) is determined considering the number of predictors that exist in the model: if variables are add in the model, the R^2 increases, while the Adj R^2 increases only if the addition let the model improve more than if it would be done by chance. To increase the model's accuracy, the variables are transformed considering three types of intervention:

(1)Some absolute variables are normalized as described in Eq. (7):

$$z_{ij} = \frac{x_{ij} - \bar{x}_j}{\sigma_j} \quad (7)$$

where, $\bar{x_j}$ is the mean of the j^{th} variable and σ_j its standard deviation {xij: i=1, …, N};

(2) Some variables are squared;

(3) Some variables are transformed and/or redefined.

The third case occurs for variables related to the *Building Construction Year* characteristic of residential buildings, and the *Education degree, Family members and Age* characteristics concerning the population.
In the example of the *Building Construction Year* characteristics, nine variables selected for the initial model describe the percentage on the total number of residential buildings built in one of the nine classes created. A single variable (*BCY)* is created to express the average age of residential buildings in each municipality, calculated as the difference between the median value in each category and the value of the corresponding year (2015), weighting the resulting average.
Reporting the other example of the *Education degree* characteristic, four initial variables are selected describing the percentage of the total population according to four education levels: primary school diploma (*P*), junior high school diploma (*JH*), senior high school diploma (*SH*) or university degree (*U*). Each variable is associated to the total number of mandatory years of study envisaged by the Italian government (respectively 5, 8, 13 and 18 years). A new single variable (*EDU)* is defined the as the weighted average in Eq. (8), expressing the average number of years of education of the population:

$$EDU = \frac{P_{tot} \cdot [(P \cdot 5) + (JH \cdot 8) + (SH \cdot 13) + (U \cdot 18)]}{P_{tot}} \quad (8)$$

Step E - Influence of independent variables.
The last assessment of model's validity is done by checking whether the observed values fall within the interval of predicted values. This is determined referring to the predicted values of the year 2015 and a 95% of confidence value. A graphical evaluation is performed, comparing observed values of

the annual electricity consumption for each of the six years of evaluation and identifying observations that fell outside the prediction interval.

2.2.3. Results.

Step A. The electric consumption is transformed into a logarithmic value, to reach a logarithmic distribution that is evaluated approximately normal according to the results shown by the goodness of fit graph (Figure 2a) in which it is compared to the probability density function (red line) typical of the normal distribution. To confirm the Log-normal distribution of the outcome (blue point), it is also compared to other theoretical distributions (asterisk), as reported in the Cullen and Frey chart (Figure 2b). In addition, it is checked that the annual electric consumption (log) does not significantly vary among the six years, as the p-value is equal to 0.271. Figures 2a-b show the results of 2015, but all years have been evaluated.

Step B. The electric consumption of residential users at municipal scale is described by the 117 variables reported in Table 3 of which 114 are *numerical* and 3 *categorical*. The number of variables analyzed is specified and variables for which percentage is calculated are indicated with an asterisk. In Figure 3a is reported the example of the linear association that exist between the *number of occupied dwellings (Od)* variable and the electric consumption. From the Wilcoxon rank sum test results, it is confirmed that the electric consumption of municipalities in climatic zone E is significantly different (p-value< 0.0001) from the ones in climate zone F (Figure 3b). Consequently, it is possible to affirm that the climatic zone significantly and not accidentally affects the energy consumption; therefore, the HDD variable is retained in the model. Non-collinear variables ($|\rho| < 0.95$) are removed (67 of 117) and percentage values are preferred to absolute values. Figure 4 presents the heatmap of the correlation matrix resulting from the PCA test: for each couple of variables (*Var 1* and *Var 2*) a direct (red scale) or inverse (violet scale) collinearity is assigned. Figures 5a-b show results of the PCA analysis: the first ten principal dimensions explained 74% of the data variability. The contribution of each variable in the definition of each dimension is evaluated, removing the less influent (9 variables). According to the cluster dendrogram of PCA (Figure 4a): the observations are divided into six homogeneous cluster, cutting off at 1.0 height. In the score plot in Figure 5b observations in the six clusters are represented as colored points, according to their eigenvalues related to their first two principal dimensions; observations whose points are nearest have the highest similarity of energy consumption. The belonging to clusters is included in the model as a factor variable.

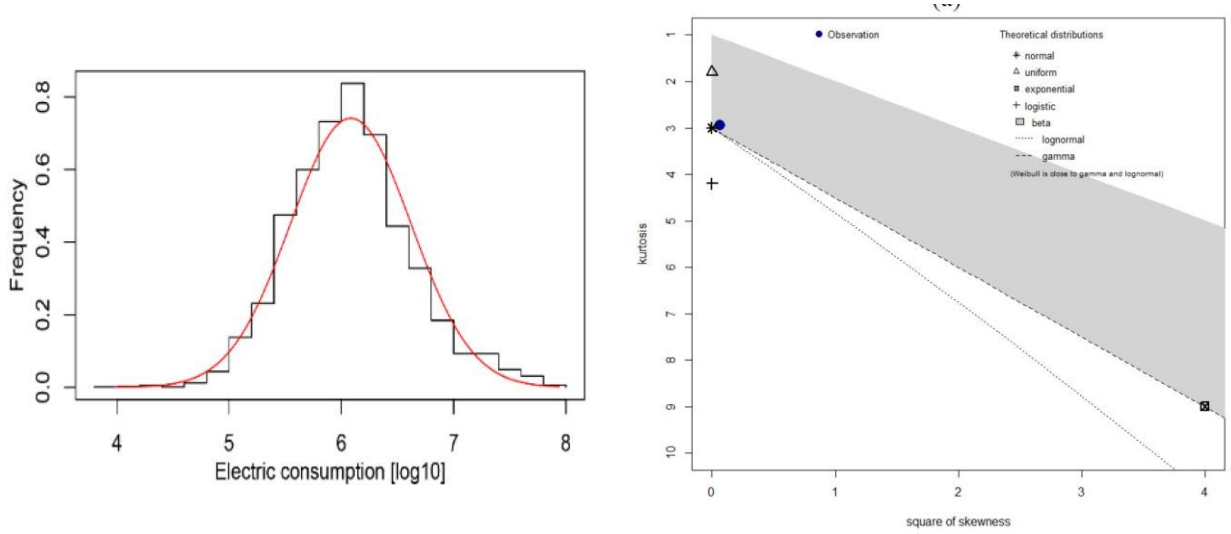

(a) (b)

Fig. 2 – The approximately normal log-distribution in the goodness of fit graph (a) and the Cullen-Frey chart (b).

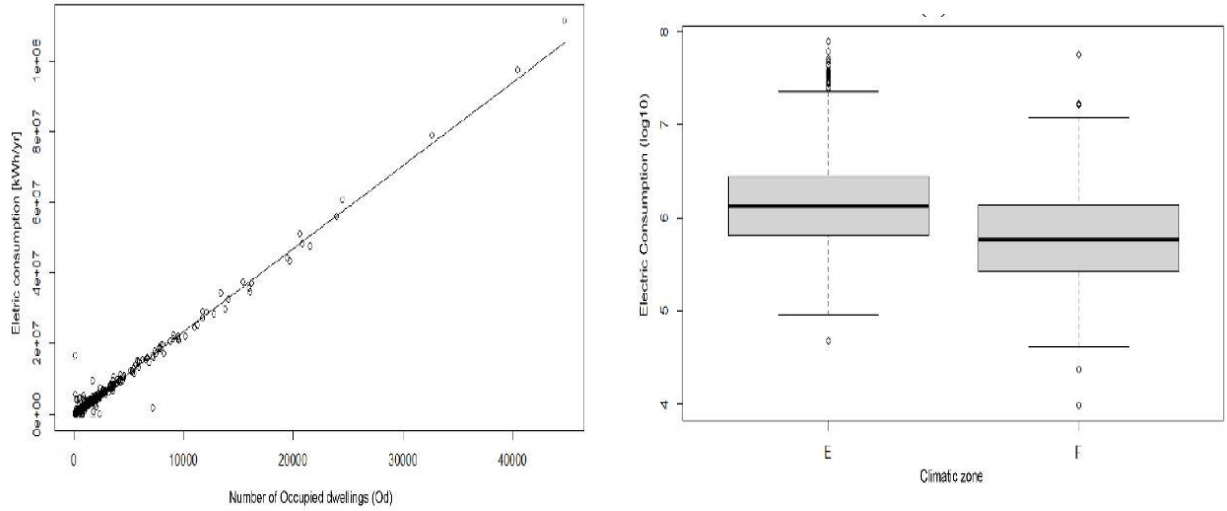

(a) (b)

Fig. 3 – Examples of linear association between dependent and indipendent variables (a) and boxplot graph (b).

Table 3. Number of variables for each feature considered.

Climatic-Environmental		Socio- economic		Residential built heritage	
Area	1	Population	7	Geometrical features	16
Altitude	1	Density	8	Construction year*	16
HDD	1	Foreigners*	2	Number of floors*	8
Climatic zone	7	Education*	8	Maintenance conditions*	8
		Occupation*	16		
		Income	5		
		Families*	13		

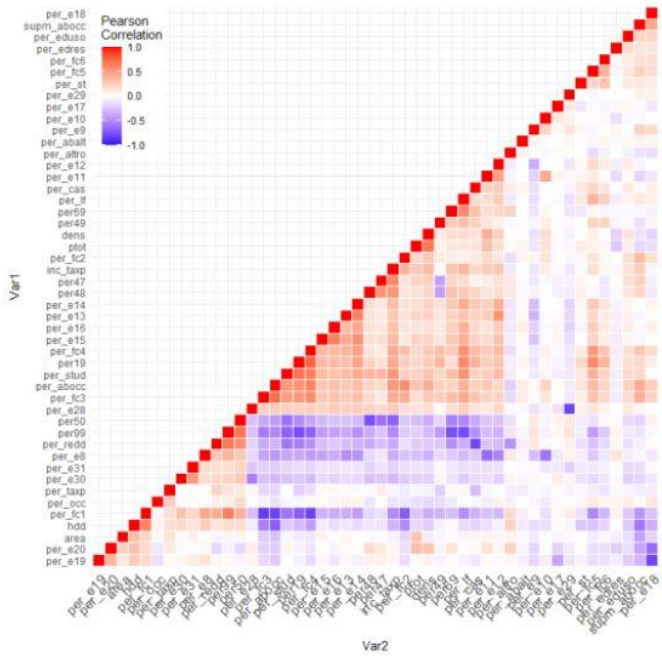

Fig. 4 – Heatmap of the correlation matrix.

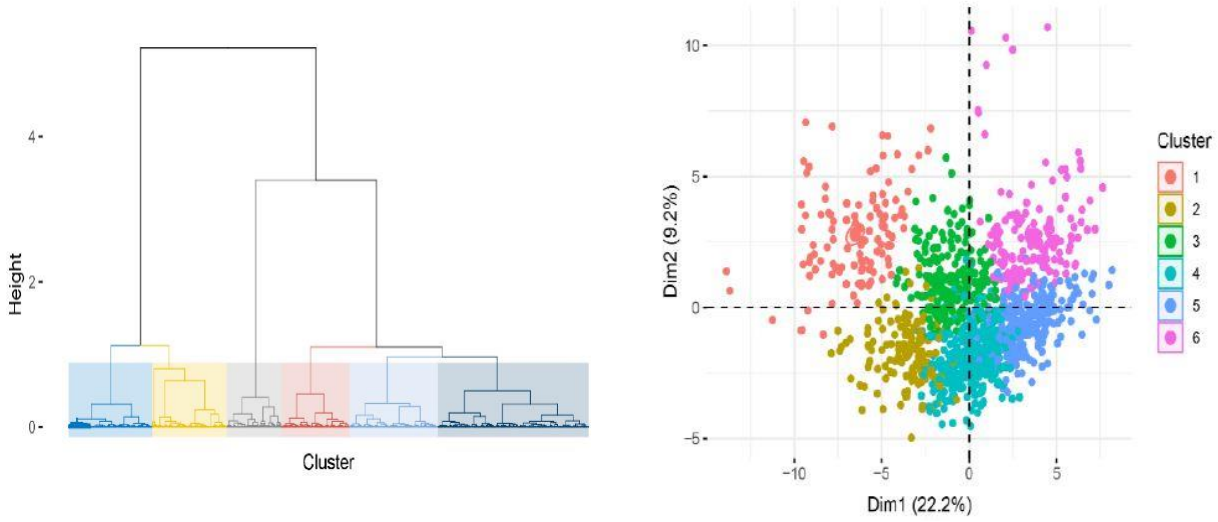

(a) (b)

Fig. 5 – The six clusters in the cluster dendrogram graph (a) and the score plot graph (b).

Step D. The R^2 and adjusted R^2 values of the initial model (41 variables, AIC = 347.30) are respectively 0.7469 and 0.7378: it means that the 74% of the variance in the annual electric consumption of municipalities is explained by these variables whose specific standard errors are shown in Table 4. Figure 6a shows the probability graph of the not normally distributed error, while in Figure 6b the patterns exposed by the scatterplot mean that the variance of residuals tends to increase together with the increase of predicted values. The *Breusch–Pagan test* shows the heteroskedastic of residuals (p-value < 0.001). Since the assumptions for a multiple lineal regression analysis are rejected, some of the independent variables (*Education degree, Family members, Age and Building Construction Year*) are transformed. Ten variables are normalized while other ten

variables are squared. Then, a new initial model (55 variables) is defined, performing the stepwise method. The resulting second model consists of 18 variables with an R^2 and an adjusted R^2 values of 0.7644 and 0.7607, respectively, explaining the 76% of the variance. The standard error, t value and VIF of the selected variables are reported in Table 5. In Figures 7a is presented the probability graph, in which it is possible to notice that the residuals are not normally distributed. Both *Breusch–Pagan* and *White tests confirm that t*he variance of the residuals is not constant (p-value < 0.001). From the resulting leverage diagnostic graph and outliers (Figure 7b), a cut off is applied at 2 times the standard deviation, eliminating 68 observations that correspond to the 5.7% of the total. A third model is then defined with 17 variables: the R^2 and Adj R^2 values reach 0.8909 and 0.8892, respectively (Table 6). In this case it is achieved an acceptable VIF. The probability graph of residuals is displayed in Figures 8a. Even though the residuals distribution is not normal, and the model does not well predict highest and lowest values, results are better. The *Breusch–Pagan test* and the *White test* still confirm unacceptable variance of residuals (p-value <0.0001). *The Heteroskedasticity-Consistent Standard Errors* is applied because no further reduction on the number of observations or in the number of variables is acceptable. A final model is defined achieving all the necessary assumptions. It counts for 17 variables that consist in quadratic and linear predictors, as reported in Table 7. The R^2 and Adj R^2 values are reported in Table 8, comparing all the models evaluated. The scatterplot presented in Figure 8b confirm that the distribution of residuals' variance is now acceptable, even if the White correction test has been used to adjust the quadratic trend observed.

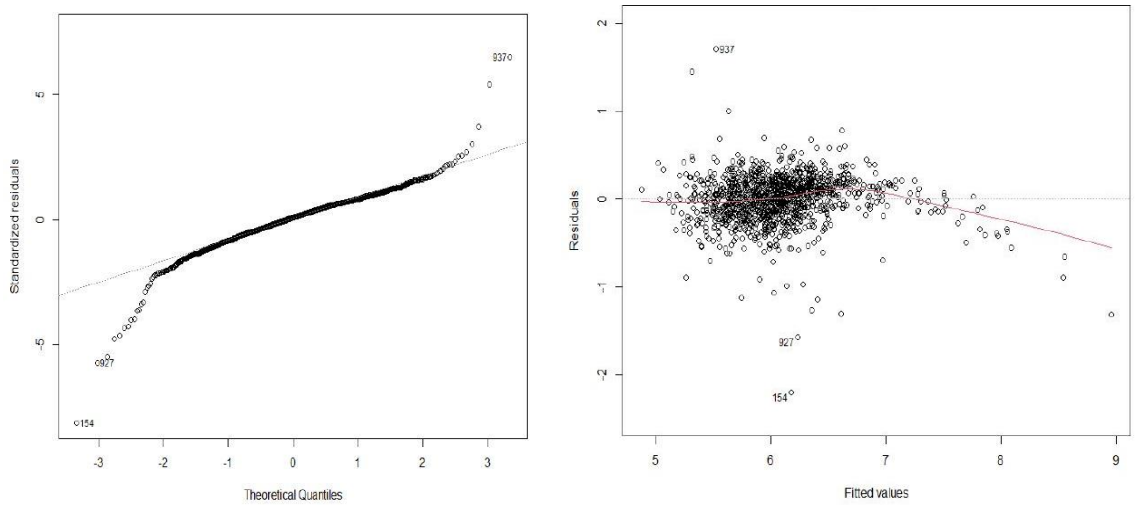

(a) (b)

Fig. 6 – The probability graph (a) and the distribution of residuals' variance oft he first model (b)

Table 4. Variables selected for each characteristic considered in the first model.

Variable	Parameter Estimate	Standard Error	T Value	Pr > |T|	VIF
Intercept	8.73e+00	1.73e+00	5.031	<0.0001	-
HDD	-8.99e-05	3.88e-05	-2.313	0.020	1.79
Total Population (Ptot)	-5.96e-04	1.61e-04	-3.695	<0.0001	**122.41**
Density	1.13e-05	5.71e-05	0.200	0.841	1.77
Age 0-19 (% on Ptot)	8.64e-01	5.94e-01	1.455	0.145	2.39
Age 20-69 (% on Ptot)	-5.45e-02	4.46e-01	-0.122	0.902	1.79
University degree (% Ptot)	2.33e-04	2.35e-04	0.989	0.322	**17.98**
Sr.H.S. Diploma (%Ptot)	6.41e-04	2.05e-04	3.115	0.0018	**45.05**
Jr.H.S. Diploma (%Ptot)	5.21e-04	2.63e-04	1.981	0.047	**60.39**
Primary Diploma (%Ptot)	1.30e-03	2.01e-04	6.445	<0.0001	**29.45**
WorkForce (W- %Ptot)	-9.90e-02	3.02e-01	-0.327	0.743	1.91
Employment rate (%Wtot)	-8.27e-02	4.04e-01	-0.205	0.837	1.09
Homeworker (% on NoW)	3.37e-01	3.65e-01	0.923	0.356	2.09
Students (% on NoW)	8.76e-01	4.73e-01	1.849	0.064	2.00
Fixed income (% on NoW)	-4.36e-01	2.94e-01	-1.486	0.137	2.64
Taxpayers Incavgy(inc_Taxp)	4.24e-05	3.78e-06	11.24	<0.0001	1.51
Fam of 1 member (%Ftot)	-4.29e+00	1.51e+00	-2.836	0.004	**19.38**
Fam of 2 member (%Ftot)	-3.45e+00	1.52e+00	-2.271	0.023	7.68
Fam of 3 member (%Ftot)	-3.76e+00	1.55e+00	-2.424	0.015	8.06
Fam of 4 member (%Ftot)	-3.27e+00	4.54e+00	-2.116	0.034	7.16
Fam of 5 member (%Ftot)	-4.97e+00	1.81e+00	-2.739	0.006	2.93
Occupied dw. (tot Od)	4.32e-05	1.10e-04	0.390	0.696	**36.33**
Occupied dw. (%RESb)	7.35e-02	7.85e-02	0.936	0.349	2.24
Avg. Area of Od (supm_Od)	-5.47e-03	9.08e-04	-6.030	<0.0001	1.68
Bcy < 1918	8.51e-01	4.20e-01	2.024	0.043	**11.2**
1919< Bcy < 1945	1.01e+00	4.27e-01	2.379	0.017	6.21
1946< Bcy < 1960	8.14e-01	4.40e-01	1.847	0.065	4.19
1961< Bcy < 1970	1.21e+00	4.54e-01	2.668	0.007	3.60
1971< Bcy < 1980	1.28e+00	4.55e-01	2.829	0.004	3.82
1981< Bcy < 1990	9.70e-01	4.97e-01	1.952	0.051	2.73
1991< Bcy <2000	1.13e-01	5.36e-01	0.211	0.832	2.45
2001< Bcy < 2005	1.91e+00	7.46e-01	2.561	0.010	2.42
2 Floors (%on RESb)	2.78e-02	9.27e-02	0.300	0.764	1.99
3 Floors (%on RESb)	1.41e-01	1.02e-01	1.374	0.169	1.90
Optimal BMS (% RESb)	1.95e-01	4.22e-01	0.463	0.643	**10.01**
Good BMS (% RESb)	1.29e-01	4.14e-01	0.312	0.755	8.26
Bad BMS (% RESb)	-6.90e-03	4.76e-01	-0.014	0.988	6.04
Cluster 1 (ref.)	-	-	-	-	1.45
Cluster 2	-2.76e-02	4.76e-02	-0.580	0.561	1.45
Cluster 3	7.08e-03	4.83e-02	0.146	0.883	1.45
Cluster 4	8.06e-03	5.69e-02	0.142	0.887	1.45
Cluster 5	-6.69e-03	6.61e-02	-0.101	0.919	1.45
Cluster 6	1.20e-01	6.55e-02	1.836	0.066	1.45

Note 1. HDD=Heating Degree Days; Ptot = Total population; Age=people age; H.S.=High School; NoW= No Workforce people; Fam= number of families; Ftot= Total families; Od= Occupied dwellings; BCY= Building Construction Year (% on total number of residential buildings- RESb); BMS= Building Maintenance Status.

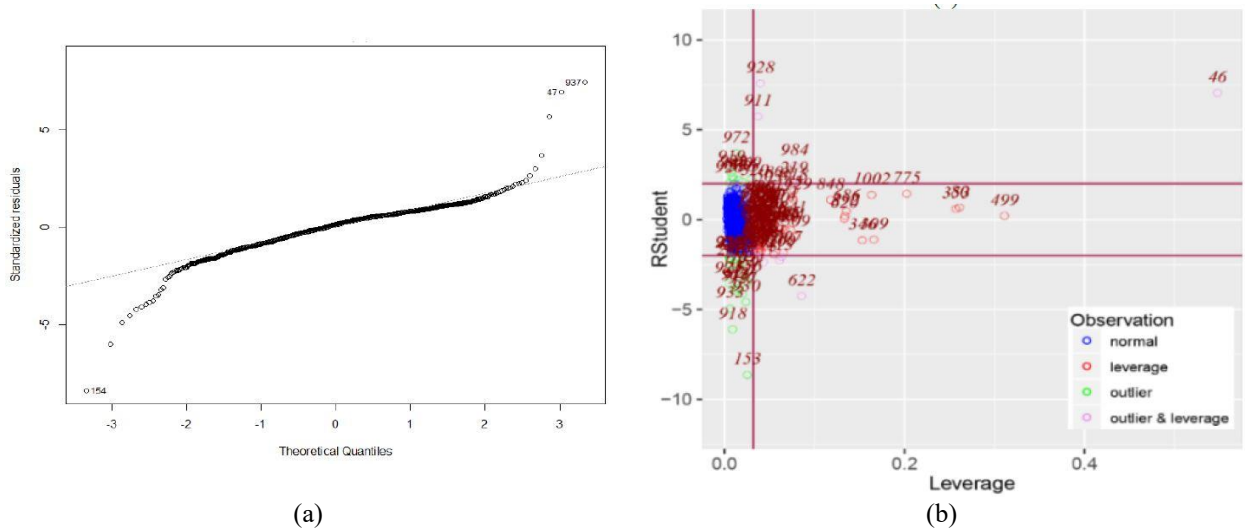

(a) (b)

Fig. 7 - The probability graph (a) and the graph of outliers and leverage diagnostic (b) of the second model.

Table 5. Variables selected for each feature in the second model.

Variable	Parameter Estimate	Standard Error	T Value	Pr > |T|	VIF
Intercept	6.45e+00	1.13e-01	56.88	<0.0001	-
nHDD	-1.51e+01	5.57e+00	-2.70	0.006	3.91
$nHDD^2$	1.07e+03+06	5.52e+02	1.94	0.051	2.48
$nPtot^2$	-1.61e+00	9.94e+04	-16.22	<0.0001	5.54
nDens	7.60e+02	5.07e+00	1.49	0.134	7.18
$nDens^2$	-3.94e-02	1.48e+02	-2.65	0.008	4.35
nEDU	-1.21e-03	7.71e-03	-1.57	0.116	2.93
$n.EDU^2$	-6.66e-01	1.56e-03	-4.27	<0.0001	1.17
Students (% on NoW)	5.84e-01	3.70e-01	1.57	0.114	2.70
Fixed income (% on NoW)	-6.21e+01	1.45e-01	-4.28	<0.0001	1.87
Taxpayers $Inc_{avg,y}$(inc_Taxp)	3.88e+02	4.00e+01	9.70	<0.0001	2.69
nFAM	1.40e-02	3.68e-03	3.82	<0.0001	4.2
$nFAM^2$	-8.22e-04	3.22e-04	-2.55	0.010	1.69
nOd	1.39e+03	5.71e+01	24.49	<0.0001	8.14
nsupm_Od	-7.94e-01	1.88e-01	-4.22	<0.0001	2.76
nBCY	-2.73e-01	1.29e-01	-2.11	0.034	1.89
$nBCY^2$	-3.14e+00	1.01e+00	-3.10	0.002	1.19
3 Floors (%on RESb)	1.39e-01	5.84e-02	2.38	0.017	1.28
Optimal BMS (% RESb)	7.80e-02	4.39e-02	1.77	0.076	1.19

Note 2. n= normalized; BCY= Building Construction Year (% on total number of residential buildings- RESb).

Table 6. Variables selected for each feature in the third model.

Variable	Parameter Estimate	Standard Error	T Value	Pr > |T0.505|	VIF
Intercept	6.53e+00	7.05e-02	92.62	<0.0001	-
nHDD	-7.41e+00	3.52e+00	-2.10	0.035	3.33
$nHDD^2$	-1.15e+03	4.59e+02	2.50	0.012	2.16
$nPtot^2$	8.51e+06	3.10e+05	-27.38	<0.0001	5.00
nDens	-4.36e+00	4.31e+00	-1.01	0.311	6.72
$nDens^2$	-3.23e+02	2.68e+02	-1.23	0.215	3.89
$n.EDU^2$	-7.06e-03	1.28e-03	-5.49	<0.0001	1.14
Students (% on NoW)	1.51e-01	2.26e-01	0.66	0.505	2.46
Fixed income (% on NoW)	-4.53e-01	8.80e-02	-5.15	<0.0001	1.62
Taxpayers $Inc_{avg,y}$(inc_Taxp)	3.00e+02	2.19e+01	13.68	<0.0001	1.94
nFAM	1.34e-02	2.14e-03	6.24	<0.0001	3.47
$nFAM^2$	-1.50e-03	2.16e-04	-6.95	<0.0001	1.62
nOd	2.63e+03	6.29e+01	41.84	<0.0001	7.73
nsupm_Od	-4.87e-01	1.15e-01	-4.23	<0.0001	2.45
nBCY	-1.07e-01	8.10e-02	-1.32	0.186	1.85
$nBCY^2$	-9.93e-01	6.42e-01	-1.54	0.122	1.20
3 Floors (%on RESb)	5.63e-02	3.69e-02	1.52	0.127	1.30
Optimal BMS (% RESb)	5.97e-02	2.80e-02	2.12	0.033	1.17

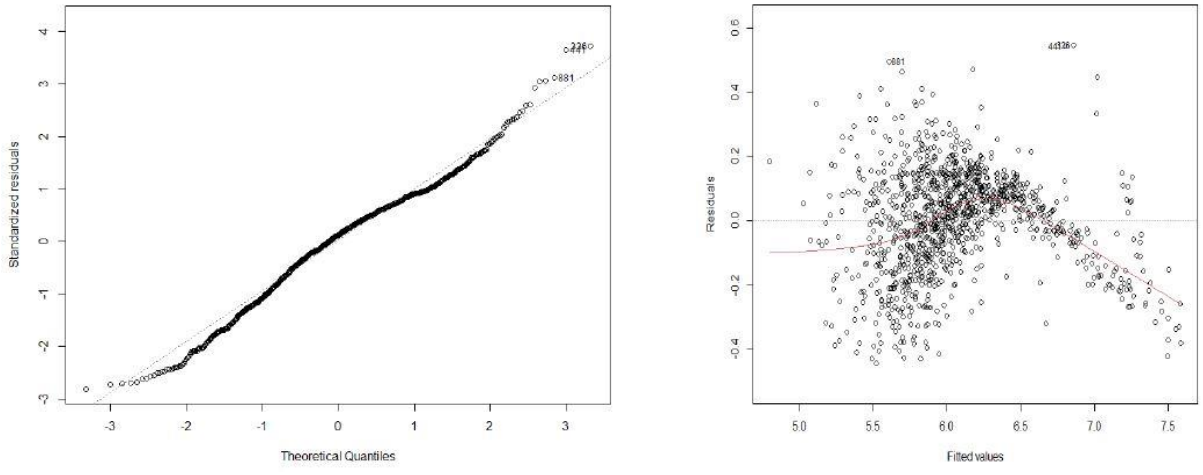

(a) (b)

Fig. 8 - Probability graph of residuals (a) of third model and variance distribution of residuals (b) of last model.

Table 7. Variables selected for each feature in the last model.

Variable	Parameter Estimate	Standard Error	T Value	Pr > |T|	VIF
Intercept	6.53e+00	7.62e-02	85.65	<0.0001	-
nHDD	-7.41e+00	3.46e+00	-2.13	0.032	3.33
$nHDD^2$	1.15e+03	5.33e+02	2.15	0.031	2.16
$nPtot^2$	-8.51e+06	5.63e+05	-15.11	<0.0001	5.00
nDens	-4.36e+00	3.73e+00	-1.16	0.242	6.72
$nDens^2$	-3.32e+02	2.29e+02	-1.44	0.147	3.89
$n.EDU^2$	-7.06e-03	1.46e-03	-4.82	<0.0001	1.14
Students (% on NoW)	1.51e-01	2.49e-01	0.60	0.544	2.46
Fixed income (% on NoW)	-4.53e-01	9.94e-02	-4.56	<0.0001	1.62
Taxpayers $Inc_{avg,y}$(inc_Taxp)	3.00e+02	2.51e+01	11.93	<0.0001	1.94
nFAM	1.34e-02	2.33e-03	5.73	<0.0001	3.47
$nFAM^2$	-1.50e-03	2.48e-04	-6.06	<0.0001	1.62
nOd	2.63e+03	8.03e+01	32.81	<0.0001	7.73
nsupm_Od	-4.87e-01	1.17e-01	-4.15	<0.0001	2.45
nBCY	-1.07e-01	8.44e-02	-1.26	0.204	1.85
$nBCY^2$	-9.93e-01	6.10e-01	-1.62	0.103	1.20
3 Floors (%on RESb)	5.63e-02	3.90e-02	1.44	0.149	1.30
Optimal BMS (% RESb)	5.97e-02	2.77e-02	2.15	0.031	1.17

Table 8. Results of the coefficients of determination in the four models.

	R^2	Adj R^2
First model	0.7469	0.7378
Second model	0.7644	0.7607
Third model	0.8909	0.8892
Last model	0.8909	0.8892

Step E. For all the analyzed years, the validity of the final model is checked on the graph showing the model's confidence and its prediction interval for the observed values of annual energy demand of all the 1186 municipalities. In Figure 9 are reported the results of the reference year 2015 (violet points) and they are referred to the *number of occupied dwellings* variable: only 59 observed values (5 % of total observation) fall outside the prediction interval (yellow points); this sustains the validity of the model in predicting electric consumption apart from very small municipalities. In Table 9 are identified observations that the model is not able to predict, reporting their main statistical parameters concerning the electric consumption, the total population variable, and the number of observed values in each cluster.

Table 9. Characteristic of the observations not predictable by the final model.

Year	N.	Electric Consumption [MWh/yr]			Total Population [n]			Cluster					
		Min	Max	Median	Min	Max	Median	1	2	3	4	5	6
2010	59	71,268	32,242,421	489,058	52	25,986	350	21	13	7	4	6	8
2012	57	72,074	30,783,835	332,997	52	25,986	323	19	15	7	4	5	7
2013	59	71,255	30,183,758	316,550	52	25,986	323	21	14	7	4	5	8
2014	60	70,938	28,586,741	281,745	52	25,986	251	18	14	6	6	6	10
2015	62	70,959	39,169,077	317,418	52	25,986	326	17	13	6	9	6	11
2016	61	67,692	28,433,423	257,178	52	25,986	250	16	13	8	8	6	10

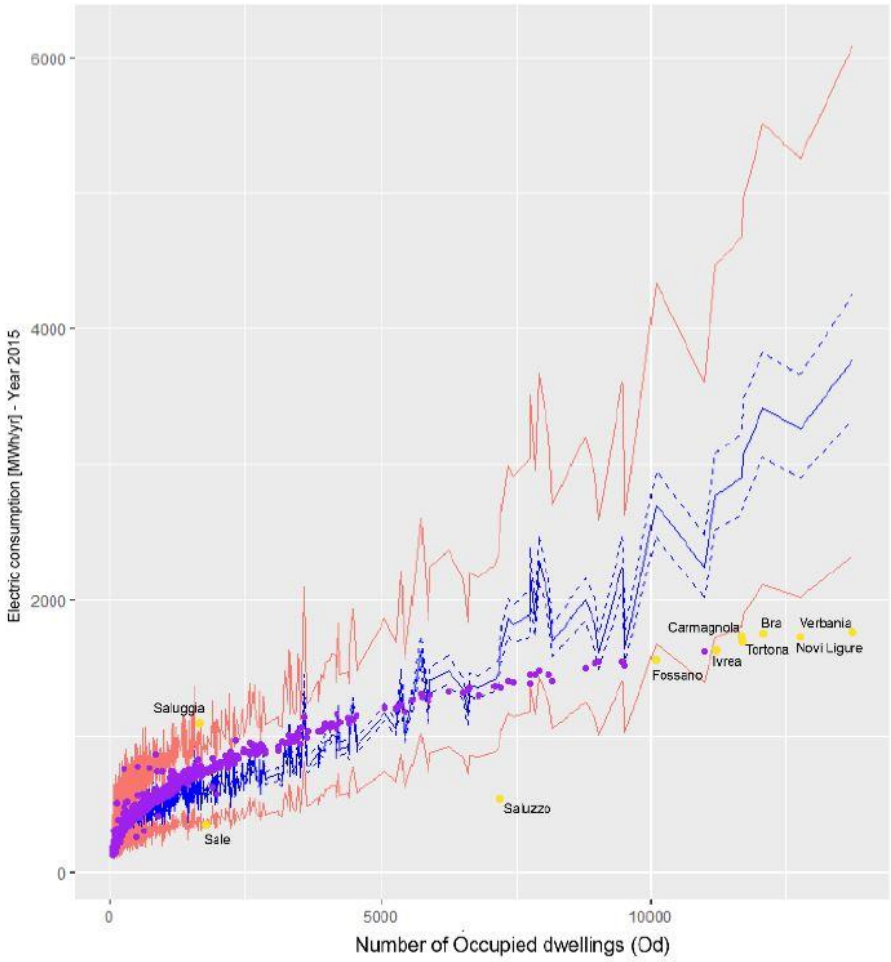

Fig. 9 - Observed values of annual energy consumption (2015) considering the confidence (blue lines) and prediction (red lines) intervals, and defining inside (violet points) and outside (yellow points) values.

The model results point out that climatic-environmental data, socio-economic features, and building characteristics are all influential variables. Even if it is possible to associate an increase of the energy consumption to the HDD and the population density variables, in both cases they have not a strong influence. A strong influence on energy consumptions is associated with the total population values, the number of occupied dwellings, and other variables (education degree, yearly average income, average number of members in a family, number of students, owners of fixed income), all are positively correlated but less significant, or negatively correlated and very significant. The (average) surface of occupied dwellings and the (average) age of buildings are significant and negatively correlated. The resulted model highlights which are the most significant variables affecting the electric energy demand of residential building at municipal scale depending on buildings' characteristics, socio-economic and environmental features. The final model is able to predict electric consumption in most cases, except for very large municipalities and the small ones. The methodology presented can be replicated to evaluate which are the influencing variables that affect the electric energy demand of other types of end users such as municipal buildings, service and companies.

2.3. GIS and Placed-based energy consumption model

This paragraph describes the mentioned GIS-based and place-based process-driven engineering energy model that this research aims to implement providing hourly values of the air change per hours parameters (ach). To better understand how this physic-based energy model works, the thermal energy balance is presented with a focus on the ventilation loads that are directly affected by the ach parameters. Then, the GIS place-based process-driven model is applied at the block of building scale with the city of Turin as a case study. The work titled *Urban-Scale Energy Models: the relationship between cooling energy demand and urban form* has been presented at the 38th International Conference on Heat and Mass Transfer (UIT) and published in the Journal of Physics: Conference Series [29].

2.3.1. The energy consumption model for residential building at urban scale

The GIS-based model is a lumped parameter model at Urban Building Scale (USBEM) and according to the classification provided in the initial paragraphs of this chapter, it corresponds to a process-driven engineering type of modeling with a bottom-up approach on input data derived from accessible open-database, based on a place-based approach. It is designed to evaluate the space heating and cooling energy consumption of residential buildings at different spatiotemporal scales.

As a USBEM, the main advantage of this type of modeling consists of the possibility to estimate energy consumption at multiple temporal and spatial detail, relating the results' accuracy with the accuracy of the input data, and ensuring relatively brief-time requests to process large amount of data. As a GIS-based model, it enables the integration, harmonization and management of variables at different scales, relying on databases normally used for urban planning, and to visualize spatiotemporal results [58].

Firstly, a monthly process-driven model has been designed by reference to the semi-steady state method and standards on buildings' energy balance, in particular the calculation method provided by ISO 52016-1:2017, ISO 52017-1:2017 and ISO 13790:2008. Starting from energy balance at building scale, three urban variables elaborated have been introduced to include urban context's characteristics: the *Sky View Factor (SVF)* is used to quantify thermal solar radiation lost to the sky , the *Main Orientation of the Street (MOS)* in order to describe exposition to the sun and the *H/Havg ratio* that is used to address the relative height of the buildings in a district. All these variables have been assessed at urban district scale using GIS software tools and plug-ins. This model has been validated referring to energy consumption data for space heating and domestic hot water of residential buildings that are connected to the District Heating Network (DHN) in Turin [59].

Starting from the monthly model, the hourly process-driven model has been developed, adding the mentioned urban parameters in the thermal balance with the aim of increase the model's accuracy [60]. An hourly model is necessary when thermal peak loads need to be managed, optimizing energy demand and supply.

The novelty of this model is the possibility to apply it at the block of buildings scale and include in the model some of the energy-related variables that can depict their urban morphology and are necessarily defined at this scale. It consists of a dynamic model based on the building energy balance equations with refence to the ISO 13786:2018, ISO 52016-1:2017, ISO 52017-1:2017, and ISO 13790:2008 standards. It can be described as a simplified engineering energy model, relying on

existing territorial database as input data and a place-based assessment with open-source GIS software and tool to manage and harmonize data in the pre-processing and post-processing phases.

The flexible methodology on which the model is based allows for its simple and quick adaptation to any scale of applications. It can guarantee accurate results at urban level starting from a reasonable number of input data and simulation times adequated than other existing tools.

The model is already be validated for the space heating simulation at urban scale [51] and [61]; the validation of the model for space cooling consumption is however missing and it is addressed in the work presented in this paragraph.

2.3.2. The hourly process-driven model

The hourly GIS-based engineering model consists of a dynamic thermal balance, and it is designed according to the standards ISO 52016-1:2017, ISO 52017:2017. As a process-driven building energy models with a bottom-up approach, the purpose is to apply physical models of heat and mass flows in and around buildings to predict thermal energy use, setting indoor and outdoor environmental conditions.

The software (ArcGIS 10.7, SOLWEIG 4.2) are used to elaborate all input data. These refer to three main categories:

- geometrical characteristics of the buildings, among which the surface-to-volume ratio (*S/V*) is one of the main important parameters, the heat loss surfaces, the heated net volume, calculated as the 75% of the gross volume, and the glazing area corresponding to 1/8 of net floor area, according to the Italian Decree 190/1975;
- thermo-physical properties of the buildings, that are assumed considering the building construction period: the thermal transmittances (*U*), the thermal capacities (*C*) of both the opaque and transparent envelopes, and the solar energy transmittance of the glass ($\boldsymbol{g}_{\perp}$);
- local climate characteristics, retrieved from data recorded by local weather station.

As the monthly model, the model's novelty stands in the application of the buildings heat balance equation at a neighborhood scale thanks to the adaptation of some variables. These are the Sky View Factor (*SVF)* and the Height-to-Width or Aspect ratio (*H/W)* that are used to assess at a neighborhood scale the heat fluxes exchanged by the heated/cooled block of buildings and the outdoor environment; in this way is possible to include in the model the mutual shading and the view factors of the surrounding built-up context.

The GIS-based lumped parameter model consists of three thermodynamic systems (TSs) that describe:

- the opaque envelope, made up by all opaque surfaces that limit the heated/cooled volume
- the glazing components, that separate the heated/cooled volume from the outdoor environment
- the indoor building elements in which are included internal partitions and structures, occupants, and furniture.

In Eq. (9) is described the dynamic heat balance with hourly time interval that is applied to each thermodynamic system (TS) at block of building scale, as shown in Figure 10.

$$C_{TS}\frac{dT_{TS}}{dt} = \varphi_{sol} + \varphi_I - (\varphi_C + \varphi_T + \varphi_V) \quad (9)$$

where, for each TS there are heat capacity C [JK^{-1}], temperature T [K], time-span t [s], heat flow rate [W] from solar gains φ_{sol}; from internal gains φ_I , from the cooling system φ_C, by transmission φ_T and by ventilation φ_V .

In the case of external temperatures lower than the internal one, the heat flow rate by transmission (φ_T) and ventilation (φ_V) are positive.

The heat capacity is assumed in relation with the different construction period and as a function of:

- the heat flow rate from internal heat sources (φ_I), it is calculated using the input data describing the net floor area of buildings and the average floor area per dwelling, the internal heat gains is calculated considering hourly profiles of occupants and equipment use typical of residential buildings;
- the heat flow by the cooling system (φ_C), it is released in the confined volume at a set point air temperature to guarantee indoor thermal comfort that in a climatic zone E corresponds to 26 °C (cooling season);
- the heat flow rate by transmission (φ_T), it is based on the thermal transmittances (U), and the heat dispersant surfaces (A) of envelope's components;
- the heat flow rate by ventilation (φ_V), it is calculated using the heat capacity of air per volume ($\rho a \cdot ca = 1{,}200\ J \cdot m^{-3} \cdot K^{-1}$) and the air change per hour parameters (**ach**) fixed at 0.5 and 0.3, according to the period of construction of the building;
- the heat flow rate from solar heat gains (φ_{sol}), it is calculated considering the absorption coefficient of opaque envelope and its area (A_{env}), the effective glazing area (A_w), the solar energy transmittance of the glasses (g_w), and the incident solar irradiance (I) that is determined by the orientation of surfaces, and the percentage of sunny surfaces (ξ).

In Italy, the humidification of indoor air volumes in residential buildings is not controlled, due to that in this model only sensible heat flow components are taken into consideration.

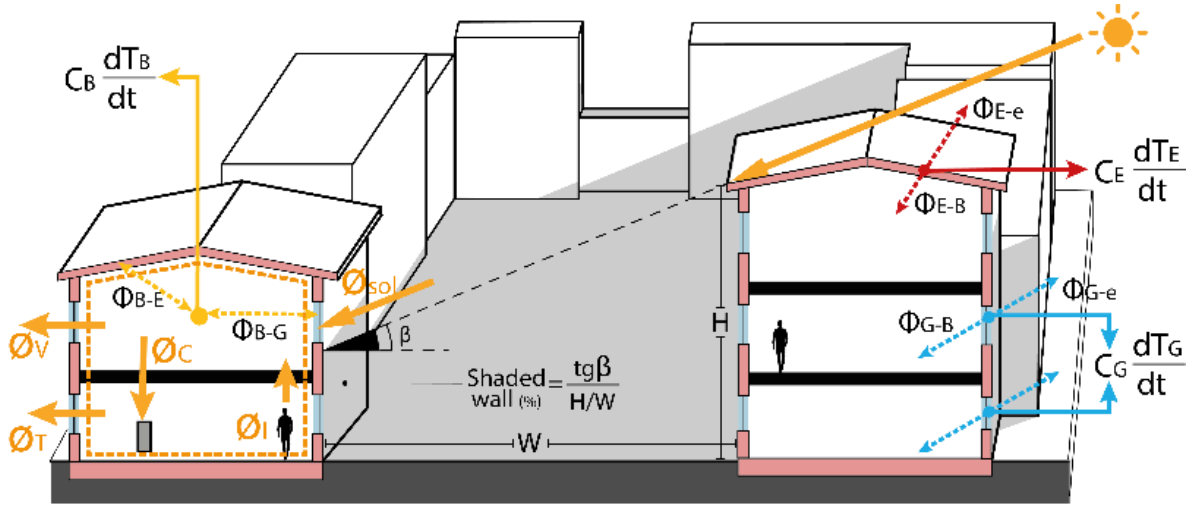

Fig. 10 – Thermodynamic system (TS) of the building (B, in yellow), the opaque envelope (E, in red), and the glazing components (G, in blue) at the block of buildings scale.

As schematized in Figure 10, in the model application at the block of building scale, the percentage of sunny surfaces (or shaded wall) is calculated according to the already presented two urban parameters: the Sky View Factor (*SVF)* and the aspect ratio (*H/W*). They describe the reciprocal shading and the view factors in the built surrounding and they allow to determine the exchanged heat

fluxes that occur between the buildings that made up the block and the outdoor environment. Depending on the solar height β [°], the shadow quota, calculated as a percentage, is equal to the ratio between *tan(β)* and the aspect ratio *H/W*. When the solar height β is lower than the angle of urban canyons, calculated as the *arctan(H/W),* the shadow quota is equal to the ratio between *tan(β)* and *H/W and when* the *arctan(H/W)* is equal to 1 (or greater) there is no shadow on the building's walls, (100% of the wall surface is irradiated).

2.3.3. Thermal Energy balance with focus on ventilation loads

Necessarily, the input data of the model's energy balance equations should be adaptable according to the available information provided at the selected scale of analysis (building, neighbourhood, districts or city scale). Equations (10) and (11) explain the components of the heat fluxes for a thermodynamic systems (TS) for the space heating and space cooling energy power release by the building, respectively:

$$C_{TS}\frac{dT_{TS}}{dt} = \varphi_{sol} + \varphi_I + \varphi_H - (\varphi_T + \varphi_V) \quad (10)$$

$$C_{TS}\frac{dT_{TS}}{dt} = \varphi_{sol} + \varphi_I - (\varphi_C + \varphi_T + \varphi_V) \quad (11)$$

Focusing on the heat flow rate from ventilation, it depends on the temperature difference, the number of the air changes per hours (ach), and the heat capacity of the air per volume, as reported in Eq. (12a), that can rewrite as Eq. (12b):

$$\varphi_V = c_a \cdot \dot{m}_a \cdot (T_{ai} - T_{ae}) \quad (12a)$$

$$\varphi_V = \rho_a \cdot c_a \cdot \frac{ach \cdot V}{3600} \cdot (T_{ai} - T_{ae}) \quad 12b)$$

where T_{ai} is the indoor air temperature and T_{ae} is the external air temperature [K]; $\dot{m}_a$ is the air mass flow rate [kg·s^{-1}], c_a is the air specific heat [J·kg^{-1}·K^{-1}], ρ_a is the air density [kg·m^{-3}], and $(\rho_a \cdot c_a)$ is the heat capacity of air per volume [J·m^{-3}·K^{-1}], *ach* is the number of air changes per hour [h^{-1}], and V is the volume of the heated/cooled air [m^3].

Regarding the air change rate (ach) parameters, this model tested different hypothesis. A constant air change rate (ach=0.5 h^{-1}) is firstly applied, during all the hours in a day (24h) and considering only natural ventilation due to infiltrations through the building envelope. Then, depending by the energy efficiency level of buildings and according to the period of construction input data, two values of ach are differentiated: 0.5 h^{-1} for old windows and 0.3 h^{-1} for new efficient windows. To improve the model accuracy, a variation during the daytime and nighttime is introduced, considering minimal ventilation heat losses at night due to the presence of shutters. Another hypothesis concerns the case when the building temperature surpasses the set-point temperature: then occupants would probably open the windows; therefore, the ach is determine considering the window opening and the infiltrations shares. Figure 11 shown the correlation between the temperature variation (ΔT) and the number of ach, measured for a typical Italian window of pre-defined dimension, according to [61].

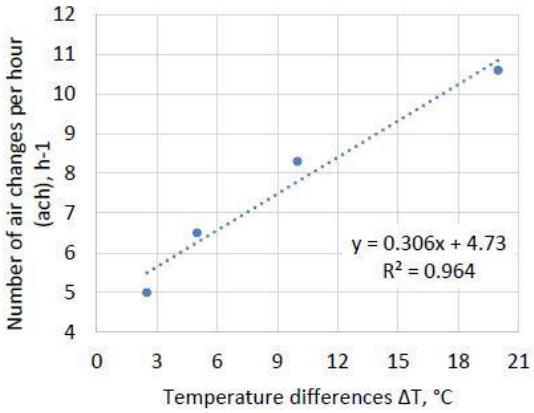

Fig. 11 - Correlation between indoor and outdoor temperature variation (ΔT) and the number of air exchanges per hours from measured data of a windows (height = 1.5 m) in Italy. Source: [61].

Deeper considerations concerning ventilation loads at urban scale have been done in the work presented at the *4th IEEE International Conference and Workshop Óbuda on Electrical and Power Engineering (CANDO-EPE)*, and published in [31], that is described in detail in Chapter 4, paragraph 4.5.5.2. In this work, the monthly ACH is studied in relation to climatic data, air permeability, shape and orientation of case study buildings and characteristics of urban morphology. Evaluations consider only the air flow rate due to infiltrations through the building envelope caused by the cross ventilation generated by the driving force of natural wind. Four scenarios of different values of air changes per hours (ach) are assessed to ensure Indoor Air Quality (IAQ) requirements; the methodology is applied to two buildings in a central urban area, as representative of the building stock of the Turin case study city, where two typical buildings' orientations exist. Results of the different scenarios are then compared. A monthly prevailing wind speed is derived from local climatic data to assess the average monthly pressure coefficients on building facades. Results show that the air change rates vary that mainly vary according to the wind direction and velocity, the buildings' height, the presence of surrounding buildings and their geometrical characteristics that represents obstacles to the driving force of wind. This encourages the deeper investigation of urban natural ventilation for the evaluation of hourly variation of ach according to the hourly variation of the local wind speed and direction.

2.3.4. GIS-based model application

Among the consequences of temperature rising due to the effect of climate change, the energy demand for cooling is expected to increase, especially in urban area [62]. In line with European policies, in order to improve the livability of high-dense built urban contexts and the sustainability of energy systems, analysis on the energy consumption of buildings for space cooling should be done; their results can orient energy urban policies in designing new neighborhoods or identifying retrofit interventions priorities in case of existing buildings.

This work sets two research objectives:

- Validate the GIS-based engineering model in simulating the hourly energy demand for space cooling of residential buildings at the block of building scale.
- Investigate the relationship between the urban form (morphology of the surrounding built-context) and the energy demand for space cooling of typical blocks of buildings, especially during summer, in order to understand how the cooling energy demand is affected by urban morphology and building typologies.

In the first part of this work, regarding the cooling demand simulation, the GIS-based engineering model is adjusted: the terms of the thermal balance equations are applied at the building scale to calibrate the model. Then, input data from existing databases and municipal technical maps are aggregated with the use of ArcGIS software and Q-GIS SOLWEIG tool, adapting the model at block of buildings scale; consequently, simulations of the hourly cooling energy demand of residential buildings are performed for thirty case-study buildings: five buildings for each of the six neighborhoods selected in the case study area.

The model validation is done comparing the cooling energy demand simulated with the results of a well-established existing tool and a reference procedure, respectively the *CitySim* tool [63] and the ISO 52016-1:2017 standard assessment.

The model validation occurs at two scales:

- at building scale, where 30 residential buildings are considered (five for each of the six selected neighborhoods); the comparison is carried out with both the *CitySim* tool and ISO 52016 standard assessment;
- at block of buildings scale, where five blocks of buildings are selected among the six neighborhoods due to their difference in urban shape; the comparison is carried out only with the *CitySim* tool.

The final part of this work concerns the model application to the already mentioned five blocks of buildings to investigate the influence of each parameters used to describe the urban morphology of the surrounding built context on the hourly energy consumption for space cooling; in addition, several buildings' typologies are considered in relation to the relative construction periods that is categorized into nine classes (see Table below).

2.3.4.1. Input data and case study

The six neighborhoods located in the city of Turin (Italy) (Figure 12) are identified as homogeneous urban zones due to their characteristics [64]. The building stock of the city of Turin consists of the 75% of residential buildings, of which the 80% is built before the 1976, considered a threshold year as it coincides with the first Italian law on the subject of energy savings in residential buildings.

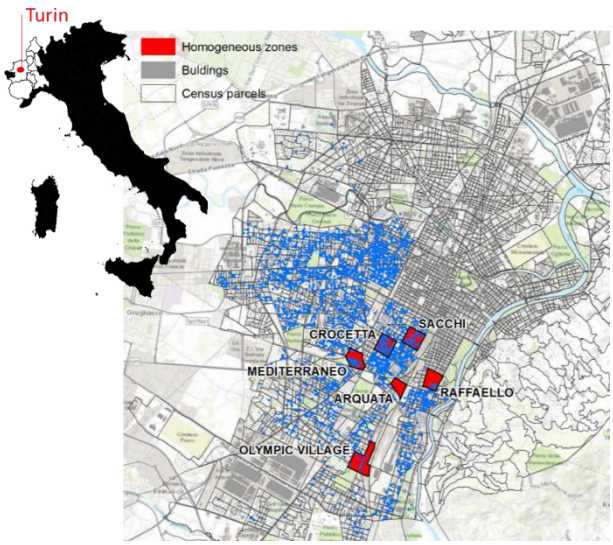

Fig. 12 - Localization of the city case study of Turin, the six homogeneous zones (in red) and the building (in blue) of which hourly energy consumption data are available, among the entire building stock (in grey), in all

census section (rectangles).

Input data is processed with the support of GIS tools and can be divided into three main groups: building data, urban morphology data and local climate data, as schematized in Figure 13.

Regarding building data, some information refers to the building scale (yellow boxes in Fig.13), others are provided at the census section scale (red boxes in Fig.13). In the first group there are: the building dimension and geometry, the period of construction, the surface-to-volume ratio (S/V), the heated net volume and the heat net floor surfaces, the glazing area (window-to-wall ratio) that here is assumed being 1/8 of the net floor area, as indicated by the Italian Decree 190/1975. In the second group there are the level of maintenance, the type of heating systems and the type of energy vector.

In this work the construction period is used as a key parameter to recognize thermo-physical properties of buildings, because real energy consumption data for space cooling are not always available. Due to that, the thermal transmittances U [$W \cdot m^{-2} \cdot K^{-1}$], the thermal capacities C [$kJ \cdot m^{-2} \cdot K^{-1}$] of the opaque and transparent building components, and the solar energy transmittance of the glass ($g+$) are shown in Table 10, for each of the nine construction periods representative of the building stock.

Table 10. Thermo-physical characteristics of buildings according to construction period.

Period	U_g	U_{wall}	U_{roof}	U_{floor}	$g_{\perp}$	$C_{envelope}$
	$W \cdot m^{-2} \cdot K^{-1}$				-	$kJ \cdot m^{-2} \cdot K^{-1}$
< 1918	5.9	1.45	1.8	1.75	0.82	504
1919-45	5.9	1.35	1.8	1.58	0.82	504
1946-60	5.9	1.18	1.8	1.23	0.82	283
1961-70	5.9	1.13	2.2	1.3	0.82	283
1971-80	5.9	1.04	2.2	1.21	0.82	257
1981-90	3.3	0.78	1.18	1.95	0.70	264
1991-00	2.7	0.7	0.68	0.8	0.70	274
2001-05	2.7	0.7	0.68	0.8	0.70	274
> 2006	1.8	0.46*	0.43*	0.43*	0.62	267

* Legislative Decree Dgls 311, 29 December 2006

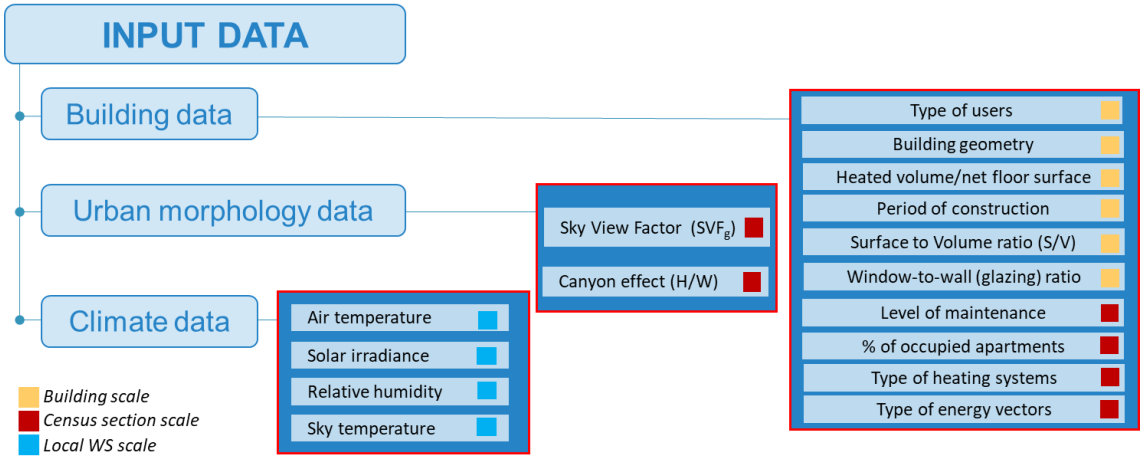

Fig. 13 - Building, urban morphology and climate input data for the space cooling energy model, according to the scale to which are provided by the original database: building (yellow boxes), census section (red boxes) and district or city (blue boxes) scales.

Regarding urban morphology input data, two main parameters are used in the model: the Sky View Factor (SVF) and the aspect ratio (H/W) or canyon effect. The first measures solar exposition, obstructions, and thermal radiation to the sky, considering real spatial characteristics of the built context; it determines the portion of the sky that is visible from a selected site.

To achieve the second objective of this work, the energy demand for space cooling is evaluated in relationship to different urban forms. It is necessary to describe the urban environment considering all influencing energy-related parameters. These are: the *Building Coverage Ratio BCR* [$m^2 \cdot m^{-2}$], the *Building Density BD* [$m^3 \cdot m^{-2}$], the *Main Orientation of the Streets and buildings MOS* [-], the *aspect ratio* or *Height-to-Width ratio H/W* [m/m], the *Sky View Factor SVF* [-], the *Green Area Ratio GAR [$m^2 \cdot m^{-2}$],* and the *Normalized Difference Vegetation Index NDVI [-],* as described in [65], [66] and [67] and schematized in Figure 14.

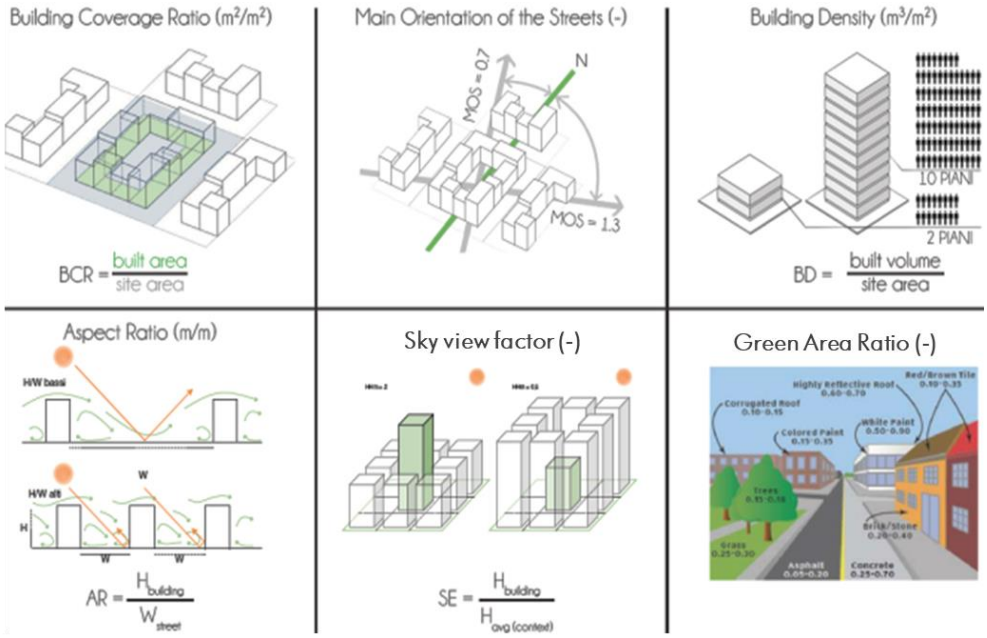

Fig. 14 - The six urban parameters used to describe morphology of urban environment at neighborhood scale Source: [64].

In Figure 15 is reported an example for each of the five blocks of buildings selected to be representative of the building stock in the case study. Different urban forms exist, according to the number of buildings that made up the block, their geometries and spatial reciprocity: the open-court buildings in block 1, the in-line rows of block 2, the tower in block 3, the courtyards in blocks 4 and 5; these two last blocks represent typical courtyards in Turin, usually characterized by high-building density and two prevalent orientations. Block of buildings input data are reported in Table 11 and concern the characteristics of the buildings and the characteristic of the block.

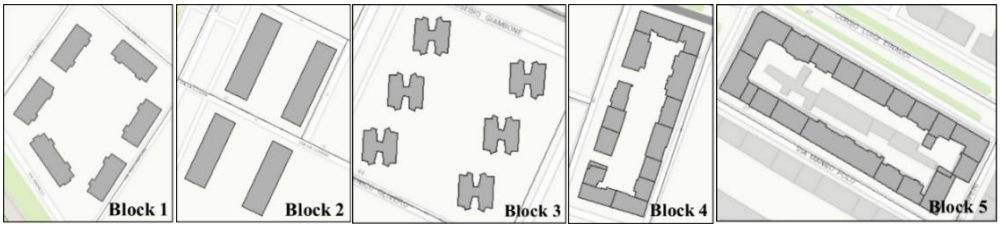

Fig. 15 - The five blocks of buildings with typical urban forms: open-court buildings (1), row (2), tower (3), courtyard (4-5).

Concerning the climate data, local climate and microclimate are evaluated relying on hourly data retrieved by near weather stations. In this work, energy simulations are assessed considering the cooling season of the year 2014. In this case study the cooling energy demand is usually quite low and it is concentrated only in few months during the years; due to this reason, the model simulated results are evaluated in the summer season. For each of the 5 months of the cooling season, the warmest monthly day are selected: May 30th, June 12th, July 18th, August 5th and September 1st. The average ($T_{ae,avg}$) air temperature [°C], the maximum daily ($T_{ae,max}$) air temperature [°C], and the global horizontal irradiation (GHI) in [kWh·m^{-2}] are indicated in Table 12. The graph in Figure 16 shows the hourly climate data of the five selected months.

Table 11. Characteristics of the five blocks of buildings.

Block of Buildings		**Block 1**	**Block 2**	**Block 3**	**Block 4**	**Block 5**
Name of the Block		Arquata	Villaggio Olimpico		Mediterraneo	Crocetta
N. of buildings per Block	-	6	4	6	15	20
Surface of flat	m^2/flat	62	114	90	79	117
Components per family	Inh/fam	1.63	2.16	2.09	1.85	2.05
Prevalent Construction Period	-	1961 - 1970	1971 - 1980	1961 - 1970	1946 - 1960	1961 - 1970
U_{wall}	W/m^2/K	1.13	0.93	1.13	1.16	1.2
U_{roof}		2.2	1.73	2.2	1.73	2.02
U_{floor}		1.3	1.55	1.3	1.20	1.40
$U_{glazing}$		5.9	4.72	5.9	5.74	5.9
$g_{\perp}$	-	0.82	0.77	0.82	0.81	0.82
$C_{envelope}$	J/m^2/K	282,518	260,199	282,518	282,094	345,277
Window-to-wall ratio	%	14	20	12	21	23
S/V	m^2/m^3	0.41	0.29	0.38	0.28	0.27
Prevalent Azimut angle	°	N/W = +125	N/W = +155	N/W = +165	N/W = +110	N/E = -150
		S/E = -55	S/E = -65	S/E = -85	S/E = -70	S/W = +30
BCR	m^2/m^2	0.16	0.31	0.12	0.31	0.38
BD	m^3/m^2	2.58	7.99	3.88	8.63	7.78
H/W	m^2/m^2	0.22	0.35	0.37	0.73	0.58
SVF	-	0.77	0.74	0.82	0.68	0.67

Table 12. Selected monthly warmest days in the cooling season 2014.

		May 30th	**June 12th**	**July 18th**	**August 5th**	**September 1st**
$T_{ae,avg}$	°C	21.4	28.7	27.6	24.3	23.0
$T_{ae,max}$	°C (hour)	25.9 (4 p.m.)	33.6 (5 p.m.)	32.1 (7 p.m.)	29.6 (6 p.m.)	28.1 (5 p.m.)
GHI	kWh/m^2/day	6.91	7.36	6.98	7.08	6.23

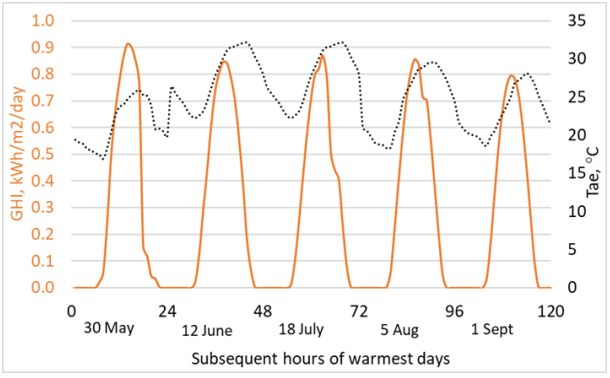

Fig. 16 - Subsequent hours of warmest day in the five months of the cooling season, considering the air temperature (dotted black line) and the global horizontal irradiation (yellow line).

2.3.4.2. Space cooling energy demand and model validation.

In this paragraph, results of the GIS-based engineering model are compared to the ones of the tool CitySim and the ISO 52016 standard to validate its capacity in predicting the hourly energy demand for space cooling in residential buildings.

Figure 17 reports simulations result of hourly cooling demand for three residential buildings built in different periods and located in different neighborhoods: the one in Crocetta built in 1919-46 (Fig.17a), the one in Mediterraneo built in 1946-60 (Fig.17a b), and the one in Villaggio Olimpico built in 1981-90 (Fig.17c). In the graphs are compared: the hourly cooling energy profiles assessed with the GIS-based model (in red), the CitySim tool (in blue) and the ISO 52016 standard (in green), considering the hourly average air temperature (in yellow).

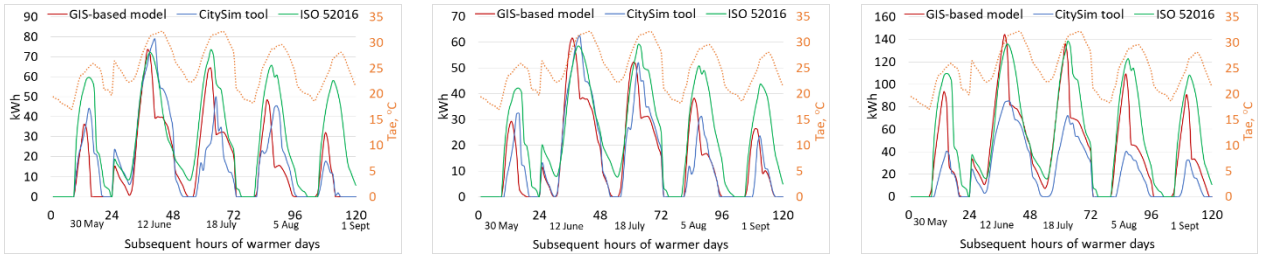

(a) Crocetta (1919-46) (b) Mediterraneo (1946-60) (b) Villaggio Olimpico (1981-90)

Fig. 17a-b - Comparison of hourly cooling demand in the five warmer days simulated by the GIS-based model (red lines), CitySim (blue lines) and ISO 52016 (green lines) for three residential building of different construction period in Crocetta (a), Mediterraneo (b) and Villaggio Olimpico (c) neighborhoods.

A trend line is recognizable in relation to external air temperature T_{ae} (and solar irradiation), by observing the hourly energy profiles. The first important consideration from the comparison between the GIS-based model and the CitySim tool is that their results are very similar: both models identify closer hourly energy peaks in all the five days and for all buildings. The energy consumption simulated by the ISO 52016 standard is higher than the other two models, especially for months with lower external air temperature (May and September). This discrepancy is explained by the fact that local climate conditions used in ISO standard refer to the typical meteorological year, and not to the year 2014. Due to that, correlations between air temperature and energy consumption are used to compare results, also specifying weather data used CitySim and GIS-based model; the same happens for the global horizontal irradiance.

The absolute relative error for the (annual) cooling season (April 15th - October 15th) is 30% (average) and 26% (median). The minimum values, respectively 21% and 22%, are reached in Raffaello and Crocetta neighbourhoods; while a maximum value of 70% occur in Villaggio Olimpico. All the listed results are in line with the trend obtained by applying the GIS-based model at urban scale and not at the building scale. It is assumed that the model accuracy mainly depends on urban form. Therefore, it is decided to design it for the typical district of the city of Turin: the courtyard, in its two prevailing orientations (NW-SE and NE-SW). This is clearly represented by the case study of Raffaello and Crocetta neighbourhoods, in which exist compact condominiums built between 1946 and 1980. On the contrary, the Villaggio Olimpico neighbourhood that is characterized by towers and big isolated condominiums, it is more recent (1981-90).

In Figure 18 is reported the daily cooling demand in the five warmest days, comparing GIS-based and CitySim models. Energy predictions of the thirty buildings are shown in Figure 18a, while the ones concerning the cooling need required by each of the five blocks are shown in Figure 18b. For

the GIS-based model a good accuracy is retrieved in both cases, especially in the warmest day of the cooling season (June 12th and July 18th), probably due to their highest external air temperatures (33.6 and 32.1 °C, respectively).

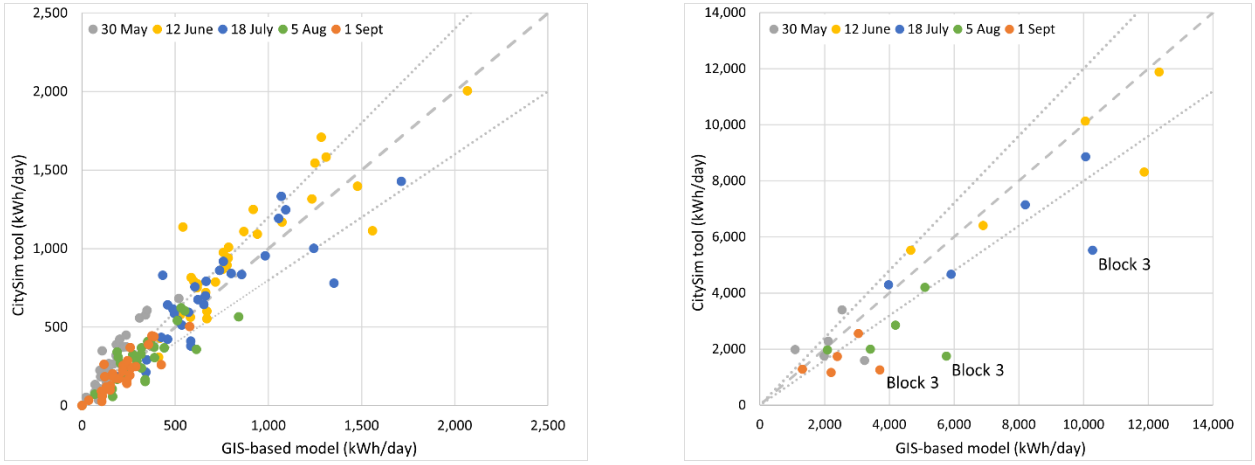

(a) Building scale: 30 buildings (b) Block of buildings scale: 5 blocks

Fig. 18 - Comparison of The daily energy demand for the five warmest days of the cooling season, comparing GIS-based model (x-axis) and CitySim tool (y-axis) at building (a) and block of building scale (b).

The last comparison between the two models concerns the hourly space cooling energy demand defined at the block of building scale, testing the GIS-based model predictions (Fig. 19, red lines) and results from CitySim simualtions (Fig. 19, blue lines) in each of the five warmer days. Confirming what is observed in Figures 17 and 18, the GIS model results are less accurate for the Villaggio Olimpico (Block 2 and Block 3 in Fig.19). The accuracy of the GIS model probably depends on the number of buildings that made up each block; also the scale of application can influence the model's accuracy, as reported in [68]. This another reason can explain why the tested model is more accurate in the evaluation of the energy cooling demand of Blocks 4 and 5, that are made up of 15-20 buildings each, and it is less accurate in the assessment of the energy demand of Blocks 2 and 3, composed by 4-6 isolated buildings.

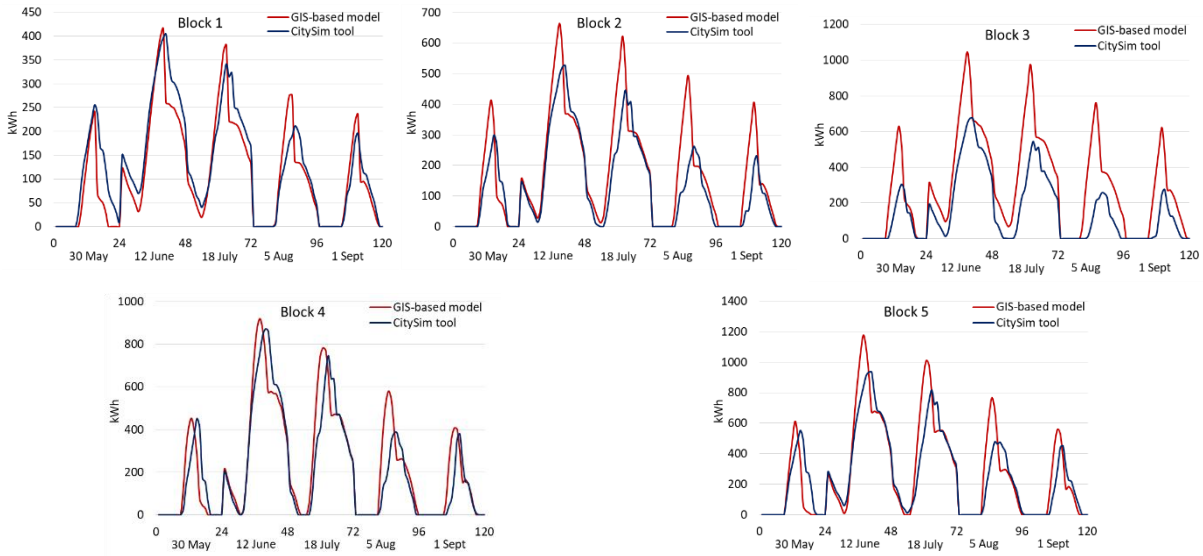

Fig. 19 - The hourly energy demand assessed at the block of buildings scale for the five warmest days of the cooling season, comparing results from the GIS-based model (red lines) and CitySim (blue lines) in application to Arquata (block 1), Villaggio(block 2-3), Mediterraneo (block 4) and Crocetta (block 5) neighborhoods.

2.3.4.3. Relation between urban form and building energy demand.

In this paragraph the effect of the urban form on space cooling energy demand of building at the block of building scale is investigated, the energy performance of the five buildings' blocks shown in Figure 15. The analysis is based on the thermo-physical properties associated to each of the four classes (until 1918, 1961-70, 1980-90, and after 2006) of construction period that are created. These have been selected after the identification of consistent variations of the thermal transmittance values (related to opaque and transparent components) and variations of the thermal capacities (related to building envelope) that characterizes buildings that made up each block.

The main findings are reported in the graphs in Figure 20, and they are summarised as follows:

- in all buildings' blocks, older buildings have lower cooling energy demand, probably because of their higher thermal capacity;
- cooling energy demand increases according to the increase of the surface to volume ratio (S/V) and the Sky View Factor (SVF)
- cooling energy demand decreases in case of high values of the aspect ratio (H/W) and the building coverage ratio (BCR);
- the lowest cooling demand is observed in the block with the courtyard typology (typical urban form in consolidated districts of the case study), and in block with South-North orientation (MOS), such as the Block 4, in Mediterraneo;
- the GIS model is not accurate in predicting energy consumption of towers (Block 3 in Villaggio Olimpico).

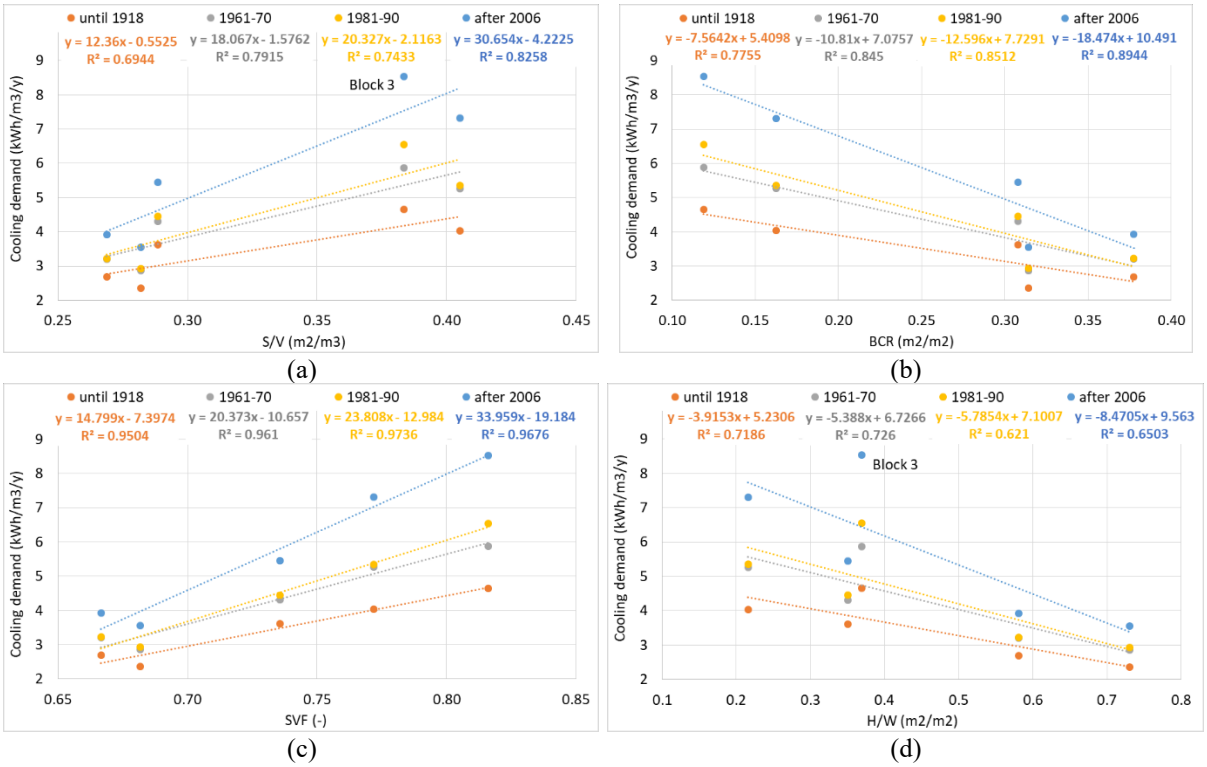

Fig. 20 - Correlation between the cooling demand (y-axis) evaluated with the GIS-based model applied at the block of building scale and influencing urban parameters: (a) the surface-to-volume ratio (S/V), (b) the building coverage ratio (BCR), (c) the sky view factor (SVF), and (d) the height-to-width ratio (H/W); considering four classes of construction periods: until 1918 (orange points), 1961-70 (grey points), 1981-90 (yellow points) and after 2006 (blue points).

In this work, the GIS-place based engineering hourly energy model is validated at a district-scale application. Then, it is applied to neighbourhoods of several urban forms to predict cooling energy demand. The main finding is the model validation at the block scale, even if the model accuracy seems to be proportional to the number of buildings in the district and some exceptions occur in case of isolated towers typology and applications at building scale.

Another important finding is the significant correlation that occur between the shape of the built environment and the cooling energy demand of residential neighbourhoods assessed at block of building scale. In particular, courtyards with East-West orientation that represent a compact urban form with high density, allow for an optimal shading on building facades that face the internal area of the courtyard and consequently a low space cooling energy demand is required by the buildings that made up the block.

From the main findings of this work, further developments concerning the implementation of the GIS-based model are listed below:

- to evaluate the contribution of heat fluxes sensibility analysis can be assessed, as it is observed that aspect ratio has important weight on solar gains;
- the contribution of the glazing TS is minimal, and it can be removed;
- to better describe the mutual shading in the building's blocks, interesting GIS pug-in can be studied (i.e., Solar Energy on Building Envelopes-SEBE).

Chapter 3 – Air flow at urban and canyon scale

Chapter overview

This chapter describes the analysis at urban and canyon scale for the evaluation of the air flow at different heights above and below interesting boundary layers in which the natural wind profiles and patterns can be described. Regarding the overall research study, the analysis in this chapter constitutes the first step, as shown in Figure 21. Since the final aim is the assessment of the hourly air changes per hour (ach), according to the building characteristics, the urban context, and the local climate conditions, the main objective of this research activity is the evaluation of urban natural ventilation at different spatial scale: from the city to the building scale. The goal is to define a place-based methodology able to integrate physic equations, describing the natural phenomena of wind and buoyancy with the use of GIS tools to consider local characteristics of the real built environment.

In this chapter the investigation concerns on how the terrain roughness and obstacles (buildings) affect the wind speed and direction inside urban canyons at urban scale, influencing wind path and momentum, generating windward/leeward zones, turbulence, and pressure variation on building facades. Firstly, an overview of current available *QGIS* tools for urban-scale wind assessment is done, reference is made to GIS-based morphometric models. Then the selected *UMEP Q-GIS plug-in* is applied to a case study and results are compared to the one of an established parametric method (*Cpcalc+),* presenting strength, limits and possible implementation of the methodology. The limit of this methodology is the impossibility of adjusting the wind speed inside urban canyons, since in these cases wind profile laws (power-law, log-law) are no longer applicable and it is necessary to use turbulent wind profiles.

The proposed model uses open-source GIS plug-in to define the spatial distribution of the displacement height parameter *zd*; it is used as a threshold value to apply the proper wind law profile in correcting the reference wind speed as a function of interesting heights from the ground at different spatial scale of analysis. In this way for any points in front of the building façades it is possible to determine the characteristics of the wind flow (laminar or turbulent) and apply the correct physical law that describe the type of wind motion and momentum. In comparison to the well-established parametric model *Cpcalc+* tool, the proposed methodology can describe the horizontal and vertical spatial distribution of the surface pressure without calculating the Cp coefficients. To overcome the limit of the application field proper of parametric type of modelling, the proposed methodology can determine surface pressure considering the real characteristics of any case study. The output data is the wind velocity as a function of the height from the ground for any building in any canyon within a city to apply the info inside the air flow modelling at building scale. However, its own limit stand in the correction of wind speed inside urban canyon: below z_d. it is no longer possible to apply the wind log law as turbulent flows occur. These are evaluated in the second part of this chapter.

A lack of investigation in the research field concerning the assessment of the wind paths and momentum inside urban street canyons, regards the evaluation of urban airflows pattern in non-isothermal conditions. The proposed methodology is based on GIS-place-based assessment integrated with CFD model simulations. It has been applied at urban level to several zones in the city of Turin, after having identified, based on statistical and spatial analysis in the GIS-environment, three aspect ratio classes and two orientation classes of the urban canyons as representative of the whole city. Seasonal hourly variations of the local climatic conditions have been assessed to include all the effective hourly variations during a whole climatic year. The results of these analyses carried out in

GIS constitute the boundary conditions provided to the research group of the *DIMEAS* department of the Polytechnic of Turin. They were responsible for the 2D CFD simulations that have been processed with the widely used *Star CCM+* software. The goal of CFD analysis is to acquire velocity vector fields in the dominium, considering the combined effect of cross wind-driven and thermal buoyancy in different local climatic conditions, and to evaluate how vortical structures are affected by the urban geometry (canyon dimension and orientation). The objective is to adjust the reference hourly wind speed obtained from local weather stations at specific points in the canyon positioned near the windward and leeward facades of buildings at interesting heights above the ground. For each simulated scenario, the velocity profiles obtained through the CFD simulations have been interpolated within the *MATLAB* environment using a fifth-grade polynomial function: the wind velocity f(x) is described as a function of the height (x) of the building, according to canyon dimension and climate condition.

Output data from CFD simulations have been used as input parameters in the second step of the research activity. It concerns the definition and application of an air flow lumped parameters model that has been outlined to consider the combined effect of cross natural ventilation, wind-driven and buoyancy on air flow rate at building level that will be presented in the next chapter.

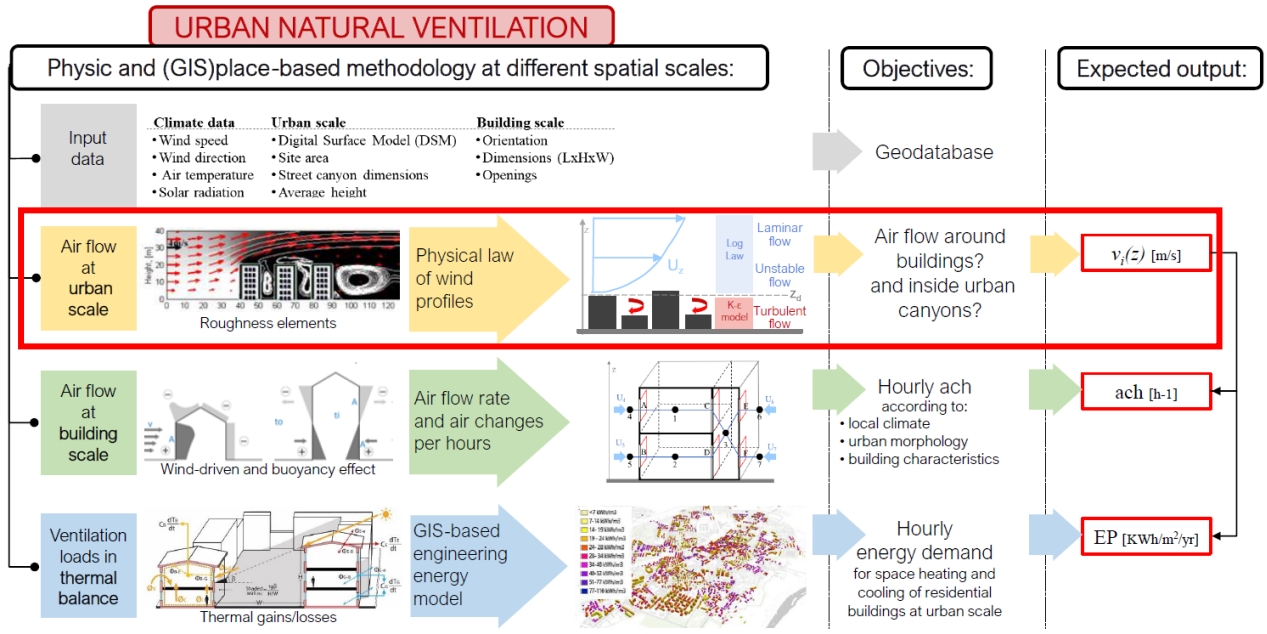

Fig. 21 - The step of the analysis investigated in this chapter (red box) in the flowchart of the overall methodology.

3.1. Introduction

Understanding and modelling the urban natural ventilation has focused the attention of many research activities. In very high-dense urban areas, the presence of different types of roughness elements, deeply affects local wind performance [69]. In recent years, the study of the air flow properties has confirmed important implications on urban design in the matter of outdoor thermal comfort and air quality, and buildings energy demand for space heating and cooling [70].

As already mentioned, the local built environment and climate conditions of any urban area can have impact on the energy performances of buildings [71]. In addition, the great number of anthropogenic heat sources and the scarcity of green surfaces contribute in the rising of local air and surface temperatures, causing the Urban Heat Island (UHI) phenomenon [72]. Urban morphology can directly modify solar access, wind speed and direction [73]. However, this can negatively or positively impact on the thermal energy performance of buildings, according to the requirements of the cooling or heating season, in most cases compensating one the other. Some studies [74], [75] show that compact urban built-contexts display lower thermal losses, with a decrease in the heating energy demand that is positive in cold climates. Whereas, in the case of warm climate conditions, very dense built environments are associated with a very high cooling energy demand because of rising air temperatures and reduced wind speed. Wider street canyons can ensure good wind conditions at the expense of an increase in exposure of the building façade on solar radiation with direct implications on solar gains on transparent components.

The evaluation of the urban wind is part of the urban climatology research field that concerns with interactions between a city and the overlying atmosphere As expressed by [76], the city is an integrated open system of living things interacting with their physical environment. The point of view should be bi-directional as it includes mutual and reciprocal influence between urban built environment and urban climate: the physical phenomena that characterize an urban climate have impact on urban infrastructure and objects; in turn, cities contribute to change climate and atmospheric composition at local, regional and even global scales. Proper descriptions of these interactions are needed to maximize beneficial aspects and minimize the consequences of exceptional events [77].

The classification of urban climate systems provided by [78] is here adopted to approach the study of urban climate phenomena as the air flows at urban scale and inside urban canyons. This classification is built on scales of surface organization set by the roughness elements and scales of atmospheric motion and vertical stratification to systematize the description.

3.2. Physical laws of wind profiles at urban-canyon scale

In an urban environment, the wind phenomenon is influenced by local phenomena depending on the surface characteristics: topography, building geometry and dimension, street width, vegetation and other features. The rugosity of the terrain ground and other objects, mainly buildings, but also vegetation, create obstacles to the undisturbed flow, changing condition of the micro-climate and increasing the terrain rugosity. Due to the presence of buildings, the wind in a urban environment loses its momentum to overcome the frictional effect of the surface roughness, and it loses its kinetic energy that is converted into turbulent kinetic energy.

Two main driving forces for natural ventilation: wind pressure and buoyancy. Differences in the temperature of earth surface due to variations of the solar radiation generate pressure difference at global scale (climate-meteorological interest) and air flows from high to low pression zones. Friction on earth's surface is generated by the action of shear stress at a solid boundary that causes a shear layer or a boundary layer. Wind velocity goes from zero at the surface of the boundary layer to velocity of free stream at the outer edge of the layer. In this region, wind flow is dominated by the effect of viscosity: laminar or turbulent flows can occur and mix. Considering a horizontal profile, when the airflow hits a sharp edge, separation occurs immediately; the vertical profile primarily depends on the surface roughness elements.

A wind profile can be defined for each environmental contexts (i.e., urban, sub-urban, rural areas); it is able to mathematically describe the wind speed (Uz) as a function of the height (z) from the ground level. At reference heights are individuated some pre-defined boundary layers: they confine air flow zones in which different type of wind motion occur that can be described by applying proper physical laws.

Wind flow in cities has lower speeds than in undisturbed areas. In case of flat (rural) areas, the wind velocity can reach the value of the upper layers more quickly. The area named Urban Canopy Layer (UCL), as shown in Figure 22 is the zone in which the building's height change wind conditions, the boundary layer develops at greater heights, and different prevalent direction can occur, substantially modifying the wind turbulence.

The Reynolds number (*Re)* is an important dimensionless parameter in fluid dynamics. It is the ratio between inertial and viscous forces within a fluid that is subjected to relative internal movement due to different fluid velocities. These movements generate fluid friction, which is a factor in developing turbulent flow, and it is counteracted by the viscosity effect of the fluid that tends to inhibit the turbulence. Then, in each case a boundary layer is defined as the region in which these two forces change behaviour. A similar effect is created by the introduction of a stream of high-velocity fluid into a low-velocity fluid, to which a wind-driven flow can be reconducted.

At low Reynolds numbers, laminar flows occur, and viscous forces are dominant: the flow is characterized by smooth, constant fluid motion.

At high Reynolds numbers, turbulent flows occur because inertial forces are dominant: chaotic eddies, vortices and other flow instabilities are produced by the differences in the fluid's speed and direction.

The Re is used to predict fluid flow patterns for any given flow conditions, quantifying the relative importance of the two types of forces (inertial and viscous) and to determine if laminar or turbulent flow regimes occur. In addition, it is used to scale similar flow situations of different-sized, such as full-size versions and wind tunnel tests; this can help in predicting fluid patterns on a larger scale, as

wind flows in local or global air movement, and thereby associating meteorological and climatological effects.

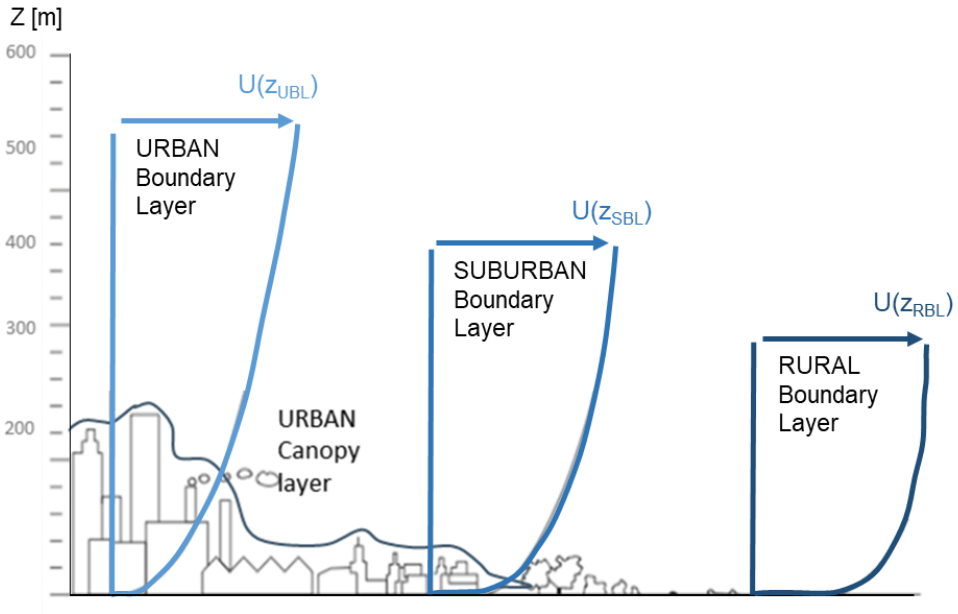

Fig. 22 - Boundary layers of the wind profile for different terrain rugosity.

3.2.1. Boundary layers and aerodynamic parameters.

As the majority of urban climate phenomena, the physical phenomenon of wind lies in the microscale, local scale and mesoscale domains and it is part of a continuum, since the atmosphere is a diffusive medium and it cannot remain discrete in it.
Regarding the horizontal scales of wind influence, three scales are individuated [79]:

1) the mesoscale, at which it is the whole city that can modify weather and climate conditions;
2) the local scale at which landscape features and topography have impact on physical phenomena;
3) the microscale, at which even short distance variations can cause great airflow perturbations.

With reference to the vertical scale of wind influence, the most important boundary layers are listed in the following paragraphs, according to what is described in [78] and with reference to the scheme in Figure 23:

- *Atmospheric Boundary Layer (ABL)*

The *ABL* is extended up to 1 or 2 km (z_{ABL} in Fig.1). In this layer the undisturbed wind flow in upper layers is progressively slowed down because of the friction with ground rugosity and obstacles. In case of flat opened terrains, as rural zones, the wind velocity reaches the values typical of the upper layers more quickly than in case of scattered urban areas.

- *Urban Boundary Layer (UBL)*

The zone of the *ABL* influenced by the presence of a large city is the *Urban Boundary Layer*. It is divided into two distinct layers, which are determined by urban surface characteristics and mesoscale conditions: the *Mixed Layer* (*ML*), whose upper limits coincides with the *UBL* (z_i, in Fig.1) and in the

lower part of the UBL, the *Surface Layer* (*SL*) whose depth corresponds to the tenth of *UBL* (z_i /10, in Fig.1). Regarding the *SL,* it can be distinguished into two sub-layers:

- *Internal Sub-Layer (ISL)*

It is located in the upper part of the *SL*, it is possible to assume the wind as a constant flux characterized by a laminar, homogeneous horizontal flow; this is due to the fact that the flow is free of wakes associated to individual obstacles; in fact, the Reynold number is lower than 2000 (Re <2000) [78]. To determine the average wind speed (*Uz*) occurring in this layer, the wind log-law can be applied.

- *Roughness Sub-Layer (RSL)*

This layer is located in the lower part of the *SL;* here, the effects of individual roughness elements are strongly evident. The *RSL* stretch out from ground level to the blending height z_{RSL} (Fig. 1). Airflow perturbation caused by individual roughness elements can persist until it reach the effect of turbulent eddies and they mix together. Blending distances depend on many factors: the eddies' magnitude, the wind speed, and fluxes' stability. In literature, the minimum height of this layer has been defined as the doubling of the average height of the main roughness elements (buildings) ($z_{RSL} = 2z_H$); it is reported by [79] base on observations in dense urban settings; it can be larger and vary according to density and height variability of roughness elements. For typical European cities, z_{RSL} is from 2 to 5 times the mean height z_H of roughness elements (mainly buildings) [80].

- *Urban Canopy Layer (UCL)*

It corresponds to the mean height z_H (Fig. 1) of the main roughness elements in the layer. Due to their presence, the wind flux loses its momentum overcoming the frictional effect of surface roughness elements: turbulent flows are generated near the surfaces and the Reynold number is greater than 4000 (Re > 4000) [78]. In this layer, it is frequent the occurrence of poor (lower) wind velocities, needing turbulent models to determine wind profiles inside urban canyons.

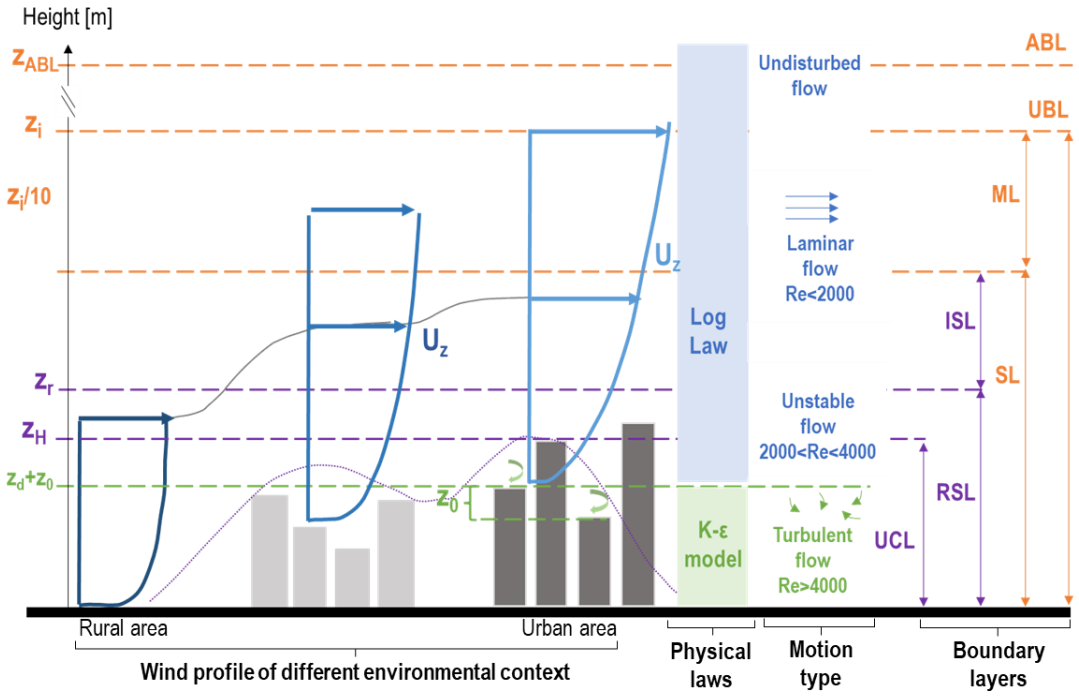

Fig. 23 – Reference heights of boundary layers (y-axis) at meso-scale (in orange), local scale (in purple) and micro-scale (in green), in association to type of wind flow motion (turbulent, unstable, laminar or undisturbed) and the proper physical law to apply to calculate the wind velocity as a function of height from the ground.

Aerodynamic parameters.

The aerodynamic parameters describe the wind velocity profile influenced by surface roughness elements (Fig. 24); they are the zero-plane displacement *(z_d)*, and the roughness length *(z_0),* and both occur at local and micro scale. These parameters may be used to estimate the spatially- and temporally averaged wind-speed profile where the air zone is free from individual turbulent wakes.

- *Zero-plane displacement height (z_d)*

The extent of vertical displacement of the (logarithmic) wind-speed profile is indicated by zd, which may correspond to the 'drag centroid' or height the mean drag appears to act. Also called displacement distance, or displacement thickness, it corresponds to the new ground level from which it is originated a (laminar) wind profile. This is due to the fact that the wind has already pass over high-density buildings [81], setting a baseline for the application of the wind log law [82]. According to [83], it can be also defined as the depth of still air that is still trapped between roughness elements. In a viscous homogeneous fluid, the depth of a boundary layer of shearing flows over a flat plate. Several formulas exist to relate this height scale as a function of the roughness element geometry (for example, spacing and silhouette area). Tabulated values for various surface types are published in most micrometeorological texts.

- *Roughness length (z_0)*

This aerodynamic parameter corresponds to the height above z_d where the wind speed becomes zero once the logarithmic wind profile can be applied; the roughness length represents the size of the eddies produced from the wind flows moving over a rough surface [83]. It directly depends on the intensity of the turbulent flows and consequently on surfaces' drag. In the log wind profile, it is equivalent to the height at which the wind speed theoretically becomes zero in the absence of wind-slowing obstacles and under neutral conditions. The roughness length does not exactly correspond to any physical length. However, it can be considered as a length-scale representation of the roughness of the surface.

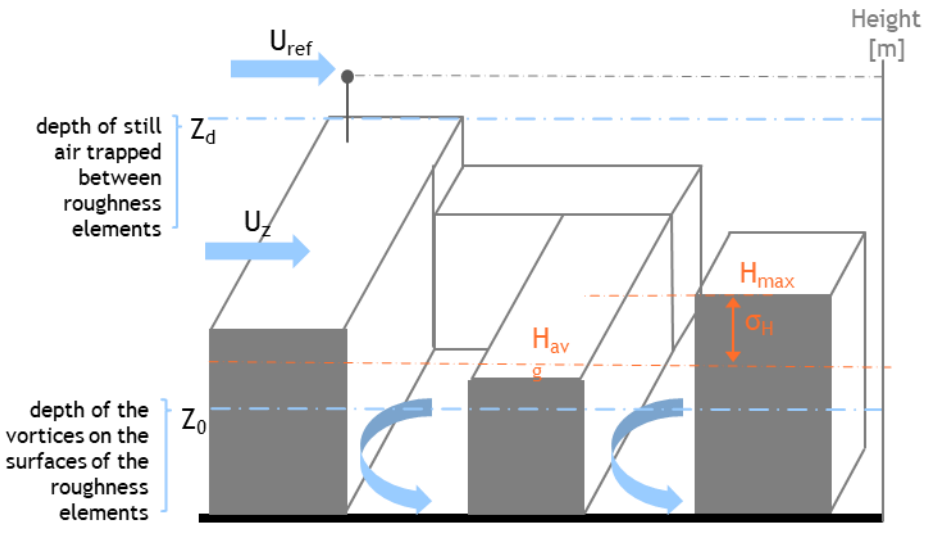

Fig. 24 - The two aerodynamic parameters *zd* and *z0* at urban micro-scale.

3.2.2. Wind law equations.

Wind data (wind speed and direction) are normally measured at 10 m above ground in some peripheral weather stations. These data need to be adjusted considering i) the height of the roughness elements and terrain roughness of the context, and ii) the wind incident angle. According to the type of wind motion, as shown in Fig. 23, the proper physical equation is applied:

- for wind fluxes occurring above z_d, characterized by the prevalence of laminar flows, the power law equation (based on roughness coefficient) or the log law equation (based on aerodynamic parameters) can be applied to adjust local wind speed; both are described in detail below.

- for turbulent fluxes occurring at a certain height z lower than z_d, the power or log laws are not valid and kinetics models should be applied: the k-epsilon (k−ϵ) and the k-omega (k-ω) models are the most common model used to simulate the characteristics of the mean turbulent flows. Both are retrieved from the Reynolds-averaged Navier Stokes (RANS) model which is considered the optimal compromise to develop accurate studied on microclimate assessments in urban environments, as described in paragraph 3.7.3.1.

The Power law wind profile.

The power law is based on empirical assumption already defined for large heights (30 m < z < 300 m) at mesoscale applications; it can be less accurate when applied at heights closer to ground level. It is defined as reported in Eq. (13) or in the simplified version in Eq. (14):

$$U_z = U_{ref} \cdot \left(\frac{\delta_{ref}}{z_{ref}}\right)^{\upsilon_{ref}} \cdot \left(\frac{z}{\delta_z}\right)^{\upsilon_z} \quad \text{Eq. (13)}$$

where U_z is the wind speed [m·s^{-1}] at height z [m], U_{ref} is the adjusted reference wind speed [m·s^{-1}] at height $z_{ref,}$ [m], δ is the height of the boundary layer [m], respectively and ν the terrain roughness coefficient (or wind velocity profile exponent) [-].

The two last parameters in the previous equation are used in application to the reference site (δ_{ref},ν_{ref}), and the analyzed site (δ_z,ν_z); they come from tabular data and empirical assumptions derived from real measurements or wind tunnel tests. Several references are present in literature, Table 13 reports typical values of the roughness parameters for some of the most frequent terrain classes; in Table 14 there is the comparison made by [84], and in Table 15 the unified terrain roughness categories given by [85].

$$U_z = U_g \cdot K \cdot z^{\alpha} \quad \text{Eq. (14)}$$

where U_z [m·s^{-1}] is the wind speed at height z [m], U_g [m·s^{-1}] is the wind speed in open country (class I) at a standard height of 10m, K and α dimensionless coefficients [-] describing the terrain roughness, according to Table 14.

The logarithmic law wind profile.

The log-law allows to approximate the wind profile occurring at lower boundary conditions where the heights are lower than 200m (z ≤ 200m). The two aerodynamic parameters identify its lower limit of application, according to the functions expressed in Equations (15) or (16):

$$U_z = U_{ref} \cdot \frac{\ln((z-z_d)/z_0)}{\ln((z_{ref}-z_d)/z_0)} \quad \text{Eq. (15)}$$

where U_z is the wind speed [m·s^{-1}] at height z [m], U_{ref} is the wind speed at height z_{ref} [m], z_d is the zero-plane displacement height [m] and z_0 is the roughness length [m].

$$U_z = \frac{u_*}{k} \cdot \ln\left(\frac{z-z_d}{z_0}\right) \quad \text{Eq. (16)}$$

where U_z is the wind speed [m·s^{-1}] at height z [m], u_* is the atmospheric friction shear velocity, k [-] is Von Karman's constant whose typical value is 0.4, z_d is the zero-plane displacement height [m], and z_0 is the roughness length [m]which represents the dimensions of eddies produced by wind flows.

Table 13. Roughness and aerodynamic parameters for different terrain roughness types.

Terrain roughness type	δ [m]	υ [-]	z_0 [m]	z_d [m]
Level surfaces, grass land	250	0.10	-	-
Flat open country	280	0.14	0.03	0.0
Rolling/level surfaces	300	0.22	0.1	0.0
Heterogeneous surface	330	0.28	-	-
Low density suburban areas	390	0.34	0.5	$0.7 \cdot z_H$
Mid-high density urban areas	450	0.40	1.0	$0.8 \cdot z_H$
Very high density city areas	510	0.45	> 2.0	$0.8 \cdot z_H$

Table 14. Typical values for terrain dependent parameters [84]

Class	*K [-]*	*α [-]*	*Terrain*	*z_0 [m]*	*z_d [m]*
I	0.68	0.17	**Open flat country**	0.03	0.0
II	0.52	0.20	**Country with scattered wind breaks**	0.10	0.0
\	\	\	**Rural**	0.50	0.7h*
III	0.35	0.25	**Urbanized**	1.0	0.8h*
IV	0.21	0.33	**City**	>2.0	0.8h*

*with h=building height [m]

Table 15. Terrain categories proposed by [85]

Category	Exposure (description)	Roughness Length z_0 [m]	Power exponent α	Current code specifications (z_0 [m])
Cat. I	Open water (open sea or lake and coastal areas with few obstructions)	0.002	0.103	AIJ Cat I – open sea (0.0014) AS/NZ Cat 1 – open terrain (0.002) BS6399 – sea (0.003) EN Cat 0 – open sea (0.003) ISO Cat 1 – open sea (0.003) ASCE Exp D – flat area & water (0.0039) GB Cat A – sea, island, desert (0.0076)
Cat. II	Open country (terrain with scattered obstructions up to 10 m high. Rural areas with a few low rise building)	0.04	0.15	AIJ Cat II – open, few obst. (0.04) AS/NZ Cat 2 – open, few small obst. (0.02) BS6399 – country (0.03) EN Cat I – lake & area without obst. (0.01) EN Cat II – area with few obst. (0.05) ISO Cat 2 – open country (0.03) ASCE Exp C – open, few med. Obst. (0.048) GB Cat B – village, countryside (0.061) NBCC Exp A – open terrain (0.025)
Cat. III	Forest/Sub-urban scattered low (3-5m) buildings (Numerous closely space 3-5m obstructions)	0.2	0.198	AIJ Cat III – suburban (0.21) AS/NZ Cat 3 – many medium obst. (0.2) BS6399 – town (0.3) EN Cat III – suburban, forest (0.3) ISO Cat 3 – suburban (0.3)
Cat. IV	Urban, large town (many medium height (10-50m) buildings)	0.5	0.241	ASCE Exp B – urban (0.58) GB Cat C – city (0.34) NBCC Exp B – suburban & urban (0.58)
Cat. V	City (medium height buildings mixed with tall (50m+) buildings)	1.0	0.289	AIJ Cat IV – city medium height bldg. (0.78) EN Cat IV – are 15% bldg>15m (1.0) GB Cat D – city all bldg. (1.13)
Cat. VI	City centre (concentration of very tall buildings mixed with other buildings)	>=2	0.362	AIJ Cat V – city tall bldg. (1.82) AS/NZ – city (2.0) ISO Cat 4 – urban (3.0) NBCC Exp C – city centre (1.97)

3.3. Research background: model and tools

The surface roughness elements influence the spatially- and temporally averaged air flow properties, as well as the turbulent characteristics. To define the structure of the urban boundary layer, an accurate representation of urban morphology is essential [86]. Several methods and tools exist to investigate the connections between the urban morphology and the wind flows. From the below lists, the main methodologies are described in detailed and compared in Table 16:

i) field measurements, whose high time and costs limitations do not let them be appropriate studies at larger scales
ii) wind tunnel experiments, that can become reference dataset, despite their high operating costs and restrictions in applications
iii) Computational Fluid Dynamic (CFD) modelling that has an unbearable computational need for larger scale applications [87]
iv) parametric models that have interesting costs-benefits ratio and limited application fields
v) Geographical Information System (GIS) based on remote sensing data and techniques dealing with roughness parameters retrieved from the analysis of their interactions with buildings' geometries at larger (whole city) scales [88].

Computational Fluid Dynamic models.

Computational fluid dynamic models (CFD) are complex finite element calculation models. They solve the equation of motion numerically. Among the three main numerical approaches: Reynold-Average Navier-Stokes (RANS), Large Eddy Simulation and Direct Numerical Simulation (DNS). They can describe turbulent motion equation of airflow inside UCL. Computations are time-consuming and require high computational demand and user expertise. The computational effort is due to the high amount of high-resolution data input, a detailed computational domain consists of mesh grid cells (smaller cell size selection to be more adjacent to obstacles and urban surface) and the high number of iterations for each simulation. The spatial scale at which CFD is usually performed occurs around individual buildings or on generic urban surfaces (idealize regular building arrays) with considerable attention in describing buildings and urban surface and form. Recently, few studies investigated actual urban areas [89], but coarser description of surrounding context is needed when large scale (i.e., district scale) simulations are made to limit cells number and simulation times.

CFDs are suitable for application concerning advanced feasibility studies. The main advantages consist in their capacity to describe highly complex patterns of turbulent flow and complex interaction between urban drivers, and the capability of generating spatially distributed microclimate data considering environmental context. The disadvantages are not negligible: they are not suitable for urban-district scale applications at early-stage studies due to high costs, and they have limits of application field; in fact, difficulties occur in the generalization of CFD results: from idealized arrays to realistic urban environments or because actual local scale case-study are not representative of neighborhoods or city-average.

Simplified parametric models.

Parametric models are based on statistical relationships between systems of variables. A parametric function (i.e., regression equation) is used to describe the result as a function of several input data (parameters). These parameters are obtained through the application of other methods, field or experimental measurements (wind tunnel tests) and usually they have a theoretical significance. The

simplification consists in loading the input parameters with reference to tabular data for which an application limit interval is defined, depending mainly on the available observation sample on which the model is derived. The simplification also consists in the limited number of input data needed with a reduced resolution: most of them concern the geometric description of buildings and their simplified relationship with the context. This is defined considering homogeneous boundary conditions and therefore not differentiating the single objects.

Parametric models can be of great descriptive and practical value by providing rapid simulations and requiring extremely low computational demand. They are suitable for early-stage studies. However, the field of application is very limited to the reference range of each parameter and the generalization of the results is limited to case studies with characteristics similar to those observed. Application on an urban scale is possible but it is limited by the inability of the model to describe the heterogeneity of urban morphological characteristics.

GIS-based tools and plug-ins.

This methodology consists of different GIS-based tools and plug-in. Geographical Information System (GIS) and remote sensing technique are able to retrieve parameters according to their interactions with spatial geometries; this analysis occur mainly at city-scale. The spatial description of phenomena integrates physical laws. Input data comes from available existing databases already used by urban planners. Application of this method can support decision making processes for early-stage project design evaluations; for this reason, it is necessary to have a detailed overview on a large spatial scale. Computational effort is limited, and it is possible to resort only to open-source software, with the possibility of modifying codes and script models, adapting and improving them. Simulation times are reduced: if compared to CFD, the lower resolution of the output data is compensated for the possibility of carrying out evaluations on a larger scale with faster simulation times. The accuracy of the results depends on the accuracy of the input data. The main advantage consists in the ability to spatially distribute input and output data, managing interaction between data with different types and measure, different details of spatial and timescales, and describing geometries with high resolution at wider scale. The less detailed description at the building scale is compensated by the ability to describe real characteristics of the built environment and the morphological urban variables at block of buildings, neighborhood, district or city-scale.

Table 16 Tools and methods to assess air flow at urban scale.

	Computational Fluid Dynamic model	**Simplified parametric model**	**GIS-based model**
Brief description	CFDs are complex finite element calculation models based on numerically motion equations	Simplified parameters models empirically based	Models and method based on Geographical Information System (GIS) tools and plug-ins
Approach	3 main numerical approaches: Reynold-Average Navier-Stokes (RANS), Large Eddy Simulation and Direct Numerical Simulation (DNS)	Statistical relationship between systems of variables (parameters) obtained from field measurements, wind tunnel tests, CFD simulation	GIS tools and remote sensing techniques retrieve parameters based on interactions with spatial geometries at city-scale.
Input data	High amount of data at high-resolution	Limited number of input parameters from reference tabular data whit defined range of application	Spatially distributed input data from accessible databases, managing integration between parameters of different natures, scale, and resolution
Modelling	Detailed computational domain consists of mesh grid cells (the smaller the cell size the higher the	Parametric function (regression equation) describing results as a	Correlation between morphological and aerodynamic urban parameters and physical laws integrated in the

	results accuracy and the number of iterations	function of several parameters with a physic-based meaning	spatial description of natural phenomena
Simulation time	Relevant time-consuming At urban scale: days	Rapid simulation time At urban scale: minutes	Moderate simulation time At urban scale: hours
Computational effort	High demand and user expertise	Simple computer application	Limited, relying on open-source software
Application field (scale)	Usually performed at the scale of individual building or idealized regular building arrays. Recent investigations on actual urban areas (limiting the number of iterations with more approximate descriptions of the context)	Usually applied at building scale with detailed description of building geometry and characteristics; easily applicable to larger scales with reduced generalization due to the simplified description of the surroundings context	Suitable for evaluation at building, block of building, neighborhood, and district scales. Less detailed description at building scale is compensated by real description of the whole urban built environment and heterogeneity of morphological urban variables
Scope of use	Advanced feasibility studies	Early-stage study	Since early-stage study
Main advantages	❖ Description of highly complex patter of turbulent flow and complex interaction between urban drivers ❖ Spatially distribution of output data at microscale considering heterogeneous environmental context	❖ Great descriptive and practical value by immediate and simple simulations	❖ Evaluation on larger spatial scale with faster simulation times (compare to CFD) ❖ Ability to spatially distribute in-output data ❖ Integrability with other urban planning tools thanks to input data from existing databases
Main disadvantages	❖ Application field limited at urban-district scale (difficult generalization of results)	❖ Simplified description of urban context (homogeneous condition of surrounding) ❖ Range of reference values used for regression analyses, depending on available observation sample on which the model is derived ❖ Limited application field to similar case studies	❖ Lower accuracy of the output data (compared to CFD) mainly depending on detail resolution of input data
Software/Tool	ANSYS Fluent, ENVI-MET, UrbaWind	CpCalc+, CpCalc2.0, TNO CpGenerator	SAGA, QGIS-UMEP plug-in

3.4. Place-based tools for wind analysis at urban scale.

Morphometric methods.

The available methods that is possible to apply to calculate the aerodynamic parameters at urban scale are grouped into three categories: i) *reference-based values from field observations,* that provide wide intervals of values but entail limitations when applied in complex and heterogenous urban areas; ii) *anemometric methods* that necessarily require large experimental campaigns and that can be applicated on limited and no-replicable scales; iii) *morphometric methods* that rely on the associations of aerodynamic parameters and roughness elements geometry, which are assessed thanks to the urban morphological parameters, already used at mesoscale [90] and local scale [91].

The morphology of roughness elements can be used to determine z_d and z_0 using morphometric methods. Therefore, elevation databases that resolve roughness-element morphology allow estimation of z_d and z_0 in cities and the associated wind speeds and surface heat fluxes [92].

In literature, numerous morphometric methods have been described [93] with specified assumptions and range of applicability. In Table 17 are listed some of the main urban morphological parameters used in the scientific reference framework. These are:

- *Plan area density (PAD)* - the ratio between the built area of buildings (considering number of floors) and the total site area - (urban structure compactness). It corresponds to the *Building Density (BD or* λp*)* and the *Urban Density (UD*).
- *Building Coverage Ratio (BCR*) – the ratio between the footprint area of buildings and the total site area. It corresponds to the *Site Coverage Ratio*.
- *Sky view factor (SVF)* – the ratio of the visible sky to the overlying hemisphere in a sky view image from a given point on the ground.
- *Building frontal area (BFA or λs*) – the total area on the frontal façade of the building facing the wind (also frontal area density).
- *Gross floor area ratio (GFAR)* - the ratio between buildings' gross floor area and the site area, also Floor Area Ratio (FAR).
- *Height Variability (HV or* σ_H*)* – it is calculated has the standard deviation of the heights of the building on a certain area.
- Aspect ratio (H/W) - the ratio between the height (H) of the building facing the street canyon and the width (W) of street canyon.
- Street Canyon Density (SCD) - the ratio between the total length of street canyons (H/W < 1.4) and the site area.
- Tall Vegetation Area Density (VEG) – the ratio between the tall vegetation cover and the site area (also urban tree cover).

Table 17. Main urban parameters used in morphological methods.

	Wong et al.	Darmanto et al.	Badach et al.	Peng et al.	Mei et al.	Kent et al.	Kent et al.	Cheng et al.	Yang et al.
	[88]	[90]	[91]	[92]	[94]	[95]	[96]	[97]	[98]
PAD		●	●	●	●	●	●	●	●
SVF			●						
BFA	●	●	●		●	●	●		
G(FAR)			●	●					●
HV		●	●			●	●	●	
H/W			●		●				
VEG			●						●
z0	●	●		●	●	●	●		●
zd		●		●	●	●	●		●

As shown in Figure 25, three main regimes of wind flows in urban areas have been already classified with morphometrically determined aerodynamic parameters [78]: i) *isolated flow*, in which each building can generate individual wakes; ii) *wake interference flow*, in which wakes reinforce each other as the space in between is even closer and the greatest roughness activity can be generated; iii) *skimming flow,* in which the main wind flows are able to skip over the top of buildings. Due to this findings, the building density (λ_p) emerges as a very important parameter, especially in cities where the variability of the roughness elements' height ($\boldsymbol{\sigma_H}$) can cause complex turbulent wakes that are challenging to be assessed.

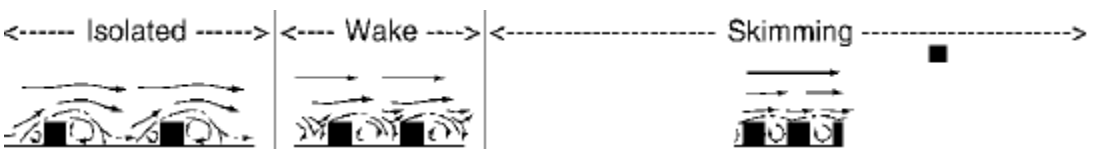

Fig. 25 - The three main flow regimes between buildings defined according to the building density. Source: [79]

GIS-based tools and plug-ins for wind analysis.

In this paragraph, two of the main GIS-based tools and plug-ins to investigate wind at urban scale are described: the SAGA and UMEP plug-ins. Both have been studied and compared (Table 18), but only the second has been deeply investigated and chosen to be applied in the proposed place-based methodology.

Table 18. QGIS-based tools for wind analysis at urban scale.

Plug-in	*Section - Tool*	*Description*	*Scale*	*Input data*	*Output data*	*Ref.*
 	Terrain analysis – Morphometry section – Wind Effect	Determine areas exposed to the wind and the shaded ones	Meso scale (above ABL)	• DEM (grid) • Wind speed and direction (vector grid)	• Dimensionless index (grid): <1 shadowed >1 exposed	[99]
	Climate and Weather – Wind Effect Correction	Calibrate the scaling factor of the wind effect, considering local observation of ABL conditions (e.g, precipitation, cloudiness		• Boundary Layer (grid) • Wind effect (grid) • Observations (grid)	• Corrected wind effect (grid)	
	Urban morphology - Morphometric calculator (*Grid or Point*)	Calculate morphometric parameters based on digital surface model and aerodynamic parameters based on morphometric methods (isotropic and anisotropic results).	Local scale	• DSM -DEM (grid) • Grid cell (polygon)	• Morphometric parameters (grid): λ_p, λ_f, z_H, z_{Hmax},$z_{\sigma H}$ • Aerodynamic parameters (grid): z_d, z_0	[100]

SAGA QGIS Tool at mesoscale.

The *System for Automated Geoscientific Analysis* (*SAGA)* software (https://saga-gis.sourceforge.io) has been developed and integrated in the open-source software Quantum-GIS (QGIS). Version 2.1.4 [99] presents some interesting tools to adjust the wind at the mesoscale, in order to consider the influence of the terrain and of the observed meteorological conditions. In the *Terrain analysis - Morphometry* section, the *Wind Effect* tool is used to classify levels of wind exposure and shades areas through a dimensionless index, according to information about terrain elevation and wind characteristics; as input data only a raster file of the Digital Terrain Model (DTM) or Digital Elevation Model (DEM) are needed, together with a vector grid containing information about interesting wind speed and direction. In the *Climate and Weather* section, the *Wind Effect Correction tool* allows to calibrate the *Wind Effect* scaling factor, previously calculated, for the determination of ABL considering meteorological observations (e.g., precipitation, cloudiness).

3.4.1. QGIS-UMEP plug-in

The *Urban Multi-scale Environmental Predictor* (UMEP) is a climate service tool, designed as a plug-in for the open-source QGIS software. The tool can be used for several applications related to climate and solar analysis, outdoor thermal comfort, urban energy consumption, climate change mitigation etc. It can be used to morphometrically determine *zd* and *z0* at local scale. The presented

UMEP plug-in refer to the version 1.6.1 [100]. Among its pre-processing tools, in the section *Urban morphology,* there are two similar tool that can be used:

- *Urban Morphology: Morphometric Calculator (Grid)*
- *Urban Morphology: Morphometric Calculator (Point)*

Both calculate five morphometric parameters (see Table 19 and Figure 26) based on the Digital Surface Models (DSM), required among the few input data, that are used to calculate the two aerodynamic parameters (z_d, z_0), according to six different morphometric methods (see Table 20). The (*Grid*) and the (*Point*) tools differ for the geometry of the interested area of a polygon vector layer on which calculation will be referred to. In the first case a single simulation will be brought back to a point (with coordinates x, y), which can be selected directly on the map, in the second case, after creating a vector polygon grid layer with a preferable resolution, an output result will be obtained for each grids' cell.

Required input data.

Only two type of input file are required, both spatially related: raster file, describing the real condition of the case study area, considering the available and preferable extension and resolution, and shape file, containing a polygon layer of regular grid cells, to which results will be reconducted. Three raster files are needed, possibly in the *geoTIFF* format and with same resolution and extension of pixels, containing information of raster cells elements height in meters above sea level. The three raster files consist of:

1) Digital Surface Model – DSM, ground and roughness elements height

2) Digital Elevation Model -DEM, only ground height

3) only roughness elements height (DSM-DEM), it can be calculated directly in QGIS as a difference between the two previous rasters, using the *Raster calculator tool.*

Settings.

The main setting of this tool deals with the extension of the study zone area that will be used to determine the morphological and aerodynamic parameters, based on the information contained in the raster files. It is possible to indicate the length of the radius (in meters) from the selected point, in the *(Point)* method or the centroid of each grid cell, in the *(Grid)* method. No unified or shared standards exist about the size of the calculation area, even though it strongly affects the accuracy of results [101]. In addition, it is possible to specify the search range of the wind direction (in degrees, from the North pole and in the clockwise direction): for each wind direction a simulation will be performed (anisotropic output file).

Definition of the five morphometric parameters.

The five morphometric parameters that are calculated by the UMEP tool are then used to describe the geometry of the roughness elements. They correspond to the most frequent urban parameters: plan area density index (λ_p), frontal area index (λ_f), average (z_H) and maximum (z_{Hmax}) buildings height and height variability (z_{Hstd}). The selection of these parameters as most correlated to the aerodynamic parameters is widely shared by numerous studies (Table 16). Table 19 reports the definition, symbology and unit of measurement of each parameter as calculated by the QGIS tool [96] . Morphological features and aerodynamic parameters can vary due to the selected wind directions, and this allows for more precise and accurate results of z_d and z_0, adding the roughness surfaces'

variability [82]. The scheme in Figure 26 reports an example of the setting variables used in UMEP tool, to determine the urban parameters in a case study area considering the wind direction.

Definition of the six morphometric methods.

In the examined plug-in it is possible to calculate the aerodynamic parameters z_d and z_0 by applying six different morphometric methods, selected from the numerous existing methods, the results of which were previously compared in [96].

As described by [96], all these methods follow some criteria: (i) both z_d and z_0 are included in the formulations; (ii) the method is applicable to a wide range of urban densities and environments; (iii) geometric data required are readily obtainable in complex urban environments; (iv) given resources available, the method is computationally feasible. Table 20 reports for each method the authors, the abbreviation, and the urban parameters used in the calculation methodology of z_d and z_0, among the five morphometric parameters listed in Table 18. In dense districts that are typical of the central areas of a city, the most suitable method is the Kanda method [102], due to the fact that it is very important to considering the height heterogeneity of the roughness elements (buildings). Based on regression algorithms, it expresses the correlation between morphometric parameters and aerodynamic parameters as output data, according to Eq. (17) and Eq. (18), respectively for the displacement height z_d and the roughness height z_0.

$$KAN_{zd} = H_{max}[c_0 \cdot X^2 + (a_0 \cdot \lambda_p^{b0} - c_0) \cdot X] \quad \text{with } X = \frac{H_{std} \cdot H_{avg}}{H_{max}}, \text{ for } 0 \leq X \leq 1 \qquad \text{Eq. (17)}$$

$$KAN_{z0} = MAC_{z0}\,(b_1 Y^2 + c_1 Y + \alpha_1) \quad \text{with } Y = \frac{\lambda_p \cdot H_{std}}{H_{avg}}, \text{ for } 0 \leq Y \qquad \text{Eq. (18)}$$

where λ_p [-] is the plan area density index, H_{std} [m] the height variability, H_{avg}, [m] the average height, H_{max}, [m] the maximum height of the buildings, and a_0, b_0, c_0, are regressed constant parameters (a_0= *1.29*, b_0= *0.36*, c_0=*-0.17).*

Table 19. Urban parameters applied in QGIS-UMEP tool.

Urban Parameters	Symbol	Unit	Definition	Formula
Plan Area Index	λ_p	[-]	Ratio between the built area (Ap) of n buildings (i) (considering number of floors) and the total site area (A_T)	$\lambda_p = (\sum_{i=1}^{n} Api)\ /A_T$
Frontal Area Index	λ_f	[-]	Ratio between the windward façade area (Af) of n buildings (i) (for each wind direction) and the total site area (AT)	$\lambda_f = (\sum_{i=1}^{n} Afi)\ /A_T$
Mean Height	z_H	[m]	Average height (H) of n buildings (i)	$z_H = (\sum_{i=1}^{n} Hi)$ /n
Maximum height	z_{Hmax}	[m]	Maximum height (H) of the building (i)	z_{Hmax} =Max (H_i)
Height variability	z_{Hstd}	[m]	Standard deviation of buildings' height	$z_{Hstd} = \sqrt{\frac{1}{n}\sum_{i=1}^{n}(Hi - z_H)^2}$

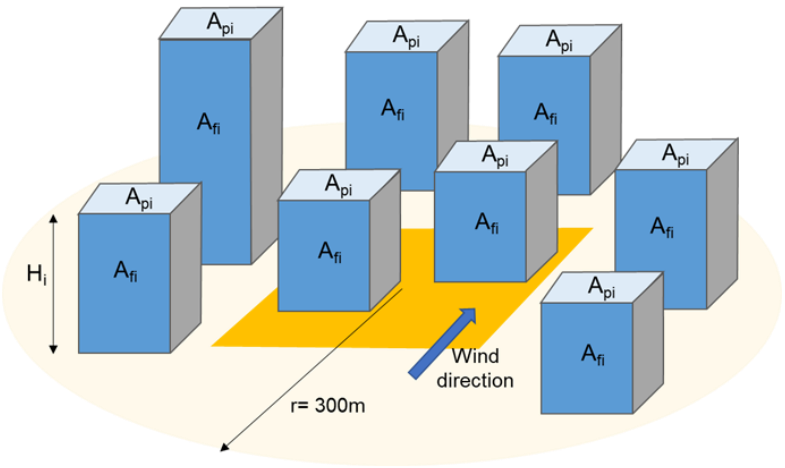

Fig. 26 - Example of main setting variables used in UMEP tool: built area *Ap*, windward façade area *Af,* and total site area A_T for all the *i* buildings (with height *H)* in a case study area (in light yellow) defined by the radius length (r) in which the investigated site (in orange) is centred, and considering the selected wind direction (blue arrow).

Table 20. Morphometric method included in QGIS-UMEP tool.

				Required urban parameter				
Method	**Ref.**	**Year**	**Abbr.**	**λ_p**	**λ_f**	**Z_H**	**Z_{Hmax}**	**Z_{Hstd}**
Rule of thumb	-	-	RT			●		
Raupach	[96]	1994	RAU		●	●		
Bottema and Mestayer	[103]	1997	BOT	●	●	●		
Macdonald	[104]	1998	MAC	●	●	●		
Millward-Hopkins	[105]	2011	MHO	●	●	●		●
Kanda	[102]	2013	KAN	●	●	●	●	●

3.5. Research objective and novelty

In this step of the research activity the main aim is to assess the urban ventilation at urban scale defining a GIS-place based methodology that fits into the subsequent steps of the overall methodology concerning air flows at building scale and building energy modelling thanks to the interoperability of the input and output data in a unique geo-database, which makes all the steps functional to each other.

The main goal is the adjustment of the refence wind speed according to the height from the ground, considering the impact of the built context and the presence of buildings together with the specificities of the real urban environment and local climate context.

The novelty of this work is the application of specific GIS tools (UMEP) and remote sensing techniques to retrieve physical-based models at urban scale based on interactions with spatial geometries. Q-GIS plug-in based on morphometric methods is chosen to define the spatial distribution of aerodynamic parameters as a function of morphometric urban parameters with digital surface model (DSM) as input data and the real environment as application field. Accessible database constitutes the few input data required, open-source software allows the replicability of the methodology in any case study; the definition of a flexible methodology makes it adaptable to the specificities of any context and scale; the relationship between the number of input data, simulation times and accuracy of the result also makes it suitable for early-stage evaluations.

The GIS-based modeling is chosen to overcome the limits of other types of modeling: the limited application field of parametric models and their simplified description of the urban context, based on tabular data, and the high computational effort of CFD simulations, not suitable for analysis at urban scale.

GIS-based modelling is intended as a good compromise as it allow to spatially distribute output data, even if not in the complete domain as CFD, but it evaluates larger spatial scale with faster simulation than CFD. In addition, it can describe complex interactions between urban drivers combining the spatial interactions and the physical laws that governed phenomena with the possibility to manage large amounts of data. The less detailed description of the buildings is compensated for by the real description of the whole urban built environment and heterogeneity of morphological urban variables. Starting from it, the place-based methodology proposed in the following paragraphs allows to calculate:

- the wind speed variation at local scale as a function of roughness elements morphology,
- the spatial distribution of the height of boundary canopy layer at neighborhood scale to apply proper wind profile laws,
- the horizontal and vertical distribution of incident wind speed along buildings' facades to determine surface pressures on both windward and leeward façade, considering only the natural wind-driven effect.

Firstly, the selected *UMEP* tool is applied to a case study, then results are compared to the one of an established parametric method (*Cpcalc+),* presenting strength, limits and possible implementation of the methodology.

The limit of this methodology is the impossibility of adjusting the wind speed inside urban canyons, since in these cases wind profile laws (power-law, log-law) are no longer applicable and it is necessary to use turbulent wind profiles. These will be evaluated from paragraph 3.7.

3.6. GIS-based method for ventilation at urban scale

The methodology described in this paragraph has been presented at the 5th Building Simulation Applications Conference (BSA 2022), in Bolzen (Italy), on June, 29th – July, 1st 2022); it has been published in the Conference Proceedings with the title *GIS-based tools to evaluate air flow rate by natural ventilation in buildings at urban scale* [30].

Firstly, the *zd methodology* has been developed to determine the spatial distribution of aerodynamic parameters, and consequently, applying the proper wind law , correct the local wind speeds of the selected case study. The QGIS UMEP plug-in has been used and the flow chart in Figure 27 summarizes the main steps of the *zd methodology*.

Secondly, the *zd methodology* has been compared to the well-established parametric methodology on which the *CpCalc+* tool is based, to validate and present strength, limits and possible implementations of the place-based methodology. The scheme in Figure 31 summarizes the main features of the two methodologies compared: the place-based model (*zd-method*) and the parametric model (*Cp-method*). The adjusted wind velocity at urban scale is then applied at building scale in order to evaluate the vertical and horizontal distribution of the surface pressure coefficient generated by the incident wind on building facades. Results of the surface pressure (p_{dyn}) are compared.

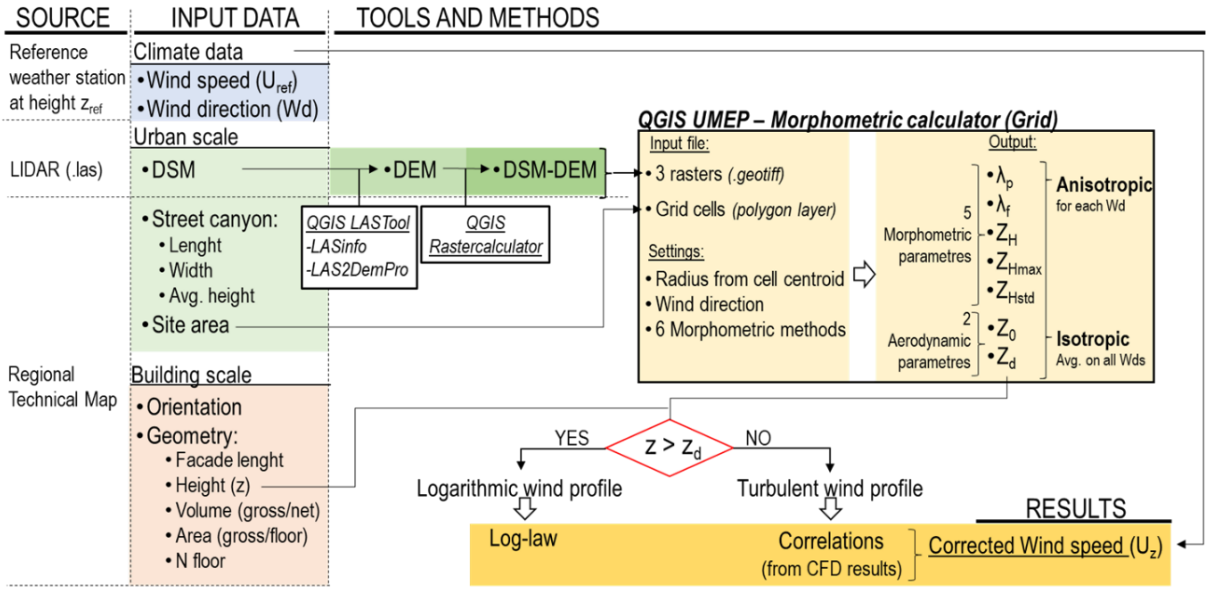

Fig. 27 - Flow chart of the *zd methodology* based on the application of the QGIS-UMEP tools.

3.6.1. Methodology and case study application

The place-based methodology is applied in a central district in the city of Turin (Figure 28a), in the North-West of Italy. For the in-depth analysis concerning the selection of the case study zone and the description of its characteristics, refer to [60]. The site area has an extension of 200m^2 (200mx200m).

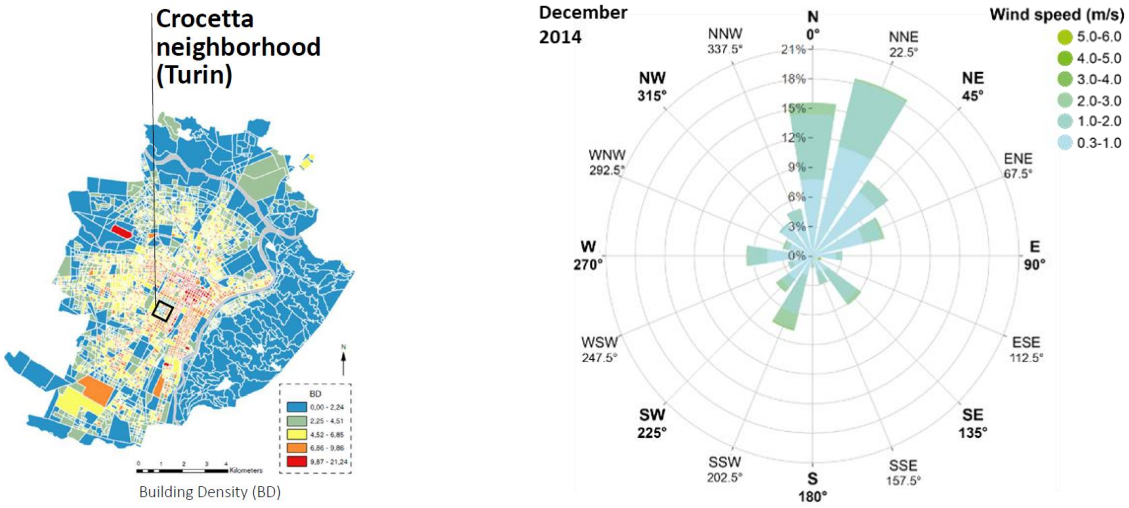

(a) (b)

Fig. 28 a-b - The localization of the Crocetta district in the centre of Turin, Italy (a) and example of the prevailing monthly wind direction and velocity for the city case study (b). .

Step A - Input data.

The locale climate data of wind speed [$m \cdot s^{-1}$] and direction [0°N] come from the nearest weather station of the Living Lab of Polytechnic of Turin, locatedat 32m from the ground (https://smartgreenbuilding.polito.it). Data are quarterly detailed and refer to the years 2010-2020. Two years have been analyzed (2013-2014), for each month, Table 21 reports the monthly prevailing wind direction (0 ° N, clockwise) and the average hourly wind speed (U_{ref}), calculated as the average of the hourly speed values for the monthly prevailing sector. The monthly prevailing wind direction (*Wd*) is from North-NorthEast and West-SouthWest, and the mean wind velocity is around 1.4 m/s (Figure 28b). Concerning the urban parameters, Table 22 shows the main parameter calculated at neighborhood level in QGIS to describe case study area and then integrated with building scale characteristics. Typological characteristics of buildings and geometrical dimensions are obtained from the Regional Technical Map for the city of Turin (i.e., BDTRE:2019, http://www.geoportale.piemonte.it/).

Table 21. Local climate input data of Crocetta district.

Month		**1**	**2**	**3**	**4**	**5**	**6**	**7**	**8**	**9**	**10**	**11**	**12**
W_d	***2013***	11	11	11	214	11	11	11	349	349	11	11	11
[°]	***2014***	11	11	11	11	11	349	11	281	349	11	11	11
U_{ref}	***2013***	1.28	1.28	1.31	1.76	1.64	1.51	1.49	1.51	1.32	1.03	1.25	1.04
[m/s]	***2014***	1.05	1.29	1.50	1.52	1.50	1.66	1.51	1.51	1.24	1.05	1.05	1.15

Table 22. Morphological characteristics of Crocetta district.

Urban parameter	**Unit**	**Study area**
Built Coverage Ratio (BCR)	[-]	0.33
Plan Area Density (PAD)	[-]	1.66
Volume Area Ratio (VAR)	[-]	0.30
Sorrounding buildings height	[m]	19.5
Height of boundary layer (z_{UBL})	[m]	450
Wind speed profile exponent (v)	[-]	0.4
Short urban canyon (L/H)	[m]	≤ 3
Long urban canyon (L/H)	[m]	> 5

Step B - UMEP settings and simulations

The tool setting is a crucial aspect in the application of the UMEP plug-in, the main features are reported in the example in Figure 29. Raster files are created from the same dataset of 1-m resolution surface elevation. It comes from a LIDAR flight: the available dataset in the format *.las* file is transformed into a raster file (Geo TIFF), using the *QGIS LAS tool*; the Digital Surface Model (DSM) and Digital Elevation Model (DEM) are retrieved according to the information stored, while the third raster (DSM-DEM) is calculated with the *QGIS Raster calculator tool*.

Considering the extension of the site area (200mx200m) and the resolution of the DSM, a grid vector polygon is created, with a 5m squared grid to assign results to each grid cell and to have more than one cell related to each building. From the centroid of each cell in the grid, a radius of 300 m length is set, defining the extension of the case study area. For each of the twelve prevalent wind directions selected, considering an interval of 30°, a simulation will be performed and, for each cell on the grid, twelve different results of morphological and aerodynamic parameters will be obtained (anisotropic results). In addition, for each cell, an isotropic result will be added, calculated as the average value between all the results from the twelve wind directions.

As mentioned before, among the six morphometric methods available in UMEP, the Kanda method is chosen to calculate the five morphometric parameters on which the two aerodynamic parameters are retrieved. For each cell of the grid (5x5m), and for each wind direction, a value of z_d is obtained.

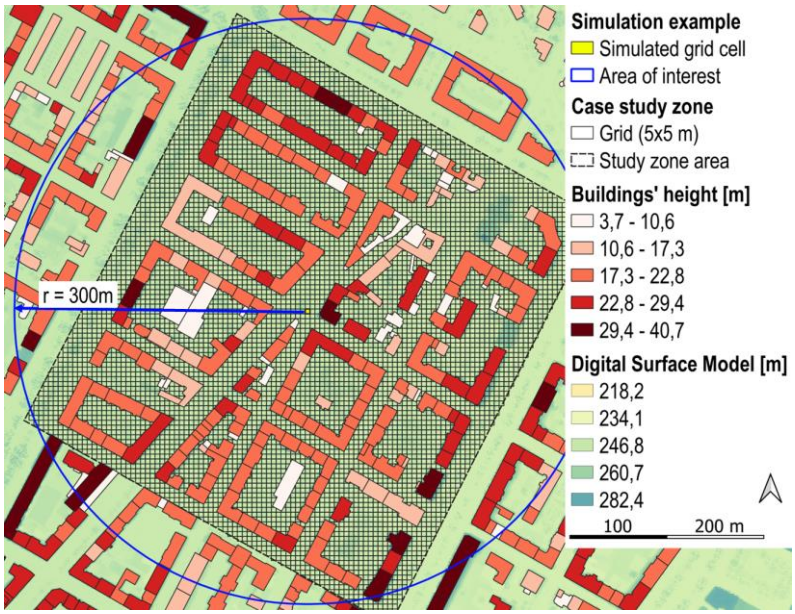

Fig. 29 - Example of the settings required by the UMEP tool: for each simulated cell (in yellow) of the grid (5x5m)in which the study zone area is divided, an area of interest (blue circle) is define with a radius r=300m, considering all the buildings present in the area and their geometrical information (height) and spatial correlation (DSM) to calculate the output parameters.

Step C - Wind profile assignment

At the building or block of buildings scale the evaluation of the wind profile occurs in order to apply the proper wind law to correct the reference wind velocity. As shown in the flow chart in Figure 27, the displacement height zd is compared to the interesting height z referred to the building height (or floor height), and the two possible conditions are tested:

- if z > z_d, for interesting heights above zd, the logarithmic wind profile is assigned and the local wind velocity *Uz* is calculated applying the wind log-law;
- if z < z_d, for interesting heights below zd, the turbulent wind profile is assigned and the local wind velocity *Uz* is calculated according to correlation from CFD results.

Then, according to building heights (*z*) or floor numbers, for each building or buildings' floor, the wind speed can be adjusted, and buildings are classified into two groups: those with both logarithmic and turbulent wind profile, occurring at different floors' heights and those with only turbulent profile. In this work, the wind velocity above z_d is calculated applying the log-law equation (Eq. 15), while the wind velocity below z_d, is based on correlations found from CFD models results [106]. Reference is made to a selected reference case study with similar characteristics of the urban morphology (Table 22); linear and exponential correlations have been previously determined for short and long canyons (Fig. 30).

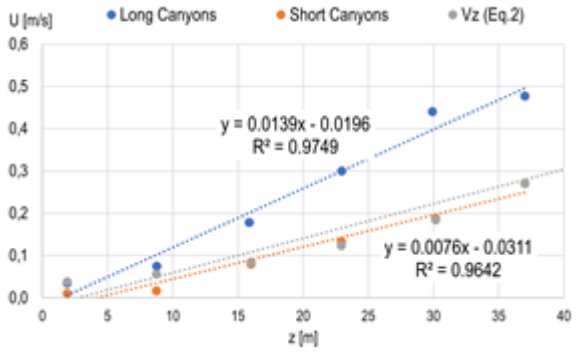

Fig. 30 - Correlation from CFD model results in [106] for long (in blue) and short (in orange) canyons.

3.6.2. Methodology validation: comparing the zd-method and cp-method

According to the second objective of this work, to validate the *zd method,* it is compared to the well-established parametric methodology on which the *CpCalc+* tool is based, defining a (*Cp-method*), with reference to the scheme in Figure 31.

To compare the two methods, the wind velocity must be analyzed at building local scale. The presented methodology is applied to a block of buildings in the case study area, well exposed to the wind considered: buildings oriented perpendicularly to the prevailing monthly wind direction (N-NE).

The wind driven effect is one of the two main driving forces that generate natural ventilation in and around buildings (the other is buoyancy or stack-effect). The incident wind generates positive pressures and negative pressures on windward and leeward facades, respectively. The aim is to compare the ability of the two methods in describing the vertical and horizontal spatial distribution of the surface pressures on both buildings' facades. The adjusted wind velocity at urban scale is then applied at building scale to evaluate the vertical and horizontal distribution of the surface pressure [Pa] generated by the incident wind on building facades. Results of the surface pressure determined by the two methods will be compared.

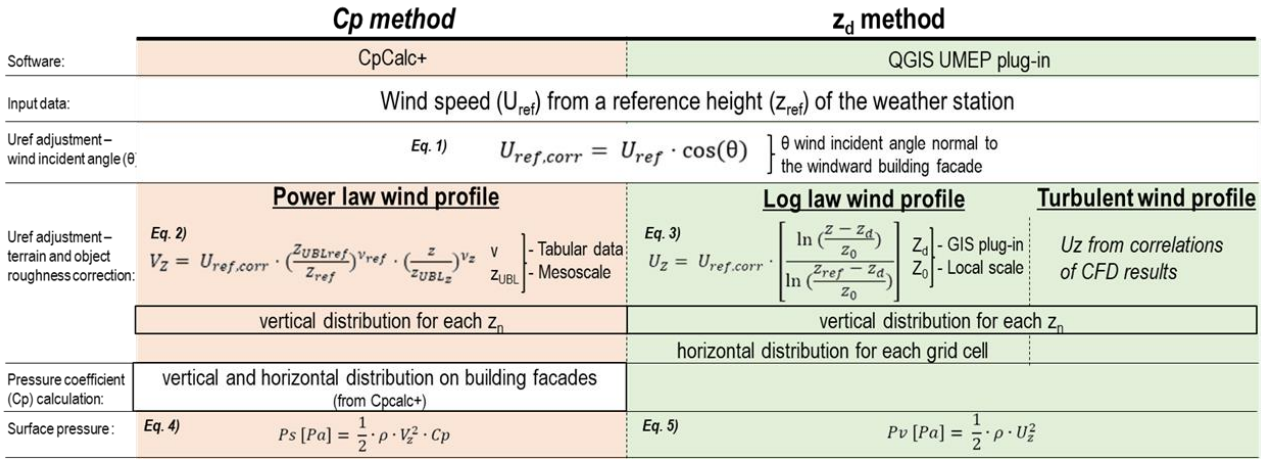

Fig. 31 - Flow chart describing the two methodologies compared: the *Cp-method* based on the CpClac+ tool and the *zd-method* based on the QGIS-UMEP tools.

As described in the flow chart in Figure 31, the *Cp-method* is based on the *CpCalc+* software, while the *zd-method* is based on the UMEP plug-in. The main features and differences between the two software are listed in Table 23.

The *CpCalc+* is a tool used to determine the pressure coefficients (Cp) that the incident wind generates on the windward and leeward facades of a building. An in-depth description of the tool is given in paragraph 4.2.1.2 of the next chapter. The Cp is a non-dimensional coefficient estimated on the basis of real scale measurements or wind tunnel tests, or CFD simulations or parametric models; among the last method there is the *Cpcalc+* software [107], whose input data concern: climate data (wind direction), urban parameter (PAD, surrounding building height, wind profile exponent) and building characteristics (dimension, orientation, slope and openings positions). In addition to the application of the power law that let it possible to determine the vertical variation of wind velocity at the local urban scale, the Cp allows to horizontally and vertically distribute wind speeds at the height of interesting points on a certain building façade, distinguishing the windward and leeward ones. It is also able to consider the building geometry and its orientation, and the density, and the roughness characteristics of its surrounding built environment. Limitations in the use of this tool are related to its application field: suitable at building scale, nor at neighborhood-district scale. This is due to the limited application range of the FAR and SAR parameters, respectively the relative building height and the aspect ratios whose threshold values are: 0.5≤FAR≤4 and 0.5≤SAR≤2.

Starting from the reference wind velocity $U_{ref,}$ [m·s^{-1}] for both methods, it is adjusted $U_{ref,corr}$ [m·s^{-1}] considering the cosine of wind incident angle (θ) on the façade, and only its normal component, as reported by Eq.(19),:

$$U_{ref_{corr}} = U_{ref} \cdot \cos(\theta) \tag{19}$$

Then the adjusted wind velocity $U_{ref,corr}$ [m·s^{-1}] is corrected applying the proper wind profile law, to consider the impact of the terrain roughness and obstacles at urban scale :

- in *Cp-method*, the power law is applied (Eq.14) with reference to tabular data (Table 13)
- in *zd-method*, the logarithmic or turbulent wind profiles are assigned to each building, according to results of the UMEP plug-in application at urban scale; consequently:
  - log law is applied (Eq.15), in case of $z > z_d$
  - correlation from CFD results is retrieved (Fig.9), in case of $z < z_d$

As final step, the surface pressures can be calculated according to Eq.(20), or Eq.(21), respectively surface pressure P_s [Pa] with *Cp-method* and surface pressure P_v [Pa] with *zd-method:*

$$Ps\ [Pa] = \frac{1}{2}\rho \cdot Cp \cdot V_{(z)}^2 \tag{20}$$

where: V_z is the adjusted wind speed ($U_{ref,corr}$) [m·s^{-1}] at the height z [m], according to the power law, ρ [kg·m^{-3}] is the outdoor air density, and Cp [-] is the pressure coefficient at height z.

$$Pv\ [Pa] = \frac{1}{2}\rho \cdot U_{(z)}^2 \tag{21}$$

where: U_z is the adjusted wind speed ($U_{ref,corr}$) [m·s^{-1}] at the height z [m], according to the log law (or CFD correlations), ρ [kg·m^{-3}] is the outdoor air density.

Table 23. Comparison between QGIS-UMEP tool and CpCalc+ software.

Software	Input data			Modelling			Supported data	Output data	
	Climatic data	Urban data	Building data	Approach	Language	Description		Variable	Application
QGIS-UMEP tool	Range of wind direction (°, from N, clockwise)	Digital Surface Model (DSM) Digital Elevation Model (DEM) Grid cell polygon	-	GIS-based model: parameters based on interactions and correlations with spatial geometries	Phyton	6 morphometric models express correlation between aerodynamic parameters (z_d, z_0) and morphological parameters (λ_p, λ_f, Z_H, Z_{Hmax}, Z_{Hstd}) used to describe roughness elements geometry, determine by the same simulation	Geospatial data: - shapefile (.shp) - raster (geotiff) - text-dbx (.csv)	Morphometric (λ_p, λ_f, Z_H, Z_{Hmax}, Z_{Hstd}), and aerodynamic parameters (z_d, z_0) for each cell of the grid and wind direction interval	Urban scale: block of buildings, neighborhood, district scale (depending on the size of cells grid) simulation time (<1min per grid cell)
CpCalc+	Wind incident angle direction (°, from N, clockwise)	Wind profile exponent (v) Plan Area Density (PAD) Surrounding building height (SbH)	Dimension and geometry Azimuth Roof type and tilt angle Opening element positioning on facades	Parametric model: statistical relationship between parameters based on regression-analyses of wind-tunnel test data on cube-shaped models	Visual Basic (CpCalc+) - Stand-alone Phyton 3.7 (CpCalc2.0)	Structured modules for a specific type of correction factor applied to a reference Cp profile as a function of parameters: -climate: wind incident angle, -urban: v, PAD, SbH, -building: azimuth, frontal aspect ratio (FAR), side aspect ratio (SAR), relative vertical positioning (zh), relative horizontal positioning (xl), roof slope tilt angle (φ)	Manual insertion of the input data; Output data in .txt or .csv format	Cp values for given points on building facade	Building scale: one simulation for each building and wind direction, simulation time (<1min)

3.6.3. Results and limits of the methodology

Figures 32a-b show the spatial distribution of two of the five morphometric parameter calculated in the simulation to retrieve the aerodynamic parameters: the Frontal Area Index [-] (Fig.32a), and the Plan Area Index [-] (Fig.32b), evaluated on the cells grid (5mx5m), considering the prevalent wind direction from Nort-NorthEast (0°-30°N). Due to how the two parameters are defined, the first can take on any value, while the second has values between 0 and 1: the higher the PAD, the higher the density in the zone, also considering the elevation of the building. In fact, the analyzed area of Crocetta reports very high PAD values, especially in correspondence with the taller blocks of buildings and except for the perimeter streets. In addition, the typical urban form of the Turin blocks in this district is the closed courtyard: this greatly influences the quantity of exposed facades.

UMEP results are distinguished in *anisotropic* and *isotropic* outputs: the first give output for each wind direction, the second report mean values for all the selected wind directions. Isotropic results of the displacement height z_d are displayed in Figure 34, while the anisotropic ones are separately provided for each of the two observed prevailing wind directions (N-NE, Fig.33a and W-SW, Fig.33b). The displacement height corresponds to a threshold value for the correction of the reference wind speed U_{ref} [m/s]. According to building heights (z) and floor numbers, for each floor, the wind speed is adjusted by the log-law (if $z > z_d$) or the turbulent motion equation (if $z \leq z_d$).

Buildings are then classified in two groups: those with both logarithmic and turbulent wind profiles occurring at different heights on the same facade (red points, in Fig. 33a-b) and those with only turbulent profiles (blue points, in Fig. 33a-b). Simulations are assessed at grid level, but results are represented in the maps at the building scale. In Figures 33a-b it is evident that urban canyons oriented parallel to the prevailing wind direction consist of buildings for which the log-law is still valid, as no elements obstacle the path of the incident wind. Results of spatial distribution of *zd* at different prevailing wind direction intervals, highlight the capability of the UMEP tool in considering the real urban built context: lower level of *zd* occur in the street whose main axes are parallel to wind direction, letting clear the presence of the wind wake core generated among buildings.

The selected block of buildings (red rectangle, Fig. 33a) is chosen as it is considered well exposed to the N-NE wind; buildings that made up the block are oriented perpendicularly to the prevailing monthly wind direction (N-NE). The block of buildings is examined in detail in Figure 35: 30 points are identified horizontally along the two facades, each point corresponding to a cell grid (with x, from 1 to 30) whose z_d is known. For each cell of the grid (5x5m), a value of z_d is calculated. Therefore, to each building it is assigned a value of z_d in correspondence to defined points on both windward and leeward facades with reference to the individual cells of the grid.

The horizontal distribution of the incident wind along the windward façade is firstly determined by the application of the *Cpcalc+* tool; while in the *z_d method,* values of z_d and z_0 are retrieved from each cell in the grid of the analyzed area: different wind velocities are extrapolated which result spatially distributed in front of facades.

The block of building (Fig. 31) has been previously selected in order to compare the results of the two different methodologies applied on it, related to the surface pressure produced by the incident wind on the windward façades. Wind speed are corrected applying both the power and the log-law, (respectively in the *Cp method* and *z_d method*), at three representative heights: z_1 at first floor, z_2 at half of the building height, and at the top floor z_3.

For the building highlighted in yellow, in Fig.35, the results in Figure 36a-b shown the adjusted wind speed U [m/s] at the three heights z_1 (in grey), z_2 (in orange) and z_3 (in blue) for 30 points on both windward (Fig.36a) and leeward façade (Fig.36b), considering the prevalent wind direction from N-NE and the displacement height z_d (violet dotted lines), specifically calculated for the selected building. Considering the three representative heights, Figure 37 represents the results of the surface pressure P_s and P_v, respectively assessed in application of the *Cp-method* and *z_d-method*.

The place-based tool (zd-method) can easily describe the horizontal and vertical distribution of wind on building facades and its variation taking into consideration the impact of real obstacles where they are sited. The lower peaks correspond to points on building facades in front of which there is not a building but the void of a street canyon, whose direction is parallel to the incident wind. For the height z_3 that are above z_d, the *z_d-method* results more precise than the other method; in fact, in describing the variations that occur on facades, the *z_d-method* has the ability to highlight the wind wakes

generated from surrounding buildings. The main limit of the C*p-method focus on* its already mentioned ranges of applicability, since the analyzed block exceeds the threshold value of the aspect ratio range (FAR>4). In the application of both methods, the surface pressure at the two heights (z_1, z_2) below z_d, result very poor, due to the extremely low wind speed occurring inside the urban canyon (Fig. 37).

(a)

(b)

Fig. 32 a-b - Frontal area index (a) and Plan Area Index (b) from QGIS-UMEP tool for a grid cell (5x5m) in the Crocetta district, considering the prevalent wind direction from N-NE.

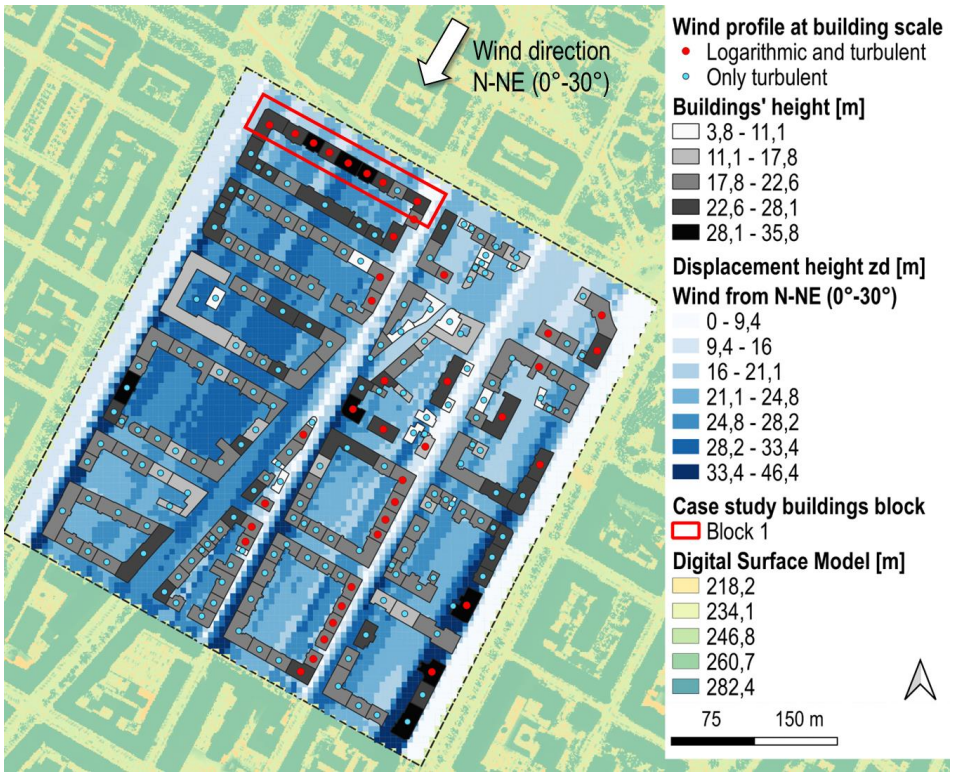

(a)

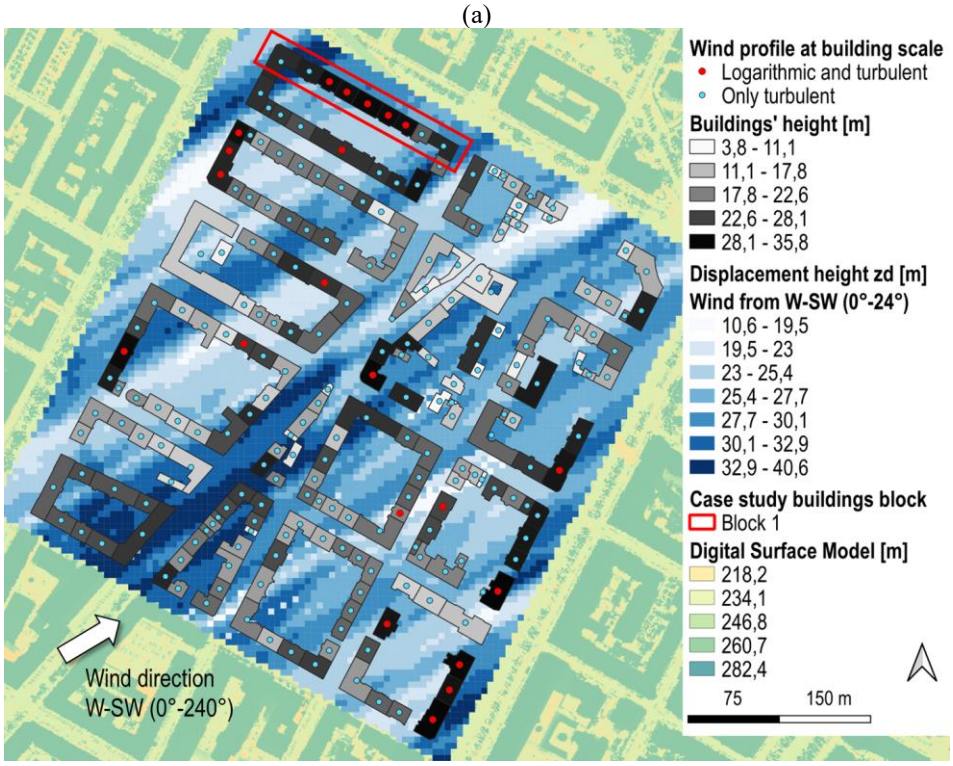

(b)

Fig. 33 a-b - Anisotropic result of the displacement height z_d, in case of the two prevailing wind directions from N-NE (a) and W-SW (b).

Fig. 34 - Isotropic result of the height oft he displacement layer z_d [m] in the case study.

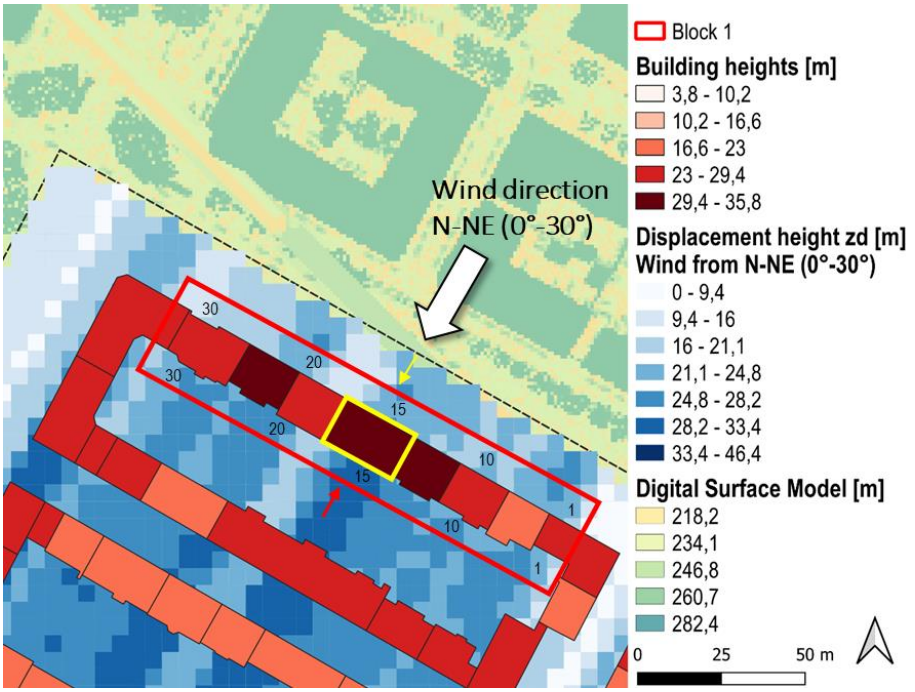

Fig. 35 - Displacement height z_d [m] for the selected building (in yellow) in the analysed buildings 'block (red box), considering the results of the *zd-method* retrieved from each of the 30 cells in the grid in front of facades.

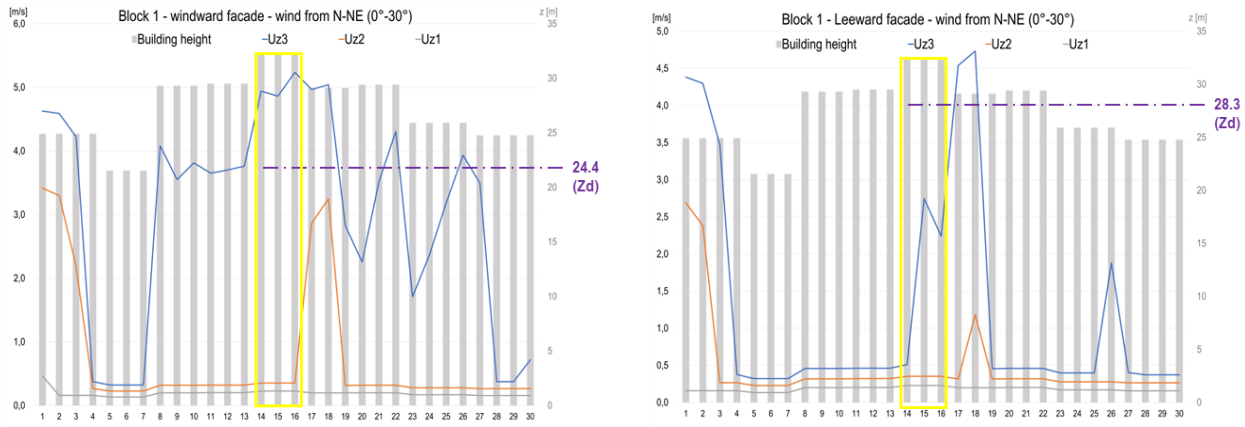

(a) (b)

Fig. 36a-b - Adjusted wind speed U [m/s] at height [m] z1 (in grey), z2 (in orange) and z3 (in blue) for 30 points on both windward (a) and leeward façade (b), considering a prevalent wind direction from N-NE and the displacement height zd (violet dotted lines) for a selected building (in yellow box) among the ones in the block.

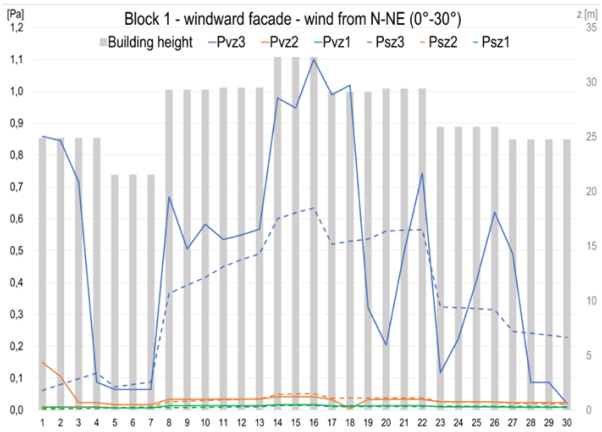

Fig. 37 - Comparison of the surface pressures calculated with the Cp-method (Ps, dotted lines) and the zd-method (Pv, straight lines) at height [m] z1 (in grey), z2 (in orange) and z3 (in blue) for 30 points on both windward considering a prevalent wind direction from N-NE for all buildings in the block.

After the comparison with the *Cp method*, it is possible to affirm that the place-based methodology (zd-method) can describe the horizontal distribution on building facades of the surface pressure due to incident flows from any wind directions. The recent implementation of the *CpCalc+* algorithm in the Python code language [107], which is the same used by the Q-GIS software, can represent an interesting opportunity two merge the two methodologies; these can happen realizing a QGIS plug-in based on *CpCalc+* algorithm to assess Cp coefficient at urban scales, or provide for the possibility to retrieve in the GIS environment all input data necessary for Cp calculations.

Strength and limits of the zd-method and QGIS UMEP plug-in applications.

As first results, the proposed GIS-based methodology (zd-method) concerns the spatialization of results with fast simulation that allow to easily apply it to the whole city, divide into homogeneous zones or districts. This can support urban energy planning in identifying critical zones and area with priority of intervention as it is a flexible methodology, adaptable to any context and scale, directly depending on the available input data. The main limits consist in the parametrization of the wind

speed inside urban canyons, below the displacement height *zd,* where turbulent fluxes occur, and the power and log law cannot be applied. The main advantages and disadvantages of the proposed methodology are listed in Table 24.

Limits are related to two main aspects: the accuracy of the input data (DSM resolution) and the tool setting (cell size of polygon grid and radius length from grid centroid): the first having a strong impact on the accuracy of the output data and the second depending from the scarcity of application of the UMEP tool to urban case study ventilation assessment in defying sensitivity analysis of this aspects. Considering the limits about input data, the DSM resolution depends on the availability of local data for the case study. In Figure 17, isotropic results of the displacement height *zd* are shown, comparing simulations based on DSM at 1m and 5m resolution, respectively in Fig.17a and Fig.17b.
Considering the limits about the tool setting, the cell size of the polygon grid depends on the research question: the bigger the size, the faster the simulation but also the less accurate the spatial description of the horizontal distribution of results, as shown in Figure 18a-b. Secondly, the radius length is a crucial variable because it can strongly impact results of the frontal area index, as shown in the scheme on Figure 19: some heights can be let out and results can be affected by this error.

Table 24. Limits and strength of the UMEP tool and zd-method.

Limits	Strength
• Parametrization of wind speed inside urban canyon • Accuracy of result depending on accuracy of available input data	• Flexible methodology, adaptable to any context and scale • Results spatialization supporting energy urban planning • Accessible input data, fast simulation and low computational costs

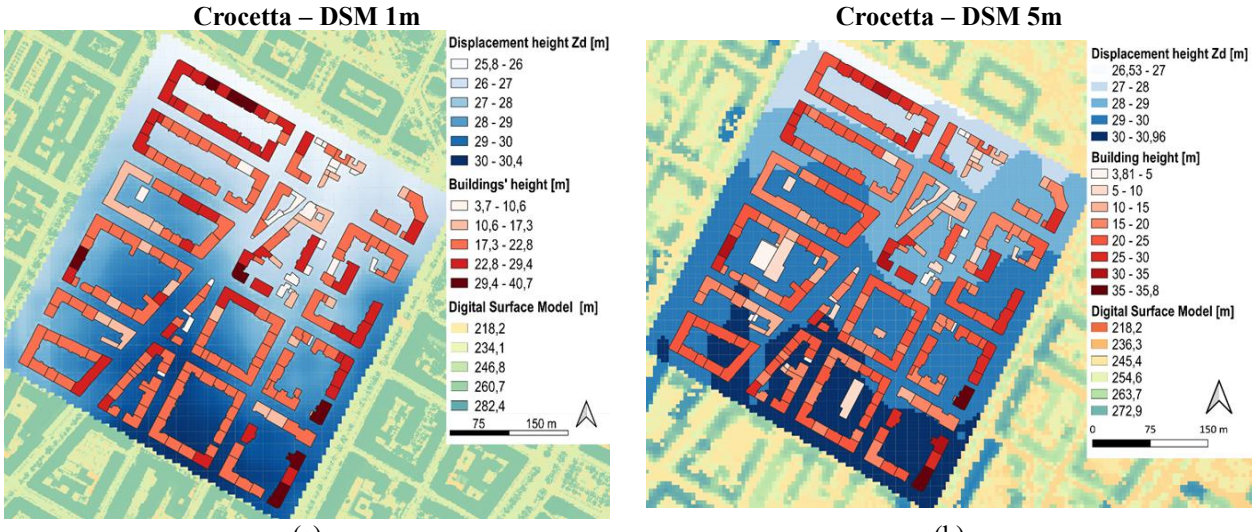

(a) (b)

Fig. 38a-b - Isotropic results of the displacement height z_d in Crocetta district based on DSM at 1-meter (a) and 5-meters (b) resolution.

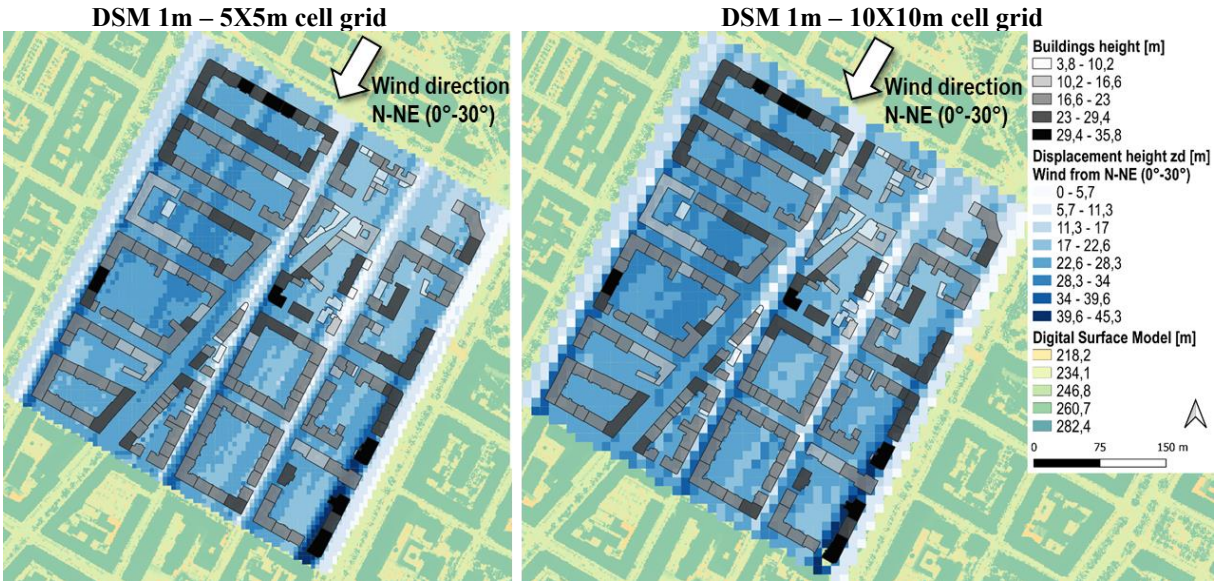

(a) (b)

Fig. 39a-b - Anisotropic results of the displacement height z_d in Crocetta district based on DSM at 1-meter, reported on a 5x5 meters (a) and 10x10m (b) cell grid for the study zone area.

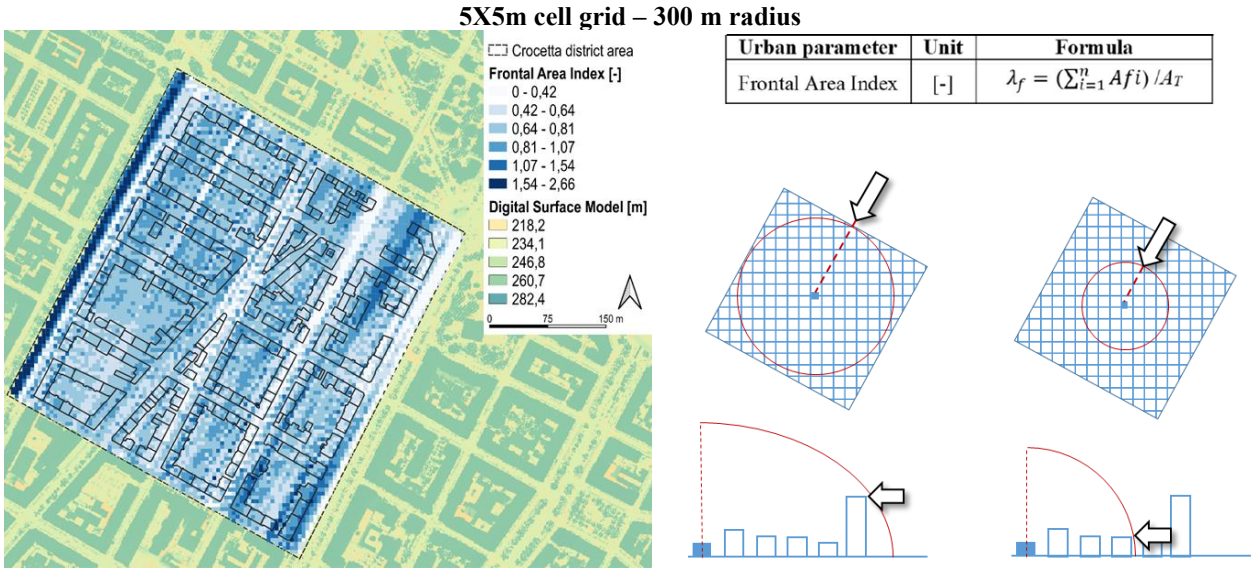

Fig. 40a-b - The radius length definition in the setting of UMEP tool and its possible impact in determining the Frontal Area Index urban morphometric parameter in the case study area.

3.7. Air flow inside urban canyon

In the reference scientific framework, the urban street canyon ventilation is becoming topical as it entails many aspects (i.e., energy demand, pollutants and heat stress exposure). The urban canyon (UC) is defined as the street unit formed by the street and its flanking buildings. The most important feature that characterizes UCs is their geometry form: canyons are described by their two-dimensional cross-section, also named *aspect ratio*. It is referred to the dimensionless ratio H/W where H [m] is the height of the buildings adjacent to the street and W [m] is the width of the street. The UC canyon length is usually considered regular and infinite [108].
This analysis takes part from the results of wind assessments with the place-based GIS methodology (par.3.6). It can assess a profile for each wind direction considering all the real obstacles, their spatial relationship, and their characteristics (size and geometry). Since it allows to determine the height of the displacement layer (*zd)* for each examined building, a wind profile is assigned to it, showing the turbulent flows generated in some urban canyons. To sum up, the displacement layer is used as a threshold value to apply proper wind law.

- Above z_d: the logarithmic law (Eq.14) is applied to correct the undisturbed (reference) wind velocity, and it is directly calculated by GIS tool at the urban scale, (as described in par.3.2.2).
- Below z_d: CFD models are needed to described vortexes and eddies generated by the turbulent motion occurring in canyons with similar characteristics, as presented in the following paragraphs.

3.7.1. Research background: 2D and 3D CFD models

As shown by current studies on urban ventilation, CFD simulations are becoming increasingly recurring, and many simplified models are designed to form urban structures including characteristics at building scale.

Based on the interesting scale and the examined phenomenon (i.e., wind speed, pollutant dispersion, etc.), it is possible to opt in favor of 2D or 3D urban canyon models. This choice can imply input variables which consist of specific morphometric parameters. The most frequent urban parameters used in 2D models are the *aspect ratio* (H/W), the *building height (Hbld)*, and the *height variation (Hσ)*. The *length-to-width* or *length-to-high*, and *plan area density* are fundamental in 3D models [89]. Two-dimensional (2D) urban models were studied to determine how the canyon aspect ratio impacts on urban ventilation and pollutant dispersion [109]. The majority of studies that rely on 3D CFD models use the generic building geometries in order to arrange idealized urban structures [110]. In the reference scientific literature, investigations on real urban areas are very few, since the physical phenomena in question are very complex to describe, and the details required by the model are of a very high level. Some of these studies are used to characterized the phenomena in specific environmental conditions [111], others are used to validate the accuracy of (computational) settings [112], others are used to describe urban parameters and wind speed correlations [113]. The work in [106] proposes data-driven models and the downscaling of certain climate variables for specific urban forms and considering extreme climate conditions, underling the difficulty of 3D CFD models in generalizing its results at urban scale. Among the requirement provided by the Best Practice Guidance (BPG) on CFD analysis for wind comfort and safety [114], it is mentioned the importance of explicitly modeling all the buildings relevant for wind analysis, even if this instruction cannot be easily achieved for neighborhood-scale applications within a city. Nevertheless, this scale is widespread considered the best one to describe physical processes and urban configurations [115].

The assessment of airflows patterns in urban canyons with non-isothermal conditions represents a lack of investigation in this scientific research fields. It implies that the effects generated by the cross wind and the thermal gradient occurring in the urban street canyons should be studied in combinations. Promising results come from [116] in which 2D CFD simulations are used to acquire the velocity vector field in three hypothetical canyons' aspect ratio, also through experimental investigation: the velocity field and its vortical structure are affected by the aspect ratio, and flow direction is influenced by the presence of irradiated building facades.

3.7.2. Research objective and novelty

This part of the work deals with the definition of a methodology to assess wind velocity inside urban canyons. The choice of the 2D CFD scheme is demanded by the aim to reach a sufficient accuracy to properly entail both physical phenomena (crosswind driven and thermal gradient) and to replicate the methodology to similar urban canyons within a city. An urban canyon of infinite length is analyzed as an ideal case study in order to deal with a limited number of parameters, as the bi-dimensional aspect ratio parameter alone describes the canyon geometry. In high-dense urban context with a regular, dense, compact built environment, canyons can be assumed to be infinite, and a 2D CFD scheme of its boundary conditions is represents by the vertical section of the street canyon. An additional dimension would be added applying a 3D CFD modeling, enhancing the description of the reality, increasing the computational effort and increasing the difficulty of replicate the results at city scale.

The novelty of the methodology proposed stands in the effort to describe the complex connection that relate canyon dimensions and its environmental context, considering combined contribution of natural phenomena (cross wind-driven and thermal gradient) to overcome the lack in the scientific research field about CFD simulation with non-isothermal conditions.

The research objective is to have a CFD place-based methodology that describes the domain in a simplified way but based on real and representative data of the case study; therefore, a methodology based only on accessible information from urban planning database that makes it easily adaptable to any context of application at urban scale (cities or homogeneous zones within a city). The methodology provides for a classification of the types of canyons in relation to the types of buildings present and for each category identified as representative, it can determine wind speed patterns in typical climatic conditions. In this way, for each case study, an atlas of wind patterns is created that describe the type of the wind motion and momentum in the different urban canyons and allow the external wind speed to be adhusted at any point of the canyon as a function of the height from the ground.

3.7.3. CFD methodology for natural ventilation in urban street canyon

The methodology proposed here has been presented at the 8th AIGE/IIETA International Conference and 18th AIGE 2023 Conference held in Turin on 2024, the 14th -15th of June.

The objectives of this work were:

- 2D CFD modeling to describe the wind velocity field inside urban canyons of three different aspect ratio, considering the combined effect of cross wind and thermal gradient.
- Scenarios of extreme windy conditions and thermal gradient in the canyon to study separately the contribution of each of the two phenomena in determining the velocity field in the domain.

- Scenarios of climate condition representative of the local meteorological year to describe all the possible combination of the two phenomena.
- Application of the wind velocity inside urban canyon in the 3-zone air flow lumped parameter model to calculate hourly air changes per hour (ach).
- Comparing the resulting hourly ach and tabular data of pressure coefficient (Cp), applying them in the calculation of incident dynamic pressure incident on case-study buildings' façades.

In this chapter only the first three objectives will be presented, since they concern air flow assessment at urban-canyon scale, while the second and third objectives are the objects of the investigation presented in the next chapter concerning the air flow at building scale and the 3-zones lumped parameter model. The results of this analysis are the adjusted wind velocity as a function of height from the ground in any interesting point inside urban canyon. This information can be calculated for any building in any urban canyon in a case study zone.

In order to understand how the steps of the overall methodology are related, the scheme in Fig. 41 synthetized it: the first step, 2D CFD modelling has been run to assess the wind velocity field and to describe the vortical structures in the domain; the output consists in the wind speed (*v)*, determined as a function of the height *(z). This result become the* input data of the second phase of analysis in which the 3-zone air flow model is applied to calculate the ach in different climate scenarios. The results of this model (applying CFD method) are then compared to a well-known method (Cp method) in particular for the calculation of the dynamic pressure (P_{dyn}).

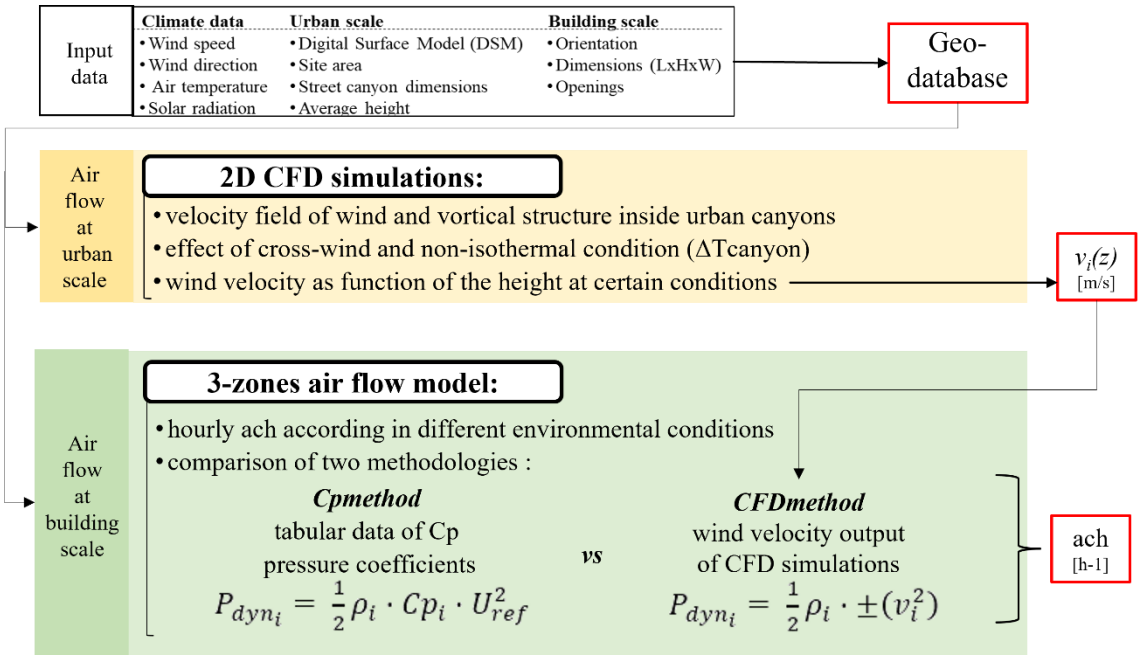

Fig. 41 - Flowchart of the methodology.of the analysis at canyon scale.

3.7.3.1. Materials and methods

In this study the 2D CFD modeling relies on the Star CCM+ software (vers. 2310), a widely used computational fluid dynamics (CFD) tool.

The 2D CFD model is designed to study the heat transfer phenomena within an urban canyon and the cross-incident reference urban wind.

The CFD modeling relies on the RANS (Reynolds-Averaged Navier-Stokes) approach that is the most widely approach used in the reference scientific literature for steady state flow regime numerical simulations. The RANS approach provides for a good compromise between the accuracy and the efficiency of solving building-terrain local climate case studies [106]. The k-ε model is generally applied due to its good performance in predicting flow and turbulence fields around buildings [110]. The choice of turbulence model depends on the specific characteristics of the flow being studied and the desired level of accuracy.

Steady and unsteady state flow regime models comparison.

In this study are applied and compared the results of:

- a k-epsilon (k-ε) model assuming a steady state flow regime
- a k-omega (k-ω) model assuming an unsteady state flow regime to consider temporal fluctuations.

In both cases, the boundary conditions of the domain are the geometry of the urban canyon, the inlet velocity of the cross-sectional wind and the gradient of temperature between the two façades of the buildings.

Regarding the steady state flow regime, it has been the first choice as the computational time for each simulation (about half an hour) is functional for urban-scale applications, just as the accuracy of the result is considered acceptable.

Regarding the unsteady state flow regime, the initialization of the physical phenomenon inside the canyon starts from a condition of absence of air velocity. Therefore, the transient of the simulation that lasts 500 seconds has been chosen considering: i) the characteristic time step, equal to 1 second, calculated as the ratio between the length of the canyon (*W*) [m] and the velocity of the inlet air (*Uref*) [m·s-1], ii) the computational time of a simulation, which for the unsteady model is approximately double that of the steady model, iii) the velocity of the air flow monitored within the canyons do not vary significantly. To let the model reaches convergence, the duration of the final part of the simulation lasts 30 seconds with a time-step of 1/10 of the characteristic time step, as it is useful to describe the equilibrium condition and the speed variations in the vortex.

For both regimes, for all the interesting points in the canyon, the normal V(x) and tangential V(y) velocity's components are evaluated over time and constitute the results of each simulation. In the steady state flow regime, the velocity profile is determined. In the unsteady state flow regime, from the results of the final part of the simulation (30 s), the mean and standard deviation are calculated. To determine whether the results of the unsteady model can be described as a stationary condition, it is decided to observe and consider acceptable the threshold of the mean ± σ (std), equivalent to 66% of all observations over time.

From the comparison between the two flow regimes, it is reasonable to expect that in case of stationary physical phenomena, the two wind velocity profiles will be identical, while in case of non-

stationary physical phenomena, the noise obtained from the steady state model will be better described through the velocity profile oscillations over time of the unsteady model's results.

Boundary conditions of the domain.

Structured and unstructured elements have been combined to map the physical domain of the CFD environment. In presence of regular grid geometry that coincide with the main canyon section, a structured mesh has been used; it provides for an efficient computation and optimal resolution. For specific regions in which high flow gradients can occur , such as corners, a refined mesh has been employed to capture the complexity of local flows.

An iterative analysis and mesh sensitivity studies have assessed the refinement level to ensure the appropriate resolution of the flow phenomena of interest. After the appropriate refinement, the whole domain contains almost 170'000 elements.

As commonly occurs in urban physics studies that analyze urban ventilation with a multidisciplinary and multiscale approach, the in-situ and/or laboratory measurements may be difficult to implement and may not constitute the appropriate investigation method for the research purpose [113].

The numerical analysis were not validated with in-situ measurements as there were no operating conditions for a measurement campaign which would have required high costs for the following reasons: it would be necessary to measure the air temperature and speed point by point and wind direction, easily subject to weather conditions, difficult to plan; furthermore, it would be difficult to have data for the entire area investigated. This study relies on the acquisition of climate data in real conditions coming from a weather station located in the same urban block where the examined case study is located.

The CFD simulations aimed to investigate the velocity field within the canyon, weighting the different contributions provided by the cross wind and thermal buoyancy. This last has been generated by an imposed ΔT between the facades of the two buildings in the canyon. To better explain the input data, settings criteria and output data used to describe the velocity field in the domain, a cross-sectional scheme of the 2D model with variables used in the CFD simulation is schematized in Figure 42.

Geometry of the urban canyon.

The 2D geometry of the street canyon is described by the *aspect ratio* parameter *H/W*. In this work three options are considered for the width of the street *W* [m] (large, medium, narrow canyon), while the average height of the building *H* [m] is fixed.

The two identical buildings that made up the urban canyon are represented as schematic volumes, with not permeable surfaces. For each building, internal partitions creating 3 zones are represented in Figure 42 only to better describe the future application of the CFD results in the 3-zones air flow lumped parameter model at building scale; details inside the buildings are not relevant for the CFD simulations. In the scheme, the heated zones (Fig. 42, in dark gray) represent the apartments, divided in two volumes (above and below the neutral pressure plan occurring in the half of the building height); the shaft (Fig. 42, in light grey) is a unique volume, and it is positioned on the building façade that face the courtyard and not the urban street canyon. To each façade facing the canyon a temperature is assigned: temperature T_1 [°C] is assigned to the building on the left, and temperature T_2 [°C] is assigned to the building on the right in Fig. 42.

Climate scenarios.

The local climate conditions are described by two main variables: the inlet reference wind speed U_{ref} [$m \cdot s^{-1}$], and the thermal gradient ΔT [-] between the temperatures of the two facades.

The reference wind speed of the inlet air in the dominium U_{ref} [m·s^{-1}] is necessarily perpendicular to the canyon axis direction, and its direction is fixed from left to right in the free stream above the canyon height (outside the canyon). The wind direction fixes the *windward façade* (WF) and *leeward façade (*LF), respectively on the right and the left of the canyon scheme in Figure 42.

The thermal gradient ΔT [-] is calculated from the difference of two temperatures: the sol-air temperature (T_{s-a}) that is assigned to the façade exposed to the incident radiation of the sun ($I_{in}c$), and the outdoor air temperature (T_{air}), assigned to the façade not exposed. Inside the canyon, the exposed facade defined as *warm* facade (W) always corresponds to the non-exposed facade defined as *cold* (C) façade.

As schematized in Fig. 42, according to the position of the sun, the sol-air temperature can be assigned to the building on the left side of the canyon (Fig. 42a, $T_2 = T_{s-a}$) and consequently, the outdoor air temperature is assigned to the building on the right side of the canyon ($T_1 = T_{air}$), or vice-versa (Fig. 42a, $T_1 = T_{air}$ and $T_2 = T_{s-a}$).

Scenarios of CFD simulations.

The CFD simulations are based on the four following criteria, each criterion has multiple options: the total number of simulations is given by all the possible permutations between the values that each criterion can take on.

<u>Criteria 1) ASPECT RATIO</u> - three options concerning the canyon width *W*, whose values are determined for each case study, as shown in Table 28 of the following paragraph:

- large canyon (LC),
- medium canyon (MC)
- narrow canyon (NC)

<u>Criteria 2) EFFECT</u> – two or four options among the following list, concerning the combination of the wind-driven and thermal gradient effects in the urban canyon considered, separately or combined. In particular:

- *Windy and no thermal gradient (WIN-nogra):* the contribution of the wind-driven effect is prevalent (strong winds and low or absent ΔT)
- *No windy but thermal gradient (nowin-GRA*): the contribution of the thermal gradient effect is prevalent (poor or absent winds and high ΔT)
- *Windy and thermal gradient (WIN-GRA):* the wind-driven and thermal gradient are concurrent and relevant (strong winds and high ΔT)
- *No windy and no thermal gradient (nowin-nogra):* neither of the two effects is relevant (poor winds and low or absent ΔT)

<u>Criteria 3) SEASON</u> – three or four options among the following list, concerning the seasonal variability of the values that climatic input data can have; it is directly related to the statistical analysis of the reference climate year (following paragraph), to described synthetically the representative conditions of windy-non windy and thermal gradient, occurring during the year:

- Winter season (WIN),
- Mid-season 1 (MID-1)
- Mid-season 2 (MID-2)
- Summer season (SUM)

Criteria42) SCENE – two options concerning the combination of the wind-driven and thermal gradient effects on the same building façade. In particular:

- Winward Warm Façade (WWF) scenario, in which the two effects are concurrent (Fig. 42a), as windward building (warm) façade is exposed to solar radiation; consequently, the other façade is named Leeward Cold Façade (LCF).
- Windward Cold Façade (WCF) scenario, in which two effects occur on opposite facades in the canyon (Fig. 42b), as the windward building (cold) façade is not exposed to solar radiation; consequently, the other façade is named Leeward Warm Façade (LWF).

The number of CFD simulations is defined based on the number of scenarios created for the two-analysis investigated: *analysis-A* and *analysis-B*. The simulation campaign of *analysis-A* foresees 36 simulations, according to criteria listed in Table 25, while for *analysis-B* the 96 simulations are based on criteria of Table 26.

Analysis-A: extreme climatic conditions.

The concurrent or disjoint phenomena (wind-driven and thermal gradient) that can create vortices structures in the velocity field are separately studied to highlight their specific contribution; for this purpose, two extreme local climate conditions have been considered:

- *U max* as the maximum hourly wind speed
- I_{inc} *max* as the maximum hourly incident radiation from which calculating thermal gradient

In this analysis, the simulation campaign foresees 36 simulations (Table 25). For each aspect ratios, the two extreme effects have been evaluated in three seasons: winter and summer representing extreme opposite conditions of outdoor air temperature (T_{air}) and height of the sun (*Hsun*), and a mid-season with intermediate conditions; the two scenes (WCF and WWF) are considered.

Table 25. Criteria for the 36 CFD simulations campaign of Analysis A-extreme climatic condition.

Aspect ratio	Effect	Season	Scene
Large Canyon (LC)	Windy-no gradient (U max)	Winter (WIN)	Windward Cold Façade (WCF)
Medium Canyon (MC)		Mid-season (MID)	
Narrow Canyon (LC)	No windy-GRADIENT (I_{inc} max)	Summer (SUM)	Windward Warm Façade (WWF)

Analysis-B: typical climatic conditions.

Based on analysis at monthly level, a typical climate year is reconduct, considering seasonal values of the climate variables. It is considered a good compromise between the possibility to describe the main climate variability of the case study without creating too many scenarios of CFD simulations on which depend the computational effort and time-consuming of analysis.

In this analysis, the simulation campaign foresees 96 simulations. For each aspect ratios, the four combinations of the two effects have been evaluated in four seasons, considering the two scenes, as describe in Table 26.

Table 26. Criteria for the 96 CFD simulations campaign of Analysis B- typical climatic condition.

Aspect ratio	Effect	Season	Scene
Large Canyon (LC)	Windy–no gradient (WINnogra)	Winter (WIN)	Windward Cold Façade (WCF)
	no windy – Gradient (nowinGRA)	Mid-season 1 (MID 1)	
Medium Canyon (MC)	Windy-Gradient (WINGRA)	Mid-season 2 (MID 2)	Windward Warm Façade (WWF)
Narrow Canyon (LC)	no windy- no gradient (nowinnogra)	Summer (SUM)	

To assess the wind velocity law in every point along the canyon's height, two probes have been located adjacent to each facade, to record the whole velocity field at different heights from the ground. For each of the three canyon dimensions tested, the probes at the 1% and 99% of the canyon length dimension (W) refer respectively to the leeward facades at T1 and the windward one at T2. Both the normal V(x) and tangential V(y) vectors' components of wind speed profile are distinctly provided by the CFD simulations, for each examined point of the two axes (probes). Both will be used to obtain the module and the direction of the flux in any interesting point in the dominium.

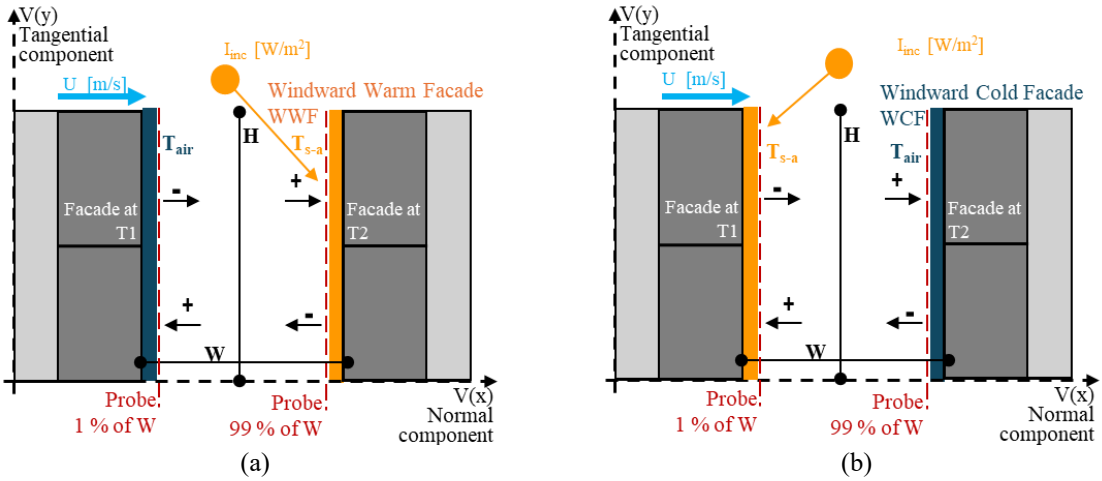

Fig. 42 - Cross section of urban street canyon with its aspect ratio (H/W), considering cross reference wind-driven speed (U) and thermal gradient (ΔT) caused by the different position of the incident solar irradiation (I_{inc}); concurrent (a) and disjointed (b) effects occurring respectively on the windward warm and windward cold facades. Both normal V(x) and tangential V(y) vectors' components of the wind velocity field are evaluated at probes (dashed red lines), generate air flows (arrow) entering (+) or outgoing (-) from facades.

Polynomial function.

The main output obtained from the CFD simulations is the profile of the wind velocity field for each scenario evaluated. These profiles have been interpolated using Matlab software in a fifth-grade polynomial function, described in Eq. (22).

The dependent variable is the wind velocity f(z) which is determined as a function of canyon's height (z) in front of each of the two façades. For each combination of aspect ratio and climate condition, a

specific function is given, considering the 36 or 96 conditions, respectively mentioned in Table 25 and Table 26:

$$f(z) = p_1 z^5 + p_2 z^4 + p_3 z^3 + p_4 z^2 + p_5 z + p_6 \quad (22)$$

where from *p1* to *p6* are the coefficients specific for each of the 36 or 96 investigated conditions.

3.7.3.2. Input data and case study

The main parameters necessary to describe the boundary conditions in the CFD domain are the geometry of the urban canyon, and the local climate conditions. Even in the CFD analysis the useful data comprehends local climate, urban morphology and building characteristics; all information has been harmonized using Q-GIS software and, then a unique geo-database has been created. In detail each type of input data is described below, reporting the example of the case study of the city of Turin.

Urban Canyons (UC) characteristics.

The two main variables that describe the characteristics of the canyon are the canyon width W_{UC} [m] and the canyon orientation θ_{UC} [0°N]. The canyon width is used to determine the canyon aspect ratio H/W [-], considering the average height H [m] of the buildings that made up the canyon.

In this paragraph is described the procedure, schematized in the flow chart in Fig.43, to define the urban canyons geometry at the city scale. The methodology proposed here is based on accessible public databases and the open-source software Q-GIS.

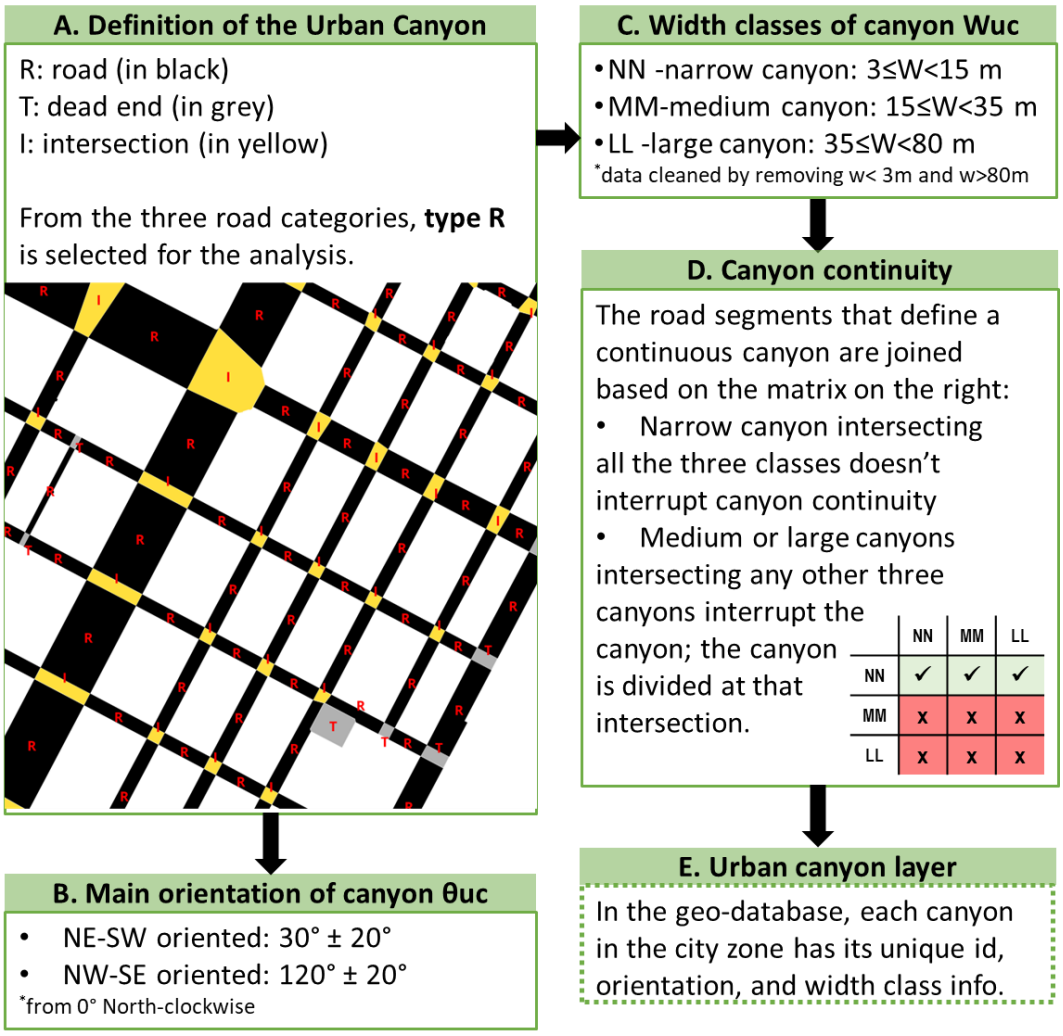

Fig. 43 - Flowchart of GIS-based procedure to define urban canyons and main attributes at city scale.

Step A – Definition of the urban canyons at city scale.

The main input data is the *grafo stradale* (polygon shapefile) provided by the municipality (*Città di Torino Settore Cartografia e sistema Informativo Cartografico, from BDTRE*, updated to 2019, available at http://www.geoportale.piemonte.it/). This layer has been chosen because its geometry describes the space occurring between buildings, including sidewalks, roads, and squares; the minimum element is named 'segment'. Three types of segments are distinguished: *road (R),* considered in the analysis, *dead end roads (D)* and *intersections (I)* (Fig.44). The R segments are used to evaluate the main street orientation and width, as representative of the whole city to define a finite number of classes for Urban Canyon (UC) orientation (θ_{UC}) and width (W_{UC}). According to the characteristics of the urban morphology:

- the definition of the main canyon orientation θ_{UC} consider 0° N clockwise;
- the number of W_{UC} classes (3 classes) is defined considering the classes already defined by the Sustainable Mobility Urban Plan (PUMS 2021) and using the Minimum Bounding Box (MOBB) and the equal interval classification method in GIS; in the pre-processing phase segments with width less than 3 meters or greater than 80 meters, outliers and wrong data have been removed.

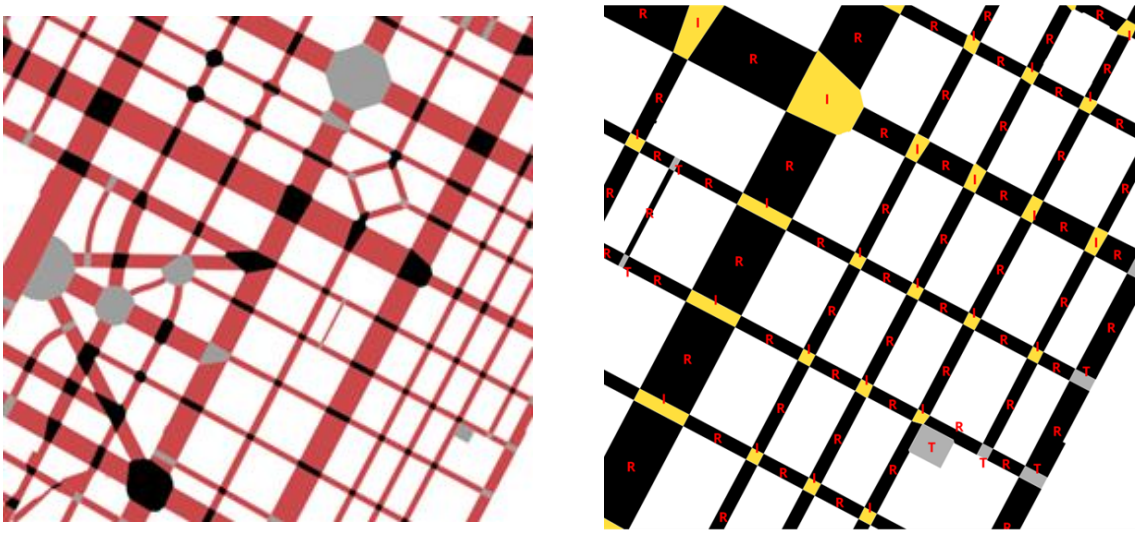

(a) (b)

Fig. 44 - The road (R), dead end roads (D) and intersections (I) segments provided by the *Torino Settore Cartografia e sistema Informativo Cartografico* (a) and elaborated in GIS environment (b).

Step B – Definition of the main orientation of the urban canyons.

The prevalent urban canyon orientations (θ_{UC}) for the whole of Turin are two: the Northeast Southwest orientation (NE-WS: +30°N) and the Northwest-Southeast (NW-SE: +120°N). These two classes are assigned to all urban canyons with actual orientation in the ranges +30° ±20° and +120° ±20°, as summarize in Table 27.

Table 27. The two classes of UC orientation for Turin.

θ_{UC} classes	θ_{UC} range
NE-SW	+30°N±20
NW-SE	+120°N ±20°

Step C – Definition of the classes of width of the urban canyons.

The three representative classes of canyon width (W_{UC}) for the whole city of Turin are described in Table 28. Where W [m] is the width of the canyon that will be used in the CFD simulation, and it is identified as the median value of all the canyon inside each W class. H [m] is the average building height in the zones that respect the prevailing urban canyon orientation in Turin.

Table 28. The three classes of UC width and relative aspect ratio for Turin.

W_{UC} classes		W_{UC} range [m]	W [m]	H [m]	Aspect ratio H/W [-]
Narrow canyon	NC	$3 \leq W < 15$	12	20	1.7
Medium canyon	MC	$15 \leq W < 35$	17	20	1.2
Large canyon	LC	$35 \leq W < 80$	46	20	0.4

Step D – Definition of the canyon continuity.

The continuity of the canyon is evaluated to ensure the validity of the Urban canyon definition about its infinitive length. Due to that the intersection between canyons whose widths are different are evaluated according to the following conditions and the matrix in Figure 43 (step D):

- narrow canyons intersecting all the three classes doesn't interrupt canyon continuity
- medium and large canyons intersecting any other three classes interrupt the canyon continuity and the canyon is divided at that intersection

Step E – Creation of the urban canyon layer.

The procedure ends creating a geo-referenced layer of the urban canyon within the case study area, as described in Figure 45. The attribute table associated contains for each canyon (id) its spatial information, geometry and orientation, according to the real values, orientation and width classes are assigned. This spatialized information will be used in the GIS-based procedure to match canyon layer and building layer in the application of the CFD results to the 3-zone parametric model; urban canyon characteristics (W_{uc}, Θ_{uc}) will be assigned in the attribute table of each building that made up the canyon, applying the procedure described in chapter 4, paragraph 4.5.7.2.1.

Fig. 45 - Example of the urban canyon layer in the geo-database with narrow (in yellow), medium (in orange) and large (in red) canyon width in a case-study zone in the city of Turin.

Climate input data and scenarios.

The input data to describe the local climate are the direction of the reference wind DirV at 0° North-clockwise, and its wind speed U_{ref} [m·s^{-1}] from the reference weather station, the outdoor air temperature $T_{C,air}$ [°C], and the solar irradiation, considering its direct normal I_b [W·m^{-2}] and diffuse I_d [W·m^{-2}] components.

Weather data are retrieved from the weather station of the Living Lab of Polytechnic of Turin (https://smartgreenbuilding.polito.it). Data are quarterly detailed and refer to the years 2010-2023. From the original database, null and missing data have been verified, clean and correct. For discrete variables, the hourly average values are determined starting from the quarterly detail information.

According to Eq. (23), the incident solar radiation I_{inc} [W·m^{-2}] is then calculated to consider only the solar components incident on building facades during daily hours (β>0):

$$I_{inc} = (I_b \cdot \cos\beta) + (SVF \cdot I_d) \quad (23)$$

where: I_b [W·m^{-2}] is the direct normal component, β [°] is the hourly evaluated incident angle of the sun, I_d [W·m^{-2}] is the diffuse solar irradiation and the Sky View Factor (SFV) is the portion of the sky visible from a given position on building's facade.

The Sky View Factor (SFV) can be retrieved applying dedicated tools of Q-GIS, requiring DSM and hourly local meteorological information as input data. The hourly information concerning the height of the sun (Hsun) to calculate β [°] , according to the elevation of the building and the geographical coordinates of the analysed case study, can be obtained from the PVGIS online plugin, provided by the European Joint Research Centre (JRC) https://re.jrc.ec.europa.eu/pvg_tools/en/.

The non-isothermal condition that occurs in the canyon is simulated as a variation (ΔT) of the outdoor air temperature inside the canyon. In particular, the temperature difference between the air layers adjacent to the exposed (warm) and not exposed (cold) façades to the incident radiation I_{inc} , as Eq. (24): to the cold façade is attribute the outdoor air temperature (in Kelvin) $T_{K,air}$ [K], to the warm one is assigned the sol-air temperature $T_{K,s\text{-}a}$ [K].

$$\Delta T_{canyon} = |T_{K,s-a} - T_{K,air}| \quad (24)$$

The sol-air temperature $T_{K,s\text{-}a}$ [K] is a fictitious parameter used to take into consideration both the convective and conductive heat exchanges that occur on the external surface of a building façade, as a result of the mixed contribution of external air temperature, the incident solar irradiation and the radiative exchange between façades, the sky and other surrounding surfaces [117]. Therefore, the sol-air temperature depends on the incident solar radiation I_{inc} [W·m^{-2}] and some properties of the building façade that are the convective exchange capacity h_e [W·m^{-2}·K^{-1}] and the absorption factor α [-]. Referring also to the UNI EN ISO 6946:2008 and UNI 10349-1:2016, it can be calculated according to Eq. (25.1):

$$T_{K,s-a} = T_{K,air} + \left(\alpha \cdot \frac{I_{inc}}{h_e}\right) - \left(\frac{\varepsilon \cdot \sigma \cdot \left(T_{K,sky}^4 - T_{K,air}^4\right)}{h_e}\right) \quad (25.1)$$

where: $T_{K,air}$ [K] is the air temperature, α [-] is the absorption factor for walls with medium colour (i.e., 0.6), I_{inc} [W·m^{-2}] is the incident solar radiation incident, h_e [W·m^{-2}·K^{-1}] the coefficient of external adduction for horizontal heat flow, ε [W·m^{-2}] is the emissivity of the surfaces (i.e., 0.9), σ is the Stefan-Boltzmann constant equal to 5.67·10^{-8} [W·m^{-2} ·K^{-4}], and $T_{K,sky}$ [K] is the apparent sky temperature. It is calculated according to Idso and Jackson equation, as reported in Eq. (25.2), specific for clear sky conditions:

$$T_{K,sky} = T_{K,air} \cdot (0.7 + 5.95 \cdot 10^{-5} \cdot e)^{0.25} \quad (25.2)$$

where: $T_{K,air}$ [K] is the air temperature, e [hPa] is the water vapor pressure.

Regarding the coefficient h_e, it can vary according to range of wind velocities; in this work, the two following ranges have been considered and applied: 25 [W·m^{-2}·K^{-1}] for high wind speed 4-5 [m·s^{-1}] and 12.5 [W·m^{-2}·K^{-1}] for poor wind speed lower than 1 [m·s^{-1}].

Table 29 shows an example of the calculation of the sol-air temperature, starting from a series of monthly air temperatures, water vapor pressure and incident solar radiation of a given location. With reference to Eq. (25), the temperature $T_{s\text{-}a}$ is calculated considering the three components $T_{s\text{-}a,3}$ and

only the first two components $T_{s\text{-}a,2}$ of the equation; then is calculated a relative error [%]. Since in all months, the discrepancy between the two results is less than 10%, it is possible to use the simplified two-component equation, in case when detailed information on sky conditions is not available.

Table 29. Calculation of the sol-air temperature according to Eq. (25)

			Months										
			1	**2**	**3**	**4**	**5**	**6**	**7**	**8**	**9**	**10**	**11**	**12**
	T_{air}	[°C]	1.3	3.2	8.4	12.0	18.1	22.2	23.7	22.7	19.2	12.4	6.9	2.7
	e	[Pa]	558	618	888	934	1355	1616	1584	2003	1659	1180	925	654
	I_{inc}	[Wh·m^{-2}]	1278	2139	3250	4444	5472	6333	6667	5611	4056	2500	1333	1083
3 components	$T_{s\text{-}a,3}$	[°C]	6.73	10.29	17.04	22.54	29.60	34.92	37.51	34.69	29.14	19.76	11.88	7.56
2 components	$T_{s\text{-}a,2}$	[°C]	5.38	8.72	15.27	20.03	26.90	31.82	33.94	32.09	26.84	18.00	10.71	6.33
	Error (relative)		-9%	-4%	-1%	1%	1%	1%	1%	1%	1%	0%	-3%	-8%

In the analysis A, extreme climate scenarios of windy condition and gradient of temperature will be assessed, considering hourly values of a specific year. For each season, the greatest hourly value of wind velocity U_{max} [m·s^{-1}] is selected to be representative of the extreme windy conditions in the canyon, while the extreme thermal gradient condition is based on the selection of the greatest hourly value of incident solar irradiation $I_{inc\ max}$ [W·m^{-2}].

In the analysis B- typical climate condition, the aim is to have a reference local climate year, based on statistical analysis of each climate parameters considering all years in the whole database 2010-2023; range values have been hypothesized to define threshold values to create the category of *windy-nonwindy* and *thermal gradient-no thermal gradient* conditions for each of the four seasons. Firstly, monthly and seasonal hourly average has been calculated for the following variables: height of the sun H_{sun} [°], air temperature T_{air} [°C], wind velocity U_{ref} [m·s^{-1}], and thermal gradient ΔT [°C].

For each month, the hourly average of the height of the sun H_{sun} [°] has been calculated (Fig.46a) to find the hours of dawn and dusk, and consequently, the number of daylights per day. Midday is the hour used to divide the create two groups: hours of dawn-midday (AM), and hours of midday-dusk (PM). The hours f the year that fall into these two groups can be evaluated, since scenarios of thermal gradient are based on the presence of solar irradiation incident (I_{inc}) on buildings facades.

For each month and considering only the (irradiated) hour, the hourly average outdoor air temperature T_{air} [°C] has been calculated (Fig.46c). Four ranges of temperature have been defined to be representative of the temperature variation during the whole year and these constitute the four seasons Table 30. For each of the four seasons, the hourly weighted average temperature has been calculated, considering all the temperature in the irradiate hours of the whole database (years 2010-2023).

Starting from the analysis of the hourly monthly average (Fig. 46b and Fig. 46d), for each of the four seasons, according to air temperature, and considering only the irradiated hours, the hourly average wind speed U_{ref} [m·s^{-1}] and the hourly average thermal gradient ΔT [°C] have been evaluated. To define the threshold values for the *windy-nowindy* and *gradient-nogradient* conditions the following hypothesis have been done.

For each season, among all observations of the hourly wind speed, the wind speed value of the 3rd quantile has been chosen as the threshold value: hourly wind speed greater than it are in the *windy* condition, hourly wind speed lower than it will be in the *no-windy* condition. The threshold values in Table 31 have been compared to the values in the Beaufort scale, in each of the four cases the limit value would fall between class 2-light breeze and class 3-gentle breeze.

For each season, among all observations of the hourly ΔT, the median value of the has been chosen as the threshold value: hourly temperature variations ΔT greater than it is in the *gradient* condition, hourly temperature variations ΔT lower than it will be in the *no-gradient* condition.

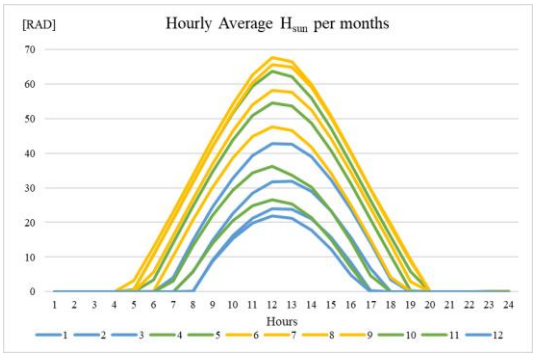

(a)

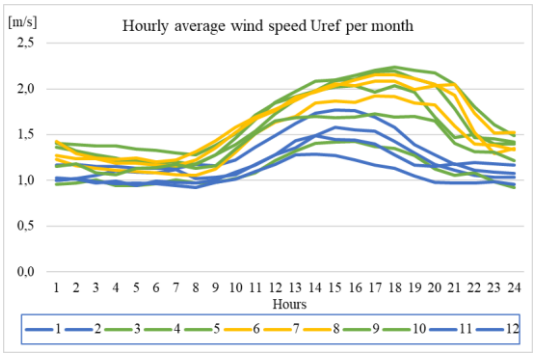

(b)

Tair avg [°C]	Months											
Hours	1	2	3	4	5	6	7	8	9	10	11	12
1	4	6	10	14	17	23	25	23	19	15	9	5
2	4	5	9	13	16	22	24	23	19	15	9	5
3	4	5	9	13	16	21	24	22	18	14	9	5
4	4	5	8	12	16	21	23	22	18	14	8	5
5	3	5	8	12	15	20	23	21	18	14	8	4
6	3	4	8	12	15	20	22	21	17	14	8	4
7	3	4	7	11	15	20	22	21	17	13	8	4
8	3	4	7	11	AM before h=12				17	13	8	4
9	3	4	8	12	16	21	23	21	17	13	8	4
10	4	5	9	13	17	22	24	23	18	14	9	5
11	5	6	11	14	18	23	26	24	19	15	10	6
12	6	8	12	15	19	25	27	25	20	16	11	7
13	7	9	13	16	20	26	28	26	21	17	12	8
14	8	10	14	17	21	26	29	27	23	18	12	9
15	9	10	14	18	PM after h=12				23	19	13	9
16	9	10	15	18	22	27	30	28	24	19	13	9
17	9	11	15	18	22	28	30	28	24	19	13	9
18	8	10	15	18	22	28	30	28	24	19	12	8
19	7	9	14	18	21	27	30	28	24	18	11	7
20	6	8	12	17	20	26	29	26	22	17	10	7
21	6	8	12	17	20	26	29	26	22	17	10	7
22	6	7	12	16	19	25	28	26	21	16	10	6
23	5	7	11	15	18	24	27	25	20	16	10	6
24	5	6	10	15	18	24	26	24	20	15	9	6

(c)

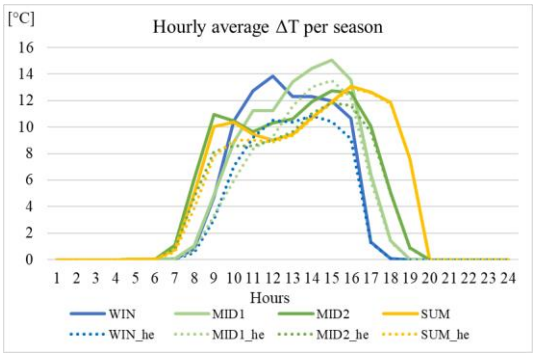

(d)

Fig. 46 - Monthly and seasonal hourly average values for interesting climate variables: height of sun (a), wind speed (b), air temperature (c) and temperature variation DT (d), considering winter (in blue), summer (in yellow), mid-season 1 (in light green) and mid-season 2 (in dark green).

Table 30. Four ranges of outdoor air temperature T_{air} to identify the four seasons.

Season	T_{air} [°C]	Hourly avg. [°C]	Hourly weighted avg. [°C]	Range [°C]
WINTER	$-4 \leq T_{air} < 11$	7.5	7.3	7 ± 2
MID-SEASON 1	$11 \leq T_{air} < 17$	13.9	13.9	14 ± 2
MID-SEASON 2	$17 \leq T_{air} < 24$	20.4	20.4	20 ± 2
SUMMER	$T_{air} \geq 24$	27.2	27.4	28 ± 2

Table 31. Threshold values of wind speed U_{ref} for the two wind conditions in each season.

Season	No windy	U_{ref} [m·s^{-1}]	Windy
WINTER	U_{ref} <	1.5	< U_{ref}
MID-SEASON 1		1.9	
MID-SEASON 2		1.8	
SUMMER		2.2	

Table 32. Threshold values of temperature variation ΔT for the two conditions in each season.

Season	No gradient	ΔT [-]	Gradient
WINTER	**ΔT** <	4.1	< **ΔT**
MID-SEASON 1		6.3	
MID-SEASON 2		7.7	
SUMMER		10.3	

CFD database for the 3-zone air flow model.

The final aim of the CFD analysis is to have for each analyzed building a database containing all the polynomial coefficient that will be used to determine the wind velocity at interesting height for the 3-zone air flow lumped parameter model. Due to that it is necessary to evaluate which are the possible scenarios that a building can assume, considering all the criteria presented here.

Considering the *scenes* of WWF and WCF, the façade of a building in the canyon can assume four possible conditions: the *WW*-Windward Warm façade, the *WC*-Windward Cold façade, the *LW*-Leeward Warm façade, and LC-Leeward Cold façade.

Since the inlet cross wind (WD) perpendicular to the canyon axis orientation, in the CFD model insists always on the windward façade, the façade of the opposite building is considered leeward. The scene is assigned to the façade of the building that faces the canyon street, as an assumption for all the buildings, the shift is placed on the opposite façade which faces the courtyard. The scene is assigned according to the scheme in Figure 47, considering:

- orientation of the canyon axis θ_{uc} equal to +30°N or +120°N;
- two wind direction WD perpendicular to the canyon: +120° or +300°N for θ_{uc} equal to 30°N, +30° or +210°N for θ_{uc} equal to 120°N;
- position of the building in the canyon: *Left* or *Right,* for θ_{uc} equal to 30°N, *Top* or *Down* for θ_{uc} equal to 120°N;
- hourly *shift* per day AM or PM, according to the position of the sun.

Since each criteria *effect*, *season* and *scene* can present four different possibilities, the total number of possible scenarios is 64. Each can occur in each of the three canyon dimension classes (Wuc). Each of the resulting 192 scenarios (64x3), listed in the scheme in Figure 49, refers to a specific polynomial function obtained from CFD simulations and describes the air motion and the magnitude of the cross wind in the canyon, according to the flow chart in Figure 48.

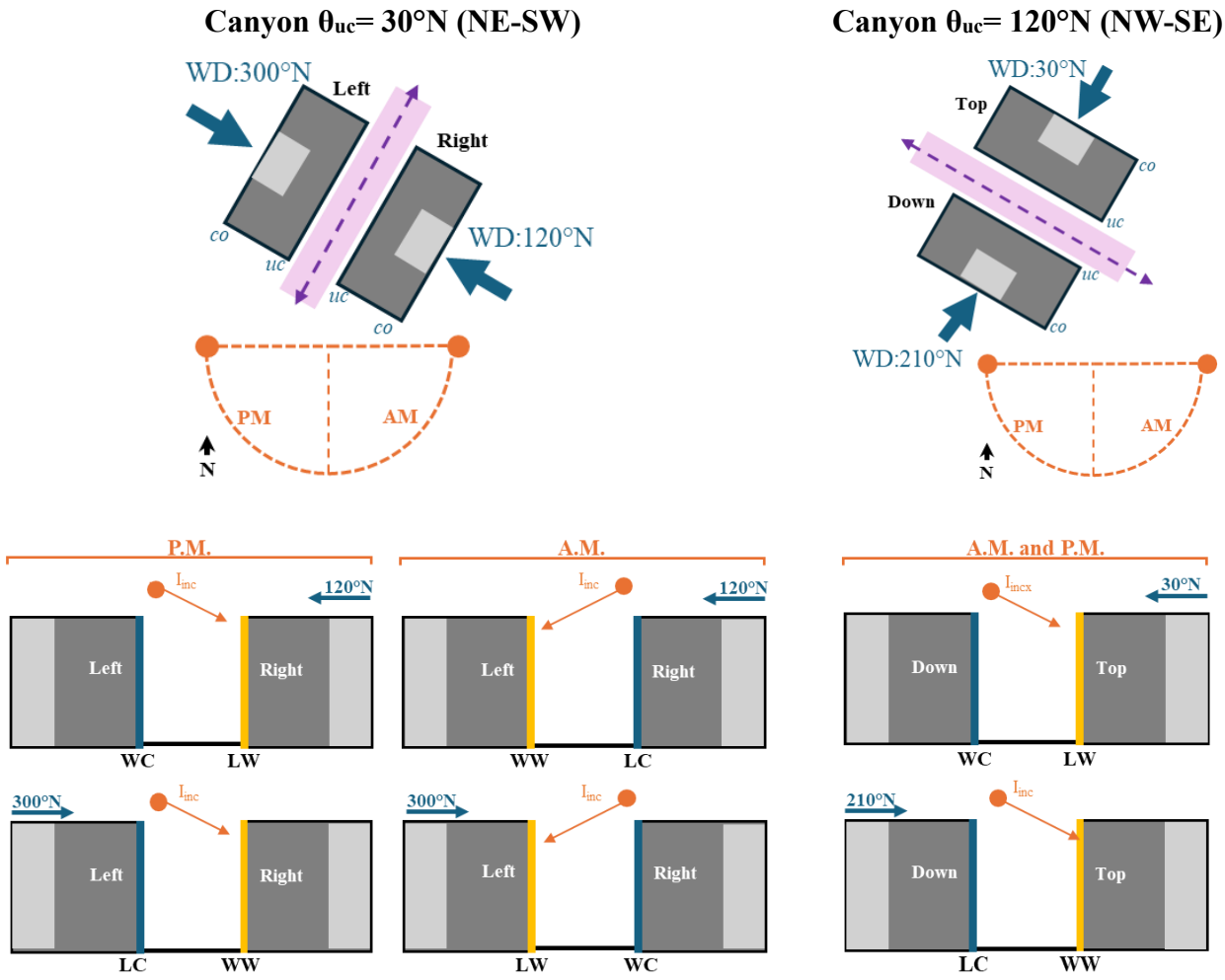

WD	Shift	Position	
		Left	Right
120°N	*A.M.*	WW	LC
	P.M.	WC	LW
300°N	*A.M.*	LW	WC
	P.M.	LC	WW

WD	Shift	Position	
		Top	Down
30°N	*A.M.*	LW	WC
	P.M.		
210°N	*A.M.*	WW	LC
	P.M.		

Fig. 47 - Four scenes that a building can assume according to its position inside the canyon, depending on the canyon orientation (θuc) and cross-sectional wind direction (WD), and from the hourly shift of the day (AM or PM) depending on the position of the sun and the incident radiation of the sun (Iinc).

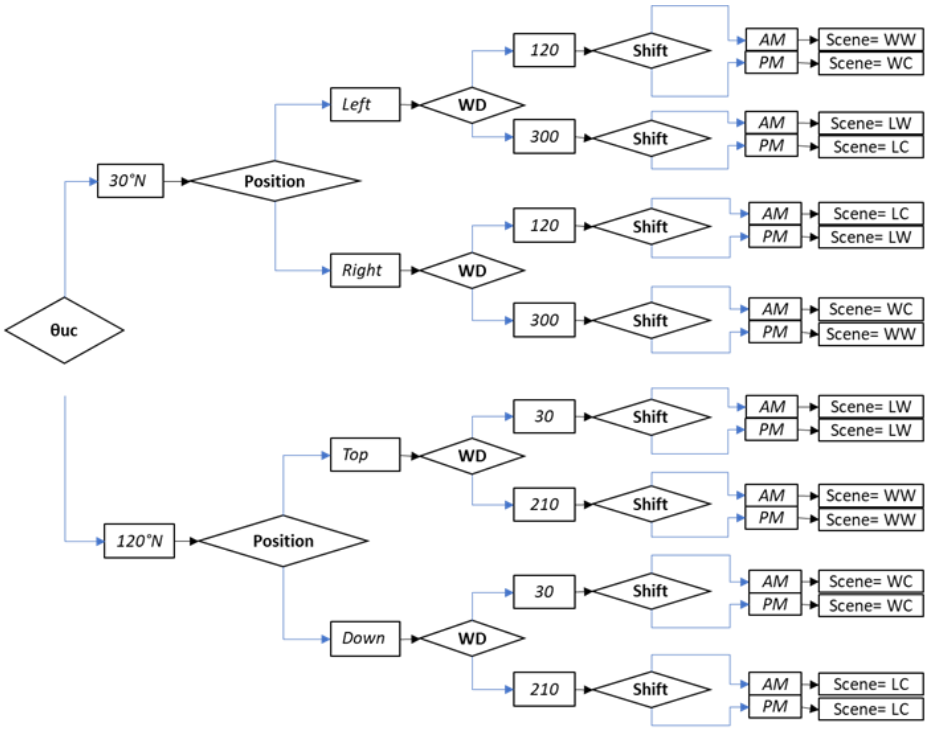

Fig. 48 - Flow chart to assign the proper *scene* to the facade of the analyzed building facing the urban canyon, according to the *canyon axis orientation θuc*, and the relative *position* of the building, the direction of the cross-wind *WD* and one of the two daily *shifts* (A.M. or P.M.).

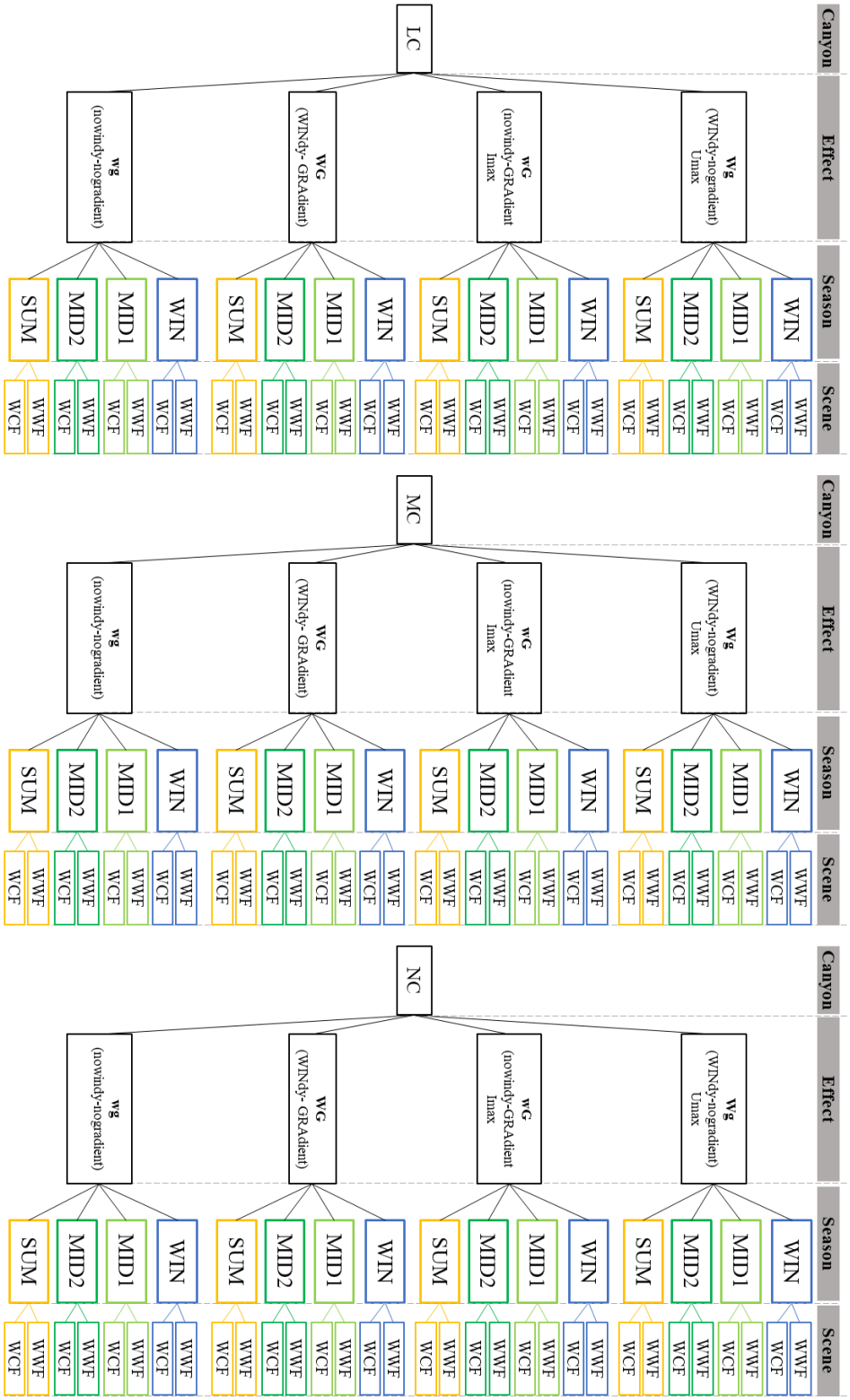

Fig. 49 - All the 96 CFD simulation condition for the analysis B- typical climatic year.

Case study application.

The case study is the same Crocetta district in the city centre of Turin (Italy). It has a regular, dense, and compact urban path; the average height of the building is 20m, the typical H/W dimension is 0.5 that considers internal courtyard of the block of buildings. The district has regular street canyons with different dimensions, and two prevailing orientations: +30°N (NE-SW) and +120°N (NW-SE) that correspond to the prevalent orientation of buildings in line with the values in Table 17. In addition, the weather station used to collect local climate data is in the same district. In Figure 50a-b are shown the three classes of urban canyon in six streets of Crocetta district that have been chosen as boundary condition for CFD analysis; three aspect ratios (H/W) are defined, according to the average street canyon width dimension (Table 18): Medium Canyons (MC) and Large Canyons (LC) are representative of the perimetral street axis of blocks, while Narrow Canyons (NC) insist on internal streets, typical of regular building blocks.

Fig. 50a-b - Localization of the urban canyons in Crocetta district for selected aspect ratios: narrow (blue), medium (green) and large (orange) (a), and the large urban canyon (LC) examined building with NE-SW axis, considering crosswind (DirV) and solar exposures (yellow dot) on the facades of building B1 and B2.

The extreme climate data conditions applied in the CFD for the *analysis A-extreme climate condition* are listed in Table 33. The prevailing local wind (DirV in Fig.50b) is from the West-Northwest direction (300°N, clockwise). For each of the three seasons (winter-WIN, mid-season-MID and summer-SUM), the highest hourly values of both wind speed (U_{max}) and incident solar irradiation ($I_{inc\ max}$) have been selected, considering the reference climate year of 2022. To the cases of Umax correspond the highest values of wind speed and poor thermal gradient, as the crosswind effect is prevalent, while in the cases of Iinc max, ΔT values are high and wind speed values are low, due to the presence of the incident solar irradiation on facades.

Two different typical meteorological seasons have been created following the approach of the *typical meteorological days*, as described in [118] in order to better characterize the local climatic seasons of the case study area. A k-means algorithm has been used to group into three clusters the meteorological data gathered for the Crocetta neighbourhood. Table 34 presents the result obtained in winter and summer seasons, as for both the minimum and maximum centroids values of clusters have been retrieved.

The extreme climate data conditions used in the CFD simulations of the *analysis B-typical climate year* are listed in Table35.

Table 33. Extreme climate conditions of hourly wind (Umax) and solar irradiation (Iinc max) in winter (WIN), summer (SUM) and mid-seasons (MID) in the reference year 2022, applied in the CFD analysis A.

Extreme condition	Period	Date (Year 2022)	U_{ref} [m· s^{-1}]	T_{air} [°C]	T_{s-a} [°C]	I_{inc} [W·m^{-2}]	ΔT [°C]
U max	WIN	02-07 08:00	6.8	9.8	15.0	215.8	5.2
	MID	04-08 17:00	10.7	22.6	32.2	401.9	9.6
	SUM	06-28 14:00	8.6	20.5	22.1	67.6	1.6
I_{inc} max	WIN	01-11 14:00	2.1	8.5	31.5	957.7	23.0
	MID	04-10 16:00	1.4	16.6	36.9	844.4	20.3
	SUM	06-10 17:00	1.6	31.0	51.1	839.5	20.1

Table 34. Typical climate winter and summer days (hourly data).

Period	U_{ref} [m· s^{-1}]	T_{air} [°C]	T_{s-a} [°C]	I_{inc} [W·m^{-2}]	ΔT [°C]
Winter	0.5	5.6	8.0	96.6	2.4
Summer	0.9	29.2	44.8	648.3	15.6

Table 35. Typical climate conditions according applied in the CFD analysis B.

Effect	Season	U_{ref} [m· s^{-1}]	T_{air} [°C]	T_{s-a} [°C]	I_{inc} [W·m^{-2}]	ΔT [°C]
Windy - no gradient	WIN	5.00	7	8.53	63.8	1.53
	MID-1	7.10	14	15.88	78.3	1.88
	MID-2	6.36	20	22.92	121.7	2.92
	SUM	6.17	28	33.98	249.2	5.98
No windy - gradient	WIN	1.48	7	24.19	716.3	17.19
	MID-1	1.88	14	31.14	714.2	17.14
	MID-2	1.78	20	34.80	616.7	14.80
	SUM	2.18	28	42.36	598.3	14.36
Windy - gradient	WIN	5.00	7	24.19	716.3	17.19
	MID-1	7.10	14	31.14	714.2	17.14
	MID-2	6.36	20	34.80	616.7	14.80
	SUM	6.17	28	42.36	598.3	14.36
no windy - no gradient	WIN	1.48	7	8.53	63.8	1.53
	MID-1	1.88	14	15.88	78.3	1.88
	MID-2	1.78	20	22.92	121.7	2.92
	SUM	2.18	28	33.98	249.2	5.98

3.7.3.3. Results and applications

In this section, results of the 2D CFD simulations are described: i) the comparison between selected profiles of wind velocity for both the windward and leeward façade in several climate scenarios, considering the steady flow regime and the unsteady flow regime for some selected boundary conditions, ii) the classification of vortices occurring in canyons, according to representative combination of aspect ratio and climate scenarios, and iii) the description of the wind velocity function.

The results shown in the following figures (Figg.51-52-53-54-55), testify the impact of canyon dimension and climate boundary conditions on wind velocity profiles.

in Figg. 51-53-55, is reported the wind driven effect contribution (Umax), while in Figg. 52-54-55b is reported the impact of thermal gradient effect (Imax), separately for narrow (NC), medium (MC), and large (LC) canyons, in the extreme condition during summer and winter seasons, and considering the Windward Cold Facade (WCF) and Windward Warm Façade (WWF) scenes.

Regarding results of the wind driven effect (Umax) in Fig.51a-f, the contribution of the crosswind in determining a central vortex is prevalent than the almost irrelevant presence of thermal gradient in both irradiated and not irradiated building facades. Therefore, since there are no significant differences between the WWF and WCF scenes, for all canyon dimensions, are presented only the results of one scene (WWF).

Figures 51 and 52 show the comparison between the wind velocity profiles of the steady flow regime (blue line) and the mean wind velocity profiles (orange line) generated from the unsteady flow regime; the latter is rated as comparable to steady-state, if it falls within a standard deviation (1σ) that comprises 66% of all simulations in the transient (grey area , Fig.51 and 52), both for the probes at leeward (1%) and windward (99%) façades.

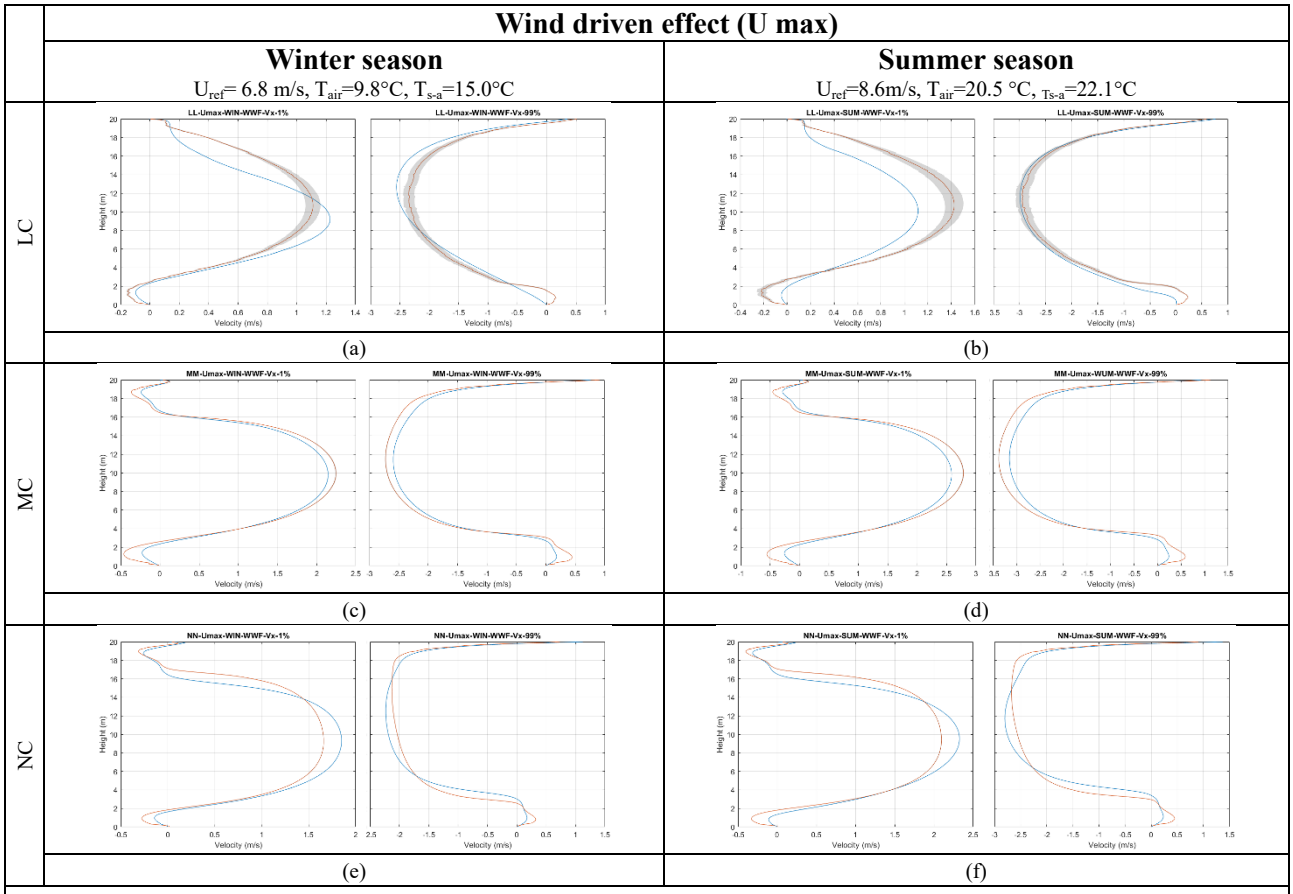

Fig. 51a-f - Wind driven (Umax) effect generating wind velocity profiles in large (LC), medium (MC), and narrow (NC) canyons, and comparison between the fitted curves of the steady-state flow regime (blue line) and the mean wind velocity profiles (orange line) from the unsteady-state regime within a standard deviation (1σ) in the transient simulations (grey area), in front of leeward (1%) and windward (99%) façades, in WWF scenarios, during winter (a-c-d) and summer (b-d-f) seasons.

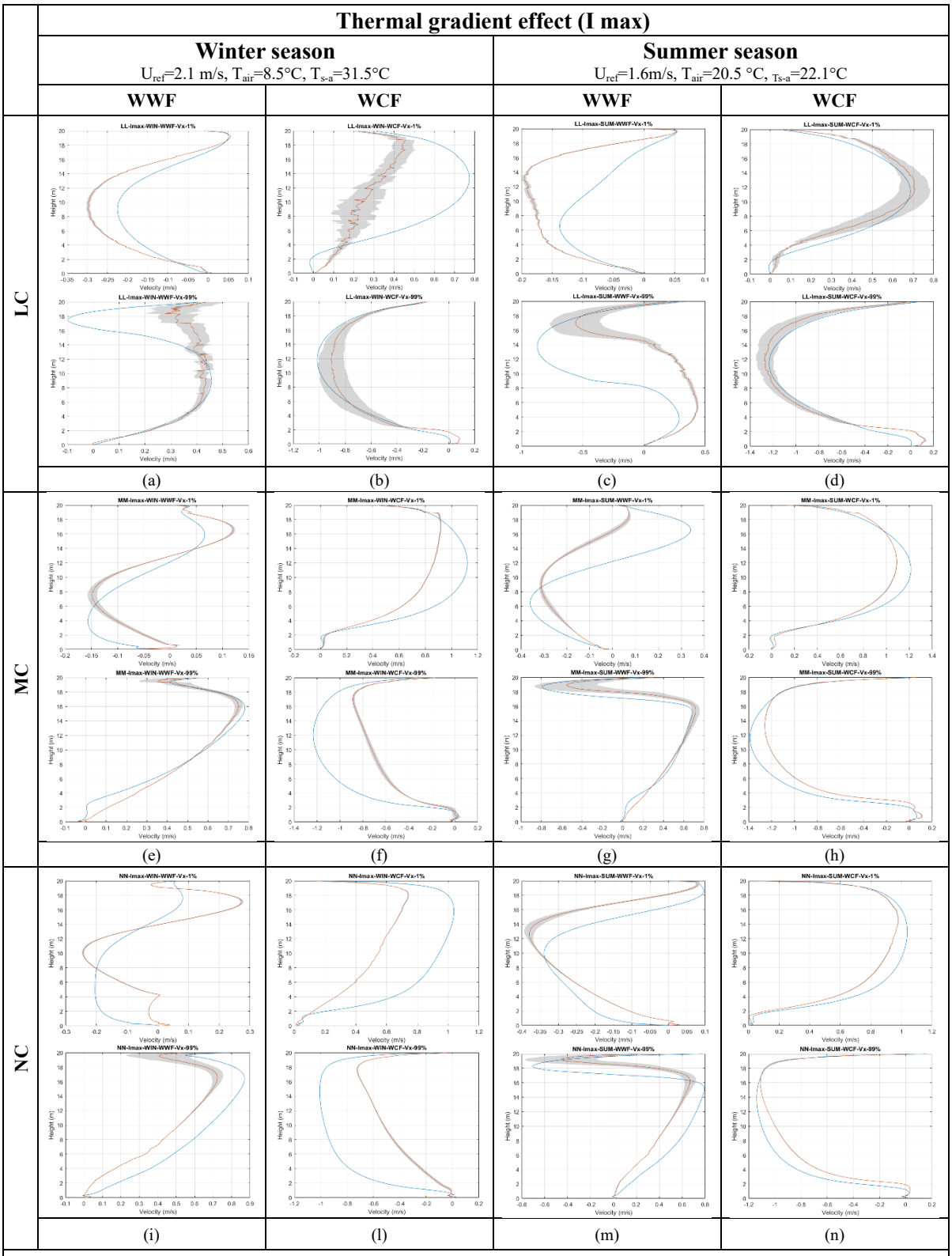

Fig. 52a-n - Effect of the extreme condition of thermal gradient (Imax) in generating the wind velocity profiles in large (LC, a-d), medium (MC, c-h), and narrow (NC, i-n) canyons, and comparison between the fitted curves of the steady flow regime (blue line) and the mean wind velocity profiles (orange line) generated from the unsteady flow regime within a standard deviation (1σ) in the transient simulations (grey area), in front of the leeward façade (probe at 1%) and the windward façade (probe at 99%), during the winter (a-b-e-f-i-l) and summer (c-d-g-h-m-n) seasons, and Windward Warm Facade (WWF, a-c-e-g-i-m) and Windward Cold Facade (WCF,b-d-f-h-l-n) scenarios.

Considering the extreme condition of the wind-driven (U_{max}) effect (Fig.51), results of the mean wind velocity profiles from the unsteady-state simulations are clearly representative of all the transient simulations, with the exception of the large canyon (LC), which is more sensitive to temporal variations , but still within the acceptable range considered; therefore, for the scenarios considered it is possible to affirm that the physical phenomenon observed in the canyon can be described with the steady-state regime: the steady-state (blue line, Fig.51) and unsteady-state (orange line, Fig.51) wind velocity profiles are similar for all boundaries conditions.

Considering the extreme condition of the thermal gradient (I_{max}) effect (Fig.52), in the medium (MC) and narrow (NC) canyons, the vortex phenomenon can be traced back to a steady-state regime more easily than in the large canyon (LC). Furthermore, for both seasons evaluated, a difference occur between the WCF and WWF scenarios in the narrow and medium canyons: i) the WCF is stationary, with a symmetric profile in the summer cases (Fig. 52h-MC and Fig. 52n-NC) and an asymmetric one in the winter cases (Fig. 52f-MC and Fig. 52 l-NC); ii) in the WWF, there is a recognizable pattern in the trend of the wind velocity profiles, when comparing the two canyons in each same climate scenario (Fig. 52e-MC and Fig.52i-NC) in winter and (Fig.52g-MC and Fig. 52m-NC) in summer; and when comparing the steady-state and unsteady-state profiles, none of them is symmetrical, as the combined effect of wind and temperature gradient creates multiple vortex structures with a different direction of rotation.

Considering the large canyon (LC), the same considerations can be applied, but it is necessary to underline that the only stationary and symmetrical velocity profile occur in summer-WCF scene (Fig. 52d); in the summer-WWF scene, the presence of multiple vortices creates an asymmetric velocity profile (Fig. 52c), while in winter there is a large discrepancy between the steady-state and unsteady-state velocity profiles, respectively for the leeward façade - WCF scene (Fig 52b) and windward façade-WWF scene (Fig. 52a).

Figures 53 and 54 reports the representation of the vortex structures that are created in the urban canyons domain, as a results of the combined or disjoined effects of the two extreme climate conditions (wind-driven and thermal gradient) different for each of the three examined aspect ratios.

Regarding the schemes in Figg 53-54, since the undisturbed reference wind U (blue arrow) is oriented from left to right, the façade on the left (building B2) is always the windward one, and it can be assumed the characteristics of the two possible scenes named Windward Warm Façade (WWF, in orange) and Windward Cold Facade (WCF, in blue).

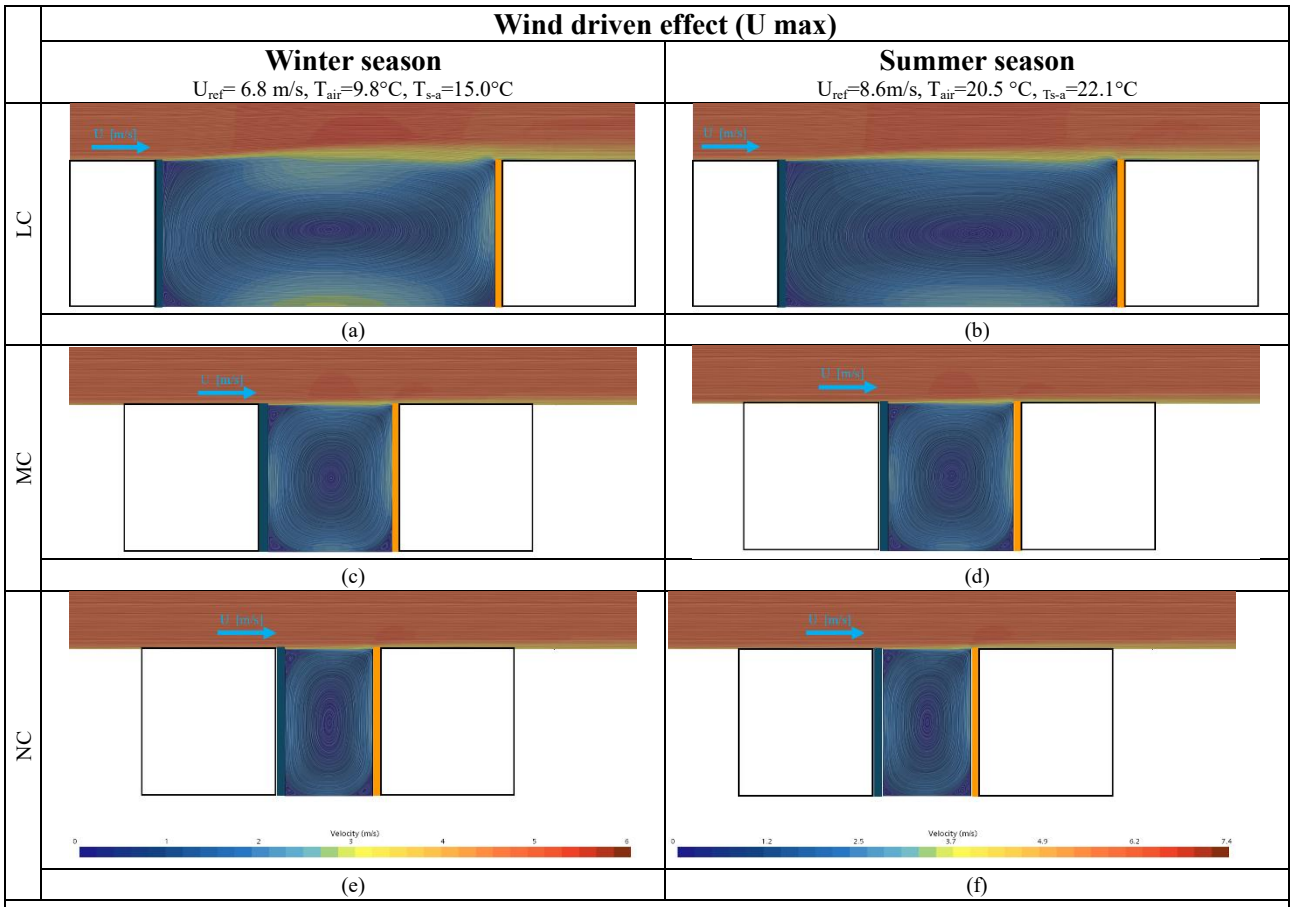

Fig. 53a-f - Vortical structures from steady-state regime, in case of extreme conditions of cross wind driven (Umax), for WWF scenes, during the winter (a-c-d) and summer (b-d-f) seasons, for large (LC, a-b), medium (MC, c-d), and narrow (NC, e-f) canyons.

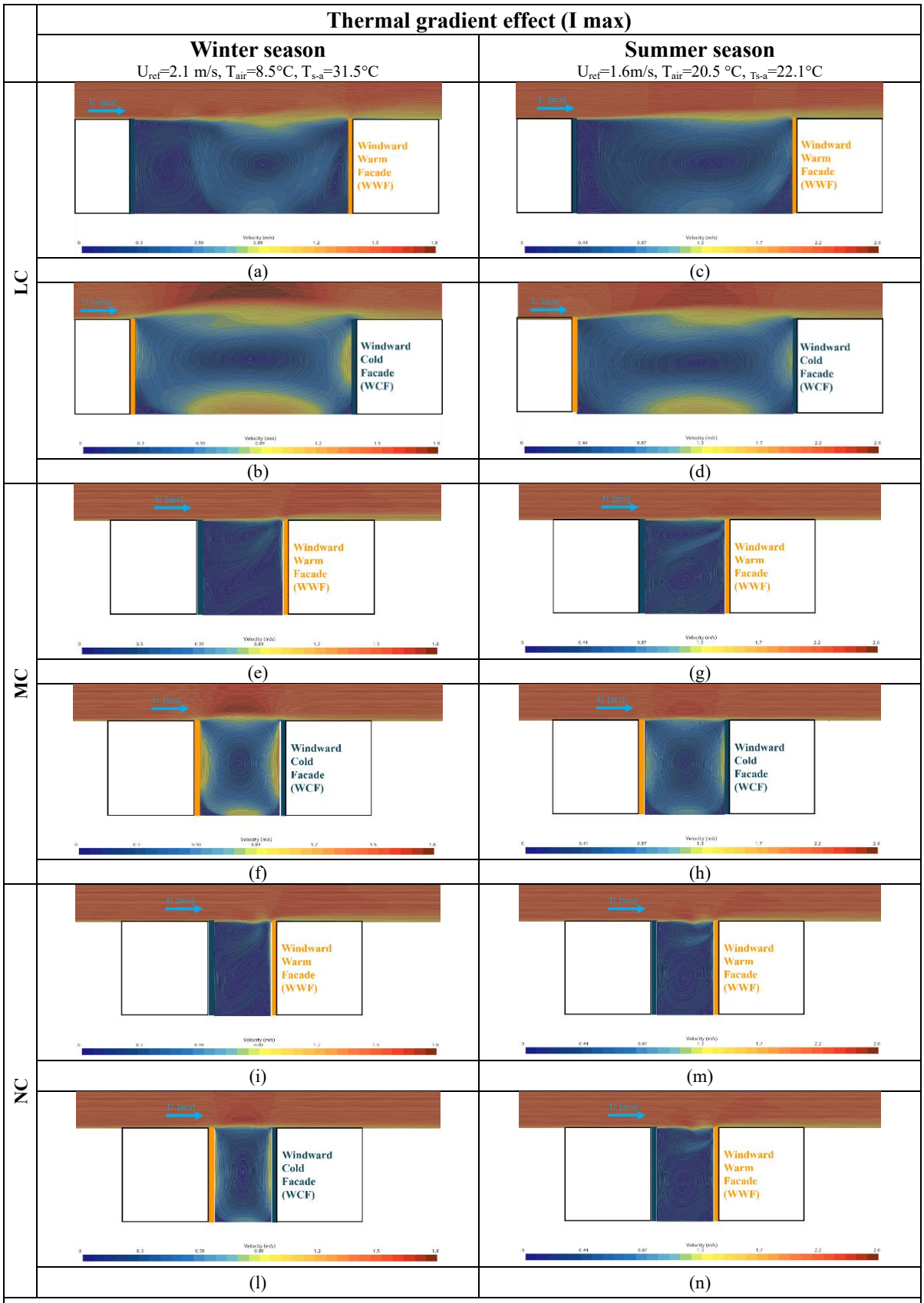

Fig. 54a-n - Vortical structures from steady-state regime, in case of extreme conditions of thermal gradient effect (Imax), for WWF (a-c-e-g-i-m) and WCF (b-d-f-h-l-n) scenes, during the winter (a-b-e-f-i-l) and summer (c-d-g-h-m-n) seasons, for large (LC, a-d), medium (MC, c-h), and narrow (NC, i-n) canyons,

Observing the results in case of cross wind-driven effect (Umax), a unique vortex is created in the Large Canyon (LC with a symmetrical behaviour in both examined seasons. Similar results are obtained for the medium and narrow canyons, each one characterized by different and unique intensity of wind velocities.

Observing the results in case of cross thermal gradient effect (Iincmax), the characterization of the vortical structures is strinctly correlated with presence of heated facades. In case of combined effects, oscillating solutions characterized the whole domain: the air flow adjacent to warmer facades flows upwards thanks to the buoyancy effect, but the presence of the external upstreaming wind with higher speed and the vortexes created in the meantime inside the canyon create conflicts, and generated multiple not symmetrical vortical structures.

In all WCF scenes, when the windward façade is not exposed, a unique symmetrical vortex is present in the domain, and this is valid for all the aspect ratios and in both winter and summer scenarios, as respectively shown in Fig. 54b-f-l and Fig.54d-h-n. Here, where the vortex is symmetrical, the air velocity field increases its magnitude near the centre of both vertical and horizontal surfaces.

Alternatively, in WWF scenes, when the windward façade is exposed, the two phenomena add up by thickening the mixing air layers; the domain is characterized by several recirculation zones, resulting not symmetrical velocity profiles (Fig. 52a-n); this occur both during in winter and summer seasons, respectively represented in Fig.54a-e-i and Fig.54c-g-m.

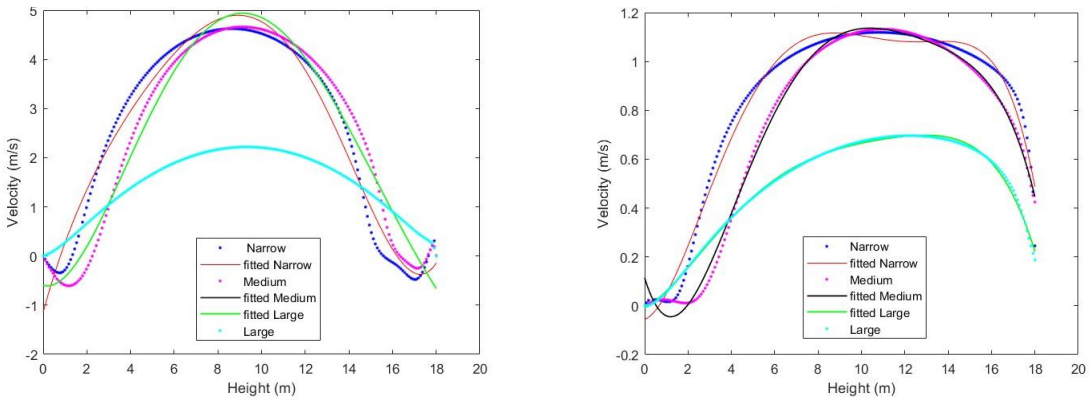

Fig. 55a-b – Comparison of the velocity fields in case of extreme cross wind-driven Umax (a) and thermal gradient I_{inc} max(b), both in WWF scene at summer season, for Narrow (blue line), Medium (violet line), and Large (green line) canyons resulting from the steady-state regime CFD simulations (dotted lines) and the interpolated fitted curves (straight lines).

Results shown in the graphs of Figure 55a-b report the comparison of velocity fields, separately for extreme condition of crosswind U_{max} (Fig.55a) and incident irradiation I_{inc} max (Fig.55b), considering the WWF scene at summer season, for the three canyons dimensions (narrow, medium, and large) resulting from the steady-state flow regime as direct output of the CFD simulations and the interpolated fitted curves; these were obtained from the fifth-grade polynomial functions in order to describe the wind speed as a function of canyon's height. As clearly represent in Fig.55a, for Umax conditions, a symmetrical velocity profile characterized all the three aspect ratios, with the highest wind speed occurring at half height. Lower velocities are obtained for Large Canyon, if compared to the medium and narrow ones. This is more evident in Fig. 55b, where the thermal gradient effects highlight this issue: caused by the buoyancy phenomenon and enhanced by the vortical structure in the domain, the warmer air flows upwards and it starts to circulate in same directions.

Chapter 4 – Air flow at building scale

Chapter overview

This chapter describes the analysis at building scale for the evaluation of the air flow through a building and its volume (Figure 56). Among the input data that will be used, there are the results of the air flow assessments at urban scale and inside urban canyon described in Chapter 3.
The presented methodology is based on the already mentioned place-based and multi-scalar approach and focuses on the creation of a 3-zones air flow lumped parameters model. It is a multizone parametric model whose input data, relating to the description of the climatic conditions, the urban morphology, and the characteristics of the building, are pre-processed to be exhaustive in the description of the real application context and to integrate the multiple scales to which the different parameters are referred. The ACH is the output parameter, evaluated at an hourly level, in relation to the hourly variation of the external and internal climatic conditions.
The aim is to define a proper methodology reaching a compromise between the accuracy of the output data and the number and accuracy of the input parameters, planning to use open and accessible databases, so that the methodology can be easily adaptable and replicable in any context.
The proposed model is applied to a case study to verify its validity in providing characteristic hourly ACH values for classes of buildings, enriching the geo-database of input parameters of the GIS-based engineering energy model presented in Chapter 2.

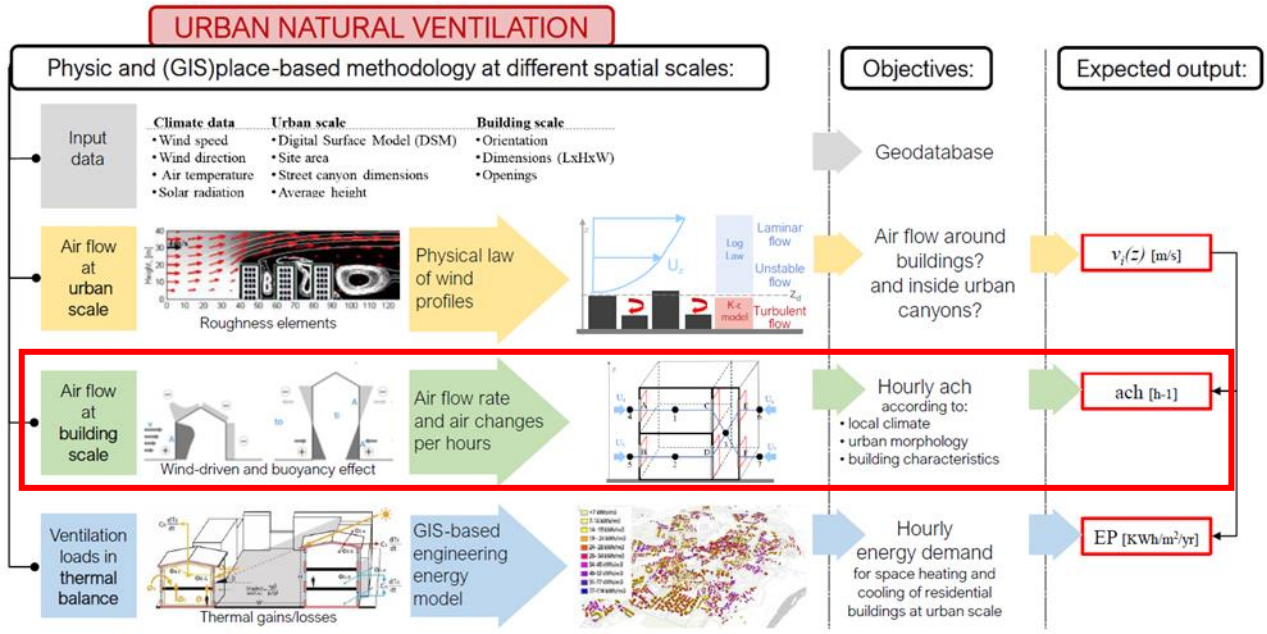

Fig. 56 - The step of the analysis investigated in this chapter (red box) in the flowchart of the overall methodology.

4.1. Introduction

The study of the air flow pattern in a building is very important to reach objective of indoor air quality and for determining space conditioning loads for energy consumption [119].
The airflows inside a building can modify infiltration and ventilation control, the indoor climate, contaminant control, energy consumption and equipment operation [120].
Air within a building needs two conditions two flows: an opening or a hole must exist for the air to flow along a path, and a driving force must exist to let the air flow in and out the building.
Air flows can be either controlled or uncontrolled. In the first case it is generate by mechanical ventilation system and devices of different type; they can be designed to increase the air flow rate, help the distribution of conditioned air, ensuring standard of indoor air quality and controlling inside air temperature for both thermal comfort and space heating/cooling purposes.
The uncontrolled, or unintentional ventilation, is a non-designed air movement and can be caused either by wind-driven flows and thermal buoyancy.

The analysed air flow is the mass air flow rate $\dot{m}$ [$kg \cdot s^{-1}$] is the air quantity that flow through a defined volume in a time unit. The analysed volume corresponds to the heated volume of a building, determined by the building envelope that delimits the internal and external environments.

As described in the scheme in Figure 57, the distribution of the air flows in a building is caused by pressure difference generated by wind, thermal buoyancy, mechanical ventilation, or, more often, a combination of these. It is also strongly influenced by the number and typology of openings and their distribution along the facades; consequently, by the leakages characteristics that influence the inner pathways together with the actions of occupants that can lead to significant and uncontrollable changes to pressure differences and air paths.
Since, the field of application of all analysis in this work will include only existing residential buildings, in which mechanical ventilation is more often absent, this work will not consider mechanical ventilation.
The focus of this investigation is the unintentional and accidental natural ventilation (NV) generated by the two natural driving forces of wind-driven and buoyancy, occurring separately and simultaneously; inhabitants' behaviour is not considered.

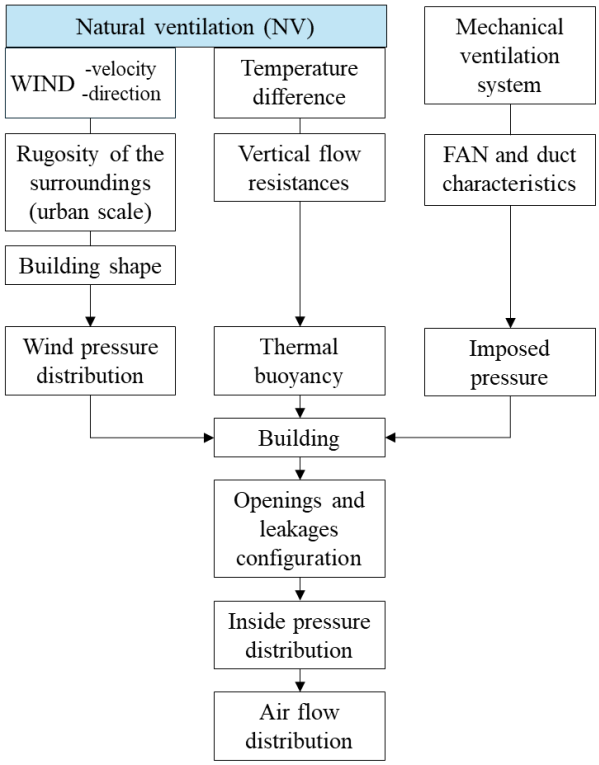

Fig. 57 - Influence on air flow distribution in a building.

Natural ventilation (NV) is considered a passive strategy to improve indoor air quality (IAQ), saving building energy costs. It is not a modern technique [97], as it has been widely applied in architectural solutions to provide acceptable indoor thermal comfort and replacing exhausted indoor air with outdoor air when the quality of the latter is suitable for NV. In fact, outdoor air can include pollutants, contaminants, and particulate matter (i.e., PM10 and PM 2.5) from unexhausted combustions, causing respiratory and other diseases on human health, especially in high-dense urban environment. In recent years, the situation has become severe, especially during winter season. Many of the drivers of air pollution (i.e. combustion of fossil fuels) are also sources of greenhouse gas emissions. Policies to reduce air pollution, therefore, offer a win-win strategy for both climate and health, lowering the burden of disease attributable to air pollution, as well as contributing to the near- and long-term mitigation of climate change [9]. Studies [121] aimed to investigate NV rate through a building to describe the airflow patterns and consequently particle transport indoor.

The NV beneficials should be evaluated case-by-case, due to the interplay of the multiple aspects that are involved on it. A systematic analysis is required, since from the early stage of building design when many key parameters about building and its context can be already determined, whereas they can significantly impact NV rate and help in predicting energy saving potential. Quick and relatively accurate method to assess NV at building scale, considering specific building parameters, ambient wind aerodynamics, and indoor thermal comfort should be developed; simple methodologies are necessary to orient new built construction project, but also retrofit interventions [97].

The NV in buildings is used as a mechanism to replace stale or noxious indoor exhausted air with fresh good air. Introducing fresh air into a heated zone can lead to additional heating or cooling loads, according to the type of ventilation present. As reported by [122] , around the 30-60% of residential building's energy consumption is accounted for ventilation. A considerable and unsolvable conflict

exists between the purpose of increasing the ventilation rate to ensure IAQ and the aim of reducing them to minimize the heating/cooling demand.

The aim of reducing heat losses and save energy consumption for space heating has led to tighter construction of building envelope and components to manage, sometimes creating other problems regarding indoor air quality [123]. Moreover, in the last decade the European regulations for the energy performance of buildings has been radically strengthened: the increase in insulation requirements has led to a strong reduction of heat losses through the building thermal envelope. Consequently, heat losses through the air-change rate has acquired a greater weight in contributing to the energy demand of buildings.

It is now clear that energy conservation must be associated with the quality of the indoor and outdoor environment. A global design for the energy efficiency of buildings considers not only the energy performance but also other quality environmental criteria, that highlights the necessity of full integration of building and surrounding characteristics [123].

Traditionally, building heat losses and gains through fresh air exchange occur for two different phenomena: ventilation and infiltration. Ventilation is a necessary feature for ensure good IAQ in buildings, infiltration is an involuntary and uncontrolled act. Therefore, despite providing an extra amount of fresh air, infiltrations alone are not enough to ensure IAQ adequate to the expected standards and can considerably increase the heating or cooling energy needs of buildings [124]. The incidence of infiltration on the total energy demand of a building has been described between 20 and 50% by [125], focusing in particular on existing buildings, for which the wide variety of energy retrofitting measures have increasingly included airtightness improvements.

This work investigates the air flows due to infiltrations through cracks or leakages in the envelope of the building and in the openings. The infiltration is one of the least investigated and most difficult to model term in the building energy balance equation. Many building energy simulation models and programs have very simplified infiltration models as it is usually intended a small load, especially in large residential building (condominiums) [126]. However, infiltration it is one of the most interesting parameters as it is strictly influenced by the characteristics of the surrounding built environment, by the variability of the climatic conditions (wind, temperature variations) that generate air movements around the building [123], and by the characteristics of the building envelope.

The airtightness or permeability level of the building's envelope and its components is an important parameter in the assessment of airflow rate, directly affecting its calculation. It requires a precise definition as close as possible to the real characteristics of the building that will be described in the next paragraphs. Awareness of infiltrations allow to manage the airflow rate and its related ventilation loads according to the purpose of the space conditioning. In fact, the air flow rate is functional to the calculation of the number of air changes per hour (ACH parameter).

The ACH is an important parameter used in many building energy models to achieve two main purposes: i) improving and maintaining indoor air quality (IAQ), according to standards; ii) controlling heat gain and losses due to ventilation loads in the building thermal energy balance that describes the energy performance of residential buildings.

Achieving objectives of IAQ means ensure supply of fresh air to a space and dilute the concentration of indoor pollution. Air quality standards (REF) are based on health-related risk-assessments that specify pre-defined threshold level of maximum permitted concentration or dose.

At Italian level, the two main reference standards today are UNI EN 16798-1:2019, and UNI 10339:95, now dated and under revision for years; other possible references are the American standard ANSI/ASHRAE Standard 62.2-2019 and voluntary certifications, such as the LEED Rating System (https://www.usgbc.org/leed), which has its own IAQ index.

The quantity (mass or volumetric air flow rate) of ventilation needed to ensure acceptable IAQ depends on the amount and nature of the dominant pollutant emitted by all sources in a confined space, during unit time period. Inside a residential building, the factors that can determine the presence of pollution sources are evaluated in relation to the number of occupants, the functions of use, the presence of construction materials and other devices or equipment.

Achieving objectives of energy saving means limiting heat losses during the heating season or increasing them during the cooling season: the operating conditions therefore are strictly related to the environmental and climate conditions of the surrounding environments. As a passive cooling technique, NV during night hours can help in cooling down the temperature of the building's structure. Considering the heat storage capacity and the thermal mass of each of the different layer of the building envelope, the air movement play a role in more rapidly dissipating the heat; greater wind speed is an advantage. If properly designed and enhance, night ventilation for cooling can delay the occurrence of peak temperature during daytime or the need of mechanical cooling system.

The aim of this chapter is to assess hourly variation of the Air Changes per hour (ACH) parameters, usually applied in building energy models as a constant value [127], according to local climate, urban morphology and building characteristics. To reach this objective, the hourly variation of the airflow rate through buildings is determined considering infiltrations created by the incident wind on building façades and the thermal buoyancy inside building zones.

As the third step of the physics and GIS-based methodology on urban ventilation presented in this work, the same criteria are used in this analysis of the NV at the building scale. Since the final objective is the application of the methodology to all the buildings in all areas within a city, the challenge has been the definition of an airflow model that represented an optimal balanced tool to properly describe physical phenomena, to rely on an efficient number of input variables, to detail buildings' characteristics; a methodology whit a schematic and synthetic description of the actual case study that is simple enough to be applied to all buildings in an urban area. A 3-zones air flow lumped parameters infiltration model has been outlined to consider the combined effect of cross natural ventilation, wind-driven and buoyancy on air flow rate at building level. According to the hourly variation of local climate condition and the characteristics of the urban canyon in which a building is sited, this methodology allow to evaluate the hourly variation of the number of ach for each building in any case study zone at urban scale. The aim is to use the resulting ACH as optimization and calibration parameters in the GIS-based engineering energy model for the hourly space heating consumption of residential building, replacing the fixed ACH values with the hourly ACH values for each building examined, according to the reference climatic year.

4.2. Fundamentals of natural ventilation at building scale

Both intentional and unintentional natural ventilation through buildings can occur in different way. Three main operational manners of the airflows can be observed, even simultaneously. These are listed below and as schematized in Figures 58a-c, these are: Single-sided ventilation, Cross ventilation, and Stack ventilation.

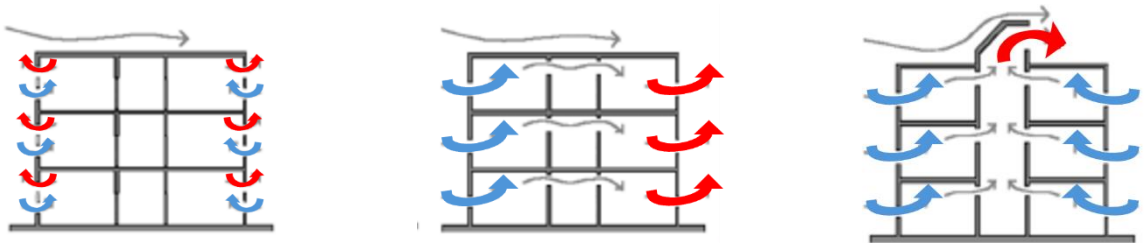

(a) (b) (c)

Fig. 58a-c - The three-operating manners of natural ventilation in a building, distinguish inlet air (blue arrows) and outlet air (red arrows): single-sided ventilation (a), cross ventilation (b), stack ventilation (c).

Single-sided ventilation can be observed when all openings in a building are positioned on the same façade, connecting internal and external environments (Fig. 58a). Each opening works as air inlet and outlet and wind-driven forces are mainly present. Despite being very frequent in residential buildings, typically in condominiums with more than two apartments per floor or not symmetrical plant, single sided ventilation does not allow the cross ventilation among opposite façades. Size, type, and shape of the openings are very important: if not appropriately designed, this system does not ensure the minimum air flow for the number of air changes per hour (ach) necessary for ensuring indoor air quality (IAQ) conditions. An increase in the ventilation rate can be reached with more openings on different heights or introducing other architectonic elements; the consequent buoyancy effect can enhance airflow through building volume.

Wind-driven cross ventilation (or cross wind-driven effect) occurs when openings are positioned on different (opposite) sides of the building (Fig. 58b). Inlet and outlet air flows are separated, respectively from the windward and leeward facades. This is regarded as the most effective strategy to reach higher Air Changes per Hour (ACH), ensuring indoor air quality and thermal comfort of occupants. Cross-ventilation is an efficient passive cooling strategy that is achieved by natural convection or evaporation rates due to the increase of air velocity or air movement inside the building. The characteristics of the wind profile (direction and velocity), the orientation of the building and the morphology of the surrounding urban context can have an important role in affecting the air flow path and air velocity through the building [128].

Buoyancy-driven stack ventilation (stack-effect or chimney-effect) is based on the physical principle that warm air tends to raise. In the confined volume of the building if warm exhausted air flow out of the upper-level, cooler air from outside flows in trough lower inlet and replaces it, generating the continuous replacement between cold and warm air and therefore a convective motion of the air (Fig.58c). Since height variation mainly affect this phenomenon, elevation is required to enhance it. In fact, this phenomenon can occur in the stairwells of buildings, usually a no-heated volume that communicates with the heated volumes (apartments) and the outside. The greater the height of the structure and the thermal variation, the greater the contribution of buoyancy force in increasing the air flow rate.

As mentioned before, the driving forces of natural ventilation that are investigated in this work are: the wind driven and thermal buoyancy.

4.2.1. Wind-driven natural ventilation.

The main driving force of natural ventilation is wind. As it flows around buildings, it generates pressures fields around buildings and across the building's envelope, in relation to the internal pressure. As schematized in Figure 59, considering the direction of the incident wind perpendicular to the bounding façade, a positive pressure is generated on it (windward façade) while on the opposite side (leeward façade) a negative pressure takes place, and suction regions occur. If compared to the static pressure associated with an undisturbed wind-velocity pattern, on the windward side, regions of over-pressure entail a decrease of wind velocity, and on the leeward side (facades parallel to the air stream) under-pressure regions are formed [123].

The morphology of the surrounding built context, the building dimension and the type of the building roof contribute to determining wake characteristics. As presented in the analysis of ventilation at urban scale and inside urban canyons (Chapter 3) tall buildings in a high-dense urban zones affect wind path and momentum at urban scale. As wake effects can be important over large distances, they are crucial for urban-flow modelling on and across different spatial scales [129]. In relation to the internal pressure, between the indoor and external environment a delta of pressure is created, and the air directly flows from the windward façade (inlet) to the leeward façade (outlet). The turbulence characteristic of the wind flow inside the urban canyons let the pressure field driven by wind on building surfaces be always unsteady and a place-based modelling is required.

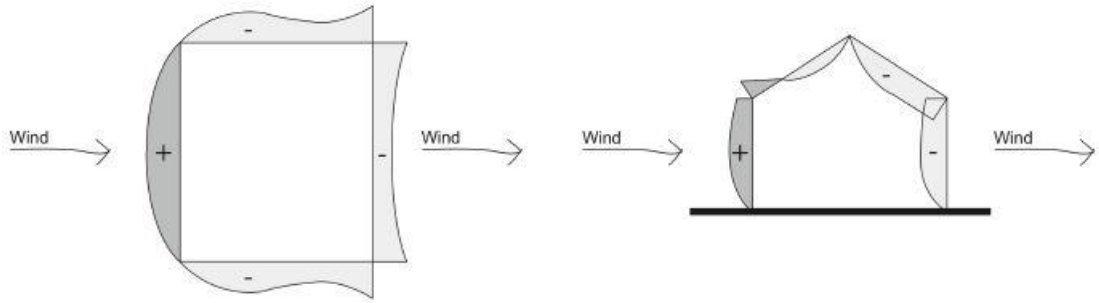

Fig. 59 - An example of the positive (+) and negative (-) pressure zones that incident wind generate on a building structure, creating respectively windward (in blue) and leeward (in red) facades, represented on both top and frontal view of the building.

Assuming constant density along the free streamline at a given height, Bernoulli's equation is simplified as Eq. (26), the contribution of static p and dynamic p_{dyn} pressures remains constant at any height of the flow field. Then, the relationship between velocity and pressure at different locations of the flow field produced by the wind around a building can be expressed as shown in Eq. (27).

$$p + p_{dyn} = \text{cost} \tag{26}$$

$$p_{dyn}(z_{ref}) = \frac{1}{2}\rho \cdot Cp \cdot U_{zref}^2 \tag{27}$$

where: U_{ref} is the undisturbed wind velocity [m·s^{-1}] at a reference height z_{ref} [m], ρ [kg·m^{-3}] is the air density, and Cp [-] is the experimental pressure coefficient.

The vertical profile of the mean wind speed U in the boundary layer of the urban canopy directly depends on the roughness of the surface of the built context. In the previous sections of this work, the

adjustment of the reference wind speed has been investigated both at urban scale and inside the building canyon, where turbulent flow occurs, comparing different methodologies. The output data of all this analysis is the adjusted wind speed *U* at any height z from the ground, with reference to results of the analysis in Chapter 3.

4.2.1.1. The surface pressure coefficient Cp

Many infiltration models rely on the dimensionless pressure coefficient Cp when assessing the wind pressures' distribution on a building's envelope. The pressure coefficient Cp represents the ratio between the surface dynamic pressure at a given height (z) and the surface dynamic pressure at measured reference height (z_{ref}) explanatory of the pattern of a undisturbed flow. Considering given point *k (x,y,z)* and wind direction (ϕ), the Cp is determined according to Eq. (28):

$$Cp_k(z_{ref}, \phi) = \frac{p_k - p_{0(z)}}{p_{dyn(z_{ref})}} \quad (28)$$

where *pk* and *p0(z)* are the surface and the reference pressures [Pa] at the height z [m] and p*dyn* is the reference dynamic pressure [Pa] at height z_{ref} [m].

The dimensionless pressure coefficient Cp [-] depends on different variables that can be grouped in three categories, reported in Table 36: wind properties, urban parameters and building geometry.

Table 36. Variables influencing the pressure coefficient parameter Cp.

Wind properties			**Urban parameters**			**Building geometry**		
Wind speed	U	[m·s^{-1}]	Plan Area Density	PAD	[%]	Orientation (azimuth)	Az	[°N]
Wind direction	Φ	[°N]	Surrounding buildings Height	SbH	[m]	Building dimension	(LxWxH)	[m]
			Wind velocity profile exponent	υ	[-]	Roof type and tilt angle	slope	[°]
						Façade elements positioning	(x,y,z)	[m]
						Side Aspect Ratio	SAR	[-]
						Frontal Area Ratio	FAR	[-]

- the *Plan Area Density (PAD)* describes the ratio between the built area (considering number of building' floors) [m^2] and the total area [m^2];
- the *Built Coverage Ratio (BCR)* that correspond to the ratio between the footprint on the ground of all buildings in the area [m^2] and the total parcel area [m^2];
- the *Surrounding building Height (SbH)* that is calculate as the mean height of all buildings;
- the *wind velocity profile exponent (υ)* indicates the terrain rugosity affecting the wind profile in the boundary layer (Chp. 3, par. 3.2.2);
- the *façade element positioning* that is evaluated in the barycentre of all the openings on each façade, reporting coordinates on both x-axis and z-axis, indicating the facades' length and height, respectively.

Estimate Cp coefficient.

The pressure coefficients Cp is still a debated topic in the deep knowledge of the natural ventilation phenomena in the reference scientific literature. Regarded as one of the main factors of uncertainty of infiltration models, it can be calculated in four different ways:

- ***Real scale measurements*****,** representing the most accurate values and detailed description of what happen on a specific building façade in a specific urban and climate setting; with very important limitations in costs and operating times, not suitable to describe all the buildings present at urban scale.

- ***Wind tunnel tests*** are done in physical chambers in scale dimension, representing idealized or real urban-building setting of a specific case study and they are used to simulate wind flows. This provides the description of the wind profile through obstacles and turbulence generators. Although not many tunnels chamber exist and the process is time consuming, they have more flexibility than real scale measurements and can provide a good basis reference.

- ***Computational Fluid Dynamics CFD simulations*** offer all benefits of wind tunnels but when the shape of the building and the surrounding environment described represent a real case study, the precision required in the modelling phase is very high so that complex turbulent flows are simulated, and the results can be considered accurate and acceptable. Furthermore, CFD simulations imply a significant computational burden. Although that, these models are constantly evolving, and today they represent a good reference for simple building geometries.

- ***Parametric models*** are based on tunnel experiments. they combine detailed measured results with the generality of the application [130]. An algorithm is found to calculate the variation of Cp on building facades, varying wind direction, environmental-urban and architectural-building conditions. These models are usually easy-to-use tools that provide the possibility to model a building and its surroundings with great flexibility and a small time/cost effort, if compared to previous methods, offering an immediate, time and cost-efficient way to model complex airflow problems. Among the most renowned tools based on parametrical models are the *TNO Cp Generator* [131] and *CpCalc+* software tool [130].

4.2.1.2. CpCalc+ tool

The *Cpcalc+* tool has been developed within the COMIS (Conjunction of Multizone Infiltration Specialists) program by the International Energy Agency [132] and was developed on FORTRAN 77 language. Then *CpCalc+* was developed on VISUAL BASIC language, within the EU PASCOOL Project (1994-96). Both software have a modular structure with a parametrical approach based on regression-analyses of wind-tunnel test data; they was generated as a module but also standalone programmes exist and are available online (https://iris.polito.it/handle/11583/2579969).

This wind pressure distribution parametrical model is based on the algorithm that focus on the context parameters, the parametrized meteorological and environmental characteristics of the site and the geometry of the analysed building to determine the pressure coefficients on the facades. The input data are the same listed in Table 36.

The tool has a graphical interface for manually entering input data. In the images in Figure 60a-d, some examples for inserting the geometric characteristics of the building under study (Fig. 60a), the

urban parameters (Fig. 60b) and the positioning of the openings on each facade of the building (Fig. 60c). Even if it can yield Cp values at any point on the surface for any specific wind angle, it has a high abstraction level, as it has to match a wide range of climatic and environmental boundary condition.

The wind pressure distribution model is based on the regression analysis of an extensive data set of wind tunnel tests, compared, and verified through a thorough accuracy and validation process to find the best reference wind pressure vertical profile on the centre of a façade as well as optimal fitting polynomial degrees with the lowest standard deviation values. The data sets used for *CpCalc* tool were related to the vertical façades of rectangular-shaped models, while for the *CpCalc+* tool wind tunnel tests were carried out on purpose on a cube-shaped model. Assuming stochastic distribution of the wind pressure around a building, empirical correlations draw algorithms which hold only within the range variation of the experimental reference data used for the analysis.

Some parameters are created by the program, and they constitute an indication of the limits of applicability of the model itself, as for each parameter the range of validity interval is indicated. These are:

- the *Relative building Height (RbH)* is the ratio of the building height (H) to the average height of the surrounding buildings (SbH) in the parcel area;
- the *Side Aspect Ratio (SAR)* is the ratio of the length of the façade adjacent to the considered one, to the facades' height;
- the *Frontal Area Ratio (FAR)* is the ratio of the length of the considered façade to its height;
- the *Wind Incidence Angle (AnwB)* is the angle between the wind direction and the normal to the considered façade.

For each parameter, or for a combination of parameters, two levels of variation range are foreseen: the larger one is the maximum range outside of which the calculation cannot be executed; the stricter one is the confidence range, outside of which results are given but the accuracy is not assured. An output file called is created by the program in a text format, as shown in the example of Figure 60d.

Limitations of this model deal with its application field due to the restricted range of the relative building height and the aspect ratios parameters, express by the FAR and SAR rages (0.5≤FAR≤4 and 0.5≤SAR≤2).

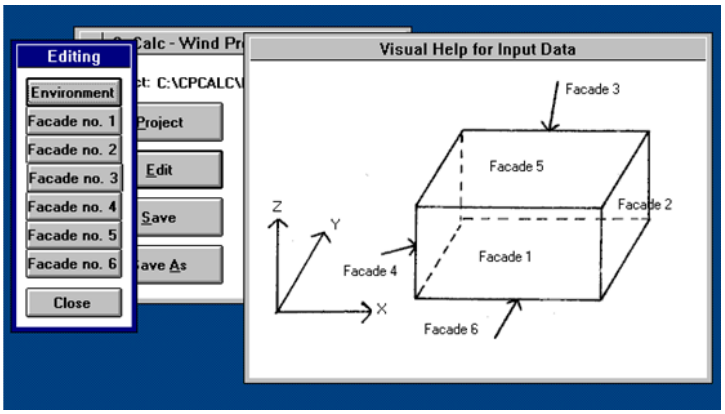

(a)

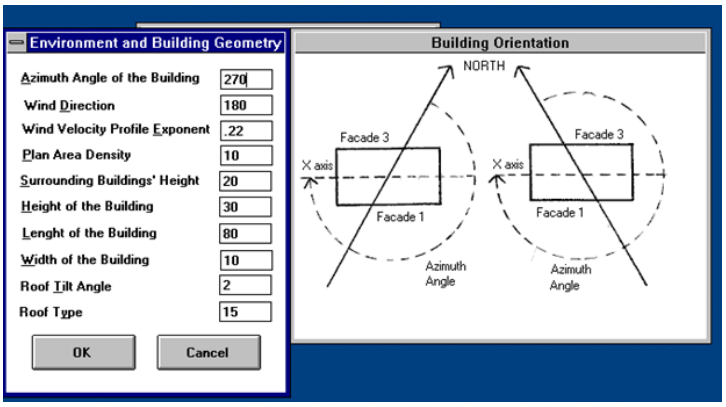

(b)

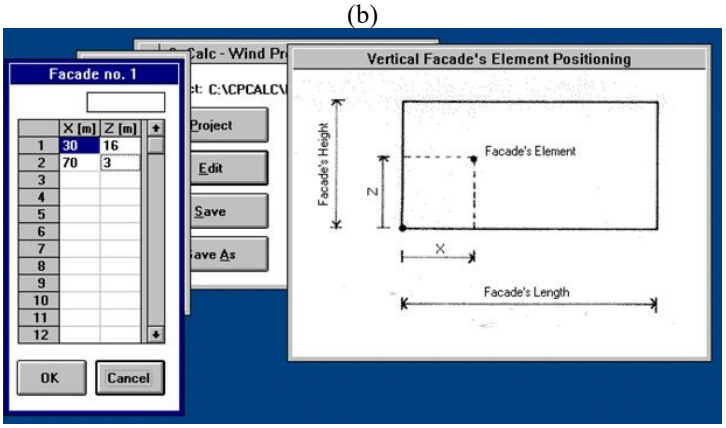

(c)

File Name: C:\Users\LENOVO\Desktop\RICERCA\2023_MODELLO\Cp_calc\case_study_bld_1 - Date: gennaio 23, 2023 - 10:00

Azimuth Angle of the Building:					255	deg.
Wind Direction:					330	deg.
Wind Velocity Profile Exponent:					0,4	
Plan Area Density:					34	%
Surronding Buildings' Height:					25	m
Height of the Building:					30	m
Lenght of the Building:					15	m
Width of the Building:					9	m
Roof Type:					double slope	
Roof Tilt Angle:					15	deg.
Facade	Element	X	Z	X/L	Z/H	CP
1	1	10	3	0,67	0,1	-0,009
1	2	10	15	0,67	0,5	-0,012
1	3	10	27	0,67	0,9	-0,021
CP average for facade n° 1						-0,014
3	4	10	3	0,67	0,1	-0,001
3	5	10	15	0,67	0,5	0,014
3	6	10	27	0,67	0,9	0,134
CP average for facade n° 3						0,049

(d)

Fig. 60a-d - Cpcalc+ tool user interface to insert input data conserning building geometry (a), boundary condition (b) and position of elements on facades (c), and example of output data for a case study building (d). Source: [107].

4.2.2. Buoyancy driven natural ventilation.

The phenomenon of thermal buoyancy is generated by the density difference between inside and outside air or between two adjacent zones of a building. The air density is function of the air temperature in the zone; the moisture content of air also affect density, but in this work is not considered. It is important to specify that this effect is not a form of convection: temperature differences inside two columns of air does not cause this phenomenon but it is due to the weight difference between two adjacent air columns [123].

The variation in density generated buoyancy forces, provokes warm air to rise and cool air to flow in by infiltrations from the bottom of the openings, as schematize in Figure 61a-b. The greater the temperature differences, the greater airflow rates. When the air in a vertical shaft is warmer and less dense than the outdoor environment, buoyant forces exert outward pressure at the top of the shaft.

In a building whit at least two openings at different heights, the neutral pressure level or neutral pressure plan (NPP) is positioned at a particular height, at which there is no difference between indoor and outdoor pressure, and the transition between inflow and outflow occurs.

The magnitude of stack pressure is a function of the zone temperature and the building height; so, at a reference height z [m], the pressure p [Pa] is given by Eq. (29):

$$p(z) = p_{0in} - \rho_{in} g z \tag{29}$$

where: p_{0in} [Pa] is the pressure at the bottom of the zone, g [m·s^{-2}] is the gravitational acceleration and, ρ_{in} [kg·m^{-3}] is the air density at the indoor temperature T_{in} [K] in the examined zone. In this work, it is assumed as valid the approximation of air as an ideal gas. So, it is given by Eq.(30):

$$\rho = \frac{\rho_0 \cdot T_0}{T} \tag{30}$$

where: ρ [kg·m^{-3}] is the air density at temperature T [K], ρ_0 [kg·m^{-3}] and T_0 [K] are the reference values for air density and temperature, respectively (T_0=273.15K and ρ_0 = 1.29 kg·m^{-3}, for dry air at 0 m a.s.l. The pressure difference between two opening, respectively at height h_1 [m] and h_2 [m], due to the stack pressure is calculated by Eq. (31), generally relatively to that of the lowest opening:

$$\Delta P = -\rho g \left[(z_1 - h_1) \cdot \left(\frac{1 - T_0}{T_1}\right) + (h_2 - z_1) \cdot \left(\frac{1 - T_0}{T_2}\right)\right] \tag{31}$$

where: z_1 [m] is the height of the lowest floor, T_1 [K] and T_2 [K] are the air temperature of zone 1 and 2, respectively. The pressure difference within a vertical shaft is determined by Eq.(32):

$$\Delta P = \rho_0 \left(\frac{T_{in} - T_0}{T_{in}}\right) g (z_{NPP} - z_{ref}) \tag{32}$$

where: ρ_0 [kg·m^{-3}] and T_0 [K] are the reference values for air density and temperature, T_{in} [K] is the indoor air temperature, z_{NPP} [m] and z_{ref} [m] are respectively the height of neutral pressure plane and the height above neutral pressure plane.

The stack effect can be a dominant force to drive air flows, especially in tall building and building vertical shafts. It can have a significant impact on the air flow distribution in multizone structures, especially in case of poor wind-driven effects due to low winds or shielding conditions [133]. When leakage (or openings) is equally distributed along the vertical axis of the shaft, the NPP will occur at mid-height of the shaft's height. As the distance from the NPP increases, the strength of the chimney effect increases. In this work, since most of the analysed building within a city are condominium, the presence of the neutral plane is always assumed at half the height of the building. In case of outdoor colder air temperature, the rise of warmer internal air creates a negative pressure variation below the NPP, increasing in strength towards the bottom of the shaft: infiltration of outdoor air occurs beneath the NPP, entering the shaft. above the NPP, a positive pressure is created by the rise of air, increasing in strength towards the top of the shaft. A vertical shaft within a multi-story building can facilitate air and contaminants from the ground floor to enter the floors above the NPP [134].

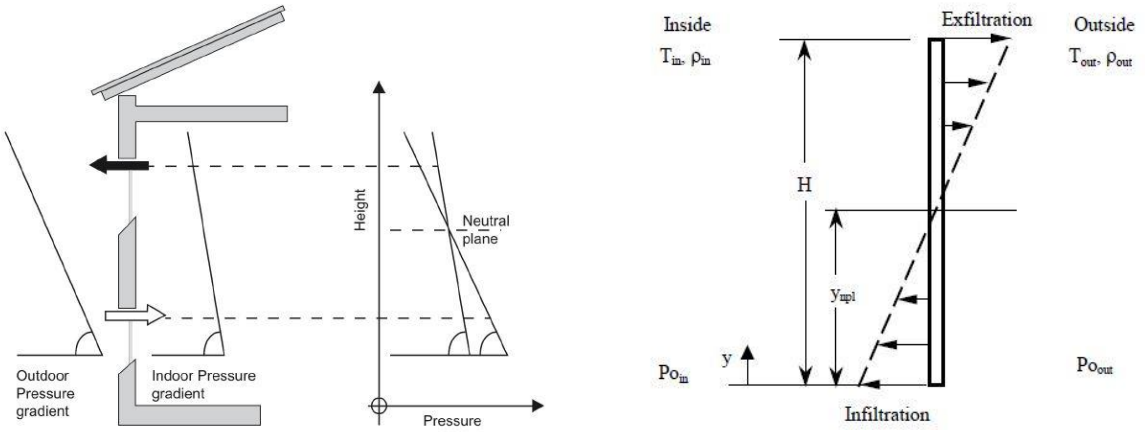

Fig. 61a-b – The buoyancy effect and the identification of the Neutral Pressure Plan (NPP). Source: [133].

4.2.3. Airflow through cracks and leakages

Pressure difference within a building can occur across holes, boundaries and barrier and are caused by one of the two natural driving forces: wind-driven and stack-effect that can occur separately or simultaneously. The amount of air that flows through a crack is governed by three factors: i) the size and dimension of the crack, ii) the magnitude of the pressure across the crack, and iii) the duration of the pressure difference. Since air always flows from a high-pressure to a low-pressure area, it will always seek the path of least resistance.

Airflows through building can be reconduct in analogy to the flow through a complex system of pipes, ducts, and orifices. In analogy to the physical phenomenon of a fluid flowing in ducts, the mass air flow rate $\dot{m}$ [$kg \cdot s^{-1}$] or the volumetric air flow rate Q [$m^3 \cdot s^{-1}$], both describe the intensity of the flow in the pipeline and they are defined as the ratio between the mass/volume of the fluid that enters a time interval and passes through a section transversal of the pipeline.

Buildings consists of numerous compartments that can be connected by leakage paths, and this is directly related to the airtightness or permeability of the building's envelope and its components.

The airtightness of a building cannot be inferred reliably just from the construction system, the building's age or inspections. Many indicators exist to characterize the airtightness level of a building, they are obtained from experimental measurements, depending on local regulation requirements and standards [124]. Reference is made to the UNI EN ISO 9972:2015 standard. The most common technique for infiltration inside building structure are of two types: air leakage measurements, which measure flow rates under large, artificially imposed pressure differences. i.e. the Blower Door Test (BDT), and air infiltration measurements which use tracer-gas measurements [135] to determine air flow rates under natural weather conditions [136]. Multizone tracer gas techniques can be used to determine either the interzonal air flows or the one occurring between the internal and external side of a building' envelope. The assessment of the interzonal air flows is necessary to better evaluate the impact of infiltration on indoor air quality [133].

Among the indicators, the most used are *q50* and *n50*. Both at a generated pressure difference of 50 Pa between the inside and the outside of an enclosure, the *q50* indicates the rate of air leakage, and the *n50* indicates the air exchange rate. The value of pressure difference of 50Pa is not correspondent to natural pressure different conditions, generally considered around 4 and 10 Pa [137]; However, it

is chosen as a standard measurement test to prevent fluctuating weather conditions from influencing the result.

In Figure 62a-c, are reported some of the average airtightness values of the envelope according to UNI EN 16798-7:2018, for different building types (single family, multi-family, industrial), 3 levels of leakages (low, average, high), at 3 pressure differences (4-10-50 Pa). The three different parameters are obtained from laboratory tests, according to standard procedures: the volumetric flow rate per outer envelope surface area (Fig.7a), the number of hourly replacements per volume (Fig.7b), and the volumetric flow rate per floor area surface area (Fig.7c).

		m^3/h per m^2 of outer envelope (exp n = 0.667)		
Leakages level		Q4Pa	Q10Pa	Q50Pa
Single family	Low	0.5	1	2.5
	Average	1	2	5
	High	2	3.5	10
Multy family, non-residential except industrial	Low	0.5	1	2.5
	Average	1	2	5
	High	2	3.5	10
Industrial	Low	1	2	5
	Average	2	3.5	10
	High	4	7	20

(a)

		n /vol.h) (exp n = 0.667)			Outer area/ vol
Leakages level		n4Pa	n10Pa	n50Pa	1/m
Single family	Low	0.4	0.8	1.9	
	Average	0.8	1.5	3.8	0.75
	High	1.5	2.6	7.5	
Multy family, non-residential except industrial	Low	0.2	0.4	1.0	
	Average	0.4	0.8	2.0	0.4
	High	0.8	1.4	4.0	
Industrial	Low	0.3	0.6	1.5	
	Average	0.6	1.1	3.0	0.3
	High	1.2	2.1	6.0	

(b)

		m^3/h per m^2 of floor area (exp n = 0.667)			Outer area/ Floor area
Leakages level		Q4Pa	Q10Pa	Q50Pa	1/m
Single family	Low	0.9	1.8	4.5	
	Average	1.8	3.6	9.0	1.8
	High	3.6	6.3	18.0	
Multy family, non-residential except industrial	Low	0.6	1.1	2.8	
	Average	1.1	2.2	5.5	1.1
	High	2.2	3.9	11.0	
Industrial	Low	1.5	3.0	7.5	
	Average	3.0	5.3	15.0	1.5
	High	6.0	10.5	30.0	

(c)

Fig. 62a-c - Average airtightness values of the envelope according to UNI 16798-7:2018, for different building types (single family, multi-family, industrial), for 3 levels of leakages (low, average, high), considering 3 different parameters: flow rate volumetric flow rate per outer envelope surface area (a), number of hourly replacements per volume (b), volumetric flow rate per floor area surface area (a).

Infiltrations are the results of the natural air flowing through openings, crack, or leakages in the building envelope, and they are affected by several factors such as climate condition and building location. Due to this complexity, the air flow rate due to infiltrations is one of the most difficult parameters to model accurately. Not only because the measurements of the leakage are challenging but also their simulation in mathematical model require some approximations. In fact, even if the location, dimension, and characteristics of all leakages in a building should be ideally know, it is impossible to precisely quantify this information and introduce them in a model. As for the wind pressure distribution on building facades, the description of leakages' characteristics is modelled based on approximate correlations derived from physical measurements.

Studies [138], [139], [140] investigated connections between the results obtained from BDT and the ones obtained from tracer-gas method. Other studies [141] defined new empirical models based on BDT results. Among these, the empirical model developed by the Lawrence Berkely Laboratory (LBL) [142], introduced in the COMIS program, is based on the effective flow area concept. It is defined as the cross-sectional area capable of producing equivalent airflow (McKeen) [134]: the approximate result is the effective leakage area, calculated in Eq. (33) (ISO 9972:2015).

$$A_e[m^2] = \frac{Q}{\sqrt{\frac{2\Delta P}{\rho}}} \tag{33}$$

where A_e [m^2] is the effective equivalent area, Q [$m^3 \cdot s^{-1}$] is the volumetric air flow rate, ρ [$kg \cdot m^{-3}$] is the air density, and ΔP [Pa] is the pressure difference between the two sides of the envelope or component.

A typical leakage area $A_{t,leak}$ [$cm^2 \cdot m^{-2}$] is associated to different types of openings, according to the category of the air tightness of the envelope or the component. For openings, like windows and doors, reference is made to UNI EN 12207:2017. Table 37 reports the description of leakages characteristic considering four different condition of airtightness (*very loose, loose, medium, tight*) and applying it to two opening types (window and door). Openings dimensions are fixed, considering normal rectangular vertical, side-hung inward typology. It is used to determine the Equivalent Leakage Area (ELA) $A_{e,leak}$, considering the area of the opening A_{op} , as shown in Eq.(34).

$$A_{e,leak}[m^2] = A_{t,leak} \cdot A_{op} \tag{34}$$

Table 37. Characteristics of the leakages for opening types and air tightness descriptions.

Type of opening	Discharge coefficient	Typical Leakage Area	Description of Air Tightness	Area of the opening	Equivalent leakage Area	Reference
	Cd [-]	$A_{t,leak}$ [cm^2/m^2]	-	A_{op} [m^2]	$A_{e,leak}$ [m^2]	
Window	0.65	12	Very Loose	(1.2x1.8)	0.0026	[134] UNI EN 12207:2017
Door				(0.9x2.2)	0.0024	
Window		6	Loose	(1.2x1.8)	0.0013	
Door				(0.9x2.2)	0.0012	
Window		3	Average	(1.2x1.8)	0.00065	
Door				(0.9x2.2)	0.00059	
Window		1.5	Tight	(1.2x1.8)	0.00032	
Door				(0.9x2.2)	0.000295	

Discharged coefficient, flow coefficient and flow exponent.

The relationship between the pressure difference across a crack or an opening in the building envelope and the mass air flow rate ṁ [kg·s^{-1}] can be expressed according to different formula, depending on the openings size and typology of the cracks.
Referring to the orifice equation and the definition of the ELA, it is possible to determine the air flow according to Eq. (35), considering the characteristics of the openings (type and dimension),

$$\dot{m} = C_d \cdot A_{e,leak} \cdot \rho \cdot \sqrt{\frac{2\Delta P}{\rho}} \tag{35}$$

where: *Cd* is the relative discharge coefficient [-], ρ the air density [kg·m^{-3}], ΔP the pressure difference and $A_{e,leak}$ is the effective flow area of all the cracks [m^2].

However, the power law equation Eq. (36) is widely used, simple and meaningful, and it consider the characteristic of the leakages (*K, n)*

$$\dot{m} = K \cdot (\Delta P)^n \tag{36}$$

where: *K* is the flow coefficient [kg·s^{-1}·Pa^{-n}] and *n* is the flow exponent [-].

Correction factors (*Cd, K, and n*) were introduced in air infiltration models to account for the influences of the air properties and shape of the cracks. The classifications of cracks, according to their physical behavior and component's types is difficult to assess, especially for real buildings. The majority of airflow modelling treats building components (e.g., walls, windows, closed doors) as single leakages in order to reduce the amount of information and input data requirements; however, this reduces the accuracy of the results of the simulations. This study considers the infiltration of cracks present in closed openings (doors and windows) of normal dimensions.

The discharge coefficient *Cd* is a dimensionless value, the theoretical model and losses in the actual opening due to frictional losses, contraction of the flow, and other geometry effects [126]. It is a function of opening height, wind pressure and direction, temperature difference and of the flow Reynolds number (Re). Its definition is a controversial matter: for small openings, a representative value of Cd=0.65 is reported by [143], for standard opening Cd=0.78, for large openings it is close to unity.

Then, the discharged coefficient *Cd* for cracks in walls and floors is usually estimated in the range of 0.6-0.7: in all the applications presented in this work, it is fixed at 0.65.

For each opening type, the *flow coefficient K* [kg·s^{-1}·Pa^{-n}] can be calculated according to Eq. (37), in its relationship with the effective leakage area, the discharged coefficient, and the air density; it is intended as the value of the flow rate induced by a unitary pressure difference.

$$K_{leak} = Cd \cdot A_{e,leak} * (2 * \rho)^{1/2} \tag{37}$$

The *flow exponent n* is a parameters used to describe the type of fluid motion, considering the dimension and the shape of cracks; it can vary from a fully turbulent flow (o.5) to a laminar one (1) [120]. Air flow through a crack is always a mixture of laminar, turbulent, and transition flow [123]. The most used values describing airflow rate for several types of leakages are reported in Table 38 and refer to the most-known scientific literature.

Air flow through large openings is difficult to predict, as it involves several different physical phenomena, including steady-state gravitational flows, recirculation flows, and fluctuating flows resulting from wind turbulence. In fact, the flow exponent n for large openings is 0.5. For small crack

opening the value of n usually applied between 0.65-0.67 depending on the reference, as shown in Table 3. In this study a value of 0.65 is considered.

Table 38. Reference values of the flow coefficient *K* and flow exponent *n*.

	Value	Unit	Specifics	Reference
K	0.67-3	[kg·s^{-1}·Pa^{-n}]	per m^2 of outer envelope at 4Pa	UNI EN 15242:2008 UNI EN 16798-7:2019
n	0.5≤n≤1	[-]	-	[144]
	0.667		-	UNI EN 15242:2008 (UNI EN 16798-7:2019)
	0.65		for array of leaks	[134]
	0.5		for large opening	[145]
	0.65		for small crack-opening	
	0.6≤n≤0.8		-	[146]

4.3. Research background: model and tools.

The topic of natural ventilation has been examined by several scientific research fields: indoor air quality and energy performance efficiency at building scale, deepening HVAC and fire safety systems [147], [148], [149].

In the reference scientific literature, the most frequent methods used to model natural ventilation at building scale and to assess the infiltration rate and the air exchange rate ACH are:

- Tabular data and empirical models
- Computational Fluid Dynamic models (CFD)
- Multizone parametric models

Tabular data and empirical models.

This type of modeling is based on an empirical approach. Measurements, field experiments and laboratory experiments are conducted on test cases. Regression methods are used to generalize the results, and reference tabular data are created according to categorizations made to describe the sample on which the test results are based. Regarding the air flow rate and ach assessment, laboratory test based on standard procedures are conducted, testing the permeability of single or multiple technological components of the building envelope. A controlled pressure difference is purposely created between two zones, and the air flow rate is directly measured, using different techniques, among which the blower door test and the tracer-gas measurements are the most frequently used. From that, ach is obtained as a tabular data according to each class of pressure difference and type of building [146]. Regression methods are used to predict infiltration rate values by analyzing the large amount of data obtained from measurements. From these results, refence tabular data are created for different classes of building typology and pressure difference.

Tabular values facilitate the application of parameters, especially in the absence of detailed information relating to the case study. They are easy to understand and immediate to use. Furthermore, the standard procedure and references to the UNI EN ISO offer a guarantee of the method and the possibility of comparing the results. The UNI EN ISO 9972:2015 concern standards on *Thermal performance of buildings*, *Determination of air permeability of buildings* and *Method of*

pressurization by fan; the UNI EN 12207:2017 deals with the classification of air permeability of windows and doors; the UNI EN 16798-7:2018 concerns methods for the evaluation of the *Energy performance of buildings*, including *Ventilation for buildings* and *Calculation methods for determining air flow rates in buildings including infiltration (Part 7).*

Despite this, the tabular values are indicative and extremely relative and may deviate significantly from reality. The main limitation in the application of this modeling is the application field of the results related to the study sample. In addition, in this type of modeling the description of the buildings and its surrounding is too general and it does not fit with the criteria of the place-based approach specific to the methodology proposed in this study, for which the description of the real characteristics of each building and its context are considered important and fundamental in determining the variation of air flow and ach.

Computational Fluid Dynamic models (CFD).

This type of modelling consists of simulations that are based on differential equations of energy, mass, and momentum: the airflows are retrieved over time and through a refine grid that describe the model geometry and its boundary conditions with many levels of accuracy. Calculations are based on the continuity equation and the Navier–Stokes equations.
These models provide for the possibility of describing the complexity of physical phenomena: the quantity and quality of the required information and input data ensure the accuracy of the results and the possibility of describing the entire field of analysis. The boundary conditions of the simulation's domain consist of the real geometry of the building and its surrounding context and can include a very high and potentially infinitesimal level of detail.
The level of accuracy of the representation of real boundary conditions is directly proportional to the computational cost of the simulations.

The main advantage of these modeling is given by its ability to facilitate the understanding of physical phenomena as well as the impact of each parameter in determining the result. Many studies have been conducted at the building scale to evaluate the air flow in the different building zones. The aim of these studies is to describe phenomena in specific contexts, verify the accuracy of computational settings or tabular methods or evaluate the correlation between parameters.

In the reference scientific literature of urban ventilation studies, numerical solutions relying on CFD simulations are acquiring importance and many simplified models are used to compose building geometries forming urban structures. Most studies apply 3D CFD model on generic building geometries that form idealized urban structures [33]. Studies on actual urban areas are still rare due to the complexity of describing the physical phenomena and the high level of detail required in modeling the built environment. The main limit is the difficulty in generalizing the results of the CFD simulations. As described in the Best Practice Guidance (BPG) on CFD analysis for wind comfort and safety [114], all buildings relevant for the wind should be modeled explicitly; but this requirement cannot be easily achieved for neighborhood-scale applications for a whole city, as it is intended to do in this study.

Multizone parametric models.

Different types of multizone parametric models exist but they can be defined as multizone models base on network-schematization that can compute the interactions between all the airflows that occur in the zones of a whole-building. The model consists of the representation of the building by a network

of nodes, representing the pressures of rooms or zones, and links connecting nodes and representing airflow disposal.

The building is represented by a simplified network scheme using a matrix of nodes, with properties of pressure, volume, temperature, and leakages. The different internal environments of the building can be divided into several zones depending on the desired quality of representation, the degree of detail that can be achieved with the available input data and the scope of the analysis. Different zones can be designed to consider and describe the interesting types of air motion that can occur in any specific case study, according to the characteristics of the building (heated volume, airtightness, openings type) and the surrounding environment and climate conditions (pressure, temperature).

For each zone that made up the network, local values of input data should be define and boundary conditions should be assumed; then, physical equations of fluid dynamics can be applied to retrieve the output variables. Based on mass conservation and energy balance equations at nodes, and considering the orifice characteristics, the air flow rate and mass transfer rate are determined due to the pressure difference between different zones. Describing the airflows as functions of the pressure differences and applying the law of conservation of air mass inside each zone leads to a system of nonlinear equations that must be solved iteratively [150].

Models with few nodes are simple and do not need high computational resources. The greater the complexity of the elements in the network, the higher the computational effort required by the model. Among well-known parametric models, CONTAM [145] and COMIS [144] are the most used ones.

The first infiltration models of residential buildings were empirical models based on measured data describing both infiltration and weather characteristics and operating with regression analysis. Regression coefficients reflected the extreme variability of the characteristics that affect the infiltration rate; therefore, empirical models have a limited field of application and are not suitable to be used as a design tool for energy analysis. Physic-based models were then studied for residential infiltration modeling.

4.4. Research objective and novelty.

The research objective of the analysis of airflow at building scale is the definition of a multizone lumped parameter model to assess hourly variation of the airflow rate through buildings and consequently determine an hourly variation of the Air Changes per hour (ACH) parameters.

To reach this objective, a 3-zones air flow lumped parameters infiltration model has been outlined to consider the combined effect of cross natural ventilation, wind-driven and buoyancy on air flow rate at building level, according to local climate, urban morphology and building characteristics.

The final objective is the application of the methodology to all the buildings in all areas within a city. The airflow model proposed in this study can represent a good balanced tool to properly describe physical phenomena, to rely on an efficient number of input variables, to detail buildings' characteristics; a methodology whit a schematic and synthetic description of the actual case study that is simple enough to be applied to all buildings in an urban area.

The novelty of this methodology consists in the definition of a physic-based and place-based model.

A GIS-place based methodology is defined to consider local climate condition, urban morphology and building characteristic in the assessment of cross natural ventilation around and inside buildings. Input data of the place-based methodology are collected from existing and accessible databases,

adapting the methodology to the characteristics of the examined context; data integration, and in some cases, transformation, or calculation, relies on the Geographical Information System (GIS) open-source software and its tools.

The presented methodology will be applied in some case studies in the city of Turin (Italy).

The aim is to use the resulting ACH as optimization and calibration parameters in the GIS-based engineering energy model for the hourly space heating consumption of residential building, replacing the fixed ACH values with the hourly ACH values for each building examined, according to the reference climatic year.

4.5. Lumped parameter model

Among the multizone parametric models, the lumped-parameter model is a zero-dimensional simplified network that is made up of a interconnected zones through which the air flows; the network is the schematization of the tridimensional structure of a building. Referring to the theory of oriented graphs, the network system is populated by nodes and links whose topological connections can be described mathematically, using matrix calculation and iterative calculation procedures for more complex problems.

The building is schematized by the network of nodes, each one representing a real or a fictitious zone of the building, and the nodes are connected by links, which represent the air flow displacement in space. Each node can be connected to one or more links so that all the possible connections that involve a movement of air from one confined environment to another are represented.

In this work, the air flows through openings' leakages generating pressure variations between every two zones due to the physical phenomena of the cross wind-driven incident on building facades and thermal buoyancy inside the building shaft.

The environment outside the building envelope is also represented at least two nodes in the network, one for each of the two opposite building façades, attributable as an external zone, whose fundamental temperature and pressure conditions are known. Internal nodes can be associated to heated zones (i.e., building apartments) or no-heated zones (i.e., building shaft) at a set internal temperature, according to the requirements specific for the heating and cooling seasons; internal pressure conditions constitute the unknown variables.

4.5.1. General assumption

All the lumped parameters models presented this work are based on the assumptions that follow:

- in each zone (node) the temperature T [K], air density ρ [kg·m-3], and physical pressure P [Pa] status are constant throughout the interesting volume;
- the air flows through leakages that characterized the examined openings, and links are one-dimensional connections between the different zones of the building to which airflow are assigned;
- both outdoor and indoor air is considered incompressible: air motion is only caused by the difference in pressure between two zones. This is generated solely by natural causes: pressure variation due to incident wind (wind effect) on the external building's envelope and/or thermal gradients (stack effect) which determine convective air motions.

Each node is associated with the physical quantities of physical pressure P [Pa], temperature T [K], air density ρ [kg·m^{-3}] and height z [m a.s.l.]; each link is associated with the physical quantities of pressure variation ΔP between two nodes [Pa], air mass flow rate $\dot{m}$ [kg·s^{-1}] and a direction of the flux. In this work, positive fluxes are the ones outgoing from a node.

Internal nodes are positioned in the barycenter of the zone's volume. In models where the buoyancy effect is considered, within each internal zone, nodes at leakage level are positioned in the barycenter of the opening and the local pressure is determined in relation to the pressure of the reference zone in the barycenter of the zone's volume. In this way the height variation of leakages belonging to the same zone is considered, affecting the local pressure variation (potential pressure contribution).

External nodes are positioned at the same height from the ground of the barycentre of the openings, depending on the number of openings considered in the model. In each model at least one opening is considered on each of the two opposite facades of the building. The number of external nodes increases as the complexity of the model increases and the detailed description of the external conditions. This depends on the ability to synthetically describe the wind velocity field incident on the facades in the urban canyon, as a function of the height from the ground, referring to the Cp-method or the CFD-method and considering the position of the neutral plane of the building.

The building should necessarily have two free opposing facades and openings uniformly distributed on both facades; the symmetrical representation of the openings (type and size) allows to consider the effect of cross ventilation and the presence of the neutral plane.

4.5.2. Physical assumptions

As the majority of multizone parametric models, the lumped parameter model presented is based on basic equations of physical laws and assumptions: the principle of mass and energy conservation and the Bernoulli's Equation.

Mass and energy conservation

Applying the fundamental equations of mass balance and energy conservation to the examined network, a mass flow balance must occur at each node, and it is led by a delta pressure; according to Eq. (38), the algebraic sum of all air flows linked to a node must be equal to zero (Eq.39 reports the equation in its vector form):

$$f(\Delta P) = \sum_{L=1}^{L_i} \pm \dot{m}_i \tag{38}$$

$$f(\Delta P) = 0 \tag{39}$$

where: i is a generic node, L_i is the number of links connected to that node, and $\dot{m}$ [kg·s^{-1}] is the mass air flow rate entering (-) to that node or outgoing (+) from it.

Conservation of the mass at each zone of the network leads to a system of equations that can be written Eq. (40):

$$\begin{cases} f(\Delta P_i) = \sum_{L=1}^{L_i} \pm \dot{m}_i = 0 \\ f(\Delta P_j) = \sum_{L=1}^{L_j} \pm \dot{m}_j = 0 \\ \dots \\ f(\Delta P_n) = \sum_{L=1}^{L_n} \pm \dot{m}_n = 0 \end{cases}. \tag{40}$$

where: each equation describes the mass energy conservation in a zone, and the number of the equations in the system correspond to the number of zones in the network.

At links, the mass flow rate $\dot{m}$ [kg·s^{-1}] can be calculated as a function of pressure difference ΔP [Pa] between two necessary nodes, here, generically nodes i and j; it can be determined applying the orifice equation Eq. (41), knowing the characteristics of the openings (type and dimension), or the power law equation Eq. (42), knowing the leakages' characteristics (*K, n*), as described in paragraph. 4.2.3:

$$\dot{m}_{ij} = C_d \cdot A_{e,leak} \cdot \rho \cdot \sqrt{\frac{2\Delta P_{ij}}{\rho}} \tag{41}$$

where: *Cd* is discharge coefficient [-], *ρ is* air density [kg·m^{-3}], *ΔP* is pressure variation and $A_{e,leak}$ is effective flow area of all cracks [m^2] existing between the two examined zones.

$$\dot{m}_{ij} = K_{ij} \cdot (\Delta P_{ij})^n \tag{42}$$

where: *K* [kg·s^{-1}·Pa^{-n}] and *n* [-] are the flow coefficient and the flow exponent, respectively.

Pressure difference – Bernoulli's equation.

As already mentioned, the difference in pressure between zones is due solely to natural causes. These are the surface pressure produced by the incident wind on the external envelope of the building (wind effect) and the spatial gradients of temperature that determine convective actions (stack effect) The air flow within two generic nodes (i,j) is assumed to be governed by Bernoulli's equation Eq. (43) :

$$p_{dyn_i} + P_i + p_{pot_i} = p_{dyn_j} + P_j + p_{pot_j} + \Delta Pij \tag{43}$$

where: *ΔPij* is a concentrated pressure variation due to the leakage, p_{dyn} [Pa] is the kinetic contribution, p_{pot} [Pa] is the potential pressure and *P* [Pa] the total pressure at each node.

The Bernoulli's equation can also be written as Eq. (44):

$$\tfrac{1}{2}\rho v_i^2 + P_i + g\rho z_i = \tfrac{1}{2}\rho v_j^2 + P_j + g\rho z_j + \Delta Pij \tag{44}$$

where ρ [kg·m^{-3}] is the air density related to the air temperature inside each zone (at each node), g [m·s^{-2}] is the gravity, *v* [m·s^{-1}] is the wind velocity at leakage's level, and *z* [m] is the height of each node from the ground, according to the reference system.

More in detail, at a generic node *i*, it can be written:

- **the dynamic pressure p_{dyn}** is generated by the effect of the surface pressure by the incident natural wind (wind-effect) on both the windward and leeward façade of the buildings. It is determined according to Eq. (45.1) or Eq. (45.2), applying the *Cp-method* or the *CFD-method*, respectively:

$$p_{dyn_i} = \tfrac{1}{2}\rho_i \cdot Cp_i \cdot U_{ref}^2 \tag{45.1}$$

where: U_{ref} is the undisturbed reference wind velocity [m·s^{-1}], ρ [kg·m^{-3}] is the outdoor air density, and *Cp* [-] is the coefficient of pressure at leakage's level assessed by *CpCalc+* tool, as explained in paragraph 4.2.1.2.

$$p_{dyn_i} = \tfrac{1}{2}\rho_i \cdot (v_i^2) \tag{45.2}$$

where: *v* [m·s^{-1}] is the wind velocity at leakage's level, retrieved from CFD simulation and consequent interpolation and ρ [kg·m^{-3}] is the outdoor air density; the effect of windward (+) and leeward (-)

dynamic pressure, generating positive or negative fluxes entering and outgoing from the façade are considered.

- **the pressure p_i** is determined correcting reference atmospheric pressure P_{atmref} [101325 Pa], according to the local altitude *alt* [m asl], and the height of the node from the ground z_i [m] , as shown in Eq. (46):

$$p_i = P_{atm_{ref}} \cdot 0.9877^{\frac{(alt+zi)}{100}} \quad (46)$$

- **the potential pressure p_{pot}** is determined by the spatial gradients of temperature that determine convective actions (stack effect), as shown in Eq. (47):

$$p_{pot_i} = \rho \cdot g \cdot z_i \quad (47)$$

where: g [$m \cdot s^{-2}$] is gravity, ρ [$kg \cdot m^{-3}$] is air density and z_i [m] is the node's height.

Since the boundary conditions of known temperature, pressure, wind speed and height are different for external and internal nodes in the network, the total pressure P_i [Pa] at a generic node i :

- in case of an external node: it is defined by summing up all the known pressure contributions, according to Eq. (48):

$$P_i = p_{dyni} + p_i + p_{poti} \quad (48)$$

- in case of an internal node: it constitutes the unknown variable, even though it should be always possible to analytically determine the contributions of the potential pressures.

The equations for determining P_i [Pa] vary in relation to the number of internal nodes and links that make up the network, directly influencing the number of non-linear equations that make up the system to be solved and progressively increasing the degree of complexity of the solutions: from the analytical calculation of the single-zone model to the iterative calculation of the 3-zones model.

4.5.3. Evolution of the model

In the following paragraphs the fundamental steps of the definition process of the final lumped parameter model are retraced. In Table 39 are presented all the models developed, according to the criteria considered to gradually insert levels of complexity into the model:

- the number of the (internal) zones, from which directly correspond the number of the internal nodes,
- the total number of nodes in the network, considering both the internal and external nodes,
- the total number of links in the network, in all cases, except the final model (3-zones v.2), the number of links is equal to the total number of nodes -1
- the physical phenomena causing pressure difference: a combination of wind-driven or cross wind-driven and buoyancy,
- the methodology for adjusting the local wind velocity: Cp-method (par.3.6.2) and CFD method (par. 3.7.3)
- the mathematical solver to determine the output data: analytical calculation or iterative calculation.

Initially a single-zone model (*Single-zone*) was analyzed, considering only the effect of wind-driven cross-ventilation, for its simplicity in calculating the unknow variable. Levels of complexity were gradually inserted into the model, moving to multidimensional models. A two-zones air flow model

(*2-zones, v.A*) was firstly developed, maintaining only the wind-driven cross ventilation and secondly (*2-zones, v.B*), combining the buoyancy effect, in this case another external node was added to the network. As the single-zone model, also in these models, the mass conservation balance can be described as a system of two equations and two unknown variables; the external boundary conditions are still enough to analytically solve the system.

Furthermore, the extreme simplification of the schematization of the buildings influenced the choice of simple case studies that easily fell within the field of application of the Cp method, initially chosen to test the proposed methodology.

The intermediate step of the two-zone model was chosen to progressively insert two internal zones heated at different temperatures (apartments and shaft), and for the simplicity of the mathematical relationships in the network; the latter allowed numerous tests to be carried out, to investigate the sensitivity of the model to the variation of values of input data. It has been possible to observe the contribution of the kinetic pressure (wind effect) and potential pressure (chimney effect) in the variation of the air flow. This served to set up the iterative calculation and be able to verify the validity of the chosen algorithms to be applied in the next model version.

The transition to the 3-zone model and the related system of 3 non-linear equations required the use of iterative calculation to determine the solutions and output parameters. The complexity of the network has also been enriched by the more detailed description of the boundary conditions in the external network nodes (two nodes on both sides at two different heights, for a total of 4 external nodes) and of the no-heated shaft zone that communicates simultaneously (4 links converging in a node) with two heated zones separated from each other.

Starting from the 3-zone model, the results of the CFD analysis were applied as input data for the correction of the wind speed that generates surface pressure on the facades; the results were compared with the cp method.

In order to better manage the analysis of the algorithm solutions, initially the 3-zone model was made simpler (3-zone, v.A), predicting the combined effect of the wind-driven and the buoyancy, but without considering the cross ventilation between the two heated zones and the external environment and therefore involving a smaller number of links compared to the subsequent version (3-zones, v.B). The latter model, which coincides with the final version of the lumped parameters model, differs exclusively for the inclusion of cross ventilation which directly links each of the two heated zones and the two nodes representing the external conditions on the same facade in which the shaft is placed.

The last model version (3-zones v.B) represents a final compromise tool that entail for the physical phenomena description, the efficient management of a great number of input variables with different nature, the detailed characterization of the case-study building, a schematic and simple model whose balance equations can be easily replicated to several buildings in urban area.

Table 39. Evolution of the lumped parameter model and main features considered.

Model name	N. of zones	N. of nodes	of which:	N. of links	Effect generating NV	Wind velocity correction method	Solver
Single-zone	1	3	2 out 1 in	2	• Cross wind-driven	Tabular data and Cp method	Analitical solution
2-zones v.A	2	4	2 out 2 in	3	• Cross wind-driven		
2-zones v.B		5	3 out 2 in	4	• Cross wind-driven Buoyancy		
3-zones v.A	3	7	4 out 3 in	6	• Wind-driven • Buoyancy	Cp method vs CFD method	Iterative calculation
3-zones v.B		7	4 out 3 in	8	• Cross wind-driven • Buoyancy		

In the following paragraphs the different models are presented in detail, showing the evolution of the methodology, the application to different case studies and the main results; this allowed us to highlight the limits, identify the objectives of further development and orient the subsequent work steps.

4.5.4. Input data.

All the models studied and proposed were tested by applying the methodology to a real case study in the city of Turin. This choice was mainly dictated by the availability and accessibility of databases relating to weather data, built heritage, and building energy consumption data. For all model presented in this section, three main categories of input data are considered:

-**climatic data** to determine the local boundary conditions of wind velocity and air temperatures, coming from available databases of the local weather station closest to each case study investigated; databases with greater data accuracy (quarter-hourly detail) allow to define the optimal time-step for the analysis depending on the objective: from the selection of extreme climatic conditions, to the average hourly, daily, monthly and seasonal conditions representative of the reference years analyzed.

Weather data has been collected from the weather station of the Living Lab of Polytechnic of Turin, located 32m from the ground (https://smartgreenbuilding.polito.it). Data are quarterly detailed and refer to the years 2010-2024. The data is continuously collected and made accessible and can be downloaded. The city of Turin is located in the climatic zone E with annual local Heating Degree Days (HDD) higher than 2100 and lower than 3000, and the heating season that lasts from October the 15th to April the 15th, according to the refence law (DPR 412/1993).

-**urban morphology parameters** to describe on an urban scale the presence of obstacles (buildings) and the roughness of the terrain that influence the speed and direction of the wind within urban canyons, influencing the path and momentum of the wind, generating windward/leeward zones, turbulence, and pressure variation on building facades. Both methodologies used and compared in this work for the analysis of wind at an urban scale (Chapter 3) use the same urban parameters. Therefore, they apply both to parametric-tabular methods (Cp method) and to the proposed GIS place-based method which uses specific GIS tools and remote sensing techniques to retrieve physical models at an urban scale based on interactions with geometries spatial.

-**building characteristics** which include the typological and dimensional characteristics of the buildings, but also the information from which it is possible to derive the characteristics of the

openings and cracks. The place-based approach used involves using existing databases for spatial planning available (i.e, public technical maps). The pre-processing phase is crucial, considering the large amount and heterogeneity of the information in these databases, the need to standardize the different types of data and geo-reference them. The management of input data is fundamental to associate information at different scales and standardize the different levels of accuracy of the input data, especially those necessary to determine the secondary variables used in the models. Furthermore, the accuracy of the input data directly influences the accuracy of the output data and the application of the entire methodology to other areas of the examined case study.

Some of the geometric and typological characteristics of the buildings used in the parametric model are common to all the models presented in the following paragraphs. Therefore, the pre-processing phase relating to this input data is presented here. Table 40a reports the main input data about building characteristics, divided into categories, indicating the variables' name and unit measure. The primary variables come directly from the municipal technical map, and from them the secondary variables have been retrieved, according to the specific calculation. All geometrical and typological buildings' features are retrieved by the technical maps (BDTRE 2019) in the GIS environment.

Table 40a. Building characteristics.

Category	Variable (primary)	Variable (secondary)	Name	Unit	Source and calculation
General	Building id		B_{id}	[n]	From municipal technical map
	Period of construction		*Period*	[Y]	From municipal technical map
Building dimension	Length		L_{bld}	[m]	From municipal technical map (using GIS query)
	Width		W_{bld}	[m]	From municipal technical map (using GIS query)
	Height		H	[m]	From municipal technical map
		Height of single floor	h_{fl}	[m]	According to Period of construction
		Number of floors	n_{fl_bld}	[n]	According to Eq. (49)
		Height	H_{bld}	[m]	According to Eq. (50)
Zones dimension	Area gross		A_{bld_gross}	[m^2]	From technical maps using GIS tools
		Area net (floor)	A_{fl}	[m^2]	According to Period of construction
		Area shaft (net)	A_{sh}	[m^2]	According to Period of construction
		Volume net	Vol_{bld}	[m^3]	According to Eq. (52)

From public technical database, usually used in urban planning, for each existing building, identified by a unique id code, general information is listed. It is intended here to be a database containing information that is already spatialized or whose non-spatialized information has been integrated with the geometric features within a GIS software in a dedicated pre-processing phase.
Among the general information the *Period of construction* should be reported. This parameter is very important in the description of the building characteristics, as it is used to determine other input data (*Height of single floor, Net floor area, Tightness description*), for each class of construction period, representative of the building stock of the analyzed case study.
For the case study applied in this work, in Table 40b are indicated the building (and leakage) characteristics as a function of the nine class of Period of construction.

Considering the *building dimensions*, the length L_{bld} [m] and width W_{bld} [m] of the building can be determined through a spatial query of the geometry which in the GIS environment is associated with the building element. Regarding the height of the building, depending on the original database, the height in meters or the number of floors may be reported. In both cases, since this parameter strongly influences the evaluation of air flows within the zones, we proceeded with the determination of secondary variables, according to a single procedure, describing the following relationships.
Starting from the height H [m] from the original database, it is possible to attribute the height of a single floor h_{fl} [m] to each building, according to its period of construction. This relationship takes into account the different construction typologies characterizing the different construction periods and obviously must be adapted to each application case study. Then, the number of floors (n_{flbld}) for each building can be determined, according to the rounded results from Eq. (49) and consequently, the final building height H_{bld} [m] is calculated from Eq. (50):

$$n_{fl_{bld}} = \frac{H}{h_{fl}} \tag{49}$$

$$H_{bld} = n_{fl_{bld}} \cdot h_{fl} \tag{50}$$

Regarding the *zone dimensions*, from the spatial query in GIS, it should be always possible to determine the gross floor area of the building A_{bld_gross} [m^2]. The net floor area A_{fl} [m^2] is an important parameter that directly affects the heated volume of the building for each zone in the multizone model. It is derived multiplying the gross floor area and the *fn* parameters. It is calculated according to Eq. (51), considering the thickness of the walls and internal partitions typical of each construction period, as described by the parameter dm in Table 40b:

$$fn = 0.9761 - 0.3055 \cdot dm \tag{51}$$

The net floor area must be adjusted, considering the presence of the shaft in the building. If it is present, the net area of the shaft A_{sh} [m^2] is determined, according to the period of construction (Table 40b), considering the shaft dimension (i.e. length of the shaft L_{sh} [m] on the building façade) and the presence of the elevator.

The net building volume Vol_{bld} [m^3] is then calculated from Eq. (52):

$$Vol_{bld} = \left(h_{fl} - 0.3\right) \cdot n_{fl_{bld}} \cdot A_{bld_{net}} \tag{52}$$

Table 40b. Building and leakage characteristics according to period of construction.

Period of construction	Building characteristics				Leakage characteristics			
	Height of single floor (h_{fl})	Area of the shaft (A_{sh})	Length of the shaft (L_{sh})	dm	Tightness description	Typical Leakage Area (At_leak_w/d)	Equivalent Leakage Area for window (Ae_leak_w)	Equivalent Leakage Area for door (Ae_leak_d)
	[m]	[m^2]	[m]	[-]		[cm^2 /m^2]	[m^2]	[m^2]
<1918	3.3	10.5	2.5	0.5	Very loose	12.0	0.00259	0.00237
1919-1945								
1946-1960		15.2	3.6	0.3				
1961-1970								
1971-1980	3.0	19.5			Loose	9.0	0.00194	0.00178
1981-1990				0.35				
1991-2000				0.4	Average	6.0	0.00130	0.00119
2001-2005								
>2006					Tight	3.0	0.00065	0.00059

4.5.5. Single zone model

The first version of the model is a single zone lumped-parameter model. The air flow motion inside the building is due only to the surface pressure on building facades generated by the incident cross natural ventilation (wind-driven effect); neither temperature and humidity gradient between indoor and outdoor air influence the air changes per hour. The network is made up of 3 nodes and 2 links: one node represents the internal zone of the heated volume of the building, whose pressure conditions are unknown, two nodes represent the external conditions on the two opposite facades, the windward and leeward façade, respectively. The wind velocity is corrected applying the *CpCalc+ method*. Since there is only one unknown variable and all boundary conditions are known, the determination of the output data (mass air flow rate $\dot{m}$) can be solved analytically.

4.5.5.1. Schematization of the building and Input data

The schematization of the building structure is represented in Figure 63: each floor is intended as an independent heated zone; no partitions and internal connections are considered. Symmetrical openings (in number and type) are positioned uniformly on both opposite facades: in this way it is possible to assume cross ventilation on each floor of the building, and so, for each zone to which the model is applied.

The input data concerns climatic data to determine the boundary conditions, urban morphology to determine the pressure coefficients on the building facades with the *CpCalc+* tool (par. 4.2.1.2.), and building characteristics, respectively listed in Tables 41, 42, and 43.

Climate condition. For each prevailing wind direction *WindDir* [°N, clockwise] the monthly wind speed *Vzws* [$m \cdot s^{-1}$] is assessed, based on the data of the nearest weather station (ws) located at height *Zws* [m]. In Figure 63, a temperature *Tin* is assigned to the internal zone in the building and the air temperature *Tout* is assigned to the external environment. Since in this case the pressure difference due to the temperature variation is not considered, the temperatures do not constitute input parameters, but serve only to distinguish and limit the internal heated volume from the external boundary conditions.

Urban scale. As described in the paragraph concerning the calculation of the pressure coefficient Cp, the two useful urban parameters are the Building Coverage Ratio (BCR) [$m^2 \cdot m\text{-}^2$] and the Height of surrounding building (Hsb) [m]. Both are calculated at census section scale in GIS environment [59]. The Plan Area Density (PAD) [$m^2 \cdot m\text{-}^2$] is used to parametrize from reference tabular data the wind velocity profile exponent (υ) [-] and height of the boundary layer (δ) [m], according to the terrain rugosity typical of dense urban areas [132].

Building scale. The general characteristics of the building comprehend its orientation and construction period. The geometrical characteristics include length (*Lbld*), height (*Hbld*), width (*Wbld*), the number of floors (*n_fl*), and the net air volume (Vol) [m^3]; all data are pre-processed as shown in Table 40. The total area of openings (*Aop*) [m^2] corresponds to 1/8 of the (net) floor area *Afl* [m^2], as it represents the minimum glazing area required by law to ensure standard of aero-illumination ratio in the internal environment of a building; then, it is distributed on exposed vertical façades, determining the Window-to-Wall Ratio (WWR). According to reference literature,[151], it is defined as the fraction of the wall area covered by fenestration, and it can be calculated as the ratio of the wall fenestration area to the gross wall area. The optimum WWR to allow the required indoor daylight and natural ventilation is 0.24 to 0.30 (ASHRAE 90.1-2013), but it can be optimized

considering the position of the windows, the orientation of the facades, and the climate conditions, as investigated in ([152]. in this work, the definition of this parameter allows to verify that the hypotheses made are in line with the typical results of residential buildings located in the same boundary conditions; for each floor, the WWR has been determined according to Eq. (53),

$$WWR\ [-] = \frac{A_{op}}{(2 \cdot L_{bld} \cdot h_{fl} \cdot n_{fl})} \quad (53)$$

where the supposed glazing area corresponds to the total area of openings (*Aop*) [m^2], the gross wall area is calculated, considering that only two opposite facades per floor have openings that ensure cross ventilation, L_{bld} [m] is the length of the facades, h_{fl} [m] the height of each floor, and n_{fl} is the total number of floors of the building. Then, the total number of openings on each façade N_{op} was determined.

Table 41. Climate condition input data

Category	Variable	Name	Unit	Source and calculation
Wind attributes	Wind direction	*WinDir*	[° N]	Local weather station (ws)
	Wind speed	*Vzws*	[$m \cdot s^{-1}$]	Local weather station (ws)

Table 42. Urban morphology input data

Category	Variable	Name	Unit	Source and calculation
Urban parameter	Building Coverage Ratio	*BCR*	[$m^2 \cdot m^{-2}$]	From technical maps using GIS tools
	Height of surrounding building	*Hsb*	[m]	From technical maps using GIS tools
	Plan Area Density	*PAD*	[$m^2 \cdot m^{-2}$]	From technical maps using GIS tools
Aerodynamic parameters	wind velocity profile exponent	υ	[-]	Tabular data
	height of the boundary layer	δ	[m]	Tabular data

Table 43. Building characteristics input data

Category	Variable	Name	Unit	Source and calculation
General	Orientation (Azimuth)	*Az*	[°N]	From technical maps using GIS tools
	Roof type (tilt angle)	*Roof*	[°]	From tabular data
Building dimension	Length	L_{bld}	[m]	From municipal technical map using GIS tools
	Width	W_{bld}	[m]	From municipal technical map using GIS tools
	Height	H_{bld}	[m]	According to Eq.(50)
	Area net (floor)	A_{fl}	[m^2]	According to Period of construction
	Volume net	Vol_{bld}	[m^3]	According to Eq.(52)
Opening dimension	Total Area of opening	A_{op}	[m^2]	According to Italian Decree July 5th, 1975
	Window-to-wall ratio	*WWR*	[-]	According to Eq.(53)
	Area of a single window	A_w	[m^2]	Fixed at 2.16
	Total number of openings per floor	N_{op}	[n]	A_{op}/A_w

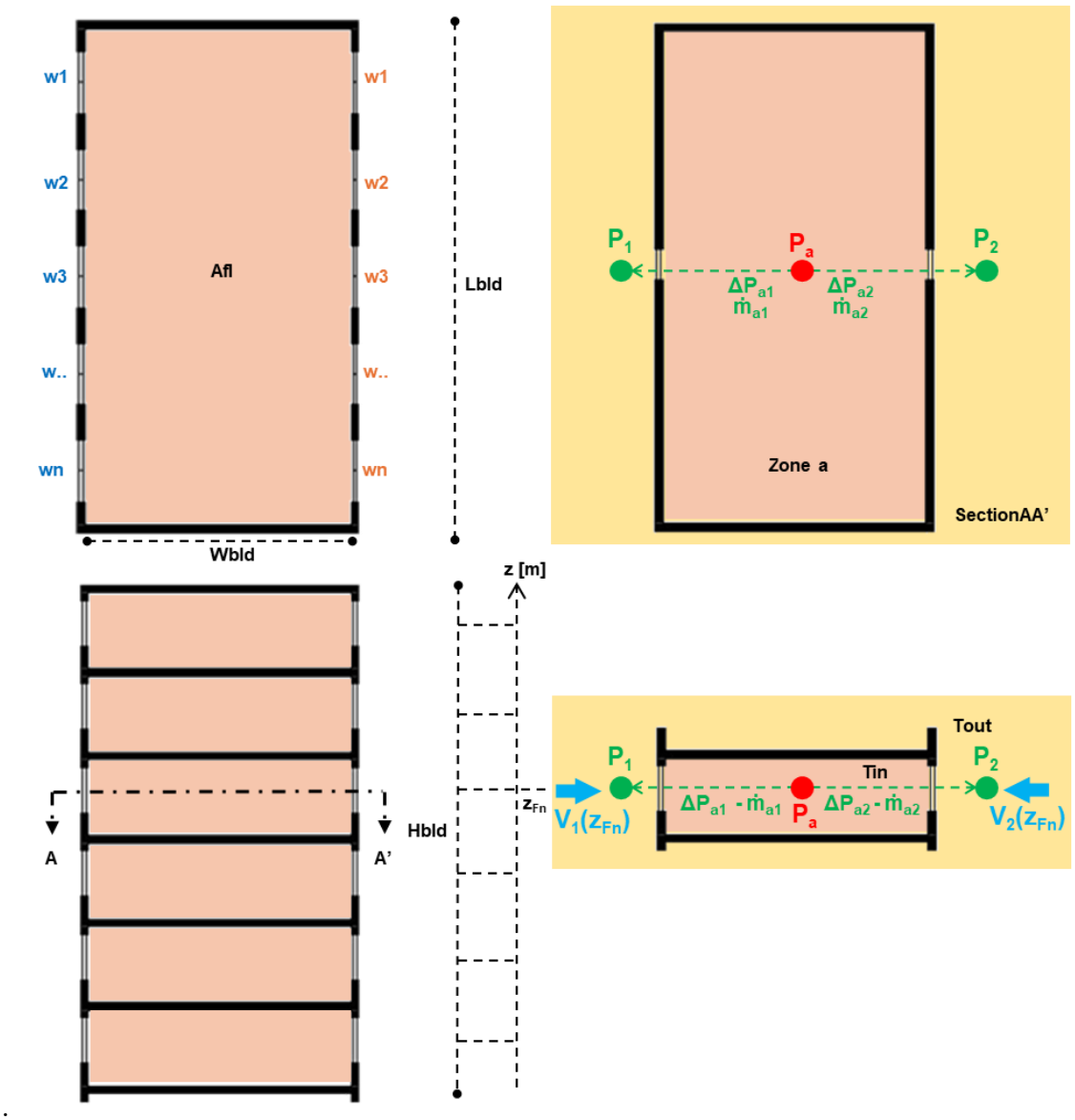

Fig. 63 - Scheme of the single-zone air flow model.

4.5.5.2. Methodology and case study application

The methodology described below has been presented at the CANDO Conference 2021 [31].
The aim of the research work is to assess ventilation loads at urban scale to implement the energy model based on thermal balance equations of residential buildings.
A place-based assessment is proposed that allows the ACH values to be varied monthly in relation to climate conditions, building permeability and the built context.
In Figure 64 is synthetized the methodology applied at two buildings case studies at different orientations whose energy consumption for space heating during the whole heating season of the years 2013-2014 is known.

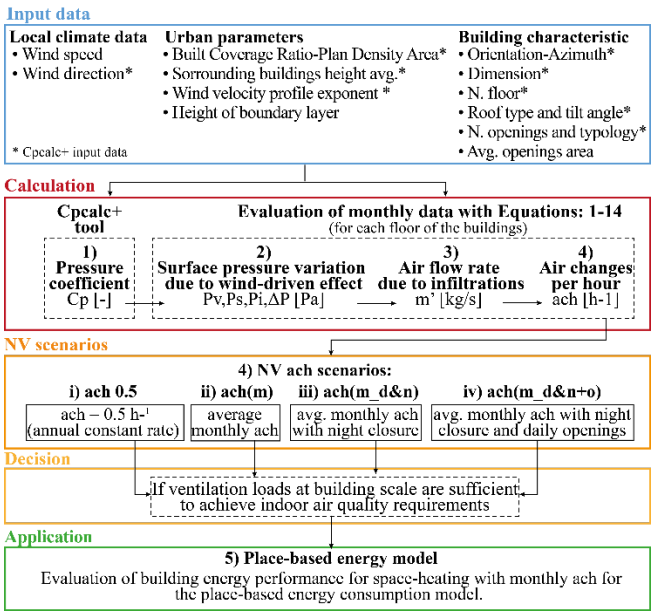

Fig. 64 – Synthetic scheme of the applied methodology in the CANDO research work.

Step A - Monthly average wind speed and direction.

Although the available climatic data were obtained at an hourly time scale, the prevailing eight sectors of wind direction (*WindDir*) (Figure 65a) are defined monthly [153], together with their prevailing frequency (%). Then, to each wind sector the wind incident angle and the monthly mean wind speed (Vz_{ws}) are associated. Figure 65a shows the example for the analysis in December 2014.

(a) (b)

Fig. 65a-b Monthly prevailing wind direction and wind speed frequency (%) on December 2014 (a) for the definition of wind incident angle (θ), according to the azimuth of the building (AzA) and wind direction (DirV) (b).

Step B - Wind speed adjustment.

As described in [154], the reference wind speed Vz_{ws} [m·s^{-1}] should be corrected by the wind incident angle, and considering the characteristics of the analysed context. For each monthly prevailing wind direction *(DirV)* measured clockwise from the north axis to the wind-tail, the incident angle θ [°N] is determined, starting from the definition of the azimuth of the building *Az* [°N] (Figure 65b).

It corresponds to the angle between the north axis and the perpendicular axis from the longitudinal windward façade of the building; consequently, an *Az* angle is monthly determined.
A described by Eq. (54), the adjusted monthly mean wind velocity (*Vzws_corr*) can be assessed by multiplying the reference wind speed (Vz_{ws}) and the cosine of incident angle (θ):

$$V_{zws_{corr}} = V_{zws} \cdot \cos(\theta) \tag{54}$$

The height of the boundary layer (δ) and the wind velocity profile exponent (υ) are chosen from the values listed in Table 44 (already presented in chapter 3), after having identify the terrain roughness types of the case study for medium-high density urban areas [132].

Table 44. Reference terrain roughnesses typologies.

Terrain roughness type	***δ* [m]**	***υ* [-]**
Level surface, surfaces of water basins, grass land	250	0.10
Flat open country with few, very small, and scattered obstructions	280	0.14
Rolling or level surfaces broken by numerous obstruction	300	0.22
Heterogeneous surface with obstacles larger than one story	330	0.28
Low density suburban areas	390	0.34
Medium-high density urban areas	450	0.40
Very high density city areas	510	0.45

The monthly average wind velocity V_H [m·s^{-1}] at the height *z* [m] of the analysed opening at each floor (Fn) of the building is determined by the power law equation for wind speed correction at urban scale (see chp.3), as presented in Eq. (55):

$$V_{H(z_{Fn})} = V_{zws\_corr} \cdot \left(\frac{\delta_{ws}}{z_{ws}}\right)^{\upsilon_{ws}} \cdot \left(\frac{\delta_{ZFn}}{z_{Fn}}\right)^{\upsilon_{zFn}} \tag{55}$$

where z_{ws} and z_{Fn} are the height of the weather station (*ws*) and the height of each of the n floors (*Fn*) of the building, respectively. Each floor is equipped with openings of equal size and with uniformed positions on facades; therefore, a monthly V_H is obtained for each of the *n* floors at height z_{Fn}. All equations that will be described in the following steps are repeated for both the Windward Façade (WF) and the Leeward Façade (LF) at every floor (Fn), and for each month during the heating season.

Step C - Wind pressure coefficients.

The wind pressure distribution on building's envelope is assessed dealing with the Cp coefficients, using the Cpcalc+ tool [107]. Most of the requested input data (Table 36) are already determined: climate parameter (wind direction), urban parameters, building typology and dimensions, respectively in Tables 41, 42, and 43. Coordinate x, respect to the façade length L_{bld}, and z respect to the façade height H_{bld}, are used to describe the position of each opening on both façades (WF and LF), distinguishing each floor Fn with n the total number of floors in the building, as schematized in Figure 66. A *Cp* value is obtained for each opening, on both the windward (WD) and the leeward (LW) façades, on each floor *Fn*, and for all months during the heating season.

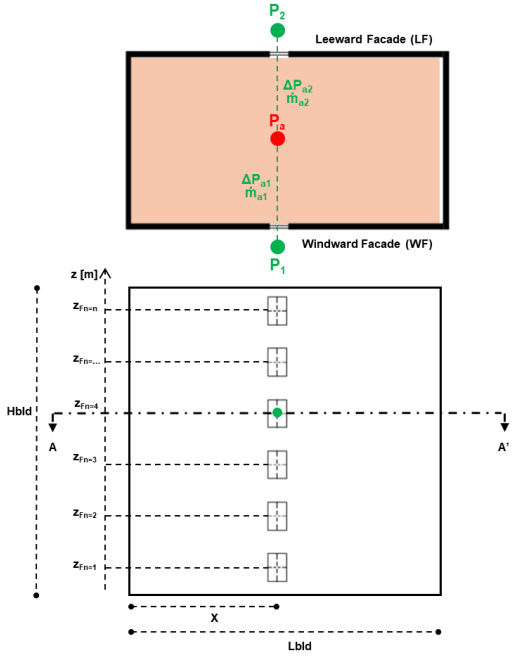

Fig. 66 - Scheme of the façade element positioning, for both the windward and leeward facades.

Step D – Surface pressure, air flow rate and ACH.

As schematized in Figure 66, each floor *Fn* is a single air flow zone, with an equal number of openings (*w)* on two opposite facades. To assess the surface pressure by the incident natural wind (wind-effect), the dynamic pressure p_{dyn} is calculated on both the windward (WF) and the leeward (LF) façades, according to Eq. (56), applying the *Cp-method*.

$$p_{dyn} = \frac{1}{2}\rho \cdot Cp \cdot V_H^2 \tag{56}$$

where: V_H is the corrected wind velocity [m·s^{-1}], ρ [kg·m^{-3}] is the outdoor air density, and Cp [-] is the pressure coefficient at leakage's position.

Applying the conservation of the mass law, at node a in the internal heated zone the mass balance of air flow rate is expressed by Eq. (57). The balance between surface pressure variations named ΔP_{a1} and ΔP_{a2} is described by Eq. (58):

$$\dot{m}_{a1} + \dot{m}_{a2} = 0 \tag{57}$$

$$\Delta P_{a1} + \Delta P_{a2} = 0 \tag{58}$$

where ΔP_{a1} is the difference between the outdoor pressure P_1 on the windward facade and the indoor pressure P_a and ΔP_{a2} is the difference between the outdoor pressure P_2 on the leeward facade and the indoor pressure P_a, (Figure 66). Consequently, the indoor pressure P_a is analytically determined in Eq. (59):

$$P_a\,[Pa] = \frac{\rho \cdot (V_H)^2}{24} \cdot (C_{p1} + C_{p2}) \tag{59}$$

where: V_H is the adjusted wind velocity [m·s^{-1}], ρ [kg·m^{-3}] is the outdoor air density, C_{p1} and C_{p2} [-] are the pressure coefficient, respectively for the windward and leeward façade.

Then the mass flow rate $\dot{m}$ is calculated applying Eq. (35), as a function of opening's leakage dimensions and typology, and the above-mentioned pressure deltas. Separately for each single zone (floor), the monthly ach is calculated (Eq. 60), since the air volume inside the building (Vol_{bld}) is known:

$$ach\ \left[\frac{1}{h}\right] = \frac{\dot{m} \cdot 3600}{\rho \cdot Vol_{bld}} \tag{60}$$

Step E – Hypothesis of ach in the energy building model

Several hypothetical scenarios are defined to investigate how the monthly ACH variations can affect the space-heating energy demand of the case study buildings: the GIS-based engineering energy model [61] is applied and its results are compared with real consumption data of the heating season 2013-14. The scenarios hypothesis for the assessment of the average monthly ACH are:

- *ach(m) scenario*, in which a constant discharge coefficient of Cd=0.65 is applied;
- *ach(m_d&n) scenario* – in which an extra closure of opening during night-time is supposed considering shutters, and different discharge coefficients Cd are applied in daily and night-time (0.65 and 0.55, respectively);
- *ach(m_d&n+o) scenario* – in which the opening of windows occurs both at night-time and three times a day (at 7 a.m., 2 p.m. and 9 p.m.) for 15 minutes each.

All the scenarios listed above are compared with the baseline *ach(0.5) scenario* in which the monthly ACH is fixed and equal to 0.5 [h^{-1}].

Case study zone and buildings

Figure 67a-b shows the buildings case-studies in the selected neighbourhood of Crocetta district, in the centre of the city of Turin, located near the weather station from which climatic data were collected. The residential buildings named ID 23534 and ID 23582 are representative of the urban building stock with two typical orientations: the NE-SW with an inclination angle of 30° (±5°) and the NW-SE with an inclination angle of -60° (±5°) [26].

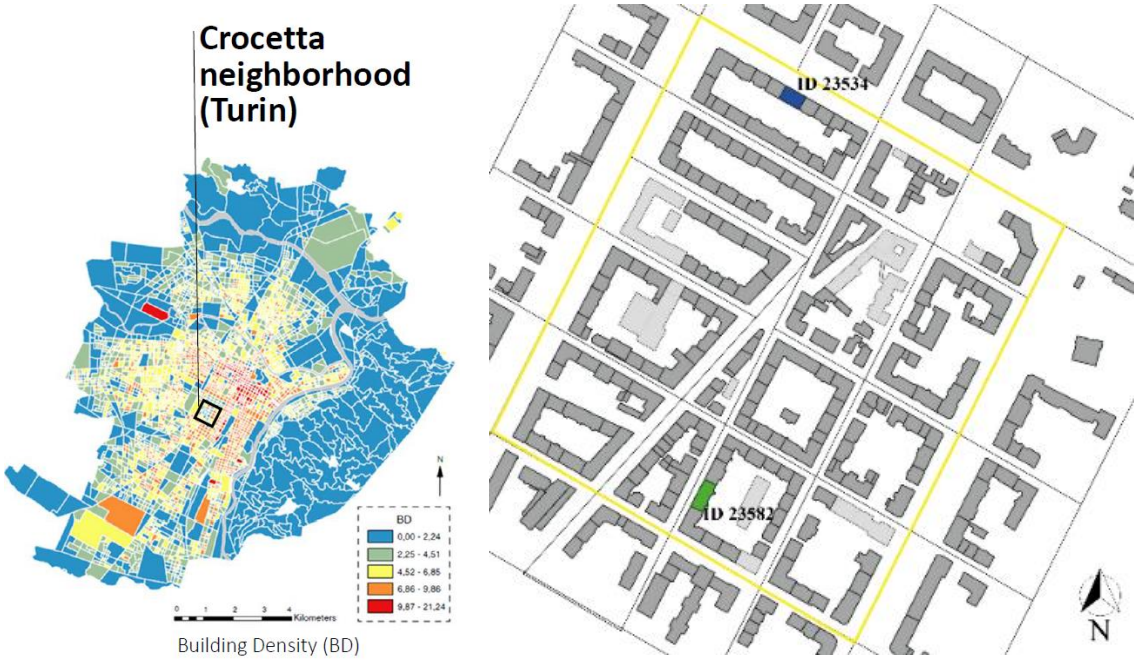

(a) (b)

Fig. 67a-b - Localization of the case study district in Turin (a) and the two selected buildings named ID23534 (blue) and ID23582 (green).

At urban scale, the two buildings refer to the same census sections [64]; so, the urban parameters are also the same for both buildings, and are listed in Table 45. Regarding building characteristics,

both buildings have a double slope roof (tilt angle of 15-20°), while they differ for their orientation, dimensions, and openings, as shown in Table 46.

Only one types of opening is considered: windows with double shutter casement, characterised by a discharge coefficient of 0.65 [-] and a very loose air tightness that correspond to the lowest typical leakage area $A_{t,leak}$ reported in Table 46.

Table 47 lists the monthly climatic data applied in the model for both years of the referring heating season(2013-14): in the brackets of columns WindDir is indicated its frequency with reference to the total hour in each month.

Table 45. Characteristics of the case study district.

Urban scale input data				
Urban parameter			*Climatic coefficient*	
Built Coverage Ratio (BCR)	**Plan Area Density (PAD)**	**Surrounding buildings height (Hsb)**	**Height of boundary layer (δ)**	**Wind velocity profile exponent (υ)**
[m^2/m^2]	**[m^2/m^2]**	**[m]**	**[m]**	**[-]**
0.38	7.78	25	450	0.4

Table 46. Characteristics of the two case-studies buildings.

Building	Construction period	Orientation	Dimension (LxHxW) [m]	Net Air Volume [m^3]	N floors	N openings	Window-to-wall ratio [-]	Opening area (avg) [m^2]
ID 23534	1916-1945	NE-SW	23x32x14	7391.6	9	54	0.3	2.88
ID23582	1946-1960	NW-SE	30x19x13	4431.9	5	45	0.22	2.97

Table 47. Climate characteristics in the years 2013-2014.

Weather input data								
	T_{avg} [°C]		I_{sol} [W/ m^2]		WindDir [°] (freq %)		Vws [m/s]	
	2013	*2014*	*2013*	*2014*	*2013*	*2014*	*2013*	*2014*
1	5.0	6.1	60.2	49.3	22.5 (41%)	**22.5 (34%)**	1.18	0.99
2	4.3	7.4	85.6	78.6	22.5 (29%)	**22.5 (29%)**	1.23	1.22
3	8.2	12.3	114.4	150.5	22.5 (22%)	**22.5 (26%)**	1.19	1.39
4	13.9	15.8	143.3	178.5	22.5 (17%)	**22.5 (22%)**	1.32	1.44
5	16.3	18.0	212.8	218.7	22.5 (16%)	22.5 (21%)	1.63	1.40
6	22.4	22.7	246.5	230.5	292.5 (18%)	337.5 (18%)	1.59	1.73
7	26.0	22.7	248.9	210.5	22.5 (19%)	22.5 (19%)	1.61	1.47
8	24.8	22.5	231.1	188.7	337.5 (17%)	292.5 (20%)	1.54	1.47
9	20.8	20.4	163.0	154.0	292.5 (16%)	292.5 (18%)	1.35	1.32
10	15.0	16.7	73.4	94.1	**22.5 (21%)**	22.5 (18%)	0.96	0.99
11	9.8	11.1	60.3	49.7	**22.5 (23%)**	22.5 (32%)	1.21	0.97
12	6.0	6.8	54.6	46.0	**22.5 (46%)**	22.5 (34%)	0.99	1.04

Three prevailing wind direction (22.5°- 292.5°- 337.5°) are observed (Table 47). Since, only the months in the heating season (from October 2013 to April 2014) will be evaluated, a unique prevailing wind direction is considered: it corresponds to 22.5° and it will be applied in the pressure coefficients calculations (Fig.68).

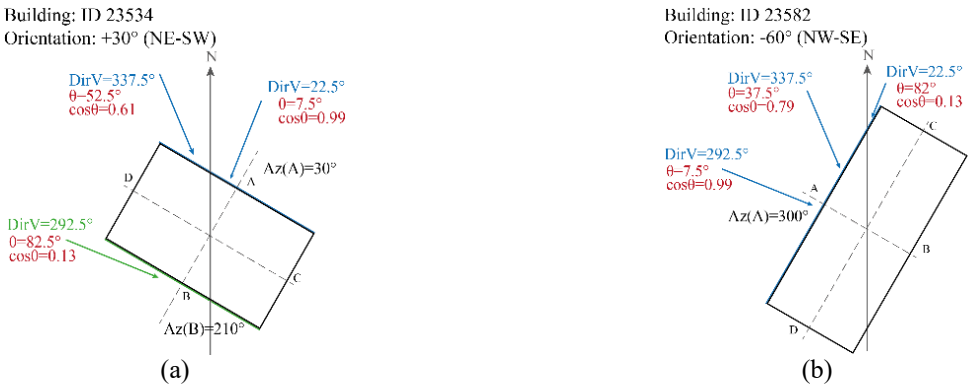

Fig. 68a-b – The azimuth angle (Az) and wind incident angle (θ) for the three prevailing wind directions (DirV) in each of the two case-studies building with NE-SW (a) and NW-SE (b) different orientations.

4.5.5.3. Results & Discussion

Results of the average monthly pressure coefficient Cp during the heating season 2013-2014 are listed in Table 48. For both case-studies buildings the results are detailed considering separately the windward (WF) and leeward (LF) façades with their orientations and floor number, five and nine floors, respectively for the ID 23582 and ID 23534 building. The higher the floor number, the higher the Cp value, due to the rise of wind speed; this is true for both buildings and in particular for the windward (WF) façades.

Table 48. Average monthly pressure coefficients at building floor F.

Building		F1	F2	F3	F4	F5	F6	F7	F8	F9
ID 23534	**WF 30°**	0.040	0.027	0.014	0.025	0.042	0.104	0.191	0.284	0.409
	LF 210°	-0.024	-0.027	-0.027	-0.028	-0.026	-0.028	-0.032	-0.045	-0.049
ID23582	**WF 300°**	-0.051	-0.018	-0.051	-0.172	-0.247	-	-	-	-
	LF 120°	-0.063	-0.079	-0.081	-0.079	-0.087	-	-	-	-

Table 49 reports the average monthly ACH results during the heating season 2013-2014, separately for the daily (d) and night (n) scenarios for each of the two buildings. High differences around the +41% are observed on monthly ACH; so, the definition of an annual average ACH value will not be accurate and representative of the whole heating season.

Table 49. Average monthly ACH in the 2013-2014 heating season.

Building		Oct-13	Nov-13	Dec-13	Jan-14	Feb-14	Mar-14	Apr-14
ID 23534	**d**	0.229	0.287	0.234	0.235	0.289	0.330	0.342
	n	0.120	0.118	0.126	0.120	0.148	0.169	0.175
ID23582	**d**	0.012	0.015	0.012	0.012	0.015	0.017	0.018
	n	0.010	0.013	0.010	0.010	0.013	0.015	0.015

The resulting average seasonal value of ACH is assessed and shown in Table 50 to compare the results of all scenarios evaluated for each of the two buildings. The not well exposed building ID23582 shows insufficient ACH values that cannot ensure good indoor air quality conditions, except in the m_d&n+o scenario, when the windows are opened 3 times a day for 15 minutes (at 7 a.m. and at 2 and 9 p.m.).

Table 50. Average seasonal ACH for the four scenarios.

Building	*Ach(0.5)*	*ach(m)*	*ach(m_d&n)*	*ach(m_d&n+o)*
ID 23534	0.5	0.276	0.225	0.466
ID23582	0.5	0.0145	0.0136	0.276

In the graphs of Figure 69a-b, results of the monthly energy demand (MWh) for the buildings' space heating in each of the four scenarios are compared to the real consumption data (Fig.69 a-b, blue histograms), showing the importance of a monthly variation of ACH parameters based on natural ventilation assessments. In fact, regarding the wind-exposed building ID 23534 (Fig. 69a), the relative errors of the energy consumption predicted by the model are equal to: 20.2% in the base-line *ach(0.5)* scenario, 11% in the *ach(m_d&n+o)* scenario, 0.9% in the *ach(m)* scenario, and 0.6% in the *ach(m_d&n)* scenario. Regarding the not-wind exposed building ID 23582 (Fig. 69b), the *ach(0.5)* scenario reports the best relative error equal to (-)7.3%; since the wind is not sufficient for guarantee air quality requirements, this is the best scenarios, followed by the *ach(m_d&n+o)* scenario in which an error of (-)16.5 % occur.

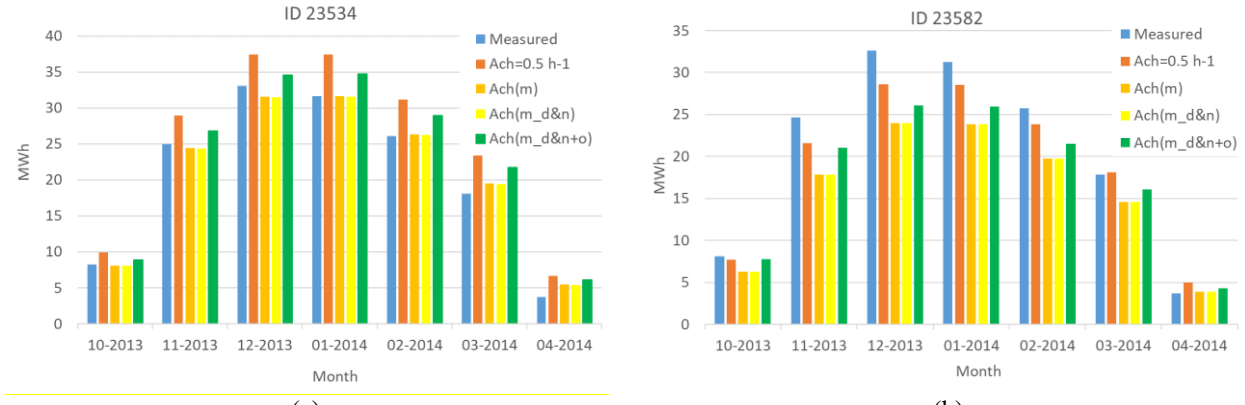

Fig. 69a-b – Comparison of the four scenarios considering the space heating energy demand of both the wind-exposed building ID23534 (a) and the not wind-exposed building ID 23582 (b).

The main finding of the analysis show that ACH values are not constant during the heating season: they are affected by the building orientation and height, and this introduces the possibility to improve the GIS place-based engineering energy model assessing hourly variation of ACH.

In fact, ventilation loads at building and block of building scale can be assessed with an hourly time-shift, for both the heating and cooling seasons.

As it has represented an introductory study, further developments are the following:

- a great number of wind directions can be considered to increase precision of input data
- openings and leakages can be better characterized in terms of size and typology
- internal partition and connection between floors can be added to assess air flow rate considering the stack effect and gradient of temperature inside-outside the building.

4.5.6. Two-zones model- versions v.A and v.B

A two-zones air flow model (2-zones, v.A) was firstly developed, maintaining only the wind-driven cross ventilation and secondly (2-zones, v.B), combining the buoyancy effect, and adding another external node to the network. As the single-zone model, also in these models, the wind velocity is corrected applying the Cp method. The mass conservation balance can be described as a system of two equations and two unknown variables; the external boundary conditions are still enough to analytically solve the system of equations.

4.5.6.1. Schematization of the building and Input data

The schematization of the building structure is represented in Figure 70a-c. The main implementation is the presence of the shaft in the real building structure (Fig.70a). Although the shaft is a connecting element between all the floors, and therefore constitutes a single volume, in both versions of the 2-zones model it is considered divided by the number of floors of the building; each floor is a separate and independent heated zone. To each floor (section AA' in Fig. 70), two internal areas correspond: the apartments (no partitions and internal connections are considered), represented by node *a,* and the shaft, represented by node *b*; the two areas are connected by a single door opening.
The openings towards the outside (windows *w*) are all the same in size, type, and position on the facade. The number of openings on the leeward facade (LF) is less than one unit compared to those on the windward facade (WF). This is due to the presence of the shaft which communicates with the

external environment through a single window of standard size in the model v.A (w1 in purple, Fig.14a). In the case of the model v.B, two windows are considered (w1 and w2 in purple, Fig.14a) , that have half the standard size and are positioned at two different heights; the barycenter of the openings is positioned respectively at 1/3 and 2/3 of the internal height of the shaft.

In the 2-zone model v.A (Fig.70b), the network is made up of 4 nodes and 3 links: two nodes (*a* and *b*) represent the two internal zones, whose pressure conditions are unknown, two nodes (P_1 and P_2) represent the external conditions on the two opposite facades, the windward (WF) and leeward (LF) façades, on which the wind velocity V_1 and V_2 occur, respectively. In the v.A version, the two internal zones are at the same temperature (T_{in} in Fig.70b) to distinguish it from the external temperature T_{out}, but both temperatures are not used as the only cause of natural ventilation is wind-driven effect.

In the 2-zone model v.B (Fig.70c), the network is made up of 5 nodes and 4 links: the two internal zones (nodes *a* and *b*) to which the temperatures T_{in} (heated apartments) and T_{sh} (unheated shaft) are assigned, respectively, to also consider the buoyancy effect inside the shaft. This effect is evaluated also considering three nodes that describe the external conditions on the two opposite facades: one node (P1) on WF and 2 nodes (P2 and P3) on LF. The last two nodes connect the shaft and the outside, each one through the window positioned at a different height, describing the wind speeds V2 and V3 respectively.

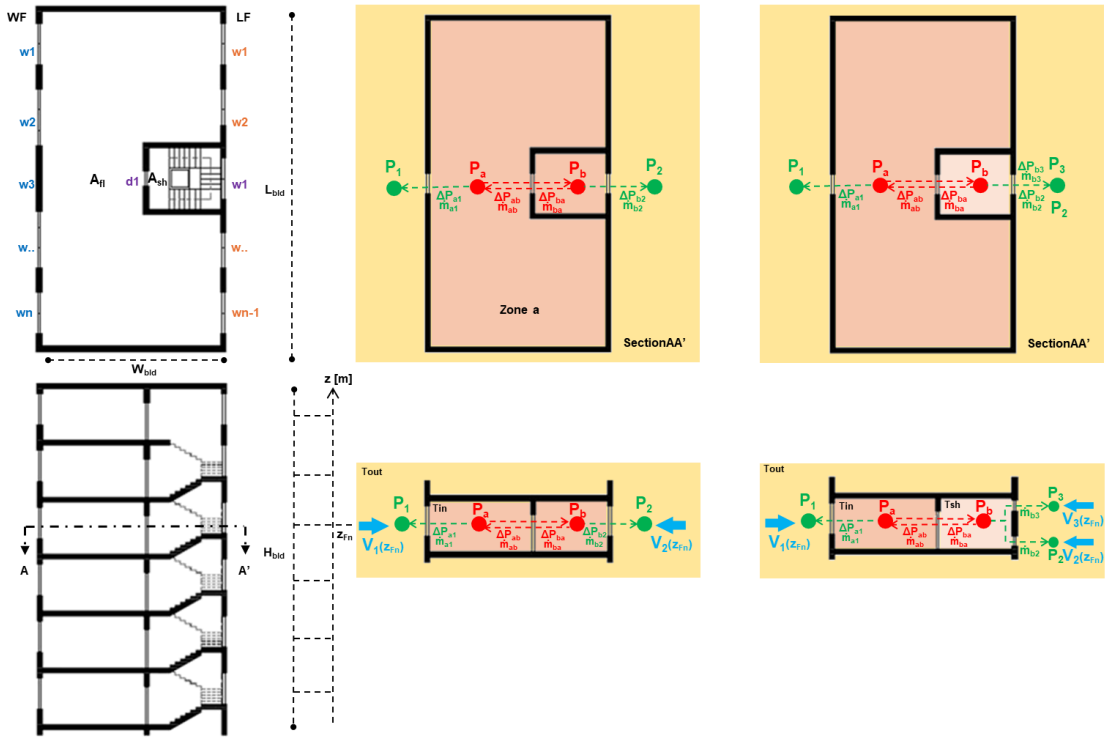

Real building (a) | Version A (b) | Version B (c)

Fig. 70a-c Scheme of the 2-zones air flow model from the real building.

The input data concerning environmental climate conditions are listed in Table 51: in addition to the variables about wind attributes, already described in the single-zone model, there are those relating to air temperatures.

The outdoor air temperature T_{out} comes from the reference weather station. The indoor air temperature T_{in} is assigned to heated zones of the building; according to local climate of the case study, it refers to a fixed set point temperature prescribed for heating and cooling seasons by the current national legislation (DPR 412/93). In this case study, the set point temperature to ensure comfort conditions inside the building are 20°C and 26°C, respectively for the heating and cooling season.

The temperature in the shaft which a no-heated zone can be assessed by Eq. (61):

$$T_{sh}[°C] = T_{out} + b_{tr,u} \cdot (T_{in} - T_{out}) \quad (61)$$

where: $b_{tr,u}$ [-] is a correction factor provided by standards in case of "*confined spaces with an external wall and one window"* (Table 5 in the Appendix A, UNI/TS 11300-1: 2014), and it equals to 0.4.

In each heated or no-heated zone, the air density [kg·m^{-3}] can be determined according to Eq. (62); it is calculated considering the reference dry air's density, which is measured at 0 m a.s.l (ρ_{ref} = 1.29 kg·m^{-3}) and at fixed temperature T_{ref} (-273.15 K); the examined temperatures (out, in and sh) should be expressed in Kelvin degrees (T_K):

$$\rho[\mathrm{kg} \cdot m^{-3}] = \frac{(\rho_{ref} \cdot T_{K,ref})}{T_K} \quad (62)$$

All the input data concerning the urban parameters and the building characteristics described in the single-zone model are considered in both versions of the 2-zones model. Due to the implementation of the building schematization and the network, new variables have been added considering the building and the leakage characteristics, these are listed in Table 52a (in bold) and Table 52b, respectively.

Table 51. Climate condition input data

Category	Variable	Name	Unit	Source and calculation
Wind attributes	Wind direction	*WinDir*	[° N]	Local weather station (ws)
	Wind speed	*Vzws*	[m·s^{-1}]	Local weather station (ws)
Air temperature	Outdoor air temperature	*Tout*	[° C, K]	Local weather station (ws)
	Indoor set temperature (heated zones)	*Tin*	[° C, K]	According to the HDD and current legislation
	Indoor air temperature (no-heated shaft)	*Tsh*	[° C, K]	According to Eq. (61)
Air density	Outdoor, indoor, in shaft	ρ	[kg·m-^{3}]	According to Eq. (62)

Table 52a. Building characteristics input data

Category	Variable	Name	Unit	Source and calculation
General	Orientation (Azimuth)	*Az*	[°N]	From technical maps using GIS tools
	Roof type (tilt angle)	*Roof*	[°]	From tabular data
Building dimension	Length	L_{bld}	[m]	From municipal technical map using GIS tools
	Width	W_{bld}	[m]	From municipal technical map using GIS tools
	Height	H_{bld}	[m]	According to Eq. (50)
	Area net (floor)	A_{fl}	[m^2]	According to Period of construction (Table 40b)
	Area shaft (net)	A_{sh}	**[m^2]**	**According to Period of construction** (Table 40b)
	Volume net	Vol_{bld}	[m^3]	According to Eq. (52)
Opening dimension	Total Area of opening	A_{op}	[m^2]	According to Italian Decree July 5th, 1975
	Window-to-wall ratio	*WWR*	[-]	According to Eq. (53)

	Area of a single window	A_w	[m^2]	Fixed at 2.16
	Area of a single door	A_d	**[m^2]**	**Fixed at 1.98**
	Total number of openings per floor	N_{op}	[n]	A_{op}/A_w

Table 52b. Leakage characteristics input data

Category	Variable	Name	Unit	Source and calculation
Leakage dimension	Typical leakage area of a single window/door	$A_{t,\ leak}$ w/d	[cm^2 /m^2]	According to Period of construction (Table 40b)
	Equivalent leakage area of a single window/door	$A_{e,leak}$ w/d	[m^2]	According to Eq. (43)
Leakage type	Discharged coefficient	Cd	[-]	Fixed at 0.65
Motion type of air	Flow coefficient	n	[-]	Fixed at 0.65
K coefficient	for a single window/door	k_{ref}	[$kg \cdot s^{-1} \cdot Pa^{-n}$]	According to Eq. (46)
	for all windows/doors in the zone	k	[$kg \cdot s^{-1} \cdot Pa^{-n}$]	According to Eq. (46)
Node heights	Internal nodes (a, b)	z_a - z_b	[m]	Barycenter of the zone'height (h_{fl})
	External nodes on façade WF	z_1	[m]	$z_1 = z_a = z_b$
	External nodes on façade LF (model v.A)	z_2	[m]	$z_2 = z_a = z_b$
	External nodes on façade LF (model v.B)	z_2 - z_3	[m]	$z_2 = 1/3\ z_b$ $z_3 = 2/3\ z_b$

4.5.6.1.1. Methodology

The aim of the analysis applying the 2-zones model version A was to implement the network (2 unknow internal nodes) just enough to still solve the system of the two non-linear equations analytically.
The aim of the analysis applying the 2-zones model version B was to enrich the calculation of the pressure variations also considering the buoyancy effect. It has been possible to observe the contribution of the kinetic pressure (wind effect) and potential pressure (buoyancy effect) in the variation of the mass air flow. This served to set up the iterative calculation and be able to verify the validity of the chosen algorithms to be applied in the next model version.
For both the 2-zone model versions (*v.A* and *v.B*), the methodology described in paragraph 4.5.5.2 has been conducted, from *step A* to *step C*; it refers to the correction of wind speed and the definition of the pressure coefficient *Cp* at each external nodes on windward façade (node 1) and on leeward façade (nodes 2-3).

As schematized in Figure 70b, each floor *Fn* is intended as a single air flow zone, so the following methodologies, different for version A (only wind-driven) and version B (wind-driven + buoyancy) are applied to a single floor, and they can be replicated for all floors of the building.

Methodology of 2-zones model version A.

Since the boundary conditions concerning the wind attributes are all know, the surface dynamic pressure incident on building façades at the height of each external node (1 and 2, respectively on windward and leeward facades) is calculated considering only the kinetic contribution, as presented in par. 4.5.2. The Eq. (45) is applied in Eq. (63.1) and Eq. (63.2), for calculating P_1 and P_2, respectively.

$$P1 = \frac{1}{2}\rho_{out} \cdot Cp_1 \cdot V_{H(z1)}^2 \quad (63.1)$$

$$P2 = \frac{1}{2}\rho_{out} \cdot Cp_2 \cdot V_{H(z2)}^2 \quad (63.2)$$

where: ρ_{out} [kg·m^{-3}] is the outdoor air density, C_{p1} and C_{p2} [-] are the pressure coefficients at leakage's position, respectively for the windward and leeward façade, V_H is the adjusted wind speed [m·s^{-1}] at leakage's height.

In this scheme, all nodes are positioned at the same height (z_a=z_b=z_1=z_2) and the pressure coefficient Cp are calculated with the *Cpcalc+* tool. The pressure conditions (P_a and P_b) of the two zones inside the building are not known.

Applying the conservation of the mass law, at each internal node (*a* and *b*) in the network (Fig.71), considering positive the outgoing fluxes, the mass balance of air flow rate $\dot{m}$ is expressed at each link, by the 2-equation system in Eq. (64). Applying the relationship between the mass air flow rate and the pressure variation ΔP, at each link between two nodes, the previous equation can be rewritten as Eq. (65):

$$\begin{cases} \dot{m}_{a1} + \dot{m}_{ab} = 0 \\ \dot{m}_{ba} + \dot{m}_{b2} = 0 \end{cases} \quad (64)$$

$$\begin{cases} K_{a1}\,(\Delta P_{a1})^n + K_{ab}\,(\Delta P_{ab})^n = 0 \\ K_{ba}\,(\Delta P_{ba})^n + K_{b2}\,(\Delta P_{b2})^n = 0 \end{cases} \quad (65)$$

where ΔP [-] are the pressure variation at each link (i.e., Pa1=Pa-P1), Ka1 and Kb2 [kg·s-1·Pa-n] are the flow coefficients at the external opening (window), Kab and Kba [kg·s-1·Pa-n] are the flow coefficients at the internal opening (door), and is the flow coefficient, fixed at 0.65 [-].

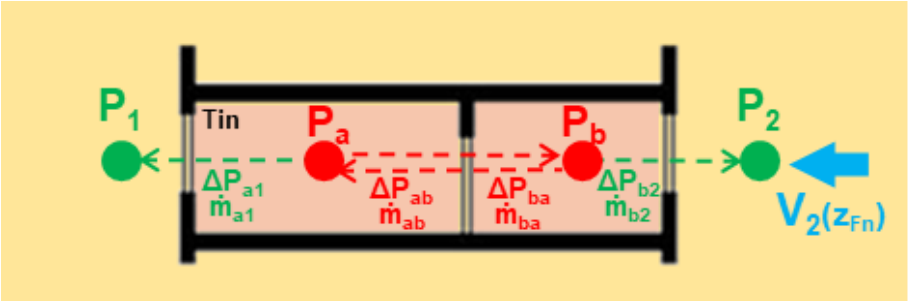

Fig. 71 – Scheme of the 2-zones model version A.

By substituting the known values of the pressures at each node, it is possible to rewrite the system as Eq. (66):

$$\begin{cases} K_{a1}\,(\boldsymbol{P_a} - P_1)^n + K_{ab}\,(\boldsymbol{P_a} - \boldsymbol{P_b})^n = 0 \\ K_{ba}\,(\boldsymbol{P_b} - \boldsymbol{P_a})^n + K_{b2}\,(\boldsymbol{P_b} - P_2)^n = 0 \end{cases} \quad (66)$$

Since only Pa and Pb are the unknow variables, they constitute the output data and the solution of the system of two equations and two unknow variables that can be solved analytically, by imposing:

$$\begin{cases} f(P_a) = P_b \\ f(P_b) = P_a \end{cases} \quad (67)$$

Since the equations of the system are not linear, the number of possible solutions is greater than one for each unknown variable. Due to this reason, after the procedure described from Equations (68.1-3), it will be necessary to verify the signs (flow directions) of the two solutions of the system, comparing them to those initially hypothesized, so that the mass balance at each node is null.

$$\begin{cases} |(\boldsymbol{P_a} - \boldsymbol{P_b})|^{n^{\frac{1}{n}}} = \alpha \cdot |(\boldsymbol{P_a} - P_1)|^{n^{\frac{1}{n}}} \\ |(\boldsymbol{P_b} - \boldsymbol{P_a})|^{n^{\frac{1}{n}}} = \beta \cdot |(\boldsymbol{P_b} - P_2)|^{n^{\frac{1}{n}}} \end{cases} \quad \text{with} \begin{cases} \alpha = |\left(-\frac{K_{a1}}{K_{ab}}\right)|^{\frac{1}{n}} \\ \beta = |(-\frac{K_{b2}}{K_{ba}})|^{\frac{1}{n}} \end{cases} \tag{68.1}$$

$$\begin{cases} \boldsymbol{P_a} = +\frac{1}{\gamma}\boldsymbol{P_b} - \frac{\alpha}{\gamma}P_1 \\ \boldsymbol{P_b} = +\frac{1}{\delta}\boldsymbol{P_a} - \frac{\beta}{\delta}P_2 \end{cases} \quad \text{with} \begin{cases} \gamma = (1-\alpha) \\ \delta = (1-\beta) \end{cases} \tag{68.2}$$

$$\begin{cases} \boldsymbol{P_a} = f(\boldsymbol{P_b}) = -\frac{\alpha}{\gamma\varepsilon}P_1 - \frac{\beta}{\delta\gamma\varepsilon}P_2 \\ \boldsymbol{P_b} = f(\boldsymbol{P_a}) = -\frac{\alpha}{\delta\gamma\varepsilon}P_1 - \frac{\beta}{\delta\varepsilon}P_2 \end{cases} \quad \text{with} \begin{cases} \varepsilon = (1 - \frac{1}{\gamma\delta}) \end{cases} \tag{68.3}$$

The signs of the results are verified imposing the following conditions Eq. (69.1-4), remembering that the positive sign indicates an air flow exiting the node, the negative sign indicates an air flow entering the node. Separately for each of the 4 links, the sign of the mass air flow rate is confirmed or made opposite in relation to the sign of the pressure difference between the two nodes connected by each link:

$$if\ \Delta P_{a1} > 0 \rightarrow (P_a - P_1) > 0 \quad then\ \dot{m}_{a1} = K_{a1}\,(\Delta P_{a1})^n \quad else\ \ \dot{m}_{a1} = -[K_{a1}\,(\Delta P_{a1})^n \tag{69.1}$$

$$if\ \Delta P_{ab} > 0 \rightarrow (P_a - P_b) > 0 \quad then\ \dot{m}_{ab} = K_{ab}\,(\Delta P_{ab})^n \quad else\ \ \dot{m}_{ab} = -[K_{ab}\,(\Delta P_{ab})^n] \tag{69.2}$$

$$if\ \Delta P_{ba} > 0 \rightarrow (P_b - P_a) > 0 \quad then\ \dot{m}_{ba} = K_{ba}\,(\Delta P_{ba})^n \quad else\ \ \dot{m}_{ba} = -[K_{ba}\,(\Delta P_{ba})^n] \tag{69.3}$$

$$if\ \Delta P_{b2} > 0 \rightarrow (P_b - P_2) > 0 \quad then\ \dot{m}_{b2} = K_{b2}\,(\Delta P_{b2})^n \quad else\ \ \dot{m}_{b2} = -[K_{b2}\,(\Delta P_{b2})^n] \tag{69.4}$$

Further condition to verify is that the sign of the airflow ṁab at link a→b is opposite to the sign of the airflow ṁab at link b→a, so Eq. (70) should be verified:

$$\dot{m}_{ab} = -\,(\dot{m}_{ba}) \tag{70}$$

Since the two links are associated with the same opening that connects the two internal areas a and b, only one direction of the air flow is possible in correspondence with the leakage, in relation to the pressure difference between the two areas.

After having calculated each mass air flow rate and substituting the resulting values in the system equations (Eq.64), if both the two equations are zero, the mass conservation balance in each node is verified and therefore, it is possible to calculate the ACH parameter, considering the net heated volume of each floor, as indicated by Eq. (60).

Methodology of 2-zones model version B.

In this version of the model the two natural driving force of NV are considered simultaneously: the wind-driven effect by the incident wind that generate surface pressures on both the windward and leeward façade and the buoyancy effect that directly depends on the air temperature variations and variation in heights. Since the external boundary conditions are all know, the total pressure at external nodes (1, 2 and 3) is calculated considering all the contributions, as presented in par. 4.5.2. The Eq. (45) is applied in Eq. (71.1-3), for calculating P_1, on the windward façade and P_2 and P_3, on the leeward façade.

$$P_1 = \frac{1}{2}\rho_{out} \cdot Cp_1 \cdot V^2_{H(z1)} + p_{atm_{ref}} \cdot 0.9877^{\frac{(alt+z1)}{100}} + \rho_{out} g z_1 \tag{71.1}$$

$$P_2 = \frac{1}{2}\rho_{out} \cdot Cp_2 \cdot V^2_{H(z2)} + p_{atm_{ref}} \cdot 0.9877^{\frac{(alt+z2)}{100}} + \rho_{out} g z_2 \quad (71.2)$$

$$P_3 = \frac{1}{2}\rho_{out} \cdot Cp_3 \cdot V^2_{H(z3)} + p_{atm_{ref}} \cdot 0.9877^{\frac{(alt+z3)}{100}} + \rho_{out} g z_3 \quad (71.3)$$

where: ρ_{out} [kg·m^{-3}] is the outdoor air density, C_{p1}, C_{p2} and C_{p3} [-] are the pressure coefficients at leakage's position, V_H is the adjusted wind speed [m·s^{-1}] at each leakage's height z [m], $p_{atm,ref}$ [Pa] is the atmospheric pressure reference (10135), *alt* [m, a.s.l] is the local altitude.

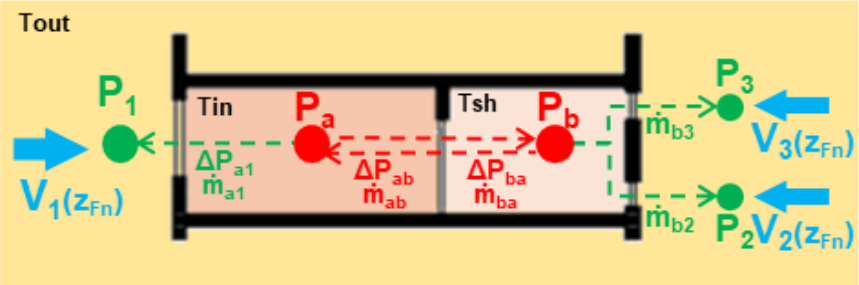

Fig. 72 – Scheme of the 2-zones model version A.

In the network scheme (Fig.72), the node 1 is positioned at the same height of the internal nodes (z_a=z_b=z_1), nodes 2 and 3 are positioned in the barycentre of the two openings (windows) in the internal side in the shaft of the leeward façade; they are placed respectively at one third (z_2 = 1/3 z_b) and two thirds (z_3 = 2/3 z_b) of the internal height of the shaft area (b) which is equivalent to that of area (a), the same for all floors of the building. The pressure coefficient Cp are calculated with the *Cpcalc+* tool. The pressure conditions of the two zones inside the building are not known; at internal nodes (a and b) only the potential pressure can be calculated, so it is possible to define:

$$Pa = p_{a0} + \rho_{in} g z_a \quad \text{with } p_{a0} = pdyn_a + p_a \quad (72.1)$$

$$Pb = p_{b0} + \rho_{in} g z_b \quad \text{with } p_{b0} = pdyn_b + p_b \quad (72.2)$$

Applying the conservation of the mass law, at each internal node in the network, considering positive the outgoing fluxes, the mass balance of air flow rate ṁ is expressed at each link, by the 2-equation system in Eq. (73). Applying the relationship between the mass air flow rate and the pressure variation ΔP, at each link between two nodes, the previous equation can be rewritten as Eq. (74):

$$\begin{cases} \dot{m}_{a1} + \dot{m}_{ab} = 0 \\ \dot{m}_{ba} + \dot{m}_{b2} + \dot{m}_{b3} = 0 \end{cases} \quad (73)$$

$$\begin{cases} K_{a1} (\Delta P_{a1})^n + K_{ab} (\Delta P_{ab})^n = 0 \\ K_{ba} (\Delta P_{ba})^n + K_{b2} (\Delta P_{b2})^n + K_{b3} (\Delta P_{b3})^n = 0 \end{cases} \quad (74)$$

where ΔP [-] are the pressure variation at each link (i.e., Pa1=Pa-P1), Ka1 , Kb2 and Kb3 [kg·s-1·Pa-n] are the flow coefficients at the external opening (window), Kab and Kba [kg·s-1·Pa-n] are the flow coefficients at the internal opening (door), and is the flow coefficient, fixed at 0.65 [-].

By substituting the known values of the pressures at each node, it is possible to rewrite the system as Eq. (74.1):

$$\begin{cases} K_{a1} (\boldsymbol{p_{a0}} + p_{pot,a} - P_1)^n + K_{ab} (\boldsymbol{p_{a0}} + p_{pot,a} - (\boldsymbol{p_{b0}} + p_{pot,b}))^n = 0 \\ K_{ba} (\boldsymbol{p_{b0}} + p_{pot,b} - (\boldsymbol{p_{a0}} + p_{pot,a}))^n + K_{b2} (\boldsymbol{p_{b0}} + p_{pot,b} - P_2)^n + K_{b3} (\boldsymbol{p_{b0}} + p_{pot,b} - P_3)^n = 0 \end{cases} \quad (74.1)$$

Since only pa0 and pb0 are the unknow variables, they constitute the output data and the solution of the system of two equations and two unknow variables that can be solved analytically, by imposing:

$$\begin{cases} f(p_{a0}) = p_{b0} \\ f(p_{b0}) = p_{a0} \end{cases} \tag{75}$$

Since the equations of the system are not linear the number of solutions is greater for each unknown variable. Due to this reason, after the simplification of the solutions in the procedure from Eq. (76.1) to Eq, (76.4), it will be necessary to verify the signs of the two solutions compared to those initially hypothesized (flow directions) so that the mass balance at each node is null.

$$\begin{cases} |(\boldsymbol{p_{a0}} + p_{pot,a} - \boldsymbol{p_{b0}} - p_{pot,b})|^{n^{\frac{1}{n}}} = \alpha \cdot |(\boldsymbol{p_{a0}} + p_{pot,a} - P_1)|^{n^{\frac{1}{n}}} \\ |(\boldsymbol{p_{b0}} + p_{pot,b} - \boldsymbol{p_{a0}} - p_{pot,a})|^{n^{\frac{1}{n}}} = \beta \cdot |(\boldsymbol{p_{b0}} + p_{pot,b} - P_2)|^{n^{\frac{1}{n}}} + \zeta \cdot |(\boldsymbol{p_{b0}} + p_{pot,b} - P_3)|^{n^{\frac{1}{n}}} \end{cases} \tag{76.1}$$

$$\text{with} \begin{cases} \alpha = |\left(-\frac{K_{a1}}{K_{ab}}\right)|^{\frac{1}{n}} \\ \beta = |(-\frac{K_{b2}}{K_{ba}})|^{\frac{1}{n}} \\ \zeta = |(-\frac{K_{b3}}{K_{ba}})|^{\frac{1}{n}} \end{cases} \tag{76.2}$$

$$\begin{cases} \boldsymbol{p_{a0}} = -p_{pot,a} + \frac{1}{\gamma}\boldsymbol{p_{b0}} + \frac{1}{\gamma}p_{pot,b} - \frac{\alpha}{\gamma}P_1 \\ \boldsymbol{p_{b0}} = -p_{pot,b} + \frac{1}{\delta}\boldsymbol{p_{a0}} + \frac{1}{\delta}p_{pot,a} - \frac{\beta}{\delta}P_2 - \frac{\zeta}{\delta}P_3 \end{cases} \quad \text{with} \begin{cases} \gamma = (1-\alpha) \\ \delta = (1-\beta-\zeta) \end{cases} \tag{76.3}$$

$$\begin{cases} \boldsymbol{p_{a0}} = f(\boldsymbol{p_{b0}}) = -p_{pot,a} - \frac{\alpha}{\gamma\varepsilon}P_1 - \frac{\beta}{\delta\gamma\varepsilon}P_2 - \frac{\zeta}{\delta\gamma\varepsilon}P_3 \\ \boldsymbol{p_{b0}} = f(\boldsymbol{p_{a0}}) = -p_{pot,b} - \frac{\alpha}{\delta\gamma\varepsilon}P_1 - \frac{\beta}{\delta\varepsilon}P_2 - \frac{\zeta}{\delta\varepsilon}P_3 \end{cases} \quad \text{with} \left\{\varepsilon = (1 - \frac{1}{\gamma\delta}) \right. \tag{76.4}$$

The signs of the results are verified imposing the following conditions Eq. (77.1-5), remembering that the positive sign indicates an air flow exiting the node, the negative sign indicates an air flow entering the node. Separately for each of the 4 links, the sign of the mass air flow rate is confirmed or made opposite in relation to the sign of the pressure difference between the two nodes connected by each link:

$$if\ \Delta P_{a1} > 0 \rightarrow (P_a - P_1) > 0 \quad then\ \dot{m}_{a1} = K_{a1}\,(\Delta P_{a1})^n \quad else\ \ \dot{m}_{a1} = -[K_{a1}\,(\Delta P_{a1})^n \tag{77.1}$$

$$if\ \Delta P_{ab} > 0 \rightarrow (P_a - P_b) > 0 \quad then\ \dot{m}_{ab} = K_{ab}\,(\Delta P_{ab})^n \quad else\ \ \dot{m}_{ab} = -[K_{ab}\,(\Delta P_{ab})^n] \tag{77.2}$$

$$if\ \Delta P_{ba} > 0 \rightarrow (P_b - P_a) > 0 \quad then\ \dot{m}_{ba} = K_{ba}\,(\Delta P_{ba})^n \quad else\ \ \dot{m}_{ba} = -[K_{ba}\,(\Delta P_{ba})^n] \tag{77.3}$$

$$if\ \Delta P_{b2} > 0 \rightarrow (P_b - P_2) > 0 \quad then\ \dot{m}_{b2} = K_{b2}\,(\Delta P_{b2})^n \quad else\ \ \dot{m}_{b2} = -[K_{b2}\,(\Delta P_{b2})^n] \tag{77.4}$$

$$if\ \Delta P_{b3} > 0 \rightarrow (P_b - P_3) > 0 \quad then\ \dot{m}_{b3} = K_{b3}\,(\Delta P_{b3})^n \quad else\ \ \dot{m}_{b3} = -[K_{b3}\,(\Delta P_{b3})^n] \tag{77.5}$$

Further condition to verify is that the sign of the airflow $\dot{m}_{ab}$ at link a→b is opposite to the sign of the airflow $\dot{m}_{ab}$ at link b→a, so Eq. (70) should be verified.

After having calculated each mass air flow rate and substituting the resulting values in the system equations (Eq.67), if both the two equations are zero, the mass conservation balance in each node is

verified and therefore, it is possible to calculate the ACH parameter, considering the net heated volume of each floor, as indicated by Eq. (60).

4.5.7. Three-zones model- versions v.A and v.B

In the transition to the 3-zones air flow model the complexity of the network has been enriched to consider a more detailed description of the outdoor boundary conditions and the internal zones.

The choice of a greater number of external nodes (2 nodes per facade at different heights) coincided with the possibility, at this point of the analysis, of applying the results of the CFD method for the correction of the wind speed incident on the facade. The results of the CFD simulations (chp.4) allow the description of the air flow field inside the urban canyons as a function of height, for the real conditions that occur in each simulated climatic and geometric scenario.

As regards the internal zones, two heated separated zones are considered in the schematization of the building structure, separated but both in communication with the no-heated shaft. This choice was motivated by the desire to simulate multistorey residential buildings (condominiums), distinguish the zone below the Neutral Pressure Plan (NPP) and the zone above it.

The complexity of the network consists of 3 unknown internal condition, one of this with 4 links converging in a single node (in the shaft); the related system of 3 non-linear equations required the use of iterative calculation to determine the solutions and output parameters.

The first version of the 3-zone model (*3-zones, v.A*) was firstly studied to simply predict the combined effect of the wind-driven and the buoyancy, but without considering the cross ventilation between the two heated zones and the external environment: only 8 links are considered.

In the second version of the 3-zone model (*3-zones, v.B*) the cross ventilation is considered which directly links each of the two heated zones with the two nodes representing the external conditions on both facades; in the final version the network counts 7 nodes of which 3 internal unknow condition and 10 links.

The last model version (3-zones v.B) represents an acceptable solution which can entail a good balance between the physical phenomena's description, the great number of input data, the detailed description of the building: a model that is synthetic enough to be applied to all buildings in an urban area.

4.5.7.1. Schematization of the building and Input data

The schematization that describes the real characteristics of a case study building in Figure 73a-c (left side) is the same for both versions A and B, since they differ only in the number of links considered in the network represented in Figure 73a-c (right side). The scheme of the network from the vertical section CC' (Fig. 73a) is valid for both versions v.A and v.B; from the horizontal sections AA' and BB', respectively at ¼ and ¾ of the building's height (H_{bld}) two different network schemes are reported, for the version A (Fig. 73b) and the version B (Fig. 73c).

The architectural sections report the geometrical characteristics of the building, the number of floors, the horizontal and vertical distribution (shaft) inside the building, and the number of openings per floor, considering two types of opening (windows-w and doors-d) and their position on the façades. Two apartments per floor are considered, but no internal partitions are studied.

A new attribute is associated with each facade of the building, to apply the results of the CFD method: the *uc facade* that faces the canyon street and the *co facade* that faces the courtyard are distinguished. As shown in Fig. 16 (left side), the shaft is assumed to be positioned in the façade *co*.

In this scheme it is no longer possible to uniquely associate the windward or leeward characteristic to the facades of the building as both conditions will be evaluated:
- uc façade windward and co facade leeward
-uc facade leeward and co facade windward.

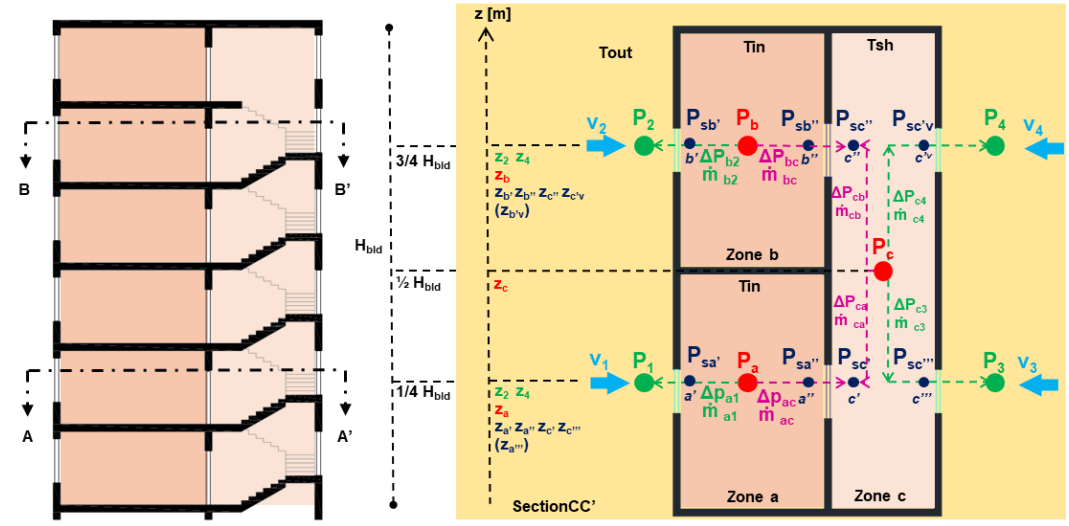

(a)

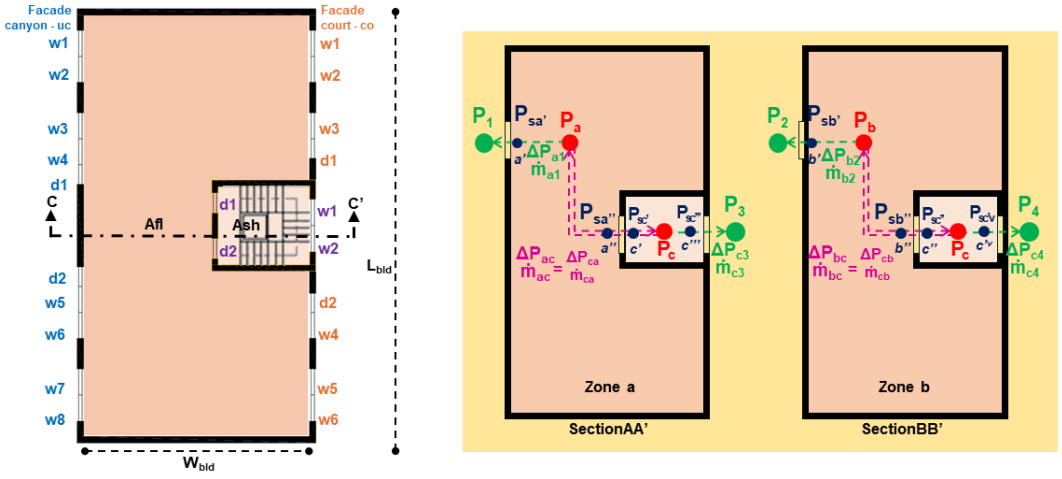

(b)

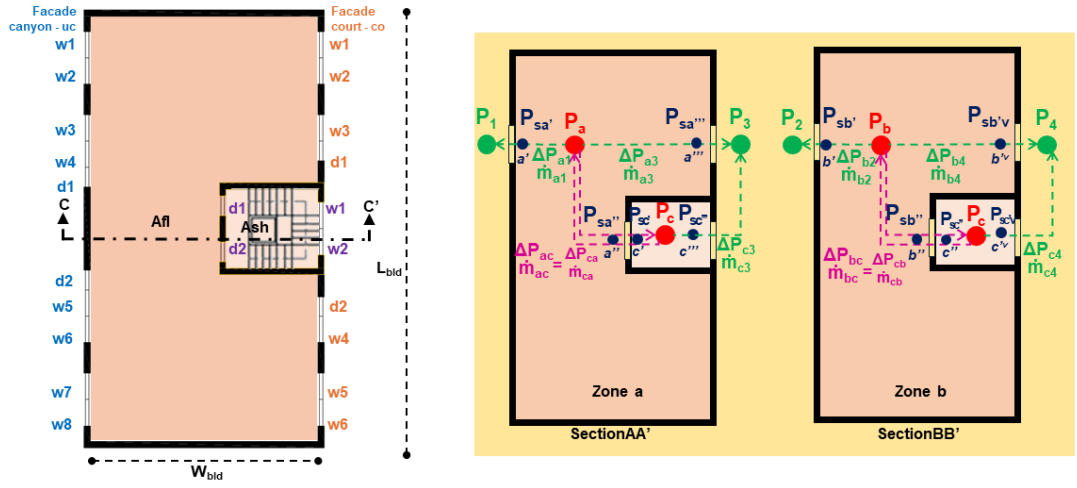

(c)

Fig. 73a-c - Schematization of buildings for the application of the 3-zones air flow model.

The vertical and horizontal sections in Figure 73 (right side) schematize the two zones (*a* and *b*), representing the apartments heated at temperature *Tin*, the no-heated zone of the shaft (*c*) at temperature *Tsh*, and the outdoor environmental context, characterized by specific conditions of wind speed (*v*) and air temperature (*Tout*). The blue arrows indicate the incident natural wind, whose velocity is determined as a function of openings' height located in correspondence with each of the two nodes on both facades: the one in the canyon (uc) and the one in the courtyard (co) to which the speeds v1, v2 and v3, v4 are associated respectively. The cross ventilation in both heated zones is considered only in the model version B (Fig. 73c); therefore, each heated zone is connected to two external nodes on both the *uc* and *co* facades, in addition to its connection to the shaft.

The shaft relates to the internal node of each heated zone and with two external nodes on the façade *co*, positioned at two different heights (below and above the height of the neutral plane, z3 and z4, respectively).

Each zone represents a generalized portion of the geometry and characteristics of the building. In particular, the volume of each zone considers the real height and floors' number of the portion of the building it represents.

In the schematization of the building network (Fig. 73 left side), since a lumped parameters model is applied, the following number of openings are considered for each zone:

- for heated zones towards outside – a single opening exists for each (uc, co) which represents all the openings w or d per facade per floor considering the number of floors per zone;

- for heated zones towards shaft and vice versa - a single opening represents all the openings (only type d), considering the number of apartments per floor (two) and the number of floors per zone;

-for shaft towards outside - two openings represent all openings (only type w) per floor, the bottom one is at the same height as node 3 and considers the number of floors in zone a, the top one is at the same height of node 4 and considers the number of floors in area b.

The number of floors per zone can vary according to the total number of floors in the building. Since the number of openings is considered uniformly distributed and symmetrical on both facades, the NPP occurs exactly at half the height of the building. In case of buildings with an even number of floors, the number of floors per area is the same; despite this, in case of buildings with an odd number

of floors, it is possible to arbitrarily choose to assign a greater number of floors to zone a or b, as indicated in Figure 74, respectively by Option 1 and 2. In this analysis, option 1 (red box) is applied.

The building is represented as a network of nodes (zones) connected by links, which describe the displacement of the air flow in space. In Fig. 73, the nodes are indicated by colored points:

- the 3 internal nodes (*Pa, Pb, Pc* in red) whose pressure condition is the unknown variable,
- the 4 external nodes (*P1, P2, P3, P4* in green) whose pressure condition is known.

In addition, two nodes are associated with the respective side of each leakage (Fig. 73, blue points), describing the height of the leakage *z* [m a.s.l.] in the barycenter of the opening, and the local pressure P_{leak} [Pa] determined in relation to the pressure of the reference zone.

In the model v.A (Fig. 73b), these are the 8 nodes at leakage (Psa',Psa'', Psb', Psb'', Psc', Psc'', Psc''', Psc'^{v}), to which are added (Psa''', Psb'^{v}) in the model v.B (Fig. 73c), for a total number of 10 nodes at leakage, correspondent to the number of links in the network.

In Fig. 73, the links are indicated by dotted lines of different colors: the green lines connect internal and external nodes, the violet lines connect nodes from the heated zones and the shaft. To each link are associated: the pressure variation ΔP [-], calculated between each couple of nodes at leakages (blue points), and the air flow rate ṁ [kg·s-1], and a direction; positive fluxes are the ones outgoing from a node.

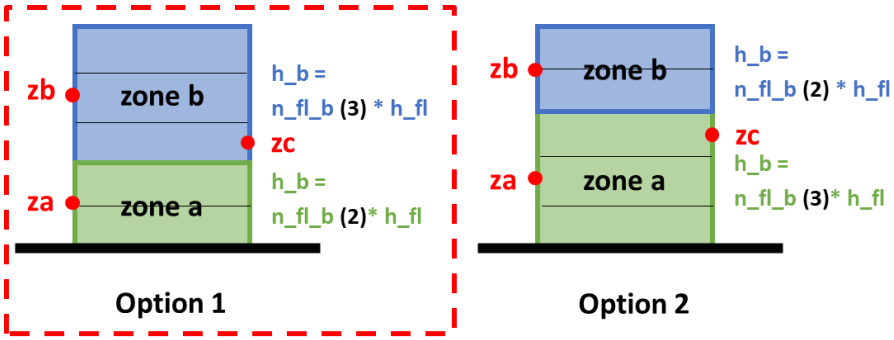

Fig. 74 - Height of the heated zones (a and b) in case of odd number of floors in the building.

According to the methodology used to correct wind velocity (Cp method or CFD method), the input data concerning the environmental climate conditions and the morphology of the built context are different, as reported in Table 53.

Table 53. Climate and urban parameter for the two methodologies investigated.

	Cp-method	**CFD-method**
Climate condition	Table 51, par. 4.5.6.1	Table 35, Chp.3, par.3.7.3.2
Urban morphology	Table 42, par. 4.5.5.1	Tables 27-28, Chp.3, par.3.7.3.2

Regarding the input data related to the building characteristics, in the 3-zone air flow model the required variables are listed in the following Tables:

- Canyon-building characteristics (Table 54a)
- Building characteristics (Table 54b)
- Opening characteristics (Table 54c)
- Leakage characteristics (Table 54d)

In Table 54a are listed the input data needed to describe the characteristics of the urban canyon in which the analyzed building is located that directly impact on the definition of the airflow around and inside the building. This input data is applied only in application of the *CFD method*, and describe the canyon dimension (W, width) separately for the façade front canyon (Wuc) and the façade front courtyard (Wco), the orientation of the canyon axis θ_{uc} according to which it is possible to determine the position of the building in the canyon. The procedure used to assess these variables is detailed in the following paragraph (pre-processing phase, step A-D).

The input data concerning the characteristics of the building (Table 54b), the opening (Table 54c) and the leakages (Table 54d) are presented implementing the input data already defined for the previous single and 2-zones models, underlying the new input variables (in bold) needed to describe the implemented network and features of the 3-zones model.

Regarding the building characteristics, new variables are added to describe the dimensions of each zone. The number of floors $n_{fl,a}$ [n] for zone *a* is always calculated by rounding down half the number of floors of the building $n_{fl,bld}$ [n] (be it odd or even); in this way, zone *a* will be assigned a number of floors equal to zone b (in the even case) or lower than that assigned to zone b (in the odd case), as described in Figure 17 (option 1).in this way an integer number will be obtained and to zone a an even number of floors (in the even case) or lower than that assigned to zone b (in the odd case), as described in Figure 17 (option 1). The height $H_{a/b}$ [m] of the zone *a* and *b* is determined multiplying the height h_{fl} [m] of a single floor by the total number of floor per zone $n_{fl,a/b}$ [n], while the height of the shaft (zone c) is calculated multiplying the height h_{fl} [m] of a single floor by the total number of floor in the building $n_{fl,bld}$ [n]. In calculating according to Eq. (78), the net volume of each zone $vol_{a/b\ or\ c}$ [m^3], it is necessary to subtract from the height of a single floor h_{fl} the thickness of a slabs (0.3 m), considering all floors in the zone, and then multiplied it by the net area of the apartments A_{fl} or the net area of the shaft A_{sh}.

$$vol_{a/\,b\ or\ c} = \left(h_{fl} - 0.3\right) \cdot n_{fl_{a/b\ or\ bld}} \cdot A_{fl\ or\ sh} \tag{78}$$

Regarding the opening characteristics, the number of openings is calculated automatically for any case study building, starting from the building dimensions, considering the fixed dimension of a single window and the fixed number of openings in the shaft (for each floor, 2 windows and 2 doors). Firstly, the total number of openings per floor $n_{op,fl,uc/co}$ is calculated separately for the *uc* and the *co* façade, according to Eq. (79.1-2):

$$n_{op,fl,uc} = \frac{L_{bld}}{Lw} \tag{79.1}$$

$$n_{op,fl,co} = \frac{(L_{bld} - L_{sh})}{Lw} \tag{79.2}$$

where L_{bld} [m] is the length of the building façade, the L_{sh} [m] is the length of the shaft, according to the construction period, L_w [m] is the length of a single opening (window). Then, if the total number of openings per façade (uc or co) is greater than 1, the type of opening is distinguished: the number of doors (balconies) per floor $n_{d,fl,uc/co}$ and the number of windows per floor $n_{d,fl,uc/co}$ correspond respectively to one third and two thirds of the total number of openings $n_{op,fl,uc/co}$.

The total number of windows and doors in the heated zone *a* or *b*, is calculated separately for the façade *uc* and *co*, multiplying the number of number of windows or doors per floor and the number of floors in the zone, as shown in Eq. (80.1); the same is done for the total number of windows and doors in the shaft, considering separately the area below (referring to zona *a*) and above (referring to zona *a*) the NPP, applying separately and respectively the Eq. (80.2)and Eq. (80.3):

$$n_{w/d,a/b,uc/co} = n_{w/d,fl,uc/co} \cdot n_{fl,a/b} \quad (80.1)$$

$$n_{w/d,sh,a} = n_{w/d,sh} \cdot n_{fl,a} \quad (80.2)$$

$$n_{w/d,sh,b} = n_{w/d,sh} \cdot n_{fl,b} \quad (80.3)$$

Regarding the leakage characteristics, the main implementations consist in calculating the flow coefficient k [kg·s^{-1}·Pa^{-n}] and the height z [m], specifying the height of internal nodes (za,zb,zc), the external nodes on uc façade (z1,z2) and co façade (z3,z4) and the height of the nodes at leakages ().

The k coefficient is determined separately for the heated zones (a and b) Eq. (81.1) and for the shaft Eq. (81.2), considering the total number of windows and doors that differ between façade uc and co:

$$k_{a/b,uc/co} = \left(k_{ref,w,hz} \cdot n_{w,a/b,uc/co}\right) + \left(k_{ref,d,hz} \cdot n_{d,a/b,uc/co}\right) \quad (81.1)$$

$$k_{w/d,sh} = \left(k_{ref,w/d,sh} \cdot n_{w/d,sh}\right) \quad (81.2)$$

Table 54a. Canyon-building characteristics

Variable	Name	Unit	Source and calculation
Canyon width – façade front canyon	Wuc	[m]	Step A-C in pre-processing phase
Canyon width – façade front courtyard	Wco	[m]	Step A-C in pre-processing phase
Canyon orientation	θuc	[°N]	Step A-C in pre-processing phase
Position of the building in the canyon	position	[-]	Step A-C in pre-processing phase

Table 54b. Building characteristics

Category	Variable	Name	Unit	Source and calculation
General	Building id	B_{id}	[n]	From municipal technical map
	Period of construction	*Period*	[Y]	From municipal technical map
	Orientation (Azimuth)	*Az*	[°N]	From technical maps using GIS tools
	Roof type (tilt angle)	*Roof*	[°]	From tabular data
Building dimension	Length	L_{bld}	[m]	From municipal technical map using GIS tools
	Width	W_{bld}	[m]	From municipal technical map using GIS tools
	Height	H_{bld}	[m]	According to Eq. (50)
	Height of single floor	h_{fl}	[m]	According to Period of construction
	Number of floors	$\boldsymbol{n_{fl,bld}}$	[n]	According to Eq. (49)
	Area net (floor)	A_{fl}	[m^2]	According to Period of construction (Table 40b)
	Area shaft (net)	A_{sh}	[m^2]	According to Period of construction (Table 40b)
	Volume net	Vol_{bld}	[m^3]	According to Eq. (78)
Zone dimension	**N of floors per zone a**	$\boldsymbol{n_{fl,a}}$	[n]	According to Figure 74 option 1
	N of floors per zone b	$\boldsymbol{n_{fl,b}}$	[n]	According to Figure 74 option 1
	Height of zone a/b	$\boldsymbol{h_{a/b}}$	[m]	$(n_{fl,a/b} * h_{fl})$
	Height of zone c	$\boldsymbol{h_c}$	[m]	$(n_{fl,bld} * h_{fl})$
	Volume of zone a/b	$\boldsymbol{vol_{a/b}}$	[m^3]	According to Eq. (78)
	Volume of zone c	$\boldsymbol{vol_c}$	[m^3]	According to Eq. (78)

Table 54c. Opening characteristics

Category	Variable	Name	Unit	Source and calculation
Openings dimension	Area of a single window (w)	A_w	[m^2]	Fixed at 2.16 (Lw x Hw: 1.2 x 1.8)
	Area of a single door (d)	A_d	[m^2]	Fixed at 1.98 (Ld x Hd: 0.9 x 2.2)
Opening number	**Number of openings per floor per façade uc and co**	$n_{op,fl,uc/co}$	[n]	According to Eq. (79.1) and Eq. (79.2)
	Number of windows/doors per floor per façade uc/co	$n_{w/d,fl,uc/co}$	[n]	Window (w): ceil (2/3 $n_{o,fl,uc/co}$) Door (d): ceil (1/3 $n_{o,fl,uc/co}$)
	Number of windows/doors per floor in the shaft	$n_{w/d,fl,sh}$	[n]	Fixed at 2
	Total number of windows/doors in zone a/b per façade uc/co	$n_{w/d,a/b,uc/co}$	[n]	According to Eq. (80.1)
	Total number of windows/doors in the shaft (below/above NPP)	$n_{w/d,sh,a/b}$	[n]	According to Eq. (80.2-3)

Table 54d. Leakage characteristics

Category	Variable	Name	Unit	Source and calculation
Leakage dimension	Typical leakage area of a single window/door	$A_{t,\ leak}$ w/d	[cm^2 /m^2]	According to Period of construction (Table 40b)
	Equivalent leakage area of a single window/door	$A_{e,leak}$ w/d	[m^2]	According to Eq. (43)
Leakage type	Discharged coefficient	Cd	[-]	Fixed at 0.65
Motion type of air	Flow coefficient	n	[-]	Fixed at 0.65
K coefficient	For a single window/door in heated zone/shaft	$k_{ref,w/d,hz/sh}$	[$kg \cdot s^{-1} \cdot Pa^{-n}$]	According to Eq. (46)
	For all windows and doors in zone a/b per façade uc/co	$k_{,a/b,uc/co}$	[$kg \cdot s^{-1} \cdot Pa^{-n}$]	According to Eq. (81.1)
	For all windows and doors in the shaft	k_{sh}	[$kg \cdot s^{-1} \cdot Pa^{-n}$]	According to Eq. (81.2)
Node heights	**Internal nodes a**	z_a	[m]	Barycenter of the zone's height (h_a/2)
	Internal nodes b	z_b	[m]	Barycenter of the zone's height from ground (h_b/2) + h_a
	Internal nodes c	z_c	[m]	Barycenter of the building's height (h_{bld}/2)
	External nodes on façade uc	$z_1 - z_2$	[m]	$z_1 = z_a$ $z_2 = z_b$
	External nodes on façade co	$z_3 - z_4$	[m]	$z_3 = z_a$ $z_4 = z_b$
	Leakages at nodes inside zone a	$z_{a'} = z_{a''} = z_{a'''}$	[m]	$z_{a'} = z_{a''} = z_{a'''} = z_a$
	Leakages at nodes inside zone b	$z_{b'} = z_{b''} = z_{b'''}$	[m]	$z_{b'} = z_{b''} = z_{b'''} = z_b$
	Leakages at nodes inside zone c	$z_{c'} = z_{c''} = z_{c'''} = z_{c'^v}$	[m]	$z_{c'} = z_{c'''} = z_a$ $z_{c''} = z_{c'^v} = z_b$

4.5.7.2. Methodology and case study application

Firstly, this paragraph presents the pre-processing phase of the geospatial input database about the buildings of a case-study zone with the aim to apply the calculation of the pressure variations and air flow rates for each building in the zone. Then, the methodology of the 3-zones air flow model is described, presenting the main difference between the 3-zone model version v.A and version v.B. The application to a case study zone helps in describing the procedure.

4.5.7.2.1. Pre-processing of input database

The pre-processing phase (Fig.75) of the geometric characteristics of the buildings is fundamental to ensure the replicability of the model to all buildings present in an examined urban area and the applicability of the 3-zone model, considering its limited field of application. This is given by the schematization of the real geometry and its simplification in the network of nodes and links described above, as well as by the calculation method of the input variables linked to the characteristics of the building, openings and leakages. Since these are geometric characteristics and spatial attributes, the pre-processing phase is carried out in a GIS environment starting from the geo-database of the buildings, created from the municipal technical paper. For each of the steps described below, examples applied to the case study are reported and reference is made to specific tools relating to the open-source QGIS software, used in this study.

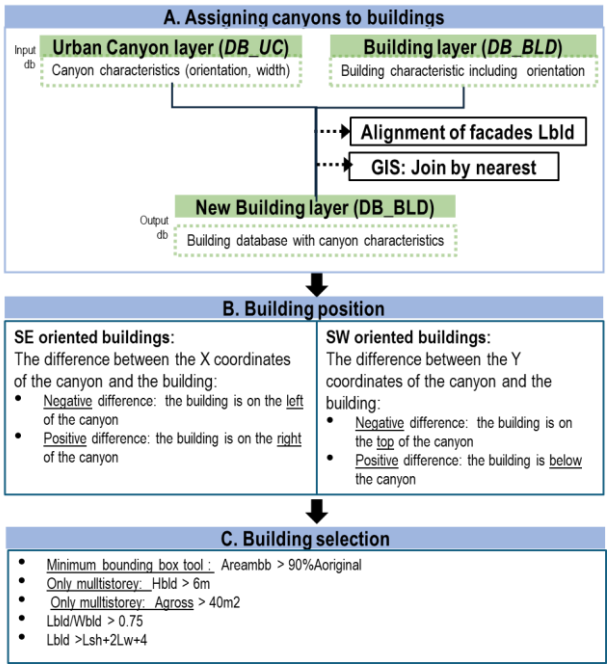

Fig. 75 – Flow chart of the methodology applied in the pre-processing phase concerning input data.

Step A. Assign canyon to buildings

In GIS environment, two input layers are added: i) the building layer (database *DB_BLD*) which contains all the general and geometrical characteristic of the buildings, ii) the canyon layer (*DB_UC*) created in the CFD method (chp.3) which contains all the characteristics of the urban canyons, derived for each case study: id, orientation (θ_{uc}), and dimension classes (W_{uc}).

The two layers are joined together using the spatial tool *join attributes by nearest*, setting the maximum distance of 2 meters, and the maximum nearest neighbors at 2 objects. In this way, a maximum of two canyons can be assigned to each building, because buildings located on a street corner are related to two different canyons; in this work, corner buildings are excluded from the analysis. The resulting joined layer consists of the updated building database *DB_BLD* on which the assigned canyon's variables are added. Before applying this spatial tool, it is necessary to check the *alignment of features*.

A building is considered aligned with the canyon if the orientation of the building coincides with that of the canyon, considering the same confidence interval used in determining the orientation of the canyon θ±45°. In a GIS environment the orientation of each geometry, a building, (Az_{bld}) is automatically calculated considering the angle between the North axis (0°N-clockwise) and the longitudinal axis of the geometry. Referring to the example in Figure 76a, buildings of type A result oriented like the assigned canyon (θ_{uc}), unlike buildings of type B.

Applying the following case sentence to all buildings in a case study zone, results for the attribute *Alignment* will be *True* (Fig. 76c) or *False* (Fig. 76d). The final step is to correctly assign the L_{bld} variable (length of the façade) to all the facades aligned with the geometry of the canyon, as in the example in Figure 76b.

Case when $\theta_{uc}=Az_{bld}$ then "True"

else "False"

end

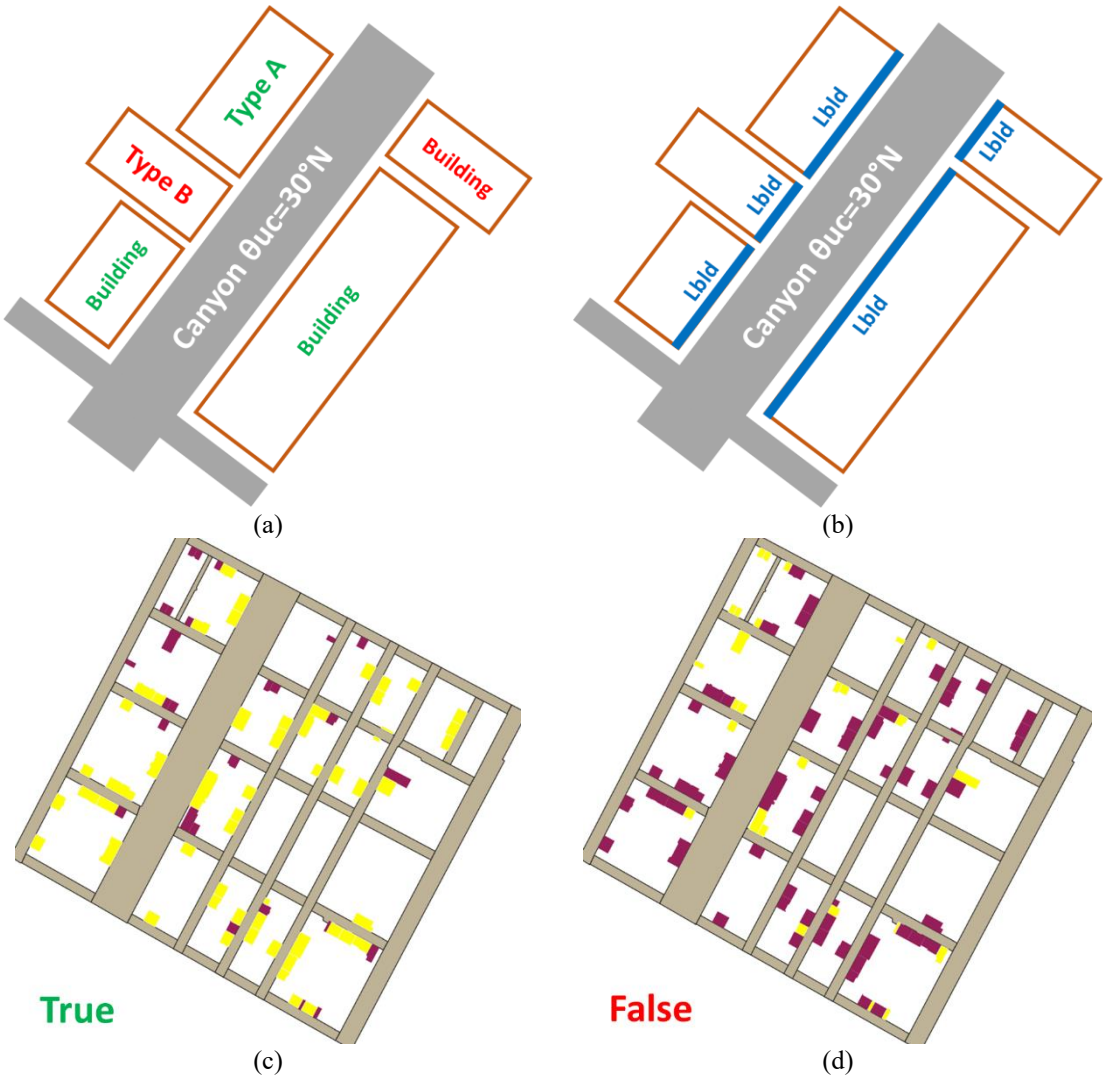

Fig. 76 – Examples from a case study application of the procedure to assign buildings and canyon geometries according to spatial and geographical correlations: orientation (a), alignment of facades (b), True (c) and False (d) results of the verification through case sentence conditions.

Step B - Define buildings' position in a canyon.

For each canyon orientation θ_{uc}, two cross wind directions *WD* are possible, to consider only perpendicular wind on building facades, according to the orientation of the building (Az_{bld}). It is necessary to know the position of the building according to the canyon side to distinguish the *uc* and *co* facades, as they will be windward or leeward, depending on which of the two opposite cross incident wind direction *WD* will occur.

As an example (Figure 77), from the analysis at urban scale of the city case study (Turin), two prevailing orientations of the urban canyon have been observed: NE-SW (30°N) and NW-SE (120°N). Buildings on a NE-SW oriented canyon can be positioned on the left or the right side of the canyon, while buildings on a NW-SE oriented canyon can be positioned on the top side or downside the canyon axis.

The position of the building is assessed in GIS environment; considering the coordinates of the elements (canyon or building), calculated from the barycenter of their geometry (polygons) and the information related to their distance. Selecting all the canyons with the same direction, it is possible to apply the following case sentences Eq. (82) to each building.

For $\theta_{uc} = 30°$ Eq. (82.1)

```
Case   when nearest x-featurex>0 then "Left"
       when nearest x-featurex<0 then "Right"
End
```

For $\theta_{uc} = 120°$ Eq. (82.2)

```
Case   when nearest y-featurey>0 then "Down"
       when nearest y-featurey<0 then "Top"
End
```

where the nearest x or y are referred to the canyon coordinates, and the feature x or y are referred to the building coordinates.

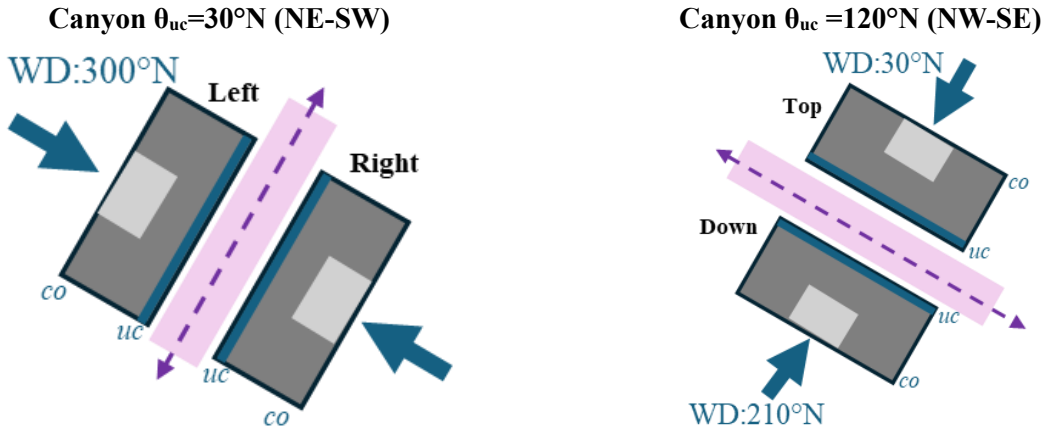

(a) (b)

Fig. 77a-b – The two main directions oft he cross-sectional wind driven (WD), for each of the two main canyon (in purple) axis orientations NE-SW (a) and NW-SE (b), for the case study of Turin.

Step C - Building selection

The field of application of the 3-zones air flow model requires the selection of residential buildings that correspond to the following criteria. For selected buildings to which a urban canyon has been assigned from the previous step of analysis, to uniform and simplify the rectangular shape of buildings geometry features in GIS (polygons), the *minimum bounding box* tool is used, verifying that the resulting area does not deviate from the original one by more than 10%.

- No buildings height less than 6 meters to consider only condominiums and multistorey buildings, and to avoid private houses and garages ($H_{bld} < 6m$).
- No buildings with a gross floor area smaller than 40 m2 ($A_{gross} < 40m^2$)
- No long and thick rectangular shaped buildings. The ratio between the building length L_{bld} [m] and width W_{bld} [m] is calculated and the 75% considered as a threshold level:

$$\frac{L_{bld}}{W_{bld}} \geq 0.75$$

- No extremely narrow building façades. The building lenght L_{bld} [m] must be greater than the length of the shaft (L_{sh}) and at least two windows, considering the length of a single window (L_w) and the minimum distance between them (1m):

$$L_{bld} \geq L_{sh} + 2L_w + 4$$

- No extremely long building façades. It is supposed that buildings with a very long façade facing the canyon L_{bld} [m] have more than one shaft (Fig.78f). Thus, the building should be splitted into portions to have one shaft for each portion, according to the following case sentence Eq.(83). The number of portions coincides with the number of shafts per building.

Case when $(\frac{L_{bld}}{2} - L_{sh}) < 7$ then 1 Eq. (83)

when $(\frac{L_{bld}}{2} - L_{sh}) \geq 7$ and when $(\frac{L_{bld}}{3} - L_{sh}) < 7$ then 2

when $(\frac{L_{bld}}{3} - L_{sh}) \geq 7$ then 3

End

As an example, in Figure 78 are shown the steps of the selection analysis at urban scale for the case study zone in the city of Turin. From the original database with 243 buildings (Fig.78a), among which 220 buildings are residential, the selected buildings on which is possible to apply the 3-zone lumped parameter model are 128 (Fig.78e); it corresponds to 58%.

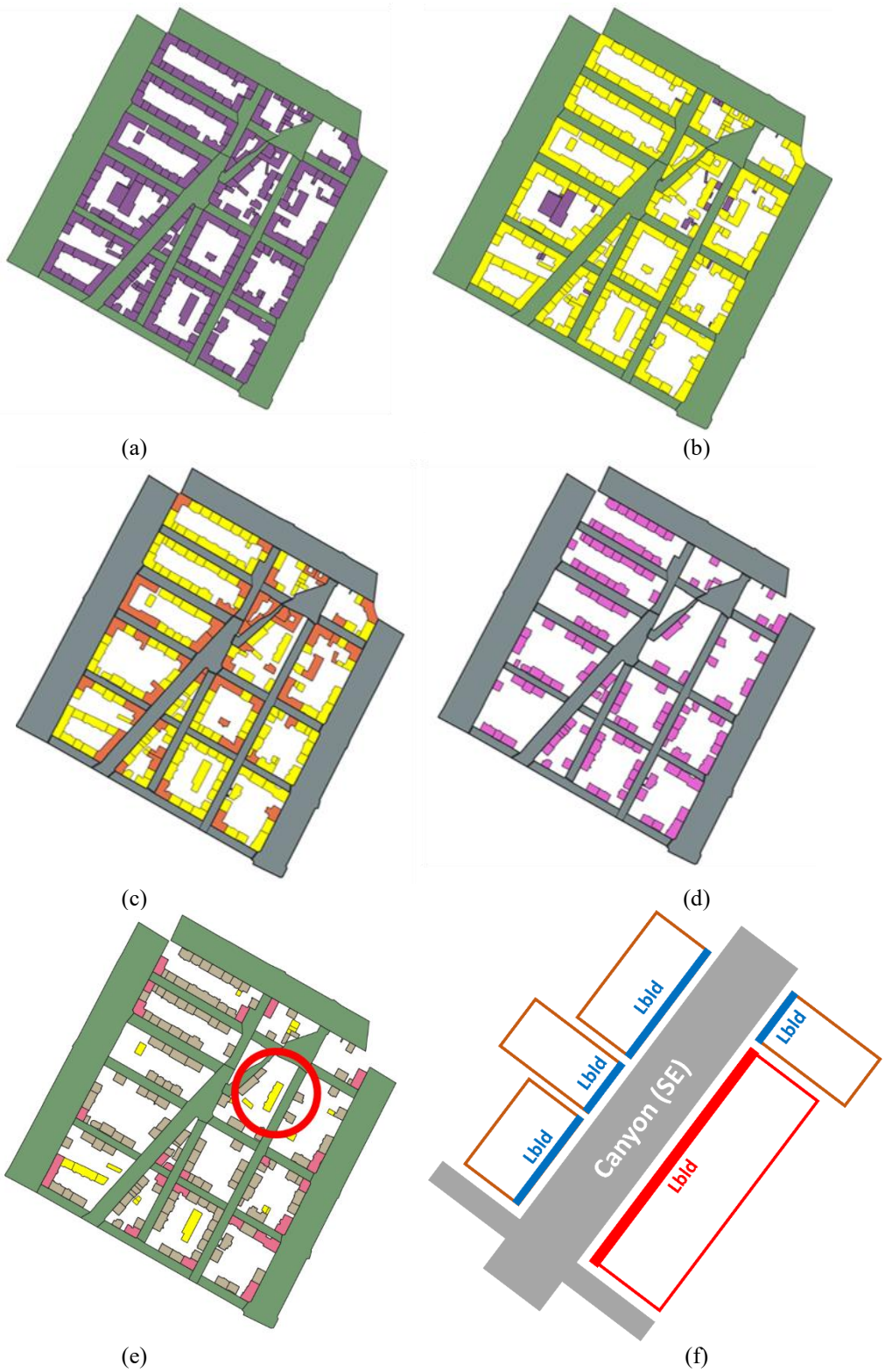

Fig. 78 – Examples of application of selection criteria to the buildings in the case study zone in the city of Turin: from the original database (a), selection of residential buildings (b), eliminating building on the corners, or in the courtyards and narrow ones (c-d), checking for long facades to split (e-f).

4.5.7.2.2. Pressure variation and air flow rate calculation

In both versions (v.A and v.B) of the 3-zone model the two natural driving force of NV are considered simultaneously: the wind-driven effect by the incident wind that generate surface pressures on both the windward and leeward façade and the buoyancy effect that directly depends on the air temperature variations and variation in heights. The cross ventilation occurs only in version v.B. The calculation of the pressure variations at external and internal nodes is the same for both model's versions; they differ for the application of the mass conservation law.

Pressure at external nodes (P at nodes 1,2,3,4).

Since the external boundary conditions are all know, the total pressure at external nodes (1, 2 ,3,4) is calculated considering the kinetic and potential pressure contributions, as presented in par. 5.5.2, and this is valid for both versions of the model (v.A, v.B).

The dynamic pressure p_{dyn} at each external node *i (with i from 1 to 4)* is because of the natural wind on both the windward and leeward façade. It is determined according to Eq. (84.1) or Eq. (84.2), in application to the *Cp-method* or *CFD-method*:

$$p_{dyn_i} = \frac{1}{2}\rho_i \cdot Cp_i \cdot U_{ref}^2 \tag{84.1}$$

where: U_{ref} is the reference wind velocity [m·s^{-1}], ρ [kg·m^{-3}] is air density, and Cp [-] is the coefficient of pressure at leakage's level assessed by CpCalc+ tool.

$$p_{dyn_i} = \frac{1}{2}\rho_i \cdot (v_i^2) \tag{84.2}$$

where: v [m·s-1] is wind velocity at leakage's level, retrieved from CFD simulation and consequent interpolation, and ρ [kg·m-3] is the outdoor air density; the effect of windward (+) and leeward (-) dynamic pressure, generating positive or negative fluxes entering and outgoing from the façade are considered.

The Eq. (85.1-4) are applied for calculating P_1 and P_1, on the façade facing the urban canyon street (uc façade) and P_3 and P_4 , on the façade facing the courtyard (co façade).

$$P_1 = p_{dyn_1} + p_{atm_{ref}} \cdot 0.9877^{\frac{(alt+z1)}{100}} + \rho_{out} g z_1 \tag{85.1}$$

$$P_2 = p_{dyn_2} + p_{atm_{ref}} \cdot 0.9877^{\frac{(alt+z2)}{100}} + \rho_{out} g z_2 \tag{85.2}$$

$$P_3 = p_{dyn_3} + p_{atm_{ref}} \cdot 0.9877^{\frac{(alt+z3)}{100}} + \rho_{out} g z_3 \tag{85.3}$$

$$P_4 = p_{dyn_4} + p_{atm_{ref}} \cdot 0.9877^{\frac{(alt+z4)}{100}} + \rho_{out} g z_4 \tag{85.4}$$

where: ρ_{out} [kg·m^{-3}] is the outdoor air density, $_{pdyn}$ is the adjusted dynamic pressure [Pa] at each leakage's height z [m], $p_{atm,ref}$ [Pa] is the atmospheric pressure reference (10135), alt [m, a.s.l] is the local altitude. In this scheme, the nodes 1 and 3 are positioned at the same height of the internal nodes z_a, nodes 2 and 4 are positioned at the same height of the internal nodes z_a.

These pressures represent the external boundary conditions at the two opposite facades of the building.

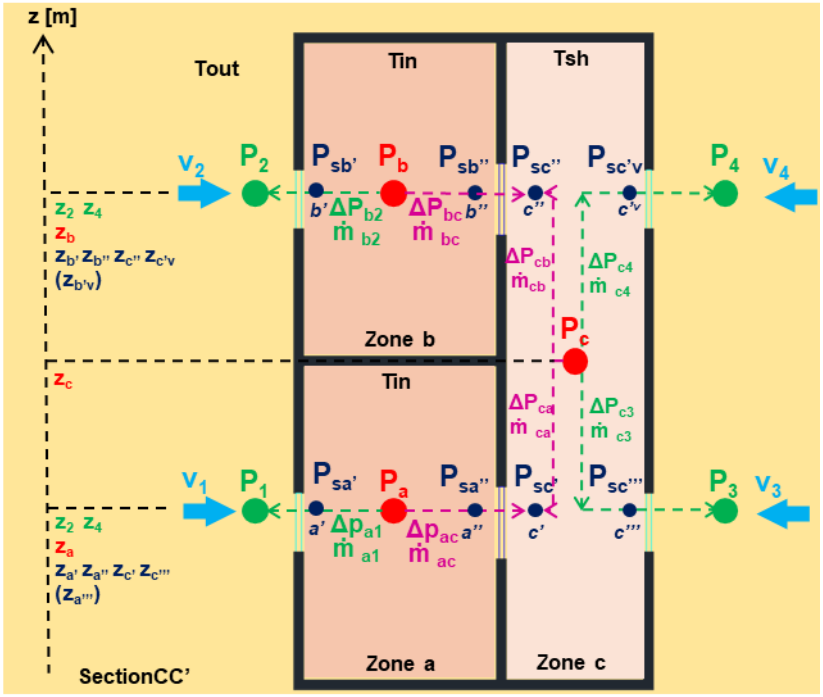

Fig. 79 – Scheme of the three-zone air flow model network version B.

Pressure at internal nodes (P at nodes a,b,c).

In all the 3 internal nodes *a,b* and *c* (red nodes in Fig.79*)*, the indoor air density in the heated zones ρ_{in} and in the shaft ρ_{in} [kg·m^{-3}], and the heights of each node *z* [m] calculated in the barycentre of the zone's volume and at leakage's level are known. But since the indoor pressure condition in the heated zones are unknown, the total pressures P_a, P_b, P_c, cannot be analytically solved.
The iterative procedure is applied to assess the pressure values at internal nodes: the starting values (p_{j0}) are defined summing pressure contributions Eq. (86.1-3):

$$p_{a0} = p_a + p_{dyna} \tag{86.1}$$

$$p_{b0} = p_b + p_{dynb} \tag{86.2}$$

$$p_{c0} = p_c + p_{dync} \tag{86.3}$$

The dynamic pressure $p_{dyn\,j}$ at a generic internal node *j* is defined by Eq. (87), due to the indoor air velocity (v_{int}) assumed to be equal in all zones,

$$p_{dyn_j} = \frac{1}{2}\rho_j \cdot (v_{int}^2) \tag{87}$$

where: v_{int} [m·s^{-1}] is the wind speed at leakage level in the heated internal zones (v_{int} =3 m·s^{-1});

The stack-effect considers the nodes' height variation between two linked nodes, and it directly impacts the contribution of the potential pressure to the total pressure of the examined zone. To each couple of nodes, the Bernoulli's equation can be applied even with the exclusion of the kinetic contribution in determining the total pressures, but it is necessary to verify the following assumptions: i) the air flow has a constant velocity, ii) no pressure drop occur within each zone. This is related to the fact that the pressure variation due to kinetic contribution is expected as infinitesimal and therefore, it could be neglected.

Then, considering the same zone and all the *n* openings in it, to each generic node *j*, identified in the barycentre of the zone's volume (Fig.79,in red) and to its correspondent node j^n at leakages' level (Fig.79 in blue) it is possible to apply Eq. (88) :

$$\cancel{p_{dyn_j}} + p_j + p_{pot_j} = \cancel{p_{dyn_{jn}}} + p_{jn} + p_{pot_{jn}} \rightarrow p_{jn} = p_j + \rho_j g(z_j - z_{jn}) \quad (88)$$

In this model version, the unique zone in which the stack-effect occurs is the shaft (zone c). Here, the height z_c in the barycentre of the zone's volume differs from the other four nodes' heights at leakages ($z_c > z_{c'}$, $z_c > z_{c'''}$, $z_c < z_{c''}$ and $z_c < z_{c'v}$). *I*n application of the Eq. (88), the following relations occur between each of the four nodes at leakage and the node c:

$$p_{c\prime} = p_c + \rho_c g(z_c - z_{c\prime}) \text{ at leakage c'} \quad (88.1)$$

$$p_{c\prime\prime} = p_c + \rho_c g(z_c - z_{c''}) \text{ at leakage c''} \quad (88.2)$$

$$p_{c\prime\prime\prime} = p_c + \rho_c g(z_c - z_{c'''}) \text{ at leakage c'''} \quad (88.3)$$

$$p_{c\prime v} = p_c + \rho_c g(z_c - z_{c\prime v}) \text{ at leakage c'}^{v} \quad (88.4)$$

For the heated zones (*a,b*), the central nodes' heights correspond to the three nodes at leakage (Fig.79 in blue), ($z_a = z_{a'} = z_{a''} = z_{a'''}$) and ($z_b = z_{b'} = z_{b''} = z_{b'v}$); in addition, within the zones' volumes, local air densities remain constant. Since, it is evident that no stack-effects occur in both zones, the following relations can be determined: $p_a = p_{a'} = p_{a''} = p_{a'''}$ and $p_b = p_{b'} = p_{b''} = p_{b'v}$, respectively in zone a and in zone *b*. As a results, in both heated zones, the pressure contributions can be calculated indiscriminately in the barycentre of the node *j* or at leakage level j_n .

For zone in which the stack effect occurs (shaft), the relation expressed by Eq. (89) must be applied to each of the four (n) leakages:

$$P_{c_n} = p_{dyn_c} + p_c + \rho_c g(z_c - z_{c_n}) + p_{pot_{c_n}} \quad (89)$$

Simplifying Eqq. (88.1-4), and considering the definition expressed by Eq.(89), then Eq. (90) can be rewrite as indicated in Eq.(90.1).

$$p_{stk_{c_n}} = \rho_c g(z_c - z_{c_n}) \quad (90)$$

$$P_{c_n} = p_{c_0} + p_{stk_{c_n}} + p_{pot_{c_n}} \quad (90.1)$$

Mass conservation law

Applying the conservation of the mass law, at each internal node in the network of the 3-zones air, considering positive the outgoing fluxes, the mass balance of air flow rate *ṁ* is expressed at each link, by the 3 non-linear equations system in Eq. (91.1) for the model version A, in which 7 links occur and in Eq. (91.2) for the model version B, in which 10 links occur.

$$\begin{cases} \dot{m}_{a1} + \dot{m}_{ac} = 0 \\ \dot{m}_{b2} + \dot{m}_{bc} = 0 \\ \dot{m}_{ca} + \dot{m}_{cb} + \dot{m}_{c3} + \dot{m}_{c4} = 0 \end{cases} \quad (91.1)$$

$$\begin{cases} \dot{m}_{a1} + \dot{m}_{a3} + \dot{m}_{ac} = 0 \\ \dot{m}_{b2} + \dot{m}_{b4} + \dot{m}_{bc} = 0 \\ \dot{m}_{ca} + \dot{m}_{cb} + \dot{m}_{c3} + \dot{m}_{c4} = 0 \end{cases} \quad (91.2)$$

Applying the relationship between the mass air flow rate and the pressure variation ΔP, at each link between two nodes, the previous equations can be rewritten, respectively for the two versions as Eq. (93.1), version A, Eq. (93.2), version B:

$$\begin{cases} K_{a1}\,(\Delta P_{a1})^n + K_{ab}\,(\Delta P_{ab})^n = 0 \\ K_{b2}\,(\Delta P_{b2})^n + K_{ba}\,(\Delta P_{ba})^n = 0 \\ K_{ca}\,(\Delta P_{ca})^n + K_{cb}\,(\Delta P_{cb})^n + K_{c3}\,(\Delta P_{c3})^n + K_{c4}\,(\Delta P_{c4})^n = 0 \end{cases} \quad (93.1)$$

$$\begin{cases} K_{a1}\,(\Delta P_{a1})^n + K_{ab}\,(\Delta P_{ab})^n + K_{a3}\,(\Delta P_{a3})^n = 0 \\ K_{b2}\,(\Delta P_{b2})^n + K_{ba}\,(\Delta P_{ba})^n + K_{b4}\,(\Delta P_{b4})^n = 0 \\ K_{ca}\,(\Delta P_{ca})^n + K_{cb}\,(\Delta P_{cb})^n + K_{c3}\,(\Delta P_{c3})^n + K_{c4}\,(\Delta P_{c4})^n = 0 \end{cases} \quad (93.2)$$

where ΔP [-] are the pressure variation at each link (i.e., P_{a1}=P_a-P_1), K_{a1}, K_{b2} [kg·s^{-1}·Pa^{-n}] are the flow coefficients at the external openings (windows + doors) in the heated zones on the uc facades, K_{a3}, K_{b4} [kg·s^{-1}·Pa^{-n}] are the flow coefficients at the external openings (windows + doors) in the heated zones on the *co* facades, K_{c3}, K_{c4} [kg·s^{-1}·Pa^{-n}] are the flow coefficients at the external openings (windows) in the shaft on the *co* facades, K_{ab} , K_{ba}, Kc_a , K_{cb} [kg·s^{-1}·Pa^{-n}] are the flow coefficients at the internal opening (door), and *n* is the flow coefficient, fixed at 0.65 [-].

For each model version, the system of equations (93) can be re-written as Eq. (94.1-3) for model v.A and as Eq. (95.1-3) for model v.B; both correspond to function F of the iterative calculation; reference is made to the nodes at leakages $j_{n'}$. The variables in bold are the unknow pressures.

$$\begin{cases} K_{a'1}\,(\boldsymbol{p_{a0}} + p_{pota} - P_1)^n + K_{a''c'}\,(\boldsymbol{p_{a0}} + p_{pota} - \boldsymbol{p_{c0}} - p_{potc'} - p_{stkc'})^n = 0 & (94.1) \\ K_{b'2}\,(\boldsymbol{p_{b0}} + p_{potb} - P_2)^n + K_{b''c''}\,(\boldsymbol{p_{b0}} + p_{potb} - \boldsymbol{p_{c0}} - p_{potc''} - p_{stkc''})^n = 0 & (94.2) \\ K_{c'a''}\left(\boldsymbol{p_{c0}} + p_{potc'} + p_{stkc'} - \boldsymbol{p_{a0}} - p_{pota}\right)^n + K_{c''b''}\left(\boldsymbol{p_{c0}} + p_{potc''} + p_{stkc''} - \boldsymbol{p_{b0}} - p_{potb}\right)^n + \cdots & \\ K_{c'''3}\left(\boldsymbol{p_{c0}} + p_{potc'''} + p_{stkc'''} - P_3\right)^n + K_{c'v4}\left(\boldsymbol{p_{c0}} + p_{potc'v} + p_{stkc'v} - P_4\right)^n = 0 & (94.3) \end{cases}$$

$$\begin{cases} K_{a'1}\,(\boldsymbol{p_{a0}} + p_{pota} - P_1)^n + K_{a'''3}\,(\boldsymbol{p_{a0}} + p_{pota} - P_3)^n + K_{a''c'}\,(\boldsymbol{p_{a0}} + p_{pota} - \boldsymbol{p_{c0}} - p_{potc'} - p_{stkc'})^n = 0 & (95.1) \\ K_{b'2}\,(\boldsymbol{p_{b0}} + p_{potb} - P_2)^n + K_{biv4}\,(P_{b0} + p_{potb} - P_4)^n + K_{b''c''}\,(\boldsymbol{p_{b0}} + p_{potb} - \boldsymbol{p_{c0}} - p_{potc''} - p_{stkc''})^n = 0 & (95.2) \\ K_{c'a''}\left(\boldsymbol{p_{c0}} + p_{potc'} + p_{stkc'} - \boldsymbol{p_{a0}} - p_{pota}\right)^n + K_{c''b''}\left(\boldsymbol{p_{c0}} + p_{potc''} + p_{stkc''} - \boldsymbol{p_{b0}} - p_{potb}\right)^n + \cdots & \\ K_{c'''3}\left(\boldsymbol{p_{c0}} + p_{potc'''} + p_{stkc'''} - P_3\right)^n + K_{c'v4}\left(\boldsymbol{p_{c0}} + p_{potc'v} + p_{stkc'v} - P_4\right)^n = 0 & (95.3) \end{cases}$$

Then, the initial value p_{j0} (with *j* the 3 internal nodes, *a, b* and *c*) of the iterative calculation, is assumed to be in a range whose lower (*low*) and upper (*upp*) limits are defined according to Eq. (96.1) and Eq. (96.2), respectively:

$$p_{j0\_low} = p_j \quad (96.1)$$

$$p_{j0\_upp} = p_j + p_{dynj} \quad (96.2)$$

4.5.7.2.3. Iterative calculation and MATLAB code

Since the solution of both Eqq. (94) and (95) cannot be analytically performed, numerical methods must be applied to find the zeros (solution) of the functions, according to which f(P)=0.

The *fsolve* function algorithm provided by the *Matlab* software has been chosen to perform the iteration process needed to find the system of equations' numerical solution. Among the several algorithms that find the solution for non-linear system of equations following the Newton-Raphson method, the *trust-region* (*tr*) algorithm has been chosen. The required initial points should be provided as vectors: three initial points (p_{a0}, p_{b0}, p_{c0}) represent the initial vector. Different combinations of them

have been randomly set to let the iterative calculation reach three convergent solutions of the three internal pressures at nodes P_a, P_b, P_c. These starting points have been defined in a range whit a lower (p_{j0_low}) and an upper limit (p_{j0_upp}). Within this interval, for each starting point, ten values are randomly tested. A single combination of three values of starting points considered its variation of one value at a time: one thousand permutations are then tested in each iterative calculation. Table 55 described the setting criteria used in the application of the *trust region* algorithm.

Table 55. Criteria of the fsolve algorithm in MatLab sofwtare.

Step Tolerance	Function Tolerance	Optimality Tolerance	Iteration number (max)
$1e^{-06}$	$1e^{-09}$	$1e^{-06}$	400

A finite number of possible fluxes direction of the mass flow entering or outgoing from the nodes in the network exists. A positive or negative sign is assigned to the K coefficient in the system of equations. The iterative procedure considers all possible signs combinations before finding the solution of Eqq. 94 and 95. For each permutation of the initial points, for each sign combination and for each iteration, a matrix can be created.

In the model version v.A, the matrix *M* has 14 combinations of the signs of the mass flow rates at each of the seven links ($\dot{m}_{a1}$- $\dot{m}_{ac}$ at node a in Eq.66.1, $\dot{m}_{b2}$- $\dot{m}_{bc}$ at node b in Eq. 66.2, $\dot{m}_{ca}$-$\dot{m}_{cb}$-$\dot{m}_{c3}$-$\dot{m}_{c4}$ at node c in Eq.66.3) was tested and the solution that minimizes the error was chosen:

$$M = \begin{bmatrix} + & - & + & - & + & - & + & - & + & - & + & - & + & - \\ - & + & - & + & - & + & - & + & - & + & - & + & - & + \\ + & - & + & - & + & - & - & + & - & + & - & + & - & + \\ - & + & - & + & - & + & + & - & + & - & + & - & + & - \\ + & - & + & - & + & - & + & - & + & - & + & - & + & - \\ + & - & + & - & + & - & - & + & - & + & - & + & - & + \\ - & + & + & - & - & + & - & + & + & - & - & + & + & - \\ - & + & - & + & + & - & - & + & + & - & + & - & - & + \end{bmatrix}$$

The solution of the three equations' system consists in the triplet of Pa, Pb and Pc values that let the system Eqq. (94.1-3) closest to the zero (mass conservation balance).

In the model version v.B, the matrix B has with 126 combinations of the signs of the mass flow rates at each of the ten links ($\dot{m}_{a1}$- $\dot{m}_{a3}$- $\dot{m}_{ac}$ at node a in Eq.95.1, $\dot{m}_{b2}$- $\dot{m}_{b4}$- $\dot{m}_{bc}$ at node b in Eq. 95.2, $\dot{m}_{ca}$-$\dot{m}_{cb}$-$\dot{m}_{c3}$-$\dot{m}_{c4}$ at node c in Eq.95.3) was tested and the solution that minimizes the error was chosen:

$$M = \begin{bmatrix} - & - & + & - & - & + & + & + & \dots & (1,10) \\ - & + & - & + & + & - & + & + & \dots & - \\ \dots & \dots & \dots & \dots & \dots & \dots & \dots & \dots & \dots & \dots \\ (126,1) & + & + & + & - & - & - & + & \dots & (126,10) \end{bmatrix}$$

The solution of the three equations' system consists in the triplet of Pa, Pb and Pc values that let the system Eqq. (95.1-3) closest to the zero (mass conservation balance).

The 126 combinations of signs are defined based on some criteria. Considering the theoretical permutations to be calculated separately for each node they would have been: 3! =6 for nodes a and b and 4!=24 for node c, then (considering 6x6x24) 864 possible combinations would be evaluated. In the 3-zone model network, with the inclusion of the physical laws that govern the air flows at each link, many of these conditions are not realistic; in fact, due to the law of conservation of mass, at least two flows of opposite sign must occur in each node. Therefore, the possible permutations are 126. In

addition, it is possible to reduce them by half as for each node there are mirrored combinations of signs. The final total number of possible sign combinations tested in the iterative calculation is 63.

Application of the 3-zone air flow model (v.B) at urban scale.

Figure 80 shows the flow-chart of the MATLAB code for the iterative and automatize application of the 3-zones air flow model to all buildings of the case study zone, according to each of the 64-climate scenario combination simulated in the CFD, for each of the three canyon's width. The code is organized in 21 Steps described below and reported in the MATLAB Code in Appendix B.

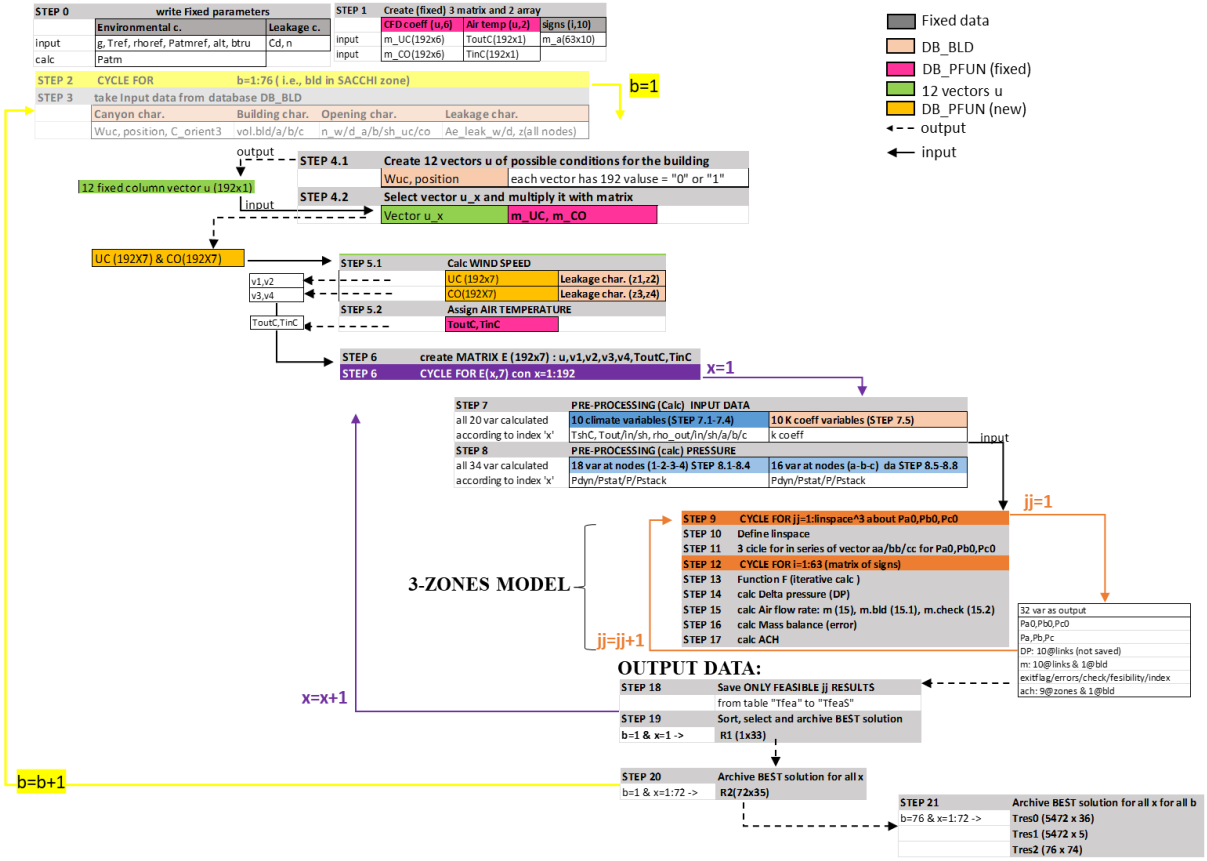

Fig. 80 - Flow chart of the MATLAB code for the iterative and automatize application of the 3-zones air flow model to all buildings of the case study zone, according to each climate scenario.

Brief description of the STEPS.

The *STEP 0* and *STEP 1* deal with the introduction of input data that do not vary and are valid for any building in any zone of the city case study.

STEP 0

The fixed input data about climate-environmental and leakage characteristics are written. In the first group there are reference parameters (g, T_{ref}, ρ_{ref}, $P_{atm,ref}$), local parameter (alt), and parameter from standard ($b_{tr,u}$), in the second group the leakage characteristics (Cd, n), according to Table 54d.

STEP 1

Then several objects (vectors, matrix) are insert in the *MATLAB* environment, as text files; all of them have been previously pre-processed:

- two matrixes (*m_UC*, *m_CO*), for each of the three canyon width (LC,MC,NC), for a total number of six matrixes; each matrix (64x12) contains the polynomial coefficients that are the results of the CFD simulation, for the 64 climate scenario combinations.
- two arrays (T_{inC}, T_{outC}) whose dimension (64x1) regards the indoor (T_{inC}) and outdoor (T_{outC}) seasonal air temperatures, for each of the 64 climate scenario combinations.
- one matrix (*m_a*) with dimension (63x10) regarding the possible combinations of sign that indicate the direction of air fluxes for the 10 links in the network that schematize the building zones. This matrix is a synthetic version of the matrix in Table

STEP 2-3

These steps have been designed but not yet implemented in the MATLAB code in Appendix B, in which this step is manually implemented, so one building a time is simulated.

A cycle for is designed to process all buildings b (b= 1: n) among the suitable number n of buildings in the case study zone. Referring to the building database DB_BLD, each *cycle for* takes the interesting input data (Table 56) from the whole database, for one building a time.

Table 56. MATLAB code input data

Canyon chr.		Building chr.		Opening chr.		Leakage chr.	
w_{uc}	From Table 54a	B_{id}	From Table 54b	$n_{w,a,uc}$ - $n_{d,a,uc}$	From Table 54c	$A_{e,leak,w}$ - $A_{e,leak,w}$	From Table 54d
w_{co}		vol_{bld}		$n_{w,a,co}$ - $n_{d,a,co}$		z_a - z_b - z_c	
θ_{uc}		vol_a		$n_{w,b,uc}$ - $n_{d,b,uc}$		z_1 - z_2 - z_3 - z_4	
Position		vol_b		$n_{w,b,co}$ - $n_{d,b,co}$		$z_a' = z_a'' = z_a'''$	
		vol_c		$n_{w,sh,a}$ - $n_{d,sh,a}$		$z_b' = z_b'' = z_b'''$	
				$n_{w,sh,b}$ - $n_{d,sh,b}$		$z_c' = z_c'' = z_c''' = z_c^y$	

In this step the height of nodes 2 and 4, respectively z_2 and z_4 are evaluated, according to the limit of the application field of this model, related to boundary condition in the CFD dominium, where the maximum height of the building simulated is 20 m. For z_2 and z_4 higher than 19 meters (z_2 and/or z_4 ≥19m), new variables (z_{22} and z_{44}) are created with height equal to 19m. These two new variables will only be used in the speed calculation (STEP 5).

STEP 4

All the following steps are done for the analyzed building b.

If the cycle for the series of multiple buildings in the same zone is active, it automatically switches between building b to the next one (b+1) and the following steps 4.1 and 4.2 will be adjusted.

STEP 4.1

A position vector *u_p* is assigned, depending on the position of the building (1=Left, 2=Right, 3=Top, 4=Down). The four *u_p* vectors are already written in the model, each with 64 parameters which can take on the value 1 or 0. The *Left* and *Right* buildings can take on all four *Scenes* for each S*eason* and each *Effect*, while the buildings in the *Top* and *Down* position, they can only take on the *WWF* and *LWF Scenes*, so half as many scenes for each season and effect, and thus a total of 32 possibilities. Therefore, for not present *Scenes*, the model avoids computing them unnecessarily.

STEP 4.2

For both the two facades, *uc* and *co*, the width of the canyon is assigned (1=Large, 2=Medium, 3=Narrow), considering the information associated with the building. Then a new coefficient vector is created, multiplying the position vector *u_p* (the same for the two facades) by the coefficient matrix *m_UC/CO_LL/MM/NN*, according to the following criterion:

IF	Wuc/Wco = 1	THEN	UC/CO = u_p · m_UC/CO_LL
ELSEIF	Wuc/Wco = 2	THEN	UC/CO = u_p · m_UC/CO_MM
ELSEIF	Wuc/Wco = 3	THEN	UC/CO = u_p · m_UC/CO_NN
END			

STEP 5.1 – Wind speed

For each row of matrix UC, the two wind speed (v1, v2) are calculated, considering the nodes' height (z1, z2) and for each row of matrix CO, the two wind speed (v3,v4) are calculated, considering nodes' heights (z3, z4). The fifth-grade polynomial function is applied (Eq.97), considering the six coefficients resulting from the CFD simulations, for each of the 64 climate scenarios.

$$f(z) = coeff_1 z^5 + coeff_2 z^4 + coeff_3 z^3 + coeff_4 z^2 + coeff_5 z + coeff_6 \quad (97)$$

All the four velocities are calculated applying the coefficient regarding the Normal (N) and the Tangential (T) components of the wind field in the dominium, see Figure 81.

STEP 5.2

For each of the four wind speeds, a resulting speed is calculated by taking the sign (+/-) from the Normal component and the magnitude from the Tangential component, with the following formula. This is because the reference system applied in the 3-zone model considers the positive incoming flows and the negative flows outgoing from the node (Fig.81b).

In the reference system of the CFD domain, the sign of the normal component refers to the x-axis V(x). Therefore, for v1 and v2 (facade T2, Fig.81a), the positive sign means an incoming flow, and a negative sign means an outgoing flow; vice versa for v3 and v4 (facade T1, Fig.81a). To apply the same reference system on both facades, corresponding to the one chosen in the 3-zone air flow model, the following corrections are applied:

IF	(v1/2_N) > 0	THEN	v1/2 = +1 · |v1/2_T|
		ELSE	v1/2 = - 1 · |v1/2_T|
END			
IF	(v3/4_N) > 0	THEN	v3/4 = - 1 · |v3/4_T|
		ELSE	v3/4 = +1 · |v3/4_T|
END			

For the speeds v1 and v2, if the normal component (v_N) is greater than zero, then the positive sign is attributed to the absolute value of the tangential component (v_T), if the v_N is less than zero, then the negative sign is attributed to the absolute value of v_T; vice versa for v3 and v4, if the v_N is greater than zero, then the negative sign is attributed to the absolute value of v_T, if the v_N is less than zero, then the positive sign is attributed to the absolute value of v_T.

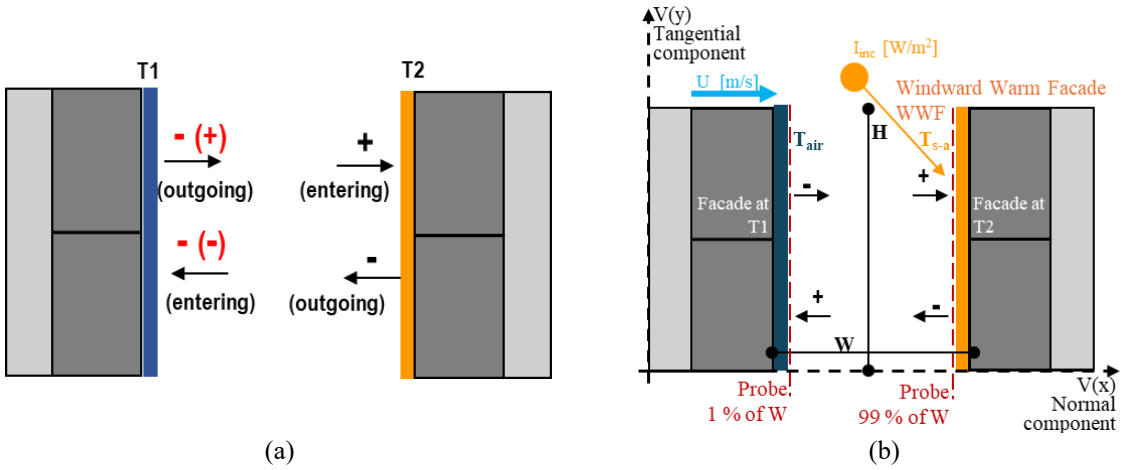

Fig. 81 - Cross section of the urban canyon, considering the signs of the fluxes (black arrow) with reference to the CFD dominium (a) and the 3-zone model assumption (b); in red the corrected signs.

STEP 6

All results are collected in a new matrix E (64x7) that contains: the id number u (from 1 to 64) of the climate scenario condition (the same for all canyon width), the four wind velocities (v1,v2,v3,v4), and the two air temperature (T_{outC}, T_{inC}).

STEP 6.1

A *cycle for* is designed to process all climate scenarios (64 or 32) for the examined building b in the calculations in Step 7 and 8; these are the pre-processing phases that will lead to additional input data (step 7) used to calculate pressure conditions (step 8).

STEP 7

For the examined building b, for each cycle on matrix E, the environmental characteristics and k coefficients are calculated. In detail, the air temperature in each zone (7.1-2), the air density in each zone (7.3-4), the k coefficient in each zone, distinguish façade uc and co (7.5-6). At the end of this step, ten climate variables and ten k coefficients are created as new input data for the 3-zone model.

STEP 7.1: define air temperature in the shaft (T_{shC})
STEP 7.2: define air temperatures in Kelvin degree (T_{outK}, $T_{inK, TshK}$)
STEP 7.3: define air density ρ [kg·m-3] external, internal and in the shaft
STEP 7.4: assign air density to each zone ($\rho_{in}=\rho_a$, $\rho_{in}=\rho_a$, $\rho_{in}=\rho_a$,)
STEP 7.5: calculate reference k coefficient for a single window and single door, distinguishing the air density of heated zones (ρ_{in}) and of the shaft (ρ_{sh})
STEP 7.6: calculate k coefficients for all windows and doors, considering the $k_{coeff,ref}$ from Step 7.5, and multiplying it for the number of all windows and doors in each zone, distinguishing *hz* or *sh* and façade *uc* or *co*.

STEP 8
For the examined building b, for each cycle on matrix E, the pressure conditions inside the zones are calculated, considering building characteristics and new input data calculated in previous steps. The Steps from 8.1 to 8.4 refer to the external nodes (1-2-3-4):
STEP 8.1: calculate reference atmospheric pressure.
STEP 8.2: calculate dynamic pressure, attention is made to keep the sign (+/-) of the wind velocity from the reference system of the domain to describe directions of the flux.
STEP 8.3: calculate potential pressure.
STEP 8.4: calculate total pressure.
Steps from 8.5 to 8.8 refer to the internal nodes (a-b-c):
STEP 8.5: calculate stack effect in the shaft (node c).
STEP 8.6: calculate potential pressure at leakages nodes
STEP 8.7: calculate dynamic pressure, assuming an indoor velocity v_{int} of maximum 3 $m \cdot s^{-1}$ in all the three zones.
STEP 8.8: calculate pressure at internal nodes.
STEP 8.8: define the interval and calculate the initial values for the iterative calculation of the internal pressure at each of the three nodes.

STEP 9
A new matrix S (64x31) has been created with all input data useful for the iterative calculation of the model. The new matrix S contains: 6 initial values (for each pa0, pb0, pc0, the left and the right limits), 10 k coefficient, one for each link in the network, 4 external total pressures at external nodes, 4 stack-pressure in the shaft, 6 potential pressures at leakages, 2 air density, and the vector u.
The iterative calculation starts with the creation of multiple cycles for linked together.

STEP 10
A cycle for with the index jj=1 is created to collect all the iterative calculations results for each simulation of the analyzed building b.
Define the *linspace* equal to 5: within the range of each initial point, 5 values are selected at a regular distance (function: *linspace*), considering the width of each interval.

STEP 11
Three *cycle for* are created, one for each vector (aa-bb-cc, where aa=bb=cc=1:length p0). Each combination considered the variation of one initial value at a time: a total of 125 permutations (for linspace=5, permutation=5^3) are applied in every iterative calculation.

STEP 12
A *cycle for* on matrix *a* of sign combination (*m_a*) is created. Each of the 125 permutations is evaluated for all the possible 63 sign combinations. The total number of cycles is 7875.

STEP 13
The iterative procedure is based on function *F* that reports the non-linear systems of three equations with the three unknown variables *Pa, Pb, Pc* (internal pressure). For each cycle (7875), the output is a triplet of these three variables.

For each iteration jj, the following steps are evaluated, from Step 14 to Step 17.

STEP 14
Knowing all total pressures at internal and external nodes, it is possible to calculate all delta pressure ΔP at each of the ten links in the network.

STEP 15
Knowing the delta pressure at each link, in this step all the mass air flow rate ṁ are calculated, according to the following conditions

IF ΔPc4 > 0 THEN m.c4 = + k coeff(c4) · $|DP.c4|^n$
ELSE m.c4 = - k coeff(c4) · $|DP.c4|^n$
END

STEP 15.1
The calculation of the total mass air flow rate of the building is calculated, considering only the fresh air entering from outside. This means summing up all the air flow rate at links with a connection to external nodes calculated in the previous step with a negative sign (entering).

STEP 15.2
In this step, all the 126 sign combinations are tested to assign to each triplet, the number (named *m.check*) that identifies the direction of each of the 10 fluxes. Iteration results without a *m.check* assigned are not acceptable solutions.

STEP 16
The mass balance is calculated at each of the 3 internal nodes (*a,b,c*), and then considering the total mass balance in the network, using this calculation to assess the absolute errors (*B.check*), as Eq.(98) and the relative error (*B.rel*), as Eq.(99):

$$\text{Absolute error: } B.check = |B.ina| + |B.inb| + |B.inc| \quad (98)$$

where *B.ina* is the deviation from zero of the mass conservation balance for the 3 links that converge at node *a*, *B.inb* is the deviation from zero of the mass conservation balance for the 3 links that converge at node b, and *B.inc* is the deviation from zero of the mass conservation balance for the 4 links that converge at node c.

$$\text{Relative error: } B.rel = \frac{B.check}{Avg(|ma1|+|mac|+|ma3|+|mb2|+|mbc|+|mb4|+|mca|+|mcb|+|mc3|+|mc4|} \quad (99)$$

STEP 17
For each zone and for the whole building, the air changes per hour (ach) parameter is calculated, according to the function ach_FNC10 that considers all the possible sign combination, and so all the possible conditions of entering fluxes.
In fact, it is necessary to distinguish between ach calculated only considering fresh air from outside, and ach considering exhausted air entering from other internal zones: in the first case, only air flow rate at link with a connection to the external nodes are considered, in the second case, only air flow rate at link with a connection to the internal nodes are considered.

STEP 18
From the 7875 jj iterations, only the feasible results are selected and then are sorted to find the best solution for each of the 64 (or 32) climate scenario of the analyzed building *b*, according to the following criteria:

1) the *exitflag* from the trust region algorithm should be equal to “1” or “2” or “3”; this means that the algorithm has reached convergence to find the result of the non-linear system of equation.
2) the *m.check* from the evaluation of sign combination should be a number from 1 to 126; results with no m.check assigned are eliminated.
3) the results with the minimum absolute (*B.check*) and relative error (*B.rel*) are selected as the final results of the iterative calculation.

STEP 19
Archive all the best (feasible) solutions of all the possible scenarios for the analysed building.
Between this step and the following, the cycle for designed to process all buildings b (b= 1: n) among the suitable number n of buildings in the case study zone is implemented of one unit: a new building b+1 is evaluated, and Step 4 to 19 are repeated.

STEP 20
Sort, select and archive as in the Step 18 all the best (feasible) solutions for each scenario and for each building, according to the same criteria.

STEP 21
Archive all the best (feasible) solutions of all the possible scenarios for all the analysed buildings (b) in the database of the case study zone.

4.5.7.3. Case study application and comparison

The methodology proposed here has been presented at the 8th AIGE/IIETA International Conference and 18th AIGE 2023 Conference held in Turin on 2024, the 14th -15th of June.

The main objectives of this paper consist in:

- 2D CFD modeling to describe the wind velocity field inside urban canyons of three different aspect ratio, considering the combined effect of cross wind and thermal gradient, already presented in paragraph 3.7.3.
- Applying the wind velocities inside urban canyon in the 3-zone air flow lumped parameter model to assess hourly values of the air changes per hour (ach).
- Comparing the resulting hourly ach and tabular data of pressure coefficient (Cp), applying them in the calculation of incident dynamic pressure incident on case-study buildings' façades.

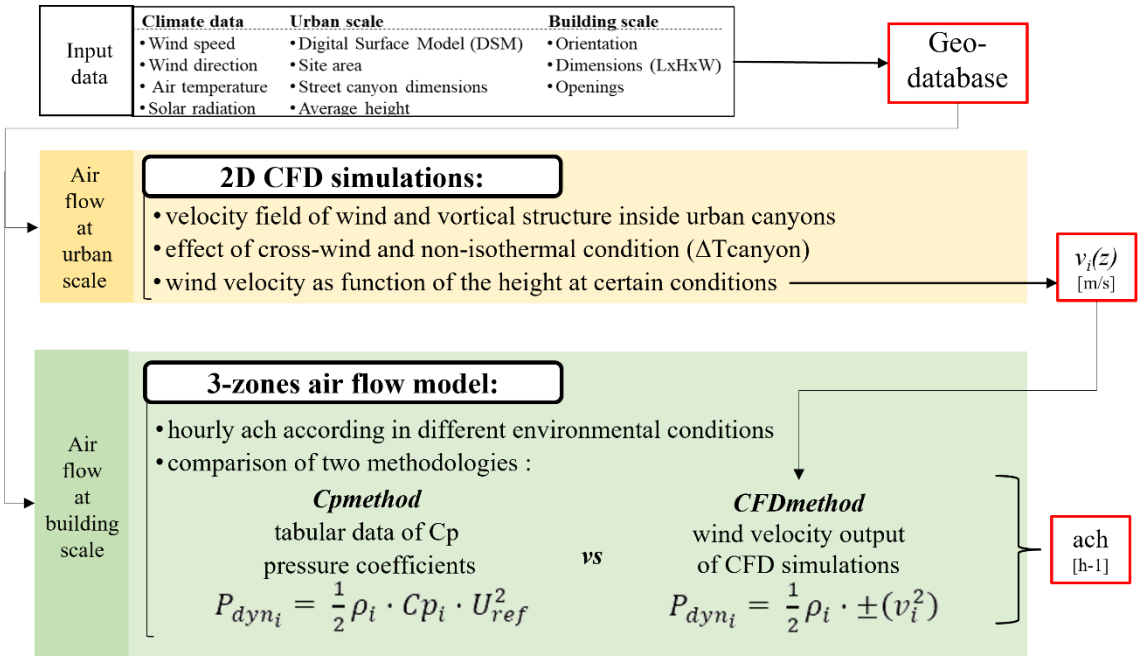

Fig. 82 - Flowchart of the methodology.

The Crocetta neighbourhood is again the case-study to which the presented methodology is applied. It is defined by a regular, dense and compact urban path, representative of the consolidated built environment of the historical city. The description of the urban morphology has been already presented in paragraph 3.7.3.2.

The three types of canyon dimension evaluated in six different street in the area are mapped in Figure 83 and listed in Table 57. These have been simulated in CFD analysis. The height of the canyon has been fixed to the average buildings' height within the whole city (20m), then the three most representative aspect ratios have been identified, considering three main street widths. Narrow canyons (NC) insist on internal streets in regular building blocks, while medium (MC) and large (LC) canyons are representative of the perimetral axis around the urban blocks.

Table 57. Canyon dimension applied in the case study.

Urban canyon	W [m]	H [m]	H/W [-]	NE-SW oriented canyon	NW-SE oriented canyon
Narrow Canyon (NC)	12	20	1.7	Lamarmora	Vochieri
Medium Canyon (MC)	17	20	1.2	Sacchi	Borsellino
Large Canyon (LC)	46	20	0.4	Vittorio	Duca

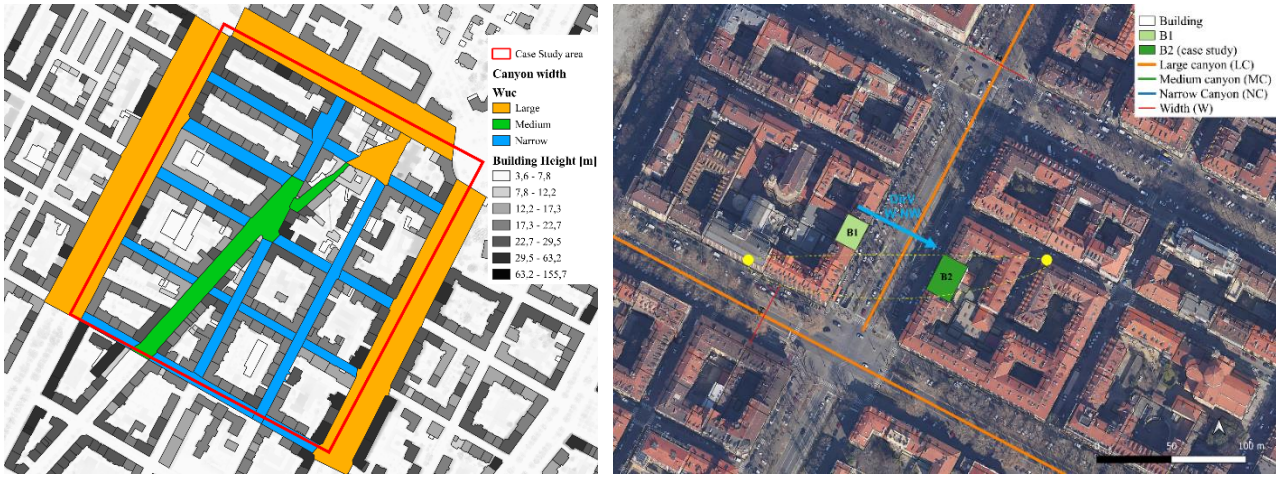

Fig. 83 - Localization of the urban canyons in Crocetta district (on the right) for selected aspect ratio: narrow (in blue), medium (in green) and large (in orange) and the examined building with NE-SW axis, considering crosswind (DirV) and solar exposures (yellow dot) on the facades of building B1 and B2.

From the reference examined year (2022), four dates have been selected and four climate scenarios have been hypothesised as representative of the typical meteorological climate days, whose characteristics are reported in Table 58 and represent input data of the three-zones air flow lumped parameter model. The resulting four configurations consider winter (WIN) and summer (SUM) seasons, both in combination with low wind (no wind) and high wind (windy) velocity conditions.

Table 58. Climate hourly data applied in the analysis.

Scenario	Date	U_{ref} [m· s^{-1}]	T_{air} [°C]	T_{in} [°C]	T_{s-a} [°C]	I_{inc} [W·m^{-2}]	ΔT [°C]
WIN-windy	04-01-2022 16:00	6.8	8.3	20	9.5	49.1	1.2
WIN-no wind	12-17-2022 08:00	1.6	-3.9	20	-3.8	2.8	0.1
SUM-windy	06-09-2022 16:00	8.6	27.9	26	48.2	844.1	20.3
SUM-no wind	07-15-2022 18:00	1.6	36.6	26	52.5	668.1	16.0

The three-zones airflow model is applied to the case study building B2 (Fig.83) whose characteristics are listed Table 59 and Table 60, respectively for building geometry and opening types, and leakages' characteristics. Since the construction period dates back before 1918, a very poor air tightness description is applied to the building's openings and leakages (Table 59).

To apply the *CpCalc* software in order to assess external pressure coefficients Cp at nodes, the correspondence to its application field requirements have been verified. In particular, the openings have been schematized and positioned at the highest and lowest points on building facades to analyse conditions of wind velocity and to enhance the buoyancy effect in the shaft.

Table 59. Building dimension and opening characteristics of the case study.

		Building geometry		Openings characteristics	
		Zone		Type	
		Heated (a,b)	Shaft (c)	window w	door d
Dimension (LxHxW)	[m]	9x9x7.7	9x18x3.3	1.2x1.8	0.9x2.2
Number	[n]	3 floors	6 floors	8 w (per floor)	2 d (per floor)
Typical Leakage Area	[cm^2/m^2]	-	-	12	12

Table 60. Heights of external and internal nodes and pressure coefficients.

		External nodes				Internal nodes			Internal nodes at leakage					
		1	2	3	4	a	b	c	a'	a''-c'	b'	b''-c''	c'''	c'v
Z	[m]	4.5	13.5	4.5	13.5	4.5	13.5	9.0	4.5	4.5	13.5	13.5	4.5	13.5
Cp	[-]	0.005	0.22	-0.03	-0.04	-	-	-	-	-	-	-	-	-

4.5.7.4. Results & Discussion

In this paragraph, results of the 3 zone-air flow model at building scale are presented: i) the air mass flows and the air changes per hour for the four typical winter and summer conditions, in no wind and windy scenarios, ii) the comparison of the results of dynamic pressure, air flow rate, and ach, considering the two applied methodologies (*CpCalc-method* and *CFD-method*).

Table 61 presents values of the dynamic pressure pdyn comparing results of the Cpmethod and CFDmethod, assessed at external nodes (1,2,3,4), considering their height (z), on both windward (WW) and leeward (LW) facades, in all climate scenarios, and for both the large (LC) and medium (MC) canyons. In both cases, the resulting pdyn at nodes 3 and 4 (leeward façade) presents a negative sign, as the direction of the surface pressure is outgoing from the building. In all cases, pdyn values determined at lower nodes, whose height (4.5m) is valid for both windward and leeward facades (respectively node 1 and node 3) is lower than the ones calculated at higher nodes, whose height (13.5m) is valid for both windward and leeward facades (respectively node 2 and node 4). The unique exception is the results from CFD method in the summer windy scenario (SUM-windy) and in application to the leeward façade on large canyon. As a common result between the two methods, considering all climate conditions, results for the medium canyon are always greater than the ones assessed for the large canyon. Even if their vortex structures and their wind velocity fields have similar profiles, in the medium canyon the magnitude of the wind increases, and this is even more evident in windy scenarios.

In each climate scenario listed inTable 61, , the p_{dynCp} result is always a lower than the correspondent p_{dynCFD} value, even if the two methods return results of the same order of magnitude. The Cpmethod is determined with no regard to the canyon dimension (width), as it described the pressure distribution along the building façade.

Observing windy scenarios, the resulting pressures calculated with the Cpmethod at the two heights on the same windward facades, show a very significant distance in their magnitude if compare to the correspondent results from CFDmethod; at lower node (1), the pressure p_{dynCp} is lower than the p_{dynCFD} one, and at higher node (3), the pressure p_{dynCp} is higher than the p_{dynCFD} one. This is probably due to the Cp coefficients' values (Table 61).

Table 61. Comparison of the results of Cp and CFD methods on windward and leeward facades for different canyon dimensions.

		Large Canyon (LC)				Medium Canyon (MC)				
	Façade	**WW**		**LW**		**WW**		**LW**		
	Node	**1**	**2**	**3**	**4**	**1**	**2**	**3**	**4**	
	z	4.5	13.5	4.5	13.5	4.5	13.5	4.5	13.5	[m]
Scenario	**Cp**	0.005	0.223	-0.032	-0.041	0.005	0.223	-0.032	-0.041	[-]
WINT-windy (U_{ref}=6.8m/s)	v_{CFD}	0.83	2.77	-0.17	-0.30	1.36	2.43	-1.06	-1.61	[ms^{-1}]
	P_{dynCFD}	0.41	4.62	-0.02	-0.05	1.11	3.55	-0.67	-1.55	[Pa]
	$Cp \cdot U_{ref}^2$	0.23	10.31	-1.48	-1.90	0.23	10.31	-1.48	-1.90	[m^2s^{-2}]
	P_{dynCp}	0.14	6.25	-0.89	-1.14	0.14	6.25	-0.89	-1.14	[Pa]
WINT-no wind (U_{ref}=1.6 m/s)	v_{CFD}	0.47	0.34	-0.17	-0.18	0.55	0.84	-0.36	-0.39	[ms^{-1}]
	P_{dynCFD}	0.13	0.07	-0.02	-0.02	0.18	0.42	-0.08	-0.09	[Pa]
	$Cp \cdot U_{ref}^2$	0.01	0.57	-0.08	-0.10	0.01	0.57	-0.08	-0.10	[m^2s^{-2}]
	P_{dynCp}	0.00	0.34	-0.05	-0.07	0.00	0.34	-0.05	-0.07	[Pa]
SUM-windy (U_{ref}=8.6 m/s)	v_{CFD}	2.06	3.20	-1.03	-1.70	2.31	3.51	-1.80	-2.68	[ms^{-1}]
	P_{dynCFD}	2.54	6.14	-0.64	-1.73	3.21	7.38	-1.93	-4.30	[Pa]
	$Cp \cdot U_{ref}^2$	0.37	16.50	-2.37	-3.03	0.37	16.50	-2.37	-3.03	[m^2s^{-2}]
	P_{dynCp}	0.21	9.55	-1.37	-1.76	0.21	9.55	-1.37	-1.76	[Pa]
SUM-no wind (U_{ref}=1.6 m/s)	v_{CFD}	0.75	1.13	-0.31	-0.57	0.87	1.32	-0.63	-1.14	[ms^{-1}]
	P_{dynCFD}	0.34	0.85	-0.05	-0.26	0.45	1.05	-0.23	-0.78	[Pa]
	$Cp \cdot U_{ref}^2$	0.01	0.57	-0.08	-0.10	0.01	0.57	-0.08	-0.10	[m^2s^{-2}]
	P_{dynCp}	0.00	0.34	-0.05	-0.07	0.00	0.34	-0.05	-0.07	[Pa]

It is possible to affirm that the *CFDmethod* is sensitive to nodes' height and the canyon dimensions; this can be explained by the fact that these parameters are considered in the CFD simulation in the assessment of the vortical structures vortex created by cross wind driven and thermal gradient effects.

Regarding the *Cpmethod,* it is possible to affirm that it overestimates the incident speed ($Cp \cdot U_{ref}^2$) for both windward and leeward facades; this can be due to the fact that :

- it can describe the surrounding built context referring to tabular data without considering neither the existence nor the characteristics of the urban canyon
- it only considers the effect of the incident wind and not the thermal gradient caused by the exposure of building facades to the solar radiation
- its application field is not suitable to application on typical buildings (condominium) in Turin positioned in regular urban canyon and characterized by closed central courtyard.

Figure 84 schematized the resulting displacement of the airflows throughout the building's zones. Similar results have been obtained for the two examined canyon dimensions. In the scheme, green arrows represent the fresh air entering in the building from the outside (outdoor airflow) and red arrows represent the exhausted air outgoing from the building to outside (indoor airflow). The four examined climate scenarios consider combination of winter (Fig.84a-b) and summer (Fig. 84c-d) seasons, both in windy (Fig. 84a-c) and no windy (Fig. 84b-d) conditions.

In all configurations, incident winds on windward façades let the outdoor fresh air (green arrows) entering the building and reaching the shaft while passing to the heated zones; the no-windy configuration during winter season (Fig. 84b) constitutes the only exception. At higher node 2

(windward façade), the exhausted air from the heated zone b exits outdoor; this is caused by the poor wind velocity inside that canyon in that scenario.

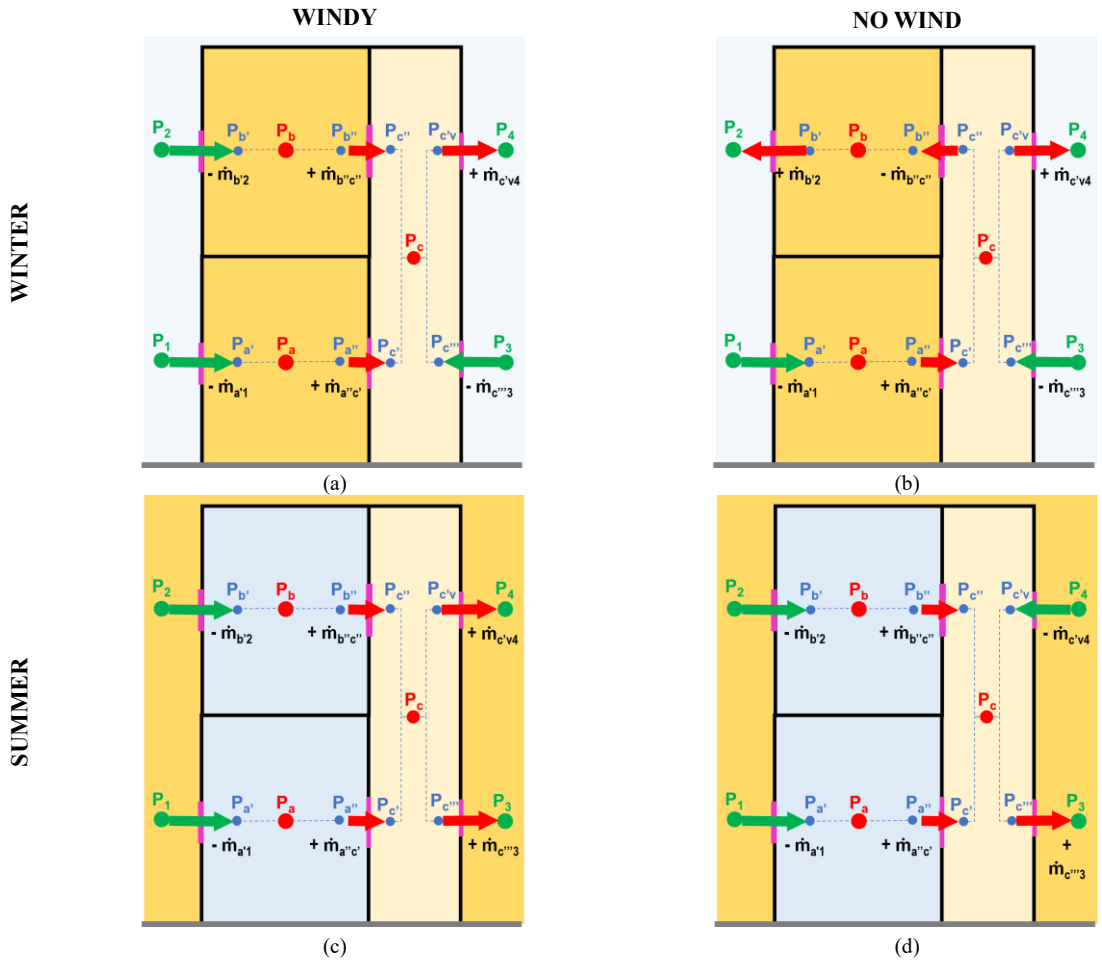

Fig. 84a-c – The displacement of airflow rates in winter-windy (a), winter-no wind (b), summer windy (c, only in MC) and summer no-wind (d) scenarios, for both large and medium canyons.

Regarding the results related to the shaft, these are the main observations:

- in all winter configurations (Fig. 84a-b), fresh air enters at ground level from node 3 and it exits at higher level from node; this is probably related to the buoyancy effect inside the shaft's volume
- in the summer windy scenario (Fig. 84c), exhausted air flows exit from the shaft both at ground and higher level (node 3 and 4, respectively)
- in the summer no windy scenario (Fig. 84d), exhausted air exits from the shaft at ground level (node4) while entering at higher level (node4)

Table 62 shows the comparison of the resulting ach values for all the examined scenarios and separately for the three zones in the buildings: the heated upper (b) and lower (a) zones and the shaft (c). The latter has been calculated considering only the external fresh airflows entering the zone from outside, as for the other zones. The ach* in Table 62 is referred to the shaft, but it has been determined considering all airflows entering the shaft (outdoor fresh air and exhausted recirculating indoor air); for this reason it has always greater ach values.

In all scenarios, lower hourly ACH values have been obtained, if compared to the reference fixed values used in the energy models (0.3-0.5).

Table 62. Comparing results of *Cpmethod* and *CFDmethod in the assessment of hourly* ach $[h^{-1}]$ for upper (b) and lower (a) heated zones and for the shaft (c) in large (LC) and medium (MC) canyons.

Scenario	Method	Canyon	ach(a)	ach(b)	ach(c)	ach(c)*
WIN-windy	Cp	LC-MC	0.05	0.08	0.18	0.28
	CFD	LC	0.06	0.04	0.32	0.38
		MC	0.08	0.03	0.41	0.57
WIN-no wind	Cp	LC-MC	0.01	0.02	0.07	0.08
	CFD	LC	0.02	0.02	0.01	0.02
		MC	0.03	0.04	0.03	0.05
SUM- windy	Cp	LC-MC	0.03	0.10	0.07	0.20
	CFD	LC	0.06	0.07	0.28	0.42
		MC	0.06	0.12	-	0.18
SUM-no wind	Cp	LC-MC	0.01	0.02	0.13	0.16
	CFD	LC	0.01	0.03	0.06	0.09
		MC	0.05	0.15	0.08	0.11

* Outdoor airflow plus airflow from zones a and b

Table 63. Comparing results of *Cpmethod* and *CFDmethod in the assessment of the e*rrors of the three non-linear system of equations at internal nodes (a,b,c), for large (LC) and medium (MC) canyons.

Scenario	Method	Canyon	Eq.a	Eq.b	Eq.c
WIN-windy	Cp	LC-MC	**-0.004**	**-0.004**	**-0.024**
	CFD	LC	0.000	0.000	-0.045
		MC	0.000	0.011	-0.077
WIN-no wind	Cp	LC-MC	0.002	0.008	0.040
	CFD	LC	-0.001	0.001	0.063
		MC	-0.003	0.008	0.059
SUM-windy	Cp	LC-MC	0.000	0.001	-0.039
	CFD	LC	0.000	0.000	-0.062
		MC	0.004	-0.007	0.065
SUM-no wind	Cp	LC-MC	-0.002	0.000	-0.033
	CFD	LC	-0.001	-0.003	-0.003
		MC	-0.008	-0.030	-0,023

The two methods report ach values with the same order of magnitude. In all climate conditions: i) the resulting achs of the medium canyon are slightly higher than the values associated to the large canyon, and this shows clearly the inverse correlation between the air velocity and the canyon dimension; ii) the resulting ach values at upper zones (b) are greater than values at lower zones (a); the only exception is the winter-windy scene.

The windy scenarios provide for greater values of ach than the no-windy ones, during both winter and summer seasons, as the contribution of the wind-driven effect is relevant in determining the airflows motion inside the canyon and the dynamic pressure contributes is relevant in determining the airflows passing through the building's zones.

The solutions of the iterative process are reported in Table 63; for each of the three non-linear equations, the results (errors) are listed.The closest to zero, the more accurate the solutions of the iterative calculation, in coherence with the mass conservation at nodes. All scenarios present very low and acceptable errors, validating the assumptions made for the modelling.

4.5.7.5. Model application: neighborhood case studies in Turin

In this paragraph, the 3-zone air flow lumped parameter model is applied to three different case study neighborhoods in the city of Turin: Crocetta (CRO), Sacchi (SAC) and Raffaello (RAF). For each zone, the canyon characteristics have been identified and the suitable building for the analysis have been selected, according to the criteria previously explained (Step C in the GIS pre-processing phase). Among the suitable buildings (in red, in Fig. 85a-c), in each neighborhood some buildings are selected (yellow point in Fig.85a-c) and listed in Table 64. The aim is to have at least one example for all possible buildings' positions in all the three classes of canyon width. An ID number identifies each building in the building database. As can be seen from Figure 85a-c, and reported in Table 64, in none of the three selected neighborhoods exist suitable buildings in a *Top* positions in a Large (LC) and Medium (MC) canyons.

Table 64. Selected building in the three neighborhoods.

	Canyon Orientation			
	30		120	
	Position			
Canyon width	Left	Right	Top	Down
LC	57511 (RAF)	41229 (SAC)	-	48906 (CRO)
MC	44723 (RAF)	41306 (SAC)	-	51472 (RAF)
NC	45913 (SAC)	41304 (CRO)	44378 (CRO)	47293 (RAF)

(a)

(b)

(c)

Fig. 85 – The three neighborhoos analyzed: Crocetta (a), Sacchi (b), and Raffaello (c) with the three classes of canyon category Large (in ornage), Medium (in green) and Narrow (in blue) in which the analyzed building (yellow points) are selected among all the suitable buildings (in red).

.Table 65. Selected building in the three neighborhoods.

		Canyon orientation and Position									
		30						120			
		Left			Right			Top	Down		
Canyon chr.	Wuc	Large	Medium	Narrow	Large	Medium	Narrow	Narrow	Large	Medium	Narrow
	Wco	MC	MC	MC	MC	LC	LC	MC	MC	MC	LC
Building chr.	Zone	RAF	RAF	SAC	SAC	SAC	CRO	CRO	CRO	RAF	RAF
	Bid	**57511**	**44723**	**45913**	41229	41306	41304	44378	**48906**	**51472**	**47293**
	Vol bld	9585.6	3512.3	2553.5	5586.2	3568.8	3106.6	3816.3	8655.9	3302.0	3306.2
	vol a	4199.6	1598.6	1182.2	2565.0	1689.9	1416.4	1498.7	4099.8	1278.2	1280.0
	volb	5039.5	1598.6	1182.2	2565.0	1689.9	1416.4	1998.2	4099.8	1704.3	1706.7
	volc	346.5	315.1	189.0	456.3	189.0	273.8	319.4	456.3	319.4	319.4
Opening chr.	n_w_a_uc	45	24	15	30	21	18	21	45	18	18
	n_w_a_co	30	18	9	15	15	3	6	10	9	9
	n_d_a_uc	10	6	3	5	6	9	15	30	3	3
	n_d_a_co	10	3	1	5	3	3	3	10	3	3
	n_w_b_uc	54	24	15	30	21	18	28	45	24	24
	n_w_b_co	36	18	9	15	15	3	8	10	12	12
	n_d_b_uc	12	6	3	5	6	9	20	30	4	4
	n_d_b_co	12	3	1	5	3	3	4	10	4	4
	n_w_sh_a	10	6	6	10	6	6	6	10	6	6
	n_d_sh_a	10	6	6	10	6	6	6	10	6	6
	n_w_sh_b	12	6	6	10	6	6	8	10	8	8
	n_d_sh_b	12	6	6	10	6	6	8	10	8	8
Leakagae chr.	Ae_leak_w	0.00259	0.00194	0.00259	0.00259	0.00259	0.002592	0.00259	0.002592	0.00259	0.00259
	Ae_leak_d	0.00238	0.00178	0.00238	0.00238	0.00238	0.002376	0.00238	0.002376	0.00238	0.00238
	za	8.3	4.5	5.0	8.3	5.0	5.0	5.0	8.3	5.0	5.0
	zb	26.4	13.5	14.9	24.8	14.9	14.8	16.5	24.8	16.5	16.5
	zc	18.2	9.0	9.9	16.5	9.9	9.9	11.5	16.5	11.6	11.6
	z1	8.3	4.5	5.0	8.3	5.0	5.0	5.0	8.3	5.0	5.0
	z2	26.4	13.5	14.9	24.8	14.9	14.8	16.5	24.8	16.5	16.5
	z3	8.3	4.5	5.0	8.3	5.0	5.0	5.0	8.3	5.0	5.0
	z4	26.4	13.5	14.9	24.8	14.9	14.8	16.5	24.8	16.5	16.5
	za1	8.3	4.5	5.0	8.3	5.0	5.0	5.0	8.3	5.0	5.0
	zac	8.3	4.5	5.0	8.3	5.0	5.0	5.0	8.3	5.0	5.0
	za3	8.3	4.5	5.0	8.3	5.0	5.0	5.0	8.3	5.0	5.0
	zb2	26.4	13.5	14.9	24.8	14.9	14.8	16.5	24.8	16.5	16.5
	zbc	26.4	13.5	14.9	24.8	14.9	14.8	16.5	24.8	16.5	16.5
	zb4	26.4	13.5	14.9	24.8	14.9	14.8	16.5	24.8	16.5	16.5
	zca	8.3	4.5	5.0	8.3	5.0	5.0	5.0	8.3	5.0	5.0
	zcb	26.4	13.5	14.9	24.8	14.9	14.8	16.5	24.8	16.5	16.5
	zc3	8.3	4.5	5.0	8.3	5.0	5.0	5.0	8.3	5.0	5.0
	zc4	26.4	13.5	14.9	24.8	14.9	14.8	16.5	24.8	16.5	16.5

In Table 65 are reported the characteristics of the ten selected buildings. considering all the input data required by the 3-zones air flow model. the buildings were also selected so that they were similar in terms of geometric characteristics. such as the volume of the building. a number of floors greater than 4 and other characteristics that strongly influence the air flow rate such as the air tightness of leakage (Ae. leak) determined according to the construction period of the building. All the buildings are in the last air permeability class. very poor leakage condition. as these are central neighborhoods in the city and the consolidated built context is mainly made up of historic buildings.

4.5.7.6. Model application: results and discussion

In this paragraph, the results from the application of the 3-zones air flow model at two buildings among the list in Table 65, are reported and discussed. In Table 66 and Table 67 are synthetized some important output from the model, respectively for the building ID 57511 in a large canyon and left position (Table 66) and for the building ID 47293 in a narrow canyon and down position (Table 67). Both buildings are in Raffaello neighborhood. The number of climatic scenarios evaluated by the model for the two buildings is different, according to the possible scenes that the building's position allows: the building in left position (ID 57511) is evaluated for all the 64 climate scenarios, while the building in down position (ID 47293) is evaluated only for 32 climate scenarios. This means that for the first building all Scenes (WWF-WCF-LWF-LCF) are evaluated, while for the second only the half (WCF-LCF). Tables 66-67 contain results for the four possible effects (WINDY-no), each one evaluated in the winter and summer seasons, and considering the Windward Warm Façade (WWF) and Windward Cold Façade (WCF) scenes, when present.

Regarding the output data listed in Tables 66-67, these are:

- **pa0, pb0, pc0 [Pa**] initial values of pressure at the three internal unknown nodes: among the 125 permutations, this triplet identifies the three initial values that have led the algorithm on which iterative calculation is based to convergence and find a solution.

- **Pa, Pb, Pc [Pa]** output values of pressure at the three internal nodes: it is the triplet of the unknow variables that solve the non-linear system of three equations and represent the internal pressures at nodes that is also the main result.

- **ACH [h^{-1}]** values for each zone (*ach(a), ach(b), ach(c)*) and for the whole building *ach(bld),* distinguish the ach calculated considering only the fresh air from outside *ach(a)* or the exhausted air *ach(a_{ex})*; the two situations are an alternative to the other, they cannot happen together and which of the two occurs depends on the direction (signs) of the flows resulting from the pressure variations between internal and external zones. In the first case, the air flow rates considered are only the ones at link connected to the external environment (ma1,ma3,mb2,mb4,mc3,mc4); in the second case, the air flow rates considered are only the ones at links that connect internal zones (mac,mbc, mca,mcb).

- **Exitflag [num]** the resulting message from the solver used in the algorithm to solve the system indicating successful convergence; values 1 to 3 are acceptable.

Table 66. Results of building ID 57511 in a large canyon and Left position.

	nowind-nogradient				nowind-GRADIENT				WINDY-GRADIENT				WINDY-nogradient			
	WINTER		SUMMER		WINTER		SUMMER		WINTER		SUMMER		WINTER		SUMMER	
	WWF	WCF	WWF	WCF	WWF	WCF	WWF	WCF	WWF	WCF	WWF	WCF	WWF	WCF	WWF	WCF
pa0	98275	98274	98274	98275	98275	98275	98275	98275	98277	98277	98274	98273	98274	98273	98271	98275
pb0	98051	98052	98052	98054	98056	98056	98052	98056	98056	98056	98054	98056	98051	98051	98054	98052
pc0	98151	98152	98151	98151	98151	98151	98152	98156	98152	98152	98151	98155	98152	98157	98154	98154
Pa	98276	98276	98270	98270	98276	98276	98270	98270	98276	98276	98269	98268	98277	98275	98270	98268
Pb	98065	98065	98049	98049	98065	98065	98049	98049	98066	98066	98049	98049	98065	98065	98050	98049
Pc	98155	98155	98150	98150	98155	98155	98150	98150	98156	98156	98151	98151	98157	98157	98151	98151
ach(bld)	**0.03**	**0.02**	**0.06**	**0.07**	**0.04**	**0.02**	**0.07**	**0.07**	**0.10**	**0.09**	**0.14**	**0.15**	**0.11**	**0.12**	**0.15**	**0.17**
ach(a)	0.02	NaN	0.08	0.08	0.03	NaN	0.08	0.09	0.16	0.13	0.23	0.26	0.18	0.21	0.25	0.30
ach (a_{ex})	0.03	0.03	NaN	NaN	0.03	0.03	NaN	NaN	0.04	0.03	NaN	NaN	0.03	0.04	NaN	NaN
ach(b)	0.02	0.02	NaN	NaN	0.02	0.02	NaN	NaN	0.04	0.04	NaN	NaN	0.03	0.03	0.01	NaN
ach (b_{ex})	NaN	NaN	0.05	0.05	NaN	NaN	0.05	0.05	NaN	NaN	0.05	0.05	NaN	NaN	0.05	0.05
ach(c)	0.35	0.34	0.84	0.85	0.35	0.34	0.85	0.86	0.23	0.22	1.05	1.07	0.30	0.36	1.11	1.15
ach (c_{ex})	0.32	0.31	0.69	0.70	0.32	0.31	0.70	0.70	0.20	0.23	0.57	0.52	0.08	0.12	0.59	0.47
exitflag	3	1	1	1	1	3	1	1	1	1	1	1	3	1	1	1
m.check	95	11	45	45	95	11	45	45	119	123	45	45	119	119	65	45
Abs err	0.0000	0.0000	0.0000	0.0000	0.0000	0.0000	0.0000	0.0000	0.0000	0.0000	0.0000	0.0000	0.0000	0.0000	0.0000	0.0000
Rel err	0.0003	0.0000	0.0000	0.0000	0.0000	0.0003	0.0000	0.0000	0.0000	0.0000	0.0000	0.0000	0.0002	0.0000	0.0000	0.0000
ma1	0.064	0.008	0.030	0.033	0.084	0.037	0.035	0.048	0.274	0.229	0.252	0.293	0.301	0.355	0.274	0.354
mac	-0.039	-0.036	0.078	0.079	-0.040	-0.038	0.079	0.079	-0.052	-0.045	0.065	0.059	-0.046	-0.057	0.067	0.053
ma3	-0.026	0.028	-0.108	-0.112	-0.044	0.000	-0.113	-0.126	-0.223	-0.183	-0.317	-0.351	-0.255	-0.297	-0.341	-0.407
mb2	-0.027	-0.022	0.040	0.019	-0.025	-0.029	0.033	0.021	-0.069	-0.072	0.020	0.022	-0.049	-0.051	-0.012	0.011
mbc	0.038	0.037	-0.081	-0.082	0.038	0.037	-0.082	-0.082	0.024	0.028	-0.086	-0.084	0.010	0.014	-0.088	-0.085
mb4	-0.011	-0.015	0.042	0.063	-0.012	-0.008	0.049	0.061	0.045	0.044	0.066	0.062	0.039	0.037	0.100	0.074
mca	0.039	0.036	-0.078	-0.079	0.040	0.038	-0.079	-0.079	0.052	0.045	-0.065	-0.059	0.046	0.057	-0.067	-0.053
mcb	-0.038	-0.037	0.081	0.082	-0.038	-0.037	0.082	0.082	-0.024	-0.028	0.086	0.084	-0.010	-0.014	0.088	0.085
mc3	0.041	0.041	-0.094	-0.096	0.039	0.041	-0.096	-0.097	-0.007	0.008	-0.119	-0.121	-0.034	-0.033	-0.125	-0.130
mc4	-0.041	-0.041	0.091	0.094	-0.041	-0.041	0.092	0.094	-0.021	-0.026	0.098	0.096	-0.002	-0.010	0.104	0.098
mbld	0.105	0.077	0.202	0.209	0.123	0.078	0.209	0.223	0.319	0.281	0.436	0.473	0.340	0.392	0.478	0.537

- **m.check [num]** the identification number of the sign combinations, among the 126 possible combinations; each number is associated with an arrangement of the flows and their directions which can be found by looking at the positive or negative sign of each of the 10 air flow rates at the bottom of the table; remembering that we assume flow exiting the node (positive sign) and entering the node (negative sign);

- **Abs_err [%] and rel_err [%],** respectively the absolute and relative errors of the non-linear system of equations; among all the iterative calculations for each climate scenario, the best solution means the solution with the lowest absolute and relative errors;

- **$\dot{m}$.bld [kg·s^{-1}]** the mass air flow rate in each of the ten link and calculated for the whole building; in this last case, the sum of all the flows entering the building is equal to the sum of all the outgoing flows, therefore only the flows relating to the links connected to the external environment are considered, regardless of the zone.

Regarding the result of ach, in both case study buildings, ach values are lower than 0.3 that is used as a fixed parameter for new or refurbished buildings and 0.5 for old buildings. This is due to the fact that observed results are assessed with the sole contribution of infiltrations and considers the openings (doors and windows) closed.

For both buildings, there are higher values of ach in the scenarios with wind conditions (WINDY-no gradient and WINDY-GRADIENT) both in the presence and absence of a thermal gradient than in the no wind conditions (no wind-GRADIENT and no wind-no gradient); as already observed in the results of the CFD simulations describing the velocity field in the domain, the presence of a thermal gradient leads to turbulent motions that disturb the effect of wind-driven, so in the WINDY-GRADIENT scenarios, the number of ach is slightly lower than the WINDY-no gradient. For each scenario, higher value of each occurs in summer season.

Observing the ach values for each single area, the values are higher, especially in the shaft area. this is both because, unlike the two heating zones, two flows at two different heights converge in the shaft, and because the total volume is smaller and finally because the chimney effect is present only in this zone and affects the pressure variation between zones.

Table 67. Results of building ID 47293 in a narrow canyon and Down position.

	nowind-nogradient		**nowind-GRADIENT**		**WINDY-GRADIENT**		**WINDY-nogradient**	
	WIN	**SUM**	**WIN**	**SUM**	**WIN**	**SUM**	**WIN**	**SUM**
	WCF	**WCF**	**WCF**	**WCF**	**WCF**	**WCF**	**WCF**	**WCF**
pa0	98316	98317	98312	98317	98314	98317	98313	98314
pb0	98175	98172	98175	98172	98177	98174	98177	98171
pc0	98237	98237	98231	98237	98231	98235	98231	98231
Pa	98314	98311	98314	98311	98314	98309	98315	98309
Pb	98180	98170	98180	98170	98177	98168	98177	98167
Pc	98234	98231	98234	98231	98233	98231	98233	98231
ach(bld)	**0.04**	**0.09**	**0.04**	**0.10**	**0.10**	**0.20**	**0.14**	**0.23**
ach(a)	NaN	0.08	NaN	0.08	0.05	0.17	0.07	0.20
ach (a_ex)	0.04	NaN	0.04	NaN	0.02	NaN	0.02	NaN
ach(b)	0.04	0.04	0.04	0.05	0.11	0.16	0.15	0.19
ach (b_ex)	NaN	0.07	NaN	0.07	0.04	0.10	0.05	0.11
ach(c)	0.18	0.42	0.18	0.42	0.25	0.51	0.33	0.55
ach (c_ex)	0.12	0.34	0.12	0.34	NaN	0.29	NaN	0.26
exitflag	1	1	1	1	1	1	1	1
m.check	19	40	19	40	113	73	113	73
Abs error	0.0000	0.0000	0.0000	0.0000	0.0000	0.0000	0.0000	0.0000
Rel err	0.0001	0.0000	0.0000	0.0000	0.0000	0.0000	0.0000	0.0000
ma1	0.015	-0.009	0.015	-0.007	0.029	0.040	0.041	0.055
mac	-0.016	0.035	-0.016	0.035	-0.007	0.030	-0.010	0.027
ma3	0.001	-0.026	0.001	-0.028	-0.023	-0.070	-0.031	-0.083
mb2	0.010	0.063	0.007	0.067	0.086	0.144	0.112	0.168
mbc	0.013	-0.040	0.013	-0.040	-0.021	-0.055	-0.027	-0.060
mb4	-0.023	-0.023	-0.020	-0.027	-0.065	-0.090	-0.085	-0.108
mca	0.016	-0.035	0.016	-0.035	0.007	-0.030	0.010	-0.027
mcb	-0.013	0.040	-0.013	0.040	0.021	0.055	0.027	0.060
mc3	0.017	-0.043	0.017	-0.044	-0.008	-0.054	-0.010	-0.057
mc4	-0.020	0.039	-0.020	0.039	-0.020	0.029	-0.026	0.025
mbld	0.043	0.102	0.040	0.106	0.116	0.213	0.153	0.248

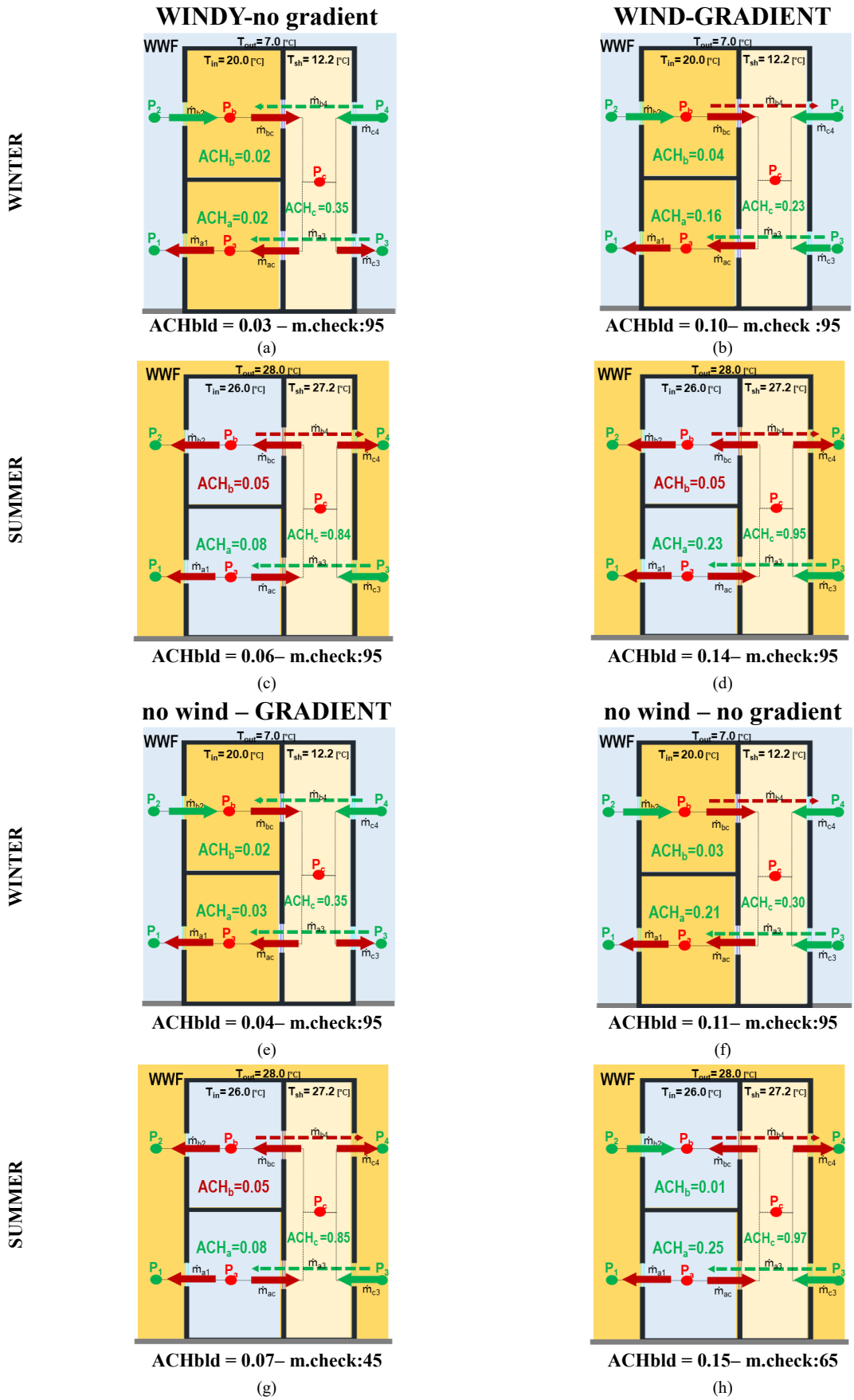

Fig. 86a-c - Airflow displacement through buildings zones of building ID-57511. in a Large Canyon and Left position. considering WWF scenes for both winter (a-b-e-f) and summer (c-d-g-h) seasons. in windy-no gradient (a-c). windy-gradient (b-d). no wind-gradient (e-g). no wind-no gradient (f-h). wind scenarios.

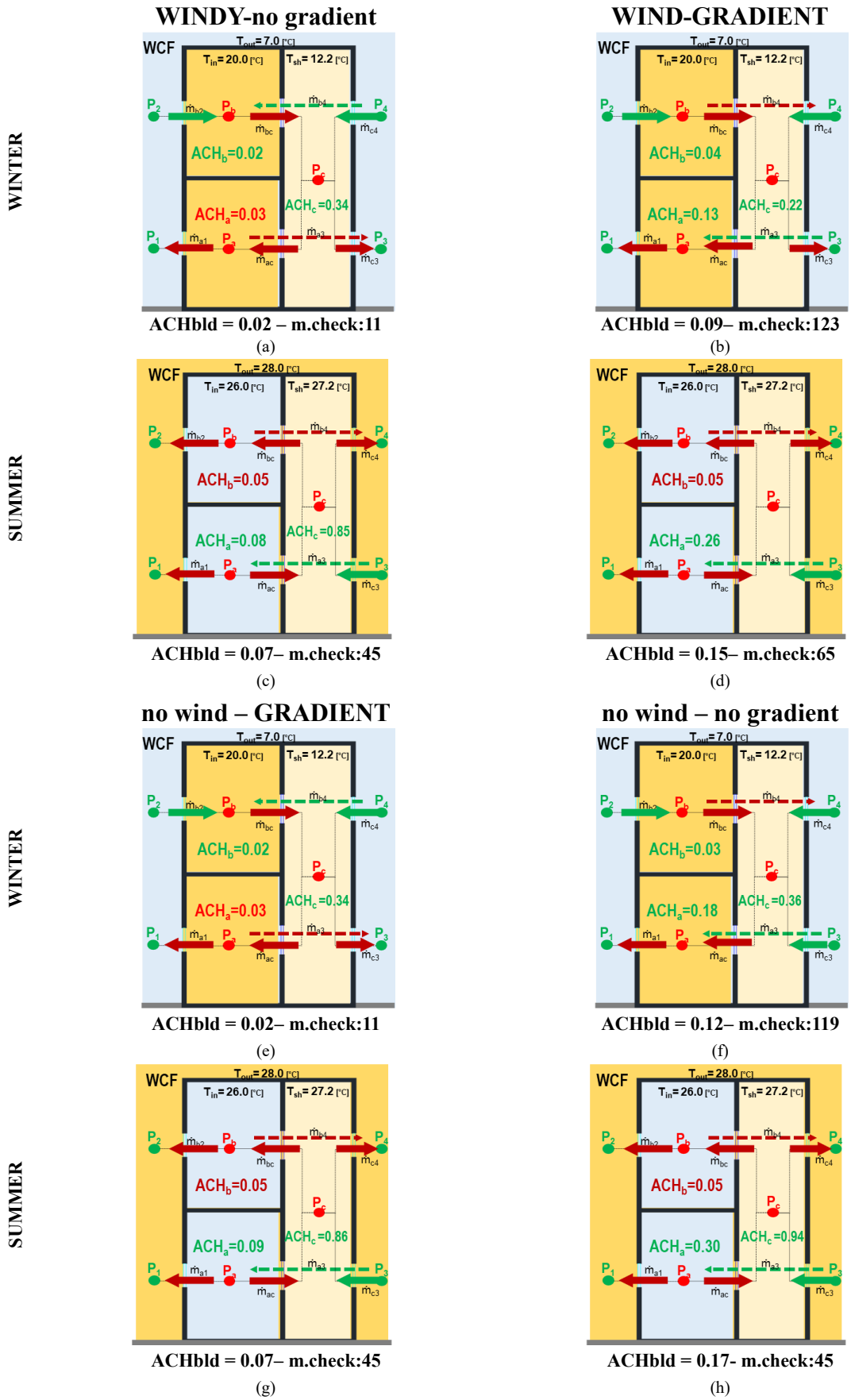

Fig. 87- Airflow displacement through buildings zones of building ID-57511. in a Large Canyon and Left position. considering WCF scenes for both winter (a-b-e-f) and summer (c-d-g-h) seasons. in windy-no gradient (a-c). windy-gradient (b-d). no wind-gradient (e-g). no wind-no gradient (f-h). wind scenarios.

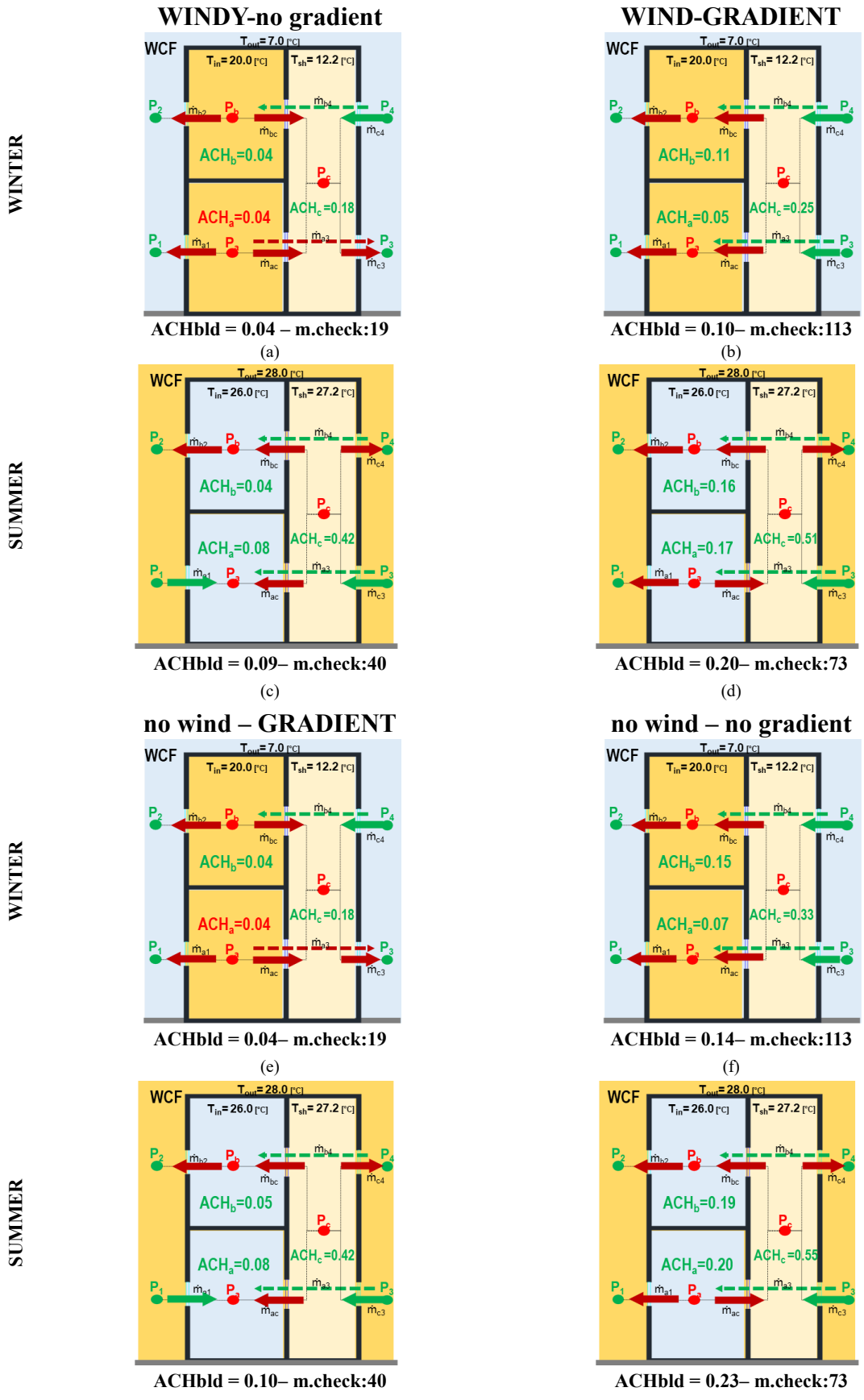

Fig. 88a-c - Airflow displacement through buildings zones of building ID-47293. in Narrow Canyon and Down position. considering WCF scenes for both winter (a-b-e-f) and summer (c-d-g-h) seasons. in windy-no gradient (a-c). windy-gradient (b-d). no wind-gradient (e-g). no wind-no gradient (f-h). wind scenarios.

For both buildings, in all scenarios considered, the results are considered acceptable, in relation to the evaluation of the relative and absolute error which is of the order of magnitude of $10^{-3.}$

Figures 86, 87 schematized the air flow displacement through the building zones of the building ID 57511, according to the results of the air flow rate m at the ten links, listed in Table 66.

The same in Figure 88 for the building ID 47293, according to the results of the air flow rate m at the ten links, listed in Table 67.

A pattern of air flow displacement and fluxes direction can be retrieved, observing results of both buildings.

Regarding the two windy scenarios, the same air flow displacement occurs, distinguishing the winter and the summer season; it is identified by the sign combination number: 113 (winter) and 73 (summer) for ID 47293 (only WCF scene). For ID 57511 the sign combination 119 (winter) in the WWF scene is the same in both effect scenarios, while it differs in WCF scene with combination sign equal to 119 and 123 for WINDY-nogradient and WINDY-GRADIENT scenarios, respectively. In the summer season the sign combination 45 occur in the WCF scene for both effect scenarios, while for the WWF scene it differs with combination sign 45 and 65 for WINDY-nogradient and WINDY-GRADIENT scenarios, respectively.

The same discussion can be done regarding the two no windy scenarios. The sign combination number of 19 (winter) and 40 (summer) occurs for ID 47293 (only WCF scene). For ID 57511 the sign combination 95 in winter season for the WWF scene is the same in both effect scenarios, and the same happens for the WCF scene with the combination sign equal to 11. In the summer season the sign combination 45 occur for both effect scenarios (no wind-no gradient and no wind-GRADIENT).

Considering the multiplicity of variables that influence the calculation of the number of achs per hour, evaluating the impact of each parameter could help to better understand the optimization and use of the 3-zones air flow lumped parameters model. Among the possible improvements of this model there is a sensitivity analysis regarding the following parameters: the level of air permeability in relation to the construction period of the building, here evaluated with 4 classes of equivalent area of leakage ($A_{e,leak}$); the influence of the width of the canyon on both building facades (W_{uc} and W_{co}), the influence of local climate boundary conditions (the 64 climate scenarios), especially considering how the WWF,WCF scenes dependent on the position of the building in the canyon affect the direction of the flows through the building zones. In addition, the low wind speed within the canyon, especially at heights below the Neutral Pressure Plane should be evaluated in order to explain part of the results.

4.5.7.7. Application of hourly ach to energy model: a case study

In this paragraph, the hourly ach results discussed in the previous chapter are applied to the hourly GIS-based engineering energy model for the evaluation of the hourly energy demand for space heating of residential buildings. Among the examined buildings, a case study building has been selected: the choice fell on a building for which real hourly heating consumption is available.

The objective of this work step is to evaluate the contribution of the hourly ach as input data of the energy model compared to the use of the fixed parameter in the definition of hourly energy consumption.

Results of the energy model with application of hourly ach will be compared with those of the model that uses the fixed parameter; both are then compared to the real consumption data to understand the model's ability to predict hourly energy consumption of the building during the heating season of an examined year.

This analysis constitutes the first test to evaluate the ability of ach hourly parameter to implement the energy model and improve its accuracy.

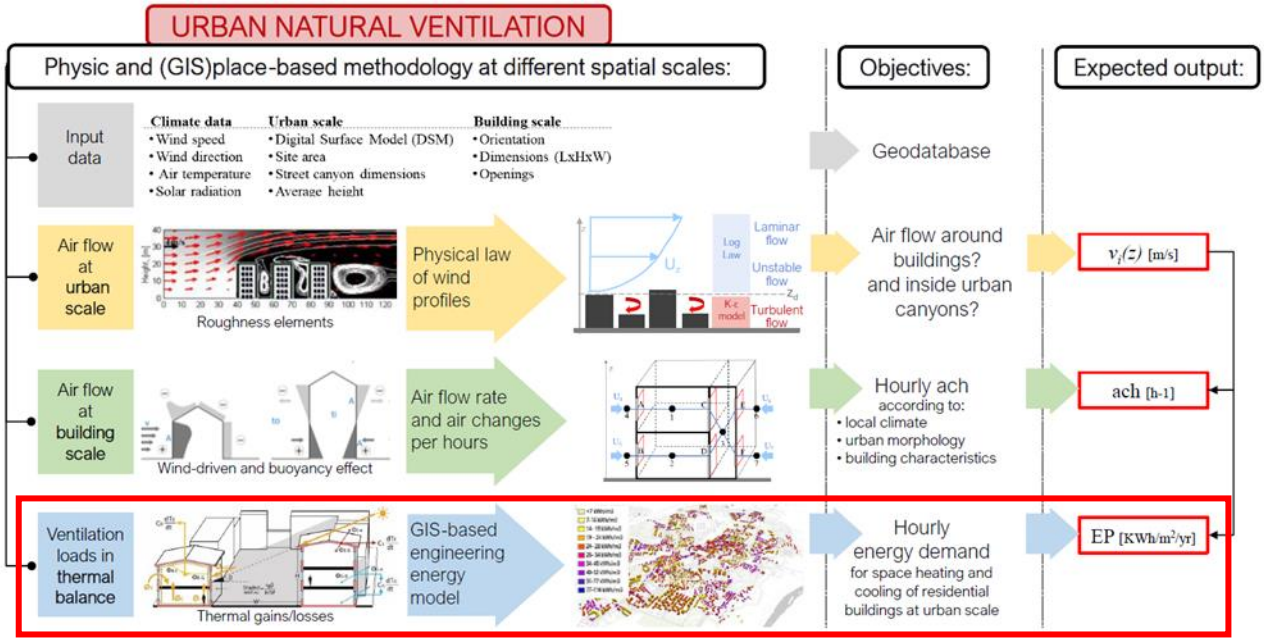

Fig. 89 - The work step investigated in this paragraph (red box) in the flowchart of the overall methodology.

Methodology, input data and case study.

Firstly, the case study building has been selected, among the already examined buildings in the three zones in the city of Turin discussed in the previous chapter. The chosen building is the ID 44723 in Raffaello zone, as it has a regular shape and whose real hourly energy consumption data were available. As indicated in Figure 90, the examined building is in a narrow canyon, NE-SW (30°N) oriented, and left positioned. The hourly energy consumption data have been collected from the local DSO and refer to the heating season 2022-2023 (15th Oct 2022 – 15th Apr 2023).

Since the examined climate years in the energy model will be the 2022 and 2023, it is necessary to assign to each hour of that years the proper hourly ach value, according to hourly meteorological

conditions of the two years with reference to the case-study building characteristics and the threshold values indicated in Table 68. These are used to assign to each hour of the examined years the proper climate scenarios that will be used to assign the correspondent ach hourly value; outdoor air temperature (T_{air}), wind velocity (U_{ref}) and temperature variation (ΔT) are used to determine the season, the windy or no-windy, and the gradient or no-gradient configuration, respectively.

Since the models considers the incident wind perpendicular to the facade of the building, it is necessary to assign an hourly value of ach only to the hours of the year with wind direction within the acceptable range, which is specifically defined for each case study building, according to its position in the canyon. In fact, the examined building is located in a canyon 30°N oriented, for which winds coming in the direction of 120°N±60° and 300°N±60° are considered acceptable.
Finally, in relation to the position of the building in the canyon, (in this case left positioned) and to the 3 shifts identified for each day (AM, PM, NIGHT), one of the four scenes foreseen by the configurations is attributed to each hour of the examined year: Windward Warm Facade (WWF), Windward Cold Facade (WCF), Leeward Warm Facade (LWF), or Leeward Cold Facade (LCF), according to the criteria explained in the schemes in Figure 47 (par.3.7.3.2).

In the assignment of hourly ach values to all hours of the years 2022 and 2023, different hypotheses are made:

i) *ACH hourly daily* - to all the night hours of the year, even those with acceptable wind direction, no ach values are assigned, considering the closing of the shielding
ii) *ACH hourly day&night* - to all night hours of the year, the values of ach corresponding to a cold facade scene are assigned, equating the absence of the sun to the condition of low thermal gradient (no-gradient scenario); the wind direction continues to be considered, thus attributing one of the only two possible conditions of windward (cold) or leeward (cold) façade
iii) *ACH all hours* - to all hours of the year with a not acceptable wind direction, the leeward façade scene is attributed; the 3 shifts identified for each day (AM, PM, NIGHT) continue to be considered.

Depending on the assumptions relating to each of the three hypotheses, the number of hours in the applied years (2022-2023) for which it is possible to associate an hourly value of ach can change, and it is reported in Table 69. Obviously, the last hypothesis (*ACH all hours*) is formulated to assign a value of ach at all hours of the year; for the first two hypotheses, however, the number of hours of the year to which a value of ach is associated is similar, with a slight increase in the case of the second hypothesis (*ACH hourly day&night*) due to the aim of considering night hours.

Table 68. Threshold values of outdoor air temperature T_{air}, wind speed U_{ref} and temperature variation ΔT in the four seasons.

Season	T_{air}	No windy	Windy	No gradient	Gradient
	[°C]	[m·s^{-1}]	[m·s^{-1}]	[-]	[-]
WINTER	$-4 \leq T_{air} < 11$	$U_{ref} < 1.5$	$U_{ref} > 1.5$	$\Delta T < 4.1$	4.1
MID-SEASON 1	$11 \leq T_{air} < 17$	$U_{ref} < 1.9$	$U_{ref} > 1.9$	$\Delta T < 6.3$	6.3
MID-SEASON 2	$17 \leq T_{air} < 24$	$U_{ref} < 1.8$	$U_{ref} > 1.8$	$\Delta T < 7.7$	7.7
SUMMER	$T_{air} \geq 24$	$U_{ref} < 2.2$	$U_{ref} > 2.2$	$\Delta T < 10.3$	10.3

Table 69. Number of ach values assigned considering all hours in the heating season 2022-2023.

	Ach values assigned	
	[n]	**[%]**
ACH hourly daily	3098	35%
ACH hourly day&night	4787	55%
ACH all hours	8760	100%
Total hours (2022-2023)	**8760**	**100%**

Fig. 90 – The examined building 44723 located in a narrow canyon Raffaello, NE-SW (30°N) oriented, and left positioned.

For a detailed description of the hourly dynamic thermal balance of three thermodynamic systems (TSs) at building scale on which the GIS-based engineering energy model is based on, reference is made to paragraph 2.3.3 of this document.

As previously detailed, the main input data refers to three main categories. These are listed below in application to the case-study building:

- **geometrical and other characteristics of the buildings archived** in georeferenced GIS database; among these, one of the main important parameters is the period of construction of the examined building according to which are assigned the fixed ach values and the thermal characteristics of building's components, as reported in Table 70.
  In this case-study the ach is equal to 0.5, as the building ID 44723 has been built in 1919-1945 period. Among the thermo-physical properties of the buildings: the thermal transmittances (*U*), the thermal capacities (*C*) of both the opaque (wall, roof, ground) and

transparent (glazing) envelopes, the solar energy transmittance of the glass ($g_{\perp}$), and the performance (η) of the centralized heating system connected to the district heating network (DHN).

- **local climate characteristics**, retrieved from data recorded by local weather station. The main input parameters are the outdoor air temperature, *Tair* [°C], the relative humidity, *HR* [%], the atmospheric pressure *Patm* [HPa], the global, direct and diffuse solar radiation [W/m^2], and the height of the sun, *Hsun* [°]. From these inputs, many parameters used in the model are subsequently calculated. In this case-study hourly climate input data refers to the years 2022-2023.
- **Heating schedule,** which contains information relating to the occupant's behavior, specific for a residential building and the operating hours of the centralized system connected to the district heating network, which is managed by the network operator (DSO). In the baseline scenario, the system's operating hours follow the indications of the national and local regulations, according to the type of user and climate zone. In this case study, to reduce primary energy consumption and manage network peaks, the DSO opted to reduce the set point temperature by 2°C at two times of the day (9 AM and 2 PM). To calibrate the GIS-based energy model based on real consumption data provided by the DSO, it has been adapted to consider this issue.

Table 70. Thermo-physical characteristics of buildings and ACH according to construction period.

	WALL		**ROOF**	**GROUND**	**GLAZING**			**ACH**	**DHN**
	$C_{envelope}$	**U_{wall}**	**U_{roof}**	**U_{floor}**	**U_g**	**WWR_l**	**$g_{\perp}$**	***Vol/h***	**η**
Period	$kJ \cdot m^{-2} \cdot K^{-1}$	$W \cdot m^{-2} \cdot K^{-1}$	$W \cdot m^{-2} \cdot K^{-1}$	$W \cdot m^{-2} \cdot K^{-1}$	$W \cdot m^{-2} \cdot K^{-1}$	-	-	-	-
< 1918	504	1.45	1.80	1.75	4.85	0.13	0.85	0.5	0.78
1919-45	**504**	**1.35**	**1.80**	**1.58**	**4.75**	**0.13**	**0.85**	**0.5**	**0.78**
1946-60	283	1.18	1.80	1.23	4.40	0.20	0.85	0.5	0.78
1961-70	283	1.13	2.20	1.30	4.90	0.20	0.85	0.5	0.79
1971-80	257	1.04	2.20	1.00	3.80	0.25	0.75	0.5	0.80
1981-90	264	0.78	1.18	0.95	3.80	0.20	0.75	0.5	0.82
1991-00	274	0.7	0.68	0.80	2.15	0.20	0.67	0.5	0.84
2001-05	274	0.7	0.68	0.80	2.15	0.20	0.67	0.3	0.84
2006-12	267	0.42	0.38	0.41	2.60	0.20	0.50	0.3	0.92
2013-15	267	0.34	0.30	0.33	2.20	0.20	0.50	0.3	0.92
2016-19	267	0.30	0.25	0.30	1.80	0.20	0.35	0.3	0.92

Then, the energy model has been applied to the case study building, considering the following scenarios:

i) *ACH constant*
ii) *ACH hourly daily*
iii) *ACH hourly day&night*
iv) *ACH all hours*

Results and discussion.

In this section, results from the application of constant and hourly ach are compared, considering the hypothesis scenarios presented in the previous part; all scenarios are then compared to the real consumption data of the case study building.

The main output of the energy model used for the comparison are the heat flow rate by ventilation (φ_V), as it directly depends on the ach values, and the heating energy demand for space heating (φ_H) required by the building.

In Figure 91 a-l are reported the hourly profiles of the energy demand for space heating φ_H [kWh] (left column) and the heat flow rate by ventilation φ_V [kWh] (right column), for selected days during the heating season. The four scenarios are compared.
Regarding consumption for heating, on all selected days the constant ach scenario maintains slightly higher values and a more regular trend. all scenarios present three upper peaks and two lower peaks, the latter due to the change in the setpoint temperature by the district heating network manager (at 9AM and 2 PM). The trend and hourly values of the profiles of the *ach hourly daily* (in yellow) and *ach d&n* (in green) scenarios coincide except for night-time hours. The trend of the *ach all hours* scenario (in purple) also does not differ much from the others, but is more irregular.
Observing the hourly profiles of the ventilation load (right column), the constant *ach scenario* (dotted pink line) reports a more regular profile and higher values than in all the other scenarios, almost double in daytime hours. On some selected days (February) the profile of the *ach hourly daily* scenario (dotted yellow line) coincides with that of the *ach d&n scenario* (dotted green line), on others (January) it coincides with that of the *ach all hours* (dotted violet line) scenario.

Table 71. Daily energy demand for space heating φ_H [kWh/d] in representative days during the heating season comparing the four ach scenarios and the real consumption data (φ_m).

Daily consumption [kWh/d]	**30th Nov**	**26th Dec**	**18th Jan**	**9th Feb**	**1st Mar**
Φ_m	548	441	633	601	501
Φ_H (ach cons)	537	486	663	632	486
Φ_H (ach hourly daily)	458	440	556	535	426
Φ_H (ach hourly d&n)	455	437	556	535	426
Φ_H (ach hourly all hours)	421	406	536	521	404

Table 72. Absolute errors [%] of the energy model in predicting the hourly daily energy demand for space heating φ_H in representative days of the heating season comparing the four ach scenarios.

Absolute errors [%]	**30th Nov**	**26th Dec**	**18th Jan**	**9th Feb**	**1st Mar**
Φ_H (ach cons)	98%	**110%**	**105%**	**105%**	97%
Φ_H (ach hourly daily)	84%	**100%**	**88%**	**89%**	85%
Φ_H (ach hourly d&n)	83%	99%	88%	89%	85%
Φ_H (ach hourly all hours)	77%	92%	85%	87%	81%

Table 71 shows the resulting daily consumption for each of the days selected in each month of the heating season, comparing the four scenarios with the actual measured data. For each scenario and day examined, Table 72 shows the absolute error values, calculated as the ratio between predicted data and measured data. Among the four scenarios, *constant ach* is the most accurate in predicting daily hourly consumption. The *ach hourly daily* and *ach day & night* scenarios are very similar and

both acceptable for estimating hourly consumption, although with a lower precision than the *constant ach* scenario. The ach *hourly all hours* scenario reports poorer results and lower predictive ability.

In Figure 92 a-f, two scenarios are compared, both in some selected days during the heating season: the *ach constant* and the *ach hourly daily* scenarios, respectively on the left and right columns.
The hourly profiles of the daily energy demand for space heating φ_H [kWh] (continuous red line) is compared to the measured data φ_m [kWh] (dashed red line); the other relevant heat flow rates [kWh] are: the heat flow rate by ventilation φ_V (blue line), the heat flow rate by internal gains φ_I (violet line), the heat flow rate by transmission from opaque envelope $\varphi_{t,e}$ (light green line), the heat flow rate by transmission from transparent envelope $\varphi_{t,g}$ (dark green line), the heat flow rate by solar irradiation φ_{sol} (orange line). In addition, the solar irradiance $I_{sol,h}$ [W·m-2] is shown (dotted orange line).

For each of the days selected in each month of the heating season, by comparing the predicted consumption (continuous red lines) and the actual measured data (dashed red lines) it is possible to state that there is correspondence in the trend of the profiles for both scenarios.

Furthermore, observing the graphs, it is evident how the hourly consumption in the case of the scenario with hourly ach are all slightly lower than the corresponding values in the scenario with constant ach.

Table 73 shows the resulting monthly and seasonal consumption [kWh] of the heating season 2022-2023, comparing the four scenarios with the actual measured data. For each scenario examined, Table 74 shows the absolute error values [%], calculated as the ratio between predicted data and measured data. Among the four scenarios, *constant ach* is the most accurate in predicting daily hourly consumption. The *ach hourly daily* and *ach day & night* scenarios are very similar and both acceptable for estimating hourly consumption, although with a lower precision than the *constant ach* scenario. The ach *hourly all hours* scenario reports poorer results and lower predictive ability.

Figure 93 a-b presents the comparison of the daily and monthly energy demand for space heating (φ_H) of the building during the heating season 2022-2023 in the four scenarios and the real consumption data (φ_m).
The early (Oct and Nov) and late (Apr and May) months of the heating season are more difficult to predict, as the energy model works best during the colder, central months of the season (Dec-Jan-Feb). The constant scenario appears to be the closest to the real data. The hourly scenarios are similar to each other, and all predict lower consumption values.
In this first test of application of the hourly ach in the model, a clear contribution of the parameter in improving the ability to estimate consumption for space heating does not emerge. This may be caused by the fact that the calibration of the energy model prior the application of hourly ach and therefore carried out only for the scenario with constant ach. Despite this, the inclusion of hourly ach does not compromise the reliability of the model and constitutes a promising parameter to investigate.

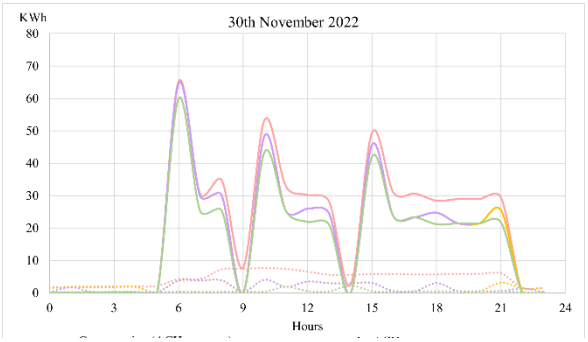

(a)

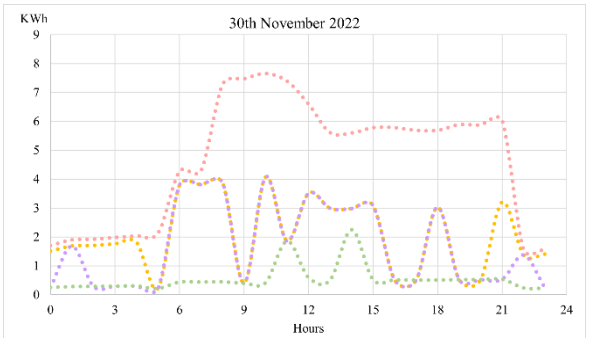

(b)

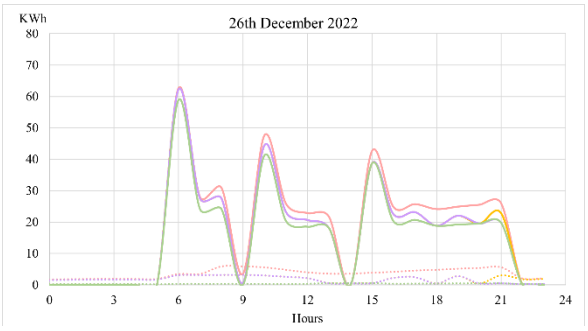

(c)

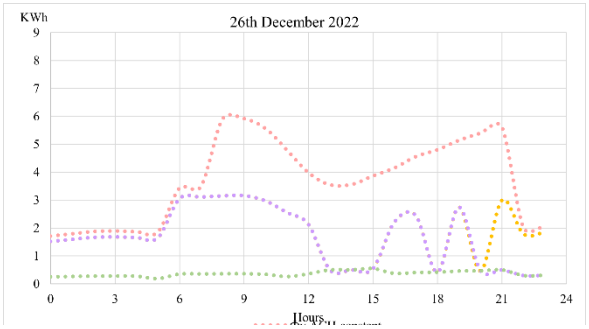

(d)

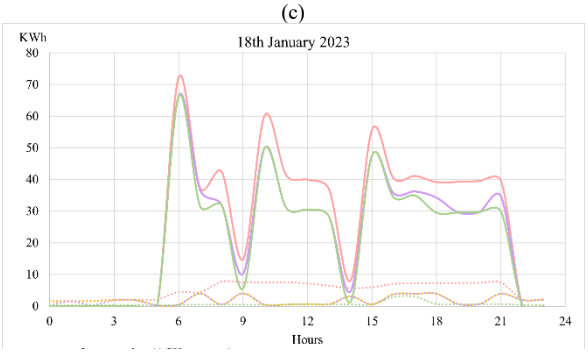

(e)

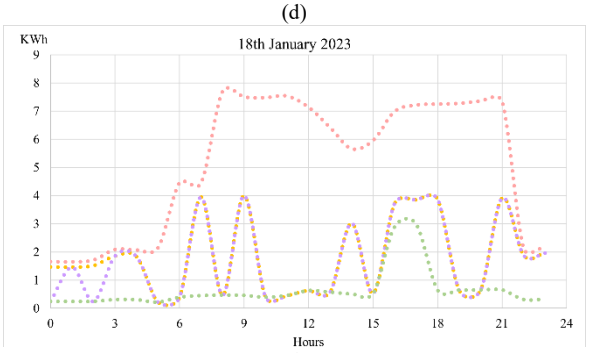

(f)

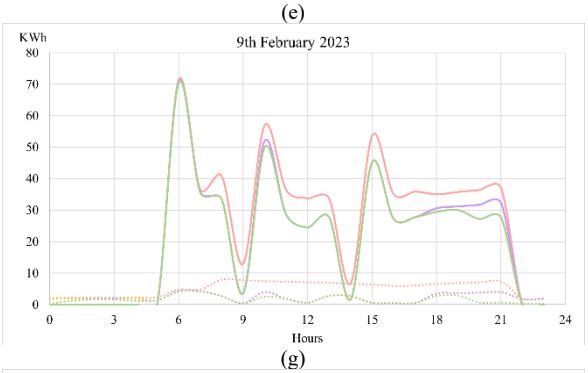

(g)

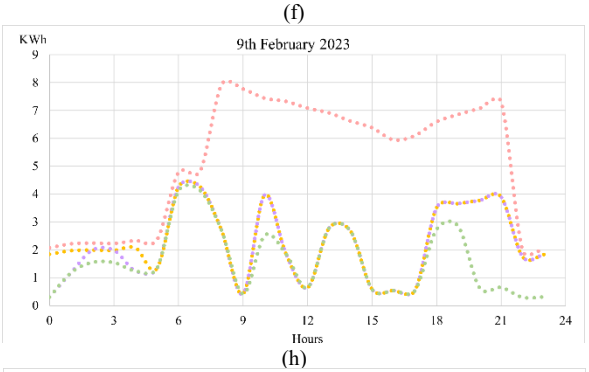

(h)

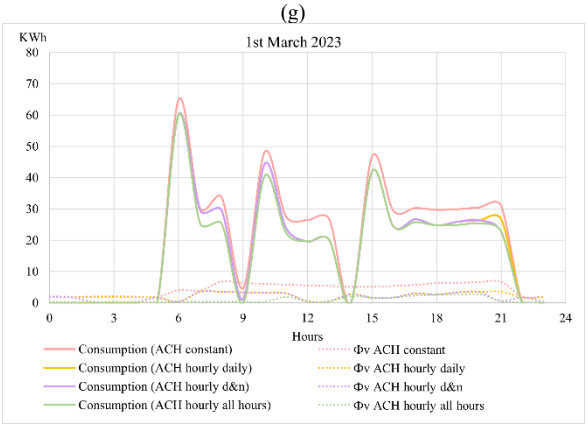

i(i)

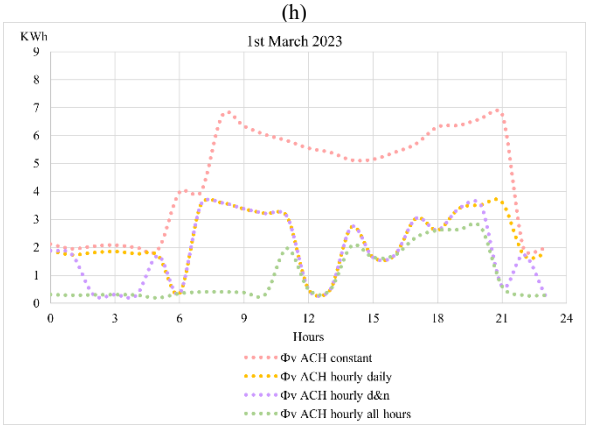

(l)

Fig. 91a-l – Hourly profiles of the energy demand for space heating φ_H [kWh] (left colum) and heat flow rate by ventilation φ_V [kWh] for selected days during the heating season for each of the four ach scenarios.

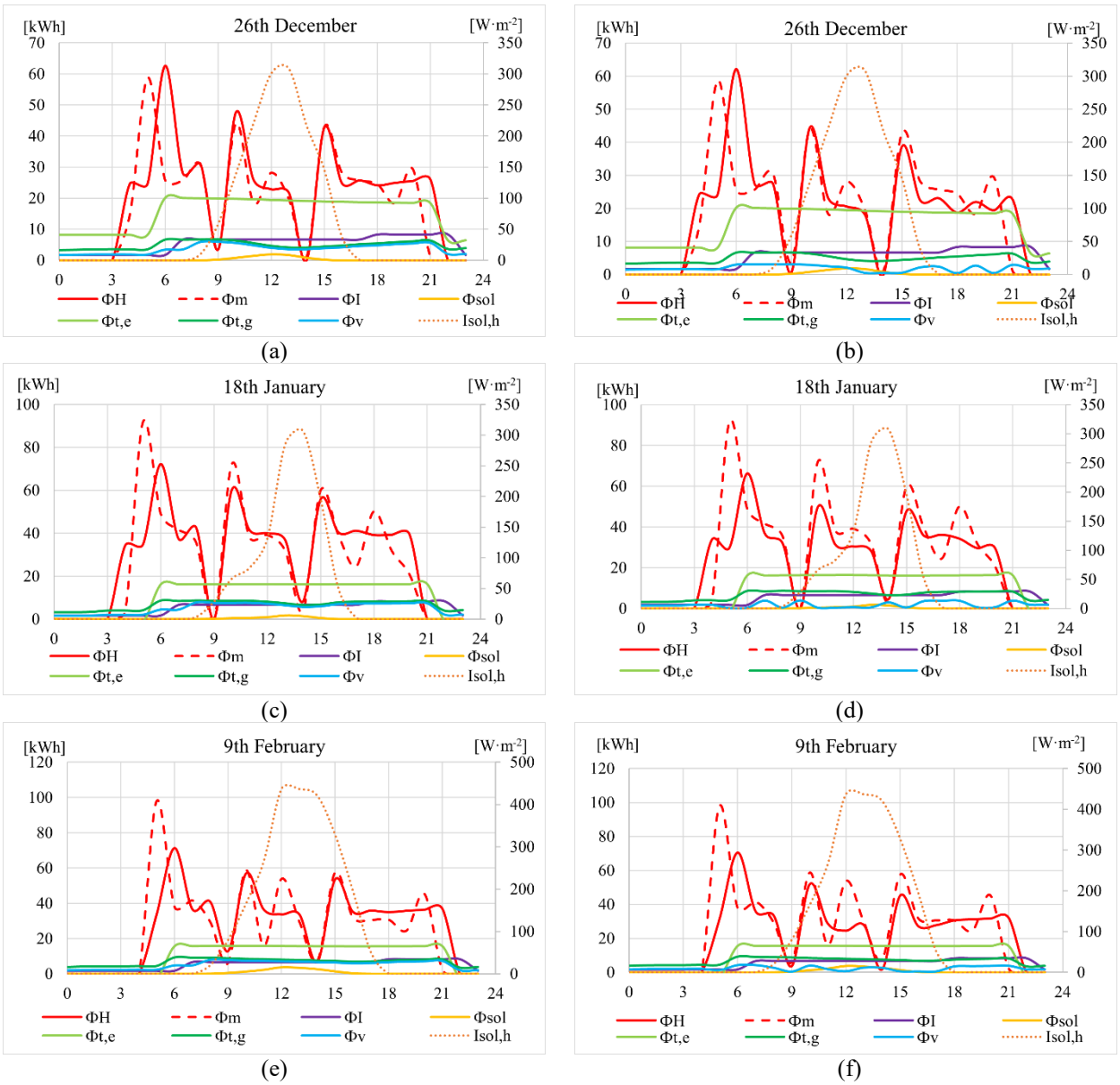

Fig. 92 a-f– Comparison of the hourly profiles of the energy demand for space heating φ_H [kWh] (continuous red line) and measured data φ_m [kWh] (dashed red line), other relevant heat flow rates [kWh], and solar irradiance $I_{sol,h}$ [W·m^{-2}] (dotted orange line), for selected days during the heating season for the *ach constant* (left column) and the *ach hourly daily* (right column) scenarios.

Table 73. Monthly and seasonal energy demand for space heating φ_H [kWh] comparing the four ach scenarios and the real consumption data (φ_m).

Montlhy consumption [kWh]	Nov 2022	Dec 2022	Jan 2023	Feb 2023	Mar 2023	Apr 2023	Seasonal
Φ_m	10.807	18.032	17.017	13.201	9.247	1.629	69.933
Φ_H (ach cons)	8.235	18.898	17.227	11.937	5.444	602	62.342
Φ_H (ach hourly daily)	6.994	16.807	14.945	10.476	4.661	535	54.419
Φ_H (ach hourly d&n)	6.965	16.765	14.899	10.429	4.641	531	54.230
Φ_H (ach hourly all h)	6.561	15.604	14.192	9.844	4.412	501	51.114

Table 74. Absolute errors [%] of the energy model in predicting the hourly monthly and seasonal energy demand for space heating φ_H comparing the four ach scenarios.

Absolute errors [%]	Nov 2022	Dec 2022	Jan 2023	Feb 2023	Mar 2023	Apr 2023	Seasonal
Φ_m	76%	105%	101%	90%	59%	37%	89%
Φ_H (ach cons)	65%	93%	88%	79%	50%	33%	78%
Φ_H (ach hourly daily)	64%	93%	88%	79%	50%	33%	78%
Φ_H (ach hourly d&n)	61%	87%	83%	75%	48%	31%	73%
Φ_H (ach hourly all h)	76%	105%	101%	90%	59%	37%	89%

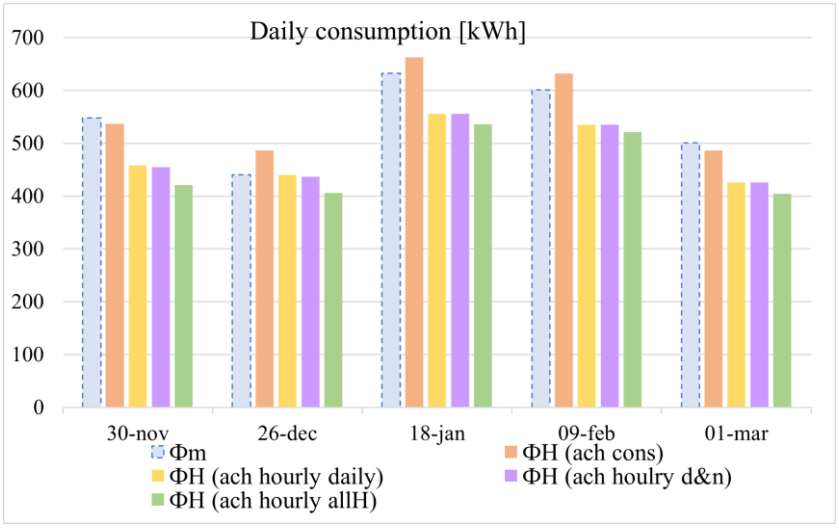

(a)

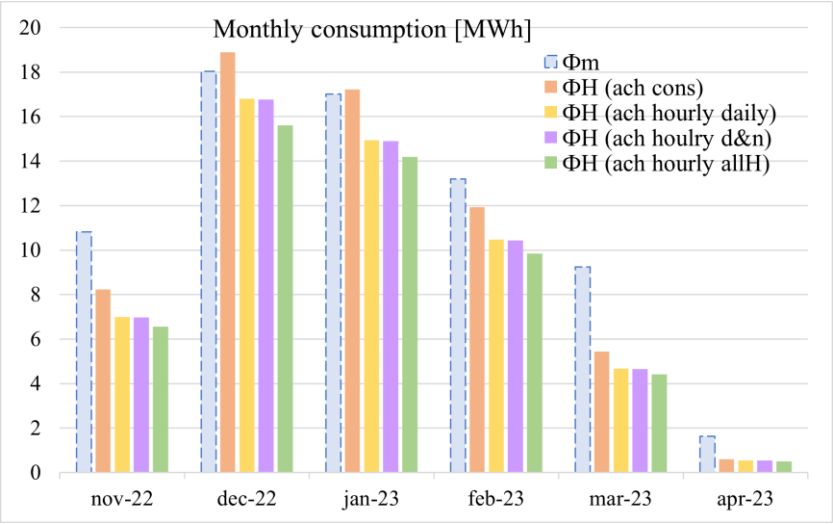

(b)

Fig. 93a-b – Comparison of the daily (a) and monthly (b) energy demand for space heating (φ_H) of the building during the heating season 2022-2023 in the scenarios based on constant ach (in pink), houlry daily ach (in yellow), hourly day and night ach (in violet), houlry ach in all hours (in green), and the real consumption data (φ_m).

Chapter 5 – Conclusion

To assess and manage the distribution of building energy consumption at urban scale, place-based USBEM are fundamental. This models and tools can be used to assessed site-specific evaluations to include in the model important parameters explaining peculiarities of each case study.

The evaluation of urban natural ventilation that affect the air flow rate at building scale and impact the energy performance of buildings requires this type of models and tools since it is strictly influenced by the local climate conditions, and the specific form of the urban built context.

This doctoral thesis has described a GIS-place based methodology to evaluate natural ventilation at different spatial scale as a physical phenomenon that varies according to scale.

The proposed methodology has integrated physic equations and the use of GIS to consider local characteristics of the real built environment. This improvement consent to increase the number and quality of energy-related variables through geo-databases, to comprehend the relationships behind spatial patterns, to rely on new tools appropriately selected to be adapted to the research's objectives, optimizing techniques to analyze any territory and city.

From the analyses at urban scale of the height zd of the displacement layer applying a place-based methodology based on the Q-GIS UMEP plug-in, the main findings concern the possibility to spatially describe the distribution of this output parameter, considering several boundary conditions with fast simulations. In this research, the height zd has been used as a threshold value to rapidly assess the type of wind motion and assign to each urban canyon within the whole city the proper wind profile. In this way, it is possible to spatially represents in which urban canyons turbulence flows are generated due, and the spatial correlation between the characteristics of the urban morphology that influence it. In this work it was highlighted how the accuracy of the initial data of the digital surface model impacts the accuracy and precision of the output data and the possibility of using the results in subsequent evaluations.

Future outlook to implement this step of analysis concern the accuracy of the model: it can be improved by investigating the influence of some parameters on the final result of the simulations; especially the setting parameters relating to the plug-in and specifically those relating to the definition of the spatial analysis grid and the observation radius for each analysed cell, as do not exist yet many scientific works assessing limits and possible implementation of the plug-in in this type of applications.

Regarding the application of a CFD model simulations to evaluate the turbulent wind field inside urban canyon, the proposed methodology has investigated urban airflows pattern in non-isothermal conditions at urban scale, in the attempt of contributing to fill the gap of this specific research field. The GIS-place based methodology has tried to integrate physical equations of turbulence together with the definition of input parameters as a result of analyses carried out in GIS environment in order to identified classes of urban canyons as representative of the whole city, considering two important parameters: the aspect ratio and the canyon axis orientation.

Future outlook regarding the step of analysis at canyon scale with CFD simulation can be the validation of the CFD results with experimental data; in addition, the implementation of input parameters can be useful to define the boundary condition of the CFD domain and to better refine the accuracy of results.

The main contribution of this doctoral research is the definition of the three-zones air flow lumped model used to assess the hourly variation of the number of air changes per hour (ach). The air displacement in a building is determined, considering only the air flow rate due to infiltrations, depending on leakages' characteristics and pressure variation due to the wind and buoyancy effect. The fsolve function has been used to solve the non-linear equations of mass conservation, through an iterative procedure.

The outdoor environmental condition of dynamic and static pressure on building façades have been determined by experimental values (Cp) and CFD simulations on urban canyons. Different climate scenarios have been considered to investigate the velocity field in the domain, evaluating the contributions of cross wind flow and thermal buoyancy in urban canyons with different dimensions. Then, polynomial function is interpolated to obtain the description of wind speed as function of the elevation.

In its application to several buildings in different case study zones in any possible climate and urban scenario assessed, the three-zones air flow model allow to easily evaluate how the ach is affected by some crucial parameters: at the building scale, the level of air permeability in relation to the construction period of the building, here evaluated with 4 classes of equivalent area of leakage (Ae,leak) and the number of opening in each zone; regarding the urban scale where geometries and spatial reciprocity between the canyon and the building are considered, the canyon width (Wuc) and the position of the building in the canyon; lastly, the local climate boundary conditions, in this work 64 climate scenarios have been identified as representative of a whole typical climate year.

The accuracy of the model can be improved by implementing and optimizing the input data or with sensitivity analysis concerning the already mentioned input variables that is evident affect strongly the number of air changes per hour.

The field of application of the model is strictly related to the level of accuracy of the main input data, i.e. the geo-referenced cartographic data base that contains information relating to the buildings. The greater the accuracy of the information, including spatial information, the greater the number of buildings that can be evaluated. In this case, the pre-processing phase can be implemented to increase the number of buildings in line with the 3-zone air flow model assumptions and suitable for its application.

The airflow model proposed in this study represent an optimal balanced tool to properly describe physical phenomena, to rely on an efficient number of input variables, to detail buildings' characteristics; a methodology whit a schematic and synthetic description of the actual case study that is simple enough to be applied to all buildings in an urban area.

The application of the three-zone air flow model to all the buildings in a case study zone results in a new dataset for each building with all the possible ach values that the building can have during the whole year. This dataset enriches the GIS-based building database used in the energy model: in fact, the new energy-related input parameters of the hourly ach can be used as optimization and calibration parameters of the GIS-based engineering energy model for the hourly space heating consumption of residential building. The new dataset of ach values provide a wide and exhaustive case history describing the hourly variation of ach values for any building examined, that can replace the fixed ach values used in the energy model. Then, in the energy assessment of the energy performance of buildings, the contribution of each thermal gain and loss in the thermal energy balance can be evaluated separately, with a focus on ventilation loads.

Relying on open-source software with high level of integrability provides for the possibility to implement the proposed methodology with existing plug-in for application at larger spatial scale with simulations that last just few hours. Among the possible applications of the presented place-based methodology, there is its integration in a digital platform to simulate urban energy scenarios, combining ventilation assessment. It provides for the possibility of mapping an entire city, helping policy makers, urban planners, public administration, and citizens in architectural and urban planning capable of exploiting the morphological peculiarities of the built environment to increase the energy efficiency of buildings and make urban space more liveable.

Reference

[1] K. Calvin *et al.*. «IPCC. 2023: Climate Change 2023: Synthesis Report. Contribution of Working Groups I. II and III to the Sixth Assessment Report of the Intergovernmental Panel on Climate Change [Core Writing Team. H. Lee and J. Romero (eds.)]. IPCC. Geneva. Switzerland.». Intergovernmental Panel on Climate Change (IPCC). lug. 2023. doi: 10.59327/IPCC/AR6-9789291691647.

[2] United Nations Environment Programme. *Emissions Gap Report 2023: Broken Record – Temperatures hit new highs. yet world fails to cut emissions (again)*. United Nations Environment Programme. 2023. doi: 10.59117/20.500.11822/43922.

[4] F. Mancini e G. Lo Basso. «How Climate Change Affects the Building Energy Consumptions Due to Cooling. Heating. and Electricity Demands of Italian Residential Sector». *Energies*. vol. 13. fasc. 2. Art. fasc. 2. gen. 2020. doi: 10.3390/en13020410.

[5] F. Peron. M. M. De Maria. F. Spinazze. e U. Mazzali. «An analysis of the urban heat island of Venice mainland». *Sust. Cities Soc.*. vol. 19. pp. 300–309. dic. 2015. doi: 10.1016/j.scs.2015.05.008.

[6] International Energy Agency (IEA), The Critical Role of Buildings Perspectives for the Clean Energy Transition – April 2019, https://www.iea.org/reports/the-critical-role-of-buildings, (last access, 2024 May the 23rd);

[7] EEA European Environment Agency - Europe's air quality status 2024, https://www.eea.europa.eu//publications/europes-air-quality-status-2024, (last access, 2024 May the 23rd);

[8] WHO – World Health Organization, Health and Energy Platform of Action (HEPA) Report 2020–2022 Building connections for better health, https://iris.who.int/bitstream/handle/10665/375840/9789240071650-eng.pdf?sequence=1 (last access, 2024 May the 23rd).

[9] United Nation UN, World Urbanization Prospects 2018 Population Division, https://population.un.org/wup/Download/ (last access, 2024 May the 23rd);

[10] «EU TRANSPORT IN FIGURES – STATISTICAL POCKETBOOK 2023». 2023.

[11] Stockholm Environment Institute. A. Dzebo. e Z. Shawoo. «Sustainable Development Goal interactions through a climate lens: a global analysis». Stockholm Environment Institute. feb. 2023. doi: 10.51414/sei2023.010.

[12] European Commision, The European Green Deal - Striving to be the first climate-neutral continent, https://commission.europa.eu/strategy-and-policy/priorities-2019-2024/european-green-deal_en, (last access, 2024 May the 23rd);

[13] United Nation Climate change UNCC , Paris Agreement 2015, https://unfccc.int/sites/default/files/english_paris_agreement.pdf, (last access, 2024 May the 23rd);

[14] *Directive (EU) 2018/2001 of the European Parliament and of the Council of 11 December 2018 on the promotion of the use of energy from renewable sources (recast) (Text with EEA relevance.)*. vol. 328. 2018. Consultato: 25 giugno 2024. [Online]. Disponibile su: http://data.europa.eu/eli/dir/2018/2001/oj/eng

[15] «DIRECTIVE (EU) 2019/ 944 OF THE EUROPEAN PARLIAMENT AND OF THE COUNCIL - of 5 June 2019 - on common rules for the internal market for electricity and amending Directive 2012/ 27/ EU».

[16] Ministero dell'Ambiente e della Sicurezza Energetica, PIANO NAZIONALE INTEGRATO PER L'ENERGIA E IL CLIMA, PNIEC, giugno 2023, https://www.mase.gov.it/sites/default/files/PNIEC_2023.pdf , (last access, 2024 May the 23rd);

[17] Consiglio dei Ministri, Piano Nazionale di Ripresa e Resilienza PNRR 2021, https://www.governo.it/sites/governo.it/files/PNRR.pdf , (last access, 2024 May the 23rd);

[18] V. Todeschi. P. Marocco. G. Mutani. A. Lanzini. e M. Santarelli. «Towards Energy Self-consumption and Self-sufficiency in Urban Energy Communities». *IJHT*. vol. 39. fasc. 1. pp. 1–11. feb. 2021. doi: 10.18280/ijht.390101.

[19] S. Bibri. «The IoT for Smart Sustainable Cities of the Future: An Analytical Framework for Sensor-Based Big Data Applications for Environmental Sustainability». *Sustainable Cities and Society*. vol. 38. feb. 2018. doi: 10.1016/j.scs.2017.12.034.

[20] P. Nageler *et al.*. «Novel validated method for GIS based automated dynamic urban building energy simulations». *Energy*. vol. 139. pp. 142–154. nov. 2017. doi: 10.1016/j.energy.2017.07.151.

[21] P. Caputo e G. Pasetti. «Boosting the energy renovation rate of the private building stock in Italy: Policies and innovative GIS-based tools». *Sust. Cities Soc.*. vol. 34. pp. 394–404. ott. 2017. doi: 10.1016/j.scs.2017.07.002.

[22] A. Alhamwi. W. Medjroubi. T. Vogt. e C. Agert. «GIS-based urban energy systems models and tools: Introducing a model for the optimisation of flexibilisation technologies in urban areas». *Appl. Energy*. vol. 191. pp. 1–9. apr. 2017. doi: 10.1016/j.apenergy.2017.01.048.

[23] G. Mutani. S. Santantonio. e D. Goulias. «Environmental protocol for Energy Communities». in *2020 IEEE 3rd International Conference and Workshop in Óbuda on Electrical and Power Engineering (CANDO-EPE)*. nov. 2020. pp. 000191–000196. doi: 10.1109/CANDO-EPE51100.2020.9337784.

[24] L. Anselin. «Interactive Techniques and Exploratory Spatial Data Analysis». *Regional Research Institute Working Papers*. gen. 1996. [Online]. Disponibile su: https://researchrepository.wvu.edu/rri_pubs/200

[25] F. Johari. G. Peronato. P. Sadeghian. X. Zhao. e J. Widén. «Urban building energy modeling: State of the art and future prospects». *Renewable and Sustainable Energy Reviews*. vol. 128. p. 109902. ago. 2020. doi: 10.1016/j.rser.2020.109902.

[26] G. Mutani e V. Todeschi. «Optimization of Costs and Self-Sufficiency for Roof Integrated Photovoltaic Technologies on Residential Buildings». *Energies*. vol. 14. fasc. 13. Art. fasc. 13. gen. 2021. doi: 10.3390/en14134018.

[27] G. Mutani e V. Todeschi. «Building energy modeling at neighborhood scale». *Energy Efficiency*. vol. 13. fasc. 7. pp. 1353–1386. ott. 2020. doi: 10.1007/s12053-020-09882-4.

[28] «Statistical Data Analysis for Energy Communities | IIETA». Consultato: 23 giugno 2024. [Online]. Disponibile su: https://www.iieta.org/journals/ti-ijes/paper/10.18280/ti-ijes.642-438

[29] G. Mutani. V. Todeschi. e S. Santantonio. «Urban-Scale Energy Models: the relationship between cooling energy demand and urban form». *J. Phys.: Conf. Ser.*. vol. 2177. fasc. 1. p. 012016. apr. 2022. doi: 10.1088/1742-6596/2177/1/012016.

[30] S. Santantonio e G. Mutani. *QGIS-based tools to evaluate air flow rate by natural ventilation in buildings at urban scale*. 2023.

[31] G. Mutani. S. Santantonio. e V. Todeschi. «Evaluation of ventilation loads in buildings energy modelling at urban scale». in *2021 IEEE 4th International Conference and Workshop Óbuda on Electrical*

and Power Engineering (CANDO-EPE). nov. 2021. pp. 37–42. doi: 10.1109/CANDO-EPE54223.2021.9667547.

[32] N. Buckley. G. Mills. C. Reinhart. e Z. M. Berzolla. «Using urban building energy modelling (UBEM) to support the new European Union's Green Deal: Case study of Dublin Ireland». *Energy and Buildings*. vol. 247. 2021. doi: 10.1016/j.enbuild.2021.111115.

[33] U. Ali. M. H. Shamsi. C. Hoare. E. Mangina. e J. O'Donnell. «Review of urban building energy modeling (UBEM) approaches. methods and tools using qualitative and quantitative analysis». *Energy and Buildings*. vol. 246. p. 111073. set. 2021. doi: 10.1016/j.enbuild.2021.111073.

[34] S. Basu. C. S. E. Bale. T. Wehnert. e K. Topp. «A complexity approach to defining urban energy systems». *Cities*. vol. 95. p. 102358. dic. 2019. doi: 10.1016/j.cities.2019.05.027.

[35] Y. Q. Ang. Z. M. Berzolla. e C. F. Reinhart. «From concept to application: A review of use cases in urban building energy modeling». *Applied Energy*. vol. 279. 2020. doi: 10.1016/j.apenergy.2020.115738.

[36] J. Allegrini. K. Orehounig. G. Mavromatidis. F. Ruesch. V. Dorer. e R. Evins. «A review of modelling approaches and tools for the simulation of district-scale energy systems». *Renewable and Sustainable Energy Reviews*. vol. 52. pp. 1391–1404. dic. 2015. doi: 10.1016/j.rser.2015.07.123.

[37] G. Pagliarini e S. Rainieri. «Restoration of the building hourly space heating and cooling loads from the monthly energy consumption». *Energy and Buildings*. vol. 49. pp. 348–355. 2012. doi: 10.1016/j.enbuild.2012.02.030.

[38] V. S. K. V. Harish e A. Kumar. «A review on modeling and simulation of building energy systems». *Renewable and Sustainable Energy Reviews*. vol. 56. pp. 1272–1292. apr. 2016. doi: 10.1016/j.rser.2015.12.040.

[39] M. Ferrando. F. Causone. T. Hong. e Y. Chen. «Urban building energy modeling (UBEM) tools: A state-of-the-art review of bottom-up physics-based approaches». *Sustainable Cities and Society*. vol. 62. p. 102408. nov. 2020. doi: 10.1016/j.scs.2020.102408.

[40] A. Doma e M. Ouf. «Modelling occupant behaviour for urban scale simulation: Review of available approaches and tools». *Build. Simul.*. ott. 2022. doi: 10.1007/s12273-022-0939-3.

[41] L. G. Swan e V. I. Ugursal. «Modeling of end-use energy consumption in the residential sector: A review of modeling techniques». *Renewable and Sustainable Energy Reviews*. vol. 13. fasc. 8. pp. 1819–1835. ott. 2009. doi: 10.1016/j.rser.2008.09.033.

[42] G. Mutani. E. Fabiano. D. A. Garcia. e F. Mancini. «Spatial energy modelling for the Metropolitan City of Rome». in *2021 IEEE 4th International Conference and Workshop Óbuda on Electrical and Power Engineering (CANDO-EPE)*. nov. 2021. pp. 43–48. doi: 10.1109/CANDO-EPE54223.2021.9667932.

[43] S. Torabi Moghadam. J. Toniolo. G. Mutani. e P. Lombardi. «A GIS-statistical approach for assessing built environment energy use at urban scale». *Sustainable Cities and Society*. vol. 37. pp. 70–84. feb. 2018. doi: 10.1016/j.scs.2017.10.002.

[44] B. Nastasi. M. Manfren. D. Groppi. M. Lamagna. F. Mancini. e D. Astiaso Garcia. «Data-driven load profile modelling for advanced measurement and verification (M&V) in a fully electrified building». *Building and Environment*. vol. 221. p. 109279. ago. 2022. doi: 10.1016/j.buildenv.2022.109279.

[45] A. Malhotra *et al.*. «Information modelling for urban building energy simulation—A taxonomic review». *Building and Environment*. vol. 208. p. 108552. gen. 2022. doi: 10.1016/j.buildenv.2021.108552.

[46] Y. Sun. F. Haghighat. e B. C. M. Fung. «A review of the-state-of-the-art in data-driven approaches for building energy prediction». *Energy and Buildings*. vol. 221. p. 110022. ago. 2020. doi: 10.1016/j.enbuild.2020.110022.

[47] X. Yang *et al.*. «Energy-saving potential prediction models for large-scale building: A state-of-the-art review». *Renewable and Sustainable Energy Reviews*. vol. 156. p. 111992. mar. 2022. doi: 10.1016/j.rser.2021.111992.

[48] G. Pagliarini e S. Rainieri. «Modeling of a thermal energy storage system coupled with combined heat and power generation for the heating requirements of a University Campus». *Applied Thermal Engineering*. vol. 30. fasc. 10. pp. 1255–1261. lug. 2010. doi: 10.1016/j.applthermaleng.2010.02.008.

[49] A. A. A. Gassar e S. H. Cha. «Energy prediction techniques for large-scale buildings towards a sustainable built environment: A review». *Energy and Buildings*. vol. 224. p. 110238. ott. 2020. doi: 10.1016/j.enbuild.2020.110238.

[50] «Building Simulation Applications BSA 2019».

[51] V. Todeschi. R. Boghetti. J. H. Kämpf. e G. Mutani. «Evaluation of Urban-Scale Building Energy-Use Models and Tools—Application for the City of Fribourg. Switzerland». *Sustainability*. vol. 13. fasc. 4. Art. fasc. 4. gen. 2021. doi: 10.3390/su13041595.

[52] V. Todeschi. K. Javanroodi. R. Castello. N. Mohajeri. G. Mutani. e J.-L. Scartezzini. «Impact of the COVID-19 pandemic on the energy performance of residential neighborhoods and their occupancy behavior». *Sustainable Cities and Society*. vol. 82. p. 103896. lug. 2022. doi: 10.1016/j.scs.2022.103896.

[53] J. Sun. M. Gong. Y. Zhao. C. Han. L. Jing. e P. Yang. «A hybrid deep reinforcement learning ensemble optimization model for heat load energy-saving prediction». *Journal of Building Engineering*. vol. 58. p. 105031. ott. 2022. doi: 10.1016/j.jobe.2022.105031.

[54] L. Wang. E. W. M. Lee. e R. K. K. Yuen. «Novel dynamic forecasting model for building cooling loads combining an artificial neural network and an ensemble approach». *Applied Energy*. vol. 228. pp. 1740–1753. ott. 2018. doi: 10.1016/j.apenergy.2018.07.085.

[55] «A Clean Energy Atlas for Energy Communities in Piedmont Region (Italy) | IIETA». Consultato: 23 giugno 2024. [Online]. Disponibile su: https://www.iieta.org/journals/ijdne/paper/10.18280/ijdne.150308

[56] Ricci, V. (2006). Principali tecniche di regressione con R Copyright 2006. https://cran.r-project.org/doc/contrib/Ricci-regression-it.pdf, accessed on May 25th, 2020.

[57] H. White. «A Heteroskedasticity-Consistent Covariance Matrix Estimator and a Direct Test for Heteroskedasticity». *Econometrica*. vol. 48. fasc. 4. pp. 817–838. 1980. doi: 10.2307/1912934.

[58] P. Caputo e G. Pasetti. «GIS tools towards a renovation of the building heritage». in *CLIMAMED 2017 - MEDITERRANEAN CONFERENCE OF HVAC HISTORICAL BUILDINGS RETROFIT IN THE MEDITERRANEAN AREA*. F. R. D. Alfano. L. Mazzarella. e P. Romagnoni. A c. di. in Energy Procedia. vol. 133. Amsterdam: Elsevier Science Bv. 2017. pp. 435–443. doi: 10.1016/j.egypro.2017.09.388.

[59] G. Mutani e V. Todeschi. «Building energy modeling at neighborhood scale». *Energy Efficiency*. vol. 13. fasc. 7. pp. 1353–1386. ott. 2020. doi: 10.1007/s12053-020-09882-4.

[60] G. Mutani e V. Todeschi. «Urban Building Energy Modeling: an hourly energy balance model of residential buildings at a district scale». *J. Phys.: Conf. Ser.*. vol. 1599. fasc. 1. p. 012035. ago. 2020. doi: 10.1088/1742-6596/1599/1/012035.

[61] G. Mutani. V. Todeschi. e S. Beltramino. «Energy Consumption Models at Urban Scale to Measure Energy Resilience». *Sustainability*. vol. 12. fasc. 14. Art. fasc. 14. gen. 2020. doi: 10.3390/su12145678.

[62] K. Lundgren e T. Kjellstrom. «Sustainability Challenges from Climate Change and Air Conditioning Use in Urban Areas». *Sustainability*. vol. 5. fasc. 7. pp. 3116–3128. lug. 2013. doi: 10.3390/su5073116.

[63] E. Walter e J. H. Kämpf. A c. di. «A verification of CitySim results using the BESTEST and monitored consumption values». *Proceedings of the 2nd Building Simulation Applications conference*. 2015.

[64] G. Mutani. M. Carozza. V. Todeschi. e A. Rolando. «Urban-Scale Energy Models: Relationship between urban form and energy performance». presentato al CANDO-EPE 2020 - Proceedings. IEEE 3rd International Conference and Workshop in Obuda on Electrical and Power Engineering. 2020. pp. 185–190. doi: 10.1109/CANDO-EPE51100.2020.9337760.

[65] Y. Ahn e D.-W. Sohn. «The effect of neighbourhood-level urban form on residential building energy use: A GIS-based model using building energy benchmarking data in Seattle». *Energy and Buildings*. vol. 196. pp. 124–133. 2019. doi: 10.1016/j.enbuild.2019.05.018.

[66] E. Ahmadian. B. Sodagar. C. Bingham. A. Elnokaly. e G. Mills. «Effect of urban built form and density on building energy performance in temperate climates». *Energy and Buildings*. vol. 236. 2021. doi: 10.1016/j.enbuild.2021.110762.

[67] A. Salvati. M. Palme. G. Chiesa. e M. Kolokotroni. «Built form. urban climate and building energy modelling: case-studies in Rome and Antofagasta». *Journal of Building Performance Simulation*. vol. 13. fasc. 2. pp. 209–225. 2020. doi: 10.1080/19401493.2019.1707876.

[68] G. Mutani e V. Todeschi. «An Urban Energy Atlas and Engineering Model for Resilient Cities». *IJHT*. vol. 37. fasc. 4. pp. 936–947. dic. 2019. doi: 10.18280/ijht.370402.

[69] Y. Peng. Z. Gao. R. Buccolieri. e W. Ding. «An Investigation of the Quantitative Correlation between Urban Morphology Parameters and Outdoor Ventilation Efficiency Indices». *Atmosphere*. vol. 10. fasc. 1. Art. fasc. 1. gen. 2019. doi: 10.3390/atmos10010033.

[70] D. Suszanowicz. «Optimisation of Heat Loss through Ventilation for Residential Buildings». *Atmosphere*. vol. 9. fasc. 3. Art. fasc. 3. mar. 2018. doi: 10.3390/atmos9030095.

[71] M. Silva. V. Oliveira. e V. Leal. «Urban Form and Energy Demand: A Review of Energy-relevant Urban Attributes». *J. Plan. Lit.*. vol. 32. fasc. 4. pp. 346–365. nov. 2017. doi: 10.1177/0885412217706900.

[72] A. Salvati. M. Palme. e L. Inostroza. «Key Parameters for Urban Heat Island Assessment in A Mediterranean Context: A Sensitivity Analysis Using the Urban Weather Generator Model». in *WORLD MULTIDISCIPLINARY CIVIL ENGINEERING-ARCHITECTURE-URBAN PLANNING SYMPOSIUM - WMCAUS*. in IoP Conference Series-Materials Science and Engineering. vol. 245. Bristol: IoP Publishing Ltd. 2017. p. 082055. doi: 10.1088/1757-899X/245/8/082055.

[73] C. Chatzipoulka e M. Nikolopoulou. «Urban geometry. SVF and insolation of open spaces: London and Paris». *Build. Res. Informat.*. vol. 46. fasc. 8. pp. 881–898. 2018. doi: 10.1080/09613218.2018.1463015.

[74] J. Grove-Smith. V. Aydin. W. Feist. J. Schnieders. e S. Thomas. «Standards and policies for very high energy efficiency in the urban building sector towards reaching the 1.5°C target». *Current Opinion in Environmental Sustainability*. vol. 30. pp. 103–114. feb. 2018. doi: 10.1016/j.cosust.2018.04.006.

[75] C. Cerezo. J. Sokol. S. AlKhaled. C. Reinhart. A. Al-Mumin. e A. Hajiah. «Comparison of four building archetype characterization methods in urban building energy modeling (UBEM): A residential case study in Kuwait City». *Energy and Buildings*. vol. 154. pp. 321–334. nov. 2017. doi: 10.1016/j.enbuild.2017.08.029.

[76] I. Douglas. *The Routledge Handbook of Urban Ecology Introduction*. London: Routledge. 2011. pp. 531–535. Consultato: 13 giugno 2024. [Online]. Disponibile su: https://www-webofscience-com.ezproxy.biblio.polito.it/wos/woscc/full-record/WOS:000290380300047

[77] T. Oke e Canada. «Initial guidance to obtain representative meteorological observations at urban sites». gen. 2006.

[78] T. R. Oke. G. Mills. A. Christen. e J. A. Voogt. *Urban Climates*. Cambridge: Cambridge University Press. 2017. doi: 10.1017/9781139016476.

[79] T. R. Oke. «The energetic basis of the urban heat island». *Quarterly Journal of the Royal Meteorological Society*. vol. 108. fasc. 455. pp. 1–24. 1982. doi: 10.1002/qj.49710845502.

[80] C. W. Kent *et al.*. «Evaluation of Urban Local-Scale Aerodynamic Parameters: Implications for the Vertical Profile of Wind Speed and for Source Areas». *Boundary-Layer Meteorol*. vol. 164. fasc. 2. pp. 183–213. ago. 2017. doi: 10.1007/s10546-017-0248-z.

[81] V. Masson. A. Lemonsu. J. Hidalgo. e J. Voogt. «Urban Climates and Climate Change». *Annual Review of Environment and Resources*. vol. 45. fasc. 1. pp. 411–444. 2020. doi: 10.1146/annurev-environ-012320-083623.

[82] C. Grimmond e T. Oke. «Aerodynamic Properties of Urban Areas Derived from Analysis of Surface Form». *Journal of Applied Meteorology*. vol. 38. pp. 1262–1292. set. 1999. doi: 10.1175/1520-0450(1999)038<1262:APOUAD>2.0.CO;2.

[83] A. Abubaker. I. Kostić. e O. Kostić. «Numerical modelling of velocity profile parameters of the atmospheric boundary layer simulated in wind tunnels». *IOP Conf. Ser.: Mater. Sci. Eng.*. vol. 393. p. 012025. ago. 2018. doi: 10.1088/1757-899X/393/1/012025.

[84] A. Davenport. C. Grimmond. T. Oke. e J. Wieringa. «Estimating the roughness of cities and sheltered country». *15th conference on probability and statistics in the atmospheric sciences/12th conference on applied climatology. Ashville. NC. American Meteorological Society*. pp. 96–99. gen. 2000.

[85] E. Choi. «Proposal for Unified Terrain Categories Exposures and Velocity Profiles». *7th Asia-Pacific Conference on Wind Engineering. APCWE-VII*. gen. 2009.

[86] S. Ferrari. F. Zagarella. P. Caputo. e G. Dall'O'. «A GIS-Based Procedure for Estimating the Energy Demand Profiles of Buildings towards Urban Energy Policies». *Energies*. vol. 14. fasc. 17. Art. fasc. 17. gen. 2021. doi: 10.3390/en14175445.

[87] R. Buccolieri e J. Hang. «Recent Advances in Urban Ventilation Assessment and Flow Modelling». *Atmosphere*. vol. 10. fasc. 3. Art. fasc. 3. mar. 2019. doi: 10.3390/atmos10030144.

[88] M. Wong *et al.*. «GIS techniques for mapping urban ventilation. using frontal area index and least cost path analysis». *International Archives of the Photogrammetry. Remote Sensing and Spatial Information Sciences - ISPRS Archives*. vol. 38. gen. 2010.

[89] O. Palusci. P. Monti. C. Cecere. H. Montazeri. e B. Blocken. «Impact of morphological parameters on urban ventilation in compact cities: The case of the Tuscolano-Don Bosco district in Rome». *Science of The Total Environment*. vol. 807. p. 150490. feb. 2022. doi: 10.1016/j.scitotenv.2021.150490.

[90] N. S. Darmanto. A. C. G. Varquez. e M. Kanda. «Urban roughness parameters estimation from globally available datasets for mesoscale modeling in megacities». *Urban Climate*. vol. 21. pp. 243–261. set. 2017. doi: 10.1016/j.uclim.2017.07.001.

[91] J. Badach. D. Voordeckers. L. Nyka. e M. Van Acker. «A framework for Air Quality Management Zones - Useful GIS-based tool for urban planning: Case studies in Antwerp and Gdańsk». *Building and Environment*. vol. 174. p. 106743. mag. 2020. doi: 10.1016/j.buildenv.2020.106743.

[92] Y. Peng. Z. Gao. e W. Ding. «An Approach on the Correlation between Urban Morphological Parameters and Ventilation Performance». *Energy Procedia*. vol. 142. pp. 2884–2891. dic. 2017. doi: 10.1016/j.egypro.2017.12.412.

[93] C. Shen *et al.*. «Spatializing the roughness length of heterogeneous urban underlying surfaces to improve the WRF simulation-part 1: A review of morphological methods and model evaluation». *Atmospheric Environment*. vol. 270. p. 118874. feb. 2022. doi: 10.1016/j.atmosenv.2021.118874.

[94] S.-J. Mei *et al.*. «Wind driven natural ventilation in the idealized building block arrays with multiple urban morphologies and unique package building density». *Energy and Buildings*. vol. 155. pp. 324–338. nov. 2017. doi: 10.1016/j.enbuild.2017.09.019.

[95] C. W. Kent. S. Grimmond. D. Gatey. e K. Hirano. «Urban morphology parameters from global digital elevation models: Implications for aerodynamic roughness and for wind-speed estimation». *Remote Sensing of Environment*. vol. 221. pp. 316–339. feb. 2019. doi: 10.1016/j.rse.2018.09.024.

[96] C. W. Kent *et al.*. «Evaluation of Urban Local-Scale Aerodynamic Parameters: Implications for the Vertical Profile of Wind Speed and for Source Areas». *Boundary-Layer Meteorol*. vol. 164. fasc. 2. pp. 183–213. ago. 2017. doi: 10.1007/s10546-017-0248-z.

[97] J. Cheng. D. Qi. A. Katal. L. Wang. e T. Stathopoulos. «Evaluating wind-driven natural ventilation potential for early building design». *J. Wind Eng. Ind. Aerodyn.*. vol. 182. pp. 160–169. nov. 2018. doi: 10.1016/j.jweia.2018.09.017.

[98] F. Yang. F. Qian. e S. S. Y. Lau. «Urban form and density as indicators for summertime outdoor ventilation potential: A case study on high-rise housing in Shanghai». *Building and Environment*. vol. 70. pp. 122–137. dic. 2013. doi: 10.1016/j.buildenv.2013.08.019.

[99] O. Conrad *et al.*. «System for Automated Geoscientific Analyses (SAGA) v. 2.1.4». *Geoscientific Model Development*. vol. 8. fasc. 7. pp. 1991–2007. lug. 2015. doi: 10.5194/gmd-8-1991-2015.

[100] F. Lindberg *et al.*. «Urban Multi-scale Environmental Predictor (UMEP): An integrated tool for city-based climate services». *Environmental Modelling & Software*. vol. 99. pp. 70–87. gen. 2018. doi: 10.1016/j.envsoft.2017.09.020.

[101] G. Lv. K. Zhao. Y. Qin. e J. Ge. «An urban-scale method for building roofs available wind resource evaluation based on aerodynamic parameters of urban sublayer surfaces». *Sustainable Cities and Society*. vol. 80. p. 103790. mag. 2022. doi: 10.1016/j.scs.2022.103790.

[102] M. Kanda. A. Inagaki. T. Miyamoto. M. Gryschka. e S. Raasch. «A New Aerodynamic Parametrization for Real Urban Surfaces». *Boundary-Layer Meteorol*. vol. 148. fasc. 2. pp. 357–377. ago. 2013. doi: 10.1007/s10546-013-9818-x.

[103] M. Bottema. «Urban roughness modelling in relation to pollutant dispersion». *Atmospheric Environment*. vol. 31. fasc. 18. pp. 3059–3075. set. 1997. doi: 10.1016/S1352-2310(97)00117-9.

[104] R. W. Macdonald. R. F. Griffiths. e D. J. Hall. «An improved method for the estimation of surface roughness of obstacle arrays». *Atmospheric Environment*. vol. 32. fasc. 11. pp. 1857–1864. giu. 1998. doi: 10.1016/S1352-2310(97)00403-2.

[105] J. T. Millward-Hopkins. A. S. Tomlin. L. Ma. D. Ingham. e M. Pourkashanian. «Estimating Aerodynamic Parameters of Urban-Like Surfaces with Heterogeneous Building Heights». *Boundary-Layer Meteorol*. vol. 141. fasc. 3. pp. 443–465. dic. 2011. doi: 10.1007/s10546-011-9640-2.

[106] K. Javanroodi. V. M. Nik. M. G. Giometto. e J.-L. Scartezzini. «Combining computational fluid dynamics and neural networks to characterize microclimate extremes: Learning the complex interactions

between meso-climate and urban morphology». *Science of The Total Environment*. vol. 829. p. 154223. lug. 2022. doi: 10.1016/j.scitotenv.2022.154223.

[107] G. Chiesa e M. Grosso. «Python-based calculation tool of wind-pressure coefficients on building envelopes». *J. Phys.: Conf. Ser.*. vol. 1343. fasc. 1. p. 012132. nov. 2019. doi: 10.1088/1742-6596/1343/1/012132.

[108] T. Samsonov. P. Konstantinov. e M. Varentsov. «Object-oriented approach to urban canyon analysis and its applications in meteorological modeling». *Urban Climate*. vol. 13. pp. 122–139. set. 2015. doi: 10.1016/j.uclim.2015.07.007.

[109] A. Di Bernardino. P. Monti. G. Leuzzi. e G. Querzoli. «Pollutant fluxes in two-dimensional street canyons». *Urban CLim.*. vol. 24. pp. 80–93. giu. 2018. doi: 10.1016/j.uclim.2018.02.002.

[110] Z. T. Ai e C. M. Mak. «CFD simulation of flow in a long street canyon under a perpendicular wind direction: Evaluation of three computational settings». *Build. Environ.*. vol. 114. pp. 293–306. mar. 2017. doi: 10.1016/j.buildenv.2016.12.032.

[111] L. Tsichritzis e M. Nikolopoulou. «The effect of building height and facade area ratio on pedestrian wind comfort of London». *J. Wind Eng. Ind. Aerodyn.*. vol. 191. pp. 63–75. ago. 2019. doi: 10.1016/j.jweia.2019.05.021.

[112] J. J. O'Neill. X.-M. Cai. e R. Kinnersley. «Stochastic backscatter modelling for the prediction of pollutant removal from an urban street canyon: A large-eddy simulation». *Atmospheric Environment*. vol. 142. pp. 9–18. ott. 2016. doi: 10.1016/j.atmosenv.2016.07.024.

[113] O. Palusci e C. Cecere. «Urban Ventilation in the Compact City: A Critical Review and a Multidisciplinary Methodology for Improving Sustainability and Resilience in Urban Areas». *Sustainability*. vol. 14. fasc. 7. p. 3948. apr. 2022. doi: 10.3390/su14073948.

[114] B. Blocken. W. D. Janssen. e T. van Hooff. «CFD simulation for pedestrian wind comfort and wind safety in urban areas: General decision framework and case study for the Eindhoven University campus». *Environ. Modell. Softw.*. vol. 30. pp. 15–34. apr. 2012. doi: 10.1016/j.envsoft.2011.11.009.

[115] H. Sanaieian. M. Tenpierik. K. van den Linden. F. M. Seraj. e S. M. M. Shemrani. «Review of the impact of urban block form on thermal performance. solar access and ventilation». *Renew. Sust. Energ. Rev.*. vol. 38. pp. 551–560. ott. 2014. doi: 10.1016/j.rser.2014.06.007.

[116] P. Mouzourides. C. Marakkos. e M. K.-A. Neophytou. «Urban street canyon flows under combined wind forcing and thermal buoyancy». *Physics of Fluids*. vol. 34. fasc. 7. p. 076606. lug. 2022. doi: 10.1063/5.0090642.

[117] Lenin. G. Krishnan. P. E. e R. R.. «Effect of various parameters on sol-air temperature Corresponding authors». vol. 7. pp. 408–415. ago. 2022.

[118] M. A. Hassan. A. Khalil. e M. Abubakr. «Selection methodology of representative meteorological days for assessment of renewable energy systems». *Renewable Energy*. vol. 177. pp. 34–51. nov. 2021. doi: 10.1016/j.renene.2021.05.124.

[119] Stuart Dols W., Polidoro B.J., CONTAM UserGuide and Program Documentation Vresion 3.4, NIST National Institute of Standards and Technology Technical Note 1887 Revision 1, 2020, U.S. Department of Commerce DOI: 10.6028/NIST.TN.1887r1 (last access, 2024 May the 23rd).

[120] F. Allard M. Herrlin, Wind-Induced Ventilation, - ASHRAE transactions, Air infiltration and Ventilation Centre (AIVC), 1989, available at: https://www.aivc.org/sites/default/files/airbase_3534.pdf (accessed on 20/7/2021).

[121] Y. Zhou. Y. Deng. P. Wu. e S.-J. Cao. «The effects of ventilation and floor heating systems on the dispersion and deposition of fine particles in an enclosed environment». *Build. Environ.*. vol. 125. pp. 192–205. nov. 2017. doi: 10.1016/j.buildenv.2017.08.049.

[122] A. Dodoo. L. Gustavsson. e R. Sathre. «Primary energy implications of ventilation heat recovery in residential buildings». *Energy Build.*. vol. 43. fasc. 7. pp. 1566–1572. lug. 2011. doi: 10.1016/j.enbuild.2011.02.019.

[123] H. E. Feustel. «COMIS-an international multizone air-flow and contaminant transport model». *Energy and Buildings*. vol. 30. fasc. 1. pp. 3–18. 1999. doi: 10.1016/S0378-7788(98)00043-7.

[124] A. Martin-Garin. J. A. Millan-Garcia. J. M. Hidalgo-Betanzos. R. J. Hernandez-Minguillon. e A. Bairi. «Airtightness Analysis of the Built Heritage-Field Measurements of Nineteenth Century Buildings through Blower Door Tests». *Energies*. vol. 13. fasc. 24. p. 6727. dic. 2020. doi: 10.3390/en13246727.

[125] J. Fernandez-Agueera. J. Jose Sendra. e S. Dominguez. «Protocols for measuring the airtightness of multi-dwelling units in Southern Europe». in *2011 INTERNATIONAL CONFERENCE ON GREEN BUILDINGS AND SUSTAINABLE CITIES*. P. Secondini. X. Wu. S. Tondelli. J. Wu. e H. Xie. A c. di. in Procedia Engineering. vol. 21. Amsterdam: Elsevier Science Bv. 2011. pp. 98–105. doi: 10.1016/j.proeng.2011.11.1992.

[126] M. Deru e P. Burns. «Infiltration and Natural Ventilation Model for Whole-Building Energy Simulation of Residential Buildings: Preprint». National Renewable Energy Lab. (NREL). Golden. CO (United States). NREL/CP-550-33698. mar. 2003. Consultato: 16 maggio 2024. [Online]. Disponibile su: https://www.osti.gov/biblio/15003730

[127] W. W. Nazaroff. «Residential air-change rates: A critical review». *Indoor Air*. vol. 31. fasc. 2. pp. 282–313. 2021. doi: 10.1111/ina.12785.

[128] A. A. Rizk. M. S. El-Morsi. e M. M. Elwan. «A Review on Wind - Driven Cross - Ventilation Techniques Inside Single Rooms». vol. 6. fasc. 8. 2015.

[129] D. Hertwig *et al.*. «Wake Characteristics of Tall Buildings in a Realistic Urban Canopy». *Boundary-Layer Meteorology*. vol. 172. fasc. 2. pp. 239–270. 2019. doi: 10.1007/s10546-019-00450-7.

[130] M. Grosso. «Wind Pressure Distribution Around Buildings - a Parametrical Model». *Energy Build.*. vol. 18. fasc. 2. pp. 101–131. 1992. doi: 10.1016/0378-7788(92)90041-E.

[131] N. V. Tam e D. T. Frank. «New Surrogate Model for Wind Pressure Coefficients in a Schematic Urban Environment with a Regular Pattern». *Atmosphere*. vol. 9. fasc. 3. p. 113. mar. 2018. doi: 10.3390/atmos9030113.

[132] International Energy Agency, Technical Note AIVC 29 – Fundamentals of the Multizone Air Flow Model-COMIS, Air Infiltration and Ventilation Centre, Bracknell, UK, 1990.

[133] R. Y. Pelletret, W. P. Keilholz, COMIS 3.0 - A new simulation environment for multizone air flow and pollutant transport modelling, IBPSA Proceedings 1997, available at: http://www.ibpsa.org/proceedings/bs1997 (accessed on 20/7/2021).

[134] P. Mckeen e Z. Liao. «The Influence of Building Airtightness on Airflow in Stairwells». *Buildings*. vol. 9. fasc. 10. Art. fasc. 10. ott. 2019. doi: 10.3390/buildings9100208.

[135] A. Mélois. F. R. Carrié. M. El Mankibi. e B. Moujalled. «Uncertainty in building fan pressurization tests: Review and gaps in research». *Journal of Building Engineering*. vol. 52. 2022. doi: 10.1016/j.jobe.2022.104455.

[136] J. H. Klems. «Methods of estimating air infiltration through windows». *Energy and Buildings*. vol. 5. fasc. 4. pp. 243–252. set. 1983. doi: 10.1016/0378-7788(83)90012-9.

[137] ASHRAE, Handbook of Fundamentals. 2009, Atlanta, USA: American Society of Heating, Refrigerating and Air Conditioning Engineers.

[138] J. Kronvall. «Testing of Houses for Air-Leakage Using a Pressure Method». *ASHRAE J.-Am. Soc. Heat Refrig. Air-Cond. Eng.*. vol. 19. fasc. 12. pp. 32–32. 1977.

[139] Persily, A.K.; Linteris, G.T. A Comparison of Measured and Predicted Infiltration Rates; ASHRAE Transactions: Peachtree Corners, GA, USA, 1983; pp. 183–200.

[140] Grimsrud, D.T.; Sherman, M.H.; Diamond, R.C.; Condon, P.E.; Rosenfeld, A.H. Infiltration: Pressuriztion Correlations: Detailed Measurement on a California House; No. LBL-7824; CONF-790112-5; Lawrence Berkeley National Laboratory: Berkeley, CA, USA, 1978.

[141] S. Zheng. X. Song. D. Lin. Y. Xue. e X. Yang. «Comparison of models to predict air infiltration rate of buildings with different surrounding environments». *Build. Simul.*. apr. 2024. doi: 10.1007/s12273-024-1118-5.

[142] M. Sherman. «Estimation of Infiltration from Leakage and Climate Indicators». *Energy Build.*. vol. 10. fasc. 1. pp. 81–86. feb. 1987. doi: 10.1016/0378-7788(87)90008-9.

[143] D. A. Asimakopoulos *et al.*. «Modelling the energy demand projection of the building sector in Greece in the 21st century». *Energy Build.*. vol. 49. pp. 488–498. giu. 2012. doi: 10.1016/j.enbuild.2012.02.043.

[144] R.-H. A. Edited by: Feustel H. E.. «TN 29: Fundamentals of the Multizone Air Flow Model-COMIS». AIVC. Consultato: 13 maggio 2022. [Online]. Disponibile su: https://www.aivc.org/resource/tn-29-fundamentals-multizone-air-flow-model-comis

[145] W. S. Dols e B. J. Polidoro. «CONTAM User Guide and Program Documentation Version 3.4». National Institute of Standards and Technology. ago. 2020. doi: 10.6028/NIST.TN.1887r1.

[146] J. Mun. J. Lee. e M. Kim. «Estimation of Infiltration Rate (ACH Natural) Using Blower Door Test and Simulation». *Energies*. vol. 14. fasc. 4. Art. fasc. 4. gen. 2021. doi: 10.3390/en14040912.

[147] M. Calì, R. Borchiellini, P. Arena, G. Mutani, G. Vannelli, Metodi di analisi e verifica delle prestazioni di codici numerici finalizzati a calcoli energetici e fluidodinamici negli edifici di uso civile e industriale, Copyright 1997 by ATIG, 1997 (in Italian).

[148] G.V. Fracastoro, G. Mutani, M. Perino, A simple tool to assess the feasibility of hybrid ventilation systems, Proceedings of the 4th IAQVEC 2001, Changsha, Hunan (China), pp. 1421-1429 (and Techincal Report IEA Annex 35 WG B4 - REPORT 1, 2002), available at: https://www.en.build.aau.dk/digitalAssets/403/403353_tr21-simpletool.pdf (accessed on 20/7/2021).

[149] R. Borchiellini, M. Cali, G. Mutani, Evaluation to adapt COMIS to smoke movements in buildings analysis, IEA.ECB.A23/93.10.13/RB, Energy in Buildings and Communities Programme (Dip. di Energetica, Politecnico di Torino, internal publication PT DE 338/FT, 1993).

[150] F. Allard, M. Santamouris, Natural ventilation in buildings. A design handbook, 1998, published by James & James Ltd, The Cromwell Press UK, ISBN 1873936729.

[151] L. Troup. R. Phillips. M. J. Eckelman. e D. Fannon. «Effect of window-to-wall ratio on measured energy consumption in US office buildings». *Energy and Buildings*. vol. 203. 2019. doi: 10.1016/j.enbuild.2019.109434.

[152] S. Sayadi. A. Hayati. e M. Salmanzadeh. «Optimization of window-to-wall ratio for buildings located in different climates: An IDA-indoor climate and energy simulation study». *Energies*. vol. 14. fasc. 7. 2021. doi: 10.3390/en14071974.

[153] T. Erhart. D. Guerlich. T. Schulze. e U. Eicker. «Experimental validation of basic natural ventilation air flow calculations for different flow path and window configurations». presentato al Energy Procedia. 2015. pp. 2838–2843. doi: 10.1016/j.egypro.2015.11.644.

[154] H. Zhang *et al.*. «A critical review of combined natural ventilation techniques in sustainable buildings». *Renewable and Sustainable Energy Reviews*. vol. 141. 2021. doi: 10.1016/j.rser.2021.110795.

Appendix A (CFD)

Canyon:			Facade on the urban canyon (uc)					
LARGE (LC)			Normal component					
Effect	Season	Scene	Coeff. 1	Coeff. 2	Coeff. 3	Coeff. 4	Coeff. 5	Coeff. 6
WINDY- no gradient	WINTER	WWF	5.52E-06	-2.26E-04	2.92E-03	-9.95E-03	-2.96E-02	6.28E-02
		WCF	6.39E-06	-2.66E-04	3.85E-03	-2.28E-02	4.23E-02	3.88E-02
		LWF	2.80E-06	-1.23E-04	1.90E-03	-1.21E-02	2.56E-02	1.15E-02
		LCF	2.38E-06	-1.09E-04	1.77E-03	-1.21E-02	2.99E-02	-4.80E-03
	MID-SEASON1	WWF	3.95E-06	-1.49E-04	1.72E-03	-4.32E-03	-1.98E-02	5.32E-03
		WCF	2.61E-07	2.87E-05	-1.38E-03	1.90E-02	-8.60E-02	2.95E-02
		LWF	3.92E-06	-1.76E-04	2.73E-03	-1.65E-02	2.98E-02	-3.42E-02
		LCF	2.14E-06	-9.52E-05	1.46E-03	-8.61E-03	1.60E-02	-1.66E-02
	MID-SEASON2	WWF	5.98E-06	-2.39E-04	2.89E-03	-5.58E-03	-6.51E-02	1.01E-01
		WCF	2.77E-06	-1.38E-04	2.65E-03	-2.16E-02	4.72E-02	4.33E-02
		LWF	3.02E-06	-1.42E-04	2.35E-03	-1.55E-02	3.11E-02	6.94E-03
		LCF	3.33E-06	-1.48E-04	2.31E-03	-1.52E-02	3.75E-02	-9.06E-03
	SUMMER	WWF	1.35E-06	-5.77E-06	-1.19E-03	2.22E-02	-1.17E-01	6.61E-02
		WCF	-3.10E-08	5.49E-05	-2.08E-03	2.64E-02	-1.15E-01	4.98E-02
		LWF	2.91E-06	-1.16E-04	1.48E-03	-5.38E-03	-5.52E-03	-1.90E-02
		LCF	3.60E-06	-1.77E-04	3.08E-03	-2.19E-02	5.34E-02	-3.24E-02
no wind - GRADIENT	WINTER	WWF	2.70E-06	-6.96E-05	-1.60E-04	1.58E-02	-1.08E-01	9.42E-02
		WCF	2.54E-06	-7.85E-05	7.74E-04	-2.48E-03	-1.40E-02	9.27E-02
		LWF	3.25E-06	-1.42E-04	2.17E-03	-1.37E-02	2.96E-02	7.79E-03
		LCF	3.37E-06	-1.52E-04	2.31E-03	-1.31E-02	1.72E-02	1.20E-02
	MID-SEASON 1	WWF	2.70E-06	-8.33E-05	5.08E-04	4.75E-03	-4.04E-02	-1.07E-02
		WCF	1.37E-06	-6.84E-06	-1.12E-03	2.01E-02	-9.94E-02	4.47E-02
		LWF	6.80E-06	-3.12E-04	5.01E-03	-3.27E-02	7.25E-02	-5.64E-02
		LCF	2.24E-06	-9.72E-05	1.39E-03	-6.65E-03	2.89E-03	-7.14E-03
	MID-SEASON 2	WWF	9.10E-06	-3.88E-04	5.48E-03	-2.57E-02	-3.14E-03	6.70E-02
		WCF	7.66E-06	-3.74E-04	6.63E-03	-4.88E-02	1.13E-01	3.61E-04
		LWF	3.81E-06	-1.74E-04	2.78E-03	-1.82E-02	4.05E-02	-8.88E-04
		LCF	3.72E-06	-1.67E-04	2.58E-03	-1.52E-02	2.40E-02	9.40E-03
	SUMMER	WWF	2.22E-06	-4.63E-05	-3.84E-04	1.32E-02	-6.66E-02	-1.31E-02
		WCF	2.48E-06	-6.25E-05	-1.28E-04	1.29E-02	-8.04E-02	2.58E-02
		LWF	4.05E-06	-1.80E-04	2.76E-03	-1.61E-02	2.74E-02	-3.14E-02
		LCF	3.08E-06	-1.34E-04	1.95E-03	-9.88E-03	8.60E-03	-1.56E-02
WINDY- GRADIENT	WINTER	WWF	1.37E-05	-5.70E-04	8.11E-03	-4.39E-02	7.25E-02	-1.39E-01
		WCF	1.20E-05	-4.81E-04	6.52E-03	-3.13E-02	1.49E-02	-8.99E-03
		LWF	9.86E-06	-4.52E-04	7.15E-03	-4.41E-02	8.06E-02	2.82E-03
		LCF	9.62E-06	-4.14E-04	5.69E-03	-2.33E-02	-1.93E-02	5.95E-02
	MID-SEASON 1	WWF	1.11E-05	-4.39E-04	5.87E-03	-2.95E-02	5.77E-02	-2.04E-01
		WCF	9.00E-06	-3.36E-04	3.90E-03	-1.16E-02	-1.34E-02	-1.39E-01
		LWF	5.09E-06	-2.18E-04	2.99E-03	-1.19E-02	-1.21E-02	-1.07E-02
		LCF	8.47E-06	-3.65E-04	4.91E-03	-1.76E-02	-3.67E-02	5.79E-02
	MID-SEASON 2	WWF	8.41E-06	-2.39E-04	8.58E-04	2.29E-02	-1.55E-01	-1.75E-02
		WCF	7.52E-06	-1.79E-04	-6.53E-04	4.05E-02	-2.43E-01	1.09E-01
		LWF	6.59E-06	-2.81E-04	3.80E-03	-1.44E-02	-2.16E-02	2.08E-02
		LCF	9.38E-06	-4.17E-04	6.14E-03	-3.15E-02	2.55E-02	5.62E-03
	SUMMER	WWF	1.16E-05	-4.15E-04	4.48E-03	-1.07E-02	-2.54E-02	-1.42E-01
		WCF	1.20E-05	-4.58E-04	5.57E-03	-1.97E-02	-5.85E-03	-1.59E-01
		LWF	7.97E-06	-3.51E-04	5.18E-03	-2.72E-02	3.11E-02	-3.87E-02
		LCF	5.90E-06	-2.44E-04	3.21E-03	-1.22E-02	-8.18E-03	-3.51E-02
no wind- no gradient	WINTER	WWF	1.84E-05	-7.66E-04	1.09E-02	-5.99E-02	1.01E-01	-1.24E-01
		WCF	1.06E-05	-3.41E-04	2.49E-03	1.34E-02	-1.49E-01	3.19E-02
		LWF	1.10E-05	-4.87E-04	7.27E-03	-4.01E-02	5.51E-02	-8.99E-03
		LCF	1.02E-05	-4.43E-04	6.35E-03	-3.13E-02	2.27E-02	-2.21E-03
	MID-SEASON 1	WWF	2.66E-05	-1.13E-03	1.63E-02	-8.94E-02	1.39E-01	-1.26E-01
		WCF	1.70E-05	-6.79E-04	9.24E-03	-5.00E-02	1.24E-01	-3.45E-01
		LWF	1.19E-06	-2.69E-05	-4.32E-04	1.54E-02	-9.45E-02	-1.44E-02
		LCF	1.15E-05	-5.23E-04	8.07E-03	-4.64E-02	6.76E-02	-1.53E-02
	MID-SEASON 2	WWF	2.00E-05	-8.36E-04	1.21E-02	-6.90E-02	1.32E-01	-1.69E-01
		WCF	1.59E-05	-6.01E-04	7.29E-03	-2.76E-02	3.12E-03	-1.15E-01
		LWF	1.14E-05	-5.05E-04	7.59E-03	-4.25E-02	6.22E-02	-1.94E-02
		LCF	1.10E-05	-4.88E-04	7.31E-03	-4.09E-02	5.98E-02	-1.82E-02
	SUMMER	WWF	1.99E-05	-8.57E-04	1.31E-02	-8.43E-02	2.25E-01	-3.40E-01
		WCF	1.39E-05	-5.34E-04	6.61E-03	-2.51E-02	6.27E-03	-2.00E-01
		LWF	5.64E-06	-2.28E-04	2.78E-03	-6.08E-03	-4.37E-02	-1.11E-02
		LCF	1.15E-05	-5.06E-04	7.26E-03	-3.36E-02	-1.10E-03	5.25E-02

Canyon:			Facade on the urban canyon (uc)					
LARGE (LC)			Tangential component					
Effect	Season	Scene	Coeff. 1	Coeff. 2	Coeff. 3	Coeff. 4	Coeff. 5	Coeff. 6
WINDY-no gradient	WINTER	WWF	1.69E-05	-8.65E-04	1.63E-02	-1.27E-01	2.51E-01	-3.20E-02
		WCF	1.46E-05	-6.55E-04	1.03E-02	-7.34E-02	2.71E-01	-8.25E-02
		LWF	-2.36E-06	1.03E-04	-1.58E-03	1.30E-02	-7.51E-02	7.92E-03
		LCF	7.41E-08	-7.74E-06	1.94E-04	-6.30E-05	-2.43E-02	-8.82E-04
	MID-SEASON 1	WWF	9.10E-06	-4.19E-04	6.99E-03	-4.44E-02	-7.17E-03	2.07E-02
		WCF	5.50E-06	-2.39E-04	3.52E-03	-1.17E-02	-1.60E-01	9.27E-02
		LWF	-7.59E-06	4.08E-04	-8.21E-03	6.94E-02	-1.37E-01	3.92E-02
		LCF	-1.97E-06	1.08E-04	-2.21E-03	1.72E-02	-1.18E-02	5.08E-04
	MID-SEASON 2	WWF	2.20E-05	-1.16E-03	2.23E-02	-1.76E-01	3.37E-01	-2.97E-02
		WCF	-1.29E-05	6.83E-04	-1.11E-02	5.07E-02	1.13E-02	7.26E-02
		LWF	4.69E-07	1.07E-06	-8.04E-04	1.61E-02	-8.20E-02	1.42E-02
		LCF	-2.56E-06	1.17E-04	-1.73E-03	1.11E-02	-5.21E-02	1.53E-02
	SUMMER	WWF	9.63E-06	-4.46E-04	7.43E-03	-4.10E-02	-1.21E-01	1.23E-01
		WCF	7.15E-06	-3.08E-04	4.42E-03	-1.34E-02	-1.88E-01	1.28E-01
		LWF	-7.06E-06	3.54E-04	-6.49E-03	4.54E-02	-8.62E-03	-3.03E-02
		LCF	-5.38E-07	6.69E-05	-2.42E-03	3.05E-02	-9.07E-02	4.42E-02
no wind - GRADIENT	WINTER	WWF	1.57E-05	-7.67E-04	1.35E-02	-9.06E-02	5.95E-02	8.07E-02
		WCF	1.13E-05	-4.07E-04	5.26E-03	-4.33E-02	2.27E-01	-8.73E-03
		LWF	-3.02E-06	1.30E-04	-1.88E-03	1.34E-02	-7.17E-02	7.98E-03
		LCF	-2.93E-06	1.91E-04	-4.41E-03	4.08E-02	-1.13E-01	2.31E-02
	MID-SEASON 1	WWF	6.79E-06	-2.82E-04	4.05E-03	-1.52E-02	-1.37E-01	4.40E-02
		WCF	8.91E-06	-3.83E-04	5.52E-03	-2.05E-02	-1.69E-01	1.24E-01
		LWF	-8.36E-06	4.63E-04	-9.69E-03	8.65E-02	-2.14E-01	8.89E-02
		LCF	-2.38E-06	1.41E-04	-3.06E-03	2.39E-02	-2.81E-03	-1.03E-02
	MID-SEASON 2	WWF	2.41E-05	-1.24E-03	2.36E-02	-1.89E-01	4.28E-01	-1.06E-01
		WCF	-8.59E-06	4.17E-04	-5.28E-03	1.07E-03	1.42E-01	-2.28E-02
		LWF	6.43E-08	7.02E-07	-1.91E-04	5.63E-03	-4.96E-02	-3.63E-04
		LCF	-2.39E-06	1.50E-04	-3.39E-03	3.14E-02	-9.06E-02	1.10E-02
	SUMMER	WWF	7.06E-06	-2.71E-04	3.22E-03	-4.85E-04	-2.37E-01	7.22E-02
		WCF	8.47E-06	-3.78E-04	5.97E-03	-2.88E-02	-1.46E-01	8.66E-02
		LWF	-6.35E-06	3.43E-04	-6.91E-03	5.61E-02	-8.37E-02	1.62E-02
		LCF	-4.35E-06	2.40E-04	-4.87E-03	3.73E-02	-1.84E-02	-9.09E-03
WINDY-GRADIENT	WINTER	WWF	1.93E-05	-8.54E-04	1.40E-02	-8.57E-02	-1.16E-01	-4.69E-02
		WCF	1.25E-05	-4.67E-04	7.39E-03	-5.73E-02	-4.58E-02	3.28E-02
		LWF	-5.42E-06	3.67E-04	-8.79E-03	8.45E-02	-2.46E-01	5.64E-02
		LCF	-1.26E-05	8.00E-04	-1.76E-02	1.45E-01	-2.39E-01	6.13E-03
	MID-SEASON 1	WWF	1.64E-05	-6.66E-04	9.12E-03	-2.79E-02	-3.70E-01	-5.67E-03
		WCF	1.55E-05	-6.57E-04	9.87E-03	-3.84E-02	-3.74E-01	5.19E-02
		LWF	-5.92E-06	3.62E-04	-8.14E-03	6.56E-02	-2.81E-03	-2.71E-02
		LCF	-7.06E-06	5.33E-04	-1.31E-02	1.13E-01	-1.23E-01	-4.93E-02
	MID-SEASON 2	WWF	2.51E-05	-1.04E-03	1.45E-02	-4.98E-02	-4.74E-01	2.01E-01
		WCF	3.15E-05	-1.39E-03	2.13E-02	-1.06E-01	-3.17E-01	2.79E-01
		LWF	-3.71E-06	2.83E-04	-7.24E-03	6.14E-02	4.10E-03	-7.50E-02
		LCF	-2.86E-06	2.67E-04	-7.50E-03	6.99E-02	-6.89E-02	-3.88E-02
	SUMMER	WWF	2.17E-05	-8.61E-04	1.12E-02	-2.92E-02	-4.69E-01	6.91E-02
		WCF	2.02E-05	-8.73E-04	1.36E-02	-6.24E-02	-3.93E-01	5.76E-02
		LWF	-4.71E-06	3.06E-04	-7.09E-03	5.67E-02	1.45E-02	-2.24E-02
		LCF	-4.33E-06	2.62E-04	-5.63E-03	3.67E-02	1.22E-01	-6.68E-02
no wind-no gradient	WINTER	WWF	3.15E-05	-1.42E-03	2.33E-02	-1.50E-01	7.74E-02	-8.32E-02
		WCF	2.95E-05	-1.29E-03	1.99E-02	-1.04E-01	-2.64E-01	1.82E-01
		LWF	-4.08E-06	3.14E-04	-7.87E-03	6.97E-02	-9.89E-02	-8.82E-03
		LCF	-3.92E-06	3.12E-04	-7.81E-03	6.37E-02	-7.01E-03	-5.65E-02
	MID-SEASON 1	WWF	4.07E-05	-1.99E-03	3.51E-02	-2.43E-01	2.56E-01	-1.38E-01
		WCF	2.55E-05	-1.02E-03	1.30E-02	-2.62E-02	-5.59E-01	-2.99E-02
		LWF	3.30E-06	-9.31E-05	-2.45E-04	-1.56E-04	3.25E-01	-1.41E-01
		LCF	-1.76E-06	2.30E-04	-7.38E-03	7.58E-02	-1.17E-01	-6.10E-04
	MID-SEASON 2	WWF	2.83E-05	-1.22E-03	1.91E-02	-1.16E-01	-4.29E-02	-6.64E-02
		WCF	2.62E-05	-1.07E-03	1.49E-02	-6.14E-02	-3.30E-01	8.99E-02
		LWF	-1.56E-06	1.74E-04	-5.16E-03	4.78E-02	-2.48E-02	-4.05E-02
		LCF	-3.47E-06	2.57E-04	-6.33E-03	5.35E-02	-3.28E-02	-3.94E-02
	SUMMER	WWF	1.81E-05	-6.64E-04	8.16E-03	-2.30E-02	-3.69E-01	-8.66E-02
		WCF	2.30E-05	-9.93E-04	1.53E-02	-6.82E-02	-4.55E-01	5.64E-02
		LWF	-5.07E-06	3.31E-04	-7.82E-03	5.94E-02	1.09E-01	-7.43E-02
		LCF	-1.22E-05	8.10E-04	-1.87E-02	1.61E-01	-2.69E-01	1.72E-03

Canyon:			Facade on the courtyard (co)					
LARGE (LC)			Normal component					
Effect	**Season**	**Scene**	**Coeff. 1**	**Coeff. 2**	**Coeff. 3**	**Coeff. 4**	**Coeff. 5**	**Coeff. 6**
WINDY- no gradient	WINTER	WWF	2.38E-06	-1.09E-04	1.77E-03	-1.21E-02	2.99E-02	-4.80E-03
		WCF	2.80E-06	-1.23E-04	1.90E-03	-1.21E-02	2.56E-02	1.15E-02
		LWF	6.39E-06	-2.66E-04	3.85E-03	-2.28E-02	4.23E-02	3.88E-02
		LCF	5.52E-06	-2.26E-04	2.92E-03	-9.95E-03	-2.96E-02	6.28E-02
	MID-SEASON 1	WWF	2.14E-06	-9.52E-05	1.46E-03	-8.61E-03	1.60E-02	-1.66E-02
		WCF	3.92E-06	-1.76E-04	2.73E-03	-1.65E-02	2.98E-02	-3.42E-02
		LWF	2.61E-07	2.87E-05	-1.38E-03	1.90E-02	-8.60E-02	2.95E-02
		LCF	3.95E-06	-1.49E-04	1.72E-03	-4.32E-03	-1.98E-02	5.32E-03
	MID-SEASON 2	WWF	3.33E-06	-1.48E-04	2.31E-03	-1.52E-02	3.75E-02	-9.06E-03
		WCF	3.02E-06	-1.42E-04	2.35E-03	-1.55E-02	3.11E-02	6.94E-03
		LWF	2.77E-06	-1.38E-04	2.65E-03	-2.16E-02	4.72E-02	4.33E-02
		LCF	5.98E-06	-2.39E-04	2.89E-03	-5.58E-03	-6.51E-02	1.01E-01
	SUMMER	WWF	3.60E-06	-1.77E-04	3.08E-03	-2.19E-02	5.34E-02	-3.24E-02
		WCF	2.91E-06	-1.16E-04	1.48E-03	-5.38E-03	-5.52E-03	-1.90E-02
		LWF	-3.10E-08	5.49E-05	-2.08E-03	2.64E-02	-1.15E-01	4.98E-02
		LCF	1.35E-06	-5.77E-06	-1.19E-03	2.22E-02	-1.17E-01	6.61E-02
no wind - GRADIENT	WINTER	WWF	3.37E-06	-1.52E-04	2.31E-03	-1.31E-02	1.72E-02	1.20E-02
		WCF	3.25E-06	-1.42E-04	2.17E-03	-1.37E-02	2.96E-02	7.79E-03
		LWF	2.54E-06	-7.85E-05	7.74E-04	-2.48E-03	-1.40E-02	9.27E-02
		LCF	2.70E-06	-6.96E-05	-1.60E-04	1.58E-02	-1.08E-01	9.42E-02
	MID-SEASON 1	WWF	2.24E-06	-9.72E-05	1.39E-03	-6.65E-03	2.89E-03	-7.14E-03
		WCF	6.80E-06	-3.12E-04	5.01E-03	-3.27E-02	7.25E-02	-5.64E-02
		LWF	1.37E-06	-6.84E-06	-1.12E-03	2.01E-02	-9.94E-02	4.47E-02
		LCF	2.70E-06	-8.33E-05	5.08E-04	4.75E-03	-4.04E-02	-1.07E-02
	MID-SEASON 2	WWF	3.72E-06	-1.67E-04	2.58E-03	-1.52E-02	2.40E-02	9.40E-03
		WCF	3.81E-06	-1.74E-04	2.78E-03	-1.82E-02	4.05E-02	-8.88E-04
		LWF	7.66E-06	-3.74E-04	6.63E-03	-4.88E-02	1.13E-01	3.61E-04
		LCF	9.10E-06	-3.88E-04	5.48E-03	-2.57E-02	-3.14E-03	6.70E-02
	SUMMER	WWF	3.08E-06	-1.34E-04	1.95E-03	-9.88E-03	8.60E-03	-1.56E-02
		WCF	4.05E-06	-1.80E-04	2.76E-03	-1.61E-02	2.74E-02	-3.14E-02
		LWF	2.48E-06	-6.25E-05	-1.28E-04	1.29E-02	-8.04E-02	2.58E-02
		LCF	2.22E-06	-4.63E-05	-3.84E-04	1.32E-02	-6.66E-02	-1.31E-02
WINDY- GRADIENT	WINTER	WWF	9.62E-06	-4.14E-04	5.69E-03	-2.33E-02	-1.93E-02	5.95E-02
		WCF	9.86E-06	-4.52E-04	7.15E-03	-4.41E-02	8.06E-02	2.82E-03
		LWF	1.20E-05	-4.81E-04	6.52E-03	-3.13E-02	1.49E-02	-8.99E-03
		LCF	1.37E-05	-5.70E-04	8.11E-03	-4.39E-02	7.25E-02	-1.39E-01
	MID-SEASON 1	WWF	8.47E-06	-3.65E-04	4.91E-03	-1.76E-02	-3.67E-02	5.79E-02
		WCF	5.09E-06	-2.18E-04	2.99E-03	-1.19E-02	-1.21E-02	-1.07E-02
		LWF	9.00E-06	-3.36E-04	3.90E-03	-1.16E-02	-1.34E-02	-1.39E-01
		LCF	1.11E-05	-4.39E-04	5.87E-03	-2.95E-02	5.77E-02	-2.04E-01
	MID-SEASON 2	WWF	9.38E-06	-4.17E-04	6.14E-03	-3.15E-02	2.55E-02	5.62E-03
		WCF	6.59E-06	-2.81E-04	3.80E-03	-1.44E-02	-2.16E-02	2.08E-02
		LWF	7.52E-06	-1.79E-04	-6.53E-04	4.05E-02	-2.43E-01	1.09E-01
		LCF	8.41E-06	-2.39E-04	8.58E-04	2.29E-02	-1.55E-01	-1.75E-02
	SUMMER	WWF	5.90E-06	-2.44E-04	3.21E-03	-1.22E-02	-8.18E-03	-3.51E-02
		WCF	7.97E-06	-3.51E-04	5.18E-03	-2.72E-02	3.11E-02	-3.87E-02
		LWF	1.20E-05	-4.58E-04	5.57E-03	-1.97E-02	-5.85E-03	-1.59E-01
		LCF	1.16E-05	-4.15E-04	4.48E-03	-1.07E-02	-2.54E-02	-1.42E-01
no wind- no gradient	WINTER	WWF	1.02E-05	-4.43E-04	6.35E-03	-3.13E-02	2.27E-02	-2.21E-03
		WCF	1.10E-05	-4.87E-04	7.27E-03	-4.01E-02	5.51E-02	-8.99E-03
		LWF	1.06E-05	-3.41E-04	2.49E-03	1.34E-02	-1.49E-01	3.19E-02
		LCF	1.84E-05	-7.66E-04	1.09E-02	-5.99E-02	1.01E-01	-1.24E-01
	MID-SEASON 1	WWF	1.15E-05	-5.23E-04	8.07E-03	-4.64E-02	6.76E-02	-1.53E-02
		WCF	1.19E-06	-2.69E-05	-4.32E-04	1.54E-02	-9.45E-02	-1.44E-02
		LWF	1.70E-05	-6.79E-04	9.24E-03	-5.00E-02	1.24E-01	-3.45E-01
		LCF	2.66E-05	-1.13E-03	1.63E-02	-8.94E-02	1.39E-01	-1.26E-01
	MID-SEASON 2	WWF	1.10E-05	-4.88E-04	7.31E-03	-4.09E-02	5.98E-02	-1.82E-02
		WCF	1.14E-05	-5.05E-04	7.59E-03	-4.25E-02	6.22E-02	-1.94E-02
		LWF	1.59E-05	-6.01E-04	7.29E-03	-2.76E-02	3.12E-03	-1.15E-01
		LCF	2.00E-05	-8.36E-04	1.21E-02	-6.90E-02	1.32E-01	-1.69E-01
	SUMMER	WWF	1.15E-05	-5.06E-04	7.26E-03	-3.36E-02	-1.10E-03	5.25E-02
		WCF	5.64E-06	-2.28E-04	2.78E-03	-6.08E-03	-4.37E-02	-1.11E-02
		LWF	1.39E-05	-5.34E-04	6.61E-03	-2.51E-02	6.27E-03	-2.00E-01
		LCF	1.99E-05	-8.57E-04	1.31E-02	-8.43E-02	2.25E-01	-3.40E-01

Canyon:			Facade on the courtyard (co)					
LARGE (LC)			Tangential component					
Effect	Season	Scene	Coeff. 1	Coeff. 2	Coeff. 3	Coeff. 4	Coeff. 5	Coeff. 6
WINDY-no gradient	WINTER	WWF	7.41E-08	-7.74E-06	1.94E-04	-6.30E-05	-2.43E-02	-8.82E-04
		WCF	-2.36E-06	1.03E-04	-1.58E-03	1.30E-02	-7.51E-02	7.92E-03
		LWF	1.46E-05	-6.55E-04	1.03E-02	-7.34E-02	2.71E-01	-8.25E-02
		LCF	1.69E-05	-8.65E-04	1.63E-02	-1.27E-01	2.51E-01	-3.20E-02
	MID-SEASON 1	WWF	-1.97E-06	1.08E-04	-2.21E-03	1.72E-02	-1.18E-02	5.08E-04
		WCF	-7.59E-06	4.08E-04	-8.21E-03	6.94E-02	-1.37E-01	3.92E-02
		LWF	5.50E-06	-2.39E-04	3.52E-03	-1.17E-02	-1.60E-01	9.27E-02
		LCF	9.10E-06	-4.19E-04	6.99E-03	-4.44E-02	-7.17E-03	2.07E-02
	MID-SEASON 2	WWF	-2.56E-06	1.17E-04	-1.73E-03	1.11E-02	-5.21E-02	1.53E-02
		WCF	4.69E-07	1.07E-06	-8.04E-04	1.61E-02	-8.20E-02	1.42E-02
		LWF	-1.29E-05	6.83E-04	-1.11E-02	5.07E-02	1.13E-02	7.26E-02
		LCF	2.20E-05	-1.16E-03	2.23E-02	-1.76E-01	3.37E-01	-2.97E-02
	SUMMER	WWF	-5.38E-07	6.69E-05	-2.42E-03	3.05E-02	-9.07E-02	4.42E-02
		WCF	-7.06E-06	3.54E-04	-6.49E-03	4.54E-02	-8.62E-03	-3.03E-02
		LWF	7.15E-06	-3.08E-04	4.42E-03	-1.34E-02	-1.88E-01	1.28E-01
		LCF	9.63E-06	-4.46E-04	7.43E-03	-4.10E-02	-1.21E-01	1.23E-01
no wind - GRADIENT	WINTER	WWF	-2.93E-06	1.91E-04	-4.41E-03	4.08E-02	-1.13E-01	2.31E-02
		WCF	-3.02E-06	1.30E-04	-1.88E-03	1.34E-02	-7.17E-02	7.98E-03
		LWF	1.13E-05	-4.07E-04	5.26E-03	-4.33E-02	2.27E-01	-8.73E-03
		LCF	1.57E-05	-7.67E-04	1.35E-02	-9.06E-02	5.95E-02	8.07E-02
	MID-SEASON 1	WWF	-2.38E-06	1.41E-04	-3.06E-03	2.39E-02	-2.81E-03	-1.03E-02
		WCF	-8.36E-06	4.63E-04	-9.69E-03	8.65E-02	-2.14E-01	8.89E-02
		LWF	8.91E-06	-3.83E-04	5.52E-03	-2.05E-02	-1.69E-01	1.24E-01
		LCF	6.79E-06	-2.82E-04	4.05E-03	-1.52E-02	-1.37E-01	4.40E-02
	MID-SEASON 2	WWF	-2.39E-06	1.50E-04	-3.39E-03	3.14E-02	-9.06E-02	1.10E-02
		WCF	6.43E-08	7.02E-07	-1.91E-04	5.63E-03	-4.96E-02	-3.63E-04
		LWF	-8.59E-06	4.17E-04	-5.28E-03	1.07E-03	1.42E-01	-2.28E-02
		LCF	2.41E-05	-1.24E-03	2.36E-02	-1.89E-01	4.28E-01	-1.06E-01
	SUMMER	WWF	-4.35E-06	2.40E-04	-4.87E-03	3.73E-02	-1.84E-02	-9.09E-03
		WCF	-6.35E-06	3.43E-04	-6.91E-03	5.61E-02	-8.37E-02	1.62E-02
		LWF	8.47E-06	-3.78E-04	5.97E-03	-2.88E-02	-1.46E-01	8.66E-02
		LCF	7.06E-06	-2.71E-04	3.22E-03	-4.85E-04	-2.37E-01	7.22E-02
WINDY-GRADIENT	WINTER	WWF	-1.26E-05	8.00E-04	-1.76E-02	1.45E-01	-2.39E-01	6.13E-03
		WCF	-5.42E-06	3.67E-04	-8.79E-03	8.45E-02	-2.46E-01	5.64E-02
		LWF	1.25E-05	-4.67E-04	7.39E-03	-5.73E-02	-4.58E-02	3.28E-02
		LCF	1.93E-05	-8.54E-04	1.40E-02	-8.57E-02	-1.16E-01	-4.69E-02
	MID-SEASON 1	WWF	-7.06E-06	5.33E-04	-1.31E-02	1.13E-01	-1.23E-01	-4.93E-02
		WCF	-5.92E-06	3.62E-04	-8.14E-03	6.56E-02	-2.81E-03	-2.71E-02
		LWF	1.55E-05	-6.57E-04	9.87E-03	-3.84E-02	-3.74E-01	5.19E-02
		LCF	1.64E-05	-6.66E-04	9.12E-03	-2.79E-02	-3.70E-01	-5.67E-03
	MID-SEASON 2	WWF	-2.86E-06	2.67E-04	-7.50E-03	6.99E-02	-6.89E-02	-3.88E-02
		WCF	-3.71E-06	2.83E-04	-7.24E-03	6.14E-02	4.10E-03	-7.50E-02
		LWF	3.15E-05	-1.39E-03	2.13E-02	-1.06E-01	-3.17E-01	2.79E-01
		LCF	2.51E-05	-1.04E-03	1.45E-02	-4.98E-02	-4.74E-01	2.01E-01
	SUMMER	WWF	-4.33E-06	2.62E-04	-5.63E-03	3.67E-02	1.22E-01	-6.68E-02
		WCF	-4.71E-06	3.06E-04	-7.09E-03	5.67E-02	1.45E-02	-2.24E-02
		LWF	2.02E-05	-8.73E-04	1.36E-02	-6.24E-02	-3.93E-01	5.76E-02
		LCF	2.17E-05	-8.61E-04	1.12E-02	-2.92E-02	-4.69E-01	6.91E-02
no wind-no gradient	WINTER	WWF	-3.92E-06	3.12E-04	-7.81E-03	6.37E-02	-7.01E-03	-5.65E-02
		WCF	-4.08E-06	3.14E-04	-7.87E-03	6.97E-02	-9.89E-02	-8.82E-03
		LWF	2.95E-05	-1.29E-03	1.99E-02	-1.04E-01	-2.64E-01	1.82E-01
		LCF	3.15E-05	-1.42E-03	2.33E-02	-1.50E-01	7.74E-02	-8.32E-02
	MID-SEASON 1	WWF	-1.76E-06	2.30E-04	-7.38E-03	7.58E-02	-1.17E-01	-6.10E-04
		WCF	3.30E-06	-9.31E-05	-2.45E-04	-1.56E-04	3.25E-01	-1.41E-01
		LWF	2.55E-05	-1.02E-03	1.30E-02	-2.62E-02	-5.59E-01	-2.99E-02
		LCF	4.07E-05	-1.99E-03	3.51E-02	-2.43E-01	2.56E-01	-1.38E-01
	MID-SEASON 2	WWF	-3.47E-06	2.57E-04	-6.33E-03	5.35E-02	-3.28E-02	-3.94E-02
		WCF	-1.56E-06	1.74E-04	-5.16E-03	4.78E-02	-2.48E-02	-4.05E-02
		LWF	2.62E-05	-1.07E-03	1.49E-02	-6.14E-02	-3.30E-01	8.99E-02
		LCF	2.83E-05	-1.22E-03	1.91E-02	-1.16E-01	-4.29E-02	-6.64E-02
	SUMMER	WWF	-1.22E-05	8.10E-04	-1.87E-02	1.61E-01	-2.69E-01	1.72E-03
		WCF	-5.07E-06	3.31E-04	-7.82E-03	5.94E-02	1.09E-01	-7.43E-02
		LWF	2.30E-05	-9.93E-04	1.53E-02	-6.82E-02	-4.55E-01	5.64E-02
		LCF	1.81E-05	-6.64E-04	8.16E-03	-2.30E-02	-3.69E-01	-8.66E-02

Canyon:			Facade on the urban canyon (uc)					
MEDIUM (MC)			Normal component					
Effect	Season	Scene	Coeff. 1	Coeff. 2	Coeff. 3	Coeff. 4	Coeff. 5	Coeff. 6
WINDY-no gradient	WINTER	WWF	3.59E-06	-1.62E-04	2.64E-03	-1.85E-02	4.75E-02	-1.88E-02
		WCF	3.65E-06	-1.67E-04	2.65E-03	-1.74E-02	4.07E-02	-1.34E-03
		LWF	1.36E-06	-5.85E-05	8.52E-04	-4.55E-03	3.52E-03	1.59E-02
		LCF	1.72E-06	-8.56E-05	1.50E-03	-1.04E-02	2.23E-02	-1.59E-03
	MID-SEASON 1	WWF	4.70E-06	-2.00E-04	2.86E-03	-1.50E-02	1.65E-02	5.15E-03
		WCF	1.25E-06	-3.31E-05	-4.31E-06	5.46E-03	-3.38E-02	9.61E-03
		LWF	2.84E-06	-1.20E-04	1.70E-03	-8.68E-03	1.06E-02	-1.89E-02
		LCF	2.12E-06	-9.39E-05	1.41E-03	-7.78E-03	1.09E-02	-8.29E-03
	MID-SEASON 2	WWF	5.39E-06	-2.48E-04	4.08E-03	-2.81E-02	6.79E-02	-2.04E-02
		WCF	5.97E-06	-2.74E-04	4.42E-03	-2.96E-02	7.30E-02	-2.40E-02
		LWF	1.76E-06	-7.50E-05	1.08E-03	-5.68E-03	4.74E-03	1.79E-02
		LCF	2.16E-06	-9.74E-05	1.46E-03	-7.71E-03	8.73E-03	-6.36E-03
	SUMMER	WWF	5.40E-06	-2.27E-04	3.20E-03	-1.61E-02	1.48E-02	6.66E-03
		WCF	3.12E-06	-1.16E-04	1.27E-03	-2.31E-03	-1.91E-02	9.43E-03
		LWF	3.94E-06	-1.69E-04	2.46E-03	-1.34E-02	2.06E-02	-2.16E-02
		LCF	2.73E-06	-1.20E-04	1.77E-03	-9.64E-03	1.31E-02	-1.04E-02
no wind - GRADIENT	WINTER	WWF	7.60E-06	-3.53E-04	5.81E-03	-3.95E-02	9.38E-02	-3.65E-02
		WCF	6.88E-06	-3.15E-04	5.05E-03	-3.34E-02	8.09E-02	-2.55E-02
		LWF	2.03E-06	-8.66E-05	1.24E-03	-6.60E-03	6.18E-03	1.89E-02
		LCF	2.29E-06	-1.07E-04	1.71E-03	-1.06E-02	1.99E-02	-9.52E-03
	MID-SEASON 1	WWF	5.87E-06	-2.48E-04	3.52E-03	-1.81E-02	1.88E-02	6.07E-03
		WCF	3.13E-06	-1.15E-04	1.21E-03	-1.66E-03	-2.07E-02	6.89E-03
		LWF	4.28E-06	-1.84E-04	2.68E-03	-1.48E-02	2.39E-02	-2.53E-02
		LCF	1.74E-06	-7.44E-05	1.03E-03	-4.41E-03	-1.81E-03	9.60E-04
	MID-SEASON 2	WWF	4.22E-06	-1.72E-04	2.50E-03	-1.59E-02	3.88E-02	-1.05E-02
		WCF	1.19E-05	-5.34E-04	8.34E-03	-5.38E-02	1.28E-01	-5.02E-02
		LWF	1.83E-06	-7.96E-05	1.24E-03	-8.09E-03	1.58E-02	1.23E-02
		LCF	-1.80E-07	3.13E-06	1.39E-04	-3.02E-03	1.27E-02	-2.88E-03
	SUMMER	WWF	5.97E-06	-2.46E-04	3.32E-03	-1.53E-02	7.51E-03	8.67E-03
		WCF	4.61E-06	-1.80E-04	2.19E-03	-7.23E-03	-1.28E-02	1.17E-02
		LWF	4.19E-06	-1.79E-04	2.57E-03	-1.35E-02	1.80E-02	-1.84E-02
		LCF	3.44E-06	-1.48E-04	2.13E-03	-1.10E-02	1.24E-02	-1.02E-02
WINDY-GRADIENT	WINTER	WWF	1.45E-05	-6.03E-04	8.34E-03	-4.09E-02	3.46E-02	1.30E-02
		WCF	1.99E-05	-8.92E-04	1.39E-02	-8.49E-02	1.57E-01	-2.31E-02
		LWF	5.16E-06	-2.22E-04	3.01E-03	-1.13E-02	-1.64E-02	2.20E-02
		LCF	5.05E-06	-2.12E-04	2.69E-03	-7.40E-03	-3.50E-02	4.12E-02
	MID-SEASON 1	WWF	1.38E-05	-5.66E-04	7.68E-03	-3.61E-02	2.38E-02	1.18E-02
		WCF	1.25E-05	-5.04E-04	6.61E-03	-2.87E-02	8.15E-03	6.60E-03
		LWF	4.05E-06	-1.53E-04	1.64E-03	-1.30E-03	-3.86E-02	1.83E-02
		LCF	3.80E-06	-1.53E-04	1.72E-03	-9.11E-04	-5.04E-02	4.74E-02
	MID-SEASON 2	WWF	1.82E-05	-7.63E-04	1.06E-02	-5.31E-02	4.97E-02	1.61E-02
		WCF	2.04E-05	-8.79E-04	1.28E-02	-6.97E-02	9.30E-02	8.53E-03
		LWF	5.83E-06	-2.46E-04	3.20E-03	-9.81E-03	-3.39E-02	3.81E-02
		LCF	5.59E-06	-2.32E-04	2.88E-03	-6.64E-03	-4.63E-02	4.85E-02
	SUMMER	WWF	1.63E-05	-6.65E-04	8.90E-03	-4.07E-02	2.22E-02	1.01E-02
		WCF	1.59E-05	-6.45E-04	8.56E-03	-3.85E-02	1.84E-02	6.30E-03
		LWF	1.36E-06	-2.06E-05	-7.58E-04	1.84E-02	-1.06E-01	6.87E-02
		LCF	2.33E-06	-7.48E-05	2.44E-04	1.13E-02	-8.95E-02	6.59E-02
no wind-no gradient	WINTER	WWF	1.78E-05	-7.35E-04	1.00E-02	-4.78E-02	3.41E-02	1.68E-02
		WCF	2.08E-05	-8.90E-04	1.29E-02	-6.87E-02	8.44E-02	1.61E-02
		LWF	5.54E-06	-2.31E-04	2.87E-03	-6.66E-03	-4.57E-02	4.46E-02
		LCF	5.15E-06	-2.09E-04	2.43E-03	-2.86E-03	-5.86E-02	5.41E-02
	MID-SEASON 1	WWF	1.69E-05	-6.91E-04	9.28E-03	-4.28E-02	2.57E-02	8.77E-03
		WCF	1.61E-05	-6.54E-04	8.64E-03	-3.85E-02	1.70E-02	4.61E-03
		LWF	1.21E-06	-1.14E-05	-9.66E-04	2.03E-02	-1.12E-01	6.94E-02
		LCF	3.35E-06	-1.23E-04	1.02E-03	6.42E-03	-7.95E-02	6.08E-02
	MID-SEASON 2	WWF	1.89E-05	-7.72E-04	1.04E-02	-4.77E-02	2.74E-02	1.31E-02
		WCF	2.22E-05	-9.41E-04	1.33E-02	-6.86E-02	7.06E-02	2.92E-02
		LWF	5.46E-06	-2.21E-04	2.56E-03	-2.77E-03	-6.34E-02	5.53E-02
		LCF	4.07E-06	-1.52E-04	1.35E-03	5.98E-03	-8.62E-02	6.43E-02
	SUMMER	WWF	1.85E-05	-7.52E-04	1.00E-02	-4.57E-02	2.54E-02	6.44E-03
		WCF	1.79E-05	-7.24E-04	9.57E-03	-4.28E-02	2.08E-02	1.03E-04
		LWF	1.47E-06	-1.84E-05	-9.67E-04	2.16E-02	-1.20E-01	7.23E-02
		LCF	3.24E-06	-1.12E-04	6.93E-04	1.03E-02	-9.55E-02	6.66E-02

Canyon:			Facade on the urban canyon (uc)					
MEDIUM (MC)			Tangential component					
Effect	Season	Scene	Coeff. 1	Coeff. 2	Coeff. 3	Coeff. 4	Coeff. 5	Coeff. 6
WINDY-no gradient	WINTER	WWF	-8.32E-06	5.11E-04	-1.00E-02	6.95E-02	-1.36E-01	5.52E-02
		WCF	-3.99E-06	1.96E-04	-3.82E-03	3.30E-02	-4.45E-02	-1.83E-03
		LWF	2.10E-07	-7.93E-06	-1.70E-04	7.85E-03	-5.64E-02	-4.94E-02
		LCF	7.48E-06	-3.19E-04	3.87E-03	-7.86E-03	-3.48E-02	-1.79E-02
	MID-SEASON 1	WWF	2.15E-05	-1.09E-03	1.97E-02	-1.45E-01	2.73E-01	-5.02E-02
		WCF	1.10E-05	-4.83E-04	6.93E-03	-2.35E-02	-2.23E-01	1.69E-01
		LWF	-1.43E-05	7.33E-04	-1.35E-02	9.55E-02	-8.78E-02	-2.21E-03
		LCF	-8.68E-06	4.74E-04	-9.44E-03	7.50E-02	-1.27E-01	2.86E-02
	MID-SEASON 2	WWF	-9.72E-06	5.15E-04	-8.44E-03	4.02E-02	-4.59E-03	3.15E-02
		WCF	-3.30E-06	1.46E-04	-2.74E-03	2.41E-02	-2.54E-02	-2.02E-02
		LWF	-4.12E-07	2.33E-05	-6.83E-04	1.11E-02	-6.71E-02	-5.25E-02
		LCF	9.99E-06	-4.01E-04	5.05E-03	-2.81E-02	1.60E-01	-1.29E-01
	SUMMER	WWF	2.48E-05	-1.24E-03	2.21E-02	-1.58E-01	2.64E-01	-1.96E-02
		WCF	1.68E-05	-7.82E-04	1.25E-02	-6.76E-02	-9.91E-02	1.42E-01
		LWF	-1.53E-05	7.90E-04	-1.46E-02	1.06E-01	-1.19E-01	1.04E-02
		LCF	-1.07E-05	5.79E-04	-1.14E-02	8.87E-02	-1.39E-01	2.88E-02
no wind - GRADIENT	WINTER	WWF	3.86E-06	-2.29E-04	6.08E-03	-7.54E-02	2.95E-01	-1.63E-01
		WCF	-3.96E-06	1.72E-04	-3.21E-03	2.91E-02	-4.59E-02	5.72E-03
		LWF	-1.09E-06	5.61E-05	-1.22E-03	1.48E-02	-7.84E-02	-5.49E-02
		LCF	5.95E-06	-2.26E-04	2.30E-03	-5.31E-03	4.18E-02	-4.62E-02
	MID-SEASON 1	WWF	2.68E-05	-1.34E-03	2.40E-02	-1.73E-01	3.07E-01	-3.67E-02
		WCF	1.60E-05	-7.25E-04	1.11E-02	-5.27E-02	-1.63E-01	1.67E-01
		LWF	-1.61E-05	8.23E-04	-1.51E-02	1.07E-01	-1.10E-01	4.58E-03
		LCF	-1.01E-05	5.52E-04	-1.10E-02	8.69E-02	-1.34E-01	1.50E-02
	MID-SEASON 2	WWF	1.34E-05	-4.03E-04	2.47E-03	3.99E-03	6.83E-03	4.00E-03
		WCF	1.91E-05	-9.36E-04	1.53E-02	-1.01E-01	3.09E-01	-1.90E-01
		LWF	-1.14E-07	-5.99E-05	1.71E-03	-5.92E-03	-6.72E-02	-4.43E-02
		LCF	1.11E-05	-6.48E-04	1.22E-02	-8.16E-02	1.47E-01	-8.23E-02
	SUMMER	WWF	2.77E-05	-1.36E-03	2.35E-02	-1.59E-01	1.89E-01	4.96E-02
		WCF	2.25E-05	-1.07E-03	1.76E-02	-1.05E-01	-2.07E-02	1.44E-01
		LWF	-1.66E-05	8.56E-04	-1.59E-02	1.15E-01	-1.30E-01	4.96E-03
		LCF	-1.41E-05	7.43E-04	-1.42E-02	1.07E-01	-1.49E-01	2.22E-02
WINDY-GRADIENT	WINTER	WWF	6.58E-05	-3.23E-03	5.64E-02	-3.92E-01	5.85E-01	3.27E-03
		WCF	6.35E-05	-3.35E-03	6.53E-02	-5.46E-01	1.45E+00	-5.22E-01
		LWF	1.52E-05	-4.72E-04	2.38E-03	8.44E-03	2.48E-01	-3.43E-01
		LCF	9.75E-06	-1.73E-04	-3.45E-03	5.35E-02	1.53E-01	-3.45E-01
	MID-SEASON 1	WWF	6.13E-05	-2.97E-03	5.09E-02	-3.40E-01	3.95E-01	9.32E-02
		WCF	5.10E-05	-2.41E-03	3.97E-02	-2.42E-01	5.86E-02	2.38E-01
		LWF	-2.56E-05	1.33E-03	-2.46E-02	1.69E-01	-5.83E-02	-1.38E-01
		LCF	7.90E-06	-1.31E-04	-3.28E-03	4.56E-02	1.95E-01	-3.69E-01
	MID-SEASON 2	WWF	8.27E-05	-4.07E-03	7.16E-02	-5.04E-01	8.13E-01	-4.26E-02
		WCF	8.81E-05	-4.45E-03	8.11E-02	-6.09E-01	1.27E+00	-2.90E-01
		LWF	1.44E-05	-3.75E-04	-5.56E-04	3.43E-02	2.58E-01	-4.19E-01
		LCF	1.25E-05	-2.76E-04	-2.39E-03	4.68E-02	2.46E-01	-4.40E-01
	SUMMER	WWF	6.97E-05	-3.33E-03	5.60E-02	-3.59E-01	2.89E-01	1.97E-01
		WCF	6.50E-05	-3.08E-03	5.12E-02	-3.19E-01	1.60E-01	2.46E-01
		LWF	-1.97E-05	1.06E-03	-2.08E-02	1.42E-01	1.05E-01	-3.38E-01
		LCF	2.13E-06	1.03E-04	-6.42E-03	5.64E-02	2.85E-01	-4.61E-01
no wind-no gradient	WINTER	WWF	7.94E-05	-3.86E-03	6.66E-02	-4.52E-01	5.83E-01	8.26E-02
		WCF	9.12E-05	-4.60E-03	8.38E-02	-6.27E-01	1.27E+00	-2.57E-01
		LWF	1.51E-05	-4.07E-04	-5.28E-05	2.87E-02	3.12E-01	-4.67E-01
		LCF	1.29E-05	-3.03E-04	-1.73E-03	3.82E-02	3.09E-01	-4.89E-01
	MID-SEASON 1	WWF	7.14E-05	-3.42E-03	5.75E-02	-3.71E-01	3.11E-01	1.90E-01
		WCF	6.47E-05	-3.06E-03	5.05E-02	-3.10E-01	1.05E-01	2.76E-01
		LWF	-1.98E-05	1.06E-03	-2.05E-02	1.37E-01	1.51E-01	-3.65E-01
		LCF	8.40E-06	-1.59E-04	-2.71E-03	3.39E-02	3.51E-01	-5.03E-01
	MID-SEASON 2	WWF	7.98E-05	-3.83E-03	6.48E-02	-4.22E-01	3.80E-01	2.04E-01
		WCF	1.00E-04	-5.02E-03	9.05E-02	-6.64E-01	1.26E+00	-1.77E-01
		LWF	1.65E-05	-4.67E-04	7.74E-04	2.02E-02	4.05E-01	-5.58E-01
		LCF	1.37E-05	-3.81E-04	4.13E-04	1.13E-02	4.79E-01	-6.05E-01
	SUMMER	WWF	7.54E-05	-3.58E-03	5.98E-02	-3.77E-01	2.34E-01	2.56E-01
		WCF	6.98E-05	-3.28E-03	5.37E-02	-3.24E-01	5.64E-02	3.21E-01
		LWF	-2.05E-05	1.10E-03	-2.13E-02	1.39E-01	2.05E-01	-4.13E-01
		LCF	1.06E-05	-2.67E-04	-7.81E-04	1.41E-02	4.86E-01	-6.01E-01

Canyon:			Facade on the courtyard (co)					
MEDIUM (MC)			Normal component					
Effect	Season	Scene	Coeff. 1	Coeff. 2	Coeff. 3	Coeff. 4	Coeff. 5	Coeff. 6
WINDY-no gradient	WINTER	WWF	1.72E-06	-8.56E-05	1.50E-03	-1.04E-02	2.23E-02	-1.59E-03
		WCF	1.36E-06	-5.85E-05	8.52E-04	-4.55E-03	3.52E-03	1.59E-02
		LWF	3.65E-06	-1.67E-04	2.65E-03	-1.74E-02	4.07E-02	-1.34E-03
		LCF	3.59E-06	-1.62E-04	2.64E-03	-1.85E-02	4.75E-02	-1.88E-02
	MID-SEASON 1	WWF	2.12E-06	-9.39E-05	1.41E-03	-7.78E-03	1.09E-02	-8.29E-03
		WCF	2.84E-06	-1.20E-04	1.70E-03	-8.68E-03	1.06E-02	-1.89E-02
		LWF	1.25E-06	-3.31E-05	-4.31E-06	5.46E-03	-3.38E-02	9.61E-03
		LCF	4.70E-06	-2.00E-04	2.86E-03	-1.50E-02	1.65E-02	5.15E-03
	MID-SEASON 2	WWF	2.16E-06	-9.74E-05	1.46E-03	-7.71E-03	8.73E-03	-6.36E-03
		WCF	1.76E-06	-7.50E-05	1.08E-03	-5.68E-03	4.74E-03	1.79E-02
		LWF	5.97E-06	-2.74E-04	4.42E-03	-2.96E-02	7.30E-02	-2.40E-02
		LCF	5.39E-06	-2.48E-04	4.08E-03	-2.81E-02	6.79E-02	-2.04E-02
	SUMMER	WWF	2.73E-06	-1.20E-04	1.77E-03	-9.64E-03	1.31E-02	-1.04E-02
		WCF	3.94E-06	-1.69E-04	2.46E-03	-1.34E-02	2.06E-02	-2.16E-02
		LWF	3.12E-06	-1.16E-04	1.27E-03	-2.31E-03	-1.91E-02	9.43E-03
		LCF	5.40E-06	-2.27E-04	3.20E-03	-1.61E-02	1.48E-02	6.66E-03
no wind - GRADIENT	WINTER	WWF	2.29E-06	-1.07E-04	1.71E-03	-1.06E-02	1.99E-02	-9.52E-03
		WCF	2.03E-06	-8.66E-05	1.24E-03	-6.60E-03	6.18E-03	1.89E-02
		LWF	6.88E-06	-3.15E-04	5.05E-03	-3.34E-02	8.09E-02	-2.55E-02
		LCF	7.60E-06	-3.53E-04	5.81E-03	-3.95E-02	9.38E-02	-3.65E-02
	MID-SEASON 1	WWF	1.74E-06	-7.44E-05	1.03E-03	-4.41E-03	-1.81E-03	9.60E-04
		WCF	4.28E-06	-1.84E-04	2.68E-03	-1.48E-02	2.39E-02	-2.53E-02
		LWF	3.13E-06	-1.15E-04	1.21E-03	-1.66E-03	-2.07E-02	6.89E-03
		LCF	5.87E-06	-2.48E-04	3.52E-03	-1.81E-02	1.88E-02	6.07E-03
	MID-SEASON 2	WWF	-1.80E-07	3.13E-06	1.39E-04	-3.02E-03	1.27E-02	-2.88E-03
		WCF	1.83E-06	-7.96E-05	1.24E-03	-8.09E-03	1.58E-02	1.23E-02
		LWF	1.19E-05	-5.34E-04	8.34E-03	-5.38E-02	1.28E-01	-5.02E-02
		LCF	4.22E-06	-1.72E-04	2.50E-03	-1.59E-02	3.88E-02	-1.05E-02
	SUMMER	WWF	3.44E-06	-1.48E-04	2.13E-03	-1.10E-02	1.24E-02	-1.02E-02
		WCF	4.19E-06	-1.79E-04	2.57E-03	-1.35E-02	1.80E-02	-1.84E-02
		LWF	4.61E-06	-1.80E-04	2.19E-03	-7.23E-03	-1.28E-02	1.17E-02
		LCF	5.97E-06	-2.46E-04	3.32E-03	-1.53E-02	7.51E-03	8.67E-03
WINDY-GRADIENT	WINTER	WWF	5.05E-06	-2.12E-04	2.69E-03	-7.40E-03	-3.50E-02	4.12E-02
		WCF	5.16E-06	-2.22E-04	3.01E-03	-1.13E-02	-1.64E-02	2.20E-02
		LWF	1.99E-05	-8.92E-04	1.39E-02	-8.49E-02	1.57E-01	-2.31E-02
		LCF	1.45E-05	-6.03E-04	8.34E-03	-4.09E-02	3.46E-02	1.30E-02
	MID-SEASON 1	WWF	3.80E-06	-1.53E-04	1.72E-03	-9.11E-04	-5.04E-02	4.74E-02
		WCF	4.05E-06	-1.53E-04	1.64E-03	-1.30E-03	-3.86E-02	1.83E-02
		LWF	1.25E-05	-5.04E-04	6.61E-03	-2.87E-02	8.15E-03	6.60E-03
		LCF	1.38E-05	-5.66E-04	7.68E-03	-3.61E-02	2.38E-02	1.18E-02
	MID-SEASON 2	WWF	5.59E-06	-2.32E-04	2.88E-03	-6.64E-03	-4.63E-02	4.85E-02
		WCF	5.83E-06	-2.46E-04	3.20E-03	-9.81E-03	-3.39E-02	3.81E-02
		LWF	2.04E-05	-8.79E-04	1.28E-02	-6.97E-02	9.30E-02	8.53E-03
		LCF	1.82E-05	-7.63E-04	1.06E-02	-5.31E-02	4.97E-02	1.61E-02
	SUMMER	WWF	2.33E-06	-7.48E-05	2.44E-04	1.13E-02	-8.95E-02	6.59E-02
		WCF	1.36E-06	-2.06E-05	-7.58E-04	1.84E-02	-1.06E-01	6.87E-02
		LWF	1.59E-05	-6.45E-04	8.56E-03	-3.85E-02	1.84E-02	6.30E-03
		LCF	1.63E-05	-6.65E-04	8.90E-03	-4.07E-02	2.22E-02	1.01E-02
no wind-no gradient	WINTER	WWF	5.15E-06	-2.09E-04	2.43E-03	-2.86E-03	-5.86E-02	5.41E-02
		WCF	5.54E-06	-2.31E-04	2.87E-03	-6.66E-03	-4.57E-02	4.46E-02
		LWF	2.08E-05	-8.90E-04	1.29E-02	-6.87E-02	8.44E-02	1.61E-02
		LCF	1.78E-05	-7.35E-04	1.00E-02	-4.78E-02	3.41E-02	1.68E-02
	MID-SEASON 1	WWF	3.35E-06	-1.23E-04	1.02E-03	6.42E-03	-7.95E-02	6.08E-02
		WCF	1.21E-06	-1.14E-05	-9.66E-04	2.03E-02	-1.12E-01	6.94E-02
		LWF	1.61E-05	-6.54E-04	8.64E-03	-3.85E-02	1.70E-02	4.61E-03
		LCF	1.69E-05	-6.91E-04	9.28E-03	-4.28E-02	2.57E-02	8.77E-03
	MID-SEASON 2	WWF	4.07E-06	-1.52E-04	1.35E-03	5.98E-03	-8.62E-02	6.43E-02
		WCF	5.46E-06	-2.21E-04	2.56E-03	-2.77E-03	-6.34E-02	5.53E-02
		LWF	2.22E-05	-9.41E-04	1.33E-02	-6.86E-02	7.06E-02	2.92E-02
		LCF	1.89E-05	-7.72E-04	1.04E-02	-4.77E-02	2.74E-02	1.31E-02
	SUMMER	WWF	3.24E-06	-1.12E-04	6.93E-04	1.03E-02	-9.55E-02	6.66E-02
		WCF	1.47E-06	-1.84E-05	-9.67E-04	2.16E-02	-1.20E-01	7.23E-02
		LWF	1.79E-05	-7.24E-04	9.57E-03	-4.28E-02	2.08E-02	1.03E-04
		LCF	1.85E-05	-7.52E-04	1.00E-02	-4.57E-02	2.54E-02	6.44E-03

Canyon:			Facade on the courtyard (co)					
MEDIUM (MC)			Tangential component					
Effect	Season	Scene	Coeff. 1	Coeff. 2	Coeff. 3	Coeff. 4	Coeff. 5	Coeff. 6
WINDY-no gradient	WINTER	WWF	7.48E-06	-3.19E-04	3.87E-03	-7.86E-03	-3.48E-02	-1.79E-02
		WCF	2.10E-07	-7.93E-06	-1.70E-04	7.85E-03	-5.64E-02	-4.94E-02
		LWF	-3.99E-06	1.96E-04	-3.82E-03	3.30E-02	-4.45E-02	-1.83E-03
		LCF	-8.32E-06	5.11E-04	-1.00E-02	6.95E-02	-1.36E-01	5.52E-02
	MID-SEASON 1	WWF	-8.68E-06	4.74E-04	-9.44E-03	7.50E-02	-1.27E-01	2.86E-02
		WCF	-1.43E-05	7.33E-04	-1.35E-02	9.55E-02	-8.78E-02	-2.21E-03
		LWF	1.10E-05	-4.83E-04	6.93E-03	-2.35E-02	-2.23E-01	1.69E-01
		LCF	2.15E-05	-1.09E-03	1.97E-02	-1.45E-01	2.73E-01	-5.02E-02
	MID-SEASON 2	WWF	9.99E-06	-4.01E-04	5.05E-03	-2.81E-02	1.60E-01	-1.29E-01
		WCF	-4.12E-07	2.33E-05	-6.83E-04	1.11E-02	-6.71E-02	-5.25E-02
		LWF	-3.30E-06	1.46E-04	-2.74E-03	2.41E-02	-2.54E-02	-2.02E-02
		LCF	-9.72E-06	5.15E-04	-8.44E-03	4.02E-02	-4.59E-03	3.15E-02
	SUMMER	WWF	-1.07E-05	5.79E-04	-1.14E-02	8.87E-02	-1.39E-01	2.88E-02
		WCF	-1.53E-05	7.90E-04	-1.46E-02	1.06E-01	-1.19E-01	1.04E-02
		LWF	1.68E-05	-7.82E-04	1.25E-02	-6.76E-02	-9.91E-02	1.42E-01
		LCF	2.48E-05	-1.24E-03	2.21E-02	-1.58E-01	2.64E-01	-1.96E-02
no wind - GRADIENT	WINTER	WWF	5.95E-06	-2.26E-04	2.30E-03	-5.31E-03	4.18E-02	-4.62E-02
		WCF	-1.09E-06	5.61E-05	-1.22E-03	1.48E-02	-7.84E-02	-5.49E-02
		LWF	-3.96E-06	1.72E-04	-3.21E-03	2.91E-02	-4.59E-02	5.72E-03
		LCF	3.86E-06	-2.29E-04	6.08E-03	-7.54E-02	2.95E-01	-1.63E-01
	MID-SEASON 1	WWF	-1.01E-05	5.52E-04	-1.10E-02	8.69E-02	-1.34E-01	1.50E-02
		WCF	-1.61E-05	8.23E-04	-1.51E-02	1.07E-01	-1.10E-01	4.58E-03
		LWF	1.60E-05	-7.25E-04	1.11E-02	-5.27E-02	-1.63E-01	1.67E-01
		LCF	2.68E-05	-1.34E-03	2.40E-02	-1.73E-01	3.07E-01	-3.67E-02
	MID-SEASON 2	WWF	1.11E-05	-6.48E-04	1.22E-02	-8.16E-02	1.47E-01	-8.23E-02
		WCF	-1.14E-07	-5.99E-05	1.71E-03	-5.92E-03	-6.72E-02	-4.43E-02
		LWF	1.91E-05	-9.36E-04	1.53E-02	-1.01E-01	3.09E-01	-1.90E-01
		LCF	1.34E-05	-4.03E-04	2.47E-03	3.99E-03	6.83E-03	4.00E-03
	SUMMER	WWF	-1.41E-05	7.43E-04	-1.42E-02	1.07E-01	-1.49E-01	2.22E-02
		WCF	-1.66E-05	8.56E-04	-1.59E-02	1.15E-01	-1.30E-01	4.96E-03
		LWF	2.25E-05	-1.07E-03	1.76E-02	-1.05E-01	-2.07E-02	1.44E-01
		LCF	2.77E-05	-1.36E-03	2.35E-02	-1.59E-01	1.89E-01	4.96E-02
WINDY-GRADIENT	WINTER	WWF	9.75E-06	-1.73E-04	-3.45E-03	5.35E-02	1.53E-01	-3.45E-01
		WCF	1.52E-05	-4.72E-04	2.38E-03	8.44E-03	2.48E-01	-3.43E-01
		LWF	6.35E-05	-3.35E-03	6.53E-02	-5.46E-01	1.45E+00	-5.22E-01
		LCF	6.58E-05	-3.23E-03	5.64E-02	-3.92E-01	5.85E-01	3.27E-03
	MID-SEASON 1	WWF	7.90E-06	-1.31E-04	-3.28E-03	4.56E-02	1.95E-01	-3.69E-01
		WCF	-2.56E-05	1.33E-03	-2.46E-02	1.69E-01	-5.83E-02	-1.38E-01
		LWF	5.10E-05	-2.41E-03	3.97E-02	-2.42E-01	5.86E-02	2.38E-01
		LCF	6.13E-05	-2.97E-03	5.09E-02	-3.40E-01	3.95E-01	9.32E-02
	MID-SEASON 2	WWF	1.25E-05	-2.76E-04	-2.39E-03	4.68E-02	2.46E-01	-4.40E-01
		WCF	1.44E-05	-3.75E-04	-5.56E-04	3.43E-02	2.58E-01	-4.19E-01
		LWF	8.81E-05	-4.45E-03	8.11E-02	-6.09E-01	1.27E+00	-2.90E-01
		LCF	8.27E-05	-4.07E-03	7.16E-02	-5.04E-01	8.13E-01	-4.26E-02
	SUMMER	WWF	2.13E-06	1.03E-04	-6.42E-03	5.64E-02	2.85E-01	-4.61E-01
		WCF	-1.97E-05	1.06E-03	-2.08E-02	1.42E-01	1.05E-01	-3.38E-01
		LWF	6.50E-05	-3.08E-03	5.12E-02	-3.19E-01	1.60E-01	2.46E-01
		LCF	6.97E-05	-3.33E-03	5.60E-02	-3.59E-01	2.89E-01	1.97E-01
no wind-no gradient	WINTER	WWF	1.29E-05	-3.03E-04	-1.73E-03	3.82E-02	3.09E-01	-4.89E-01
		WCF	1.51E-05	-4.07E-04	-5.28E-05	2.87E-02	3.12E-01	-4.67E-01
		LWF	9.12E-05	-4.60E-03	8.38E-02	-6.27E-01	1.27E+00	-2.57E-01
		LCF	7.94E-05	-3.86E-03	6.66E-02	-4.52E-01	5.83E-01	8.26E-02
	MID-SEASON 1	WWF	8.40E-06	-1.59E-04	-2.71E-03	3.39E-02	3.51E-01	-5.03E-01
		WCF	-1.98E-05	1.06E-03	-2.05E-02	1.37E-01	1.51E-01	-3.65E-01
		LWF	6.47E-05	-3.06E-03	5.05E-02	-3.10E-01	1.05E-01	2.76E-01
		LCF	7.14E-05	-3.42E-03	5.75E-02	-3.71E-01	3.11E-01	1.90E-01
	MID-SEASON 2	WWF	1.37E-05	-3.81E-04	4.13E-04	1.13E-02	4.79E-01	-6.05E-01
		WCF	1.65E-05	-4.67E-04	7.74E-04	2.02E-02	4.05E-01	-5.58E-01
		LWF	1.00E-04	-5.02E-03	9.05E-02	-6.64E-01	1.26E+00	-1.77E-01
		LCF	7.98E-05	-3.83E-03	6.48E-02	-4.22E-01	3.80E-01	2.04E-01
	SUMMER	WWF	1.06E-05	-2.67E-04	-7.81E-04	1.41E-02	4.86E-01	-6.01E-01
		WCF	-2.05E-05	1.10E-03	-2.13E-02	1.39E-01	2.05E-01	-4.13E-01
		LWF	6.98E-05	-3.28E-03	5.37E-02	-3.24E-01	5.64E-02	3.21E-01
		LCF	7.54E-05	-3.58E-03	5.98E-02	-3.77E-01	2.34E-01	2.56E-01

Canyon:			Facade on the urban canyon (uc)					
NARROW (NC)			Normal component					
Effect	Season	Scene	Coeff. 1	Coeff. 2	Coeff. 3	Coeff. 4	Coeff. 5	Coeff. 6
WINDY-no gradient	WINTER	WWF	2.86E-06	-1.23E-04	1.86E-03	-1.18E-02	2.79E-02	-1.03E-02
		WCF	2.61E-06	-1.18E-04	1.86E-03	-1.19E-02	2.56E-02	1.64E-03
		LWF	1.39E-06	-5.94E-05	8.66E-04	-4.85E-03	6.91E-03	7.32E-03
		LCF	4.42E-07	-2.21E-05	4.26E-04	-3.64E-03	1.06E-02	-1.23E-03
	MID-SEASON 1	WWF	3.32E-06	-1.44E-04	2.14E-03	-1.25E-02	2.29E-02	-8.70E-03
		WCF	2.11E-06	-8.84E-05	1.28E-03	-7.49E-03	1.80E-02	-2.71E-02
		LWF	2.02E-06	-8.56E-05	1.24E-03	-7.22E-03	1.55E-02	-2.08E-02
		LCF	1.62E-06	-7.00E-05	1.03E-03	-5.99E-03	1.17E-02	-1.02E-02
	MID-SEASON 2	WWF	3.53E-06	-1.51E-04	2.27E-03	-1.44E-02	3.37E-02	-1.20E-02
		WCF	3.80E-06	-1.74E-04	2.78E-03	-1.82E-02	4.21E-02	-9.38E-03
		LWF	1.78E-06	-7.55E-05	1.09E-03	-5.95E-03	7.84E-03	9.50E-03
		LCF	6.17E-07	-2.67E-05	4.42E-04	-3.32E-03	8.59E-03	2.81E-03
	SUMMER	WWF	3.79E-06	-1.63E-04	2.38E-03	-1.35E-02	2.38E-02	-9.71E-03
		WCF	2.89E-06	-1.22E-04	1.74E-03	-9.86E-03	2.01E-02	-2.25E-02
		LWF	2.37E-06	-1.01E-04	1.47E-03	-8.55E-03	1.79E-02	-2.07E-02
		LCF	2.07E-06	-8.87E-05	1.30E-03	-7.50E-03	1.47E-02	-1.32E-02
no wind - GRADIENT	WINTER	WWF	3.44E-06	-1.51E-04	2.36E-03	-1.57E-02	3.89E-02	-1.72E-02
		WCF	4.23E-06	-1.93E-04	3.06E-03	-2.00E-02	4.62E-02	-1.04E-02
		LWF	1.89E-06	-8.06E-05	1.17E-03	-6.54E-03	9.46E-03	8.59E-03
		LCF	1.49E-06	-7.50E-05	1.37E-03	-1.05E-02	2.80E-02	-8.76E-03
	MID-SEASON 1	WWF	4.45E-06	-1.94E-04	2.91E-03	-1.71E-02	3.19E-02	-1.13E-02
		WCF	3.06E-06	-1.29E-04	1.86E-03	-1.07E-02	2.27E-02	-2.63E-02
		LWF	2.52E-06	-1.07E-04	1.57E-03	-9.12E-03	1.94E-02	-2.27E-02
		LCF	1.71E-06	-7.25E-05	1.04E-03	-5.59E-03	8.98E-03	-8.93E-03
	MID-SEASON 2	WWF	4.51E-06	-1.93E-04	2.89E-03	-1.81E-02	4.24E-02	-1.47E-02
		WCF	8.08E-06	-3.60E-04	5.60E-03	-3.59E-02	8.36E-02	-3.19E-02
		LWF	2.32E-06	-9.97E-05	1.47E-03	-8.56E-03	1.52E-02	4.74E-03
		LCF	7.81E-07	-3.21E-05	4.97E-04	-3.56E-03	8.70E-03	5.28E-03
	SUMMER	WWF	4.41E-06	-1.88E-04	2.72E-03	-1.52E-02	2.66E-02	-1.34E-02
		WCF	3.88E-06	-1.64E-04	2.36E-03	-1.33E-02	2.53E-02	-2.17E-02
		LWF	2.85E-06	-1.21E-04	1.77E-03	-1.03E-02	2.11E-02	-2.22E-02
		LCF	2.69E-06	-1.15E-04	1.69E-03	-9.73E-03	1.92E-02	-1.78E-02
WINDY-GRADIENT	WINTER	WWF	1.17E-05	-5.07E-04	7.55E-03	-4.40E-02	8.07E-02	-2.89E-02
		WCF	1.01E-05	-4.56E-04	7.38E-03	-5.09E-02	1.31E-01	-6.21E-02
		LWF	4.67E-06	-2.31E-04	4.13E-03	-3.06E-02	7.66E-02	-1.59E-02
		LCF	4.84E-06	-2.08E-04	2.96E-03	-1.51E-02	1.88E-02	-1.44E-02
	MID-SEASON 1	WWF	1.11E-05	-4.79E-04	7.03E-03	-4.02E-02	7.12E-02	-2.83E-02
		WCF	1.03E-05	-4.39E-04	6.36E-03	-3.58E-02	6.43E-02	-3.59E-02
		LWF	5.08E-06	-2.13E-04	3.02E-03	-1.62E-02	2.75E-02	-2.99E-02
		LCF	4.01E-06	-1.68E-04	2.30E-03	-1.07E-02	7.99E-03	-9.12E-03
	MID-SEASON 2	WWF	1.53E-05	-6.72E-04	1.02E-02	-6.09E-02	1.17E-01	-4.09E-02
		WCF	1.82E-05	-8.37E-04	1.36E-02	-9.05E-02	2.13E-01	-9.58E-02
		LWF	7.60E-06	-3.48E-04	5.51E-03	-3.40E-02	6.41E-02	-1.46E-02
		LCF	6.61E-06	-2.90E-04	4.31E-03	-2.42E-02	4.13E-02	-3.29E-02
	SUMMER	WWF	1.34E-05	-5.74E-04	8.38E-03	-4.75E-02	8.38E-02	-3.72E-02
		WCF	1.31E-05	-5.57E-04	8.10E-03	-4.57E-02	8.10E-02	-4.05E-02
		LWF	4.20E-06	-1.68E-04	2.16E-03	-8.96E-03	3.07E-03	-1.49E-02
		LCF	4.10E-06	-1.67E-04	2.17E-03	-8.89E-03	8.58E-04	-9.65E-03
no wind-no gradient	WINTER	WWF	1.47E-05	-6.37E-04	9.44E-03	-5.47E-02	9.91E-02	-3.61E-02
		WCF	1.76E-05	-7.92E-04	1.24E-02	-7.83E-02	1.65E-01	-5.86E-02
		LWF	7.52E-06	-3.42E-04	5.39E-03	-3.38E-02	7.41E-02	-5.83E-02
		LCF	6.07E-06	-2.61E-04	3.72E-03	-1.92E-02	2.50E-02	-2.16E-02
	MID-SEASON 1	WWF	1.40E-05	-6.03E-04	8.83E-03	-5.03E-02	8.91E-02	-3.76E-02
		WCF	1.35E-05	-5.75E-04	8.37E-03	-4.72E-02	8.39E-02	-4.24E-02
		LWF	4.35E-06	-1.74E-04	2.24E-03	-9.28E-03	3.09E-03	-1.52E-02
		LCF	5.02E-06	-2.11E-04	2.89E-03	-1.36E-02	1.17E-02	-1.54E-02
	MID-SEASON 2	WWF	1.60E-05	-6.91E-04	1.02E-02	-5.85E-02	1.05E-01	-4.10E-02
		WCF	1.87E-05	-8.29E-04	1.27E-02	-7.79E-02	1.54E-01	-4.93E-02
		LWF	8.05E-06	-3.63E-04	5.61E-03	-3.42E-02	7.17E-02	-5.89E-02
		LCF	6.56E-06	-2.81E-04	3.99E-03	-2.03E-02	2.56E-02	-2.37E-02
	SUMMER	WWF	1.57E-05	-6.72E-04	9.85E-03	-5.61E-02	9.98E-02	-4.27E-02
		WCF	1.49E-05	-6.36E-04	9.24E-03	-5.21E-02	9.32E-02	-4.96E-02
		LWF	4.78E-06	-1.90E-04	2.43E-03	-9.87E-03	2.45E-03	-1.72E-02
		LCF	5.96E-06	-2.52E-04	3.52E-03	-1.72E-02	1.84E-02	-2.05E-02

Canyon:			Facade on the urban canyon (uc)					
NARROW (NC)			Tangential component					
Effect	Season	Scene	Coeff. 1	Coeff. 2	Coeff. 3	Coeff. 4	Coeff. 5	Coeff. 6
WINDY-no gradient	WINTER	WWF	1.53E-05	-5.94E-04	7.46E-03	-3.98E-02	1.22E-01	-5.19E-02
		WCF	-2.18E-06	7.70E-05	-8.15E-04	-7.78E-04	1.03E-01	-1.28E-02
		LWF	-3.43E-06	1.57E-04	-2.66E-03	2.31E-02	-9.82E-02	-5.18E-02
		LCF	1.02E-05	-5.79E-04	1.07E-02	-6.93E-02	1.05E-01	-8.56E-02
	MID-SEASON 1	WWF	1.80E-05	-8.88E-04	1.55E-02	-1.09E-01	1.78E-01	-2.14E-02
		WCF	4.39E-06	-1.15E-04	-4.69E-04	3.62E-02	-3.48E-01	8.94E-02
		LWF	-1.14E-05	5.06E-04	-7.46E-03	3.39E-02	1.15E-01	-4.77E-02
		LCF	-7.13E-06	3.50E-04	-6.03E-03	3.77E-02	5.75E-03	-2.10E-02
	MID-SEASON 2	WWF	2.26E-05	-9.24E-04	1.25E-02	-7.15E-02	2.09E-01	-9.56E-02
		WCF	-3.72E-06	1.22E-04	-1.22E-03	6.26E-04	9.72E-02	-3.92E-02
		LWF	-3.90E-06	1.81E-04	-3.05E-03	2.52E-02	-9.87E-02	-7.45E-02
		LCF	1.19E-07	-1.18E-04	3.46E-03	-2.21E-02	-2.75E-02	-4.01E-02
	SUMMER	WWF	1.98E-05	-9.54E-04	1.61E-02	-1.06E-01	1.17E-01	2.84E-02
		WCF	7.92E-06	-2.87E-04	2.53E-03	1.49E-02	-3.04E-01	1.26E-01
		LWF	-1.24E-05	5.60E-04	-8.51E-03	4.21E-02	9.37E-02	-5.10E-02
		LCF	-8.95E-06	4.30E-04	-7.20E-03	4.26E-02	2.64E-02	-3.60E-02
no wind - GRADIENT	WINTER	WWF	-8.49E-07	2.26E-04	-6.74E-03	5.70E-02	-1.19E-01	7.63E-02
		WCF	-1.13E-06	1.41E-05	3.79E-04	-9.86E-03	1.30E-01	-5.45E-02
		LWF	-4.44E-06	2.07E-04	-3.51E-03	2.88E-02	-1.12E-01	-6.98E-02
		LCF	2.03E-05	-1.01E-03	1.64E-02	-9.16E-02	1.06E-01	-8.65E-02
	MID-SEASON 1	WWF	2.45E-05	-1.23E-03	2.19E-02	-1.59E-01	2.98E-01	-5.97E-02
		WCF	8.17E-06	-2.92E-04	2.42E-03	1.80E-02	-3.28E-01	1.27E-01
		LWF	-1.28E-05	5.74E-04	-8.61E-03	4.10E-02	1.11E-01	-5.27E-02
		LCF	-7.19E-06	3.55E-04	-6.18E-03	3.71E-02	4.43E-02	-5.49E-02
	MID-SEASON 2	WWF	3.38E-05	-1.42E-03	2.02E-02	-1.20E-01	3.44E-01	-1.64E-01
		WCF	3.00E-05	-1.46E-03	2.42E-02	-1.66E-01	5.01E-01	-2.50E-01
		LWF	-7.14E-06	3.25E-04	-5.10E-03	3.59E-02	-1.32E-01	-4.91E-02
		LCF	-5.93E-06	1.36E-04	-1.58E-04	8.47E-04	-1.04E-01	-2.21E-02
	SUMMER	WWF	2.13E-05	-9.97E-04	1.61E-02	-9.60E-02	2.15E-02	8.95E-02
		WCF	1.34E-05	-5.57E-04	7.26E-03	-1.84E-02	-2.42E-01	1.49E-01
		LWF	-1.29E-05	5.86E-04	-9.04E-03	4.51E-02	1.05E-01	-7.08E-02
		LCF	-1.07E-05	5.08E-04	-8.28E-03	4.57E-02	6.48E-02	-6.06E-02
WINDY-GRADIENT	WINTER	WWF	6.71E-05	-3.31E-03	5.84E-02	-4.17E-01	7.59E-01	-1.27E-01
		WCF	-1.57E-05	1.18E-03	-2.54E-02	1.74E-01	-2.51E-01	1.39E-01
		LWF	4.74E-05	-2.32E-03	3.60E-02	-1.72E-01	4.63E-02	-1.63E-01
		LCF	1.96E-05	-7.81E-04	1.03E-02	-7.88E-02	5.86E-01	-4.75E-01
	MID-SEASON 1	WWF	6.22E-05	-3.01E-03	5.14E-02	-3.46E-01	4.82E-01	2.07E-02
		WCF	4.54E-05	-2.09E-03	3.29E-02	-1.85E-01	-4.83E-02	2.41E-01
		LWF	-1.56E-05	7.07E-04	-1.06E-02	3.90E-02	3.40E-01	-2.41E-01
		LCF	1.81E-05	-7.72E-04	1.13E-02	-9.33E-02	6.48E-01	-5.17E-01
	MID-SEASON 2	WWF	8.32E-05	-4.20E-03	7.64E-02	-5.73E-01	1.21E+00	-3.27E-01
		WCF	3.49E-05	-1.93E-03	4.15E-02	-4.03E-01	1.31E+00	-6.97E-01
		LWF	1.04E-05	-2.03E-04	-4.58E-03	1.03E-01	-2.70E-01	-6.86E-02
		LCF	2.68E-05	-1.09E-03	1.45E-02	-1.04E-01	7.04E-01	-5.01E-01
	SUMMER	WWF	7.04E-05	-3.35E-03	5.60E-02	-3.60E-01	3.64E-01	1.28E-01
		WCF	6.28E-05	-2.94E-03	4.78E-02	-2.90E-01	1.34E-01	2.23E-01
		LWF	-1.08E-05	4.62E-04	-6.31E-03	4.41E-04	5.56E-01	-4.37E-01
		LCF	1.34E-05	-6.23E-04	1.03E-02	-1.04E-01	8.02E-01	-6.21E-01
no wind-no gradient	WINTER	WWF	8.37E-05	-4.11E-03	7.20E-02	-5.07E-01	8.72E-01	-1.11E-01
		WCF	7.54E-05	-3.96E-03	7.68E-02	-6.37E-01	1.68E+00	-6.51E-01
		LWF	2.90E-05	-1.20E-03	1.59E-02	-9.73E-02	5.70E-01	-2.76E-01
		LCF	2.60E-05	-1.07E-03	1.49E-02	-1.17E-01	8.04E-01	-6.26E-01
	MID-SEASON 1	WWF	7.58E-05	-3.64E-03	6.16E-02	-4.07E-01	4.98E-01	7.38E-02
		WCF	6.42E-05	-3.01E-03	4.89E-02	-2.95E-01	1.29E-01	2.31E-01
		LWF	-1.05E-05	4.47E-04	-6.04E-03	-2.74E-03	5.82E-01	-4.51E-01
		LCF	2.23E-05	-9.76E-04	1.49E-02	-1.27E-01	8.60E-01	-6.61E-01
	MID-SEASON 2	WWF	8.85E-05	-4.30E-03	7.41E-02	-5.06E-01	7.51E-01	-1.36E-02
		WCF	9.42E-05	-4.86E-03	9.12E-02	-7.21E-01	1.73E+00	-5.62E-01
		LWF	3.11E-05	-1.29E-03	1.75E-02	-1.17E-01	7.22E-01	-3.96E-01
		LCF	2.86E-05	-1.20E-03	1.73E-02	-1.38E-01	9.28E-01	-7.13E-01
	SUMMER	WWF	8.34E-05	-4.00E-03	6.76E-02	-4.44E-01	5.29E-01	9.03E-02
		WCF	6.85E-05	-3.18E-03	5.08E-02	-2.97E-01	3.95E-02	2.95E-01
		LWF	-1.00E-05	4.03E-04	-4.79E-03	-2.02E-02	7.04E-01	-5.32E-01
		LCF	2.65E-05	-1.15E-03	1.73E-02	-1.45E-01	9.63E-01	-7.31E-01

Canyon:			Facade on the courtyard (co)					
NARROW (NC)			Normal component					
Effect	Season	Scene	Coeff. 1	Coeff. 2	Coeff. 3	Coeff. 4	Coeff. 5	Coeff. 6
WINDY-no gradient	WINTER	WWF	4.42E-07	-2.21E-05	4.26E-04	-3.64E-03	1.06E-02	-1.23E-03
		WCF	1.39E-06	-5.94E-05	8.66E-04	-4.85E-03	6.91E-03	7.32E-03
		LWF	2.61E-06	-1.18E-04	1.86E-03	-1.19E-02	2.56E-02	1.64E-03
		LCF	2.86E-06	-1.23E-04	1.86E-03	-1.18E-02	2.79E-02	-1.03E-02
	MID-SEASON 1	WWF	1.62E-06	-7.00E-05	1.03E-03	-5.99E-03	1.17E-02	-1.02E-02
		WCF	2.02E-06	-8.56E-05	1.24E-03	-7.22E-03	1.55E-02	-2.08E-02
		LWF	2.11E-06	-8.84E-05	1.28E-03	-7.49E-03	1.80E-02	-2.71E-02
		LCF	3.32E-06	-1.44E-04	2.14E-03	-1.25E-02	2.29E-02	-8.70E-03
	MID-SEASON 2	WWF	6.17E-07	-2.67E-05	4.42E-04	-3.32E-03	8.59E-03	2.81E-03
		WCF	1.78E-06	-7.55E-05	1.09E-03	-5.95E-03	7.84E-03	9.50E-03
		LWF	3.80E-06	-1.74E-04	2.78E-03	-1.82E-02	4.21E-02	-9.38E-03
		LCF	3.53E-06	-1.51E-04	2.27E-03	-1.44E-02	3.37E-02	-1.20E-02
	SUMMER	WWF	2.07E-06	-8.87E-05	1.30E-03	-7.50E-03	1.47E-02	-1.32E-02
		WCF	2.37E-06	-1.01E-04	1.47E-03	-8.55E-03	1.79E-02	-2.07E-02
		LWF	2.89E-06	-1.22E-04	1.74E-03	-9.86E-03	2.01E-02	-2.25E-02
		LCF	3.79E-06	-1.63E-04	2.38E-03	-1.35E-02	2.38E-02	-9.71E-03
no wind - GRADIENT	WINTER	WWF	1.49E-06	-7.50E-05	1.37E-03	-1.05E-02	2.80E-02	-8.76E-03
		WCF	1.89E-06	-8.06E-05	1.17E-03	-6.54E-03	9.46E-03	8.59E-03
		LWF	4.23E-06	-1.93E-04	3.06E-03	-2.00E-02	4.62E-02	-1.04E-02
		LCF	3.44E-06	-1.51E-04	2.36E-03	-1.57E-02	3.89E-02	-1.72E-02
	MID-SEASON 1	WWF	1.71E-06	-7.25E-05	1.04E-03	-5.59E-03	8.98E-03	-8.93E-03
		WCF	2.52E-06	-1.07E-04	1.57E-03	-9.12E-03	1.94E-02	-2.27E-02
		LWF	3.06E-06	-1.29E-04	1.86E-03	-1.07E-02	2.27E-02	-2.63E-02
		LCF	4.45E-06	-1.94E-04	2.91E-03	-1.71E-02	3.19E-02	-1.13E-02
	MID-SEASON 2	WWF	7.81E-07	-3.21E-05	4.97E-04	-3.56E-03	8.70E-03	5.28E-03
		WCF	2.32E-06	-9.97E-05	1.47E-03	-8.56E-03	1.52E-02	4.74E-03
		LWF	8.08E-06	-3.60E-04	5.60E-03	-3.59E-02	8.36E-02	-3.19E-02
		LCF	4.51E-06	-1.93E-04	2.89E-03	-1.81E-02	4.24E-02	-1.47E-02
	SUMMER	WWF	2.69E-06	-1.15E-04	1.69E-03	-9.73E-03	1.92E-02	-1.78E-02
		WCF	2.85E-06	-1.21E-04	1.77E-03	-1.03E-02	2.11E-02	-2.22E-02
		LWF	3.88E-06	-1.64E-04	2.36E-03	-1.33E-02	2.53E-02	-2.17E-02
		LCF	4.41E-06	-1.88E-04	2.72E-03	-1.52E-02	2.66E-02	-1.34E-02
WINDY-GRADIENT	WINTER	WWF	4.84E-06	-2.08E-04	2.96E-03	-1.51E-02	1.88E-02	-1.44E-02
		WCF	4.67E-06	-2.31E-04	4.13E-03	-3.06E-02	7.66E-02	-1.59E-02
		LWF	1.01E-05	-4.56E-04	7.38E-03	-5.09E-02	1.31E-01	-6.21E-02
		LCF	1.17E-05	-5.07E-04	7.55E-03	-4.40E-02	8.07E-02	-2.89E-02
	MID-SEASON 1	WWF	4.01E-06	-1.68E-04	2.30E-03	-1.07E-02	7.99E-03	-9.12E-03
		WCF	5.08E-06	-2.13E-04	3.02E-03	-1.62E-02	2.75E-02	-2.99E-02
		LWF	1.03E-05	-4.39E-04	6.36E-03	-3.58E-02	6.43E-02	-3.59E-02
		LCF	1.11E-05	-4.79E-04	7.03E-03	-4.02E-02	7.12E-02	-2.83E-02
	MID-SEASON 2	WWF	6.61E-06	-2.90E-04	4.31E-03	-2.42E-02	4.13E-02	-3.29E-02
		WCF	7.60E-06	-3.48E-04	5.51E-03	-3.40E-02	6.41E-02	-1.46E-02
		LWF	1.82E-05	-8.37E-04	1.36E-02	-9.05E-02	2.13E-01	-9.58E-02
		LCF	1.53E-05	-6.72E-04	1.02E-02	-6.09E-02	1.17E-01	-4.09E-02
	SUMMER	WWF	4.10E-06	-1.67E-04	2.17E-03	-8.89E-03	8.58E-04	-9.65E-03
		WCF	4.20E-06	-1.68E-04	2.16E-03	-8.96E-03	3.07E-03	-1.49E-02
		LWF	1.31E-05	-5.57E-04	8.10E-03	-4.57E-02	8.10E-02	-4.05E-02
		LCF	1.34E-05	-5.74E-04	8.38E-03	-4.75E-02	8.38E-02	-3.72E-02
no wind-no gradient	WINTER	WWF	6.07E-06	-2.61E-04	3.72E-03	-1.92E-02	2.50E-02	-2.16E-02
		WCF	7.52E-06	-3.42E-04	5.39E-03	-3.38E-02	7.41E-02	-5.83E-02
		LWF	1.76E-05	-7.92E-04	1.24E-02	-7.83E-02	1.65E-01	-5.86E-02
		LCF	1.47E-05	-6.37E-04	9.44E-03	-5.47E-02	9.91E-02	-3.61E-02
	MID-SEASON 1	WWF	5.02E-06	-2.11E-04	2.89E-03	-1.36E-02	1.17E-02	-1.54E-02
		WCF	4.35E-06	-1.74E-04	2.24E-03	-9.28E-03	3.09E-03	-1.52E-02
		LWF	1.35E-05	-5.75E-04	8.37E-03	-4.72E-02	8.39E-02	-4.24E-02
		LCF	1.40E-05	-6.03E-04	8.83E-03	-5.03E-02	8.91E-02	-3.76E-02
	MID-SEASON 2	WWF	6.56E-06	-2.81E-04	3.99E-03	-2.03E-02	2.56E-02	-2.37E-02
		WCF	8.05E-06	-3.63E-04	5.61E-03	-3.42E-02	7.17E-02	-5.89E-02
		LWF	1.87E-05	-8.29E-04	1.27E-02	-7.79E-02	1.54E-01	-4.93E-02
		LCF	1.60E-05	-6.91E-04	1.02E-02	-5.85E-02	1.05E-01	-4.10E-02
	SUMMER	WWF	5.96E-06	-2.52E-04	3.52E-03	-1.72E-02	1.84E-02	-2.05E-02
		WCF	4.78E-06	-1.90E-04	2.43E-03	-9.87E-03	2.45E-03	-1.72E-02
		LWF	1.49E-05	-6.36E-04	9.24E-03	-5.21E-02	9.32E-02	-4.96E-02
		LCF	1.57E-05	-6.72E-04	9.85E-03	-5.61E-02	9.98E-02	-4.27E-02

Canyon:			Facade on the courtyard (co)					
NARROW (NC)			Tangential component					
Effect	Season	Scene	Coeff. 1	Coeff. 2	Coeff. 3	Coeff. 4	Coeff. 5	Coeff. 6
WINDY-no gradient	WINTER	WWF	1.02E-05	-5.79E-04	1.07E-02	-6.93E-02	1.05E-01	-8.56E-02
		WCF	-3.43E-06	1.57E-04	-2.66E-03	2.31E-02	-9.82E-02	-5.18E-02
		LWF	-2.18E-06	7.70E-05	-8.15E-04	-7.78E-04	1.03E-01	-1.28E-02
		LCF	1.53E-05	-5.94E-04	7.46E-03	-3.98E-02	1.22E-01	-5.19E-02
	MID-SEASON 1	WWF	-7.13E-06	3.50E-04	-6.03E-03	3.77E-02	5.75E-03	-2.10E-02
		WCF	-1.14E-05	5.06E-04	-7.46E-03	3.39E-02	1.15E-01	-4.77E-02
		LWF	4.39E-06	-1.15E-04	-4.69E-04	3.62E-02	-3.48E-01	8.94E-02
		LCF	1.80E-05	-8.88E-04	1.55E-02	-1.09E-01	1.78E-01	-2.14E-02
	MID-SEASON 2	WWF	1.19E-07	-1.18E-04	3.46E-03	-2.21E-02	-2.75E-02	-4.01E-02
		WCF	-3.90E-06	1.81E-04	-3.05E-03	2.52E-02	-9.87E-02	-7.45E-02
		LWF	-3.72E-06	1.22E-04	-1.22E-03	6.26E-04	9.72E-02	-3.92E-02
		LCF	2.26E-05	-9.24E-04	1.25E-02	-7.15E-02	2.09E-01	-9.56E-02
	SUMMER	WWF	-8.95E-06	4.30E-04	-7.20E-03	4.26E-02	2.64E-02	-3.60E-02
		WCF	-1.24E-05	5.60E-04	-8.51E-03	4.21E-02	9.37E-02	-5.10E-02
		LWF	7.92E-06	-2.87E-04	2.53E-03	1.49E-02	-3.04E-01	1.26E-01
		LCF	1.98E-05	-9.54E-04	1.61E-02	-1.06E-01	1.17E-01	2.84E-02
no wind - GRADIENT	WINTER	WWF	2.03E-05	-1.01E-03	1.64E-02	-9.16E-02	1.06E-01	-8.65E-02
		WCF	-4.44E-06	2.07E-04	-3.51E-03	2.88E-02	-1.12E-01	-6.98E-02
		LWF	-1.13E-06	1.41E-05	3.79E-04	-9.86E-03	1.30E-01	-5.45E-02
		LCF	-8.49E-07	2.26E-04	-6.74E-03	5.70E-02	-1.19E-01	7.63E-02
	MID-SEASON 1	WWF	-7.19E-06	3.55E-04	-6.18E-03	3.71E-02	4.43E-02	-5.49E-02
		WCF	-1.28E-05	5.74E-04	-8.61E-03	4.10E-02	1.11E-01	-5.27E-02
		LWF	8.17E-06	-2.92E-04	2.42E-03	1.80E-02	-3.28E-01	1.27E-01
		LCF	2.45E-05	-1.23E-03	2.19E-02	-1.59E-01	2.98E-01	-5.97E-02
	MID-SEASON 2	WWF	-5.93E-06	1.36E-04	-1.58E-04	8.47E-04	-1.04E-01	-2.21E-02
		WCF	-7.14E-06	3.25E-04	-5.10E-03	3.59E-02	-1.32E-01	-4.91E-02
		LWF	3.00E-05	-1.46E-03	2.42E-02	-1.66E-01	5.01E-01	-2.50E-01
		LCF	3.38E-05	-1.42E-03	2.02E-02	-1.20E-01	3.44E-01	-1.64E-01
	SUMMER	WWF	-1.07E-05	5.08E-04	-8.28E-03	4.57E-02	6.48E-02	-6.06E-02
		WCF	-1.29E-05	5.86E-04	-9.04E-03	4.51E-02	1.05E-01	-7.08E-02
		LWF	1.34E-05	-5.57E-04	7.26E-03	-1.84E-02	-2.42E-01	1.49E-01
		LCF	2.13E-05	-9.97E-04	1.61E-02	-9.60E-02	2.15E-02	8.95E-02
WINDY-GRADIENT	WINTER	WWF	1.96E-05	-7.81E-04	1.03E-02	-7.88E-02	5.86E-01	-4.75E-01
		WCF	4.74E-05	-2.32E-03	3.60E-02	-1.72E-01	4.63E-02	-1.63E-01
		LWF	-1.57E-05	1.18E-03	-2.54E-02	1.74E-01	-2.51E-01	1.39E-01
		LCF	6.71E-05	-3.31E-03	5.84E-02	-4.17E-01	7.59E-01	-1.27E-01
	MID-SEASON 1	WWF	1.81E-05	-7.72E-04	1.13E-02	-9.33E-02	6.48E-01	-5.17E-01
		WCF	-1.56E-05	7.07E-04	-1.06E-02	3.90E-02	3.40E-01	-2.41E-01
		LWF	4.54E-05	-2.09E-03	3.29E-02	-1.85E-01	-4.83E-02	2.41E-01
		LCF	6.22E-05	-3.01E-03	5.14E-02	-3.46E-01	4.82E-01	2.07E-02
	MID-SEASON 2	WWF	2.68E-05	-1.09E-03	1.45E-02	-1.04E-01	7.04E-01	-5.01E-01
		WCF	1.04E-05	-2.03E-04	-4.58E-03	1.03E-01	-2.70E-01	-6.86E-02
		LWF	3.49E-05	-1.93E-03	4.15E-02	-4.03E-01	1.31E+00	-6.97E-01
		LCF	8.32E-05	-4.20E-03	7.64E-02	-5.73E-01	1.21E+00	-3.27E-01
	SUMMER	WWF	1.34E-05	-6.23E-04	1.03E-02	-1.04E-01	8.02E-01	-6.21E-01
		WCF	-1.08E-05	4.62E-04	-6.31E-03	4.41E-04	5.56E-01	-4.37E-01
		LWF	6.28E-05	-2.94E-03	4.78E-02	-2.90E-01	1.34E-01	2.23E-01
		LCF	7.04E-05	-3.35E-03	5.60E-02	-3.60E-01	3.64E-01	1.28E-01
no wind-no gradient	WINTER	WWF	2.60E-05	-1.07E-03	1.49E-02	-1.17E-01	8.04E-01	-6.26E-01
		WCF	2.90E-05	-1.20E-03	1.59E-02	-9.73E-02	5.70E-01	-2.76E-01
		LWF	7.54E-05	-3.96E-03	7.68E-02	-6.37E-01	1.68E+00	-6.51E-01
		LCF	8.37E-05	-4.11E-03	7.20E-02	-5.07E-01	8.72E-01	-1.11E-01
	MID-SEASON 1	WWF	2.23E-05	-9.76E-04	1.49E-02	-1.27E-01	8.60E-01	-6.61E-01
		WCF	-1.05E-05	4.47E-04	-6.04E-03	-2.74E-03	5.82E-01	-4.51E-01
		LWF	6.42E-05	-3.01E-03	4.89E-02	-2.95E-01	1.29E-01	2.31E-01
		LCF	7.58E-05	-3.64E-03	6.16E-02	-4.07E-01	4.98E-01	7.38E-02
	MID-SEASON 2	WWF	2.86E-05	-1.20E-03	1.73E-02	-1.38E-01	9.28E-01	-7.13E-01
		WCF	3.11E-05	-1.29E-03	1.75E-02	-1.17E-01	7.22E-01	-3.96E-01
		LWF	9.42E-05	-4.86E-03	9.12E-02	-7.21E-01	1.73E+00	-5.62E-01
		LCF	8.85E-05	-4.30E-03	7.41E-02	-5.06E-01	7.51E-01	-1.36E-02
	SUMMER	WWF	2.65E-05	-1.15E-03	1.73E-02	-1.45E-01	9.63E-01	-7.31E-01
		WCF	-1.00E-05	4.03E-04	-4.79E-03	-2.02E-02	7.04E-01	-5.32E-01
		LWF	6.85E-05	-3.18E-03	5.08E-02	-2.97E-01	3.95E-02	2.95E-01
		LCF	8.34E-05	-4.00E-03	6.76E-02	-4.44E-01	5.29E-01	9.03E-02

Appendix B (MATLAB code)

```
close all

clearvars

clear all

clc

addpath 'C:\Users\LENOVO\Desktop\2_PhD\ESAME_FINALE\MOD_12_man'

addpath 'C:\Users\LENOVO\Desktop\2_PhD\ESAME_FINALE\MOD_12_man\functions'

addpath 'C:\Users\LENOVO\Desktop\2_PhD\ESAME_FINALE\MOD_12_man\DB'


%_________

%%% STEP 0

%% Input data regarding environmental-climate characteristics

% Define gravity (g). reference Temperature (Tref). reference air density (rhoref @Tref). reference
atmosferic pressure (Patmref). altitude. coeff btru;

g=9.81; Tref= 273.15; rhoref=1.29; Patmref=101325; alt=239; btru=0.4;

% Calculate local atmosferic pressure (Patm);

Patm=Patmref*0.9877^(alt/100);

%% Input data regarding leakage characteristic

% Define fixed discharge coefficient (Cd) and flow coefficient (n)

Cd=0.65; n=0.65;

_____

%%% STEP 1

%% Input data regarding CFD coefficient or 64 climate scenario

% Load the 6 matrixes (64x12): 2 matrixes (UC and CO) per 3 canyon width (LC.MC.NC)

load -ascii m_UC_LC.txt

load -ascii m_UC_MC.txt

load -ascii m_UC_NC.txt

load -ascii m_CO_LC.txt

load -ascii m_CO_MC.txt

load -ascii m_CO_NC.txt
```

```
%% Input data regarding Temparature for 64 climate scenario
% Load the 2 vectors (64x1):
load -ascii ToutC.txt
load -ascii TinC.txt
%% Input data regarding the sign combination
% Load matrix a (126x19):
load -ascii a.txt
%_____
%%% STEP 2
%% Cycle FOR about BUILDINGS (not implemented)
% Identification of the analyzed building b
%_____
%%% STEP 3
%% Input data regarding characterstics of the analyzed building b
%id building
B_id=63;
%canyon_characteristics: orientation (Ouc); width (Wuc.Wco); position;
Ouc=30; Wuc=1; Wco=1; position=2;
%building_characteristics: volumes (vol.bld.vol.a.vol.b.vol.c)
vol.bld  =10624.6; vol.a=4624.0; vol.b=5548.8; vol.c=451.7;
%opening characteristic: numer of openings (windows or doors)
%zone a
n_w_a_uc=50;n_d_a_uc=20;n_w_a_co=40;n_d_a_co=15;
%zone b
n_w_b_uc=60;n_d_b_uc=24;n_w_b_co=48;n_d_b_co=18;
%zone c
n_w_sha          =10;n_d_sha=18;n_w_shb=10;n_d_shb=18;
%leakage characteristics: equivalent leakage area (Ae_leak_w/d) and nodes' heights (z)
Ae_leak_w=0.001944; Ae_leak_d=0.001782;
za=7.5; zb=24; zc=16.5;
z1=7.5; z2=24; z3=7.5;   z4=24;
```

```
za1=7.5; zac=7.5; za3=7.5; zb2=24; zbc=24; zb4=24; zca=7.5; zcb=24; zc3=7.5; zc4=24;

% Evaluate height z2 and z4

if      z2>= 19

        z22 = 19;

else    z22 = z2;

end

if      z4>= 19

        z44 = 19;

else    z44 = z4;

end

%_____________

%%% STEP 4.1

%% Assign the position vector according to the building position (1=Left. 2=Right.3=Top. 4=Down)

if position==1

  u_p = [1      1      1      1      1      1      1      1      1      1      1      1
         1      1      1      1      1      1      1      1      1      1      1      1
         1      1      1      1      1      1      1      1      1      1      1      1
         1      1      1      1      1      1      1      1      1      1      1      1
         1      1      1      1      1      1      1      1      1      1      1      1]';

elseif position==2

  u_p = [1      1      1      1      1      1      1      1      1      1      1      1
         1      1      1      1      1      1      1      1      1      1      1      1
         1      1      1      1      1      1      1      1      1      1      1      1
         1      1      1      1      1      1      1      1      1      1      1      1
         1      1      1      1      1      1      1      1      1      1      1      1]';

elseif position==3

  u_p = [1      0      1      0      1      0      1      0      1      0      1      0      1
         0      1      0      1      0      1      0      1      0      1      0      1      0
         1      0      1      0      1      0      1      0      1      0      1      0      1
         0      1      0      1      0      1      0      1      0      1      0      1      0
         1      0      1      0      1      0      1      0      1      0      1      0]';

elseif position==4

  u_p = [0      1      0      1      0      1      0      1      0      1      0      1      0
         1      0      1      0      1      0      1      0      1      0      1      0      1
         0      1      0      1      0      1      0      1      0      1      0      1      0
         1      0      1      0      1      0      1      0      1      0      1      0      1
         0      1      0      1      0      1      0      1      0      1      0      1]';
```

```
end

%_____________
%%% STEP 4.2
%% Assing the canyon widht (1=Large (LC). 2=Medium (MC). 3=Narrow (NC)
%% Calculate the resulting matric UC
if Wuc==1
   UC=u_p.*m_UC_LL;
elseif Wuc==2
   UC=u_p.*m_UC_MM;
elseif Wuc==3
   UC=u_p.*m_UC_NN;
end
%% Calculate the resulting matric CO
if Wco==1
   CO=u_p.*m_CO_LL;
elseif Wco==2
   CO=u_p.*m_CO_MM;
elseif Wco==3
   CO=u_p.*m_CO_NN;
end
%u_p. (the point transform the vector (64X1)->(1x64)

%_____________
%%% STEP 5.1
%% Calculate wind speed at 4 external nodes (v1.v2.v3.v4) according to normal (N) and tangential (T) components
% Calculate wind speed at nodes 1 and 2
v1_N=[];v2_N=[]; v1_T=[]; v2_T=[];
for u=1:size(UC.1)
   v1_N = [v1_N. UC(u.1)*(z1)^5+UC(u.2)*(z1)^4+UC(u.3)*(z1)^3+UC(u.4)*(z1)^2+UC(u.5)*(z1)+UC(u.6)];
```

```
   v2_N = [v2_N.
UC(u.1)*(z22)^5+UC(u.2)*(z22)^4+UC(u.3)*(z22)^3+UC(u.4)*(z22)^2+UC(u.5)*(z22)+UC(u.6)];
   v1_T = [v1_T. UC(u.7)*(z1)^5+UC(u.8)*(z1)^4+UC(u.9)*(z1)^3+UC(u.10)*(z1)^2+UC(u.11)*(z1)+UC(u.12)];
   v2_T = [v2_T.
UC(u.7)*(z22)^5+UC(u.8)*(z22)^4+UC(u.9)*(z22)^3+UC(u.10)*(z22)^2+UC(u.11)*(z22)+UC(u.12)];
end
v1_N=v1_N'; v2_N=v2_N'; v1_T=v1_T'; v2_T=v2_T';

% Calculate wind speed at nodes 1 and 2
v3_N=[]; v4_N=[]; v3_T=[]; v4_T=[];
for u=1:size(CO.1)
   v3_N = [v3_N. CO(u.1)*(z3)^5+CO(u.2)*(z3)^4+CO(u.3)*(z3)^3+CO(u.4)*(z3)^2+CO(u.5)*(z3)+CO(u.6)];
   v4_N = [v4_N.
CO(u.1)*(z44)^5+CO(u.2)*(z44)^4+CO(u.3)*(z44)^3+CO(u.4)*(z44)^2+CO(u.5)*(z44)+CO(u.6)];
   v3_T = [v3_T. CO(u.7)*(z3)^5+CO(u.8)*(z3)^4+CO(u.9)*(z3)^3+CO(u.10)*(z3)^2+CO(u.11)*(z3)+CO(u.12)];
   v4_T = [v4_T.
CO(u.7)*(z44)^5+CO(u.8)*(z44)^4+CO(u.9)*(z44)^3+CO(u.10)*(z44)^2+CO(u.11)*(z44)+CO(u.12)];
end
v3_N=v3_N'; v4_N=v4_N'; v3_T=v3_T'; v4_T=v4_T';

% Create matrix of all resulting velocities
V_all= [v1_N.v1_T.v2_N.v2_T.v3_N.v3_T.v4_N.v4_T];

%_____________
%%% STEP 5.2
%% Assign proper sign
v1=[]; v2=[]; v3=[]; v4=[];
for v=1:size(V_all.1)
   if V_all(v.1)>0
      v1=[v1.1*abs(V_all(v.2))];
   else
      v1=[v1.-1*abs(V_all(v.2))];
```

```
    end
    if V_all(v.3)>0
        v2=[v2.1*abs(V_all(v.4))];
    else
        v2=[v2.-1*abs(V_all(v.4))];
    end
    if V_all(v.5)>0
        v3=[v3.-1*abs(V_all(v.6))];
    else
        v3=[v3.1*abs(V_all(v.6))];
    end
    if V_all(v.7)>0
        v4=[v4.-1*abs(V_all(v.8))];
    else
        v4=[v4.1*abs(V_all(v.8))];
    end
end
v1=v1';v2=v2';v3=v3';v4=v4';
% Create matrix of all resulting velocities
v_R_all = [v1.v2.v3.v4];

%_________
%%% STEP 6
%% Create a new matrix of the resulting velocities and temperature conditions
% Load the vector u that indicate the id of the 64 climate scenarios analyzed
load -ascii u.txt
E= [u.v1.v2.v3.v4.ToutC.TinC];

%____________
%%% STEP 6.1
%% Create a cycle to iterate automatically steps 7-8 on matrix E (x.7) where x=1:64
```

```
% Create useful vectors for all variables that will be calculated

TshC=[];Tout=[];Tin=[];Tsh=[];

rho_out=[];rho_in=[];rho_sh=[];

kw_ref_hz=[];kd_ref_hz=[];kw_ref_sh=[];kd_ref_sh=[];k_a_uc=[];k_a_co=[];k_b_uc=[];k_b_co=[];kw_sha=[];
kd_sha=[];kw_shb=[];kd_shb=[];


%_____________

%%% STEP 7

%% Calculate environmental characteristics and K coefficients input data

% Temperatures in the three zones (7.1-7.2). air density (7.3-4). k coefficient (7.5-6)

%_____________

%%% STEP 7.1

%% Calculate Temperature in the shaft: TshC=ToutC+(btru*(TinC-ToutC))

for x=1:size(E.1)

TshC=[TshC. E(x.6) + (btru*(E(x.7) - E(x.6)))];

%_____________

%%% STEP 7.2

%% Calculate air temperature (from Celsius to kelvin)

Tout= [Tout. E(x.6) + 273.15];

Tin = [Tin. E(x.7) + 273.15];

Tsh = [Tsh. TshC(x) + 273.15];

end

TshC=TshC'; Tout=Tout';Tin=Tin';Tsh=Tsh';

T_all=[Tout. Tin. Tsh];


%_____________

%%% STEP 7.3

%% Calculate air density (rho)

for x=1:size(T_all.1)

rho_out= [rho_out. (rhoref*Tref)/T_all(x.1)];

rho_in = [rho_in. (rhoref*Tref)/T_all(x.2)];
```

```
rho_sh = [rho_sh.(rhoref*Tref)/T_all(x.3)];
end
rho_out=rho_out';rho_in= rho_in';rho_sh=rho_sh';
rho_all=[rho_out.rho_in.rho_sh];
%_____________
%%% STEP 7.4
%% Assign air density to each zone
rho_abc=[rho_in. rho_in.rho_sh];

%_____________
%%% STEP 7.5
%% Calculate K coeff for a single window/door for heated zones/shaft
for x=1:size(rho_all.1)
kw_ref_hz = [kw_ref_hz.Cd*Ae_leak_w*sqrt(2*rho_all(x.2))];
kd_ref_hz = [kd_ref_hz.Cd*Ae_leak_d*sqrt(2*rho_all(x.2))];
kw_ref_sh = [kw_ref_sh. Cd*Ae_leak_w*sqrt(2*rho_all(x.3))];
kd_ref_sh = [kd_ref_sh .Cd*Ae_leak_d*sqrt(2*rho_all(x.3))];
end
kw_ref_hz=kw_ref_hz'; kd_ref_hz=kd_ref_hz'; kw_ref_sh=kw_ref_sh'; kd_ref_sh=kd_ref_sh';
k_ref_all=[kw_ref_hz.kd_ref_hz.kw_ref_sh.kd_ref_sh];
%_____________
%%% STEP 7.6
%% Calculate K coefficient for all windows and doors in the building in zone a/b/shaft
for x=1:size(k_ref_all.1)
k_a_uc=[k_a_uc.(k_ref_all(x.1)*n_w_a_uc)+(k_ref_all(x.2)* n_d_a_uc)];
k_a_co=[k_a_co.(k_ref_all(x.1)*n_w_a_co)+(k_ref_all(x.2)* n_d_a_co)];
k_b_uc=[k_b_uc.(k_ref_all(x.1)*n_w_b_uc)+(k_ref_all(x.2)*n_d_b_uc)];
k_b_co=[k_b_co.(k_ref_all(x.1)*n_w_b_co)+(k_ref_all(x.2)*n_d_b_co)];
kw_sha=[kw_sha.(k_ref_all(x.3)*n_w_sha)];
kd_sha=[kd_sha.(k_ref_all(x.4)*n_d_sha)];
kw_shb=[kw_shb.(k_ref_all(x.3)*n_w_shb)];
```

```
kd_shb=[kd_shb.(k_ref_all(x.4)*n_d_shb)];
end
k_a_uc=k_a_uc'; k_a_co=k_a_co'; k_b_uc=k_b_uc'; k_b_co=k_b_co';
kw_sha=kw_sha'; kd_sha=kd_sha'; kw_shb=kw_shb'; kd_shb=kd_shb';
k_all=[k_a_uc.k_a_co.k_b_uc.k_b_co.kw_sha.kd_sha.kw_shb.kd_shb];

%_____
%%% STEP 8
%% Steps 8.1 to 8.4: calculate the known pressure conditions at external nodes (1-2-3-4)
Patm1=[];Patm2=[];Patm3=[];Patm4=[];
Pdyn1=[];Pdyn2=[];Pdyn3=[];Pdyn4=[];
Ppot1=[];Ppot2=[];Ppot3=[];Ppot4=[];
P1=[];P2=[];P3=[];P4=[];
%_____
%%% STEP 8.1
%% Calculate atmospheric pressure at external nodes
Patm1=[Patm1. Patmref*0.9877^((alt+z1)/100)];
Patm2=[Patm2. Patmref*0.9877^((alt+z2)/100)];
Patm3=[Patm3. Patmref*0.9877^((alt+z3)/100)];
Patm4=[Patm4. Patmref*0.9877^((alt+z4)/100)];
Patm1=Patm1'; Patm2=Patm2'; Patm3=Patm3'; Patm4=Patm4';
Patm_est_temp=[Patm1. Patm2. Patm3. Patm4];
Patm_est_all=repmat(Patm_est_temp. 64.1);
%_____
%%% STEP 8.2
%% Calculate dynamic pressure at external nodes
% for v1(x)=E(x.2) and v2(x)=E(x.3) and v3(x)=E(x.4) and v4(x)=E(x.5)
E2=[E.rho_out];
for x=1:size(E2.1)
    if (E2(x.2)>0)
        Pdyn1=[Pdyn1. 0.5*E2(x.8)*E2(x.2)^2];
```

```
    else
      Pdyn1=[Pdyn1. 0.5*E2(x.8)*-(E2(x.2)^2)];
    end
    if (E2(x.3)>0)
      Pdyn2=[Pdyn2. 0.5*E2(x.8)*E2(x.3)^2];
    else
      Pdyn2=[Pdyn2. 0.5*E2(x.8)*-(E2(x.3)^2)];
    end
    if (E2(x.4)>0)
      Pdyn3=[Pdyn3. 0.5*E2(x.8)*E2(x.4)^2];
    else
      Pdyn3=[Pdyn3. 0.5*E2(x.8)*-(E2(x.4)^2)];
    end
    if (E2(x.5)>0)
      Pdyn4=[Pdyn4. 0.5*E2(x.8)*E2(x.5)^2];
    else
      Pdyn4=[Pdyn4. 0.5*E2(x.8)*-(E2(x.5)^2)];
    end
  end
Pdyn1=Pdyn1';Pdyn2=Pdyn2';Pdyn3=Pdyn3';Pdyn4=Pdyn4';
Pdyn_est_all=[Pdyn1.Pdyn2.Pdyn3.Pdyn4];
%% Transform results with null velocities (=0. zero) in "nan" values
Pdyn_est_all(Pdyn_est_all==0)=NaN;
%_____
%%% STEP 8.3
%% Calculate potential pressure at external nodes
for x=1:size(rho_all.1)
  Ppot1=[Ppot1. (g*rho_all(x.1)*z1)];
  Ppot2=[Ppot2. (g*rho_all(x.1)*z2)];
  Ppot3=[Ppot3. (g*rho_all(x.1)*z3)];
  Ppot4=[Ppot4. (g*rho_all(x.1)*z4)];
```

```
end
Ppot1=Ppot1';Ppot2=Ppot2';Ppot3=Ppot3';Ppot4=Ppot4';
Ppot_est_all=[Ppot1.Ppot2.Ppot3.Ppot4];
P_est_temp=[Patm_est_all.Pdyn_est_all. Ppot_est_all];
%_____________
%%% STEP 8.4
%% Calculate total pressure at external nodes
for x=1:size(P_est_temp.1)
   P1=[P1. P_est_temp(x.1)+P_est_temp(x.5)+P_est_temp(x.9)];
   P2=[P2. P_est_temp(x.2)+P_est_temp(x.6)+P_est_temp(x.10)];
   P3=[P3. P_est_temp(x.3)+P_est_temp(x.7)+P_est_temp(x.11)];
   P4=[P4. P_est_temp(x.4)+P_est_temp(x.8)+P_est_temp(x.12)];
end
P1=P1'; P2=P2';P3=P3';P4=P4';
P_est=[P1.P2.P3.P4];

%_____________________
%% Steps 8.5 to 8.8: calculate the known pressure conditions at internal nodes (a-b-c)
pstkc1=[];pstkc2=[];pstkc3=[];pstkc4=[];
ppota=[];ppotb=[];ppotca=[];ppotcb=[];ppotc3=[];ppotc4=[];
pdyna=[];pdynb=[];pdync=[];
pstata=[];pstatb=[];pstatc=[];
pa0_l=[];pa0_r=[];pb0_l=[];pb0_r=[];pc0_l=[];pc0_r=[];
%_____________
%%% STEP 8.5
%% Calculate stack effect in the shaft
for x=1:size(rho_all.1)
pstkc1=[pstkc1. rho_all(x.3)*g*(zc-zca)];
pstkc2=[pstkc2. rho_all(x.3)*g*(zc-zcb)];
pstkc3=[pstkc3. rho_all(x.3)*g*(zc-zc3)];
pstkc4=[pstkc4. rho_all(x.3)*g*(zc-zc4)];
```

```
end
pstkc1=pstkc1';pstkc2=pstkc2';pstkc3=pstkc3';pstkc4=pstkc4';
pstk_int_all=[pstkc1.pstkc2.pstkc3.pstkc4];
%_____________
%%% STEP 8.6
%% Calculate potential pressure at leakages nodes
for x=1:size(rho_all.1)
ppota=[ppota.rho_all(x.2)*g*za];
ppotb=[ppotb.rho_all(x.2)*g*zb];
ppotca=[ppotca.rho_all(x.3)*g*zca];
ppotcb=[ppotcb.rho_all(x.3)*g*zcb];
ppotc3=[ppotc3.rho_all(x.3)*g*zc3];
ppotc4=[ppotc4.rho_all(x.3)*g*zc4];
end
ppota=ppota'; ppotb=ppotb'; ppotca=ppotca'; ppotcb=ppotcb'; ppotc3=ppotc3'; ppotc4=ppotc4';
ppot_int_all=[ppota.ppotb.ppotca.ppotcb.ppotc3.ppotc4];
%_____________
%%% STEP 8.7
%% Calculate dynamic pressure at internal nodes (assuming va=vb=vc=)
vint= 3;
for x=1:size(rho_all.1)
pdyna=[pdyna. 0.5*rho_all(x.2)*(vint)^2];
pdynb=[pdynb. 0.5*rho_all(x.2)*(vint)^2];
pdync=[pdync. 0.5*rho_all(x.3)*(vint)^2];
end
pdyna=pdyna';pdynb=pdynb';pdync=pdync';
pdyn_int_all=[pdyna.pdynb.pdync];
%_____________
%%% STEP 8.8
%% Calculate pressure at internal nodes
pstata=Patmref*0.9877^((alt+za)/100);
```

```
pstatb=Patmref*0.9877^((alt+zb)/100);
pstatc=Patmref*0.9877^((alt+zc)/100);
pstata=pstata'; pstatb=pstatb'; pstatc=pstatc';
pstat_int_temp=[pstata. pstatb. pstatc];
pstat_int_all=repmat(pstat_int_temp. 64.1);
%_____________
%%% STEP 8.9
%% Create a new matrix with the dynamic contribution and pressure at internal nodes
p_int_temp=[pdyn_int_all. pstat_int_all];
%% Define interval for initial values pa0. pb0. pc0
for x=1:size(p_int_temp.1)
pa0_l=[pa0_l. p_int_temp(x.4)];
pa0_r=[pa0_r. p_int_temp(x.4)+p_int_temp(x.1)];
pb0_l=[pb0_l. p_int_temp(x.5)];
pb0_r=[pb0_r. p_int_temp(x.5)+p_int_temp(x.2)];
pc0_l=[pc0_l. p_int_temp(x.6)];
pc0_r=[pc0_r. p_int_temp(x.6)+p_int_temp(x.3)];
end
pa0_l=pa0_l'; pa0_r=pa0_r'; pb0_l=pb0_l';pb0_r=pb0_r';pc0_l=pc0_l';pc0_r=pc0_r';
p0_all=[pa0_l.pa0_r.pb0_l.pb0_r.pc0_l.pc0_r];

%__________
%%% STEP 9
%% Create a new matrix S with all input data useful to the iterative calculation
% Define matrix S1
S1=[p0_all.k_all.P_est.pstk_int_all. ppot_int_all.rho_in. rho_sh.u];
% Define matrix S
S=S1(sum(isnan(S1).2)==0.:);
%___________
%%% STEP 10
%% Create a cycle for jj
```

```
%% Define the LINSPACE (=5)
Pa0=[];Pb0=[];Pc0=[];
%_________
%% STEP 11
%% Create 3 cycle for vectors aa-bb-cc
%_________
%% STEP 12
%% Create cycle for for matrix a of sign combination

jj = 1;
tic
for w=1:size(S.1)
Pa0 = linspace(S(w.1).S(w.2).5);
Pb0 = linspace(S(w.3).S(w.4).5);
Pc0 = linspace(S(w.5).S(w.6).5);
   for aa=1:length(Pa0)
    for bb=1:length(Pb0)
      for cc=1:length(Pc0)
         for i=1:size(a.1)
%%%_______
%% STEP 13
%% Define the function F
%   F = @(x) [+a(i.1)*kauc*abs(Pa-P1+ppota))^n+a(i.2)*kaco*abs(Pa-P3+ppota)^n+a(i.3)*kdsha*abs(Pa-Pc+ppota-ppotca-pstkc1)^n;
%         +a(i.4)*kbuc*abs(Pb-P2+ppotb))^n+a(i.5)*kbco*abs(Pb-P4+ppotb))^n+a(i.6)*kdshb*abs(Pb-Pc+ppotb-ppotcb-pstkc2)^n;
%         +a(i.7)*kdsha*abs(Pc-Pa+pstkc1+ppotca-ppota)^n+a(i.8)*kdshb*abs(Pc-Pb+pstkc2+ppotcb-ppotb)^n+a(i.9)*kwsha*abs(Pc-P3+pstkc3+ppotc3)^n+a(i.10)*kwshb*abs(Pc-P4+pstkc4+ppotc4)^n];

        F = @(x) [+a(i.1)*S(w.7)*abs(x(1)-S(w.15)+S(w.23))^n+a(i.2)*S(w.8)*abs(x(1)-S(w.17)+S(w.23))^n+a(i.3)*S(w.12)*abs(x(1)-x(3)+S(w.23)-S(w.25)-S(w.19))^n;
                  a(i.4)*S(w.9)*abs(x(2)-S(w.16)+S(w.24))^n+a(i.5)*S(w.10)*abs(x(2)-S(w.18)+S(w.24))^n+a(i.6)*S(w.14)*abs(x(2)-x(3)+S(w.24)-S(w.26)-S(w.20))^n;
```

```
        a(i.7)*S(w.12)*abs(x(3)-x(1)+S(w.19)+S(w.25)-S(w.23))^n+a(i.8)*S(w.14)*abs(x(3)-
x(2)+S(w.20)+S(w.26)-S(w.24))^n+a(i.9)*S(w.11)*abs(x(3)-S(w.17)+S(w.21)+S(w.27))...

        ^n+a(i.10)*S(w.13)*abs(x(3)-S(w.18)+S(w.22)+S(w.28))^n];


    x0(jj.:) = [Pa0(aa) Pb0(bb) Pc0(cc)];

    options = optimoptions('fsolve'.'Display'.'off'.'Algorithm'.'trust-region'.'StepTolerance'.10e-6);


     [x.fval.message]= fsolve(F.x0(jj.:).options);


     exitflag(jj) = message;


%% Save output data (results of f.solve function: x(1). x(2). x(3)) in a unique table. considering the 7875
cycles

     Pa = x(1);

     Pb = x(2);

     Pc = x(3);

     P_solution (jj.:)=[Pa.Pb.Pc];


     %_____________________________________

     %%% STEP 14

        %% Calculate Delta pressure at 10 link

     %DP.a1=Pa-P1+ppota;

     %DP.ac=Pa-Pc+ppota-ppotca-pstkc1;

     %DP.a3=Pa-P3+ppota;

     %DP.b2=Pb-P2+ppotb;

     %DP.bc=Pb-Pc+ppotb-ppotcb-pstkc2;

     %DP.b4=Pb-P4+ppotb;

     %DP.ca=Pc-Pa+pstkc1+ppotca-ppota;

     %DP.cb=Pc-Pb+pstkc2+ppotcb-ppotb;

     %DP.c3=Pc-P3+pstkc3+ppotc3;

     %DP.c4=Pc-P4+pstkc4+ppotc4;
```

```
DP.a1=Pa-S(w.15)+S(w.23);
DP.ac=Pa-Pc+S(w.23)-S(w.25)-S(w.19);
DP.a3=Pa-S(w.17)+S(w.23);
DP.b2=Pb-S(w.16)+S(w.24);
DP.bc=Pb-Pc+S(w.24)-S(w.26)-S(w.20);
DP.b4=Pb-S(w.18)+S(w.24);
DP.ca=Pc-Pa+S(w.19)+S(w.25)-S(w.23);
DP.cb=Pc-Pb+S(w.20)+S(w.26)-S(w.24);
DP.c3=Pc-S(w.17)+S(w.21)+S(w.27);
DP.c4=Pc-S(w.18)+S(w.22)+S(w.28);



    %_____________________________________________
%%% STEP 15
    %% Calculate mass air flow rate at 10 link
if DP.a1>0
   m.a1 =S(w.7)*(abs(DP.a1)^n);
else
   m.a1 =-S(w.7)*(abs(DP.a1)^n);
end
 if DP.ac>0
   m.ac =S(w.12)*(abs(DP.ac)^n);
else
   m.ac =-S(w.12)*(abs(DP.ac)^n);
end
 if DP.a3>0
   m.a3 =S(w.8)*(abs(DP.a3)^n);
else
   m.a3 =-S(w.8)*(abs(DP.a3)^n);
end
```

```
 if DP.b2>0
    m.b2 =S(w.9)*(abs(DP.b2)^n);
else
    m.b2 =-S(w.9)*(abs(DP.b2)^n);
end
if DP.bc>0
    m.bc =S(w.14)*(abs(DP.bc)^n);
else
    m.bc =-S(w.14)*(abs(DP.bc)^n);
end
if DP.b4>0
    m.b4 =S(w.10)*(abs(DP.b4)^n);
else
    m.b4 =-S(w.10)*(abs(DP.b4)^n);
end
 if DP.ca>0
    m.ca =S(w.12)*(abs(DP.ca)^n);
else
    m.ca =-S(w.12)*(abs(DP.ca)^n);
end
 if DP.cb>0
    m.cb =S(w.14)*(abs(DP.cb)^n);
else
    m.cb=-S(w.14)*(abs(DP.cb)^n);
 end
if DP.c3>0
    m.c3 =S(w.11)*(abs(DP.c3)^n);
else
    m.c3=-S(w.11)*(abs(DP.c3)^n);
end
if DP.c4>0
```

```
        m.c4 =S(w.13)*(abs(DP.c4)^n);
    else
        m.c4=-S(w.13)*(abs(DP.c4)^n);
    end

%_____
%%% STEP 15.1
%% Calculate mass air flow rate of the building
% only fresh air from outside (negative m at links with external nodes)
if      m.a1<0 &&   m.a3<0 &&   m.b2<0 &&   m.b4<0 &&   m.c3<0 &&   m.c4<0
m.bld=  abs(m.a1+m.a3+m.b2+m.b4+m.c3+m.c4);
elseif  m.a1<0 &&   m.a3<0 &&   m.b2<0 &&   m.b4>0 &&   m.c3<0 &&   m.c4<0
m.bld=  abs(m.a1+m.a3+m.b2+m.c3+m.c4);
elseif  m.a1<0 &&   m.a3<0 &&   m.b2>0 &&   m.b4<0 &&   m.c3<0 &&   m.c4<0
m.bld=  abs(m.a1+m.a3+m.b4+m.c3+m.c4);
elseif  m.a1<0 &&   m.a3<0 &&   m.b2>0 &&   m.b4>0 &&   m.c3<0 &&   m.c4<0
m.bld=  abs(m.a1+m.a3+m.c3+m.c4);
elseif  m.a1<0 &&   m.a3>0 &&   m.b2<0 &&   m.b4<0 &&   m.c3<0 &&   m.c4<0
m.bld=  abs(m.a1+m.b2+m.b4+m.c3+m.c4);
elseif  m.a1<0 &&   m.a3>0 &&   m.b2<0 &&   m.b4>0 &&   m.c3<0 &&   m.c4<0
m.bld=  abs(m.a1+m.b2+m.c3+m.c4);
elseif  m.a1<0 &&   m.a3>0 &&   m.b2>0 &&   m.b4<0 &&   m.c3<0 &&   m.c4<0
m.bld=  abs(m.a1+m.b4+m.c3+m.c4);
elseif  m.a1<0 &&   m.a3>0 &&   m.b2>0 &&   m.b4>0 &&   m.c3<0 &&   m.c4<0
m.bld=  abs(m.a1+m.c3+m.c4);
elseif  m.a1>0 &&   m.a3<0 &&   m.b2<0 &&   m.b4<0 &&   m.c3<0 &&   m.c4<0
m.bld=  abs(m.a3+m.b2+m.b4+m.c3+m.c4);
elseif  m.a1>0 &&   m.a3<0 &&   m.b2<0 &&   m.b4>0 &&   m.c3<0 &&   m.c4<0
m.bld=  abs(m.a3+m.b2+m.c3+m.c4);
elseif  m.a1>0 &&   m.a3<0 &&   m.b2>0 &&   m.b4<0 &&   m.c3<0 &&   m.c4<0
m.bld=  abs(m.a3+m.b4+m.c3+m.c4);
```

```
elseif m.a1>0 && m.a3<0 && m.b2>0 && m.b4>0 && m.c3<0 && m.c4<0
m.bld= abs(m.a3+m.c3+m.c4);
elseif m.a1>0 && m.a3>0 && m.b2<0 && m.b4<0 && m.c3<0 && m.c4<0
m.bld= abs(m.b2+m.b4+m.c3+m.c4);
elseif m.a1>0 && m.a3>0 && m.b2<0 && m.b4>0 && m.c3<0 && m.c4<0
m.bld= abs(m.b2+m.c3+m.c4);
elseif m.a1>0 && m.a3>0 && m.b2>0 && m.b4<0 && m.c3<0 && m.c4<0
m.bld= abs(m.b4+m.c3+m.c4);
elseif m.a1>0 && m.a3>0 && m.b2>0 && m.b4>0 && m.c3<0 && m.c4<0
m.bld= abs(m.c3+m.c4);
elseif m.a1<0 && m.a3<0 && m.b2<0 && m.b4<0 && m.c3>0 && m.c4<0
m.bld= abs(m.a1+m.a3+m.b2+m.b4+m.c4);
elseif m.a1<0 && m.a3<0 && m.b2<0 && m.b4>0 && m.c3>0 && m.c4<0
m.bld= abs(m.a1+m.a3+m.b2+m.c4);
elseif m.a1<0 && m.a3<0 && m.b2>0 && m.b4<0 && m.c3>0 && m.c4<0
m.bld= abs(m.a1+m.a3+m.b4+m.c4);
elseif m.a1<0 && m.a3<0 && m.b2>0 && m.b4>0 && m.c3>0 && m.c4<0
m.bld= abs(m.a1+m.a3+m.c4);
elseif m.a1<0 && m.a3>0 && m.b2<0 && m.b4<0 && m.c3>0 && m.c4<0
m.bld= abs(m.a1+m.b2+m.b4+m.c4);
elseif m.a1<0 && m.a3>0 && m.b2<0 && m.b4>0 && m.c3>0 && m.c4<0
m.bld= abs(m.a1+m.b2+m.c4);
elseif m.a1<0 && m.a3>0 && m.b2>0 && m.b4<0 && m.c3>0 && m.c4<0
m.bld= abs(m.a1+m.b4+m.c4);
elseif m.a1<0 && m.a3>0 && m.b2>0 && m.b4>0 && m.c3>0 && m.c4<0
m.bld= abs(m.a1+m.c4);
elseif m.a1>0 && m.a3<0 && m.b2<0 && m.b4<0 && m.c3>0 && m.c4<0
m.bld= abs(m.a3+m.b2+m.b4+m.c4);
elseif m.a1>0 && m.a3<0 && m.b2<0 && m.b4>0 && m.c3>0 && m.c4<0
m.bld= abs(m.a3+m.b2+m.c4);
elseif m.a1>0 && m.a3<0 && m.b2>0 && m.b4<0 && m.c3>0 && m.c4<0
```

```
m.bld= abs(m.a3+m.b4+m.c4);
elseif m.a1>0 && m.a3<0 && m.b2>0 && m.b4>0 && m.c3>0 && m.c4<0
m.bld= abs(m.a3+m.c4);
elseif m.a1>0 && m.a3>0 && m.b2<0 && m.b4<0 && m.c3>0 && m.c4<0
m.bld= abs(m.b2+m.b4+m.c4);
elseif m.a1>0 && m.a3>0 && m.b2<0 && m.b4>0 && m.c3>0 && m.c4<0
m.bld= abs(m.b2+m.c4);
elseif m.a1>0 && m.a3>0 && m.b2>0 && m.b4<0 && m.c3>0 && m.c4<0
m.bld= abs(m.b4+m.c4);
elseif m.a1>0 && m.a3>0 && m.b2>0 && m.b4>0 && m.c3>0 && m.c4<0
m.bld= abs(m.c4);
elseif m.a1<0 && m.a3<0 && m.b2<0 && m.b4<0 && m.c3<0 && m.c4>0
m.bld= abs(m.a1+m.a3+m.b2+m.b4+m.c3);
elseif m.a1<0 && m.a3<0 && m.b2<0 && m.b4>0 && m.c3<0 && m.c4>0
m.bld= abs(m.a1+m.a3+m.b2+m.c3);
elseif m.a1<0 && m.a3<0 && m.b2>0 && m.b4<0 && m.c3<0 && m.c4>0
m.bld= abs(m.a1+m.a3+m.b4+m.c3);
elseif m.a1<0 && m.a3<0 && m.b2>0 && m.b4>0 && m.c3<0 && m.c4>0
m.bld= abs(m.a1+m.a3+m.c3);
elseif m.a1<0 && m.a3>0 && m.b2<0 && m.b4<0 && m.c3<0 && m.c4>0
m.bld= abs(m.a1+m.b2+m.b4+m.c3);
elseif m.a1<0 && m.a3>0 && m.b2<0 && m.b4>0 && m.c3<0 && m.c4>0
m.bld= abs(m.a1+m.b2+m.c3);
elseif m.a1<0 && m.a3>0 && m.b2>0 && m.b4<0 && m.c3<0 && m.c4>0
m.bld= abs(m.a1+m.b4+m.c3);
elseif m.a1<0 && m.a3>0 && m.b2>0 && m.b4>0 && m.c3<0 && m.c4>0
m.bld= abs(m.a1+m.c3);
elseif m.a1>0 && m.a3<0 && m.b2<0 && m.b4<0 && m.c3<0 && m.c4>0
m.bld= abs(m.a3+m.b2+m.b4+m.c3);
elseif m.a1>0 && m.a3<0 && m.b2<0 && m.b4>0 && m.c3<0 && m.c4>0
m.bld= abs(m.a3+m.b2+m.c3);
```

```
elseif m.a1>0 && m.a3<0 && m.b2>0 && m.b4<0 && m.c3<0 && m.c4>0
m.bld= abs(m.a3+m.b4+m.c3);
elseif m.a1>0 && m.a3<0 && m.b2>0 && m.b4>0 && m.c3<0 && m.c4>0
m.bld= abs(m.a3+m.c3);
elseif m.a1>0 && m.a3>0 && m.b2<0 && m.b4<0 && m.c3<0 && m.c4>0
m.bld= abs(m.b2+m.b4+m.c3);
elseif m.a1>0 && m.a3>0 && m.b2<0 && m.b4>0 && m.c3<0 && m.c4>0
m.bld= abs(m.b2+m.c3);
elseif m.a1>0 && m.a3>0 && m.b2>0 && m.b4<0 && m.c3<0 && m.c4>0
m.bld= abs(m.b4+m.c3);
elseif m.a1>0 && m.a3>0 && m.b2>0 && m.b4>0 && m.c3<0 && m.c4>0
m.bld= abs(m.c3);
elseif m.a1<0 && m.a3<0 && m.b2<0 && m.b4<0 && m.c3>0 && m.c4>0
m.bld= abs(m.a1+m.a3+m.b2+m.b4);
elseif m.a1<0 && m.a3<0 && m.b2<0 && m.b4>0 && m.c3>0 && m.c4>0
m.bld= abs(m.a1+m.a3+m.b2);
elseif m.a1<0 && m.a3<0 && m.b2>0 && m.b4<0 && m.c3>0 && m.c4>0
m.bld= abs(m.a1+m.a3+m.b4);
elseif m.a1<0 && m.a3<0 && m.b2>0 && m.b4>0 && m.c3>0 && m.c4>0
m.bld= abs(m.a1+m.a3);
elseif m.a1<0 && m.a3>0 && m.b2<0 && m.b4<0 && m.c3>0 && m.c4>0
m.bld= abs(m.a1+m.b2+m.b4);
elseif m.a1<0 && m.a3>0 && m.b2<0 && m.b4>0 && m.c3>0 && m.c4>0
m.bld= abs(m.a1+m.b2);
elseif m.a1<0 && m.a3>0 && m.b2>0 && m.b4<0 && m.c3>0 && m.c4>0
m.bld= abs(m.a1+m.b4);
elseif m.a1<0 && m.a3>0 && m.b2>0 && m.b4>0 && m.c3>0 && m.c4>0
m.bld= abs(m.a1);
elseif m.a1>0 && m.a3<0 && m.b2<0 && m.b4<0 && m.c3>0 && m.c4>0
m.bld= abs(m.a3+m.b2+m.b4);
elseif m.a1>0 && m.a3<0 && m.b2<0 && m.b4>0 && m.c3>0 && m.c4>0
```

```
m.bld= abs(m.a3+m.b2);
elseif  m.a1>0 &&   m.a3<0 &&   m.b2>0 &&   m.b4<0 &&   m.c3>0 &&   m.c4>0
m.bld= abs(m.a3+m.b4);
elseif  m.a1>0 &&   m.a3<0 &&   m.b2>0 &&   m.b4>0 &&   m.c3>0 &&   m.c4>0
m.bld= abs(m.a3);
elseif  m.a1>0 &&   m.a3>0 &&   m.b2<0 &&   m.b4<0 &&   m.c3>0 &&   m.c4>0
m.bld= abs(m.b2+m.b4);
elseif  m.a1>0 &&   m.a3>0 &&   m.b2<0 &&   m.b4>0 &&   m.c3>0 &&   m.c4>0
m.bld= abs(m.b2);
elseif  m.a1>0 &&   m.a3>0 &&   m.b2>0 &&   m.b4<0 &&   m.c3>0 &&   m.c4>0
m.bld= abs(m.b4);
elseif  m.a1>0 &&   m.a3>0 &&   m.b2>0 &&   m.b4>0 &&   m.c3>0 &&   m.c4>0
m.bld= 0;
end

%_____________________________________________________________________________
%%% STEP 15.2
%% Define variable m.check as a number that identify sign combination (from 1 to 126)
 %% Assign m.check to each iteration
%% Iteration result without m.check assigned are not acceptable solutions.
if      m.a1<0 &&   m.a3<0 &&   m.ac>0 &&   m.b2<0 &&   m.b4<0 &&   m.bc>0 &&
        m.ca<0 &&   m.cb<0 &&   m.c3>0 &&   m.c4>0
   m.check=    2;
elseif  m.a1<0 &&   m.a3<0 &&   m.ac>0 &&   m.b2<0 &&   m.b4<0 &&   m.bc>0 &&
        m.ca<0 &&   m.cb<0 &&   m.c3>0 &&   m.c4<0
   m.check=    4;
elseif  m.a1<0 &&   m.a3<0 &&   m.ac>0 &&   m.b2<0 &&   m.b4<0 &&   m.bc>0 &&
        m.ca<0 &&   m.cb<0 &&   m.c3<0 &&   m.c4>0
   m.check=    6;
elseif  m.a1<0 &&   m.a3<0 &&   m.ac>0 &&   m.b2>0 &&   m.b4>0 &&   m.bc<0 &&
        m.ca<0 &&   m.cb>0 &&   m.c3>0 &&   m.c4>0
   m.check=    8;
```

```
elseif  m.a1<0 &&   m.a3<0 &&   m.ac>0 &&   m.b2>0 &&   m.b4>0 &&   m.bc<0 &&
        m.ca<0 &&   m.cb>0 &&   m.c3>0 &&   m.c4<0

  m.check=    10;

elseif  m.a1<0 &&   m.a3<0 &&   m.ac>0 &&   m.b2>0 &&   m.b4>0 &&   m.bc<0 &&
        m.ca<0 &&   m.cb>0 &&   m.c3<0 &&   m.c4>0

  m.check=    12;

elseif  m.a1<0 &&   m.a3<0 &&   m.ac>0 &&   m.b2>0 &&   m.b4>0 &&   m.bc<0 &&
        m.ca<0 &&   m.cb>0 &&   m.c3<0 &&   m.c4<0

  m.check=    14;

elseif  m.a1<0 &&   m.a3<0 &&   m.ac>0 &&   m.b2<0 &&   m.b4>0 &&   m.bc<0 &&
        m.ca<0 &&   m.cb>0 &&   m.c3>0 &&   m.c4>0

  m.check=    16;

elseif  m.a1<0 &&   m.a3<0 &&   m.ac>0 &&   m.b2<0 &&   m.b4>0 &&   m.bc<0 &&
        m.ca<0 &&   m.cb>0 &&   m.c3>0 &&   m.c4<0

  m.check=    18;

elseif  m.a1<0 &&   m.a3<0 &&   m.ac>0 &&   m.b2<0 &&   m.b4>0 &&   m.bc<0 &&
        m.ca<0 &&   m.cb>0 &&   m.c3<0 &&   m.c4>0

  m.check=    20;

elseif  m.a1<0 &&   m.a3<0 &&   m.ac>0 &&   m.b2<0 &&   m.b4>0 &&   m.bc<0 &&
        m.ca<0 &&   m.cb>0 &&   m.c3<0 &&   m.c4<0

  m.check=    22;

elseif  m.a1<0 &&   m.a3<0 &&   m.ac>0 &&   m.b2>0 &&   m.b4<0 &&   m.bc>0 &&
        m.ca<0 &&   m.cb<0 &&   m.c3>0 &&   m.c4>0

  m.check=    24;

elseif  m.a1<0 &&   m.a3<0 &&   m.ac>0 &&   m.b2>0 &&   m.b4<0 &&   m.bc>0 &&
        m.ca<0 &&   m.cb<0 &&   m.c3>0 &&   m.c4<0

  m.check=    26;

elseif  m.a1<0 &&   m.a3<0 &&   m.ac>0 &&   m.b2>0 &&   m.b4<0 &&   m.bc>0 &&
        m.ca<0 &&   m.cb<0 &&   m.c3<0 &&   m.c4>0

  m.check=    28;

elseif  m.a1<0 &&   m.a3<0 &&   m.ac>0 &&   m.b2<0 &&   m.b4>0 &&   m.bc>0 &&
        m.ca<0 &&   m.cb<0 &&   m.c3>0 &&   m.c4>0

  m.check=    30;

elseif  m.a1<0 &&   m.a3<0 &&   m.ac>0 &&   m.b2<0 &&   m.b4>0 &&   m.bc>0 &&
        m.ca<0 &&   m.cb<0 &&   m.c3>0 &&   m.c4<0
```

```
   m.check=     32;

elseif  m.a1<0 &&    m.a3<0 &&    m.ac>0 &&    m.b2<0 &&    m.b4>0 &&    m.bc>0 &&
        m.ca<0 &&    m.cb<0 &&    m.c3<0 &&    m.c4>0

   m.check=     34;

elseif  m.a1<0 &&    m.a3<0 &&    m.ac>0 &&    m.b2>0 &&    m.b4<0 &&    m.bc<0 &&
        m.ca<0 &&    m.cb>0 &&    m.c3>0 &&    m.c4>0

   m.check=     36;

elseif  m.a1<0 &&    m.a3<0 &&    m.ac>0 &&    m.b2>0 &&    m.b4<0 &&    m.bc<0 &&
        m.ca<0 &&    m.cb>0 &&    m.c3>0 &&    m.c4<0

   m.check=     38;

elseif  m.a1<0 &&    m.a3<0 &&    m.ac>0 &&    m.b2>0 &&    m.b4<0 &&    m.bc<0 &&
        m.ca<0 &&    m.cb>0 &&    m.c3<0 &&    m.c4>0

   m.check=     40;

elseif  m.a1<0 &&    m.a3<0 &&    m.ac>0 &&    m.b2>0 &&    m.b4<0 &&    m.bc<0 &&
        m.ca<0 &&    m.cb>0 &&    m.c3<0 &&    m.c4<0

   m.check=     42;

elseif  m.a1<0 &&    m.a3>0 &&    m.ac<0 &&    m.b2<0 &&    m.b4<0 &&    m.bc>0 &&
        m.ca>0 &&    m.cb<0 &&    m.c3>0 &&    m.c4>0

   m.check=     44;

elseif  m.a1<0 &&    m.a3>0 &&    m.ac<0 &&    m.b2<0 &&    m.b4<0 &&    m.bc>0 &&
        m.ca>0 &&    m.cb<0 &&    m.c3>0 &&    m.c4<0

   m.check=     46;

elseif  m.a1<0 &&    m.a3>0 &&    m.ac<0 &&    m.b2<0 &&    m.b4<0 &&    m.bc>0 &&
        m.ca>0 &&    m.cb<0 &&    m.c3<0 &&    m.c4>0

   m.check=     48;

elseif  m.a1<0 &&    m.a3>0 &&    m.ac<0 &&    m.b2<0 &&    m.b4<0 &&    m.bc>0 &&
        m.ca>0 &&    m.cb<0 &&    m.c3<0 &&    m.c4<0

   m.check=     50;

elseif  m.a1<0 &&    m.a3>0 &&    m.ac<0 &&    m.b2>0 &&    m.b4>0 &&    m.bc<0 &&
        m.ca>0 &&    m.cb>0 &&    m.c3>0 &&    m.c4<0

   m.check=     52;

elseif  m.a1<0 &&    m.a3>0 &&    m.ac<0 &&    m.b2>0 &&    m.b4>0 &&    m.bc<0 &&
        m.ca>0 &&    m.cb>0 &&    m.c3<0 &&    m.c4>0

   m.check=     54;
```

```
elseif  m.a1<0 &&   m.a3>0 &&   m.ac<0 &&   m.b2>0 &&   m.b4>0 &&   m.bc<0 &&
        m.ca>0 &&   m.cb>0 &&   m.c3<0 &&   m.c4<0

  m.check=    56;

elseif  m.a1<0 &&   m.a3>0 &&   m.ac<0 &&   m.b2<0 &&   m.b4>0 &&   m.bc<0 &&
        m.ca>0 &&   m.cb>0 &&   m.c3>0 &&   m.c4<0

  m.check=    58;

elseif  m.a1<0 &&   m.a3>0 &&   m.ac<0 &&   m.b2<0 &&   m.b4>0 &&   m.bc<0 &&
        m.ca>0 &&   m.cb>0 &&   m.c3<0 &&   m.c4>0

  m.check=    60;

elseif  m.a1<0 &&   m.a3>0 &&   m.ac<0 &&   m.b2<0 &&   m.b4>0 &&   m.bc<0 &&
        m.ca>0 &&   m.cb>0 &&   m.c3<0 &&   m.c4<0

  m.check=    62;

elseif  m.a1<0 &&   m.a3>0 &&   m.ac<0 &&   m.b2>0 &&   m.b4<0 &&   m.bc>0 &&
        m.ca>0 &&   m.cb<0 &&   m.c3>0 &&   m.c4>0

  m.check=    64;

elseif  m.a1<0 &&   m.a3>0 &&   m.ac<0 &&   m.b2>0 &&   m.b4<0 &&   m.bc>0 &&
        m.ca>0 &&   m.cb<0 &&   m.c3>0 &&   m.c4<0

  m.check=    66;

elseif  m.a1<0 &&   m.a3>0 &&   m.ac<0 &&   m.b2>0 &&   m.b4<0 &&   m.bc>0 &&
        m.ca>0 &&   m.cb<0 &&   m.c3<0 &&   m.c4>0

  m.check=    68;

elseif  m.a1<0 &&   m.a3>0 &&   m.ac<0 &&   m.b2>0 &&   m.b4<0 &&   m.bc>0 &&
        m.ca>0 &&   m.cb<0 &&   m.c3<0 &&   m.c4<0

  m.check=    70;

elseif  m.a1<0 &&   m.a3>0 &&   m.ac<0 &&   m.b2<0 &&   m.b4>0 &&   m.bc>0 &&
        m.ca>0 &&   m.cb<0 &&   m.c3>0 &&   m.c4>0

  m.check=    72;

elseif  m.a1<0 &&   m.a3>0 &&   m.ac<0 &&   m.b2<0 &&   m.b4>0 &&   m.bc>0 &&
        m.ca>0 &&   m.cb<0 &&   m.c3>0 &&   m.c4<0

  m.check=    74;

elseif  m.a1<0 &&   m.a3>0 &&   m.ac<0 &&   m.b2<0 &&   m.b4>0 &&   m.bc>0 &&
        m.ca>0 &&   m.cb<0 &&   m.c3<0 &&   m.c4>0

  m.check=    76;

elseif  m.a1<0 &&   m.a3>0 &&   m.ac<0 &&   m.b2<0 &&   m.b4>0 &&   m.bc>0 &&
        m.ca>0 &&   m.cb<0 &&   m.c3<0 &&   m.c4<0
```

```
   m.check=     78;

elseif  m.a1<0 &&    m.a3>0 &&    m.ac<0 &&    m.b2>0 &&    m.b4<0 &&    m.bc<0 &&
        m.ca>0 &&    m.cb>0 &&    m.c3>0 &&    m.c4<0

   m.check=     80;

elseif  m.a1<0 &&    m.a3>0 &&    m.ac<0 &&    m.b2>0 &&    m.b4<0 &&    m.bc<0 &&
        m.ca>0 &&    m.cb>0 &&    m.c3<0 &&    m.c4>0

   m.check=     82;

elseif  m.a1<0 &&    m.a3>0 &&    m.ac<0 &&    m.b2>0 &&    m.b4<0 &&    m.bc<0 &&
        m.ca>0 &&    m.cb>0 &&    m.c3<0 &&    m.c4<0

   m.check=     84;

elseif  m.a1<0 &&    m.a3>0 &&    m.ac>0 &&    m.b2<0 &&    m.b4<0 &&    m.bc>0 &&
        m.ca<0 &&    m.cb<0 &&    m.c3>0 &&    m.c4>0

   m.check=     86;

elseif  m.a1<0 &&    m.a3>0 &&    m.ac>0 &&    m.b2<0 &&    m.b4<0 &&    m.bc>0 &&
        m.ca<0 &&    m.cb<0 &&    m.c3>0 &&    m.c4<0

   m.check=     88;

elseif  m.a1<0 &&    m.a3>0 &&    m.ac>0 &&    m.b2<0 &&    m.b4<0 &&    m.bc>0 &&
        m.ca<0 &&    m.cb<0 &&    m.c3<0 &&    m.c4>0

   m.check=     90;

elseif  m.a1<0 &&    m.a3>0 &&    m.ac>0 &&    m.b2>0 &&    m.b4>0 &&    m.bc<0 &&
        m.ca<0 &&    m.cb>0 &&    m.c3>0 &&    m.c4>0

   m.check=     92;

elseif  m.a1<0 &&    m.a3>0 &&    m.ac>0 &&    m.b2>0 &&    m.b4>0 &&    m.bc<0 &&
        m.ca<0 &&    m.cb>0 &&    m.c3>0 &&    m.c4<0

   m.check=     94;

elseif  m.a1<0 &&    m.a3>0 &&    m.ac>0 &&    m.b2>0 &&    m.b4>0 &&    m.bc<0 &&
        m.ca<0 &&    m.cb>0 &&    m.c3<0 &&    m.c4>0

   m.check=     96;

elseif  m.a1<0 &&    m.a3>0 &&    m.ac>0 &&    m.b2>0 &&    m.b4>0 &&    m.bc<0 &&
        m.ca<0 &&    m.cb>0 &&    m.c3<0 &&    m.c4<0

   m.check=     98;

elseif  m.a1<0 &&    m.a3>0 &&    m.ac>0 &&    m.b2<0 &&    m.b4>0 &&    m.bc<0 &&
        m.ca<0 &&    m.cb>0 &&    m.c3>0 &&    m.c4>0

   m.check=     100;
```

```
elseif  m.a1<0 &&   m.a3>0 &&   m.ac>0 &&   m.b2<0 &&   m.b4>0 &&   m.bc<0 &&
        m.ca<0 &&   m.cb>0 &&   m.c3>0 &&   m.c4<0

  m.check=    102;

elseif  m.a1<0 &&   m.a3>0 &&   m.ac>0 &&   m.b2<0 &&   m.b4>0 &&   m.bc<0 &&
        m.ca<0 &&   m.cb>0 &&   m.c3<0 &&   m.c4>0

  m.check=    104;

elseif  m.a1<0 &&   m.a3>0 &&   m.ac>0 &&   m.b2<0 &&   m.b4>0 &&   m.bc<0 &&
        m.ca<0 &&   m.cb>0 &&   m.c3<0 &&   m.c4<0

  m.check=    106;

elseif  m.a1<0 &&   m.a3>0 &&   m.ac>0 &&   m.b2>0 &&   m.b4<0 &&   m.bc>0 &&
        m.ca<0 &&   m.cb<0 &&   m.c3>0 &&   m.c4>0

  m.check=    108;

elseif  m.a1<0 &&   m.a3>0 &&   m.ac>0 &&   m.b2>0 &&   m.b4<0 &&   m.bc>0 &&
        m.ca<0 &&   m.cb<0 &&   m.c3>0 &&   m.c4<0

  m.check=    110;

elseif  m.a1<0 &&   m.a3>0 &&   m.ac>0 &&   m.b2>0 &&   m.b4<0 &&   m.bc>0 &&
        m.ca<0 &&   m.cb<0 &&   m.c3<0 &&   m.c4>0

  m.check=    112;

elseif  m.a1<0 &&   m.a3>0 &&   m.ac>0 &&   m.b2<0 &&   m.b4>0 &&   m.bc>0 &&
        m.ca<0 &&   m.cb<0 &&   m.c3>0 &&   m.c4>0

  m.check=    114;

elseif  m.a1<0 &&   m.a3>0 &&   m.ac>0 &&   m.b2<0 &&   m.b4>0 &&   m.bc>0 &&
        m.ca<0 &&   m.cb<0 &&   m.c3>0 &&   m.c4<0

  m.check=    116;

elseif  m.a1<0 &&   m.a3>0 &&   m.ac>0 &&   m.b2<0 &&   m.b4>0 &&   m.bc>0 &&
        m.ca<0 &&   m.cb<0 &&   m.c3<0 &&   m.c4>0

  m.check=    118;

elseif  m.a1<0 &&   m.a3>0 &&   m.ac>0 &&   m.b2>0 &&   m.b4<0 &&   m.bc<0 &&
        m.ca<0 &&   m.cb>0 &&   m.c3>0 &&   m.c4>0

  m.check=    120;

elseif  m.a1<0 &&   m.a3>0 &&   m.ac>0 &&   m.b2>0 &&   m.b4<0 &&   m.bc<0 &&
        m.ca<0 &&   m.cb>0 &&   m.c3>0 &&   m.c4<0

  m.check=    122;

elseif  m.a1<0 &&   m.a3>0 &&   m.ac>0 &&   m.b2>0 &&   m.b4<0 &&   m.bc<0 &&
        m.ca<0 &&   m.cb>0 &&   m.c3<0 &&   m.c4>0
```

```
   m.check=     124;

elseif  m.a1<0 &&    m.a3>0 &&    m.ac>0 &&    m.b2>0 &&    m.b4<0 &&    m.bc<0 &&
        m.ca<0 &&    m.cb>0 &&    m.c3<0 &&    m.c4<0

   m.check=     126;

elseif  m.a1>0 &&    m.a3>0 &&    m.ac<0 &&    m.b2>0 &&    m.b4>0 &&    m.bc<0 &&
        m.ca>0 &&    m.cb>0 &&    m.c3<0 &&    m.c4<0

   m.check=     1;

elseif  m.a1>0 &&    m.a3>0 &&    m.ac<0 &&    m.b2>0 &&    m.b4>0 &&    m.bc<0 &&
        m.ca>0 &&    m.cb>0 &&    m.c3<0 &&    m.c4>0

   m.check=     3;

elseif  m.a1>0 &&    m.a3>0 &&    m.ac<0 &&    m.b2>0 &&    m.b4>0 &&    m.bc<0 &&
        m.ca>0 &&    m.cb>0 &&    m.c3>0 &&    m.c4<0

   m.check=     5;

elseif  m.a1>0 &&    m.a3>0 &&    m.ac<0 &&    m.b2<0 &&    m.b4<0 &&    m.bc>0 &&
        m.ca>0 &&    m.cb<0 &&    m.c3<0 &&    m.c4<0

   m.check=     7;

elseif  m.a1>0 &&    m.a3>0 &&    m.ac<0 &&    m.b2<0 &&    m.b4<0 &&    m.bc>0 &&
        m.ca>0 &&    m.cb<0 &&    m.c3<0 &&    m.c4>0

   m.check=     9;

elseif  m.a1>0 &&    m.a3>0 &&    m.ac<0 &&    m.b2<0 &&    m.b4<0 &&    m.bc>0 &&
        m.ca>0 &&    m.cb<0 &&    m.c3>0 &&    m.c4<0

   m.check=     11;

elseif  m.a1>0 &&    m.a3>0 &&    m.ac<0 &&    m.b2<0 &&    m.b4<0 &&    m.bc>0 &&
        m.ca>0 &&    m.cb<0 &&    m.c3>0 &&    m.c4>0

   m.check=     13;

elseif  m.a1>0 &&    m.a3>0 &&    m.ac<0 &&    m.b2>0 &&    m.b4<0 &&    m.bc>0 &&
        m.ca>0 &&    m.cb<0 &&    m.c3<0 &&    m.c4<0

   m.check=     15;

elseif  m.a1>0 &&    m.a3>0 &&    m.ac<0 &&    m.b2>0 &&    m.b4<0 &&    m.bc>0 &&
        m.ca>0 &&    m.cb<0 &&    m.c3<0 &&    m.c4>0

   m.check=     17;

elseif  m.a1>0 &&    m.a3>0 &&    m.ac<0 &&    m.b2>0 &&    m.b4<0 &&    m.bc>0 &&
        m.ca>0 &&    m.cb<0 &&    m.c3>0 &&    m.c4<0

   m.check=     19;
```

```
elseif  m.a1>0 &&   m.a3>0 &&   m.ac<0 &&   m.b2>0 &&   m.b4<0 &&   m.bc>0 &&
        m.ca>0 &&   m.cb<0 &&   m.c3>0 &&   m.c4>0

  m.check=    21;

elseif  m.a1>0 &&   m.a3>0 &&   m.ac<0 &&   m.b2<0 &&   m.b4>0 &&   m.bc<0 &&
        m.ca>0 &&   m.cb>0 &&   m.c3<0 &&   m.c4<0

  m.check=    23;

elseif  m.a1>0 &&   m.a3>0 &&   m.ac<0 &&   m.b2<0 &&   m.b4>0 &&   m.bc<0 &&
        m.ca>0 &&   m.cb>0 &&   m.c3<0 &&   m.c4>0

  m.check=    25;

elseif  m.a1>0 &&   m.a3>0 &&   m.ac<0 &&   m.b2<0 &&   m.b4>0 &&   m.bc<0 &&
        m.ca>0 &&   m.cb>0 &&   m.c3>0 &&   m.c4<0

  m.check=    27;

elseif  m.a1>0 &&   m.a3>0 &&   m.ac<0 &&   m.b2>0 &&   m.b4<0 &&   m.bc<0 &&
        m.ca>0 &&   m.cb>0 &&   m.c3<0 &&   m.c4<0

  m.check=    29;

elseif  m.a1>0 &&   m.a3>0 &&   m.ac<0 &&   m.b2>0 &&   m.b4<0 &&   m.bc<0 &&
        m.ca>0 &&   m.cb>0 &&   m.c3<0 &&   m.c4>0

  m.check=    31;

elseif  m.a1>0 &&   m.a3>0 &&   m.ac<0 &&   m.b2>0 &&   m.b4<0 &&   m.bc<0 &&
        m.ca>0 &&   m.cb>0 &&   m.c3>0 &&   m.c4<0

  m.check=    33;

elseif  m.a1>0 &&   m.a3>0 &&   m.ac<0 &&   m.b2<0 &&   m.b4>0 &&   m.bc>0 &&
        m.ca>0 &&   m.cb<0 &&   m.c3<0 &&   m.c4<0

  m.check=    35;

elseif  m.a1>0 &&   m.a3>0 &&   m.ac<0 &&   m.b2<0 &&   m.b4>0 &&   m.bc>0 &&
        m.ca>0 &&   m.cb<0 &&   m.c3<0 &&   m.c4>0

  m.check=    37;

elseif  m.a1>0 &&   m.a3>0 &&   m.ac<0 &&   m.b2<0 &&   m.b4>0 &&   m.bc>0 &&
        m.ca>0 &&   m.cb<0 &&   m.c3>0 &&   m.c4<0

  m.check=    39;

elseif  m.a1>0 &&   m.a3>0 &&   m.ac<0 &&   m.b2<0 &&   m.b4>0 &&   m.bc>0 &&
        m.ca>0 &&   m.cb<0 &&   m.c3>0 &&   m.c4>0

  m.check=    41;

elseif  m.a1>0 &&   m.a3<0 &&   m.ac>0 &&   m.b2>0 &&   m.b4>0 &&   m.bc<0 &&
        m.ca<0 &&   m.cb>0 &&   m.c3<0 &&   m.c4<0
```

```
   m.check=     43;

elseif  m.a1>0 &&    m.a3<0 &&    m.ac>0 &&    m.b2>0 &&    m.b4>0 &&    m.bc<0 &&
        m.ca<0 &&    m.cb>0 &&    m.c3<0 &&    m.c4>0

   m.check=     45;

elseif  m.a1>0 &&    m.a3<0 &&    m.ac>0 &&    m.b2>0 &&    m.b4>0 &&    m.bc<0 &&
        m.ca<0 &&    m.cb>0 &&    m.c3>0 &&    m.c4<0

   m.check=     47;

elseif  m.a1>0 &&    m.a3<0 &&    m.ac>0 &&    m.b2>0 &&    m.b4>0 &&    m.bc<0 &&
        m.ca<0 &&    m.cb>1 &&    m.c3>0 &&    m.c4>0

   m.check=     49;

elseif  m.a1>0 &&    m.a3<0 &&    m.ac>0 &&    m.b2<0 &&    m.b4<0 &&    m.bc>0 &&
        m.ca<0 &&    m.cb<0 &&    m.c3<0 &&    m.c4>0

   m.check=     51;

elseif  m.a1>0 &&    m.a3<0 &&    m.ac>0 &&    m.b2<0 &&    m.b4<0 &&    m.bc>0 &&
        m.ca<0 &&    m.cb<0 &&    m.c3>0 &&    m.c4<0

   m.check=     53;

elseif  m.a1>0 &&    m.a3<0 &&    m.ac>0 &&    m.b2<0 &&    m.b4<0 &&    m.bc>0 &&
        m.ca<0 &&    m.cb<0 &&    m.c3>0 &&    m.c4>0

   m.check=     55;

elseif  m.a1>0 &&    m.a3<0 &&    m.ac>0 &&    m.b2>0 &&    m.b4<0 &&    m.bc>0 &&
        m.ca<0 &&    m.cb<0 &&    m.c3<0 &&    m.c4>0

   m.check=     57;

elseif  m.a1>0 &&    m.a3<0 &&    m.ac>0 &&    m.b2>0 &&    m.b4<0 &&    m.bc>0 &&
        m.ca<0 &&    m.cb<0 &&    m.c3>0 &&    m.c4<0

   m.check=     59;

elseif  m.a1>0 &&    m.a3<0 &&    m.ac>0 &&    m.b2>0 &&    m.b4<0 &&    m.bc>0 &&
        m.ca<0 &&    m.cb<0 &&    m.c3>0 &&    m.c4>0

   m.check=     61;

elseif  m.a1>0 &&    m.a3<0 &&    m.ac>0 &&    m.b2<0 &&    m.b4>0 &&    m.bc<0 &&
        m.ca<0 &&    m.cb>0 &&    m.c3<0 &&    m.c4<0

   m.check=     63;

elseif  m.a1>0 &&    m.a3<0 &&    m.ac>0 &&    m.b2<0 &&    m.b4>0 &&    m.bc<0 &&
        m.ca<0 &&    m.cb>0 &&    m.c3<0 &&    m.c4>0

   m.check=     65;
```

```
elseif  m.a1>0 &&   m.a3<0 &&   m.ac>0 &&   m.b2<0 &&   m.b4>0 &&   m.bc<0 &&
        m.ca<0 &&   m.cb>0 &&   m.c3>0 &&   m.c4<0

  m.check=    67;

elseif  m.a1>0 &&   m.a3<0 &&   m.ac>0 &&   m.b2<0 &&   m.b4>0 &&   m.bc<0 &&
        m.ca<0 &&   m.cb>0 &&   m.c3>0 &&   m.c4>0

  m.check=    69;

elseif  m.a1>0 &&   m.a3<0 &&   m.ac>0 &&   m.b2>0 &&   m.b4<0 &&   m.bc<0 &&
        m.ca<0 &&   m.cb>0 &&   m.c3<0 &&   m.c4<0

  m.check=    71;

elseif  m.a1>0 &&   m.a3<0 &&   m.ac>0 &&   m.b2>0 &&   m.b4<0 &&   m.bc<0 &&
        m.ca<0 &&   m.cb>0 &&   m.c3<0 &&   m.c4>0

  m.check=    73;

elseif  m.a1>0 &&   m.a3<0 &&   m.ac>0 &&   m.b2>0 &&   m.b4<0 &&   m.bc<0 &&
        m.ca<0 &&   m.cb>0 &&   m.c3>0 &&   m.c4<0

  m.check=    75;

elseif  m.a1>0 &&   m.a3<0 &&   m.ac>0 &&   m.b2>0 &&   m.b4<0 &&   m.bc<0 &&
        m.ca<0 &&   m.cb>0 &&   m.c3>0 &&   m.c4>0

  m.check=    77;

elseif  m.a1>0 &&   m.a3<0 &&   m.ac>0 &&   m.b2<0 &&   m.b4>0 &&   m.bc>0 &&
        m.ca<0 &&   m.cb<0 &&   m.c3<0 &&   m.c4>0

  m.check=    79;

elseif  m.a1>0 &&   m.a3<0 &&   m.ac>0 &&   m.b2<0 &&   m.b4>0 &&   m.bc>0 &&
        m.ca<0 &&   m.cb<0 &&   m.c3>0 &&   m.c4<0

  m.check=    81;

elseif  m.a1>0 &&   m.a3<0 &&   m.ac>0 &&   m.b2<0 &&   m.b4>0 &&   m.bc>0 &&
        m.ca<0 &&   m.cb<0 &&   m.c3>0 &&   m.c4>0

  m.check=    83;

elseif  m.a1>0 &&   m.a3<0 &&   m.ac<0 &&   m.b2>0 &&   m.b4>0 &&   m.bc<0 &&
        m.ca>0 &&   m.cb>0 &&   m.c3<0 &&   m.c4<0

  m.check=    85;

elseif  m.a1>0 &&   m.a3<0 &&   m.ac<0 &&   m.b2>0 &&   m.b4>0 &&   m.bc<0 &&
        m.ca>0 &&   m.cb>0 &&   m.c3<0 &&   m.c4>0

  m.check=    87;

elseif  m.a1>0 &&   m.a3<0 &&   m.ac<0 &&   m.b2>0 &&   m.b4>0 &&   m.bc<0 &&
        m.ca>0 &&   m.cb>0 &&   m.c3>0 &&   m.c4<0
```

```
   m.check=     89;

elseif  m.a1>0 &&    m.a3<0 &&    m.ac<0 &&    m.b2<0 &&    m.b4<0 &&    m.bc>0 &&
        m.ca>0 &&    m.cb<0 &&    m.c3<0 &&    m.c4<0

   m.check=     91;

elseif  m.a1>0 &&    m.a3<0 &&    m.ac<0 &&    m.b2<0 &&    m.b4<0 &&    m.bc>0 &&
        m.ca>0 &&    m.cb<0 &&    m.c3<0 &&    m.c4>0

   m.check=     93;

elseif  m.a1>0 &&    m.a3<0 &&    m.ac<0 &&    m.b2<0 &&    m.b4<0 &&    m.bc>0 &&
        m.ca>0 &&    m.cb<0 &&    m.c3>0 &&    m.c4<0

   m.check=     95;

elseif  m.a1>0 &&    m.a3<0 &&    m.ac<0 &&    m.b2<0 &&    m.b4<0 &&    m.bc>0 &&
        m.ca>0 &&    m.cb<0 &&    m.c3>0 &&    m.c4>0

   m.check=     97;

elseif  m.a1>0 &&    m.a3<0 &&    m.ac<0 &&    m.b2>0 &&    m.b4<0 &&    m.bc>0 &&
        m.ca>0 &&    m.cb<0 &&    m.c3<0 &&    m.c4<0

   m.check=     99;

elseif  m.a1>0 &&    m.a3<0 &&    m.ac<0 &&    m.b2>0 &&    m.b4<0 &&    m.bc>0 &&
        m.ca>0 &&    m.cb<0 &&    m.c3<0 &&    m.c4>0

   m.check=     101;

elseif  m.a1>0 &&    m.a3<0 &&    m.ac<0 &&    m.b2>0 &&    m.b4<0 &&    m.bc>0 &&
        m.ca>0 &&    m.cb<0 &&    m.c3>0 &&    m.c4<0

   m.check=     103;

elseif  m.a1>0 &&    m.a3<0 &&    m.ac<0 &&    m.b2>0 &&    m.b4<0 &&    m.bc>0 &&
        m.ca>0 &&    m.cb<0 &&    m.c3>0 &&    m.c4>0

   m.check=     105;

elseif  m.a1>0 &&    m.a3<0 &&    m.ac<0 &&    m.b2<0 &&    m.b4>0 &&    m.bc<0 &&
        m.ca>0 &&    m.cb>0 &&    m.c3<0 &&    m.c4<0

   m.check=     107;

elseif  m.a1>0 &&    m.a3<0 &&    m.ac<0 &&    m.b2<0 &&    m.b4>0 &&    m.bc<0 &&
        m.ca>0 &&    m.cb>0 &&    m.c3<0 &&    m.c4>0

   m.check=     109;

elseif  m.a1>0 &&    m.a3<0 &&    m.ac<0 &&    m.b2<0 &&    m.b4>0 &&    m.bc<0 &&
        m.ca>0 &&    m.cb>0 &&    m.c3>0 &&    m.c4<0

   m.check=     111;
```

```
elseif  m.a1>0 &&  m.a3<0 &&  m.ac<0 &&  m.b2>0 &&  m.b4<0 &&  m.bc<0 &&
        m.ca>0 &&  m.cb>0 &&  m.c3<0 &&  m.c4<0

   m.check=  113;

elseif  m.a1>0 &&  m.a3<0 &&  m.ac<0 &&  m.b2>0 &&  m.b4<0 &&  m.bc<0 &&
        m.ca>0 &&  m.cb>0 &&  m.c3<0 &&  m.c4>0

   m.check=  115;

elseif  m.a1>0 &&  m.a3<0 &&  m.ac<0 &&  m.b2>0 &&  m.b4<0 &&  m.bc<0 &&
        m.ca>0 &&  m.cb>0 &&  m.c3>0 &&  m.c4<0

   m.check=  117;

elseif  m.a1>0 &&  m.a3<0 &&  m.ac<0 &&  m.b2<0 &&  m.b4>0 &&  m.bc>0 &&
        m.ca>0 &&  m.cb<0 &&  m.c3<0 &&  m.c4<0

   m.check=  119;

elseif  m.a1>0 &&  m.a3<0 &&  m.ac<0 &&  m.b2<0 &&  m.b4>0 &&  m.bc>0 &&
        m.ca>0 &&  m.cb<0 &&  m.c3<0 &&  m.c4>0

   m.check=  121;

elseif  m.a1>0 &&  m.a3<0 &&  m.ac<0 &&  m.b2<0 &&  m.b4>0 &&  m.bc>0 &&
        m.ca>0 &&  m.cb<0 &&  m.c3>0 &&  m.c4<0

   m.check=  123;

elseif  m.a1>0 &&  m.a3<0 &&  m.ac<0 &&  m.b2<0 &&  m.b4>0 &&  m.bc>0 &&
        m.ca>0 &&  m.cb<0 &&  m.c3>0 &&  m.c4>0

   m.check=  125;

else

   m.check= NaN;

end


%_____________________________________________________________________________________

%%% STEP 16

%% Calculate the mass balance (B) at each of the three internal nodes

      B.ina=m.a1+m.ac+m.a3;

      B.inb=m.b2+m.bc+m.b4;

      B.inc=m.ca+m.cb+m.c3+m.c4;

%% Calculate the total mass balance of the network as the (absolute error)

      B.check= abs(B.ina) + abs(B.inb)+abs(B.inc);

%% Calculate the mass balance in the network as the (relative error)
```

```
      B.rel=
B.check/((abs(m.a1)+abs(m.ac)+abs(m.a3)+abs(m.b2)+abs(m.bc)+abs(m.b4)+abs(m.ca)+abs(m.cb)+abs(m.c
3)+abs(m.c4))/10);
%_____
%%% STEP 17
%% Calculate the ach parameter according to function named ach_FNC10
    H.bld= (m.bld*3600)/(S(w.29)*vol.bld);
    pfun.pfun=S(w.31);
     ach(jj) = ach_FNC10(m.S.w.vol.message.jj.B.H.pfun);


jj = jj+1;
          end
        end
    end
 end
end
toc
%_____
%%% STEP 18
%% Selection of the feasible jj results
% Create table of results
ach_table = struct2table (ach);
x0_table = array2table (x0);
P_table = array2table(P_solution);
% Selection according to index of feasibility
index_feasibility = find(strcmp(ach_table.feasibility.'feasibile'));
index_nofeasibility = setdiff([1:height(ach_table)].index_feasibility.'stable')';
% Create tables with only acceptable (feasible) results
ach_fea = ach_table(index_feasibility.:);
x0_fea = x0_table(index_feasibility.:);
P_fea = P_table(index_feasibility.:);
% Create a unique table. reporting the main input and output data
```

```
Tfea = [x0_fea. P_fea. ach_fea];

% Sort rows. for each climate scenario. according to the absolute error (B.check)

TfeaS = sortrows(Tfea.[19 21].'ascend');


%%Save result in an Excel or csv file

writetable(TfeaS. 'C:\Users\LENOVO\Desktop\30_EDIFICI\MOD_11_man\RESULTS\B63_soloUC.xlsx')

%_____

%%% STEP 19 (not yet implemented)

%% For all the 64 (or 32) climate scenarios for the analyzed building b save the best solution

%% Create a vector R from Table TfeaS

%_____

%%% STEP 20 (not yet implemented)

%% the analysis for the building b is finished (end of cycle b=1)

%% the cycle for steps to b=b+1;

%_____

%%% STEP 21(not yet implemented)

%% the analysis for all the builing in the analysed zone is finished (end of cycle b=n)

%% For each building in the zone. the best solution of ach is reported for each of the 64 (or 32) climate scenarios that have been evaluated

% Save results in a final output database

%**********ACH FUNCTION: ach_FNC10**********

function ach = ach_FNC10 (m.S.w.vol.message.jj.B.H.pfun)

if      m.check==2

  ach.a=(abs(m.a1+m.a3)*3600)/(S(w.29)*vol.a);      ach.a_ex='NaN';      ach.atot='NaN';
      ach.b=(abs(m.b2+m.b4)*3600)/(S(w.29)*vol.b);ach.b_ex='NaN';      ach.btot='NaN';ach.c='NaN';
      ach.c_ex=(abs(m.ca+m.cb)*3600)/(S(w.30)*vol.c);      ach.ctot='NaN';

elseif  m.check==4

  ach.a=(abs(m.a1+m.a3)*3600)/(S(w.29)*vol.a);      ach.a_ex='NaN';      ach.atot='NaN';
      ach.b=(abs(m.b2+m.b4)*3600)/(S(w.29)*vol.b);ach.b_ex='NaN';      ach.btot='NaN';
      ach.c=(abs(m.c4)*3600)/(S(w.30)*vol.c);      ach.c_ex=(abs(m.ca+m.cb)*3600)/(S(w.30)*vol.c);
      ach.ctot=(abs(m.ca+m.cb+m.c4)*3600)/(S(w.30)*vol.c);

elseif  m.check==6

  ach.a=(abs(m.a1+m.a3)*3600)/(S(w.29)*vol.a);      ach.a_ex='NaN';      ach.atot='NaN';
      ach.b=(abs(m.b2+m.b4)*3600)/(S(w.29)*vol.b);ach.b_ex='NaN';      ach.btot='NaN';
```

```
        ach.c=(abs(m.c3)*3600)/(S(w.30)*vol.c);          ach.c_ex=(abs(m.ca+m.cb)*3600)/(S(w.30)*vol.c);
        ach.ctot=(abs(m.ca+m.cb+m.c3)*3600)/(S(w.30)*vol.c);

elseif  m.check==8

   ach.a=(abs(m.a1+m.a3)*3600)/(S(w.29)*vol.a);      ach.a_ex='NaN';          ach.atot='NaN';ach.b='NaN';
        ach.b_ex=(abs(m.bc)*3600)/(S(w.29)*vol.b);   ach.btot='NaN';ach.c='NaN';
        ach.c_ex=(abs(m.ca)*3600)/(S(w.30)*vol.c);   ach.ctot='NaN';

elseif  m.check==10

   ach.a=(abs(m.a1+m.a3)*3600)/(S(w.29)*vol.a);      ach.a_ex='NaN';          ach.atot='NaN';ach.b='NaN';
        ach.b_ex=(abs(m.bc)*3600)/(S(w.29)*vol.b);   ach.btot='NaN';
        ach.c=(abs(m.c4)*3600)/(S(w.30)*vol.c);      ach.c_ex=(abs(m.ca)*3600)/(S(w.30)*vol.c);
        ach.ctot=(abs(m.ca+m.c4)*3600)/(S(w.30)*vol.c);

elseif  m.check==12

   ach.a=(abs(m.a1+m.a3)*3600)/(S(w.29)*vol.a);      ach.a_ex='NaN';          ach.atot='NaN';ach.b='NaN';
        ach.b_ex=(abs(m.bc)*3600)/(S(w.29)*vol.b);   ach.btot='NaN';
        ach.c=(abs(m.c3)*3600)/(S(w.30)*vol.c);      ach.c_ex=(abs(m.ca)*3600)/(S(w.30)*vol.c);
        ach.ctot=(abs(m.ca+m.c3)*3600)/(S(w.30)*vol.c);

elseif  m.check==14

   ach.a=(abs(m.a1+m.a3)*3600)/(S(w.29)*vol.a);      ach.a_ex='NaN';          ach.atot='NaN';ach.b='NaN';
        ach.b_ex=(abs(m.bc)*3600)/(S(w.29)*vol.b);   ach.btot='NaN';
        ach.c=(abs(m.c3+m.c4)*3600)/(S(w.30)*vol.c); ach.c_ex=(abs(m.ca)*3600)/(S(w.30)*vol.c);
        ach.ctot=(abs(m.ca+m.c3+m.c4)*3600)/(S(w.30)*vol.c);

elseif  m.check==16

   ach.a=(abs(m.a1+m.a3)*3600)/(S(w.29)*vol.a);      ach.a_ex='NaN';          ach.atot='NaN';
        ach.b=(abs(m.b2)*3600)/(S(w.29)*vol.b);      ach.b_ex=(abs(m.bc)*3600)/(S(w.29)*vol.b);
        ach.btot=(abs(m.b2+m.bc)*3600)/(S(w.29)*vol.b);      ach.c='NaN';
        ach.c_ex=(abs(m.ca)*3600)/(S(w.30)*vol.c);   ach.ctot='NaN';

elseif  m.check==18

   ach.a=(abs(m.a1+m.a3)*3600)/(S(w.29)*vol.a);      ach.a_ex='NaN';          ach.atot='NaN';
        ach.b=(abs(m.b2)*3600)/(S(w.29)*vol.b);      ach.b_ex=(abs(m.bc)*3600)/(S(w.29)*vol.b);
        ach.btot=(abs(m.b2+m.bc)*3600)/(S(w.29)*vol.b);      ach.c=(abs(m.c4)*3600)/(S(w.30)*vol.c);
        ach.c_ex=(abs(m.ca)*3600)/(S(w.30)*vol.c);   ach.ctot=(abs(m.ca+m.c4)*3600)/(S(w.30)*vol.c);

elseif  m.check==20

   ach.a=(abs(m.a1+m.a3)*3600)/(S(w.29)*vol.a);      ach.a_ex='NaN';          ach.atot='NaN';
        ach.b=(abs(m.b2)*3600)/(S(w.29)*vol.b);      ach.b_ex=(abs(m.bc)*3600)/(S(w.29)*vol.b);
        ach.btot=(abs(m.b2+m.bc)*3600)/(S(w.29)*vol.b);      ach.c=(abs(m.c3)*3600)/(S(w.30)*vol.c);
        ach.c_ex=(abs(m.ca)*3600)/(S(w.30)*vol.c);   ach.ctot=(abs(m.ca+m.c3)*3600)/(S(w.30)*vol.c);

elseif  m.check==22

   ach.a=(abs(m.a1+m.a3)*3600)/(S(w.29)*vol.a);      ach.a_ex='NaN';          ach.atot='NaN';
        ach.b=(abs(m.b2)*3600)/(S(w.29)*vol.b);      ach.b_ex=(abs(m.bc)*3600)/(S(w.29)*vol.b);
```

```
        ach.btot=(abs(m.b2+m.bc)*3600)/(S(w.29)*vol.b);
        ach.c=(abs(m.c3+m.c4)*3600)/(S(w.30)*vol.c);  ach.c_ex=(abs(m.ca)*3600)/(S(w.30)*vol.c);
        ach.ctot=(abs(m.ca+m.c3+m.c4)*3600)/(S(w.30)*vol.c);

elseif  m.check==24

   ach.a=(abs(m.a1+m.a3)*3600)/(S(w.29)*vol.a);        ach.a_ex='NaN';         ach.atot='NaN';
        ach.b=(abs(m.b4)*3600)/(S(w.29)*vol.b);        ach.b_ex='NaN';         ach.btot='NaN';ach.c='NaN';
        ach.c_ex=(abs(m.ca+m.cb)*3600)/(S(w.30)*vol.c);      ach.ctot='NaN';

elseif  m.check==26

   ach.a=(abs(m.a1+m.a3)*3600)/(S(w.29)*vol.a);        ach.a_ex='NaN';         ach.atot='NaN';
        ach.b=(abs(m.b4)*3600)/(S(w.29)*vol.b);        ach.b_ex='NaN';         ach.btot='NaN';
        ach.c=(abs(m.c4)*3600)/(S(w.30)*vol.c);        ach.c_ex=(abs(m.ca+m.cb)*3600)/(S(w.30)*vol.c);
        ach.ctot=(abs(m.ca+m.cb+m.c4)*3600)/(S(w.30)*vol.c);

elseif  m.check==28

   ach.a=(abs(m.a1+m.a3)*3600)/(S(w.29)*vol.a);        ach.a_ex='NaN';         ach.atot='NaN';
        ach.b=(abs(m.b4)*3600)/(S(w.29)*vol.b);        ach.b_ex='NaN';         ach.btot='NaN';
        ach.c=(abs(m.c3)*3600)/(S(w.30)*vol.c);        ach.c_ex=(abs(m.ca+m.cb)*3600)/(S(w.30)*vol.c);
        ach.ctot=(abs(m.ca+m.cb+m.c3)*3600)/(S(w.30)*vol.c);

elseif  m.check==30

   ach.a=(abs(m.a1+m.a3)*3600)/(S(w.29)*vol.a);        ach.a_ex='NaN';         ach.atot='NaN';
        ach.b=(abs(m.b2)*3600)/(S(w.29)*vol.b);        ach.b_ex='NaN';         ach.btot='NaN';ach.c='NaN';
        ach.c_ex=(abs(m.ca+m.cb)*3600)/(S(w.30)*vol.c);      ach.ctot='NaN';

elseif  m.check==32

   ach.a=(abs(m.a1+m.a3)*3600)/(S(w.29)*vol.a);        ach.a_ex='NaN';         ach.atot='NaN';
        ach.b=(abs(m.b2)*3600)/(S(w.29)*vol.b);        ach.b_ex='NaN';         ach.btot='NaN';
        ach.c=(abs(m.c4)*3600)/(S(w.30)*vol.c);        ach.c_ex=(abs(m.ca+m.cb)*3600)/(S(w.30)*vol.c);
        ach.ctot=(abs(m.ca+m.cb+m.c4)*3600)/(S(w.30)*vol.c);

elseif  m.check==34

   ach.a=(abs(m.a1+m.a3)*3600)/(S(w.29)*vol.a);        ach.a_ex='NaN';         ach.atot='NaN';
        ach.b=(abs(m.b2)*3600)/(S(w.29)*vol.b);        ach.b_ex='NaN';         ach.btot='NaN';
        ach.c=(abs(m.c3)*3600)/(S(w.30)*vol.c);        ach.c_ex=(abs(m.ca+m.cb)*3600)/(S(w.30)*vol.c);
        ach.ctot=(abs(m.ca+m.cb+m.c3)*3600)/(S(w.30)*vol.c);

elseif  m.check==36

   ach.a=(abs(m.a1+m.a3)*3600)/(S(w.29)*vol.a);        ach.a_ex='NaN';         ach.atot='NaN';
        ach.b=(abs(m.b4)*3600)/(S(w.29)*vol.b);        ach.b_ex=(abs(m.bc)*3600)/(S(w.29)*vol.b);
        ach.btot=(abs(m.b4+m.bc)*3600)/(S(w.29)*vol.b);      ach.c='NaN';
        ach.c_ex=(abs(m.ca)*3600)/(S(w.30)*vol.c);     ach.ctot='NaN';

elseif  m.check==38

   ach.a=(abs(m.a1+m.a3)*3600)/(S(w.29)*vol.a);        ach.a_ex='NaN';         ach.atot='NaN';
        ach.b=(abs(m.b4)*3600)/(S(w.29)*vol.b);        ach.b_ex=(abs(m.bc)*3600)/(S(w.29)*vol.b);
```

```
        ach.btot=(abs(m.b4+m.bc)*3600)/(S(w.29)*vol.b);      ach.c=(abs(m.c4)*3600)/(S(w.30)*vol.c);
        ach.c_ex=(abs(m.ca)*3600)/(S(w.30)*vol.c);    ach.ctot=(abs(m.ca+m.c4)*3600)/(S(w.30)*vol.c);

elseif  m.check==40

  ach.a=(abs(m.a1+m.a3)*3600)/(S(w.29)*vol.a);       ach.a_ex='NaN';         ach.atot='NaN';
        ach.b=(abs(m.b4)*3600)/(S(w.29)*vol.b);       ach.b_ex=(abs(m.bc)*3600)/(S(w.29)*vol.b);
        ach.btot=(abs(m.b4+m.bc)*3600)/(S(w.29)*vol.b);      ach.c=(abs(m.c3)*3600)/(S(w.30)*vol.c);
        ach.c_ex=(abs(m.ca)*3600)/(S(w.30)*vol.c);    ach.ctot=(abs(m.ca+m.c3)*3600)/(S(w.30)*vol.c);

elseif  m.check==42

  ach.a=(abs(m.a1+m.a3)*3600)/(S(w.29)*vol.a);       ach.a_ex='NaN';         ach.atot='NaN';
        ach.b=(abs(m.b4)*3600)/(S(w.29)*vol.b);       ach.b_ex=(abs(m.bc)*3600)/(S(w.29)*vol.b);
        ach.btot=(abs(m.b4+m.bc)*3600)/(S(w.29)*vol.b);
        ach.c=(abs(m.c3+m.c4)*3600)/(S(w.30)*vol.c);  ach.c_ex=(abs(m.ca)*3600)/(S(w.30)*vol.c);
        ach.ctot=(abs(m.ca+m.c3+m.c4)*3600)/(S(w.30)*vol.c);

elseif  m.check==44

  ach.a=(abs(m.a1)*3600)/(S(w.29)*vol.a);      ach.a_ex=(abs(m.ac)*3600)/(S(w.29)*vol.a);
        ach.atot=(abs(m.a1+m.ac)*3600)/(S(w.29)*vol.a);
        ach.b=(abs(m.b2+m.b4)*3600)/(S(w.29)*vol.b);ach.b_ex='NaN';         ach.btot='NaN';ach.c='NaN';
        ach.c_ex=(abs(m.cb)*3600)/(S(w.30)*vol.c);    ach.ctot='NaN';

elseif  m.check==46

  ach.a=(abs(m.a1)*3600)/(S(w.29)*vol.a);      ach.a_ex=(abs(m.ac)*3600)/(S(w.29)*vol.a);
        ach.atot=(abs(m.a1+m.ac)*3600)/(S(w.29)*vol.a);
        ach.b=(abs(m.b2+m.b4)*3600)/(S(w.29)*vol.b);ach.b_ex='NaN';         ach.btot='NaN';
        ach.c=(abs(m.c4)*3600)/(S(w.30)*vol.c);         ach.c_ex=(abs(m.cb)*3600)/(S(w.30)*vol.c);
        ach.ctot=(abs(m.cb+m.c4)*3600)/(S(w.30)*vol.c);

elseif  m.check==48

  ach.a=(abs(m.a1)*3600)/(S(w.29)*vol.a);      ach.a_ex=(abs(m.ac)*3600)/(S(w.29)*vol.a);
        ach.atot=(abs(m.a1+m.ac)*3600)/(S(w.29)*vol.a);
        ach.b=(abs(m.b2+m.b4)*3600)/(S(w.29)*vol.b);ach.b_ex='NaN';         ach.btot='NaN';
        ach.c=(abs(m.c3)*3600)/(S(w.30)*vol.c);         ach.c_ex=(abs(m.cb)*3600)/(S(w.30)*vol.c);
        ach.ctot=(abs(m.cb+m.c3)*3600)/(S(w.30)*vol.c);

elseif  m.check==50

  ach.a=(abs(m.a1)*3600)/(S(w.29)*vol.a);      ach.a_ex=(abs(m.ac)*3600)/(S(w.29)*vol.a);
        ach.atot=(abs(m.a1+m.ac)*3600)/(S(w.29)*vol.a);
        ach.b=(abs(m.b2+m.b4)*3600)/(S(w.29)*vol.b);ach.b_ex='NaN';         ach.btot='NaN';
        ach.c=(abs(m.c3+m.c4)*3600)/(S(w.30)*vol.c);  ach.c_ex=(abs(m.cb)*3600)/(S(w.30)*vol.c);
        ach.ctot=(abs(m.cb+m.c3+m.c4)*3600)/(S(w.30)*vol.c);

elseif  m.check==52

  ach.a=(abs(m.a1)*3600)/(S(w.29)*vol.a);      ach.a_ex=(abs(m.ac)*3600)/(S(w.29)*vol.a);
        ach.atot=(abs(m.a1+m.ac)*3600)/(S(w.29)*vol.a);       ach.b='NaN';
```

```
        ach.b_ex=(abs(m.bc)*3600)/(S(w.29)*vol.b);    ach.btot='NaN';
        ach.c=(abs(m.c4)*3600)/(S(w.30)*vol.c);       ach.c_ex='NaN';       ach.ctot='NaN';

elseif  m.check==54

  ach.a=(abs(m.a1)*3600)/(S(w.29)*vol.a);     ach.a_ex=(abs(m.ac)*3600)/(S(w.29)*vol.a);
        ach.atot=(abs(m.a1+m.ac)*3600)/(S(w.29)*vol.a);     ach.b='NaN';
        ach.b_ex=(abs(m.bc)*3600)/(S(w.29)*vol.b);    ach.btot='NaN';
        ach.c=(abs(m.c3)*3600)/(S(w.30)*vol.c);       ach.c_ex='NaN';       ach.ctot='NaN';

elseif  m.check==56

  ach.a=(abs(m.a1)*3600)/(S(w.29)*vol.a);     ach.a_ex=(abs(m.ac)*3600)/(S(w.29)*vol.a);
        ach.atot=(abs(m.a1+m.ac)*3600)/(S(w.29)*vol.a);     ach.b='NaN';
        ach.b_ex=(abs(m.bc)*3600)/(S(w.29)*vol.b);    ach.btot='NaN';
        ach.c=(abs(m.c3+m.c4)*3600)/(S(w.30)*vol.c);  ach.c_ex='NaN';       ach.ctot='NaN';

elseif  m.check==58

  ach.a=(abs(m.a1)*3600)/(S(w.29)*vol.a);     ach.a_ex=(abs(m.ac)*3600)/(S(w.29)*vol.a);
        ach.atot=(abs(m.a1+m.ac)*3600)/(S(w.29)*vol.a);     ach.b=(abs(m.b2)*3600)/(S(w.29)*vol.b);
        ach.b_ex=(abs(m.bc)*3600)/(S(w.29)*vol.b);    ach.btot=(abs(m.b2+m.bc)*3600)/(S(w.29)*vol.b);
        ach.c=(abs(m.c4)*3600)/(S(w.30)*vol.c);       ach.c_ex='NaN';       ach.ctot='NaN';

elseif  m.check==60

  ach.a=(abs(m.a1)*3600)/(S(w.29)*vol.a);     ach.a_ex=(abs(m.ac)*3600)/(S(w.29)*vol.a);
        ach.atot=(abs(m.a1+m.ac)*3600)/(S(w.29)*vol.a);     ach.b=(abs(m.b2)*3600)/(S(w.29)*vol.b);
        ach.b_ex=(abs(m.bc)*3600)/(S(w.29)*vol.b);    ach.btot=(abs(m.b2+m.bc)*3600)/(S(w.29)*vol.b);
        ach.c=(abs(m.c3)*3600)/(S(w.30)*vol.c);       ach.c_ex='NaN';       ach.ctot='NaN';

elseif  m.check==62

  ach.a=(abs(m.a1)*3600)/(S(w.29)*vol.a);     ach.a_ex=(abs(m.ac)*3600)/(S(w.29)*vol.a);
        ach.atot=(abs(m.a1+m.ac)*3600)/(S(w.29)*vol.a);     ach.b=(abs(m.b2)*3600)/(S(w.29)*vol.b);
        ach.b_ex=(abs(m.bc)*3600)/(S(w.29)*vol.b);    ach.btot=(abs(m.b2+m.bc)*3600)/(S(w.29)*vol.b);
        ach.c=(abs(m.c3+m.c4)*3600)/(S(w.30)*vol.c);  ach.c_ex='NaN';       ach.ctot='NaN';

elseif  m.check==64

  ach.a=(abs(m.a1)*3600)/(S(w.29)*vol.a);     ach.a_ex=(abs(m.ac)*3600)/(S(w.29)*vol.a);
        ach.atot=(abs(m.a1+m.ac)*3600)/(S(w.29)*vol.a);     ach.b=(abs(m.b4)*3600)/(S(w.29)*vol.b);
        ach.b_ex='NaN';       ach.btot='NaN';ach.c='NaN';   ach.c_ex=(abs(m.cb)*3600)/(S(w.30)*vol.c);
        ach.ctot='NaN';

elseif  m.check==66

  ach.a=(abs(m.a1)*3600)/(S(w.29)*vol.a);     ach.a_ex=(abs(m.ac)*3600)/(S(w.29)*vol.a);
        ach.atot=(abs(m.a1+m.ac)*3600)/(S(w.29)*vol.a);     ach.b=(abs(m.b4)*3600)/(S(w.29)*vol.b);
        ach.b_ex='NaN';       ach.btot='NaN';ach.c=(abs(m.c4)*3600)/(S(w.30)*vol.c);
        ach.c_ex=(abs(m.cb)*3600)/(S(w.30)*vol.c);    ach.ctot=(abs(m.cb+m.c4)*3600)/(S(w.30)*vol.c);

elseif  m.check==68
```

```
  ach.a=(abs(m.a1)*3600)/(S(w.29)*vol.a);      ach.a_ex=(abs(m.ac)*3600)/(S(w.29)*vol.a);
       ach.atot=(abs(m.a1+m.ac)*3600)/(S(w.29)*vol.a);      ach.b=(abs(m.b4)*3600)/(S(w.29)*vol.b);
       ach.b_ex='NaN';          ach.btot='NaN';ach.c=(abs(m.c3)*3600)/(S(w.30)*vol.c);
       ach.c_ex=(abs(m.cb)*3600)/(S(w.30)*vol.c);     ach.ctot=(abs(m.cb+m.c3)*3600)/(S(w.30)*vol.c);

elseif   m.check==70

  ach.a=(abs(m.a1)*3600)/(S(w.29)*vol.a);      ach.a_ex=(abs(m.ac)*3600)/(S(w.29)*vol.a);
       ach.atot=(abs(m.a1+m.ac)*3600)/(S(w.29)*vol.a);      ach.b=(abs(m.b4)*3600)/(S(w.29)*vol.b);
       ach.b_ex='NaN';          ach.btot='NaN';ach.c=(abs(m.c3+m.c4)*3600)/(S(w.30)*vol.c);
       ach.c_ex=(abs(m.cb)*3600)/(S(w.30)*vol.c);
       ach.ctot=(abs(m.cb+m.c3+m.c4)*3600)/(S(w.30)*vol.c);

elseif   m.check==72

  ach.a=(abs(m.a1)*3600)/(S(w.29)*vol.a);      ach.a_ex=(abs(m.ac)*3600)/(S(w.29)*vol.a);
       ach.atot=(abs(m.a1+m.ac)*3600)/(S(w.29)*vol.a);      ach.b=(abs(m.b2)*3600)/(S(w.29)*vol.b);
       ach.b_ex='NaN';          ach.btot='NaN';ach.c='NaN';     ach.c_ex=(abs(m.cb)*3600)/(S(w.30)*vol.c);
       ach.ctot='NaN';

elseif   m.check==74

  ach.a=(abs(m.a1)*3600)/(S(w.29)*vol.a);      ach.a_ex=(abs(m.ac)*3600)/(S(w.29)*vol.a);
       ach.atot=(abs(m.a1+m.ac)*3600)/(S(w.29)*vol.a);      ach.b=(abs(m.b2)*3600)/(S(w.29)*vol.b);
       ach.b_ex='NaN';          ach.btot='NaN';ach.c=(abs(m.c4)*3600)/(S(w.30)*vol.c);
       ach.c_ex=(abs(m.cb)*3600)/(S(w.30)*vol.c);     ach.ctot=(abs(m.cb+m.c4)*3600)/(S(w.30)*vol.c);

elseif   m.check==76

  ach.a=(abs(m.a1)*3600)/(S(w.29)*vol.a);      ach.a_ex=(abs(m.ac)*3600)/(S(w.29)*vol.a);
       ach.atot=(abs(m.a1+m.ac)*3600)/(S(w.29)*vol.a);      ach.b=(abs(m.b2)*3600)/(S(w.29)*vol.b);
       ach.b_ex='NaN';          ach.btot='NaN';ach.c=(abs(m.c3)*3600)/(S(w.30)*vol.c);
       ach.c_ex=(abs(m.cb)*3600)/(S(w.30)*vol.c);     ach.ctot=(abs(m.cb+m.c3)*3600)/(S(w.30)*vol.c);

elseif   m.check==78

  ach.a=(abs(m.a1)*3600)/(S(w.29)*vol.a);      ach.a_ex=(abs(m.ac)*3600)/(S(w.29)*vol.a);
       ach.atot=(abs(m.a1+m.ac)*3600)/(S(w.29)*vol.a);      ach.b=(abs(m.b2)*3600)/(S(w.29)*vol.b);
       ach.b_ex='NaN';          ach.btot='NaN';ach.c=(abs(m.c3+m.c4)*3600)/(S(w.30)*vol.c);
       ach.c_ex=(abs(m.cb)*3600)/(S(w.30)*vol.c);
       ach.ctot=(abs(m.cb+m.c3+m.c4)*3600)/(S(w.30)*vol.c);

elseif   m.check==80

  ach.a=(abs(m.a1)*3600)/(S(w.29)*vol.a);      ach.a_ex=(abs(m.ac)*3600)/(S(w.29)*vol.a);
       ach.atot=(abs(m.a1+m.ac)*3600)/(S(w.29)*vol.a);      ach.b=(abs(m.b4)*3600)/(S(w.29)*vol.b);
       ach.b_ex=(abs(m.bc)*3600)/(S(w.29)*vol.b);     ach.btot=(abs(m.b4+m.bc)*3600)/(S(w.29)*vol.b);
       ach.c=(abs(m.c4)*3600)/(S(w.30)*vol.c);          ach.c_ex='NaN';          ach.ctot='NaN';

elseif   m.check==82

  ach.a=(abs(m.a1)*3600)/(S(w.29)*vol.a);      ach.a_ex=(abs(m.ac)*3600)/(S(w.29)*vol.a);
       ach.atot=(abs(m.a1+m.ac)*3600)/(S(w.29)*vol.a);      ach.b=(abs(m.b4)*3600)/(S(w.29)*vol.b);
```

```
        ach.b_ex=(abs(m.bc)*3600)/(S(w.29)*vol.b);    ach.btot=(abs(m.b4+m.bc)*3600)/(S(w.29)*vol.b);
        ach.c=(abs(m.c3)*3600)/(S(w.30)*vol.c);       ach.c_ex='NaN';          ach.ctot='NaN';

elseif  m.check==84

  ach.a=(abs(m.a1)*3600)/(S(w.29)*vol.a);     ach.a_ex=(abs(m.ac)*3600)/(S(w.29)*vol.a);
        ach.atot=(abs(m.a1+m.ac)*3600)/(S(w.29)*vol.a);     ach.b=(abs(m.b4)*3600)/(S(w.29)*vol.b);
        ach.b_ex=(abs(m.bc)*3600)/(S(w.29)*vol.b);    ach.btot=(abs(m.b4+m.bc)*3600)/(S(w.29)*vol.b);
        ach.c=(abs(m.c3+m.c4)*3600)/(S(w.30)*vol.c); ach.c_ex='NaN';          ach.ctot='NaN';

elseif  m.check==86

  ach.a=(abs(m.a1)*3600)/(S(w.29)*vol.a);     ach.a_ex='NaN';          ach.atot='NaN';
        ach.b=(abs(m.b2+m.b4)*3600)/(S(w.29)*vol.b);ach.b_ex='NaN';          ach.btot='NaN';ach.c='NaN';
        ach.c_ex=(abs(m.ca+m.cb)*3600)/(S(w.30)*vol.c);     ach.ctot='NaN';

elseif  m.check==88

  ach.a=(abs(m.a1)*3600)/(S(w.29)*vol.a);     ach.a_ex='NaN';          ach.atot='NaN';
        ach.b=(abs(m.b2+m.b4)*3600)/(S(w.29)*vol.b);ach.b_ex='NaN';          ach.btot='NaN';
        ach.c=(abs(m.c4)*3600)/(S(w.30)*vol.c);       ach.c_ex=(abs(m.ca+m.cb)*3600)/(S(w.30)*vol.c);
        ach.ctot=(abs(m.ca+m.cb+m.c4)*3600)/(S(w.30)*vol.c);

elseif  m.check==90

  ach.a=(abs(m.a1)*3600)/(S(w.29)*vol.a);     ach.a_ex='NaN';          ach.atot='NaN';
        ach.b=(abs(m.b2+m.b4)*3600)/(S(w.29)*vol.b);ach.b_ex='NaN';          ach.btot='NaN';
        ach.c=(abs(m.c3)*3600)/(S(w.30)*vol.c);       ach.c_ex=(abs(m.ca+m.cb)*3600)/(S(w.30)*vol.c);
        ach.ctot=(abs(m.ca+m.cb+m.c3)*3600)/(S(w.30)*vol.c);

elseif  m.check==92

  ach.a=(abs(m.a1)*3600)/(S(w.29)*vol.a);     ach.a_ex='NaN';          ach.atot='NaN';ach.b='NaN';
        ach.b_ex=(abs(m.bc)*3600)/(S(w.29)*vol.b);    ach.btot='NaN';ach.c='NaN';
        ach.c_ex=(abs(m.ca)*3600)/(S(w.30)*vol.c);    ach.ctot='NaN';

elseif  m.check==94

  ach.a=(abs(m.a1)*3600)/(S(w.29)*vol.a);     ach.a_ex='NaN';          ach.atot='NaN';ach.b='NaN';
        ach.b_ex=(abs(m.bc)*3600)/(S(w.29)*vol.b);    ach.btot='NaN';
        ach.c=(abs(m.c4)*3600)/(S(w.30)*vol.c);       ach.c_ex=(abs(m.ca)*3600)/(S(w.30)*vol.c);
        ach.ctot=(abs(m.ca+m.c4)*3600)/(S(w.30)*vol.c);

elseif  m.check==96

  ach.a=(abs(m.a1)*3600)/(S(w.29)*vol.a);     ach.a_ex='NaN';          ach.atot='NaN';ach.b='NaN';
        ach.b_ex=(abs(m.bc)*3600)/(S(w.29)*vol.b);    ach.btot='NaN';
        ach.c=(abs(m.c3)*3600)/(S(w.30)*vol.c);       ach.c_ex=(abs(m.ca)*3600)/(S(w.30)*vol.c);
        ach.ctot=(abs(m.ca+m.c3)*3600)/(S(w.30)*vol.c);

elseif  m.check==98

  ach.a=(abs(m.a1)*3600)/(S(w.29)*vol.a);     ach.a_ex='NaN';          ach.atot='NaN';ach.b='NaN';
        ach.b_ex=(abs(m.bc)*3600)/(S(w.29)*vol.b);    ach.btot='NaN';
```

```
        ach.c=(abs(m.c3+m.c4)*3600)/(S(w.30)*vol.c);  ach.c_ex=(abs(m.ca)*3600)/(S(w.30)*vol.c);
        ach.ctot=(abs(m.ca+m.c3+m.c4)*3600)/(S(w.30)*vol.c);

elseif    m.check==100

   ach.a=(abs(m.a1)*3600)/(S(w.29)*vol.a);       ach.a_ex='NaN';          ach.atot='NaN';
        ach.b=(abs(m.b2)*3600)/(S(w.29)*vol.b);          ach.b_ex=(abs(m.bc)*3600)/(S(w.29)*vol.b);
        ach.btot=(abs(m.b2+m.bc)*3600)/(S(w.29)*vol.b);        ach.c='NaN';
        ach.c_ex=(abs(m.ca)*3600)/(S(w.30)*vol.c);      ach.ctot='NaN';

elseif    m.check==102

   ach.a=(abs(m.a1)*3600)/(S(w.29)*vol.a);       ach.a_ex='NaN';          ach.atot='NaN';
        ach.b=(abs(m.b2)*3600)/(S(w.29)*vol.b);          ach.b_ex=(abs(m.bc)*3600)/(S(w.29)*vol.b);
        ach.btot=(abs(m.b2+m.bc)*3600)/(S(w.29)*vol.b);        ach.c=(abs(m.c4)*3600)/(S(w.30)*vol.c);
        ach.c_ex=(abs(m.ca)*3600)/(S(w.30)*vol.c);      ach.ctot=(abs(m.ca+m.c4)*3600)/(S(w.30)*vol.c);

elseif    m.check==104

   ach.a=(abs(m.a1)*3600)/(S(w.29)*vol.a);       ach.a_ex='NaN';          ach.atot='NaN';
        ach.b=(abs(m.b2)*3600)/(S(w.29)*vol.b);          ach.b_ex=(abs(m.bc)*3600)/(S(w.29)*vol.b);
        ach.btot=(abs(m.b2+m.bc)*3600)/(S(w.29)*vol.b);        ach.c=(abs(m.c3)*3600)/(S(w.30)*vol.c);
        ach.c_ex=(abs(m.ca)*3600)/(S(w.30)*vol.c);      ach.ctot=(abs(m.ca+m.c3)*3600)/(S(w.30)*vol.c);

elseif    m.check==106

   ach.a=(abs(m.a1)*3600)/(S(w.29)*vol.a);       ach.a_ex='NaN';          ach.atot='NaN';
        ach.b=(abs(m.b2)*3600)/(S(w.29)*vol.b);          ach.b_ex=(abs(m.bc)*3600)/(S(w.29)*vol.b);
        ach.btot=(abs(m.b2+m.bc)*3600)/(S(w.29)*vol.b);
        ach.c=(abs(m.c3+m.c4)*3600)/(S(w.30)*vol.c);  ach.c_ex=(abs(m.ca)*3600)/(S(w.30)*vol.c);
        ach.ctot=(abs(m.ca+m.c3+m.c4)*3600)/(S(w.30)*vol.c);

elseif    m.check==108

   ach.a=(abs(m.a1)*3600)/(S(w.29)*vol.a);       ach.a_ex='NaN';          ach.atot='NaN';
        ach.b=(abs(m.b4)*3600)/(S(w.29)*vol.b);          ach.b_ex='NaN';          ach.btot='NaN';ach.c='NaN';
        ach.c_ex=(abs(m.ca+m.cb)*3600)/(S(w.30)*vol.c);        ach.ctot='NaN';

elseif    m.check==110

   ach.a=(abs(m.a1)*3600)/(S(w.29)*vol.a);       ach.a_ex='NaN';          ach.atot='NaN';
        ach.b=(abs(m.b4)*3600)/(S(w.29)*vol.b);          ach.b_ex='NaN';          ach.btot='NaN';
        ach.c=(abs(m.c4)*3600)/(S(w.30)*vol.c);          ach.c_ex=(abs(m.ca+m.cb)*3600)/(S(w.30)*vol.c);
        ach.ctot=(abs(m.ca+m.cb+m.c4)*3600)/(S(w.30)*vol.c);

elseif    m.check==112

   ach.a=(abs(m.a1)*3600)/(S(w.29)*vol.a);       ach.a_ex='NaN';          ach.atot='NaN';
        ach.b=(abs(m.b4)*3600)/(S(w.29)*vol.b);          ach.b_ex='NaN';          ach.btot='NaN';
        ach.c=(abs(m.c3)*3600)/(S(w.30)*vol.c);          ach.c_ex=(abs(m.ca+m.cb)*3600)/(S(w.30)*vol.c);
        ach.ctot=(abs(m.ca+m.cb+m.c3)*3600)/(S(w.30)*vol.c);

elseif    m.check==114
```

```
  ach.a=(abs(m.a1)*3600)/(S(w.29)*vol.a);      ach.a_ex='NaN';          ach.atot='NaN';
        ach.b=(abs(m.b2)*3600)/(S(w.29)*vol.b);      ach.b_ex='NaN';          ach.btot='NaN';ach.c='NaN';
        ach.c_ex=(abs(m.ca+m.cb)*3600)/(S(w.30)*vol.c);      ach.ctot='NaN';

elseif  m.check==116

  ach.a=(abs(m.a1)*3600)/(S(w.29)*vol.a);      ach.a_ex='NaN';          ach.atot='NaN';
        ach.b=(abs(m.b2)*3600)/(S(w.29)*vol.b);      ach.b_ex='NaN';          ach.btot='NaN';
        ach.c=(abs(m.c4)*3600)/(S(w.30)*vol.c);      ach.c_ex=(abs(m.ca+m.cb)*3600)/(S(w.30)*vol.c);
        ach.ctot=(abs(m.ca+m.cb+m.c4)*3600)/(S(w.30)*vol.c);

elseif  m.check==118

  ach.a=(abs(m.a1)*3600)/(S(w.29)*vol.a);      ach.a_ex='NaN';          ach.atot='NaN';
        ach.b=(abs(m.b2)*3600)/(S(w.29)*vol.b);      ach.b_ex='NaN';          ach.btot='NaN';
        ach.c=(abs(m.c3)*3600)/(S(w.30)*vol.c);      ach.c_ex=(abs(m.ca+m.cb)*3600)/(S(w.30)*vol.c);
        ach.ctot=(abs(m.ca+m.cb+m.c3)*3600)/(S(w.30)*vol.c);

elseif  m.check==120

  ach.a=(abs(m.a1)*3600)/(S(w.29)*vol.a);      ach.a_ex='NaN';          ach.atot='NaN';
        ach.b=(abs(m.b4)*3600)/(S(w.29)*vol.b);      ach.b_ex=(abs(m.bc)*3600)/(S(w.29)*vol.b);
        ach.btot=(abs(m.b4+m.bc)*3600)/(S(w.29)*vol.b);      ach.c='NaN';
        ach.c_ex=(abs(m.ca)*3600)/(S(w.30)*vol.c);      ach.ctot='NaN';

elseif  m.check==122

  ach.a=(abs(m.a1)*3600)/(S(w.29)*vol.a);      ach.a_ex='NaN';          ach.atot='NaN';
        ach.b=(abs(m.b4)*3600)/(S(w.29)*vol.b);      ach.b_ex=(abs(m.bc)*3600)/(S(w.29)*vol.b);
        ach.btot=(abs(m.b4+m.bc)*3600)/(S(w.29)*vol.b);      ach.c=(abs(m.c4)*3600)/(S(w.30)*vol.c);
        ach.c_ex=(abs(m.ca)*3600)/(S(w.30)*vol.c);      ach.ctot=(abs(m.ca+m.c4)*3600)/(S(w.30)*vol.c);

elseif  m.check==124

  ach.a=(abs(m.a1)*3600)/(S(w.29)*vol.a);      ach.a_ex='NaN';          ach.atot='NaN';
        ach.b=(abs(m.b4)*3600)/(S(w.29)*vol.b);      ach.b_ex=(abs(m.bc)*3600)/(S(w.29)*vol.b);
        ach.btot=(abs(m.b4+m.bc)*3600)/(S(w.29)*vol.b);      ach.c=(abs(m.c3)*3600)/(S(w.30)*vol.c);
        ach.c_ex=(abs(m.ca)*3600)/(S(w.30)*vol.c);      ach.ctot=(abs(m.ca+m.c3)*3600)/(S(w.30)*vol.c);

elseif  m.check==126

  ach.a=(abs(m.a1)*3600)/(S(w.29)*vol.a);      ach.a_ex='NaN';          ach.atot='NaN';
        ach.b=(abs(m.b4)*3600)/(S(w.29)*vol.b);      ach.b_ex=(abs(m.bc)*3600)/(S(w.29)*vol.b);
        ach.btot=(abs(m.b4+m.bc)*3600)/(S(w.29)*vol.b);
        ach.c=(abs(m.c3+m.c4)*3600)/(S(w.30)*vol.c);  ach.c_ex=(abs(m.ca)*3600)/(S(w.30)*vol.c);
        ach.ctot=(abs(m.ca+m.c3+m.c4)*3600)/(S(w.30)*vol.c);

elseif  m.check==1

  ach.a='NaN';  ach.a_ex=(abs(m.ac)*3600)/(S(w.29)*vol.a);      ach.atot='NaN';ach.b='NaN';
        ach.b_ex=(abs(m.bc)*3600)/(S(w.29)*vol.b);      ach.btot='NaN';
        ach.c=(abs(m.c3+m.c4)*3600)/(S(w.30)*vol.c);  ach.c_ex='NaN';          ach.ctot='NaN';

elseif  m.check==3
```

```
  ach.a='NaN'; ach.a_ex=(abs(m.ac)*3600)/(S(w.29)*vol.a);     ach.atot='NaN';ach.b='NaN';
        ach.b_ex=(abs(m.bc)*3600)/(S(w.29)*vol.b);     ach.btot='NaN';
        ach.c=(abs(m.c3)*3600)/(S(w.30)*vol.c);          ach.c_ex='NaN';          ach.ctot='NaN';

elseif    m.check==5

  ach.a='NaN'; ach.a_ex=(abs(m.ac)*3600)/(S(w.29)*vol.a);     ach.atot='NaN';ach.b='NaN';
        ach.b_ex=(abs(m.bc)*3600)/(S(w.29)*vol.b);     ach.btot='NaN';
        ach.c=(abs(m.c4)*3600)/(S(w.30)*vol.c);          ach.c_ex='NaN';          ach.ctot='NaN';

elseif    m.check==7

  ach.a='NaN'; ach.a_ex=(abs(m.ac)*3600)/(S(w.29)*vol.a);     ach.atot='NaN';
        ach.b=(abs(m.b2+m.b4)*3600)/(S(w.29)*vol.b);ach.b_ex='NaN';          ach.btot='NaN';
        ach.c=(abs(m.c3+m.c4)*3600)/(S(w.30)*vol.c);  ach.c_ex=(abs(m.cb)*3600)/(S(w.30)*vol.c);
        ach.ctot=(abs(m.cb+m.c3+m.c4)*3600)/(S(w.30)*vol.c);

elseif    m.check==9

  ach.a='NaN'; ach.a_ex=(abs(m.ac)*3600)/(S(w.29)*vol.a);     ach.atot='NaN';
        ach.b=(abs(m.b2+m.b4)*3600)/(S(w.29)*vol.b);ach.b_ex='NaN';          ach.btot='NaN';
        ach.c=(abs(m.c3)*3600)/(S(w.30)*vol.c);          ach.c_ex=(abs(m.cb)*3600)/(S(w.30)*vol.c)
        ach.ctot=(abs(m.cb+m.c3)*3600)/(S(w.30)*vol.c);

elseif    m.check==11

  ach.a='NaN'; ach.a_ex=(abs(m.ac)*3600)/(S(w.29)*vol.a);     ach.atot='NaN';
        ach.b=(abs(m.b2+m.b4)*3600)/(S(w.29)*vol.b);ach.b_ex='NaN';          ach.btot='NaN';
        ach.c=(abs(m.c4)*3600)/(S(w.30)*vol.c);          ach.c_ex=(abs(m.cb)*3600)/(S(w.30)*vol.c);
        ach.ctot=(abs(m.cb+m.c4)*3600)/(S(w.30)*vol.c);

elseif    m.check==13

  ach.a='NaN'; ach.a_ex=(abs(m.ac)*3600)/(S(w.29)*vol.a);     ach.atot='NaN';
        ach.b=(abs(m.b2+m.b4)*3600)/(S(w.29)*vol.b);ach.b_ex='NaN';          ach.btot='NaN';ach.c='NaN';
        ach.c_ex=(abs(m.cb)*3600)/(S(w.30)*vol.c);     ach.ctot='NaN';

elseif    m.check==15

  ach.a='NaN'; ach.a_ex=(abs(m.ac)*3600)/(S(w.29)*vol.a);     ach.atot='NaN';
        ach.b=(abs(m.b4)*3600)/(S(w.29)*vol.b);          ach.b_ex='NaN';          ach.btot='NaN';
        ach.c=(abs(m.c3+m.c4)*3600)/(S(w.30)*vol.c);  ach.c_ex=(abs(m.cb)*3600)/(S(w.30)*vol.c);
        ach.ctot=(abs(m.cb+m.c3+m.c4)*3600)/(S(w.30)*vol.c);

elseif    m.check==17

  ach.a='NaN'; ach.a_ex=(abs(m.ac)*3600)/(S(w.29)*vol.a);     ach.atot='NaN';
        ach.b=(abs(m.b4)*3600)/(S(w.29)*vol.b);          ach.b_ex='NaN';          ach.btot='NaN';
        ach.c=(abs(m.c3)*3600)/(S(w.30)*vol.c);          ach.c_ex=(abs(m.cb)*3600)/(S(w.30)*vol.c);
        ach.ctot=(abs(m.cb+m.c3)*3600)/(S(w.30)*vol.c);

elseif    m.check==19

  ach.a='NaN'; ach.a_ex=(abs(m.ac)*3600)/(S(w.29)*vol.a);     ach.atot='NaN';
        ach.b=(abs(m.b4)*3600)/(S(w.29)*vol.b);          ach.b_ex='NaN';          ach.btot='NaN';
```

```
        ach.c=(abs(m.c4)*3600)/(S(w.30)*vol.c);          ach.c_ex=(abs(m.cb)*3600)/(S(w.30)*vol.c);
        ach.ctot=(abs(m.cb+m.c4)*3600)/(S(w.30)*vol.c);

elseif  m.check==21

  ach.a='NaN'; ach.a_ex=(abs(m.ac)*3600)/(S(w.29)*vol.a);    ach.atot='NaN';
        ach.b=(abs(m.b4)*3600)/(S(w.29)*vol.b);          ach.b_ex='NaN';          ach.btot='NaN';ach.c='NaN';
        ach.c_ex=(abs(m.cb)*3600)/(S(w.30)*vol.c);     ach.ctot='NaN';

elseif  m.check==23

  ach.a='NaN'; ach.a_ex=(abs(m.ac)*3600)/(S(w.29)*vol.a);    ach.atot='NaN';
        ach.b=(abs(m.b2)*3600)/(S(w.29)*vol.b);          ach.b_ex=(abs(m.bc)*3600)/(S(w.29)*vol.b);
        ach.btot=(abs(m.b2+m.bc)*3600)/(S(w.29)*vol.b);
        ach.c=(abs(m.c3+m.c4)*3600)/(S(w.30)*vol.c); ach.c_ex='NaN';          ach.ctot='NaN';

elseif  m.check==25

  ach.a='NaN'; ach.a_ex=(abs(m.ac)*3600)/(S(w.29)*vol.a);    ach.atot='NaN';
        ach.b=(abs(m.b2)*3600)/(S(w.29)*vol.b);          ach.b_ex=(abs(m.bc)*3600)/(S(w.29)*vol.b);
        ach.btot=(abs(m.b2+m.bc)*3600)/(S(w.29)*vol.b);       ach.c=(abs(m.c3)*3600)/(S(w.30)*vol.c);
        ach.c_ex='NaN';          ach.ctot='NaN';

elseif  m.check==27

  ach.a='NaN'; ach.a_ex=(abs(m.ac)*3600)/(S(w.29)*vol.a);    ach.atot='NaN';ach.b=
        (abs(m.b2)*3600)/(S(w.29)*vol.b);       ach.b_ex=(abs(m.bc)*3600)/(S(w.29)*vol.b);
        ach.btot=(abs(m.b2+m.bc)*3600)/(S(w.29)*vol.b);       ach.c=(abs(m.c4)*3600)/(S(w.30)*vol.c);
        ach.c_ex='NaN';          ach.ctot='NaN';

elseif  m.check==29

  ach.a='NaN'; ach.a_ex=(abs(m.ac)*3600)/(S(w.29)*vol.a);    ach.atot='NaN';
        ach.b=(abs(m.b4)*3600)/(S(w.29)*vol.b);          ach.b_ex=(abs(m.bc)*3600)/(S(w.29)*vol.b);
        ach.btot=(abs(m.b4+m.bc)*3600)/(S(w.29)*vol.b);
        ach.c=(abs(m.c3+m.c4)*3600)/(S(w.30)*vol.c); ach.c_ex='NaN';          ach.ctot='NaN';

elseif  m.check==31

  ach.a='NaN'; ach.a_ex=(abs(m.ac)*3600)/(S(w.29)*vol.a);    ach.atot='NaN';
        ach.b=(abs(m.b4)*3600)/(S(w.29)*vol.b);          ach.b_ex=(abs(m.bc)*3600)/(S(w.29)*vol.b);
        ach.btot=(abs(m.b4+m.bc)*3600)/(S(w.29)*vol.b);       ach.c=(abs(m.c3)*3600)/(S(w.30)*vol.c);
        ach.c_ex='NaN';          ach.ctot='NaN';

elseif  m.check==33

  ach.a='NaN'; ach.a_ex=(abs(m.ac)*3600)/(S(w.29)*vol.a);    ach.atot='NaN';
        ach.b=(abs(m.b4)*3600)/(S(w.29)*vol.b);          ach.b_ex=(abs(m.bc)*3600)/(S(w.29)*vol.b);
        ach.btot=(abs(m.b4+m.bc)*3600)/(S(w.29)*vol.b);       ach.c=(abs(m.c4)*3600)/(S(w.30)*vol.c);
        ach.c_ex='NaN';          ach.ctot='NaN';

elseif  m.check==35

  ach.a='NaN'; ach.a_ex=(abs(m.ac)*3600)/(S(w.29)*vol.a);    ach.atot='NaN';
        ach.b=(abs(m.b2)*3600)/(S(w.29)*vol.b);          ach.b_ex='NaN';          ach.btot='NaN';
```

```
        ach.c=(abs(m.c3+m.c4)*3600)/(S(w.30)*vol.c);  ach.c_ex=(abs(m.cb)*3600)/(S(w.30)*vol.c);
        ach.ctot=(abs(m.cb+m.c3+m.c4)*3600)/(S(w.30)*vol.c);

elseif    m.check==37

   ach.a='NaN';  ach.a_ex=(abs(m.ac)*3600)/(S(w.29)*vol.a);     ach.atot='NaN';
        ach.b=(abs(m.b2)*3600)/(S(w.29)*vol.b);          ach.b_ex='NaN';          ach.btot='NaN';
        ach.c=(abs(m.c3)*3600)/(S(w.30)*vol.c);          ach.c_ex=(abs(m.cb)*3600)/(S(w.30)*vol.c);
        ach.ctot=(abs(m.cb+m.c3)*3600)/(S(w.30)*vol.c);

elseif    m.check==39

   ach.a='NaN';  ach.a_ex=(abs(m.ac)*3600)/(S(w.29)*vol.a);     ach.atot='NaN';
        ach.b=(abs(m.b2)*3600)/(S(w.29)*vol.b);          ach.b_ex='NaN';          ach.btot='NaN';
        ach.c=(abs(m.c4)*3600)/(S(w.30)*vol.c);          ach.c_ex=(abs(m.cb)*3600)/(S(w.30)*vol.c);
        ach.ctot=(abs(m.cb+m.c4)*3600)/(S(w.30)*vol.c);

elseif    m.check==41

   ach.a='NaN';  ach.a_ex=(abs(m.ac)*3600)/(S(w.29)*vol.a);     ach.atot='NaN';
        ach.b=(abs(m.b2)*3600)/(S(w.29)*vol.b);          ach.b_ex='NaN';          ach.btot='NaN';ach.c='NaN';
        ach.c_ex=(abs(m.cb)*3600)/(S(w.30)*vol.c);     ach.ctot='NaN';

elseif    m.check==43

   ach.a=(abs(m.a3)*3600)/(S(w.29)*vol.a);       ach.a_ex='NaN';          ach.atot='NaN';ach.b='NaN';
        ach.b_ex=(abs(m.bc)*3600)/(S(w.29)*vol.b);     ach.btot='NaN';
        ach.c=(abs(m.c3+m.c4)*3600)/(S(w.30)*vol.c);  ach.c_ex=(abs(m.ca)*3600)/(S(w.30)*vol.c);
        ach.ctot=(abs(m.ca+m.c3+m.c4)*3600)/(S(w.30)*vol.c);

elseif    m.check==45

   ach.a=(abs(m.a3)*3600)/(S(w.29)*vol.a);       ach.a_ex='NaN';          ach.atot='NaN';ach.b='NaN';
        ach.b_ex=(abs(m.bc)*3600)/(S(w.29)*vol.b);     ach.btot='NaN';
        ach.c=(abs(m.c3)*3600)/(S(w.30)*vol.c);          ach.c_ex=(abs(m.ca)*3600)/(S(w.30)*vol.c);
        ach.ctot=(abs(m.ca+m.c3)*3600)/(S(w.30)*vol.c);

elseif    m.check==47

   ach.a=(abs(m.a3)*3600)/(S(w.29)*vol.a);       ach.a_ex='NaN';          ach.atot='NaN';ach.b='NaN';
        ach.b_ex=(abs(m.bc)*3600)/(S(w.29)*vol.b);     ach.btot='NaN';
        ach.c=(abs(m.c4)*3600)/(S(w.30)*vol.c);          ach.c_ex=(abs(m.ca)*3600)/(S(w.30)*vol.c);
        ach.ctot=(abs(m.ca+m.c4)*3600)/(S(w.30)*vol.c);

elseif    m.check==49

   ach.a=(abs(m.a3)*3600)/(S(w.29)*vol.a);       ach.a_ex='NaN';          ach.atot='NaN';ach.b='NaN';
        ach.b_ex=(abs(m.bc)*3600)/(S(w.29)*vol.b);     ach.btot='NaN';ach.c='NaN';
        ach.c_ex=(abs(m.cb)*3600)/(S(w.30)*vol.c);     ach.ctot='NaN';

elseif    m.check==51

   ach.a=(abs(m.a3)*3600)/(S(w.29)*vol.a);       ach.a_ex='NaN';          ach.atot='NaN';
        ach.b=(abs(m.b2+m.b4)*3600)/(S(w.29)*vol.b);ach.b_ex='NaN';          ach.btot='NaN';
```

```
        ach.c=(abs(m.c3)*3600)/(S(w.30)*vol.c);          ach.c_ex=(abs(m.ca+m.cb)*3600)/(S(w.30)*vol.c);
        ach.ctot=(abs(m.ca+m.cb+m.c3)*3600)/(S(w.30)*vol.c);

elseif  m.check==53

  ach.a=(abs(m.a3)*3600)/(S(w.29)*vol.a);      ach.a_ex='NaN';          ach.atot='NaN';
        ach.b=(abs(m.b2+m.b4)*3600)/(S(w.29)*vol.b);ach.b_ex='NaN';          ach.btot='NaN';
        ach.c=(abs(m.c4)*3600)/(S(w.30)*vol.c);          ach.c_ex=(abs(m.ca+m.cb)*3600)/(S(w.30)*vol.c);
        ach.ctot=(abs(m.ca+m.cb+m.c4)*3600)/(S(w.30)*vol.c);

elseif  m.check==55

  ach.a=(abs(m.a3)*3600)/(S(w.29)*vol.a);      ach.a_ex='NaN';          ach.atot='NaN';
        ach.b=(abs(m.b2+m.b4)*3600)/(S(w.29)*vol.b);ach.b_ex='NaN';          ach.btot='NaN';ach.c='NaN';
        ach.c_ex=(abs(m.cb)*3600)/(S(w.30)*vol.c);     ach.ctot='NaN';

elseif  m.check==57

  ach.a=(abs(m.a3)*3600)/(S(w.29)*vol.a);      ach.a_ex='NaN';          ach.atot='NaN';
        ach.b=(abs(m.b4)*3600)/(S(w.29)*vol.b);          ach.b_ex='NaN';          ach.btot='NaN';
        ach.c=(abs(m.c3)*3600)/(S(w.30)*vol.c);          ach.c_ex=(abs(m.ca+m.cb)*3600)/(S(w.30)*vol.c);
        ach.ctot=(abs(m.ca+m.cb+m.c3)*3600)/(S(w.30)*vol.c);

elseif  m.check==59

  ach.a=(abs(m.a3)*3600)/(S(w.29)*vol.a);      ach.a_ex='NaN';          ach.atot='NaN';
        ach.b=(abs(m.b4)*3600)/(S(w.29)*vol.b);          ach.b_ex='NaN';          ach.btot='NaN';
        ach.c=(abs(m.c4)*3600)/(S(w.30)*vol.c);          ach.c_ex=(abs(m.ca+m.cb)*3600)/(S(w.30)*vol.c);
        ach.ctot=(abs(m.ca+m.cb+m.c4)*3600)/(S(w.30)*vol.c);

elseif  m.check==61

  ach.a=(abs(m.a3)*3600)/(S(w.29)*vol.a);      ach.a_ex='NaN';          ach.atot='NaN';
        ach.b=(abs(m.b4)*3600)/(S(w.29)*vol.b);          ach.b_ex='NaN';          ach.btot='NaN';ach.c='NaN';
        ach.c_ex=(abs(m.cb)*3600)/(S(w.30)*vol.c);     ach.ctot='NaN';

elseif  m.check==63

  ach.a=(abs(m.a3)*3600)/(S(w.29)*vol.a);      ach.a_ex='NaN';          ach.atot='NaN';
        ach.b=(abs(m.b2)*3600)/(S(w.29)*vol.b);          ach.b_ex=(abs(m.bc)*3600)/(S(w.29)*vol.b);
        ach.btot=(abs(m.b2+m.bc)*3600)/(S(w.29)*vol.b);
        ach.c=(abs(m.c3+m.c4)*3600)/(S(w.30)*vol.c);  ach.c_ex=(abs(m.ca)*3600)/(S(w.30)*vol.c);
        ach.ctot=(abs(m.ca+m.c3+m.c4)*3600)/(S(w.30)*vol.c);

elseif  m.check==65

  ach.a=(abs(m.a3)*3600)/(S(w.29)*vol.a);      ach.a_ex='NaN';          ach.atot='NaN';
        ach.b=(abs(m.b2)*3600)/(S(w.29)*vol.b);          ach.b_ex=(abs(m.bc)*3600)/(S(w.29)*vol.b);
        ach.btot=(abs(m.b2+m.bc)*3600)/(S(w.29)*vol.b);       ach.c=(abs(m.c3)*3600)/(S(w.30)*vol.c);
        ach.c_ex=(abs(m.ca)*3600)/(S(w.30)*vol.c);     ach.ctot=(abs(m.ca+m.c3)*3600)/(S(w.30)*vol.c);

elseif  m.check==67

  ach.a=(abs(m.a3)*3600)/(S(w.29)*vol.a);      ach.a_ex='NaN';          ach.atot='NaN';
        ach.b=(abs(m.b2)*3600)/(S(w.29)*vol.b);          ach.b_ex=(abs(m.bc)*3600)/(S(w.29)*vol.b);
```

```
        ach.btot=(abs(m.b2+m.bc)*3600)/(S(w.29)*vol.b);      ach.c=(abs(m.c4)*3600)/(S(w.30)*vol.c);
        ach.c_ex=(abs(m.ca)*3600)/(S(w.30)*vol.c);     ach.ctot=(abs(m.ca+m.c4)*3600)/(S(w.30)*vol.c);

elseif    m.check==69

   ach.a=(abs(m.a3)*3600)/(S(w.29)*vol.a);      ach.a_ex='NaN';          ach.atot='NaN';
        ach.b=(abs(m.b2)*3600)/(S(w.29)*vol.b);         ach.b_ex=(abs(m.bc)*3600)/(S(w.29)*vol.b);
        ach.btot=(abs(m.b2+m.bc)*3600)/(S(w.29)*vol.b);      ach.c='NaN';
        ach.c_ex=(abs(m.cb)*3600)/(S(w.30)*vol.c);     ach.ctot='NaN';

elseif    m.check==71

   ach.a=(abs(m.a3)*3600)/(S(w.29)*vol.a);      ach.a_ex='NaN';          ach.atot='NaN';
        ach.b=(abs(m.b4)*3600)/(S(w.29)*vol.b);         ach.b_ex=(abs(m.bc)*3600)/(S(w.29)*vol.b);
        ach.btot=(abs(m.b4+m.bc)*3600)/(S(w.29)*vol.b);
        ach.c=(abs(m.c3+m.c4)*3600)/(S(w.30)*vol.c); ach.c_ex=(abs(m.ca)*3600)/(S(w.30)*vol.c);
        ach.ctot=(abs(m.ca+m.c3+m.c4)*3600)/(S(w.30)*vol.c);

elseif    m.check==73

   ach.a=(abs(m.a3)*3600)/(S(w.29)*vol.a);      ach.a_ex='NaN';          ach.atot='NaN';
        ach.b=(abs(m.b4)*3600)/(S(w.29)*vol.b);         ach.b_ex=(abs(m.bc)*3600)/(S(w.29)*vol.b);
        ach.btot=(abs(m.b4+m.bc)*3600)/(S(w.29)*vol.b);      ach.c=(abs(m.c3)*3600)/(S(w.30)*vol.c);
        ach.c_ex=(abs(m.ca)*3600)/(S(w.30)*vol.c);     ach.ctot=(abs(m.ca+m.c3)*3600)/(S(w.30)*vol.c);

elseif    m.check==75

   ach.a=(abs(m.a3)*3600)/(S(w.29)*vol.a);      ach.a_ex='NaN';          ach.atot='NaN';
        ach.b=(abs(m.b4)*3600)/(S(w.29)*vol.b);         ach.b_ex=(abs(m.bc)*3600)/(S(w.29)*vol.b);
        ach.btot=(abs(m.b4+m.bc)*3600)/(S(w.29)*vol.b);      ach.c=(abs(m.c4)*3600)/(S(w.30)*vol.c);
        ach.c_ex=(abs(m.ca)*3600)/(S(w.30)*vol.c);     ach.ctot=(abs(m.ca+m.c4)*3600)/(S(w.30)*vol.c);

elseif    m.check==77

   ach.a=(abs(m.a3)*3600)/(S(w.29)*vol.a);      ach.a_ex='NaN';          ach.atot='NaN';
        ach.b=(abs(m.b4)*3600)/(S(w.29)*vol.b);         ach.b_ex=(abs(m.bc)*3600)/(S(w.29)*vol.b);
        ach.btot=(abs(m.b4+m.bc)*3600)/(S(w.29)*vol.b);      ach.c='NaN';
        ach.c_ex=(abs(m.cb)*3600)/(S(w.30)*vol.c);     ach.ctot='NaN';

elseif    m.check==79

   ach.a=(abs(m.a3)*3600)/(S(w.29)*vol.a);      ach.a_ex='NaN';          ach.atot='NaN';
        ach.b=(abs(m.b2)*3600)/(S(w.29)*vol.b);         ach.b_ex='NaN';          ach.btot='NaN';
        ach.c=(abs(m.c3)*3600)/(S(w.30)*vol.c);         ach.c_ex=(abs(m.ca+m.cb)*3600)/(S(w.30)*vol.c);
        ach.ctot=(abs(m.ca+m.cb+m.c3)*3600)/(S(w.30)*vol.c);

elseif    m.check==81

   ach.a=(abs(m.a3)*3600)/(S(w.29)*vol.a);      ach.a_ex='NaN';          ach.atot='NaN';
        ach.b=(abs(m.b2)*3600)/(S(w.29)*vol.b);         ach.b_ex='NaN';          ach.btot='NaN';
        ach.c=(abs(m.c4)*3600)/(S(w.30)*vol.c);         ach.c_ex=(abs(m.ca+m.cb)*3600)/(S(w.30)*vol.c);
        ach.ctot=(abs(m.ca+m.cb+m.c4)*3600)/(S(w.30)*vol.c);

elseif    m.check==83
```

```
  ach.a=(abs(m.a3)*3600)/(S(w.29)*vol.a);      ach.a_ex='NaN';          ach.atot='NaN';
        ach.b=(abs(m.b2)*3600)/(S(w.29)*vol.b);      ach.b_ex='NaN';          ach.btot='NaN';ach.c='NaN';
        ach.c_ex=(abs(m.cb)*3600)/(S(w.30)*vol.c);   ach.ctot='NaN';

elseif  m.check==85

  ach.a=(abs(m.a3)*3600)/(S(w.29)*vol.a);      ach.a_ex=(abs(m.ac)*3600)/(S(w.29)*vol.a);
        ach.atot=(abs(m.a3+m.ac)*3600)/(S(w.29)*vol.a);      ach.b='NaN';
        ach.b_ex=(abs(m.bc)*3600)/(S(w.29)*vol.b);   ach.btot='NaN';
        ach.c=(abs(m.c3+m.c4)*3600)/(S(w.30)*vol.c); ach.c_ex='NaN';          ach.ctot='NaN';

elseif  m.check==87

  ach.a=(abs(m.a3)*3600)/(S(w.29)*vol.a);      ach.a_ex=(abs(m.ac)*3600)/(S(w.29)*vol.a);
        ach.atot=(abs(m.a3+m.ac)*3600)/(S(w.29)*vol.a);      ach.b='NaN';
        ach.b_ex=(abs(m.bc)*3600)/(S(w.29)*vol.b);   ach.btot='NaN';
        ach.c=(abs(m.c3)*3600)/(S(w.30)*vol.c);      ach.c_ex='NaN';          ach.ctot='NaN';

elseif  m.check==89

  ach.a=(abs(m.a3)*3600)/(S(w.29)*vol.a);      ach.a_ex=(abs(m.ac)*3600)/(S(w.29)*vol.a);
        ach.atot=(abs(m.a3+m.ac)*3600)/(S(w.29)*vol.a);      ach.b='NaN';
        ach.b_ex=(abs(m.bc)*3600)/(S(w.29)*vol.b);   ach.btot='NaN';
        ach.c=(abs(m.c4)*3600)/(S(w.30)*vol.c);      ach.c_ex='NaN';          ach.ctot='NaN';

elseif  m.check==91

  ach.a=(abs(m.a3)*3600)/(S(w.29)*vol.a);      ach.a_ex=(abs(m.ac)*3600)/(S(w.29)*vol.a);
        ach.atot=(abs(m.a3+m.ac)*3600)/(S(w.29)*vol.a);
        ach.b=(abs(m.b2+m.b4)*3600)/(S(w.29)*vol.b);ach.b_ex='NaN';          ach.btot='NaN';
        ach.c=(abs(m.c3+m.c4)*3600)/(S(w.30)*vol.c); ach.c_ex=(abs(m.cb)*3600)/(S(w.30)*vol.c);
        ach.ctot=(abs(m.cb+m.c3+m.c4)*3600)/(S(w.30)*vol.c);

elseif  m.check==93

  ach.a=(abs(m.a3)*3600)/(S(w.29)*vol.a);      ach.a_ex=(abs(m.ac)*3600)/(S(w.29)*vol.a);
        ach.atot=(abs(m.a3+m.ac)*3600)/(S(w.29)*vol.a);
        ach.b=(abs(m.b2+m.b4)*3600)/(S(w.29)*vol.b);ach.b_ex='NaN';          ach.btot='NaN';
        ach.c=(abs(m.c3)*3600)/(S(w.30)*vol.c);      ach.c_ex=(abs(m.cb)*3600)/(S(w.30)*vol.c);
        ach.ctot=(abs(m.cb+m.c3)*3600)/(S(w.30)*vol.c);

elseif  m.check==95

  ach.a=(abs(m.a3)*3600)/(S(w.29)*vol.a);      ach.a_ex=(abs(m.ac)*3600)/(S(w.29)*vol.a);
        ach.atot=(abs(m.a3+m.ac)*3600)/(S(w.29)*vol.a);
        ach.b=(abs(m.b2+m.b4)*3600)/(S(w.29)*vol.b);ach.b_ex='NaN';          ach.btot='NaN';
        ach.c=(abs(m.c4)*3600)/(S(w.30)*vol.c);      ach.c_ex=(abs(m.cb)*3600)/(S(w.30)*vol.c);
        ach.ctot=(abs(m.cb+m.c4)*3600)/(S(w.30)*vol.c);

elseif  m.check==97

  ach.a=(abs(m.a3)*3600)/(S(w.29)*vol.a);      ach.a_ex=(abs(m.ac)*3600)/(S(w.29)*vol.a);
        ach.atot=(abs(m.a3+m.ac)*3600)/(S(w.29)*vol.a);
```

```
        ach.b=(abs(m.b2+m.b4)*3600)/(S(w.29)*vol.b);ach.b_ex='NaN';          ach.btot='NaN';ach.c='NaN';
        ach.c_ex=(abs(m.cb)*3600)/(S(w.30)*vol.c);     ach.ctot='NaN';

elseif  m.check==99

  ach.a=(abs(m.a3)*3600)/(S(w.29)*vol.a);      ach.a_ex=(abs(m.ac)*3600)/(S(w.29)*vol.a);
        ach.atot=(abs(m.a3+m.ac)*3600)/(S(w.29)*vol.a);      ach.b=(abs(m.b4)*3600)/(S(w.29)*vol.b);
        ach.b_ex='NaN';          ach.btot='NaN';ach.c=(abs(m.c3+m.c4)*3600)/(S(w.30)*vol.c);
        ach.c_ex=(abs(m.cb)*3600)/(S(w.30)*vol.c);
        ach.ctot=(abs(m.cb+m.c3+m.c4)*3600)/(S(w.30)*vol.c);

elseif  m.check==101

  ach.a=(abs(m.a3)*3600)/(S(w.29)*vol.a);      ach.a_ex=(abs(m.ac)*3600)/(S(w.29)*vol.a);
        ach.atot=(abs(m.a3+m.ac)*3600)/(S(w.29)*vol.a);      ach.b=(abs(m.b4)*3600)/(S(w.29)*vol.b);
        ach.b_ex='NaN';          ach.btot='NaN';ach.c=(abs(m.c3)*3600)/(S(w.30)*vol.c);
        ach.c_ex=(abs(m.cb)*3600)/(S(w.30)*vol.c);     ach.ctot=(abs(m.cb+m.c3)*3600)/(S(w.30)*vol.c);

elseif  m.check==103

  ach.a=(abs(m.a3)*3600)/(S(w.29)*vol.a);      ach.a_ex=(abs(m.ac)*3600)/(S(w.29)*vol.a);
        ach.atot=(abs(m.a3+m.ac)*3600)/(S(w.29)*vol.a);      ach.b=(abs(m.b4)*3600)/(S(w.29)*vol.b);
        ach.b_ex='NaN';          ach.btot='NaN';ach.c=(abs(m.c4)*3600)/(S(w.30)*vol.c);
        ach.c_ex=(abs(m.cb)*3600)/(S(w.30)*vol.c);     ach.ctot=(abs(m.cb+m.c4)*3600)/(S(w.30)*vol.c);

elseif  m.check==105

  ach.a=(abs(m.a3)*3600)/(S(w.29)*vol.a);      ach.a_ex=(abs(m.ac)*3600)/(S(w.29)*vol.a);
        ach.atot=(abs(m.a3+m.ac)*3600)/(S(w.29)*vol.a);      ach.b=(abs(m.b4)*3600)/(S(w.29)*vol.b);
        ach.b_ex='NaN';          ach.btot='NaN';ach.c='NaN';    ach.c_ex=(abs(m.cb)*3600)/(S(w.30)*vol.c);
        ach.ctot='NaN';

elseif  m.check==107

  ach.a=(abs(m.a3)*3600)/(S(w.29)*vol.a);      ach.a_ex=(abs(m.ac)*3600)/(S(w.29)*vol.a);
        ach.atot=(abs(m.a3+m.ac)*3600)/(S(w.29)*vol.a);      ach.b=(abs(m.b2)*3600)/(S(w.29)*vol.b);
        ach.b_ex=(abs(m.bc)*3600)/(S(w.29)*vol.b);    ach.btot=(abs(m.b2+m.bc)*3600)/(S(w.29)*vol.b);
        ach.c=(abs(m.c3+m.c4)*3600)/(S(w.30)*vol.c); ach.c_ex='NaN';          ach.ctot='NaN';

elseif  m.check==109

  ach.a=(abs(m.a3)*3600)/(S(w.29)*vol.a);      ach.a_ex=(abs(m.ac)*3600)/(S(w.29)*vol.a);
        ach.atot=(abs(m.a3+m.ac)*3600)/(S(w.29)*vol.a);      ach.b=(abs(m.b2)*3600)/(S(w.29)*vol.b);
        ach.b_ex=(abs(m.bc)*3600)/(S(w.29)*vol.b);    ach.btot=(abs(m.b2+m.bc)*3600)/(S(w.29)*vol.b);
        ach.c=(abs(m.c3)*3600)/(S(w.30)*vol.c);          ach.c_ex='NaN';          ach.ctot='NaN';

elseif  m.check==111

  ach.a=(abs(m.a3)*3600)/(S(w.29)*vol.a);      ach.a_ex=(abs(m.ac)*3600)/(S(w.29)*vol.a);
        ach.atot=(abs(m.a3+m.ac)*3600)/(S(w.29)*vol.a);      ach.b=(abs(m.b2)*3600)/(S(w.29)*vol.b);
        ach.b_ex=(abs(m.bc)*3600)/(S(w.29)*vol.b);    ach.btot=(abs(m.b2+m.bc)*3600)/(S(w.29)*vol.b);
        ach.c=(abs(m.c4)*3600)/(S(w.30)*vol.c);          ach.c_ex='NaN';          ach.ctot='NaN';

elseif  m.check==113
```

```
  ach.a=(abs(m.a3)*3600)/(S(w.29)*vol.a);      ach.a_ex=(abs(m.ac)*3600)/(S(w.29)*vol.a);
       ach.atot=(abs(m.a3+m.ac)*3600)/(S(w.29)*vol.a);      ach.b=(abs(m.b4)*3600)/(S(w.29)*vol.b);
       ach.b_ex=(abs(m.bc)*3600)/(S(w.29)*vol.b);    ach.btot=(abs(m.b4+m.bc)*3600)/(S(w.29)*vol.b);
       ach.c=(abs(m.c3+m.c4)*3600)/(S(w.30)*vol.c); ach.c_ex='NaN';          ach.ctot='NaN';

elseif   m.check==115

  ach.a=(abs(m.a3)*3600)/(S(w.29)*vol.a);      ach.a_ex=(abs(m.ac)*3600)/(S(w.29)*vol.a);
       ach.atot=(abs(m.a3+m.ac)*3600)/(S(w.29)*vol.a);      ach.b=(abs(m.b4)*3600)/(S(w.29)*vol.b);
       ach.b_ex=(abs(m.bc)*3600)/(S(w.29)*vol.b);    ach.btot=(abs(m.b4+m.bc)*3600)/(S(w.29)*vol.b);
       ach.c=(abs(m.c3)*3600)/(S(w.30)*vol.c);          ach.c_ex='NaN';          ach.ctot='NaN';

elseif   m.check==117

  ach.a=(abs(m.a3)*3600)/(S(w.29)*vol.a);      ach.a_ex=(abs(m.ac)*3600)/(S(w.29)*vol.a);
       ach.atot=(abs(m.a3+m.ac)*3600)/(S(w.29)*vol.a);      ach.b=(abs(m.b4)*3600)/(S(w.29)*vol.b);
       ach.b_ex=(abs(m.bc)*3600)/(S(w.29)*vol.b);    ach.btot=(abs(m.b4+m.bc)*3600)/(S(w.29)*vol.b);
       ach.c=(abs(m.c4)*3600)/(S(w.30)*vol.c);          ach.c_ex='NaN';          ach.ctot='NaN';

elseif   m.check==119

  ach.a=(abs(m.a3)*3600)/(S(w.29)*vol.a);      ach.a_ex=(abs(m.ac)*3600)/(S(w.29)*vol.a);
       ach.atot=(abs(m.a3+m.ac)*3600)/(S(w.29)*vol.a);      ach.b=(abs(m.b2)*3600)/(S(w.29)*vol.b);
       ach.b_ex='NaN';          ach.btot='NaN';ach.c=(abs(m.c3+m.c4)*3600)/(S(w.30)*vol.c);
       ach.c_ex=(abs(m.cb)*3600)/(S(w.30)*vol.c);
       ach.ctot=(abs(m.cb+m.c3+m.c4)*3600)/(S(w.30)*vol.c);

elseif   m.check==121

  ach.a=(abs(m.a3)*3600)/(S(w.29)*vol.a);      ach.a_ex=(abs(m.ac)*3600)/(S(w.29)*vol.a);
       ach.atot=(abs(m.a3+m.ac)*3600)/(S(w.29)*vol.a);      ach.b=(abs(m.b2)*3600)/(S(w.29)*vol.b);
       ach.b_ex='NaN';          ach.btot='NaN';ach.c=(abs(m.c3)*3600)/(S(w.30)*vol.c);
       ach.c_ex=(abs(m.cb)*3600)/(S(w.30)*vol.c);     ach.ctot=(abs(m.cb+m.c3)*3600)/(S(w.30)*vol.c);

elseif   m.check==123

  ach.a=(abs(m.a3)*3600)/(S(w.29)*vol.a);      ach.a_ex=(abs(m.ac)*3600)/(S(w.29)*vol.a);
       ach.atot=(abs(m.a3+m.ac)*3600)/(S(w.29)*vol.a);      ach.b=(abs(m.b2)*3600)/(S(w.29)*vol.b);
       ach.b_ex='NaN';          ach.btot='NaN';ach.c=(abs(m.c4)*3600)/(S(w.30)*vol.c);
       ach.c_ex=(abs(m.cb)*3600)/(S(w.30)*vol.c);     ach.ctot=(abs(m.cb+m.c4)*3600)/(S(w.30)*vol.c);

elseif   m.check==125

  ach.a=(abs(m.a3)*3600)/(S(w.29)*vol.a);      ach.a_ex=(abs(m.ac)*3600)/(S(w.29)*vol.a);
       ach.atot=(abs(m.a3+m.ac)*3600)/(S(w.29)*vol.a);      ach.b=(abs(m.b2)*3600)/(S(w.29)*vol.b);
       ach.b_ex='NaN';          ach.btot='NaN';ach.c='NaN';     ach.c_ex=(abs(m.cb)*3600)/(S(w.30)*vol.c);
       ach.ctot='NaN';

else

    ach.a= 'NaN'; ach.a_ex= 'NaN'; ach.atot= 'NaN';

    ach.b= 'NaN'; ach.b_ex= 'NaN'; ach.btot= 'NaN';

    ach.c= 'Nan'; ach.c_ex='Nan'; ach.ctot= 'Nan';
```

```
end
ach.exitflag = message;
if (message == 1 || message == 2 || message == 3) && (isnan(m.check) == 0)
   ach.feasibility = 'feasibile';
%       if isnan(ach.c) || isnan(ach.ctot)
%           ach.feasibily = 'no feasibility';
else
   ach.feasibility = 'no feasibility';
end
ach.index = jj; ach.w=w;
ach.check = m.check;ach.error = B.check; ach.err_rel= B.rel;
ach.ma1 = m.a1; ach.mac = m.ac; ach.ma3 = m.a3; ach.mb2 = m.b2; ach.mbc = m.bc; ach.mb4 = m.b4;
ach.mca = m.ca; ach.mcb = m.cb; ach.mc3 = m.c3; ach.mc4 = m.c4; ach.mbld = m.bld; ach.bld = H.bld;
ach.pfun=pfun.pfun;
end
```